

1984

Ground Reaction And Behaviour Of Tunnels In Soft Clays

Robert Man Ng

Follow this and additional works at: <https://ir.lib.uwo.ca/digitizedtheses>

Recommended Citation

Ng, Robert Man, "Ground Reaction And Behaviour Of Tunnels In Soft Clays" (1984). *Digitized Theses*. 1392.
<https://ir.lib.uwo.ca/digitizedtheses/1392>

This Dissertation is brought to you for free and open access by the Digitized Special Collections at Scholarship@Western. It has been accepted for inclusion in Digitized Theses by an authorized administrator of Scholarship@Western. For more information, please contact tadam@uwo.ca, wlsadmin@uwo.ca.

The author of this thesis has granted The University of Western Ontario a non-exclusive license to reproduce and distribute copies of this thesis to users of Western Libraries. Copyright remains with the author.

Electronic theses and dissertations available in The University of Western Ontario's institutional repository (Scholarship@Western) are solely for the purpose of private study and research. They may not be copied or reproduced, except as permitted by copyright laws, without written authority of the copyright owner. Any commercial use or publication is strictly prohibited.

The original copyright license attesting to these terms and signed by the author of this thesis may be found in the original print version of the thesis, held by Western Libraries.

The thesis approval page signed by the examining committee may also be found in the original print version of the thesis held in Western Libraries.

Please contact Western Libraries for further information:

E-mail: libadmin@uwo.ca

Telephone: (519) 661-2111 Ext. 84796

Web site: <http://www.lib.uwo.ca/>

CANADIAN THESES ON MICROFICHE

I.S.B.N.

THESES CANADIENNES SUR MICROFICHE



National Library of Canada
Collections Development Branch

Canadian Theses on
Microfiche Service

Ottawa, Canada
K1A 0N4

Bibliothèque nationale du Canada
Direction du développement des collections

Service des thèses canadiennes
sur microfiche

NOTICE

The quality of this microfiche is heavily dependent upon the quality of the original thesis submitted for microfilming. Every effort has been made to ensure the highest quality of reproduction possible.

If pages are missing, contact the university which granted the degree.

Some pages may have indistinct print especially if the original pages were typed with a poor typewriter ribbon or if the university sent us a poor photocopy.

Previously copyrighted materials (journal articles, published tests, etc.) are not filmed.

Reproduction in full or in part of this film is governed by the Canadian Copyright Act, R.S.C. 1970, c. C-30. Please read the authorization forms which accompany this thesis.

**THIS DISSERTATION
HAS BEEN MICROFILMED
EXACTLY AS RECEIVED**

AVIS

La qualité de cette microfiche dépend grandement de la qualité de la thèse soumise au microfilmage. Nous avons tout fait pour assurer une qualité supérieure de reproduction.

S'il manque des pages, veuillez communiquer avec l'université qui a conféré le grade.

La qualité d'impression de certaines pages peut laisser à désirer, surtout si les pages originales ont été dactylographiées à l'aide d'un ruban usé ou si l'université nous a fait parvenir une photocopie de mauvaise qualité.

Les documents qui font déjà l'objet d'un droit d'auteur (articles de revue, examens publiés, etc.) ne sont pas microfilmés.

La reproduction, même partielle, de ce microfilm est soumise à la Loi canadienne sur le droit d'auteur, SRC 1970, c. C-30. Veuillez prendre connaissance des formules d'autorisation qui accompagnent cette thèse.

**LA THÈSE A ÉTÉ
MICROFILMÉE TELLE QUE
NOUS L'AVONS REÇUE**

GROUND REACTION AND BEHAVIOUR OF TUNNELS

IN SOFT CLAYS

VOLUME I

by

Robert Man Chiu Ng

Faculty of Engineering Science

Submitted in partial fulfillment
of the requirements for the degree of
Doctor of Philosophy

Faculty of Graduate Studies
The University of Western Ontario

London, Ontario

August, 1984

© Robert Man Chiu Ng 1984

ABSTRACT

A consistent, systematic approach for predicting settlements above tunnels in soft clay is presented. This predictive scheme provides firstly, a simple method for calculating the maximum surface settlement, and secondly, a detailed method for determining the overall pattern of displacements. In the simple method, the maximum surface settlement is estimated from its relationship with the crown displacement which can be calculated theoretically. The detailed method requires finite element analysis and comprehensive field and laboratory testing. Since the detailed analysis may be used for predicting subsurface as well as surface displacements, it is considered to be very useful for analyzing critical sections of a tunnel. The development of this technique is described and its validity and applicability are examined.

Settlement due to tunnelling is generally attributed to loss of ground and volume change in soil. In this thesis, a gap parameter is used to quantify ground loss and to model approximately the effect of soil reconsolidation in the remoulded area above the crown. The components of the gap parameter are i) the three-dimensional elasto-plastic deformation at the advancing face of the tunnel, ii) the physical gap defined by the shield-lining geometry, iii) the displacement associated with workmanship which includes the effect of grouting. An additional component due to consolidation of remoulded soil above the crown may

be included as part of the gap where appropriate. The practicality of using this parameter derives from its simplicity in calculation and only conventional soil parameters are required. Comparison of the calculated gap with available field observations showed reasonable agreement. From a study of thirteen case records, an empirical relationship is established for predicting surface settlement from the gap parameter.

A method of detailed analysis using the finite element method is presented. This analysis which is used in conjunction with the concept of the gap parameter, adopts an anisotropic elastic-perfectly plastic model for soil behaviour. The analysis is also formulated to permit consideration of the construction procedure, soil-filler interaction and variation of soil properties with depth.

An extensive field and laboratory investigation of the Thunder Bay soil is performed. The stratigraphy of the instrumented arrays to be examined is well defined. It is shown that the consideration of the appropriate soil stress path is essential in the selection of soil parameters for use in the analysis. In particular, it is pointed out that the operative elastic modulus used in the analysis should correspond to the unloading mode. For the Thunder Bay silty and varved clay, the modulus in unloading is approximately twice the modulus in loading, and Poisson's ratio in unloading is approximately three times that obtained in loading. However, the independent shear modulus, effective friction angle and cohesion are relatively independent of

stress path.

Using the results of the comprehensive test program, analyses have been performed with the method developed for the prediction of the magnitude and distribution of surface and subsurface settlements. The validity of the method is investigated by comparing the results of analysis with the detailed results of two years of field measurements at two sections of the Thunder Bay Tunnel. It is found that the proposed procedure yields reasonable agreement with the observed overall displacement pattern including the magnitude and distribution of surface settlement.

It is suggested that the "simple method" may be effectively used in preliminary design considerations, while the "detailed method" is recommended for design analysis of critical sections for tunnelling projects in soft clays.

ACKNOWLEDGEMENTS

The author is most profoundly indebted to Dr. K.Y. Lo, his supervisor, who suggested the topic for this thesis and who, patiently and persistently, has given continual guidance, invaluable advice and the most rewarding and constructive criticisms throughout the course of the study.

The author is also grateful for the guidance of Dr. R.K. Rowe who, with unfailing assistance, has provided the author with helpful information on numerical techniques and has contributed valuable discussions on the finite element method.

The author also wishes to express sincere appreciation to Dr. R.M. Quigley for his interest in the thesis and the advice and incentive that he has provided in the study of clay mineralogy.

Special thanks are due to Dr. J.H.L. Palmer of the National Research Council for his discussions concerning the field behaviour of the Thunder Bay Tunnel and for his advice during site investigation at Thunder Bay.

Thanks are also directed to the following personnel of The University of Western Ontario:

Mr. G. Lusk for his assistance in all aspects of field and laboratory work, and his precise and careful drafting of the drawings presented in the thesis.

Mr. G.J. Kack for his contribution and assistance in field and experimental work and his pertinent discussions.

Mr. G. Muckle for performing the stress path tests recorded in this thesis.

Ms. J. Lemon for her typing of the thesis.

The study described in this thesis was supported by the Department of Supply and Services Canada and The National Research Council of Canada. Their support is gratefully acknowledged. In addition, the author would like to express his gratitude to the Ontario Ministry of Colleges and Universities for the award of the Ontario Graduate Scholarship (1980-1982) and The University of Western Ontario for awarding the University Scholarship (1979-1980, 1983-1984).

Finally, the author's warmest thanks are expressed to his wife, Stephanie, for her immense understanding, loving support and faithful encouragement throughout the course of this study.

VOLUME I

TABLE OF CONTENTS

	Page
CERTIFICATE OF EXAMINATION.....	ii
ABSTRACT.....	iii
ACKNOWLEDGEMENTS.....	vi
TABLE OF CONTENTS.....	viii
LIST OF TABLES.....	xiv
LIST OF FIGURES.....	xvii
LIST OF SYMBOLS.....	xxxiv
LIST OF TUNNELLING TERMS.....	xxxix
CHAPTER 1 - INTRODUCTION.....	1
CHAPTER 2 - REVIEW OF METHODS OF PREDICTION OF GROUND MOVEMENTS.....	5
2.1 Stochastic and Empirical Approach.....	6
2.2 Model Tunnel Tests on Ground Movements.....	13
2.3 Theoretical Approach.....	21
2.4 Conclusions From Review of Previous Research.....	32
CHAPTER 3 - A SEMI-THEORETICAL APPROACH FOR PREDICTING SETTLEMENTS DUE TO TUNNELLING IN CLAY.....	38
3.1 Introduction.....	38
3.2 Definition of the Gap Parameter.....	39
3.3 Solutions for Radial Displacements at the Crown..	43
3.3.1 Elastic Solution.....	43
3.3.2 Undrained Analysis of Stresses and Displace- ments in the Plastic Region Around the Tunnel..	44
3.4 Procedure for Estimating the Crown Displacement..	48
3.5 Comparison Between Calculated and Measured Crown Displacements.....	50
3.5.1 Mississauga Sewer Tunnel.....	51
3.5.2 Green Park Underground.....	53
3.5.3 Regents Park.....	56
3.5.3.1 Southbound Tunnel.....	57
3.5.3.2 Northbound Tunnel.....	58
3.5.4 Thunder Bay Tunnel.....	58
3.5.5 Summary of Observation on Detailed Case Histories.....	61
3.6 Additional Case Records.....	62
3.6.1 Ottawa Outfall Sewer Tunnel.....	63
3.6.2 Mexico City Siphon Tunnel.....	64
3.6.3 Grangemouth Sewer Tunnel.....	66
3.6.4 Bart (Market Street).....	68
3.6.5 Tyneside Tunnel.....	70

	Page
3.6.6 Heathrow Cargo Tunnel.....	71
3.6.7 Buenos Aires Tunnel.....	72
3.6.8 Edmonton Rapid Transit Tunnel - 1st Tunnel.....	73
3.7 Results of Analyses of Case Records.....	75
3.8 Conclusion.....	77
CHAPTER 4 - FUNDAMENTAL CONCEPTS AND METHOD OF SOLUTION IN A DETAILED ANALYSIS.....	95
4.1 Sources of Ground Subsidence.....	96
4.1.1 Changes in Volume Associated With Stress Changes.....	96
4.2 Component of Gap Due to Consolidation of Remoulded Zone.....	99
4.3 Elasto-Plastic Soil Model Adopted in the Finite Element Analysis.....	102
4.4 Method of Analysis.....	106
4.4.1 Finite Element Mesh and Beam Elements.....	106
4.4.2 2-D Simulation of Tunnel Construction.....	108
4.4.2.1 Effect of Advancing Face Modelled as Construction Sequences.....	109
4.4.2.2 Construction Simulation With Consideration of Machine Weight.....	111
4.4.3 Consideration of Grouting.....	111
4.4.4 Implementation of Soil-Structure Interaction Theory.....	112
CHAPTER 5 - TEST REQUIREMENTS FOR THE DETERMINATION OF SOIL PARAMETERS IN SOFT GROUND TUNNELLING.....	121
5.1 Introduction.....	121
5.2 Stress Paths in Tunnel Excavation.....	122
5.3 Anisotropy of Elastic Deformation in Soft Clay..	124
5.4 Plastic Behaviour in Soft Clay.....	128
5.5 Insitu Stress Condition.....	130
5.6 Summary.....	131
CHAPTER 6 - SITE INVESTIGATION AND GENERAL SOIL PROPERTIES... 136	136
6.1 Stratigraphy.....	136
6.1.1 Geology of Fort William, Thunder Bay.....	136
6.1.2 Tunnel and Borehole Locations.....	139
6.1.3 Subsoil Conditions.....	140
6.1.3.1 Previous Soil Investigation.....	140
6.1.3.2 Present Soil Investigation.....	140
6.2 Coefficient of Lateral Earth Pressure, K_0	146
6.3 Summary of Field Investigations at Array ⁰¹ and Array 2.....	148

	Page
CHAPTER 7 - RESULTS OF TRIAXIAL TESTS.....	164
7.1 Isotropically-Consolidated Undrained (CIU) Tests (with pore water pressure measurement).....	165
7.1.1 Undrained Stress-Strain Behaviour.....	166
7.1.2 Effect of Consolidation Pressure on the Modulus of Deformation.....	169
7.1.3 Anisotropy in CIU Behaviour.....	170
7.2 Isotropically Consolidated Drained (CID) Tests..	171
7.2.1 Stress-Strain Behaviour in CID Tests.....	172
7.2.2 Anisotropy of Drained Behaviour.....	173
7.3 Determination of Plasticity Parameters Using Conventional Triaxial Testing - CIU.....	174
7.4 Variation of Undrained Modulus and Undrained Shear Strength With Depth.....	175
7.5 Variation of Drained Modulus With Depth.....	177
7.6 Triaxial Test on Thunder Bay Sand.....	178
7.6.1 Stress-Strain Behaviour in CID Tests.....	179
7.6.2 The Effective Friction Angle.....	181
7.6.3 Poisson's Ratio At Low Strain Level.....	182
7.6.4 Determination of the Vertical Drained Modulus..	183
7.6.5 CID Extension Tests on Silty Sand.....	184
7.7 Summary of Results of Triaxial Tests.....	185
CHAPTER 8 - RESULTS OF SPECIAL TESTS.....	250
8.1 Definition of Deformation Modulus.....	250
8.2 Large Diameter Consolidation Tests Under Loading and Unloading.....	251
8.2.1 Results of Large Diameter Consolidation Tests..	253
8.2.2 Comparison of Drained Modulus From Consolida- tion Tests and CID Tests.....	255
8.3 Measurement of Elastic Anisotropic Parameters by the Anisotropic Parameter Apparatus.....	255
8.3.1 Experimental Procedure.....	256
8.3.2 Results of Tests.....	257
8.3.2.1 Stress-Axial Strain Relationship.....	257
8.3.2.2 Volumetric Strain and Axial Strain Relationship.....	258
8.3.3 Evaluation of Anisotropic Elastic Parameters..	259
8.4 Determination of Shear Modulus G_{vh} From Direct Simple Shear Test.....	260
8.4.1 Simple Shear Apparatus.....	261
8.4.2 Constant Volume Test.....	262
8.4.3 Results of Simple Shear Tests.....	264
8.5 Anisotropically Consolidated Triaxial Tests and Controlled Stress Path Tests.....	265
8.5.1 Anisotropically Consolidated, Strain- Controlled Triaxial Tests.....	265

	Page
8.5.2 Results of Tests.....	266
8.5.3 Controlled Stress Path Triaxial Tests.....	267
8.5.3.1a Total Stress Controlled Test.....	267
8.5.3.1b Servo-Test.....	268
8.5.3.2 Results of Tests.....	269
8.6 Strength From Anisotropic Consolidated Triaxial Tests and Controlled Stress Path Tests.....	271
8.7 Summary on Special Tests Performed on the Clay at Array 1 and Array 2 on the Thunder Bay Tunnel.....	272
CHAPTER 9 TUNNELLING PROCEDURE AND FIELD OBSERVATIONS AT THE THUNDER BAY TUNNEL.....	320
9.1 Tunnelling System and Procedure.....	320
9.1.1 Tunnelling Machine and Construction Cycle.....	320
9.1.2 Typical Observations During Tunnelling Operation.....	322
9.1.3 Tunnel Lining.....	322
9.2 Observed Ground Deformations.....	323
9.2.1 Undrained and Drained Settlements.....	323
9.2.2 Surface Settlements.....	325
9.2.3 Distribution of Subsurface Displacements.....	327
9.2.3.1 Vertical Displacements With Depth On Centreline.....	327
9.2.3.2 Horizontal Displacements.....	328
9.2.3.3 Displacement Vectors in the Vertical Plane..	329
9.3 Pore Water Pressure Due to Tunnelling.....	330
CHAPTER 10 - ANALYSES OF THE RESULTS OF FIELD INSTRUMENTA- TION IN THE THUNDER BAY TUNNEL.....	356
10.1 Introduction.....	356
10.2 Details of the Analysis.....	356
10.3 Selection of Drained Parameters for Analysis....	358
10.3.1 Description of Soil Stratigraphy.....	358
10.3.2 Selection of Soil Properties for Analysis of Array 1.....	359
10.3.2.1 Sand and Silt.....	359
10.3.2.2 Silty Clay and Varved Clay.....	362
10.3.3 Selection of Soil Properties for Analysis of Array 2.....	364
10.4 Results of Drained Analysis.....	364
10.4.1 Long Term Surface Settlement.....	365
10.4.1.1 Array 1.....	365
10.4.1.2 Array 2.....	366
10.4.2 Horizontal Displacement Perpendicular to the Tunnel Axis at Array 1.....	366
10.4.3 Distribution of Subsurface Settlement at Array 2.....	367

	Page
10.5 Selection of Undrained Parameters for Analysis.....	368
10.6 Results of Undrained Analysis.....	370
10.6.1 Centreline Settlement.....	370
10.6.2 Distribution of Surface Settlement.....	372
10.7 Lining Deformation.....	374
10.8 Variation of Centreline Settlement With Depth Above the Tunnel.....	375
10.9 Summary of Comparison Between Results of Field Measurements and Analysis.....	377
CHAPTER 11 - SUMMARY, CONCLUSIONS AND RECOMMENDATIONS FOR FURTHER RESEARCH.....	392
11.1 Summary and Conclusions.....	392
11.2 Recommendations for Further Research.....	399
APPENDIX 1 - SCHEME OF CONSTRUCTION SIMULATION WITH CONSIDERATION OF MACHINE WEIGHT DURING TUNNEL ADVANCE.....	402
APPENDIX 2 - UNDRAINED AND DRAINED SETTLEMENTS DUE TO TUNNELLING.....	411
APPENDIX A - SAMPLING WITH 152 mm DIAMETER PISTON SAMPLER....	416
APPENDIX B - APPARATUS AND FIELD TECHNIQUE USED IN K_0 - DETERMINATION.....	421
APPENDIX C - CONVENTIONAL LABORATORY TEST RESULTS.....	446
C.1 Grain Size Analysis.....	446
C.2 Determination of Unit Weight.....	446
C.3 One-Dimensional Consolidation Tests.....	447
C.4 Results of CIU Tests On Vertically and Hori- zontally Oriented Clay Samples.....	449
C.5 Drained Triaxial Tests On Silty Fine Sand.....	449
APPENDIX D - CONSOLIDATION TESTS PERFORMED USING THE ROWE CELL.....	476
D.1 Description of Apparatus.....	476
D.2 Specimen Preparation and Test Procedure.....	477
D.3 Coefficient of Consolidation.....	479
APPENDIX E - TESTS FOR DETERMINING ANISOTROPIC ELASTIC PARAMETERS.....	483
E.1 Theoretical Background.....	483
E.2 Formulation of Stress-Strain Relationship for CID Tests.....	484
E.3 Description of the Apparatus and Method of Measurement.....	488

	Page
APPENDIX F - DETERMINATION OF PERMEABILITY.....	493
F.1 Program of Testing and Procedure.....	493
F.2 Results of Permeability Test.....	494
REFERENCES.....	497
VITA.....	508

LIST OF TABLES

Table	Description	Page
3.1	Summary of Data of Case Records Analysed.....	79
3.2	Index Properties of London Clay at Green Park, Regents Park and Ashford Common.....	80
6.1a	Composition of Non-Clay Minerals in Whole Soil in Varved Clay (-74 μ).....	150
6.1b	Composition of -2 μ Fraction Soil.....	150
6.2a	Composition of Non-Clay Minerals in Whole Soil in Silty Clay (-74 μ).....	151
6.2b	Composition of -2 μ Fraction Soil.....	151
6.3	Summary of General Soil Properties.....	152
6.4	Groundwater Level in Array 2.....	153
6.5	Measured K_0 Values.....	154
6.6	Average Soil Properties and Measured K_0 Values at Different Locations.....	155
7.1a	Summary of the Number of Various Triaxial Tests Performed.....	187
7.1b	Summary of Numbers of Various Laboratory Tests Performed.....	187
7.2	CIU Test Results.....	188
7.3a	Isotropically Consolidated Undrained Test Results of Silty Clay (Array 2).....	189
7.3b	Modulus Determination of Grey Silty Clay At 10.7 m - 11.1 m.....	189
7.4a	Isotropically Consolidated Undrained Test Results of Varved Clay (Array 2).....	190
7.4b	Modulus Determination of Varved Clay At 14.7 m - 15.2 m.....	190

Table	Description	Page
7.5	CID Test Result on Vertically Trimmed Sample.....	191
7.6	Summary of CID Triaxial Compression Test Data on Thunder Bay Silty Sand.....	192
7.7	Summary of Drained Vertical Modulus of Thunder Bay Silty Sand.....	193
7.8	Summary of K and a Values of Thunder Bay Sand.....	193
8.1a	Results Obtained From the Large Oedometer For Silty Clay ('Crust') (7.24 m).....	277
8.1b	Results Obtained From the Large Oedometer For Silty Clay (9.78 m).....	277
8.1c	Results Obtained From the Large Oedometer For Varved Clay (13.1 m).....	278
8.2	Anisotropic Elastic Parameters From CID Tests on Silty Clay (Array 2, Depth 10.15 m).....	279
8.3	Anisotropic Elastic Parameters From CID Tests on Varved Clay (Array 2, Depth 13.4 m).....	280
8.4	Results From Simple-Shear Tests on the Thunder Bay Soil (Constant Volume Test).....	281
8.5	Comparison of Moduli From Different Types of Tests.....	282
9.1	Tunnelling Observations at Array 2.....	333, 334
9.2a	Observed Centreline Surface Settlements at Different Stages of Development (Array 1).....	335
9.2b	Observed Centreline Surface Settlements at Different Stages of Development (Array 2).....	335
9.3	Comparison Between Observed Maximum Negative Excess Pore Pressure and Theoretical Excess Pore Pressure.....	336
A1.1	Effects of Simulation of Excavation Procedure on Theoretical Results.....	406

Table	Description	Page
B.1	Effect of Rate of Water Injection on Results of K_0 Test.....	426
C.1	Conventional One-Dimensional Oedometer Consolidation Test Results.....	452
F.1	Results of Permeability Tests.....	496
F.2	Ratio of Horizontal Permeability to Vertical Permeability for Silty Clay and Varved Clay.....	496

LIST OF FIGURES

Figure	Description	Page
2.1	Properties of Normal Probability Curve as Used to Represent Surface Settlement Trough.....	34
2.2	Relation Between Width of Settlement Trough i/R , With Depth of Cover z/D , for Different Soil Conditions.....	35
2.3a	Geometric Similarity Between Model and Prototype..	36
2.3b	Dynamic Similarity Between Model and Prototype....	36
2.4	Field and Model Relationships Between Ratio of Near Surface Settlement to Settlement Near Tunnel Crown (S_s/S_c) and Cover to Diameter Ratio (c/D)...	37
3.1	Definition of Gap.....	81
3.2	Stress Condition and Geometry of Problem Analysed.	82
3.3	Variation of Normalized Critical Pressure and Plastic Radius With Stability Number ($p_i = 0$).....	83
3.4	Variation of Normalized Radial Crown Displacement With Stability Number for Different Values of E_u/C_u	84
3.5	Sewer Tunnel, Mississauga, Ontario.....	85
3.6	Tunnel at Green Park, London Underground.....	86
3.7	Northbound and Southbound Tunnels at Regents Park, London Underground.....	87
3.8	Measured Displacements for Tunnels at Regents Park.....	88
3.9	General Soil Properties - Array 2, Thunder Bay Tunnel.....	89
3.10	Measured Displacements at Array 1 and Array 2, Thunder Bay Tunnel.....	90
3.11	Comparison of Measured and Calculated Normalized Crown Displacements.....	91

Figure	Description	Page
3.12	Soil Properties and Measured Ground Displacements, Ottawa Sewer Tunnel.....	92
3.13	Relationship Between Measured Surface Settlements and Calculated Crown Displacements.....	93
3.14	Influence of Depth to Radius Ratio on Surface Settlement to Crown Displacement Ratio.....	94
4.1	Flow Trends for Drawdown and Recharge Conditions....	117
4.2	Plot of Centreline Settlements at Array 1 With Time Showing the Effect of Consolidation of Remoulded Soil.....	118
4.3a,b	Stress Strain Relationships for a Perfect Elastic Plastic Solid.....	119
4.3c	Yield Surface for a Perfectly Plastic Material.....	119
4.4	Finite Element Mesh Used in the Analysis of the Thunder Bay Tunnel.....	120
5.1	Location of Typical Points at (B) Crown, (A) Spring-line and Point (C).....	133
5.2	Stress Paths for Conventional Triaxial Tests.....	134
5.3	Stress Paths for Typical Elements in Soil Due to Tunnelling.....	135
6.1	Tunnel Location.....	156
6.2	Plan of Borehole Locations - Array 1.....	157
6.3	Plan of Borehole Locations - Array 2.....	158
6.4	Soil Section and Summary of Test Results.....	159
6.5	General Soil Properties - Array 1.....	160
6.6	General Soil Properties - Array 2.....	161
6.7	Variation of Water Content in Varved Clay.....	162
6.8	Silty Clay and Varved Clay Samples (Photograph).....	163
7.1	Stress-Strain Relationship From CIU Tests for Vertically Oriented Silty Clay and Varved Clay Samples.....	194

Figure	Description	Page
7.2	Stress Ratio-Strain Relationship From CIU Tests for Vertically Oriented Silty Clay and Varved Clay Samples.....	195
7.3	Excess Pore Water Pressure-Strain Relationship From CIU Tests for Vertically Oriented Silty Clay and Varved Clay Samples.....	196
7.4	Pore Pressure Parameter A-Strain Relationship From CIU Tests on Vertically Oriented Silty Clay and Varved Clay Samples.....	197
7.5	Effective p-q Stress Path Plot From CIU Tests On Vertically Oriented Silty Clay and Varved Clay Samples.....	198
7.6	Effective $\sigma_1-\sigma_3$ Stress Path Plot From CIU Tests On Vertically Oriented Silty Clay and Varved Clay Samples.....	199
7.7	Stress-Strain Relationship From CIU Tests For Horizontally Oriented Silty Clay and Varved Clay Samples.....	200
7.8	Stress Ratio-Strain Relationship From CIU Tests For Horizontally Oriented Silty Clay and Varved Clay Samples.....	201
7.9	Excess Pore Water Pressure-Strain Relationship For Horizontally Oriented Silty Clay and Varved Clay Samples.....	202
7.10	Pore Pressure Parameter A-Strain Relationship From CIU Tests On Horizontally Oriented Silty Clay and Varved Clay Samples.....	203
7.11	Effective p-q Stress Path Plot From CIU Tests On Horizontally Oriented Silty Clay and Varved Clay Samples.....	204
7.12	Effective $\sigma_1-\sigma_3$ Stress Path Plot From CIU Tests On Horizontally Oriented Silty Clay and Varved Clay Samples.....	205
7.13	Stress-Strain Relationship From CIU Tests For Vertically Oriented Silty Clay Samples.....	206

Figure	Description	Page
7.14	Stress Ratio-Strain Relationship From CIU Tests for Vertically Oriented Silty Clay Samples.....	207
7.15	Excess Pore Water Pressure-Strain Relationship From CIU Tests on Vertically Oriented Silty Clay Samples.....	208
7.16	Pore Pressure Parameter A-Strain Relationship From CIU Tests on Vertically Oriented Silty Clay Samples.....	209
7.17	Stress-Strain Relationship From CIU Tests for Vertically and Horizontally Oriented Varved Clay Samples.....	210
7.18	Stress Ratio-Strain Relationship From CIU Tests for Vertically and Horizontally Oriented Varved Clay Samples.....	211
7.19	Excess Pore Water Pressure-Strain Relationship From CIU Tests on Vertically and Horizontally Oriented Varved Clay Samples.....	212
7.20	Pore Water Pressure Parameter A-Strain Relationship From CIU Tests on Vertically and Horizontally Oriented Varved Clay Samples.....	213
7.21	Effective p-q Stress Path Plot From CIU Tests on Vertically and Horizontally Oriented Varved Clay Samples.....	214
7.22	Effective σ_1 - σ_3 Stress Path Plot From CIU Tests on Vertically and Horizontally Oriented Varved Clay Samples.....	215
7.23	E_{u30} vs σ'_c for Grey Silty Clay.....	216
7.24	E_{u30} vs σ'_c for Varved Clay.....	217
7.25	Stress-Strain Relationship For Silty Clay and Varved Clay From CID Triaxial Tests.....	218
7.26	Stress Ratio-Strain Relationship For Silty Clay and Varved Clay From CID Triaxial Tests.....	219
7.27	Volumetric Strain-Axial Strain Relationship For Silty Clay and Varved Clay From CID Triaxial Tests	220

Figure	Description	Page
7.28	Stress-Strain Relationship For Silty Clay and Varved Clay From CID Triaxial Tests.....	221
7.29	Stress Ratio-Strain Relationship For Silty Clay and Varved Clay From CID Triaxial Tests.....	222
7.30	Volumetric Strain-Axial Strain Relationship For Silty Clay and Varved Clay From CID Triaxial Tests	223
7.31	Stress-Strain Relationship For Silty Clay From CID Tests on Vertically and Horizontally Oriented Samples.....	224
7.32	Stress Ratio-Strain Relationship for Silty Clay From CID Tests on Vertically and Horizontally Oriented Samples.....	225
7.33	Volumetric Strain-Axial Strain Relationship From CID Tests on Vertically and Horizontally Oriented Samples.....	226
7.34	Stress-Strain Relationship For Varved Clay From CID Tests on Vertically and Horizontally Oriented Samples.....	227
7.35	Stress Ratio-Strain Relationship For Varved Clay From CID Tests on Vertically and Horizontally Oriented Samples.....	228
7.36	Volumetric Strain-Axial Strain Relationship For Varved Clay From CID Tests on Vertically and Horizontally Oriented Samples.....	229
7.37	Strength Envelope-Grey Silty Clay at Thunder Bay (Array 2).....	230
7.38	Strength Envelope-Varved Clay at Thunder Bay (Array 2).....	231
7.39	Variation of Undrained Shear Strength C_u With Depth.....	232
7.40	Variation of Undrained Modulus With Depth.....	233
7.41	Variation of E_u/C_u With Depth.....	234

Figure	Description	Page
7.42	Variation of Drained Modulus E'_v (From CID Tests) With Depth.....	235
7.43	Stress-Strain Curves From CID Triaxial Compression Tests on Loose Silty Sand.....	236
7.44	Volumetric Strain-Axial Strain Curves For Loose Silty Sand From CID Triaxial Tests.....	237
7.45	Stress-Strain Curves From CID Triaxial Compression Tests On Medium Dense Silty Sand.....	238
7.46	Volumetric Strain-Axial Strain Curves For Medium Silty Sand From CID Triaxial Tests.....	239
7.47	Stress-Strain Curves From CID Triaxial Compression Tests on Dense Silty Sand.....	240
7.48	Volumetric Strain-Axial Strain Curves for Dense Silty Sand From CID Triaxial Tests.....	241
7.49	Stress-Strain Curves For Loose, Medium and Dense Silty Sand (Consolidation Pressure \approx 100 kPa).....	242
7.50	Volumetric Strain-Axial Strain Curves For Loose, Medium and Dense Sand (Consolidation Pressure \approx 100 kPa).....	243
7.51	Stress-Strain Curves for Loose, Medium and Dense Silty Sand (Consolidation Pressure \approx 200 kPa).....	244
7.52	Volumetric Strain-Axial Strain Curves For Loose, Medium and Dense Silty Sand (Consolidation Pressure \approx 200 kPa).....	245
7.53a	Variation of Effective Friction Angle With Initial Porosity.....	246
7.53b	Variation of Effective Friction Angle With Final Porosity.....	246
7.54	Relationship Between Vertical Drained Modulus E'_v and (σ'_c/P_a) Ratio.....	247
7.55	Typical Range of Variations of Modulus Number 'K' and Exponent 'a' With Porosity.....	248

Figure	Description	Page
7.56	Stress-Strain Relationships From CID Compression and Extension Triaxial Tests on Silty Sand.....	249
8.1	1-Dimensional Compressive Strain vs Time for Loading Stage in Large Oedometer Test.....	283
8.2	1-Dimensional Compressive Strain vs Time for Loading Stage in Large Oedometer Test.....	284
8.3	1-Dimensional Swelling Strain vs Time for Unloading Stage in Large Oedometer Test.....	285
8.4	1-Dimensional Compressive Strain vs Time for Loading Stage in Large Oedometer Test.....	286
8.5	1-Dimensional Swelling Strain vs Time for Unloading Stage in Large Oedometer Test.....	287
8.6	1-Dimensional Compressive Strain vs Time for Loading Stage in Large Oedometer Test.....	288
8.7	1-Dimensional Swelling Strain vs Time for Unloading Stage in Large Oedometer Test.....	289
8.8	Relationship Between Pore Pressure Dissipation With Time.....	290
8.9	Relationship Between Pore Pressure Dissipation With Time.....	291
8.10	Relationship Between Pore Pressure Dissipation With Time.....	292
8.11	Variation of Drained Modulus E'_v With Depth.....	293
8.12	Results of CID Test on a Vertically Oriented Specimen of Silty Clay ($i = 0^\circ$).....	294
8.13	Results of CID Test on an Inclined Specimen ($i = 45^\circ$) of Silty Clay.....	295
8.14	Results of CID Test on a Horizontally Oriented Specimen of Silty Clay ($i = 90^\circ$).....	296
8.15	Results of CID Test on a Vertically Oriented Specimen of Varved Clay ($i = 0^\circ$).....	297

Figure	Description	Page
8.16	Results of CID Test on an Inclined Specimen of Varved Clay ($i = 45^\circ$).....	298
8.17	Results of CID Test on a Horizontally Oriented Sample of Varved Clay ($i = 90^\circ$).....	299
8.18	Simple Shear Test Apparatus.....	300
8.19	Result of Constant-Volume Simple Shear Test on Silty Clay.....	301
8.20	Result of Constant-Volume Simple Shear Test on Silty Clay.....	302
8.21	Result of Constant-Volume Simple Shear Test on Silty Clay.....	303
8.22	Result of Constant-Volume Simple Shear Test on Layered Clay in 'Transitional Zone'.....	304
8.23	Result of Constant-Volume Simple Shear Test on Varved Clay.....	305
8.24	Variation of G_{vh} With Depth.....	306
8.25	Sketch of K_0 -Cell Set Up For Extension Test.....	307
8.26	Stress Paths on p' - q' Space for Four Modes of Triaxial Tests on Silty Clay.....	308
8.27	Stress-Strain Relationships for Four Modes of Triaxial Tests on Silty Clay.....	308
8.28	Volumetric Strain-Axial Strain Relationships From CK_0D Compression and Extension Tests on Silty Clay	309
8.29	Excess Pore Water Pressure-Axial Strain Relationships From CK_0U Compression and Extension Tests on Silty Clay.....	309
8.30	Stress Paths on p' - q' Space for Four Modes of Triaxial Tests on Varved Clay.....	310
8.31	Stress-Strain Relationships for Four Modes of Triaxial Tests on Varved Clay.....	310

Figure	Description	Page
8.32	Volumetric Strain-Axial Strain Relationships From CK _D Compression and Extension Tests on Varved Clay.....	311
8.33	Excess Pore Water Pressure-Axial Strain Relationships From CK _U Compression and Extension Tests on Varved Clay.....	311
8.34	Stress Path Tests on p'-q' Space For the Crown Region.....	312
8.35	Stress-Strain Relationships From Triaxial Tests For the Crown Region.....	313
8.36	Stress Path Tests in p'-q' Space for the Springline Region.....	314
8.37	Stress-Strain Relationships From Triaxial Tests For the Springline Region.....	315
8.38	Modulus Values Deduced From K ₀ Consolidated Tests.	316
8.39	p'-q' Plot of Shear Strength From Anisotropic Consolidated Triaxial Tests and Controlled Stress Path Test (Silty Clay).....	317
8.40	p'-q' Plot of Shear Strength From Anisotropic Consolidated Triaxial Tests (Varved Clay).....	318
8.41a	Anisotropic Parameter Apparatus and Data-Acquisition System (Photograph).....	319
8.41b	Test Sample and Floating Transducer Units Within Triaxial Cell (Photograph).....	319
9.1	Plan of Instrumentation at Array 1.....	337
9.2	Plan of Instrumentation at Array 2.....	338
9.3	Dimensions of Tunnelling Machine.....	339
9.4a	Schematic Section of Tunnelling Operation.....	340
9.4b	Details of Tunnel Liner.....	340
9.5	Time, Settlement, Tunnel-Progress Relationships...	341

Figure	Description	Page
9.6	Vertical Soil Displacement Over Centreline of Tunnel at Array 1.....	342
9.7	Vertical Soil Displacement Over Centreline of Tunnel at Array 2.....	343
9.8	Surface Settlement Over Tunnel Centreline at Array 1 and Array 2.....	344
9.9	Settlement Over Centreline.....	345
9.10a	Surface Settlement Over Centreline of Tunnel at Array 1.....	346
9.10b	Surface Settlement Along Line Through Settlement Pin 27 at Array 1.....	346
9.11a	Surface Settlement Over Centreline of Tunnel at Array 2.....	347
9.11b	Surface Settlement Along Line Through Settlement Pin 5 at Array 2.....	347
9.11c	Plan View of Conceptual 'Bowl' of Settlement Trough Above the Advancing Tunnel at Array 2.....	347
9.12	Slope Indicator Data Perpendicular to Tunnel Axis at Array 1.....	348
9.13	Horizontal Displacement Vectors at Springline (A,C,D) and 0.96 m Above Crown (B) During Shield Advance (Array 1).....	349
9.14	Horizontal Displacement Vectors at Springline (A,B,C,E) and 1.2 m Above Crown (D) During Shield Advance (Array 2).....	350
9.15	Displacement Vectors in Vertical Plane at Array 1 Perpendicular to Tunnel Axis (Face at 10.8 m)....	351
9.16	Displacement Vectors in Vertical Plane at Array 2 Perpendicular to Tunnel Axis (After 20 Days).....	352
9.17	Changes in Pore Pressure at Array 2.....	353

Figure	Description	Page
9.18	Shield Tunnel in Plastic Clay: (a) Successive Positions of Originally Vertical Line in Soil Beside Tunnel as Shield Approached and Passed; (b) Settlement of Reference Points Above Tunnel As Shield Approached, Passed Beneath, and Continued Beyond the Points.....	354
9.19a	Oblique Rear View of Tunnel Machine Assembly (Photograph).....	355
9.19b	Oblique Front View of Tunnel Machine Assembly (Photograph).....	355
10.1	Soil Profile Adopted in the Analysis of Array 1...	381
10.2	Soil Profile Adopted in the Analysis of Array 2...	382
10.3a	Observed and Calculated Long Term Surface Settlement Profile at Array 1.....	383
10.3b	Observed and Calculated Long Term Normalized Surface Settlement at Array 1.....	383
10.4a	Observed and Calculated Long Term Surface Settlement Profile at Array 2.....	384
10.4b	Observed and Calculated Long Term Normalized Surface Settlement Profile at Array 2.....	384
10.5	Comparison of Observed Slope Indicator Data Perpendicular to Tunnel Axis With Calculated Data (Array 1).....	385
10.6	Displacement Vectors in Vertical Plane Perpendicular to Tunnel Axis (20 Days) at Array 2.....	386
10.7	Undrained Strength Profile for Undrained Analysis.	387
10.8	Relationship Between S_v and G Calculated by F.E.M.	388
10.9a	Observed and Calculated Surface Settlement Profile at Array 1 - Undrained Condition.....	389
10.9b	Observed and Calculated Normalized Surface Settlement Profile at Array 1 - Undrained Condition.....	389
10.10a	Observed and Calculated Surface Settlement Profile at Array 2 - Undrained Condition.....	390

Figure	Description	Page
10.10b	Observed and Calculated Normalized Surface Settlement Profile at Array 2 - Undrained Condition.....	390
10.11a	Comparison of Calculated and Observed Settlement Variation With Depth Above the Tunnel Axis at Array 1.....	391
10.11b	Comparison of Calculated and Observed Settlement Variation With Depth Above the Tunnel Axis at Array 2.....	391
A1.1	Simulation of 3-D Effect in 2-D Analysis by Means of Unloading Sequences.....	407
A1.2	Variation of Dimensionless Radial Displacement With Normalized Distance to the Advancing Face - Elastic Solution.....	408
A1.3	Physical Interpretation of Sequential Unloading Procedure.....	409
A1.4a	Surface Settlement Profile for Modified '2-D' Approach.....	410
A1.4b	Normalized Surface Settlement Profile for Modified '2-D' Approach.....	410
A.1	Stress Changes and Deformations of Soil Layers Below Bottom of Borehole (Boring by Removal of Soil).....	420
A.2	Stress Changes and Deformations of Soil Layers Below Bottom of Borehole (Boring by Displacement of Soil).....	420
A.3	Schematic Sketch of a Piston Sampler.....	420
B.1	Sketch of Hydraulic Fracturing Apparatus.....	427
B.2	Excess Pore Pressures Developed During Piezometer Driving at Array 2.....	428
B.3a	Dissipation Curve for Hydraulic Fracturing Test 1-P1 (1st Fracture).....	429

Figure	Description	Page
B.3b	Dissipation Curve for Hydraulic Fracturing Test 1-P1 (2nd Fracture).....	430
B.4a	Dissipation Curve for Hydraulic Fracturing Test 1-P2 (1st Fracture).....	431
B.4b	Dissipation Curve for Hydraulic Fracturing Test 1-P2 (2nd Fracture).....	432
B.4c	Dissipation Curve for Hydraulic Fracturing Test 1-P2 (3rd Fracture).....	433
B.5a	Dissipation Curve for Hydraulic Fracturing Test 1-P3 (1st Fracture).....	434
B.5b	Dissipation Curve for Hydraulic Fracturing Test 1-P3 (2nd Fracture).....	435
B.5c	Dissipation Curve for Hydraulic Fracturing Test 1-P3 (3rd Fracture).....	436
B.6a	Dissipation Curve for Hydraulic Fracturing Test 2-P1 (1st Fracture).....	437
B.6b	Dissipation Curve for Hydraulic Fracturing Test 2-P1 (2nd Fracture).....	438
B.6c	Dissipation Curve for Hydraulic Fracturing Test 2-P1 (3rd Fracture).....	439
B.7a	Dissipation Curve for Hydraulic Fracturing Test 2-P2 (1st Fracture).....	440
B.7b	Dissipation Curve for Hydraulic Fracturing Test 2-P2 (2nd Fracture).....	441
B.7c	Dissipation Curve for Hydraulic Fracturing Test 2-P2 (3rd Fracture).....	442
B.8a	Dissipation Curve for Hydraulic Fracturing Test 2-P3 (1st Fracture).....	443
B.8b	Dissipation Curve for Hydraulic Fracturing Test 2-P3 (2nd Fracture).....	444
B.8c	Dissipation Curve for Hydraulic Fracturing Test 2-P3 (3rd Fracture).....	445

Figure	Description	Page
C.1	Hydrometer Analysis - Array 1.....	453
C.2	Hydrometer Analysis - Array 2.....	454
C.3	Consolidation Curve for One Dimensional Conventional Oedometer Test.....	455
C.4	Consolidation Curve for One Dimensional Conventional Oedometer Test.....	455
C.5	Consolidation Curve for One Dimensional Conventional Oedometer Test.....	456
C.6	Consolidation Curve for One Dimensional Conventional Oedometer Test.....	456
C.7	Consolidation Curve for One Dimensional Conventional Oedometer Test.....	457
C.8	Consolidation Curve for One Dimensional Conventional Oedometer Test.....	458
C.9	Consolidation Curve for One Dimensional Conventional Oedometer Test.....	459
C.10	Consolidation Curve for One Dimensional Conventional Oedometer Test.....	459
C.11	Consolidation Curve for One Dimensional Conventional Oedometer Test.....	460
C.12	Consolidation Curve for One Dimensional Conventional Oedometer Test.....	460
C.13	Consolidation Curve for One Dimensional Conventional Oedometer Test.....	461
C.14	Stress-Strain Relationship From CIU Tests on Vertically and Horizontally Oriented Silty Clay Samples.....	461
C.15	Stress Ratio-Strain Relationship From CIU Tests on Vertically and Horizontally Oriented Silty Clay Samples.....	462
C.16	Excess Pore Water Pressure-Strain Relationship From CIU Tests on Vertically and Horizontally Oriented Silty Clay Samples.....	

Figure	Description	Page
C.17	Pore Pressure Parameter A-Strain Relationship From CIU Tests on Vertically and Horizontally Oriented Silty Clay Samples.....	462
C.18	Effective p-q Stress Path Plot From CIU Tests on Vertically and Horizontally Oriented Silty Clay Samples.....	463
C.19	Effective $\sigma_1 - \sigma_3$ Stress Path Plot From CIU Tests on Vertically and Horizontally Oriented Silty Clay Samples.....	463
C.20	Stress-Strain Relationship From CIU Tests on Vertically and Horizontally Oriented Silty Clay Samples.....	464
C.21	Stress Ratio-Strain Relationship From CIU Tests on Vertically and Horizontally Oriented Silty Clay Samples.....	464
C.22	Excess Pore Water Pressure-Strain Relationship From CIU Tests on Vertically and Horizontally Oriented Silty Clay Samples.....	465
C.23	Pore Pressure Parameter A-Strain Relationship From CIU Tests on Vertically and Horizontally Oriented Silty Clay Samples.....	465
C.24	Effective p-q Stress Path Plot From CIU Tests on Vertically and Horizontally Oriented Silty Clay Samples.....	466
C.25	Effective $\sigma_1 - \sigma_3$ Stress Path Plot From CIU Tests on Vertically and Horizontally Oriented Silty Clay Samples.....	466
C.26	Stress-Strain Relationship From CIU Tests on Vertically and Horizontally Oriented Silty Clay Samples.....	467
C.27	Stress Ratio-Strain Relationship From CIU Tests on Vertically and Horizontally Oriented Silty Clay Samples.....	467
C.28	Excess Pore Water Pressure-Strain Relationship From CIU Tests on Vertically and Horizontally Oriented Silty Clay Samples.....	468

Figure	Description	Page
C.29	Pore Pressure Parameter A-Strain Relationship From CIU Tests on Vertically and Horizontally Oriented Silty Clay Samples.....	468
C.30	Effective p-q Stress Path Plot From CIU Tests on Vertically and Horizontally Oriented Silty Clay Samples.....	469
C.31	Effective $\sigma_1 - \sigma_3$ Stress Path Plot From CIU Tests on Vertically and Horizontally Oriented Silty Clay Samples.....	469
C.32	Stress-Strain Relationship From CIU Tests on Vertically and Horizontally Oriented Varved Clay Samples.....	470
C.33	Stress Ratio-Strain Relationship From CIU Tests on Vertically and Horizontally Oriented Varved Clay Samples.....	470
C.34	Excess Pore Water Pressure-Strain Relationship From CIU Tests on Vertically and Horizontally Oriented Varved Clay Samples.....	471
C.35	Pore Pressure Parameter A-Strain Relationship From CIU Tests on Vertically and Horizontally Oriented Varved Clay Samples.....	471
C.36	Effective p-q Stress Path Plot From CIU Tests on Vertically and Horizontally Oriented Varved Clay Samples.....	472
C.37	Effective $\sigma_1 - \sigma_3$ Stress Path Plot for CIU Tests on Vertically and Horizontally Oriented Varved Clay Samples.....	472
C.38	Stress-Strain Relationship From CIU Tests on Vertically and Horizontally Oriented Varved Clay Samples.....	473
C.39	Stress Ratio-Strain Relationship From CIU Tests on Vertically and Horizontally Oriented Varved Clay Samples.....	473
C.40	Excess Pore Water Pressure-Strain Relationship From CIU Tests on Vertically and Horizontally Oriented Varved Clay Samples.....	474

Figure	Description	Page
C.41	Pore Pressure Parameter A-Strain Relationship From CIU Tests on Vertically and Horizontally Oriented Varved Clay Samples.....	474
C.42	Effective p-q Stress Path Plot From CIU Tests on Vertically and Horizontally Oriented Varved Clay Samples.....	475
C.43	Effective $\sigma_1' - \sigma_3'$ Stress Path Plot From CIU Tests on Vertically and Horizontally Oriented Varved Clay Samples.....	475
D.1	Sectional Diagram of Large Oedometer (Modified Rowe Cell).....	482
E.1	Schematic Layout of Testing Equipment.....	490
E.2	General Arrangement of Supports for Vertical Transducer Units.....	491
E.3	Set-Up for Lateral Displacement Measurement.....	492

A

LIST OF SYMBOLS

a	radius of tunnel; or empirical constant for estimated modulus for sand (see Eq. 7.1)
A	pore water pressure parameter
A_f	pore water pressure parameter at failure
B	$(\Delta u/\Delta \sigma)$ Skempton's B value
c'	effective cohesion intercept
c_u, C_u	undrained shear strength
c_{uH}	undrained shear strength in the horizontal direction
c_{uV}	undrained shear strength in the vertical direction
CK_{0UC}	K_0 consolidated undrained compression test
CK_{0DC}	K_0 consolidated drained compression test
CK_{0UE}	K_0 consolidated undrained extension test
CK_{0DE}	K_0 consolidated drained extension test
CIU	isotropically consolidated undrained (compression) test
CID	isotropically consolidated drained (compression) test
CIDC	isotropically consolidated drained compression test
CIDE	isotropically consolidated drained extension test
c_v	coefficient of consolidation in loading
c_R	coefficient of consolidation in unloading
C_c	compression index
d or D	tunnel diameter
E_{30}	secant modulus at 1/3 failure stress
E_u	(E_{u30}) undrained modulus (secant modulus taken at 1/3 failure stress)

E'	drained modulus
E_V	vertical drained modulus
E_h	horizontal drained modulus
e_0	initial void ratio
f	subscript f , e.g. ϵ_f , A_f , $(\sigma_1'/\sigma_3')_f$ indicates value of parameter at failure
G_{vh}	independent shear modulus
G_s	specific gravity of solids
H	length of drainage path
i	angle of inclination of axis of sample to the vertical; or trough width
I_p	plasticity index
I_L	liquidity index
K'_0	coefficient of earth pressure at rest
K	empirical constant for estimated modulus of silty sand and sand (see Eq. 7.1)
l	distance of the instrumented section to the tunnel face
l_1	distance of the instrumented section to the shield tail
L_s	length of shield
m_V	coefficient of volume compressibility (loading)
m_R	coefficient of volume compressibility (unloading)
n	porosity of sand
N	blow counts per 300 mm (1 foot) in SPT
p'_0	overburden pressure
p'_c	preconsolidation pressure
p	$(\sigma_1 + \sigma_3)/2$ = mean stress; consolidation pressure in simple shear test

P_a	atmospheric pressure
q	$(\sigma_1 - \sigma_3)/2$ = deviator stress
r or a	tunnel radius
S_t	sensitivity
T_v	dimensionless time factor = $c_v t/H^2$
t	time
u	pore water pressure
u_f	excess pore water pressure at failure
u_0	initial pore water pressure
U	degree of consolidation
$\Delta V/V$ (%)	volumetric strain due to initial consolidation
V_s	volume of the surface settlement trough
w_0, w_n	natural water content
w_L	liquid limit
w_p	plastic limit
z	embedment depth of tunnel
δ_d	dry density
ϕ'	effective friction angle
(ϕ'_0/c)	friction angle in overconsolidated range
δ	surface settlement
δ_{max}	maximum surface settlement
γ	shear strain or unit weight
ϵ	strain
ϵ_f	strain at failure
σ'_c	consolidation pressure in triaxial test

σ_1'	effective major principal stress
σ_3'	effective minor principal stress
σ_v'	effective vertical stress
σ_h'	effective horizontal stress
$\sigma_1' - \sigma_3'$	deviator stress
(σ_1' / σ_3')	stress ratio
τ	shear stress

The following symbols are used in Chapter 3:

a	radius of excavated opening
C_u	undrained shear strength
D	external diameter of the tunnelling shield
d	external diameter of the tunnel lining
E	elastic modulus
E_u	undrained elastic modulus
G	gap = maximum displacement that the crown can undergo
H	depth of the tunnel axis
K_0	ratio of initial total lateral stress to vertical stress
N	stability number
P_i	internal pressure
$P_{i,cr}$	critical pressure
P_0	isotropic initial stress ($= P_z$)
P_z	total vertical stress at the springline level
r	radial distance from centre of the excavated circular opening
r_e	current radius of the plastic zone

r_{eo}	radius of the plastic zone
r_i	current radius of the opening
S_s	surface settlement
U	component of G due to three-dimensional movement at the face and quality of workmanship ($u_{e,p}^* + \omega$)
u_c	"actual" crown displacement with or without restraint
u_{ee}	radial displacement at the interface of the elastic and the plastic zone
$u_{e,p}^*$	three-dimensional elasto-plastic crown displacement at the face
u_i	plain strain radial displacement of an unlined tunnel
u_r	radial displacement at radius r
ω	crown deformation related to quality of workmanship
Δ	thickness of the tailpiece
δ	the clearance required for erection of the lining
ν	Poisson's ratio
ν_u	Poisson's ratio in undrained condition
γ	unit weight

LIST OF TUNNELLING TERMS

A glossary of terms is provided for convenience in tunnel design, construction and geology. The list of terms includes those used in the thesis and additional ones commonly used in tunnelling.

- Adit.** A short tunnel from the surface to a main tunnel or connecting two main tunnels.
- Arch.** The configuration of the upper portion of a tunnel section above the springline; the crown, roof, or back of a tunnel.
- Bench.** Part of the tunnel section left temporarily unexcavated as excavation of a heading is advanced on top of it.
- Breasting.** Partial or completely braced support of the tunnel face which maintains stability of the ground during tunnel driving.
- Closed Shield.** A shield used in tunnelling in which the working face can be closed during shoving.
- Cover.** The ground between the crown of a tunnel and the surface.
- Crown.** The highest part of a circular- or horseshoe-shaped tunnel.
- Cutterhead.** The front end of a mechanical excavator.
- Drift.** A horizontal underground passage or tunnel.
- Extensometer.** A device for precisely measuring the convergence or divergence of reference points along a common axis.
- Face.** Nearly vertical wall at the farthest advance of a tunnel.
- Final Support.** Tunnel support or lining installed following and independent of excavation to satisfy user requirements.
- Firm Ground.** Ground in which a heading may be advanced several feet or more without immediate support, eg. stiff clay and cohesive granular materials.

Flowing Ground. Ground that may intrude like a thick liquid into the heading.

Footblocks. Blocks of wood, sacked concrete, steel, or precast concrete placed under ribs or posts in non-circular tunnels to provide bearing.

Forepoling. Sharpened planks or steel sections driven ahead and over the top of supports into the soft ground of headings as a protection against raveling earth.

Free Air. Air at standard atmospheric pressure.

Gravelling. The process of injecting pea gravel into the tail void created by a shield to prevent ground settlement. The process is usually followed by injection of grout.

Ground. The material through which a tunnel is driven, whether it is solid rock or soil.

Grout. A fluid with suspended solids or solutes that is injected directly into soil and rock or along the interface between tunnel supports and the adjacent ground. The fluid solidifies and hardens to fill voids and provide a water barrier and some reinforcement.

Grouting. The process of pressure injecting grout. Contact grouting is the pressure injection of grout into voids between a monolithic or segmental lining and the excavated surface of the adjacent ground. Envelope grouting is the pressure injection of grout into voids and discontinuities in the adjacent soil or rock to prevent or retard water flow.

Hard Ground. Material that responds to excavation in a rock-like manner, generally characterized by strength and resiliency that requires special cutting or drill-and-blast techniques for excavation.

Heading. A smaller tunnel excavated ahead of the main tunnel or a general term used to refer to the tunnel face.

Hog Rod. A steel turnbuckle rod set horizontally across a shield-driven tunnel to keep the initial support from being distorted. It is removed when gravelling and contact grouting are completed and the tendency of the initial support to distort has ceased.

ID.OD. Inside diameter, outside diameter.

Inclinometer. A device for precisely measuring the inclination from vertical of a casing or structure to which the inclinometer is attached. Lateral displacements at specific locations along a common axis are obtained by multiplying the sines of the inclination angles by the distance separating the locations at which the measurements are taken.

Initial Support. Tunnel support placed at the heading following excavation to maintain stability and safety of the opening and to minimize ground movement.

Invert. In a circular- or horseshoe-shaped tunnel, the invert is the bottom portion of the arc of the tunnel. In a flat-bottom tunnel, it is the bottom of the tunnel.

Lagging. Wood planking or other structural material installed between ribs.

Liner Plates. Metal plates which are fastened together to support the arch, sides, and, in some cases, the invert of a tunnel.

Mole. A tunnelling machine.

Monolithic Lining. A tunnel lining that is cast in place and continuous.

Muck. The soil or rock materials generated in excavating a tunnel. Included with these materials are by-products of the tunnelling operation such as waste cement, scrap timber and steel, debris, and blasting products residue.

Open Shield. A shield with an 'open' work face.

Pitching. Upward movement of shield from grade during advance.

Poling Boards. See forepoling.

Portal. An entrance, not involving a sudden change in gradient, to a tunnel.

Posts. The vertical members of a steel rib or timber support system of initial support.

Primary Lining. Lining placed as a temporary support for the ground during tunnel drive. In shield tunnel, the primary lining may be designed to support the ground permanently without a secondary lining.

Ravelling Ground. Ground in which the materials above the tunnel or in the upper part of the working face may flake off and fall into the heading.

Rib. A part of the tunnel support, usually of structural steel, curved to suit the shape of the tunnel section.

Ribs and Lagging. Elements of an initial tunnel support system consisting of steel ribs and wood, steel, or precast concrete lagging.

Roadheader. A partial face tunnel boring machine, which excavates by means of boom-mounted system of rotating picks.

Running Ground. Ground consisting of perfectly cohesionless materials such as dry sand or clean loose gravel which run from any unsupported lateral face until a stable pile is built up at the angle of repose.

Secondary Lining. Permanent tunnel lining that is usually placed after mining operations have been completed.

Segmental Lining. Tunnel lining made of sections which fit together to form a ring; commonly of steel, cast iron, or precast concrete. Segments may be bolted together, or keyed together without bolts.

Set. Initial support of the sides and crown of a tunnel; used more when tunnel supports were built up with wood members.

Shaft. A vertical excavation to gain access from the surface to tunnels or mines, or to perform in-situ exploration and testing.

Shield. A circular structural enclosure for tunnelling in soft ground that provides protection for construction personnel and space for excavation and support operations.

Shotcrete. Pneumatically placed concrete; a mixture of sand, gravel, cement, and water which is projected with compressed air against the ground. Accelerating agents may be added to speed hardening of the concrete.

Shove. The act of advancing a tunnel shield forward with hydraulic jacks.

Shoving Blind. The process of advancing a tunnel shield while its face is closed.

Slurry. A pumpable suspension, usually of clay minerals and water, used to stabilize borehole sidewalls, interface voids, and trenches.

Soft Ground. Material that responds to excavation in a soil-like manner, generally characterized by ravelling, sloughing, and occasional running or flowing behaviour. The material usually requires rapid support and can be excavated with scraping, digging, and pneumatic spade equipment.

Spoil. See muck.

Springline. The axis-level of the tunnel.

Squeezing Ground. Ground that undergoes a time-dependent deformation in the vicinity of a tunnel as the result of load intensities exceeding its strength.

Swelling Ground. Ground that undergoes a volumetric expansion resulting from the addition of water. Swelling ground may appear to be stable when exposed, with the swelling developing later.

Tail Void or Tailpiece Void. The annular space between the OD of the shield and the OD of the primary lining.

Tunnel Boring Machine (TBM). A machine that uses various mechanical processes for rock or soil excavation. The machines may provide either full-face or partial face excavation. Full-face tunnel boring machines are mechanical devices that provide continuous excavation by means of a rotating cutter head. The machines are outfitted with equipment for rock or soil support and connected to a skid-mounted system of conveyors and related devices for muck removal. For partial face machines see roadheader.

Yawing. Sideward movement of shield from alignment during advance.

CHAPTER 1

INTRODUCTION

With the advent of tunnel boring machines and innovative lining systems, tunnelling technology has been significantly improved in recent years. This new advance in tunnelling technology has reduced construction time and expenditures in tunnelling projects. Although tunnels have been constructed successfully under difficult soil conditions, experience has shown that ground subsidence invariably occurs over tunnels passing through clay deposits.

In spite of the large number of soft ground tunnels constructed in the past, the ability to predict surface settlements which control the design of tunnels has failed to keep pace with the technological advancements. At present, there is no generally valid theoretical method for predicting ground subsidence before construction. Methods which are based on empirical relationships have often been found to be unsatisfactory and this precarious situation has sometimes lead to expensive and time-consuming litigations among the parties involved. Therefore, improvements in the predictive capacity will result in more economical tunnel design and better contractual arrangements for underground constructions.

The objectives of this thesis are, therefore:

- a) To review and evaluate the validity and limitations of the present settlement prediction methods.

- b) To delineate the mechanisms of settlement during and after construction.
- c) To derive a simple method for predicting the maximum crown and surface settlements.
- d) To develop experimental procedures appropriate for the tunnelling problem and performing the laboratory tests to determine the soil parameters for subsequent analytical study.
- e) To develop an improved, theoretical approach for predicting both the surface and subsurface displacements due to tunnelling.

This thesis presents the results of a five-year study on the subject of ground behaviour associated with tunnelling in clays. The framework of the research consists of detailed literature review, case studies, finite element analyses, field and laboratory investigations, as well as the development of simple approximate and detailed theoretical method of analysis. An in-depth study of the settlement behaviour of a tunnel constructed in Thunder Bay will be given to illustrate the validity and practicality of the proposed procedure for settlement prediction.

A review of the present empirical, experimental and theoretical methods of settlement prediction is summarized in Chapter 2. Consideration will be given to the improvements and shortcomings in these methods.

In Chapter 3, a simple method for predicting undrained surface

3

settlement due to tunnelling in clays is proposed. The sources of subsidence are discussed and a gap parameter which can be theoretically calculated is introduced to quantify ground loss. The validity of the approach is examined by comparing the calculated crown displacements with the field measurements in five detailed case histories. Subsequently, a relationship between surface settlement and the gap parameter is developed by analyzing thirteen case records.

In Chapter 4, additional ground subsidence arising from consolidation of the remoulded zone caused by machine advance was firstly discussed; a method of analysis for soil displacements with the finite element formulation is then presented. The description of an anisotropic elasto-plastic soil model, a technique of construction simulation and the theory of soil-structure interaction are included.

The test requirements for the determination of soil parameters in soft ground tunnelling are summarized in Chapter 5. The significant difference between stress paths experienced by soils in conventional soil testing and those followed in the excavation process is pointed out. The experimental methods in the determination of the elastic anisotropic deformation parameters in a finite element analysis of settlement are also discussed.

Chapter 6 contains the descriptions of the soil stratigraphy, results of field investigation and insitu stress measurements. The index properties, mineralogical compositions of the Thunder Bay silty clay and varved clay are also summarized.

Results of conventional triaxial testing on clay, as well as drained triaxial tests on reconstituted silty sand are presented in Chapter 7.

The experimental results of special tests are reported in Chapter 8. The program of special tests includes tests for determination of the complete set of elastic anisotropic deformation parameters, simple shear tests, large diameter consolidation tests, K_0 -consolidated drained and undrained triaxial tests and controlled stress path tests.

The tunnelling procedures and field observations at the Thunder Bay Tunnel are presented in Chapter 9. The tunnelling system and construction procedure will be described first, followed by the presentation of field observations of ground settlements and changes in pore pressure during and after tunnelling.

The drained and undrained analyses for the settlement behaviour of the Thunder Bay Tunnel using the parameters determined and the proposed method of analysis are performed. In Chapter 10, the results of the analysis are compared with the detailed results of field measurements at two instrumented sections of the tunnel so that the validity of the proposed method may be examined.

Finally, based on the research performed, conclusions and recommendations that are of importance to the design and analysis of tunnels in soft ground are made in Chapter 11.

CHAPTER 2

REVIEW OF PREDICTION METHODS OF GROUND MOVEMENTS

During recent years, the research on the topic of surface settlement caused by tunnelling has been very active. This led to a much better understanding of the problem but a simple reliable method of settlement prediction has not yet been developed on a rational basis. The subject of settlement prediction has mainly been approached in the following three ways:

- 1) Stochastic and empirical method - the surface settlement distribution is determined empirically using the normal probability curve (eg: Peck, 1969). The design parameters to be used in the "error function" are compiled from previous field measurements in tunnel projects in different soil conditions (eg. Peck, 1969; Cording and Hansmire, 1975).
- 2) Laboratory model tunnel tests - Model tunnel tests in cohesive and cohesionless materials are conducted to study the mechanism of ground movements and collapse in sand and clay (eg. Atkinson and Potts, 1977a; Kimura and Mair, 1981). It is suggested that the deformation parameters determined in the model tests may be used for estimating maximum surface settlement (Atkinson and Potts, 1977b). The results of tests are also useful for checking the validity of numerical solutions.

- 3) Theoretical models - The ground stresses and movements are calculated analytically. Most of the theoretical studies are performed by the finite element analysis and nonlinear soil models such as the modified Cam clay model (Mair et al., 1981), the Duncan and Chang model (Kawamoto and Okuzono, 1977), among others have been adopted in addition to the linear elastic model. Realistic simulation of the tunnelling procedures in 'modified 2-D analysis' has also been performed (eg. Lo and Rowe, 1982; Rowe, Lo and Kack, 1983; Ghaboussi et al., 1983).

2.1 STOCHASTIC AND EMPIRICAL APPROACH

The mathematical model for predicting the subsidence of a 'stochastic medium' was first investigated by Litwinsky (1956). The 'stochastic' ground is represented by a collection of many discrete spheres. When movement is created in the medium by removing a sphere from the base of the stacked assemblage of bodies, the spheres will move under the influence of gravity according to the laws of probability. The removal of the sphere is regarded as analogous to the effect of a point source of lost ground, similar to that of excavation of a tunnel. For small disturbances created in the medium, Sweet and Bogdanoff (1965) have shown that the surface subsidence equation has the same form as a normal probability function.

It was proposed by Peck (1969) and Schmidt (1969) that the shape of the surface settlement trough over a single tunnel may be represented

7

within reasonable limits by the normal probability curve. From available field data, settlement profile above a tunnel in soft clay was shown to fit well to this distribution. In highly overconsolidated, stiff to hard clay, the settlement profile resembles the Gaussian distribution curve but it may not necessarily follow the shape of the probability function very closely.

The form of the normal probability curve used by Peck (1969) is shown in Figure 2.1. The settlement trough is characterized by the maximum settlement δ_{\max} , the "trough width" i which is the horizontal distance from the tunnel centreline to the point where the settlement $\delta = 0.61 \delta_{\max}$, and the volume of the settlement trough V_s . Provided δ_{\max} and i are known, the surface settlement at any distance x from the tunnel centreline is given by the equation

$$\delta = \delta_{\max} \exp\left(-\frac{x^2}{2i^2}\right) \quad (2.1)$$

and the volume is given by $V_s = \sqrt{2\pi} i \delta_{\max}$. The parameters i and δ_{\max} in equation 2.1 are determined empirically.

Peck (1969) plotted field observed data of i/D versus Z/D , where D is the tunnel diameter and Z is the depth to the tunnel axis level. He showed that there is a recognizable trend relating the two variables according to the type of soil. At present, the value of i is usually determined from the design curves shown in Figure 2.2. However, the i values observed in the field do not always agree well with the proposed design curves. For example, Lo and Rowe (1982) have

plotted the field value of i/R (R = radius of tunnel) of five case histories on Peck's figure. They observed that these points do not in general all lie within the classification boundaries in Figure 2.2.

Attewell and Farmer (1974) and Schmidt (1974) proposed an empirical relationship between tunnel depth Z and i in the form

$$2i/D = (Z/D)^n \quad (2.2)$$

Schmidt proposed a value of n of 0.8 while Attewell and Farmer proposed that $n = 1$ for clays. The validity of the relationship has not been tested rigorously.

The magnitude of the maximum surface settlement, δ_{\max} , is even more difficult to obtain. It is dependent on the amount of 'ground loss' and hence it varies considerably depending upon the soil condition, tunnel depth and construction procedure. Peck et al. (1972) suggested that the maximum settlement can be estimated on the assumption that the volume of the surface settlement trough V_s will be 1% of the "volume of the tunnel". For most situations, this 'rule of thumb' may give a conservative solution. However, settlement volumes for the Mexico City Siphon Tunnels have nevertheless been reported to be as high as 40% of the tunnel volume (Cording and Hansmire, 1975).

The ground movements in seventeen tunnelling case histories, most of which were in stiff clay and granular material, were summarized by Cording and Hansmire (1975). The volume of lost ground per

unit length of the tunnel V_L was defined as the volume of soil that displaces across the perimeter of the tunnel. For cases where the settlement point was located 0 to 2 m above the crown, the volume lost, V_L , was evaluated empirically from observed vertical movement near the crown. According to the authors, the volume lost may be divided into four stages, namely: 1) ahead of the face, 2) over the shield, 3) during the erection of the lining (i.e. at the shield tail), and 4) with time and with further advance of the heading as the lining deflects. The approximate empirical method to estimate the first two components of volume losses and the factors which influenced the four components were also discussed. The volumes of ground lost into the tunnels, V_L , were compared with the volumes of surface settlement troughs, V_S . (The surface trough volume V_S equals $2.5 i \cdot \delta_{max}$ as defined by a normal probability distribution curve.) It is evident from the field data presented that the volume of surface trough V_S is related to the ground lost V_L and it was proposed that

$$V_S = V_L - V_E + V_C \quad (2.3)$$

where V_E is the volume expansion of soil over the tunnel and V_C is the volume decrease in soil outside the springline. Most of the tunnel cases reported developed V_S that were approximately equal to V_L . The exceptions were the Washington D.C. Metro tunnel (Hansmire, 1975) and the Mexico City Siphon tunnel (Tinajero and Vieitez, 1971). Appreciable volume increase was observed in the medium to dense sands and gravels

in the Washington D.C. case, while significant consolidation of the Mexico City clay might have taken place in the 28-day period of measurement. For the estimation of V_C and V_E , the use of the finite element analysis was suggested. It certainly appears that by evaluating each component of volume lost or volume change, the surface settlement volume may be determined. However, the quantity of volume lost may only be inferred from previous tunnelling experiences because simple reliable theoretical based estimation techniques have not yet been formulated. Nevertheless, Cording and Hansmire have made a significant contribution to the problem of settlement prediction by identifying the components of the surface settlement volume.

Although the empirical approach to the prediction of settlement may be criticized, it does have practical attraction in its simplicity. This method has been widely used in tunnel design and settlement prediction in tunnelling projects (eg. Norgrove et al., 1979).

The empirical approach discussed has been restricted to prediction of transverse surface settlements. Attewell and Woodman (1982) have extended the empirical approach by developing equations for the prediction of three-dimensional ground movements and strains. The expression of 3-D settlements is derived by assuming that the centre-line settlements along the tunnel axis have the shape of a cumulative probability distribution, and the transverse settlements take the form

of a normal probability distribution. The width of the transverse displacement profile at depth Z is assumed to be described by

$$\frac{i}{a} = K_a \left(\frac{Z_0 - Z}{2a} \right)^n \quad (2.4)$$

where i is the transverse horizontal distance between the points of maximum settlement and inflection at depth Z .

n is usually an empirical parameter, but may sometimes be derived theoretically

a is a material parameter

K_a is a parameter of the equation

Z_0 is the depth of the tunnel.

At the surface, $Z = 0$. If K_a is chosen to be 1, equation 2.4 will be reduced to the form of equation 2.2. It was suggested that this is the experimental justification of the equation. However, since it has not been shown in the literature whether the field observed transverse settlement profile in the ground does follow the distribution, the validity of equation 2.4 may be questioned. Further, the parameters in equation 2.4 may not be readily obtained. Six British tunnelling case histories were presented. In the comparative study, the theoretical shape of the longitudinal surface settlement profile along the tunnel alignment generally approximated well to the longitudinal field settlement profile. However, an 'offset' between the measured and the predicted curve in four cases arose because it was assumed that 50% of the total surface settlement had occurred

when the tunnel face was beneath the measurement point (i.e., $S/S_{\max} = 50\%$, where S = surface settlement, S_{\max} = maximum surface settlement). The choice of $S/S_{\max} = 50\%$ appeared to be a matter of convenience rather than a theoretical requirement. Theoretically, if the face is stable and elastic, the crown settlement at the face would be about 1/3 of the total crown settlement (Lo et al., 1984). From elastic 3-D study of surface subsidence (Ito and Hisatake, 1982) S/S_{\max} approximately equals 1/3 as a lower bound value; in practice, this settlement ratio at the face may vary widely.

More results of three-dimensional deformation measurement are required in order to provide a better basis for improving the solution and for the choice of the input parameters. Although the approach is not precise, it may be justified on the ground that better 3-D solutions are not available at present. The above approach may be useful for preliminary design and planning purposes. However, it may not be able to predict the settlement patterns accurately in a specific tunnelling project.

From a critical review of the stochastic and empirical approach on settlements prediction due to tunnelling, the following comments may be made:

- 1) The stochastic approach predicts that the surface subsidence due to a point source of lost ground will have the same shape as a normal probability curve. This distribution is generally observed in settlement troughs over tunnels in clays.

- 2) The empirical approach proposed by Peck (1969) and Schmidt (1969) requires the estimation of parameters such as δ_{\max} (maximum surface settlement) and i (trough width).
- 3) Equations for the prediction of three-dimensional ground movements and strains caused by tunnelling have been formulated from basic probability equations. However, due to the inherent assumptions in the mathematical model, it may only be suitable for preliminary design purposes.
- 4) The simple empirical approach has provided a practical predictive method for the engineer. However, the development of a more accurate method to estimate maximum settlement, loss of ground and trough width is required in order to improve the reliability of the prediction. A rational semi-theoretical approach in settlement prediction will be discussed in the next chapter.

2.2 MODEL TUNNEL TESTS ON GROUND MOVEMENTS

Model tunnel tests have been carried out in order to study the mechanisms of deformation and collapse in sand and clay (eg. Atkinson and Potts, 1977a; Kimura and Mair, 1981). The tests were conducted either under static condition or in the centrifuge. In the earlier experiments, plane-strain models were set up to study the unlined tunnel behaviour away from the face (Atkinson and Potts, 1977a; Mair et al., 1981). In later experiments, the behaviour of the tunnel heading was also investigated (Kimura and Mair, 1981). Both the

behaviour of a completely lined tunnel and the behaviour of a length of unsupported heading of a lined tunnel were examined.

These model tests are useful for illustrating the pattern of soil movements around a circular cavity as the cavity pressure is reduced. Collapse mechanisms in both cohesive and cohesionless soils have been identified and this led to improved upper bound plasticity solutions of safe tunnel pressure (Davis et al., 1980; Atkinson and Potts, 1977b). Since the nature of deformations around an idealized tunnel can be studied in detail in a well controlled manner, the results of model tests are also useful for comparison with results of numerical solutions for the general displacement field and the collapse loads. However, it is important to recognize that these model tests are not intended to reproduce precisely the behaviour of a real tunnel together with the details of construction, and the results acquired in a model study cannot be directly generalized for the designs for particular tunnel projects.

It appears that the investigators on model tunnel tests have seldom outlined the principles required in a model system. A model test is a methodology by which the characteristics of other similar systems can be predicted. If accurate quantitative data are to be obtained from a model study, there must be similitude between model and prototype (Albertson, 1960; Streeter, 1975).

The types of similarity are geometric similarity, kinematic similarity and dynamic similarity. Their definitions are as follows:

1. Geometric similarity requires that all length ratios from model to prototype be the same.
2. Kinematic similarity requires that the streamline pattern be the same in the model and the prototype so that the displacement ratios, velocity ratios and the acceleration ratios are constant from model to prototype.
3. Dynamic similarity requires that the shear ratios, the pressure ratios and the force ratios be the same from model to prototype.

For geometric similitude between model and prototype, if the model is one-hundredth the size of the prototype, then the grain size of the model material and the prototype must be in the same ratio. For example, in the model tunnel in sand described by Atkinson and Potts (1977a), the diameter of the opening is 60 mm, with $c/D = 1.48$, $e/D = 0.017$ (see Figure 2.3a) where c is the cover and e the grain size of the material surrounding the tunnel. The model was filled with fairly uniform dry sand of grain size of about 1 mm (i.e., $e = 1$ mm). It would represent the behaviour of a 6 m tunnel in cobbles of 0.1 m in size.

According to the principle of similarity in modelling, it appears that the grain size (and hence the strength) of the modelling material may not adequately reflect most earth materials.

The use of the centrifuge is an appropriate method to satisfy some of the requirements of dynamic similarity which demands that the shear ratios, the pressure ratios and the force ratios be the same

from model to prototype. For example, a centrifugal model in Kaolin whose shear modulus and mass density are G_0 and ρ_0 respectively becomes apparently n times larger when accelerated to ng ; G_0 and ρ_0 may be considered identical in the prototype and model under this condition (see Figure 2.3b). Alternatively, a static model would simulate a larger tunnel at a lower stress level or in stronger and stiffer soil.

The principal disadvantage of model studies is the fact that complete similarity in the model and prototype is sometimes difficult or impossible to obtain. In these cases, it is only possible to obtain a partial (qualitative) answer by means of a model. Therefore, the results of all model tests, when used to investigate behaviour of tunnels, must be interpreted with care, bearing in mind the insufficient similarity between the model and the actual tunnels.

On the basis of experimental data from model tests on shallow tunnels, Atkinson and Potts (1977a) suggested a simple relationship between the ratio of surface settlement to crown settlement and ratio of cover to diameter:

$$S_s/S_c = 1 - \alpha(c/D) \geq 0 \quad (2.5)$$

where S_s , S_c are the settlements at the ground surface and at the crown respectively, c is depth to crown and D is the diameter of the tunnel, α represents the average dilation of the ground and it is shown to be a constant for a particular category of soil in model tests (Atkinson

and Potts, 1977a). Values of α for overconsolidated kaolin and dense Leighton Buzzard sand obtained in model tests are shown in Figure 2.4.

Ward and Pender (1981) have plotted the values of S_s/S_c from 28 case records against c/D and these were compared with the relationship in equation 2.4 and they suggested that all the complex tunneling variables are not reflected by the simple plot of Figure 2.4.

A load factor (LF) was defined by Mair et al. (1981) as the ratio between the actual stability ratio (N) and the stability ratio at collapse (NC). At collapse, LF = 1. The authors suggested that ground loss might be better related to load factor rather than stability ratio alone. From results of the model tests conducted in the centrifuge, the volume of ground loss per unit tunnel volume was seen to increase with load factor. When LF exceeded 0.5 in the kaolin models, the rate of increase was very rapid. It is certainly interesting to investigate at this point whether S_s/S_c also changes with LF. According to Atkinson and Potts (1977a), there is a constant ratio between S_s and S_c in a particular test before collapse; however, they have not indicated clearly on the plot of S_c/D vs S_s/D whether the centrifuge result is included. From theoretical considerations, S_s/S_c must be constant if soils are elastic, i.e., at low LF. When plastic zone in soft ground develops around the tunnel, say LF > 0.5, the ratio of S_s/S_c may increase nonlinearly with LF. As LF approaches or equals to one, soils above the tunnel are fully plastic, movement would be block-like and S_s/S_c approaches one. (The above comment

applies only to soils which show little dilation during tunnelling.) It does appear that the linear relationship between S_s and S_c at different LF before collapse only applies to certain model settings. The effects of LF on the magnitude of S_s/S_c for constant values of c/D were also noted by Ward and Pender (1981).

It should be noted that S_s and S_c in Figure 2.4 were measured at some variable distances from the actual surface and tunnel crown. Therefore, the S_s/S_c ratios are all in error and they are generally higher than the actual ratios.

All the settlement trough shapes from model tests in both sands and kaolin resembled the form of an error function, supporting the proposal by Peck (1969). The other interesting aspect is the volume strain measured. Very small dilation was observed in the drained overconsolidated kaolin tunnel model. Laboratory controlled stress path tests and triaxial unloading tests on soft clays from Thunder Bay also showed little volume changes as will be discussed in Chapters 7 and 8. Thus, it may be suggested that there is only moderate to small difference in drained and undrained deformation behaviour in grounds above a tunnel in clay. This phenomenon was also observed in the case history of Thunder Bay Array 2 (Palmer and Belshaw, 1980). The tunnel was constructed in soft clay with good workmanship and surface settlements had essentially terminated within 20 days after construction.

Atkinson et al. (1975) demonstrated that, in dense, dry, dilatant sand, prior to collapse, movements were initially restricted to a wedge-like zone immediately above the tunnel where relatively large dilations occurred. The collapse mechanism for final equilibrium was a block of soil descending along two vertical slip surfaces above the tunnel. This appears to be consistent with 'roof raveling' observed in the field. At collapse, the movement of soil above the model tunnel in clay was also block-like (Mair et al., 1981). Clay was seen to be 'squeezing' into the tunnel opening.

Kimura and Mair (1981) performed a series of model tests in overconsolidated kaolin in the centrifuge to investigate the behaviour of three-dimensional tunnel headings. The result revealed that tunnel stability is strongly influenced by the length of the unlined tunnel heading. For a completely lined tunnel, clay entered the tunnel heading from the surrounding soil. Within the moving body of clay, intense shearing was seen. For the model with $P/D = 2.0$, where P = length of unlined heading, D = diameter of tunnel, it exhibited a kinematic mechanism approaching two-dimensional behaviour; the soil movement was mainly vertical in a plane normal to the tunnel axis. The transition from three-dimensional to two-dimensional behaviour was accompanied by a decrease in stability in the partially lined tunnel.

The pattern of soil movements in the two cases is very illustrative. The fully-lined tunnel may approximate the situation of

tunnelling with an open face shield. The soil displacement represents movement ahead of the face. Where sufficient pressure is applied at the face, it may be anticipated that the movements can be reduced. When too large a pressure is applied, it may be expected that the soil would be displaced in the same pattern but in the reverse direction, i.e., ground heaving. The soil displacement ahead of the face in shield tunnels is strongly influenced by both the details of construction procedure and support pressure at the face. However, very little information is available in the literature describing the detail events at the face.

The apparently two-dimensional soil behaviour for a partially lined tunnel suggested that soil movements over the shield or into the tail void may be essentially two-dimensional. Such a phenomenon implies that the plane strain solution may be appropriate for predicting settlements above a shield excavated tunnel.

From the results of model tests discussed, the following observations may be made:

- 1) The model study illustrates qualitatively the soil displacement pattern around a circular cavity. This led to improved collapse load solution in plasticity theory by using the observed failure mechanism.
- 2) Surface settlement profile of the model resembles the shape of an error function. Three-dimensional soil movement is

strongly influenced by the support condition provided at the face.

- 3) The constant ratio of (S_s) surface settlement to (S_c) crown settlement observed by Atkinson and Potts (1977a) may only be valid in certain laboratory conditions. The ratio would most likely vary with changes in load factor.
- 4) The quantitative results of a model study may be applied in the design of an actual tunnel only if the similarity requirements between the model and the prototype are satisfied.

2.3 THEORETICAL APPROACH

Most of the recent analytical studies on stresses and displacements around a tunnel have employed numerical models using the finite element method. In these analyses, nonlinear elastic and elasto-plastic soil models were used in place of simple linear elastic models in many studies to characterize the representative stress-strain behaviour of soft ground. For example, the nonlinear elastic Duncan and Chang (1970) model, and the elasto-plastic modified Cam-clay model were used respectively by Kawamoto and Okuzono (1977) and Mair et al. (1981) in two-dimensional plane-strain analysis of a tunnel. A displacement boundary condition (specified by crown displacement) was used by Rowe, Lo and Kack (1983), Ghaboussi et al. (1979) and Eisenstein and Thomson (1978) in two-dimensional analyses of surface settlements. Analyses of advancing tunnels have also been performed.

Ghaboussi et al. (1983) predicted the elastic liner behaviour of existing twin subways due to the advance of a crossing sewer tunnel by a plane strain analysis. Similar 'pseudo-3D' analyses were also reported by Romo and Diazm (1981) and Ohnishi et al. (1982). Non-linear elastic three-dimensional analysis for the NATM in Frankfurt clay was carried out by Katzenbach and Breth (1981) and the numerical analysis involved a three-dimensional mesh of 990 elements. Three-dimensional surface subsidence in elastic ground was also analyzed with the linear boundary element method by Ito and Hisatake (1982).

The two-dimensional plane strain analysis will be reviewed first.

Kawamoto and Okuzono (1977) investigated the surface settlement profile over a shield tunnel in Nagoya City. Both linear and nonlinear elastic analyses were performed. The nonlinear finite element calculation was based on the stress-strain relationship proposed by Duncan and Chang (1970). The nonlinear analysis gave significantly better modelling of the measured profile than that of the linear elastic analysis.

Thomson and El-Nahhas (1980) investigated the ground deformation around the White-Mud Creek tunnel in clay-shale by performing linear-elastic plane strain analysis. The deformation calculations were made for a tunnel in insitu stress condition of $K_0 = 0.67$ and 1.0, and for a tunnel with a peripheral softened zone with a reduced

modulus of deformation ($K_0 = 1.0$). The finite element analysis suggested that this softened zone is as important a consideration with regard to tunnel deformation as increasing K_0 from 0.67 to 1.0. The calculated surface settlements were similar in the three cases. Though the analyses of Thomson and El-Nahas (1980) were far from being comprehensive, the result of their findings lends support to the concept of plasticity of soil around the tunnel. Ward and Pender (1981) had also expressed the view that the squatting behaviour of the lining appeared to be independent of the insitu stress conditions. For example, the horizontal diameter of the Heathrow cargo tunnel (Muir-Wood, 1969) showed small increase in diameter after its construction in London clay. This is contrary to expectation from linear elastic theory because the K_0 in London clay is greater than one. The local properties of the ground and the initial K_0 condition may be altered due to excavation and soil-lining interaction.

Another notable advance in the techniques of finite element analysis is the use of specified displacement boundary conditions. Ghaboussi et al. (1978) analyzed the surface settlement of a six-inch (152.4 mm) diameter model tunnel in sand. An elasto-plastic model, based on the critical state concept was used in the analysis. They showed that while the unlined tunnel analysis would overestimate the displacement, the lined tunnel analysis would underestimate the displacement. Realistic displacements could only be obtained by imposing a specified tunnel crown displacement. A maximum crown displacement

of 0.3 inches (7.6 mm, i.e., 5% of diameter) was required to reproduce the correct surface settlement. The same concept was also used by Eisenstein and Thomson (1978) in a linear elastic finite element analysis of the twin tunnels of the Rapid Transit System in Edmonton, Alberta. Both these two examples illustrate that the simulation of a displacement boundary will improve the accuracy of settlement prediction.

Lo and Rowe (1982), Rowe, Lo and Kack (1983) have proposed the use of a 'gap parameter' in settlement analysis due to tunnelling. The 'gap' quantifies ground losses as a result of tunnelling and it defines the maximum crown displacement. The gap may be calculated theoretically and it can be used in conjunction with either simple or sophisticated analytical methods of prediction. In their finite element analysis, the general soil-structure interaction theory (Rowe et al., 1978) and an elasto-plastic soil model were adopted. Six well documented case histories have been analyzed. It is found that the method yields settlement which is in reasonable agreement with field measurements. The theoretical calculation of the gap parameter and its use in a simple semi-theoretical method for maximum surface settlement has been discussed by Lo, Ng and Rowe (1984). This discussion will also be included in the subsequent chapter.

Rowe, Lo and Kack (1983) have adopted an elasto-plastic soil model in the analysis of a lined tunnel. The soil was assumed to have an elastic-perfectly plastic constitutive relationship defined by ten

cross-anisotropic elastic parameters*, a Mohr-Coulomb failure criterion and a non-associated flow rule. The analysis was used in a parametric study to identify the potential factors affecting the prediction of settlement in soft ground tunnelling. A number of significant observations regarding the geotechnical characterization of soil behaviour may be summarized as follows:

- 1) Linear elastic analyses will not provide a good estimate of distribution of surface settlements because of plastic failure within the soil.
- 2) The stress path experienced by soil during tunnel excavation is different from that experienced by the soil beneath a foundation. The modulus of the soil during tunnelling is closer to the extension modulus which is likely to be greater than the compression modulus (see also Lo and Rowe, 1982).
- 3) It is not necessarily conservative to adopt a low modulus of deformation for soft clays, because this suppresses the magnitude of plastic strains leading to the occurrence of 'wide settlement troughs'.
- 4) The elastic anisotropic parameters, especially the independent shear modulus G_{yh} , are important soil properties to be incorporated in the numerical soil model.

Mair et al. (1981) attempted to predict the surface settlement profile of a Cambridge centrifugal model test in kaolin. The modified
* five in loading and five in unloading *

Cam-clay model was used. Though this elasto-plastic model had previously yielded reasonable results for settlement analysis in other geotechnical problems, results of the analysis of settlement due to tunnelling have not led to satisfactory comparison with model test results. The shape of the predicted settlement profile was "too wide" compared with the measured curve. The authors suggested that the soil model which assumes isotropy in elastic response may not be very suitable for describing the behaviour of anisotropically consolidated clay and it is limited in its ability to simulate elastic behaviour in regions beyond the plastic zones around the tunnel opening. This observation is consistent with the view of Rowe, Lo and Kack (1983) that elastic anisotropy plays an important role in surface settlement prediction.

Many of the finite element analyses performed support the idea that the ground around a tunnel seldom remains linear elastic. Eisenstein et al. (1981) derived the resultant strain field from displacement measurements around a deep tunnel driven in dense till and he also reached this conclusion. The concept of plasticity and nonlinearity in soil behaviour have been in general recognized, but not every analysis has made use of the appropriate elasto-plastic description of soil behaviour, such as the consideration of anisotropy in clays.

The study of the soil deformation and lining behaviour of an advancing tunnel by using modified two-dimensional finite element

method was reported by Ohnishi et al. (1982) and Ghaboussi et al. (1983). Romo and Diazm (1981) have examined the stability of a pseudo-3D tunnel face.

Ohnishi et al. (1982) proposed a 'multiple element method' to simulate approximately the advancing tunnel face in a two-dimensional finite element analysis. The solution was carried out incrementally and the stiffness coefficients of the elements in each excavation step were assigned according to an assumed displacement history of a point on the tunnel boundary. The displacement history with the advancing face may be obtained from field measurements in similar ground or from a three-dimensional elastic axisymmetric analysis. Since the deformation history is required prior to the analysis, this approach is actually rather impractical.

Ghaboussi et al. (1983) analyzed a sewer tunnel crossing over existing twin subway tunnels in New York City. Since the clearance between the crossing tunnels was small, it was necessary to investigate the potential detrimental influence on the lining of the subway during driving of the new tunnel. Two-dimensional analysis on this critical section was performed. In their two-dimensional finite element mesh, the subways appeared as circles, perpendicular to the plane of the mesh; whereas, the circular sewer tunnel was modelled approximately as a plane strain tunnel with the longitudinal axis coinciding with the plane of the mesh. In such a case, an equivalent modulus was adopted for elements representing regions to be excavated.

The ground was assumed to be linear elastic. The analysis was carried out by an incremental nonlinear solution scheme such that the stiffness matrix and the load vectors were reformulated in each step. Construction was simulated by deactivating soil elements and activating lining elements and adding jacking forces on the appropriate elements. Consistent trends of lining deformation were correctly predicted prior to construction and the two-dimensional finite element simulation generally yielded conservative results when compared with measured lining deformations. The analytic simulation demonstrated the value of detailed analytical study prior to a tunnel project in providing information for engineering judgement in arriving at the final design recommendations.

Romo and Diazm (1981) examined the stability of an infinitely long tunnel face by finite element modelling of a soil with an elastic hyperbolic stress-strain relationship. The analytical results show that face yielding occurs even at stability ratios of as low as 0.51, as stated by the authors. The size of the potential failure surface increases with the stability ratio for constant tunnel depth. However, the problem investigated by Romo and Diazm is not truly three-dimensional; the result is more applicable to a long wall face in coal mining than in the case of a circular heading. The analysis illustrates the likely occurrence of soil yielding at the face of a long rectangular tunnel heading.

Three-dimensional surface subsidence caused by shallow tunnel

driving in elastic ground was studied by Ito and Hisatake (1982).

The boundary element technique was used to analyze the problem. Since Kelvin's solution of a point load in an infinite medium was implemented in the integration for the displacement solution in a semi-infinite medium, the solution involved an implicit assumption which might not be very realistic, especially for cases with depth to radius (h/a) ratio of less than three (h = distance from surface to axis of tunnel, a = radius of tunnel). However, the assumption may be approximately satisfied for tunnels having a depth ratio of greater than three and their analytical results are certainly of theoretical interest. The following observations may be made for tunnelling in isotropic elastic ground under gravitational stress condition with a h/a ratio greater than three:

- 1) The magnitude of the centreline surface settlement is not very sensitive to the change in h/a ratio for $h/a > 3$.
- 2) The extent and width of the transverse settlement trough and the longitudinal subsidence curve increases with increasing h/a ratio.
- 3) The magnitude of maximum subsidence and maximum gradient in both the transverse and longitudinal subsidence curves increases with decreasing Poisson's ratio of the ground (say from $\nu = 0.45$ to $\nu = 0.15$).
- 4) Between 20% to 40% of the total surface settlement would have occurred when the face passes beneath the cross-section.

Some observations may be made on the above theoretical findings. For point (1), since the maximum elastic surface settlement remains relatively constant with variation in h/a , it becomes apparent that little advantage may be gained by locating a tunnel deep in very stiff to hard ground. Point (2) is in general agreement with Peck's proposed design curve (Peck, 1969) for trough widths. Point (3) is interesting because the field settlement curve generally widens and flattens with time due to consolidation of remoulded soil around the tunnel; clearly, this is not an elastic character of the soil. Point (4) suggests that a correction factor of $1/3$ may be applied to the calculated plane strain surface displacement to obtain the three-dimensional surface settlement developed when the tunnel face is beneath the measurement point (see also Lo et al., 1984).

The results of the linear elastic three-dimensional analysis have been very instructive, but the general analytical solution of the realistic elasto-plastic behaviour of a three-dimensional tunnel in shallow ground is far from being resolved at the present time.

Katzenbach and Breth (1981) presented the result of a three-dimensional analysis of a tunnel constructed by the NATM method in Frankfurt clay. A three-dimensional mesh of 990 elements was used. The finite element analysis simulated the construction details by numerical modelling of the stepwise excavation and application of sprayed concrete. The Duncan and Chang (1970) nonlinear elastic constitutive law was adopted and in the calculation procedure

consideration was given to the effect of loading and unloading on deformation behaviour. The analysis computed surface settlements that were in reasonable agreement with the measured settlement profiles in both the transverse and longitudinal cross-sections. The plot of stress contours in the finite element mesh indicates that the soil surrounding the tunnel is overstressed. Since the analysis was aimed particularly at an evaluation of the NATM method in Frankfurt clay, a better general understanding of behaviour of tunnels cannot be readily gained.

From a critical review of the recent analytical studies on settlements due to tunnelling, the following comments may be made:

- 1) While most analyses have concentrated on the study of surface displacements and lining stresses, the analyses on distribution of settlements in the ground are few if any.
- 2) The soil around the tunnel is likely to become overstressed, therefore a nonlinear soil model would generally give better analytical results than a linear one.
- 3) It is not necessarily conservative to adopt low modulus of deformation in an elasto-plastic analysis because it suppresses the magnitude of plastic strains within the soil leading to a 'wide settlement trough'.
- 4) The gap parameter or displacement boundary condition is an important factor to be considered in the finite element formulation.

- 5) There are only a few three-dimensional analyses reported in the literature due to its high cost and enormous task of preparing input data; modified two-dimensional approaches have been used to simulate the three-dimensional condition of the advancing tunnel. The result appears to be conservative.
- 6) The three-dimensional elastic surface subsidence due to an advancing tunnel was solved by the BE method. However, the general theoretical behaviour of the three-dimensional elasto-plastic stress and displacement behaviour in soft ground remains unresolved.

2.4 CONCLUSIONS FROM REVIEW OF PREVIOUS RESEARCH

From a study of previous research on model tests, field measurements and theoretical analyses of settlements due to tunnelling, the following conclusions may be drawn:

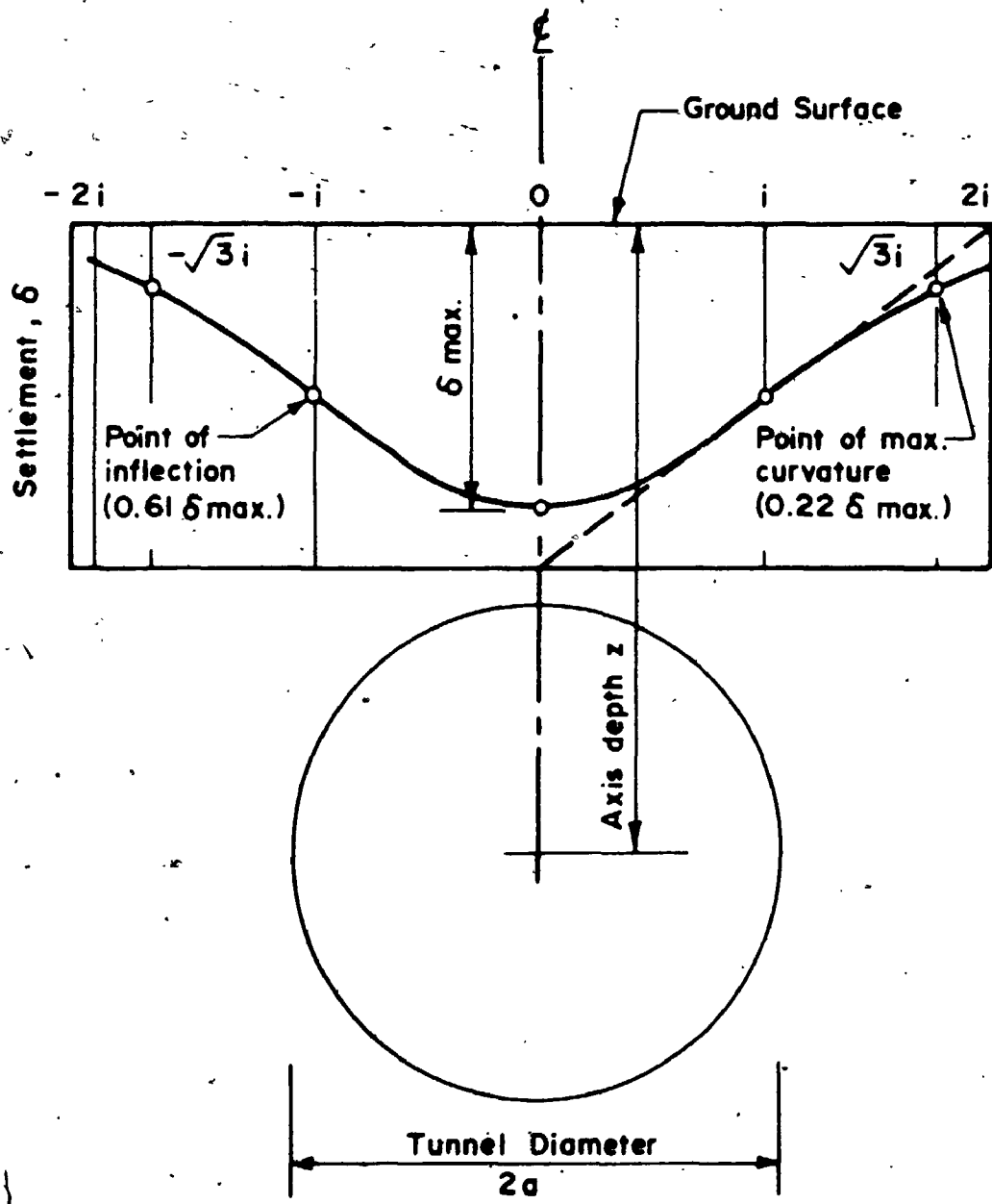
- 1) The occurrence of surface settlement is usually attributed to loss of ground caused by tunnelling and the surface subsidence profile is normally represented by a Gaussian Distribution Curve. However, there is no consistent and theoretically based method to estimate the amount of volume of ground loss. Many investigators have compiled settlement data in various tunnelling projects and the amount of empirical observations have steadily increased. These data are usually site specific and they may not be correctly extrapolated to new locations without a self-consistent theoretical framework taking into

account of the stress-strain behaviour of the soil and construction constraints.

2) Results of model tests have shown that the maximum surface settlement may be related to the crown settlement rather than the volume of ground loss which is in practice difficult to measure directly.

3) The finite element method is the most commonly used numerical technique in analysing tunnelling problems. Linear elastic analyses are generally not applicable for calculating settlements in soft ground because of yielding of soil around the tunnel. It may also be noted that some non-linear elasto-plastic models also do not yield reasonable results when compared with laboratory or field observations. This implies that any chosen soil model must represent closely the soil behaviour. Further, the modulus required in an analysis should be derived from appropriate tests following the stress paths undergone by soil elements surrounding the tunnel. It has also been shown that it is not necessarily conservative to adopt a low modulus of deformation in an analysis.

4) Model studies on tunnels provide a good source of 'idealized' tunnel settlement data. The information may be used for comparison with numerical results or developing kinematic collapse mechanism in plasticity solution. The results of the model studies would be more useful if the laws of similarity are obeyed between the prototype and model tunnel.



Ratio $\frac{z}{a}$ is function of $\frac{z}{2a}$ and soil conditions
 Volume of trough $\approx 2.5i\delta_{max}$.

FIGURE 2.1 Properties of Normal Probability Curve as Used to Represent Surface Settlement Trough (Peck, 1969)

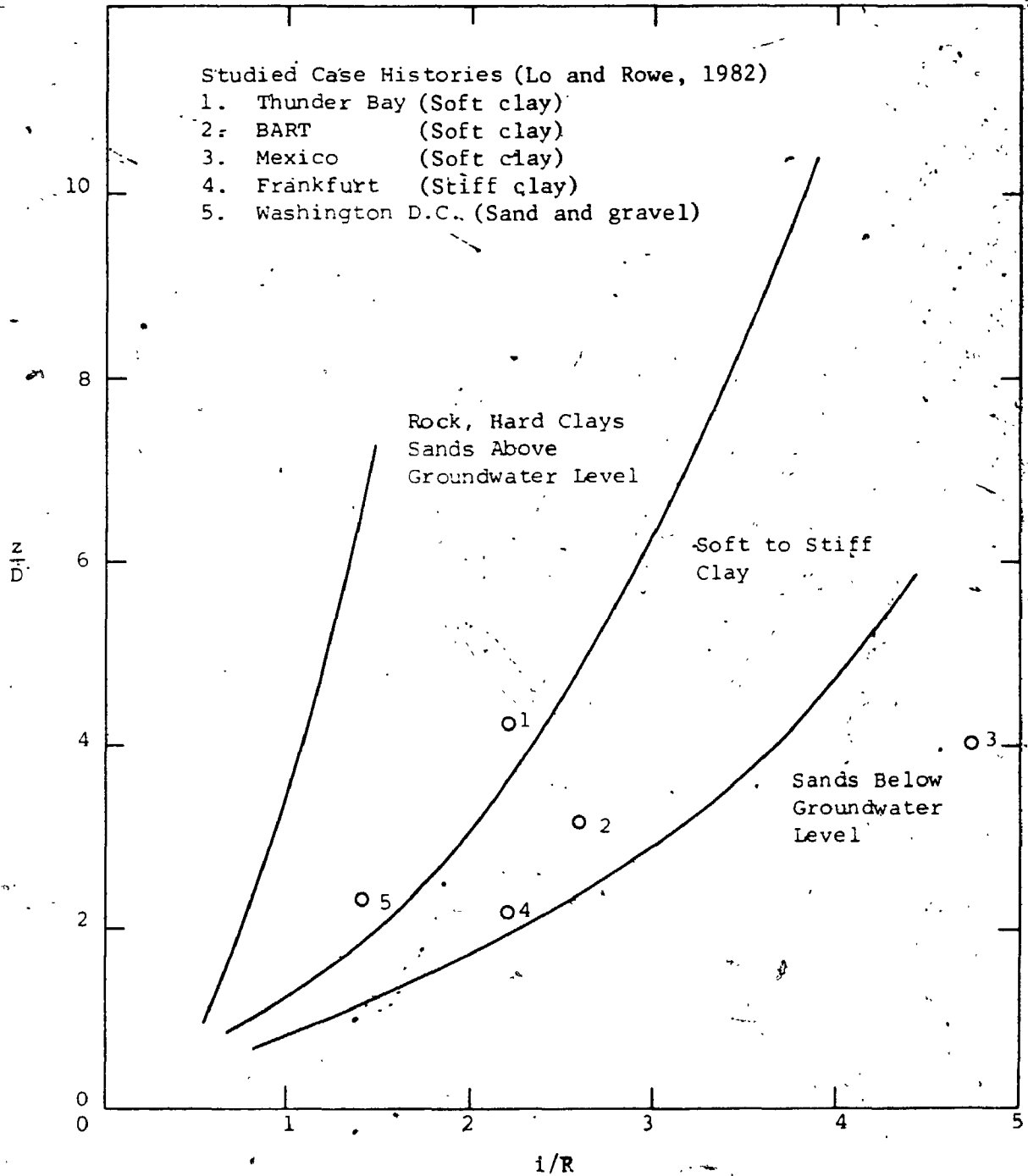


FIGURE 2.2 Relation between Width of Settlement Trough i/R , with Depth of Cover z/D , for Different Soil Conditions (Peck, 1969).

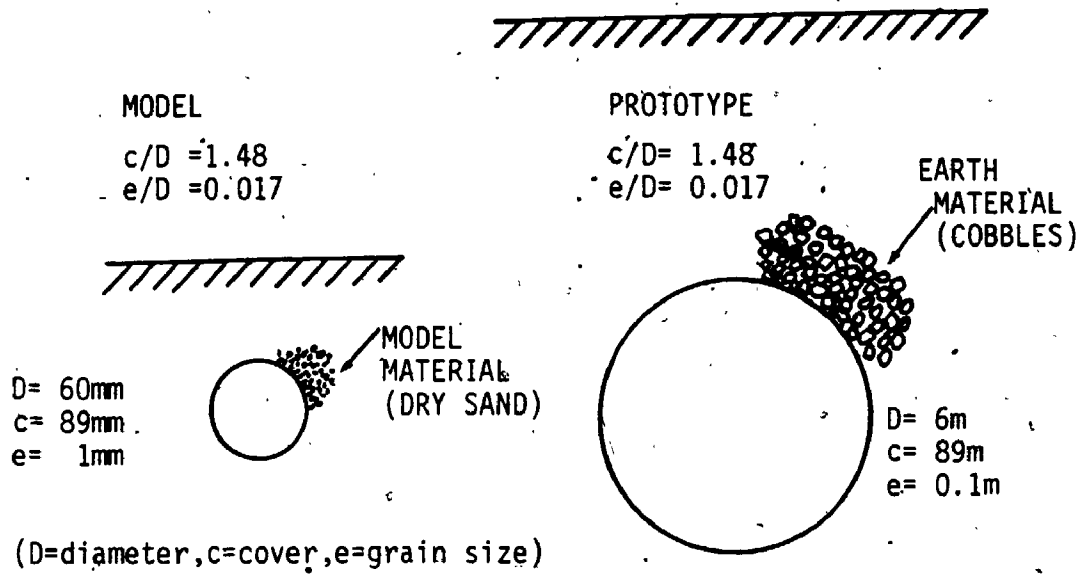
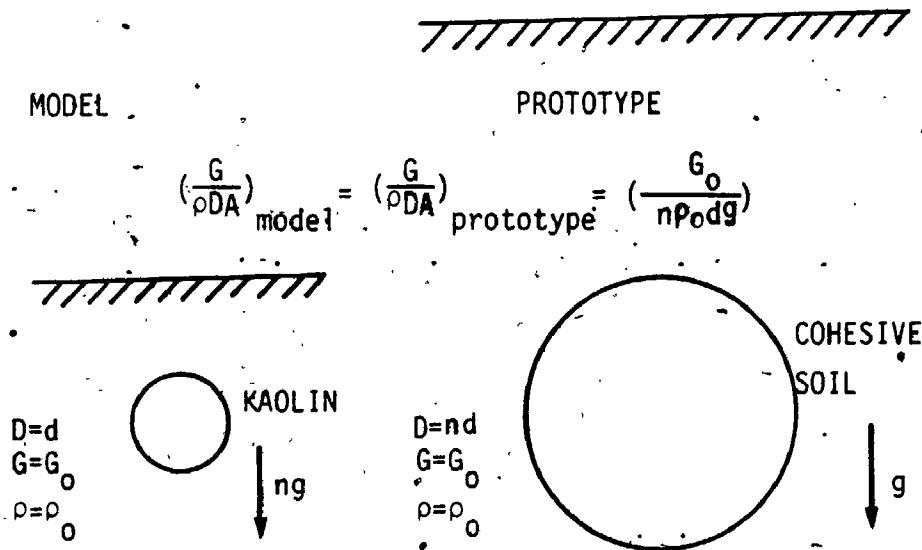


FIGURE 2.3a Geometric Similarity between Model and Prototype



(D=diameter, G=shear modulus,
rho=density, g=acceleration due to gravity,
A=acceleration)

FIGURE 2.3b Dynamic Similarity between Model and Prototype

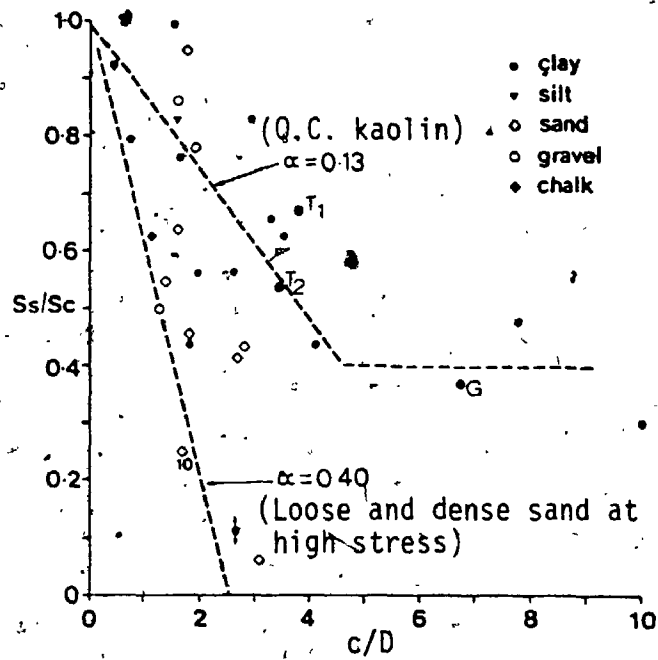


FIGURE 2.4 Field and Model Relationships between Ratio of Near Surface Settlement to Settlement Near Tunnel Crown (S_s/S_c) and Cover to Diameter Ratio (c/D) (after Ward and Pender(1981))

Note:

Points G, T_1 and T_2 respectively represent the S_s/S_c ratios for the tunnels at London Green Park, Thunder Bay Array 1 and Array 2. The original points plotted by Ward and Pender(1981) were in error.

CHAPTER 3

A SEMI-THEORETICAL APPROACH FOR PREDICTING SETTLEMENTS DUE TO TUNNELLING IN CLAY

3.1 INTRODUCTION

In Chapter 2, the methods in predicting ground movements have been reviewed. The estimation of surface settlement is usually based on an empirical relationship proposed by Peck (1969) or alternatively, Cording and Hansmire (1975). The limitations of these empirically-based methods have been discussed.

A theoretically based method for the prediction of settlements at the surface and at various depths has been suggested by Lo and Rowe (1982), Rowe, Lo and Kack (1983). An important aspect of this approach is the use of a displacement boundary condition in the finite element analysis. A gap parameter is introduced. This parameter takes into account the ground loss as a function of strength and deformation behaviour in the elastic and plastic state; the physical clearance between the lining and the excavated surface and workmanship. Retrospective analyses on well documented case histories have been performed with this approach (Lo and Rowe, 1982; Rowe and Kack, 1983). Given appropriate characterization of ground properties, the method yields settlement profiles that are in reasonable agreement with field measurements, provided that the gap parameter is correctly chosen.

The above method is subjected to two limitations for practical

applications:

- a) an estimate of the gap parameter is required,
- b) the amount of computations can only be justified for critical sections in major projects.

It is necessary, therefore, to develop i) a method for estimating the gap parameter and ii) a simple method for estimating the maximum surface settlement. The development of these methods will be discussed in this chapter and thirteen case histories are analyzed using this approach. Since only simple equations and conventional soil properties are required, the method may be readily applied in preliminary design of tunnels in clay.

3.2 DEFINITION OF THE GAP PARAMETER

The action of tunnel excavation produces two physical changes in the soil mass: (a) the creation of a new boundary within the soil mass and (b) the removal of the insitu stresses along the excavated circumference.

Excavation of the tunnel provides an opening into which the soil can deform and the constraint to soil movement is primarily a function of the machine characteristics, workmanship, lining geometry and lining flexibility. The movement of the soil into the opening can be related to the "loss of ground" resulting from the tunnelling process. The volume of soil that displaces across the perimeter of the tunnel is termed "loss of ground" (Cording and Hansmire, 1975). Alternatively, the "loss of ground" may be defined as volume of material that has been excavated or displaced in excess of the theoretical volume within the outer diameter of the final tunnel lining. This loss of ground

may be considered to occur in three stages as the boring machine advances in the soil mass: (1) ahead of the face, (2) over the shield, and (3) upon the erection of the lining. Additional loss of ground may result from creep and consolidation and a change in hydraulic condition under long term conditions.

Irrespective of methods of ground control that are used, some three-dimensional movements at and in front of the face usually take place during excavation of the working face. Therefore, a volume of lost ground is developed equal to the amount of overexcavated or displaced material at the face.

The loss of ground which occurs over the shield corresponds to the volume of soil that is displaced or mined in excess of the diameter of the cutting shield. Causes of such loss in ground are primarily due to alignment problems encountered when steering the shield. If a shield is pitched upward or downward at an inclination other than that dictated by the path of shield movement required to maintain tunnel grade, additional material may be excavated or displaced. Over the length of the shield, a point above the crown will settle an amount equal to the length of shield times the pitch of the shield in excess of the actual grade (Cording and Hansmire, 1975). Loss of ground in a similar fashion occurs due to yawing, when the shield is allowed to move irregularly from side to side. Shields are often fitted with a bead or extension to provide axial adjustments, and the space created outside this shield skin allows ground to cave in. If the shield has to negotiate tight curves, further loss of ground results from

overcutting due to curvature of the alignment.

The loss of ground which occurs upon erection of the tunnel lining results because the tunnel lining usually insufficiently replaces the cross-sectional area of the tail of the shield. This component of loss of ground may be zero if an expanded lining is used. Tunnel liners are frequently required to be erected under the protection of a shield tail with certain clearance. As the shield moves forward, the change in stress-state induced in the clay by the excavation causes the ground to squeeze into the void left by the combination of the thickness of the tail skin and the clearance. Peck (1969) indicated that frictional forces between the skin of the shield and the surrounding soil can develop longitudinal tensile stresses in the clay which may tend to cause failure and plastic flow of the clay into the annular space as soon as the tailpiece clears the lining. While articulate shields require thin tail skins and relatively small clearances, the size of this void remains a significant factor contributing to the overall settlement. Some reduction in ground subsidence has been obtained by backfilling the void with grout upon advance of the shield and thereby decreasing possible ground loss. The effectiveness of grouting however depends on the rate of soil movement into the void.

Once the soil comes into contact with the tunnel lining, the lining will deflect under the applied loading. It has been observed that the crown of the tunnel usually will compress under this loading.

while the springline will expand (Ward, 1969; Peck et al., 1972).

This may be considered directly by using the lining flexibility in the analysis or alternatively, if a rigid lining is used in the analysis, the deflected shape may be represented as an additional component of lost ground; however, for most cases, the magnitude of this component will not be as significant as the other sources described.

The components of loss of ground discussed above may be represented quantitatively by introducing a gap parameter. The gap parameter is a measure of the volume of ground lost into the tunnel. The definition is illustrated in Figure 3.1. As the tunnel face advances, the soil mass in front will move towards the face. A typical soil element C', originally at some distance above the crown will move predominantly downwards to C as shown. This component of radial deformation generally includes both elastic and plastic deformation ($u_{e,p}^*$) due to relief of insitu stresses, and represents the three-dimensional movement ahead and at the face. It is determined assuming the machine is advanced in perfect alignment. If the machine is pitched upward or downward, additional material will have to be excavated or displaced. This quantity is related to workmanship and is denoted by w . The soil will move into the geometric clearance between the outer skin of the shield and the lining until it comes into contact with the lining. Thus, the physical gap is composed of the thickness of the tailpiece (Δ) and the clearance required for erection

of the lining (δ). It follows, therefore, that the total gap (G) may be expressed as

$$G = 2\Delta + \delta + U \quad (3.1)$$

where $U = u_{e,p}^* + \omega$

It may be seen that the physical gap is readily determined once a machine and lining system are chosen. The three-dimensional elastoplastic deformation, $u_{e,p}^*$ at the face may be computed from plane strain solutions by applying a correction factor as described in the following sections. The term ω which takes into account the quality of workmanship is a factor for engineering judgement and may be related to local experience, or to empirical correlations derived from case histories.

3.3 SOLUTIONS FOR RADIAL DISPLACEMENTS AT THE CROWN

3.3.1 Elastic Solution

For the case of a deep tunnel in strong soils, the radial crown displacement u_i may be adequately given by the elastic solution of a circular opening in elastic infinite medium due to the relief of initial stresses:

$$u_i = \frac{1+\nu}{2E} a p_z [(1+K_0) + (1-K_0)(3-4\nu)] \quad (3.2a)$$

where ν, E = Poisson's ratio and elastic modulus
 a = radius of the excavated opening

p_z = total vertical stress at the springline level

K_0 = ratio of initial total lateral to vertical stress.

For the undrained condition, $\nu = 0.5$, the crown displacement is independent of K_0 and equation 3.2a reduces to

$$u_i = \frac{1+\nu}{E_u} a p_z \quad (3.2b)$$

It may be noted that Mindlin (1948) has shown that for $H/a = 3$, where H is the depth of the tunnel at the springline level, the stress conditions surrounding the opening approach those for "deep" tunnels and equations 3.2a and 3.2b are applicable.

Similarly, the radial displacement, u_r , at any radius r (i.e., settlement above the crown) is given by

$$\frac{u_r}{a} = \frac{1+\nu}{2E} p_z \frac{a}{r} [(3-K_0) + (K_0-1)\frac{a^2}{r^2}] \quad (3.3)$$

It may be noted that the term $(3-K_0)$ within the bracket dominates. For the range of K_0 commonly encountered in clays, no great accuracy is required for the value of K_0 for calculating radial displacements.

3.3.2 Undrained Analysis of Stresses and Displacements in the Plastic Region Around the Tunnel

For soft clays, a plastic zone invariably occurs as a result of stress redistribution due to relief of the initial stresses at the circumference of the excavation. It is difficult to obtain an

explicit solution for the stresses and displacement under general initial stress condition, however an approximate solution for hydrostatic initial stresses ($K_0=1$) may be developed based on De Beer and Buttien (1966) and Ladanyi (1974).

The geometry of the problem is defined in Figure 3.2. Consider a circular opening being excavated in an infinite medium subjected to isotropic initial stresses $p_0 (= p_z)$. The excavation removes the boundary stresses around the circumference and the process may be simulated by gradually reducing an internal (support) pressure p_i . The initial excavated radius is a . As p_i is reduced, a plastic zone is formed, the radial displacement u_i occurs and the radius is now r_i . At the interface of the elastic and the plastic zone, a displacement from the elastic zone u_{ee} occurs and the radius of the plastic zone is reduced to the current value of r_e from r_{e0} . The results of the solution yield the following equations of engineering interest:

(a) Critical pressure. The critical pressure, $p_{i,cr}$, is the internal pressure below which plastic flow around the tunnel will occur.

$$p_{i,cr} = p_0 - C_u \quad (3.4a)$$

$$\text{or } p_{i,cr} = \gamma H - C_u$$

where γ is the total unit weight of the clay, H is the depth of the tunnel axis and C_u the undrained shear strength of the clay.

In terms of the stability number $N = \gamma H / C_u$ (Broms and Bennermark,

1967; Peck, 1969), equation 3.4a may be written as

$$\frac{p_{i,cr}}{p_0} = \frac{N-1}{N} \quad (3.4b)$$

Within the framework of assumptions made, for a tunnel at a given depth, the transition from elastic to elasto-plastic state is governed by a single soil parameter C_u (or N). The critical pressure may be decreased (i.e., condition made more favourable) by using air pressure, which may be treated as an internal pressure p_i , so that

$$p_{i,cr} = p_0 - p_i - C_u$$

(b) Radius of plastic zone. The radius r_e of the plastic zone is given by

$$\frac{r_e}{r_i} = \exp\left(\frac{p_0 - p_i - C_u}{2C_u}\right) \quad (3.5)$$

The current radius of the opening r_i is the cut radius a minus the radial displacement u_i . For small values of u_i , r_i may be approximated by a .

(c) Radial displacement u_i . The radial displacement in the elasto-plastic state is given by

$$\frac{u_i}{a} = 1 - \left\{ \frac{1}{1 + \frac{2(1+\nu_u)C_u}{E_u} \left(\frac{r_e}{r_i}\right)^2} \right\}^{1/2} \quad (3.6)$$

where r_e/r_i is given by equation 3.5.

The implications of equations 3.4 to 3.6 may be examined. The

critical pressure $p_{i,cr}$ and the plastic radius are plotted in Figure 3.3 against the stability N , for the case of $p_i=0$. This condition represents the extreme condition where a tunnel is excavated unsupported to the plane strain condition, without air pressure or support reaction pressure from the lining. It may be seen that both critical pressure and the plastic radius increase with the stability number N . If the soil were to remain in the elastic state, N would have to be 1 or smaller. In other words, some plastic zone around the tunnel will develop in most practical situations (see values of N in Table 3.1). Peck (1969) suggested that tunnelling may be carried out without unusual difficulty (no air pressure), if N is less than 5. The undrained shear strengths used in obtaining this value correspond to those determined on specimens from conventional tube sampling. It is known, however, that sampling disturbance may reduce the strength by a factor of 0.5 to 0.7 (see eg. Lo (1973)). Thus, the actual N value lies in the range of 2.5 to 3.5. Taking a typical value of $N=3$, the corresponding plastic radius is about 3 times the radius of the tunnel. It appears, therefore, that experience suggests that a confined plastic zone of radius approximately $3a$ may be tolerated in tunnelling in soft ground.

The plane strain radial displacements are plotted against the stability number for three values of the modulus ratio E_u/C_u commonly encountered in clays in Figure 3.4. It may be seen that deformation increases rapidly as N exceeds a value of about 3. This increase in rate of displacement is due to an increase in the extent of the plastic

zone. It may also be noted that the displacement is rather sensitive to E_u/C_u , implying that a reliable value of the modulus ratio must be obtained to predict the radial displacement.

3.4 PROCEDURE FOR ESTIMATING THE CROWN DISPLACEMENT

The methods of analysis described in the preceding paragraphs are developed under idealized conditions. In applying these solutions to practical cases, each case must be carefully considered to evaluate whether the fundamental assumptions are satisfied. The following comments may be helpful in using these methods in tunnelling projects in clays:

(a) An initial estimate of the crown displacement, u_i , is obtained from the plane strain solution. If $N \leq 1$, the soil mass around the opening remains in the elastic state and the crown displacement is given by equation 3.2a. If $N > 1$, plastic zones will develop around the tunnel and the plane strain crown displacement will be given by equation 3.6.

(b) Plane strain conditions will be satisfied when the physical gap is larger than the crown displacement calculated in (a) above. Thus the crown displacement $u_c = u_i$ if $u_i \leq 2\Delta + \delta + \omega$.

(c) If the physical gap is small and support follows closely behind the tail of the shield, or an expanded lining is used, the plane strain condition cannot develop and the crown displacement will be largely

restricted to the three-dimensional movement at the tunnel face. Lo et al. (1984) have shown that for an elastic medium, the three-dimensional radial displacement is approximately 1/3 of the calculated plane strain displacement. The author is not aware of any similar solution for the elasto-plastic case, but the gradual development of plastic zone suggests that the factor 1/3 may be approximately correct, at least for small radii of plastic zone, i.e., $u_{e,p}^* = u_i/3$.

In this case, the crown displacement u_c is given by

$$u_c = G = 2\Delta + \delta + \omega + u_i/3 \quad \text{if } u_i > G$$

(d) Three-dimensional movement ahead of the face can be virtually eliminated by the use of appropriate construction technique (eg. appropriate use of an earth pressure balance machine). In this case, $u_{e,p}^* = 0$ and the crown displacement u_c is given by $u_c = G = 2\Delta + \delta + \omega$ where $u_i > G$.

(e) The effectiveness of grouting the tailpiece void depends upon the rate of soil movement into the void. In most cases, the grout is injected after soil movements have occurred and is ineffective. However, if special care is taken to ensure that the grout is injected before movements occur (eg. by maintaining compressed air pressure until grouting of the void is achieved) then the gap will be reduced. This reduction in gap may be incorporated in the workmanship term ω . Thus with good workmanship and effective grouting, ω may be negative. (For example; in the BART case to be discussed subsequently,

$\omega = -45$ mm.)

(f) Ideally, the undrained shear strength and modulus should be determined in triaxial tests following the stress path of the soil surrounding the tunnel during excavation. However, for the approximate analysis described herein, it is adequate to employ vane strength for soft clays and anisotropically consolidated-undrained triaxial tests, on good quality samples, for the determination of modulus. If conventional tube samples are used, a correction for sample disturbance must be applied.

(g) To obtain the gap G in equation 3.1, it is implicitly assumed that only radial displacement at the crown occurs and invert displacement is suppressed by the weight of the excavation system.

In the following sections, the validity of the theoretical model will firstly be assessed by comparing the calculated and measured crown displacements in several comprehensive case histories. A study of additional, though less complete, case records will then be made to arrive at a semi-theoretical method of estimating the ground surface settlements.

3.5 COMPARISON BETWEEN CALCULATED AND MEASURED CROWN DISPLACEMENTS

Five cases of tunnelling in clays are available in which settlement measurements at different radii above the crown have been performed so that the crown displacement may be reasonably extrapolated.

Fortunately, these records encompass very stiff to soft clays so that a range of tunnelling in clays of vastly different strength and deformation properties may be examined. The crown displacements of the tunnels would therefore range from elastic behaviour to predominantly plastic behaviour. In the following sections, each case record will be examined individually and the results then will be synthesized.

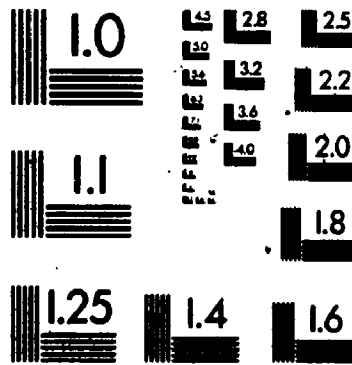
3.5.1 Mississauga Sewer Tunnel (DeLory et al. (1979))

A sewer tunnel 4.27 m in bored diameter, 3.05 m in finished inside diameter, and nearly 4.8 km in length was constructed in Mississauga, Ontario. It was excavated through very dense sand-clay till. The depth to axis level at the instrumented section was 13.1 m.

The excavation was advanced by a full face 'Alpine miner' mounted in the shield. The undercutting method was used. A slightly under-sized diameter hole was mined 0.6 m ahead of the shield and then it was advanced by shaving off a layer of soil. A temporary lining consisting of steel rings and concrete planks was assembled inside the shield. As the lining emerged from the shield, it rested on the tunnel floor leaving a physical gap of 100 mm at the crown. Pea gravel was injected 12 to 18 m behind the face and grouting was pumped in several weeks later. From these procedures and construction schedule it is clear that the plane strain condition is satisfied in this case.

The dense till was overconsolidated with liquid limit of 22%,

2



plastic limit of 15% and water contents varying from 7% to 10%. The undrained shear strength determined from unconfined compression tests on specimens trimmed from large chunks of soil from the tunnel face was 360 kPa. The unit weight was 23.9 kN/m^3 .

Based on results of unconsolidated-undrained triaxial tests and pressuremeter tests, a careful evaluation of the elastic modulus was carried out by DeLory et al. (1979) who suggested that E_u is most probably 170 MPa, with 70 MPa as a lower limit. These values are used to calculate the range of crown displacement.

The stability number N is 0.86. Since N is below unity, the deformation around the tunnel is elastic according to the analysis described in the previous sections. In the field, it was observed that the till face remained self-supporting for more than a week and no load was transmitted to the temporary lining. Both of these observations confirmed that the ground behaviour was elastic. The calculated crown displacements are 6 mm ($E_u = 170 \text{ MPa}$) and 14 mm ($E_u = 70 \text{ MPa}$) giving values of u_c/a of 0.28% and 0.67% respectively.

The distribution of measured settlement at different depths above the crown is shown in Figure 3.5. The cross-hatched area represents possible range of extrapolated values of settlement. The crown settlement may range from 7.5 mm to 12 mm, giving values of u_c/a between 0.35% to 0.56%. The possible range of measured crown settlement therefore falls within the range of calculated settlement and

the agreement is reasonable.

Using the elastic solution (equation 3.3) and a modulus value of 100 MPa, the theoretical distribution of settlement above the crown is computed and shown in Figure 3.5. It may be seen that this theoretical distribution of settlement agrees well with field data. The value of $E_u = 100$ MPa may therefore be considered representative. The corresponding E_u/C_u ratio is 280.

Surface settlement readings were reported to be erratic and small, ranging from 0 to 3 mm. These results are, however, consistent with the measurements at depth and the elastic behaviour of the soil mass. The ratio of surface settlement, S_s , to the crown displacement, u_c , is therefore between 0 to 0.21, with a probable value of S_s/u_c of 0.15. (In this case, the soil remains elastic and the gap exceeds the plane strain displacement. This case corresponds to condition (b) in the previous section.)

3.5.2 Green Park Underground (Attewell and Farmer (1974))

The Green Park Underground Tunnel was shield driven in stiff, heavily overconsolidated London clay. The shield was 3.348 m long and 4.146 m in diameter, the depth to tunnel axis level was 29.3 m.

The tunnel was mined by hand excavation. The upper part of the face was excavated 0.6 m ahead of the shield and was "boxed-in". The shield was then jacked forward and the lower part subsequently

excavated. The lining was a seven-segment bolted cast-iron lining, 4.070 m external diameter and 0.6 m in width erected inside the shield tail.

Grout was injected into the space between the cut clay surface and the lining ring when there was a 1.2 m unsupported length of tunnel between the rear of the tail and the last grouted portion. Grout injection progressed from bottom upwards at low pressures. Attewell and Farmer (1974) found that the settlement rate near the crown was of the order of 0.33 mm/hr. The average rate of advance of the shield was 0.13 m/hr. Thus, it is clear that grout could be injected into the void without difficulty and that the grouting should have been effective.

The maximum physical gap is equal to the size of the bead (6.5 mm) plus the tail void (76 mm) i.e., 82.5 mm. Grouting at the tail would have filled the tail void, however, the movement of soil into the space created by the bead would have already occurred and so the physical gap approximately corresponds to the size of the bead (i.e., 6.5 mm).

The properties of the clay are shown in Figure 3.6. The undrained shear strength obtained from unconsolidated undrained (UU) triaxial tests on tube samples at the axis level is 266 kPa which is consistent with the quoted stability number N of 2.2. The elastic modulus of the clay was not reported but this may be assumed to be

200 times C_u . This E_u/C_u ratio is obtained from UU tests on block samples from a shaft in London clay at Ashford Common at approximately the same depth (Ward et al., 1965). The Atterberg limits for London clay at Ashford Common, Green Park and Regents Park are shown in Table 3.2; it may be seen that the index properties of the clays at these locations are similar. Reasonable accuracy should be obtained using the extrapolated soil data from Ashford Common.

Using these geometric and soil parameters, the unrestricted plane strain elasto-plastic displacement at the crown is computed to be 49 mm. From the construction method described, and the effective grouting procedure adopted, it is clear that plane strain deformation could not have been realized in this case and the displacement is restricted mainly to the three-dimensional movement at the face. Applying a correction factor of 1/3 to the plane strain deformation and including the physical gap of 6.5 mm, the calculated crown displacement is 23 mm giving a value of u_c/a of 1.1%.

Vertical settlements above the crown were measured at boreholes Y1 and Z1, and the results are shown in Figure 3.6. If the data at Z1 is extrapolated to crown level, a possible range of crown displacements of 23 to 28 mm would be obtained. (It is believed that measurements at Z1 are more representative because Y1 may be affected by a 5-day tunnel stoppage within 1 m of the face.) The extrapolated u_c/a measured ranged between 1.12% to 1.37% which is in close agreement with the calculated u_c/a of 1.1%. The surface settlement measured was 6.1 mm. The settlement ratio, S_s/u_c , is 0.27.

3.5.3 Regents Park (Barratt and Tyler (1976))

Two tunnels, 4.146 m in cut diameter were constructed with expanded concrete linings at depths of 34.1 m and 20.1 m at Regents Park as part of the Fleet Line of the London Underground. The cross-sections of the tunnels are shown in Figure 3.7. The ratio of vertical distance between tunnel axes to radius was 7 while the ratio of horizontal distance between tunnel axes to radius was 9. Since the plastic radius is computed to be within one diameter of the tunnels, the behaviour of the twin tunnels may be treated as two individual tunnels. It may be noted that the southbound tunnel was excavated first so that the results of analysis for this tunnel will not be affected irrespective of the assumption made above.

Both tunnels were hand driven with the aid of a shield similar to that used at Green Park having a 3 mm bead. The concrete lining was expanded against the ground immediately after erection. The fast rate of erection reduced ground loss and settlement. In this case, the tail void space was small and the physical gap is governed only by the size of the overcutter on the shield.

The index properties of the London clay at Regents Park have been shown in Table 3.2, and they are similar to those of London clay in other localities. The value of C_u at 20 m (the depth of the axis of the northbound, second tunnel) obtained from unconsolidated undrained triaxial test was 230 kPa. This is consistent with the stability number N of 1.7 used by Ward and Pender (1981). At 34 m (the depth

of the axis of the southbound, first tunnel) the C_u value was not given. The undrained strength C_u calculated from the stability number N quoted by Ward and Pender (1981) is 230 kPa. This value appears to be too low since there is evidence that the C_u value from the borehole increases with depth (Figure 6 in Barratt and Tyler, 1976). The undrained strength of London clay at Ashford Common (Ward et al., 1965) and Chelsea (Marsland, 1973) also shows increase with depth. The extrapolated value of C_u is 280 kPa, giving a revised, more probable stability number of 2.4. The value of E_u/C_u is taken to be 140 and 200 respectively at depths of 20 m and 34 m based on the results from Ashford Common (Ward et al., 1965).

3.5.3.1 Southbound Tunnel

The vertical settlement along the centreline of the tunnel is plotted in Figure 3.8. Since the closest magnetic ring for settlement measurement was 4.5 m above the crown, a rather wide range of possible extrapolated crown displacement may be obtained (17 to 30 mm) giving u_c/a of 0.82% to 1.5%. Assuming that the expanded concrete lining reduced the tail void to zero and the construction method limited the displacements to those occurring at the tunnel face plus the size of bead, the calculated crown displacement is 23 mm, giving a u_c/a value of 1.1%. This value falls within the range of the extrapolated observed value. The settlements recorded two months after construction of the tunnel were essentially identical to the 'immediate' settlements suggesting the effect of consolidation is

minimal. (This behaviour was also observed in the Northbound tunnel.) The surface settlement is 5.5 mm, the settlement ratio (S_s/u_c) is 0.24.

3.5.3.2 Northbound Tunnel

The distribution of measured settlement above the crown is shown in Figure 3.8. The closest measurement near the crown was 2 m above the crown and the crown displacement may therefore be extrapolated with reasonable accuracy to a value of 23 mm, or u_c/a of 1.1%. The calculated elasto-plastic radial displacement at the crown, taking into account the three-dimensional effect at the face and bead size, is 17 mm giving u_c/a of 0.8%. The settlement at the surface was reported to be 7 mm so that the S_s/u_c ratio is 0.40.

3.5.4 Thunder Bay Tunnel (Belshaw and Palmer (1978), Palmer and Belshaw (1980) and Lo and Rowe (1982))

A 3.3 km sanitary trunk sewer in the city of Thunder Bay, Ontario was constructed through soft clay using a Lovat tunnel boring machine together with a segmented precast concrete tunnel lining. Since this construction technique was being used for the first time in North America, an extensive field instrumentation program was undertaken. Two arrays of instrumentation, referred to as Array 1 and Array 2 were installed.

The mined diameter of the tunnel is 2.47 m and the depth to the

tunnel axis is 10.7 m at array 1, giving an H/a ratio of 8.66. (The depth to axis in Array 2 is 10.5 m, practically the same as in Array 1.)

The detailed description of the tunnelling procedure has been given (Morton et al., 1977). A full-face tunnelling machine was used in the excavation and the tunnel was supported by an unbolted, pre-cast, segmented concrete lining. A maximum progress rate of 29 m per 8 hour shift was achieved with this tunnelling system. The lining was assembled in the tailpiece and the machine advanced by thrusting on the completed lining. Since the mined diameter is 2.47 m while the outside diameter of the completed lining is 2.38 m, a physical gap of 90 mm was left between the concrete rings and the excavated surface. During the advance, a clay grout was injected into the tail void, however, the grouting was reported to be ineffective. This is to be expected since the rate of plastic deformation in soft clay is usually very rapid. Without any internal support pressure, the remolded clay soil will fill the gap as soon as the lining leaves the shield tail.

Arrays 1 and 2 are about 1.25 km apart, but the stratigraphy is similar. The stratigraphy and soil properties are shown in Figure 3.9. The tunnel is located in a soft grey silty clay deposit which underlies postglacial fluvial deposits of loose sand and silty sand. Beneath the invert of the tunnel is a layer of varved clay which extends to shale bedrock.

The grey silty clay is slightly overconsolidated with a sensitivity of about 6 from field vane tests. The average water content w_n is 56%, while the liquid limit and the plastic limit are 65% to 75% and 20% to 25% respectively. The shear strength, as determined from Geonor vane tests increases with depth with a $C_u/\Delta p$ ratio of about 0.3. The vane strength varied from 25 to 50 kPa and is 35 kPa at the axis level. The stability number of the tunnel is 5.5. The undrained modulus of deformation E_u determined from anisotropically consolidated undrained triaxial tests on specimens trimmed from 152 mm diameter specimens is 13 MPa, and the corresponding ratio of E_u/C_u is 370.

Results of deformation measurements have been presented (Palmer and Belshaw, 1980; Belshaw and Palmer, 1978). Only the short term centreline settlement observed at the end of construction of the arrays is of interest in this discussion.

The vertical settlements measured by magnetic extensometer installed in boreholes along the tunnel alignment in Array 1 and Array 2 are shown in Figure 3.10. The crown settlement, extrapolated from the field displacements with depth may vary between 110 mm and 150 mm. The corresponding dimensionless crown settlements u_1/a are 8.9% and 12.2% respectively.

In calculating the crown displacement for this particular case, two factors need to be considered. Firstly, during advance the

tunnelling machine is almost closed-face and the remolded clay entered the face as a thick slurry through four hydraulically-controlled ports which were kept very narrow. Thus, a hydrostatic pressure from the slurry is created at the tunnel face and this virtual pressure, assumed to be 20 kPa, is taken into account in the calculation. The unconstrained displacement computed is 197 mm. The physical gap was 90 mm, however the reported pitching and yawing of the TBM was likely to result in a gap parameter which was considerably larger. The first assumption that may be made is that the geometric constraint is sufficiently large for the plane strain deformation to occur and this gives u_1/a of 16%. One possible condition is that three-dimensional deformation occurs at the face, with the residual deformation limited by the physical gap. This latter assumption gives u_1/a of 12.6%. (For comparison, the gap parameter associated with closure of the physical gap alone is 90 mm; and the ratio of u_1/a would be 7.3%.) It may be seen that these calculated values do not vary too widely from the extrapolated measured values.

The ground surface settlements vary from 49 to 54 mm giving settlement ratio S_s/u_c between 0.31 to 0.35.

3.5.5 Summary of Observations on Detailed Case Histories

Some remarks on the term ω related to workmanship may be made in the case histories analyzed. In the case of the Mississauga Tunnel, where the physical gap is large compared to the plane strain crown displacement and the soil remains elastic, ω does not play any role. In the case of the tunnel at Green Park, the effective grouting procedure adopted essentially eliminates the tailpiece void so that, in effect, $\omega = -76$ mm. For the two tunnels at Regents Park, the use of the

expanded lining, erected rapidly compared to the rate of soil displacement, yields virtually zero tailpiece void and the physical gap consists of only the bead thickness. For the Thunder Bay Tunnel in soft clay, steering of the shield may lead to variations in pitch and dive such that additional displacement over the crown may occur. Since grouting was also ineffective, the value of ω in this case is positive, and may vary from zero to as large as 41 mm. Clearly, the term is particularly significant in tunnelling in soft clays.

The measured and calculated crown displacements for the five case records are plotted against the stability number N in Figure 3.11. Considering the simplifications that have to be made regarding the construction procedure and schedule, the agreement between calculated and measured displacement is considered to be quite encouraging. Both the measured and calculated displacements show a trend for the crown displacement increasing logarithmically with N . This is consistent with the results of the theoretical analysis.

It appears, therefore, that the proposed approximate method yields results consistent with field measurements and may be used for estimating the gap parameter. It remains to be shown that the maximum surface settlement is predominantly controlled by the gap parameter.

3.6 ADDITIONAL CASE RECORDS

Five case records of tunnelling in clays have been analyzed in

the previous section where comparison between measured and calculated crown displacement have been made. Additional case histories in which the field measurements are less extensive and soil information has sometimes to be extrapolated, but reasonable interpretation can be made, are dealt with in this section. The procedure is to calculate the gap parameter from an evaluation of the construction method and geometry and soil properties so that the gap may be related to the measured surface settlements.

3.6.1 Ottawa Outfall Sewer Tunnel (Eden and Bozozuk (1969))

The tunnel passed through extremely sensitive, moderately over-consolidated Leda clay in Ottawa. The tunnel axis was at a depth of 18.3 m. The outside diameter of the tunnel was 3.04 m and the inside diameter was 2.44 m.

The tunnel was driven by a rotary tunnelling machine and was lined immediately with corrugated segmental steel liner rings. This temporary liner ring consisted of eight segments, the top segment was first placed. Good contact with the clay was ensured by jacking the bottom liner against the neighbouring segments. When necessary, grout was pumped into any space between the clay and the liner. However, it was reported that in general, the liner was in close contact with the surrounding clay and little grouting was required. Thus it is reasonable to assume that the 'physical gap' is small. An air pressure of about 29 kPa was maintained in the tunnel during excavation.

The soil conditions in the clay section of the tunnel are uniform and the stratigraphy and soil properties are shown in Figure 3.12. The liquid limit and plastic limit of the clay are respectively 34% and 23%, with water content of about 47%. The shear strength increase with depth and the average, ~~vane~~ strength of the clay at the tunnel level is 90 kPa (Eden, 1970). The stability number M considering the effect of the air pressure is 3.2. Sensitivity of the clay is very high, in the order of 600, but the undisturbed clay behaved as a stiff brittle material during excavation. The E_u/C_u ratio of a similar sensitive clay determined from unconsolidated-undrained tests on specimens trimmed from block samples at Heron Road is 300 (Law, 1975). The centreline settlement was 6 mm but no measurements of settlement at depths were made. The calculated plane strain elasto-plastic crown displacement is 64 mm. Since the liner was immediately placed and jacked against the excavated surface, the inward 'squeeze' towards the tunnel was restricted. The actual ground movement above the crown would therefore be restricted to three-dimensional movement at the face of 21 mm. The settlement ratio (S_s/u_c) is therefore 0.28.

3.6.2 Mexico City Siphon Tunnel (Tinajero and Vieitez (1971))

A sewer tunnel with an excavated diameter of 2.95 m located at a depth of 11.7 m ($H/a = 7.9$) was constructed in the soft, highly compressible clay in Mexico City.

The tunnel was constructed using a 2.95 m diameter shield equipped with a rotating full-face excavator. The oscillating cutters took up 1/3 of the area of the face. The front of the tunnelling shield was inclined at 25° with respect to the vertical so as to provide a hood which was designed to allow easier maneuverability within the soft deposit.

The tunnel lining consisted of steel segments 6 mm thick with 5 cm flange reinforcement as a primary support, followed by a concrete secondary lining that was cast after the excavation was completed. The diameter of the primary lining was approximately equal to 2.82 m and was installed within the protective shield. A sand-cement grout was injected 8 m behind the shield at a pressure approximately equal to the overburden pressure. The degree of success of the grouting technique was not mentioned, but it may be noted that grouting is seldom effective in soft clays.

The Mexico City clay is very compressible, having a high montmorillonite content, a water content close to 300% and a plasticity index as high as 400 (Tinajero and Vieitez, 1971). On the basis of published data relating to Mexico City clay (Marsal, 1957; Mesri et al., 1975; Lo, 1962; Alberro and Santoyo, 1973) it would appear that the soil is slightly overconsolidated with a typical overconsolidation ratio of 1.3, an undrained shear strength of 35 kPa, an undrained Young's modulus of 4 MPa. The stability number N is therefore 5.

Observations of the vertical settlement as a function of time

indicated an initial heave prior to passing of the shield. Upon passage of the shield the majority of the deep movement that was recorded above the tunnel centreline was observed to occur within ten days, however a significant rate of vertical movement continued both near the tunnel crown and at the ground surface 28 days after tunnel construction.

The calculated unrestricted plane strain displacement at the crown is 530 mm, which is greater than the physical gap of 130 mm. Therefore, the gap parameter is composed of the movement at the face and the physical gap, i.e., 307 mm. The undrained surface settlement observed was 105 mm. The settlement ratio (S_s/u_c) is therefore 0.34.

3.6.3 Grangemouth Sewer Tunnel (Henry (1974))

The tunnel was constructed as part of the Grangemouth Town Council's drainage modernization project. It is 1.60 km in length and one section was mined in soft to very soft brown laminated silty clay.

The mined diameter of the tunnel varied because a number of shield sizes were used. Since the finished diameter was between 2.44 m to 1.99 m and the insitu concrete lining had a minimum thickness of 125 mm, the minimum mined radius would be about 1.3 m. The depth to axis level was about 10 m, giving a H/a ratio of 7.7.

The tunnel was handmined with the protection of a shield. Compressed air of at least 62 kPa was employed to increase the stability of the excavation. The tunnel support was cast-in-place concrete lining over ribs of precast tunnel rings. Bentonite grout was also used during tunnelling. Since specific details regarding the tail void thickness and the effectiveness of the grouting were not given, the size of the physical gap is unknown.

The subsoil in the area is, in general, a silty clay of low shear strength. Typical field shear vane tests performed in boreholes along the tunnel route showed that $C_u = 22$ kPa at about the axis level. The undrained deformation modulus E_u was not reported and its value may only be assumed. Due to the very soft nature of the silty clay, E_u/C_u ratio of 500 is adopted. The initial stability number of the tunnel was 8.2, with the application of air pressure of 62 kPa, the ratio $N = (P_o - P_i)/C_u$ was reduced to 5.4.

Ground surface settlements started in front of the shield and up to 25 mm of settlements were measured above the compressed air tunnel. The gap parameter, calculated from the above available soil and tunnelling information may vary from 75 mm to 226 mm. The 226 mm displacement is the calculated plane strain settlement; however, settlements behind the shield were likely to be limited by the lining support and grouting. It is anticipated that the gap parameter should be close to the three-dimensional settlement of 75 mm. Thus the representative settlement ratio S_s/u_c would be 0.33.

3.6.4 BART (Market Street) (Kuesel (1972,1969))

The ~~first~~ tunnel at Market Street which forms part of the Bay Area Rapid Transit (BART) system in San Francisco is dealt with in this section.

The Market Street tunnel was constructed by a 5.65 m diameter closed face shield. The tunnel axis is located at 19 m below the surface ($H/a = 6.7$).

The machine had narrow slots or doors through which the soil was brought in as it was scraped from the tunnel face; care was also taken to ensure that the machine advance was kept equal to the volume of excavated soil. These measures permitted the face to be firmly supported. In addition, compressed air at 83 kPa was being used which reduced the value of stability number N from about 6 to 4.6. The tunnel was lined with a bolted, segmental lining with an outside diameter of 5.49 m. Advancing the shield left an annular void of approximately 160 mm and special attention was given to filling the tail void as promptly and fully as possible. Two optional methods for filling the tail void were specified: either ring by ring grouting or a two-shot process by injecting pea gravel immediately behind the shield, with grouting following within 45 m behind the heading. The grouting details were left to the contractor's discretion but both methods were used successfully.

The section of the Lower Market Street tunnel under construction

was excavated in San Francisco Bay Mud. The Bay mud is a soft, plastic, normally consolidated clay. The clay deposit, about 33 m thick, is underlain by a layer of dense sand and about 30 m of firm silt and clay. Bedrock is found at a depth of 70 m.

The settlement due to tunnelling was reported to be generally less than 50 mm and often less than 25 mm. The generally small magnitude of settlement was attributed to the good tunnelling technique employed. The surface settlement observations (Kuesel, 1972) indicated that the maximum subsidence due to the first tunnel was 36 mm. The trough was observed to spread to a lateral distance of 18 m on either side of the tunnel centreline, giving an average slope of the final trough of approximately 1:500. Subsurface horizontal movement measured by a slope indicator installed midway between the two tunnels showed that soil was heaved away from the tunnel as the face approached; but the ground moved in towards the tunnel, filling the tail void as soon as the heading had passed.

Since the three-dimensional movement ahead of the face could not have developed in this case due to the construction method, the crown settlement should equal the size of the tail void (160 mm). Thus, the initial estimate of S_s/u_c ratio would be 0.23. However, the tail void or the physical gap was in fact reduced by grouting. According to results of recent analyses reported (Lo and Rowe, 1982; Rowe and Kack, 1983), a gap of 115 mm is required in a finite element analysis to obtain the correct settlement of 36 mm. This implies a

value of w of -45 mm. Thus, the S_s/u_c ratio should be 0.31 instead of 0.23.

3.6.5. Tyneside Tunnel (Attewell and Farmer (1975))

The tunnel is shield driven. The external shield diameter is 2.02 m while the depth to axis is 7.5 m. The H/a ratio is 7.43.

The length of the shield is 2.86 m and it has a thick continuous bead around the hood of the shield of 10 mm. The average rate of advance is 0.18 m/hr.

The clay is laminated, the unit weight is 19.2 kN/m^3 , the undrained strength is 75 kPa and the stability number is 2. The E_u/C_u ratio may be assumed to be 200.

The physical gap at the crown was not reported. For the calculations of the crown displacement, therefore, two bracketing assumptions may be made: either the physical gap will be assumed to be zero so that all movements will be restricted to the face loss, or the gap sufficiently large to accommodate the unrestricted plane strain deformation. The first assumption yields a gap parameter of 16 mm while the second assumption gives a value of 19 mm. It may be seen that, for this particular case, the calculated gap is not unduly sensitive to the assumptions made.

The surface settlement was reported to be 7.9 mm. The settlement ratio (S_s/u_c) therefore lies between 0.41 to 0.48.

3.6.6 Heathrow Cargo Tunnel (Muir Wood (1969), Muir Wood and Gibbs (1971))

The Heathrow Cargo Tunnel is a two lane highway tunnel linking the Central Area of Heathrow Airport, London, to the new Cargo Terminal Area.

The Heathrow Cargo Tunnel is 10.9 m in diameter and it is shield driven. The crown is generally 7 m to 8 m below the ground surface, giving a small cover to diameter ratio of only 0.6. H/a being 2.34.

In order to limit the settlement of the runways above the tunnel, the shield was designed to provide support to the face and it was equipped with platform rams and face rams. The excavated face was supported by these rams while the tunnel was used as the primary lining. These rings of lining were assembled before the shield was shoved forward and were expanded immediately so that roof support was always provided. A bead of 3 mm at the leading edge of the hood facilitated the steering of the shield.

The Heathrow Tunnel is located in London Clay. Above the London Clay are deposits of gravel about 3 to 5 m in thickness. The extent of weathering at the top of the clay was confined to the upper 0.3 to 0.6 m. The index properties of the London Clay at this location are similar to those in other locations as described earlier. The undrained shear strength increases with depth from a minimum of 72 kPa to 275 kPa. Adopting the $\Delta C_u/\Delta z$ value of 10 kPa/m at Chelsea

(Marsland, 1973), the C_u value at the axis level would be 165 kPa. It follows that the stability number is 1.5. The representative average Young's modulus chosen by Muir Wood is 27 MPa, giving a E_u/C_u ratio of 165.

The results of instrumentation indicated a centreline surface settlement of 11.4 mm. Generally, the pattern of movement occurred radially into the tunnel. The vertical movement of a point 1 m above the crown was only 14 mm and the extrapolated crown displacement is 17 mm. These are very modest subsurface movements considering the size of the excavation.

The calculation of the crown settlement is complicated by the existence of the gravel layer which lies only 2 m above the crown. The crown settlement, u_c , calculated with the properties of London Clay, and assuming a negligible physical gap because of the use of an expanded lining, is 30 mm. This certainly seems to be an overestimate and it shows that the gravels above the London Clay have a significant influence on settlement. The ratio of surface settlement to the extrapolated measured crown displacement is 0.67.

3.6.7 Buenos Aires Tunnel (Moretto (1969))

This tunnel was constructed using a digger shield under atmospheric pressure. The temporary support used was steel ribs with planks expanded against the soil. The cut radius of the tunnel was 2.35 m and the depth of the tunnel axis was 16.4 m, giving a H/a ratio

of 7. Along the length of the tunnel where surface settlements were recorded, the subsoil condition consists of 7 m of silty sand, followed by a soft clay overlying a firm clay. A dense sand stratum starts at about 18 m depth.

The face of the tunnel intersected the boundary between the soft clay and the firm clay. Along the instrumented sections, the portion of the face which the firm clay occupied varied from about half of the face to none. This variation in soil stratigraphy accounts for, at least in part, the range of surface settlements measured from 130 mm to 180 mm.

Detailed information is not available for the strength and deformation properties of the clays, but undrained shear strength may be estimated to be about 35 kPa, giving a stability number N of 8.6. This value appears to be consistent with the difficulties encountered during construction. The ratio of E_u/C_u may be taken as 800.

Using these soil parameters, the calculated gap is about 500 mm. Taking the average settlement as 150 mm, the ratio of S_s/u_c is 0.3.

3.6.8 Edmonton Rapid Transit Tunnel - 1st Tunnel (Eisenstein and Thomson (1978))

Two tunnels located entirely within the dense, jointed Edmonton till were built as part of the Edmonton Rapid Transit System. The tunnels were 6 m in diameter, with an average depth of 10.2 m to the springline. The surface settlement associated with the first tunnel

will be analyzed.

The tunnels were advanced by a fully-shielded mole. The cutting profile of the mole was 20 mm in excess of the shield diameter. Temporary support system of steel ribs and timber lagging was assembled inside the shield and it was expanded into place as soon as it left the tail. A second expansion was carried out during the expansion of the next rib. The procedure was designed to reduce ground loss.

Detailed site investigation results were not reported but the soil properties in the Central Edmonton locations had been reported (Dejong and Harris, 1971). The bulk unit weight is about 20 kN/m^3 and SPT N value is of the order of 100. On the average, the till is composed of 40% to 45% sand, 25% to 35% silt and 20% to 30% clay. The undrained shear strength of the till at the springline level is 190 kPa (Eisenstein, 1984). The stability number, computed with $C_u = 190 \text{ kPa}$ is 1.1, and at this low value the ground should remain nearly elastic. The undrained modulus E_u obtained from consolidated undrained tests at overburden pressure is 58 MPa. The E_u/C_u ratio is 305. It may be noted that the E_u/C_u ratio obtained for the Edmonton till is very close to the E_u/C_u ratio of Mississauga till, which is 280 (see Table 3.1).

The surface settlement adjacent to the Treasury Branch Building was monitored. The centreline surface settlement due to the first tunnel was not observed directly. From the observed settlement measured at the same cross-section and assuming that the settlement profile

followed the typical Gaussian distribution, the maximum settlement may be estimated to be 12 mm.

Eisenstein and Thomson (1978) observed that the construction technique could allow for a typical physical gap as high as 50 mm. The plane strain elasto-plastic crown displacement is computed to be 16 mm, which is smaller than the physical gap and could have occurred unrestricted. The ratio of surface to crown displacement is 0.75.

Due to the jointing and discontinuities of the till system, some local instability occurred and blocks were observed to fall from the face on a few occasions. Sand seams and pockets had also created difficulties in the tunnelling operations. The local loosened zone might have filled up the physical gap during construction activities. This local additional movement is considered to be confined to the proximity of the tunnel heading and did not significantly affect the overall displacement pattern.

3.7 RESULTS OF ANALYSES OF CASE RECORDS

A total of thirteen case histories of settlements due to tunnelling in clays has been analyzed in the preceding sections. The gap parameter for each case was calculated from the approximate methods of analysis developed using the undrained elastic modulus and undrained shear strength of the clay, together with an evaluation of the construction method and geometry of the support system. The

essential data for the case histories are summarized in Table 3.1.* It may be seen that the tunnels studied range in radius from 1 m to 5 m at depths varying from 7 m to 34 m. The H/a ratio, however, generally varies from 6 to 17 (with the exception of the Heathrow Tunnel) and therefore satisfies the geometric condition assumed in the analysis. The tunnels were located in clays covering a wide range of undrained shear strength from 22 kPa to 360 kPa.

The measured surface settlements at the centreline of the tunnel are plotted against the crown settlement in Figure 3.13. It may be seen that the surface settlement increases approximately linearly with crown settlement, yielding an equation $S_s = 0.33 u_c$. This relationship suggests that once the gap parameter is determined, the crown settlement can be estimated and the surface settlement can be predicted.

The above relationship also suggests that the gap, which implicitly takes into account the initial stresses, strength and deformation behaviour of the clay and construction method and constraint, is the single most important parameter in controlling surface settlement. A careful examination of Figure 3.13 shows this is approximately correct for soft clays probably because the ratio of H/a varied over small ranges in these case histories. For stiff clays, the values of S_s and u_c are small and the scatter is masked. Further consideration is therefore required.

* Table 3.1 deals with undrained settlements. A further discussion on the undrained and drained settlements and the development of settlement with time can be found in Appendix 2.

The ratio of measured surface settlement to the calculated crown settlement (using the gap parameter) S_s/u_c is plotted against H/a in Figure 3.14. It is evident that, for stiff clays, the ratio of S_s/u_c decreases with increasing H/a . However, for the surface settlement to approach zero, H/a will have to be very large in general.

3.8 CONCLUSION

The concept of loss of ground in tunnelling in clays, as originally developed by Peck (1969) is quantified by the introduction of a gap parameter. The gap is the sum of the three-dimensional elasto-plastic deformation at the face and the physical gap which is related to the machine, shield and lining geometry. Methods for calculating the elasto-plastic deformation are described and the physical gap is determinable once the machine-support system is chosen.

Using this approach, analyses of thirteen case histories involving tunnelling in clays of widely different strengths and geometries have been performed. This study showed that

(a) For five case histories where measurements of displacements at different distances above the crown are available, the calculated displacements agree reasonably well with measured displacements at the crown.

(b) For soft clays, the maximum surface settlement increases linearly with the gap giving an equation $S_s = 0.33 u_c$. (In these cases the

crown settlement is equal to the gap G .) The effect of the ratio depth to radius of the tunnel (H/a) on settlement appears to be insignificant for the range of cases examined.

(c) For stiff clays, the ratio of surface settlement to crown settlement decreases with increasing H/a . However, H/a has to be very large to reduce the settlement to zero unless the behaviour of the soil surrounding the tunnel is entirely elastic.

It is suggested that the procedure developed for predicting the gap and therefore the surface settlement may be used for preliminary design purposes, provided that the undrained shear strength and modulus of the clay are reliably determined. This gap can also be used in conjunction with more sophisticated numerical methods to predict the variation in settlement with position and depth at critical sections of the tunnelling project.

TABLE 3.1 SUMMARY OF DATA OF CASE RECORDS ANALYZED

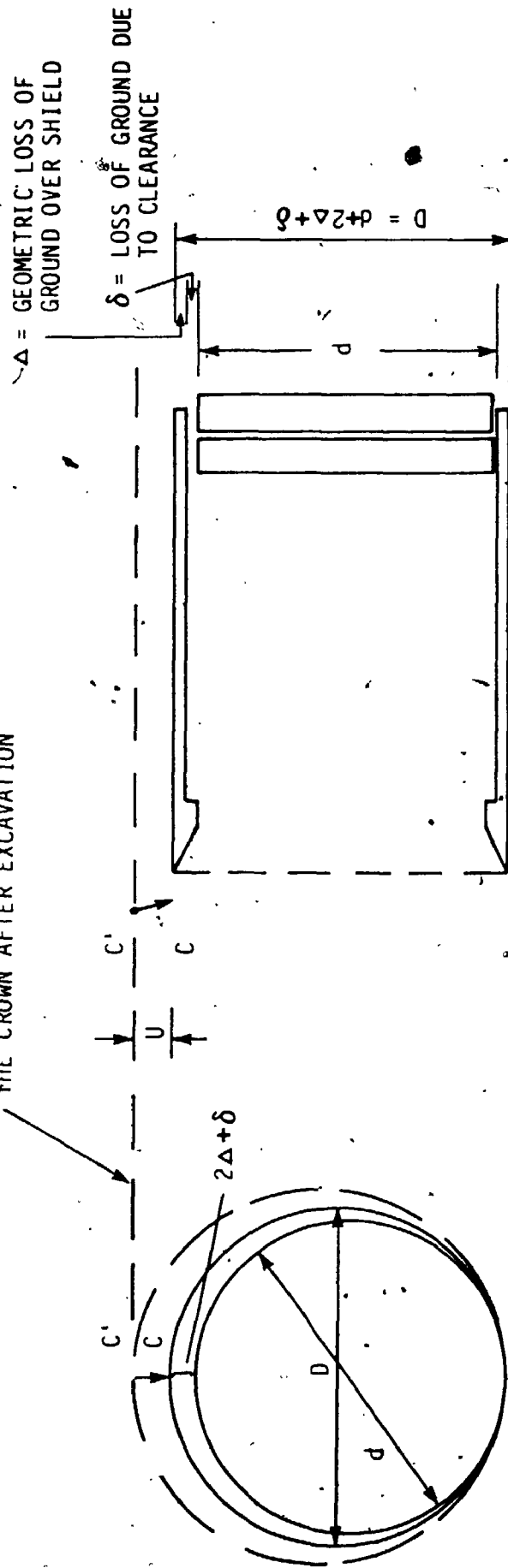
No.	Location	Reference	a (m)	H (m)	H/a	C _u (kPa)	E _u (MPa)	E _u /C _u	N	Soil Type	G (mm)	S _s (mm)	S _s /u _c
1	Mississauga	Delory et al. (1979)	2.14	13.1	6.16	360	100	280	0.86	Dense glacial till	10	1.5	0.15
2	Green Park	Attewell & Farmer (1974)	2.07	29.3	14.2	266	53	200	2.2	London clay	23	6.1	0.27
3	Regents Park (Northbound)	Barrett & Tyler (1976)	2.07	20.1	9.69	230	32	140	1.7	London clay	17	7	0.41
4	Regents Park (Southbound)	Barrett & Tyler (1976)	2.07	34.1	16.6	280	56	200	2.4	London clay	23	5.5	0.24
5	Thunder Bay 1 & 11	Belshaw & Palmer (1978)	1.24	10.7	8.66	35	13	370	5.5	Soft silty clay	156	49 to 54	0.31 to 0.35
6	Ottawa	Belshaw (1980)	1.52	18.3	12.04	90	27	300	3.2	Leda clay	21	6	0.28
7	Mexico	Tinajero & Vitez (1971)	1.48	11.7	7.9	35	4	115	5	Mexico City clay	307	105	0.34
8	Grangemouth	Henry (1974)	1.30	10.0	7.7	22	11	500	5.4	Silty clay	75	25	0.33
9	BART	Kiesel (1969, 1972)	2.83	19.0	6.73	50	-	-	4.6	San Francisco Bay mud	116	36	0.31
10	Buenos Aires	Moretto (1969)	2.35	16.4	7.0	35	28	800	8.6	Silty clay	500	130 to 160	0.26 to 0.32
11	Tyneside	Attewell & Farmer (1975)	1.01	7.5	7.43	75	15	200	2	Laminated clay	16 to 19	7.9	0.41 to 0.48
12	Heathrow	Air Wood (1969)	5.45	12.8	2.34	165	27	165	1.5	London clay	*	11.4	0.67
13	Edmonton (LRT)	Eisenstein & Thomson (1978)	3	10.2	3.4	190	58	305	1.1	Edmonton till	16	12	0.75

* At 1 m above crown, u_c was measured to be 14 mm. Extrapolated value was 17 mm.

TABLE 3.2 Index Properties of London Clay at Green Park, Regents Park and Ashford Common

	Liquid Limit %	Plastic Limit %	Natural Water Content %
Green Park	70-80	27-33	25-28
Regents Park	62-94	24-31	22-31
Ashford Common	60-71	24-29	22-26

INITIAL POSITION OF POINTS ON WHAT WILL BECOME THE CROWN AFTER EXCAVATION



$$\text{GAP} = 2\Delta + \delta + U$$

$$U = u_{e,p}^* + \omega$$

FIGURE 3.1 Definition of Gap

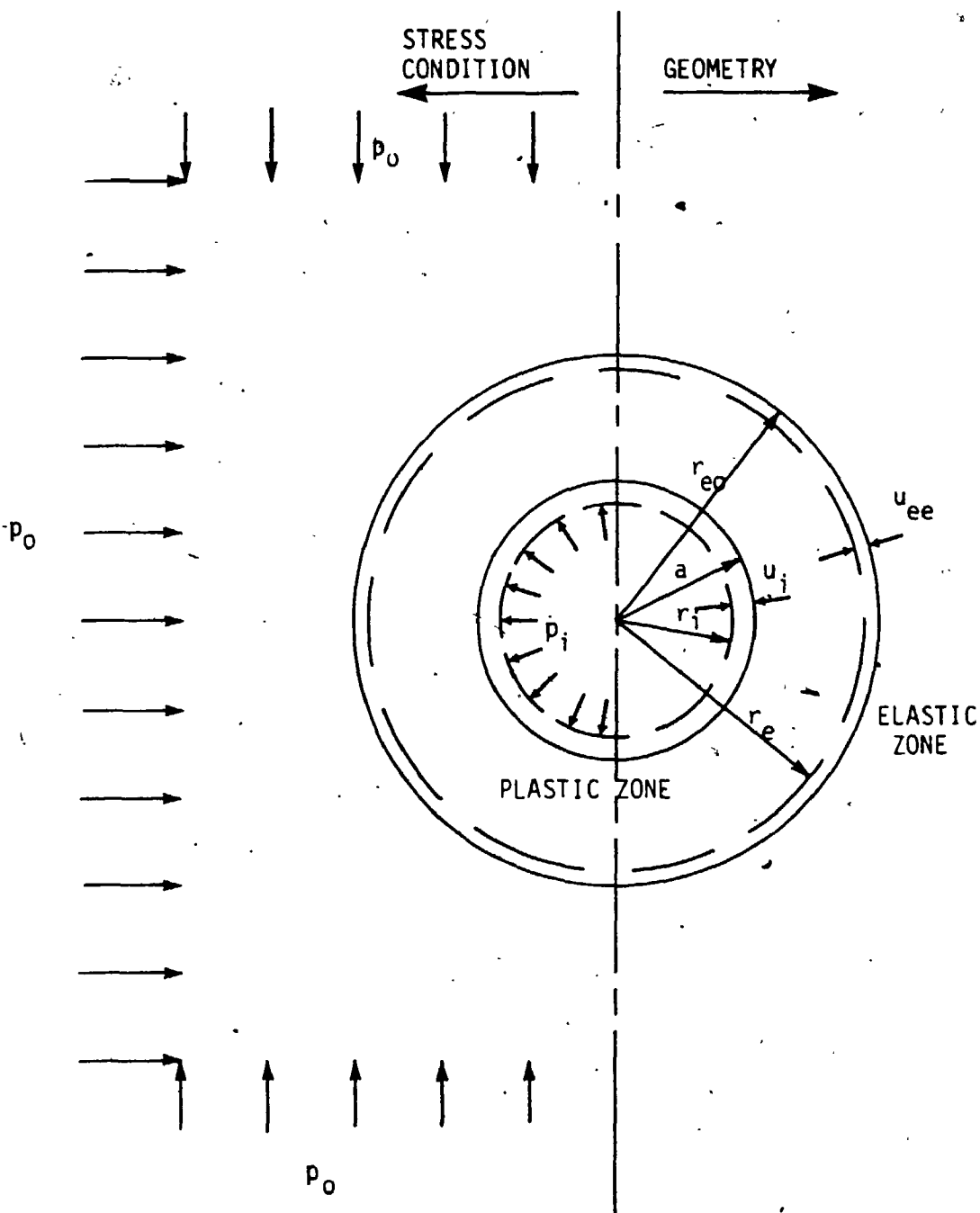


FIGURE 3.2 Stress Condition and Geometry of Problem Analyzed

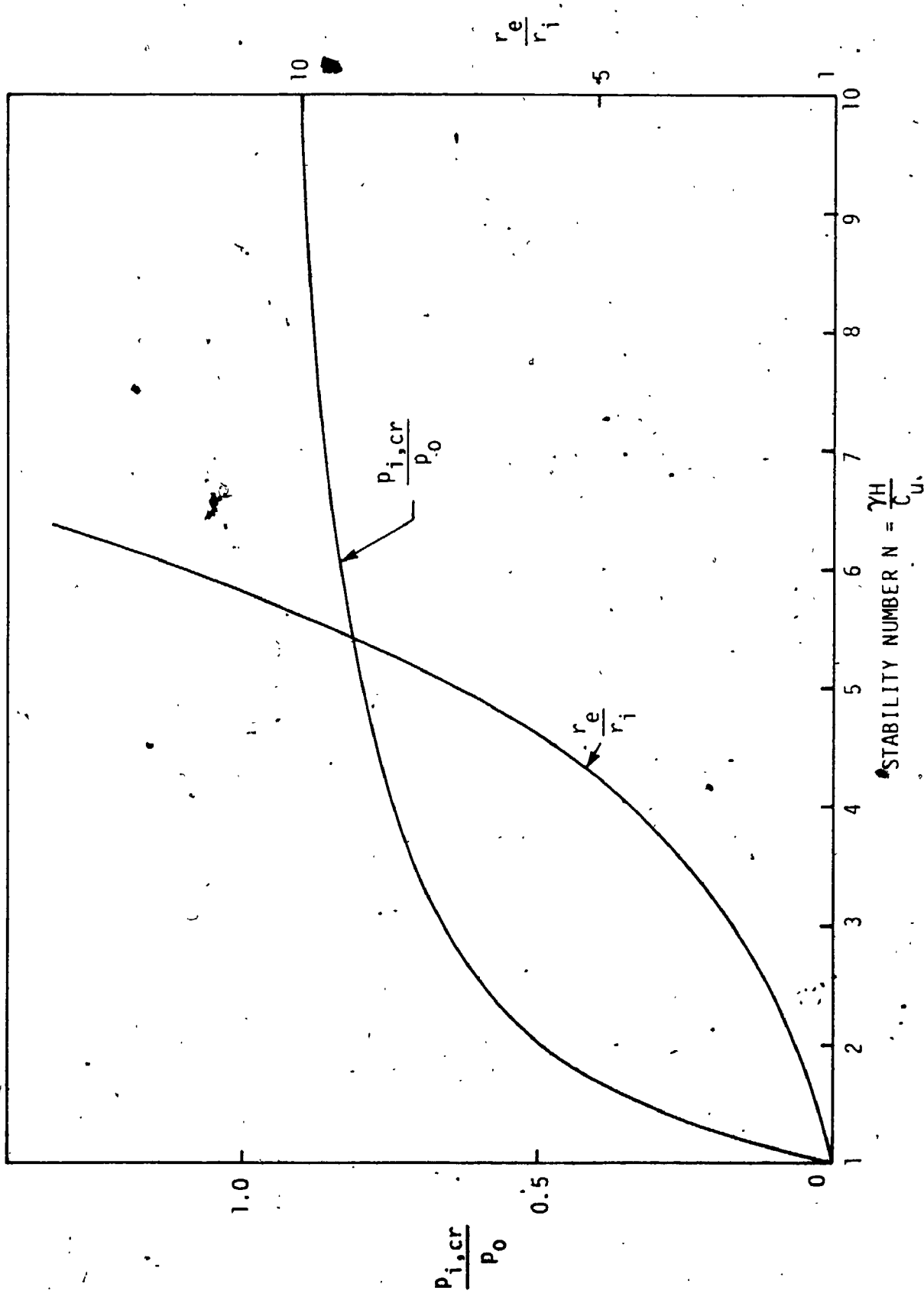


FIGURE 3.3 Variation of Normalized Critical Pressure and Plastic Radius with Stability Number ($P_i=0$)

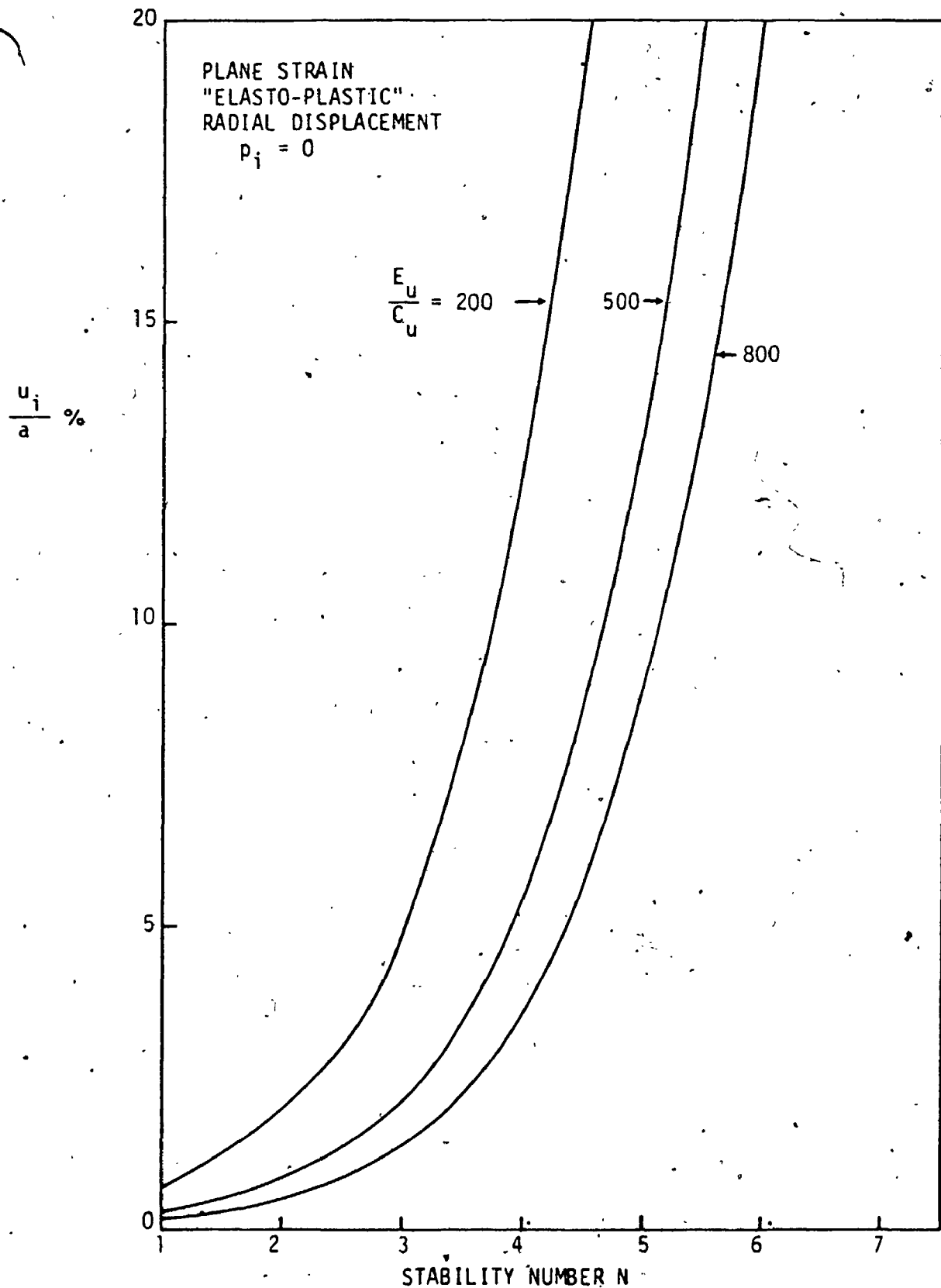


FIGURE 3.4 Variation of Normalized Radial Crown Displacement with Stability Number for Different Values of E_u/C_u

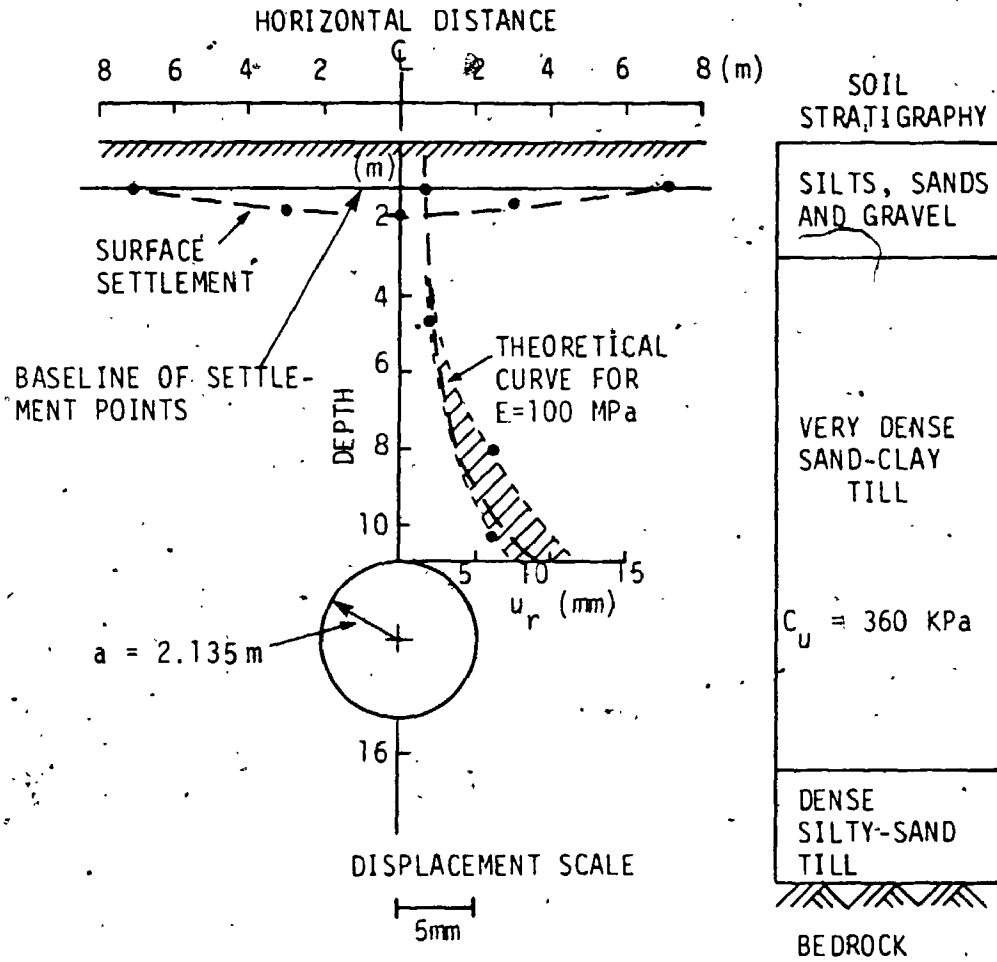


FIGURE 3.5 Sewer Tunnel, Mississauga, Ontario

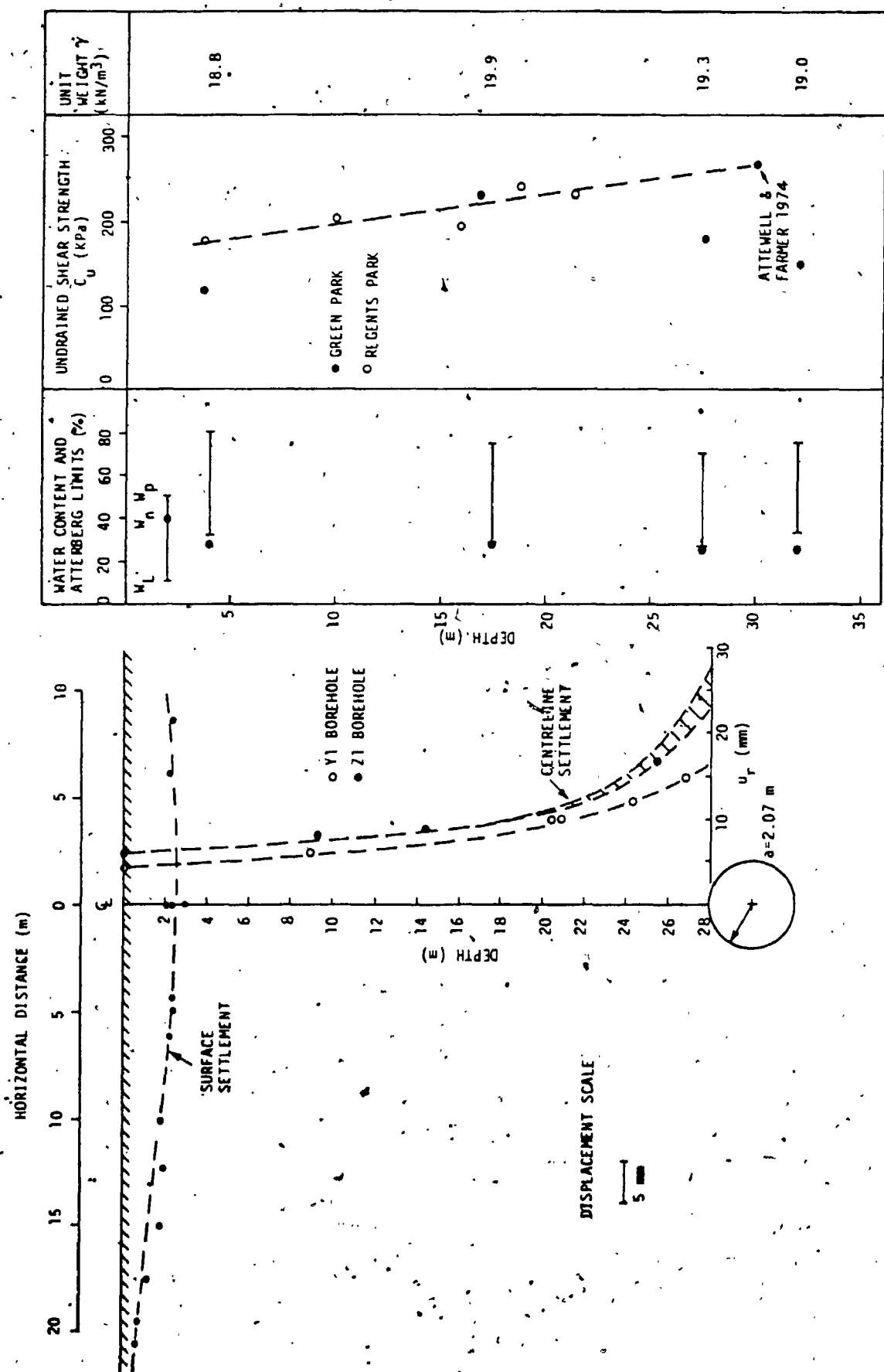


FIGURE 3.6 Tunnel at Green Park, London Underground

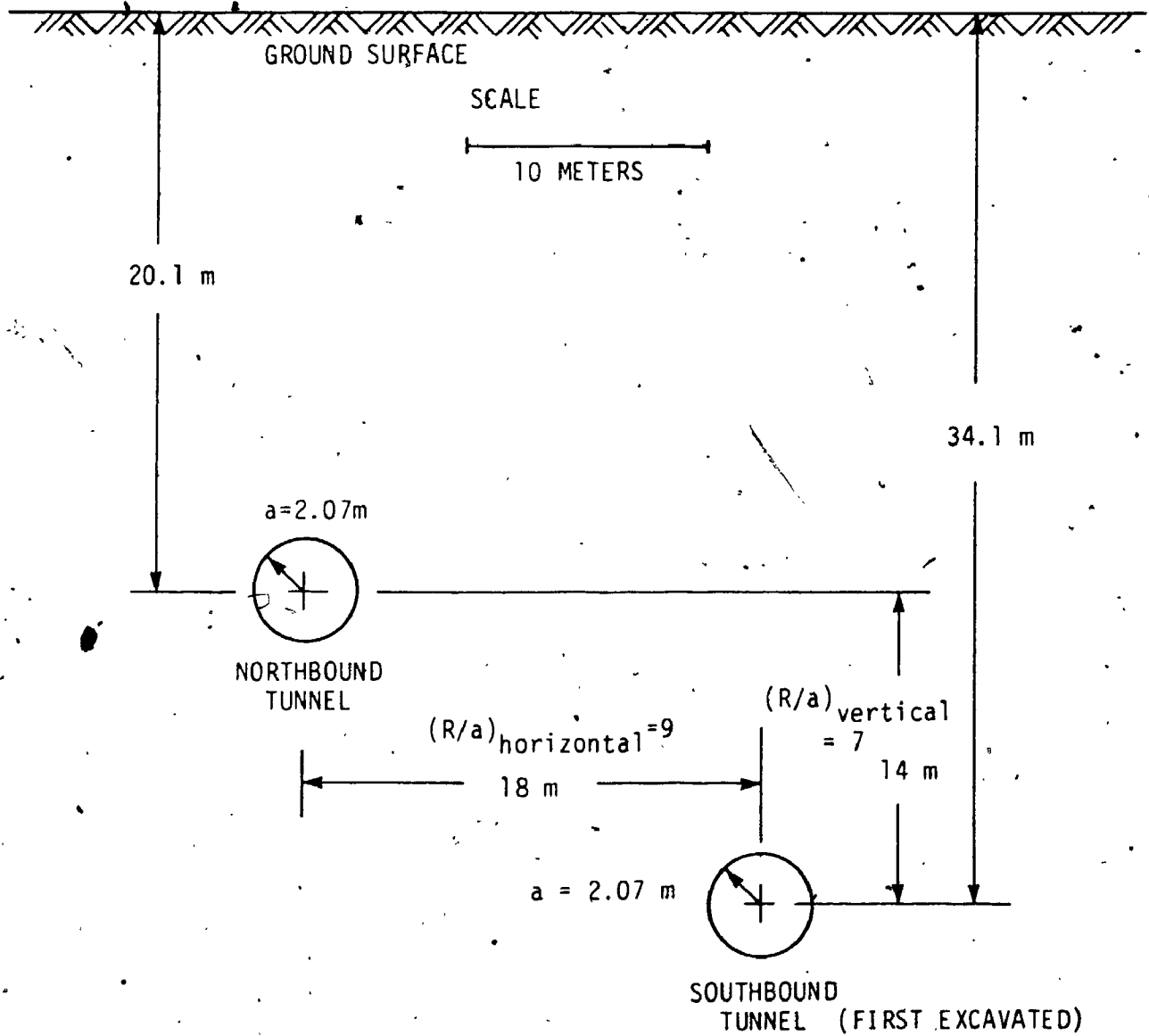


FIGURE 3.7 Northbound and Southbound Tunnels at Regents Park, London Underground

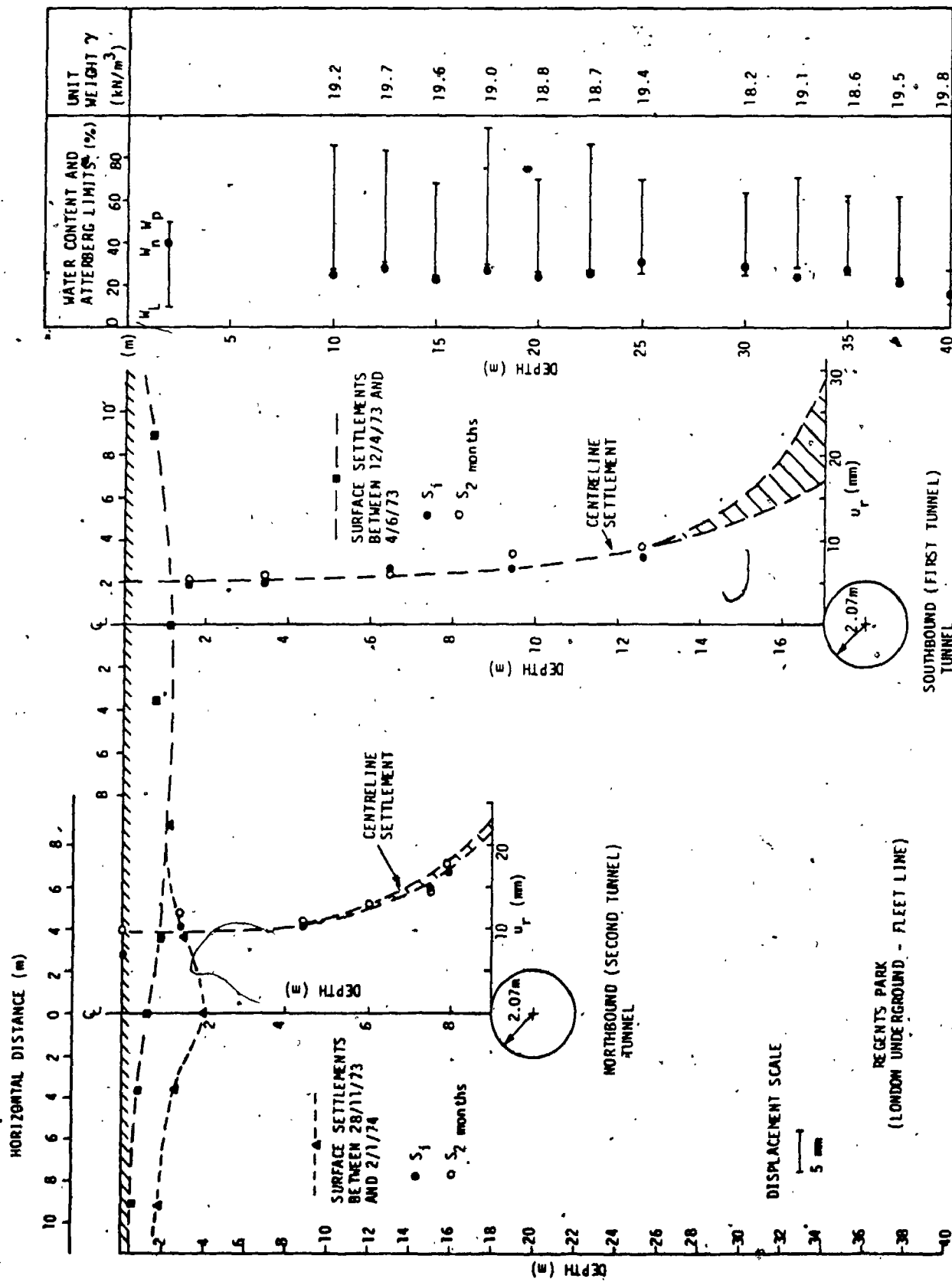


FIGURE 3.8 Measured Displacements for Tunnels at Regents Park

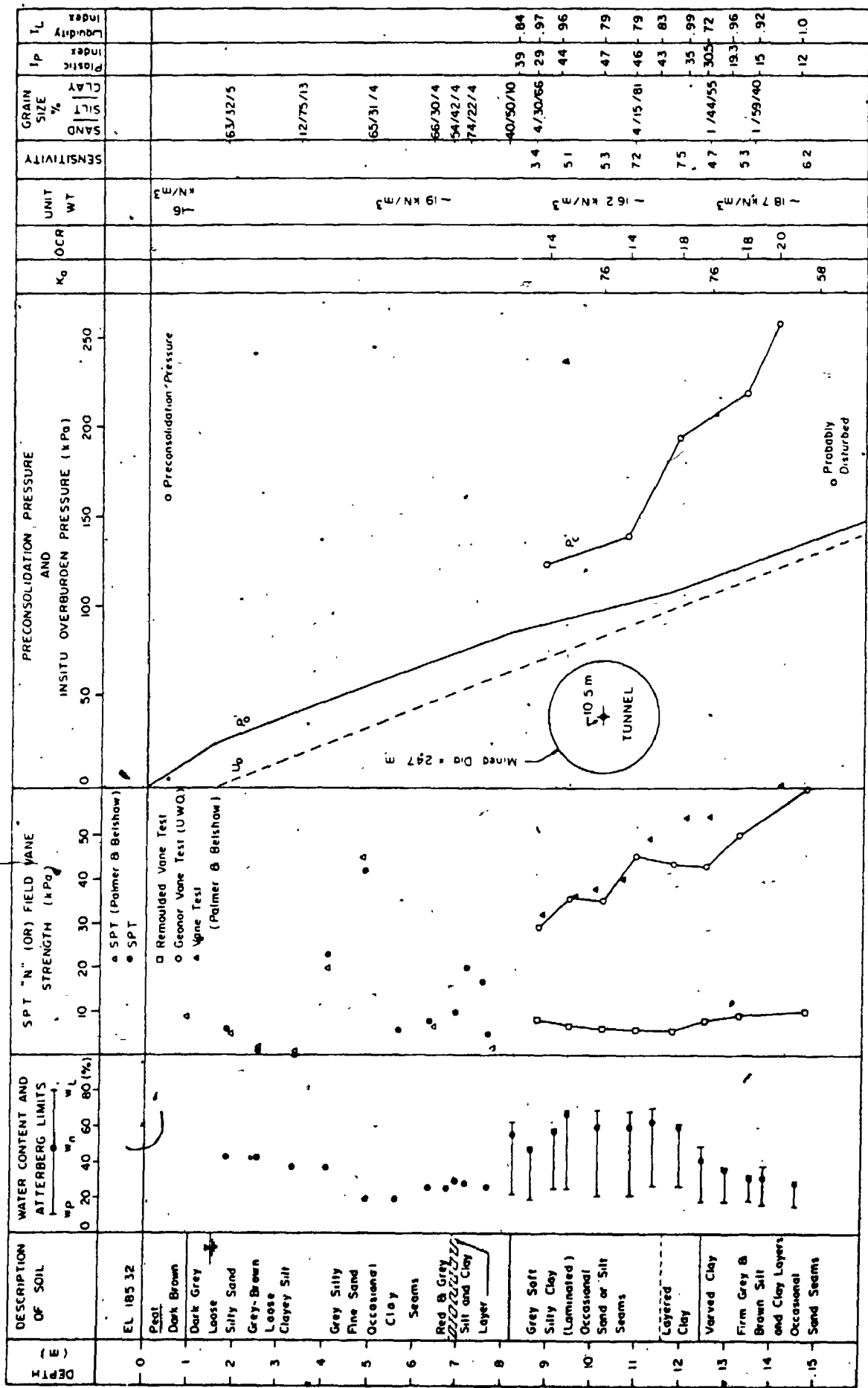


FIGURE 3.9 General Soil Properties - Array 2, Thunder Bay Tunnel

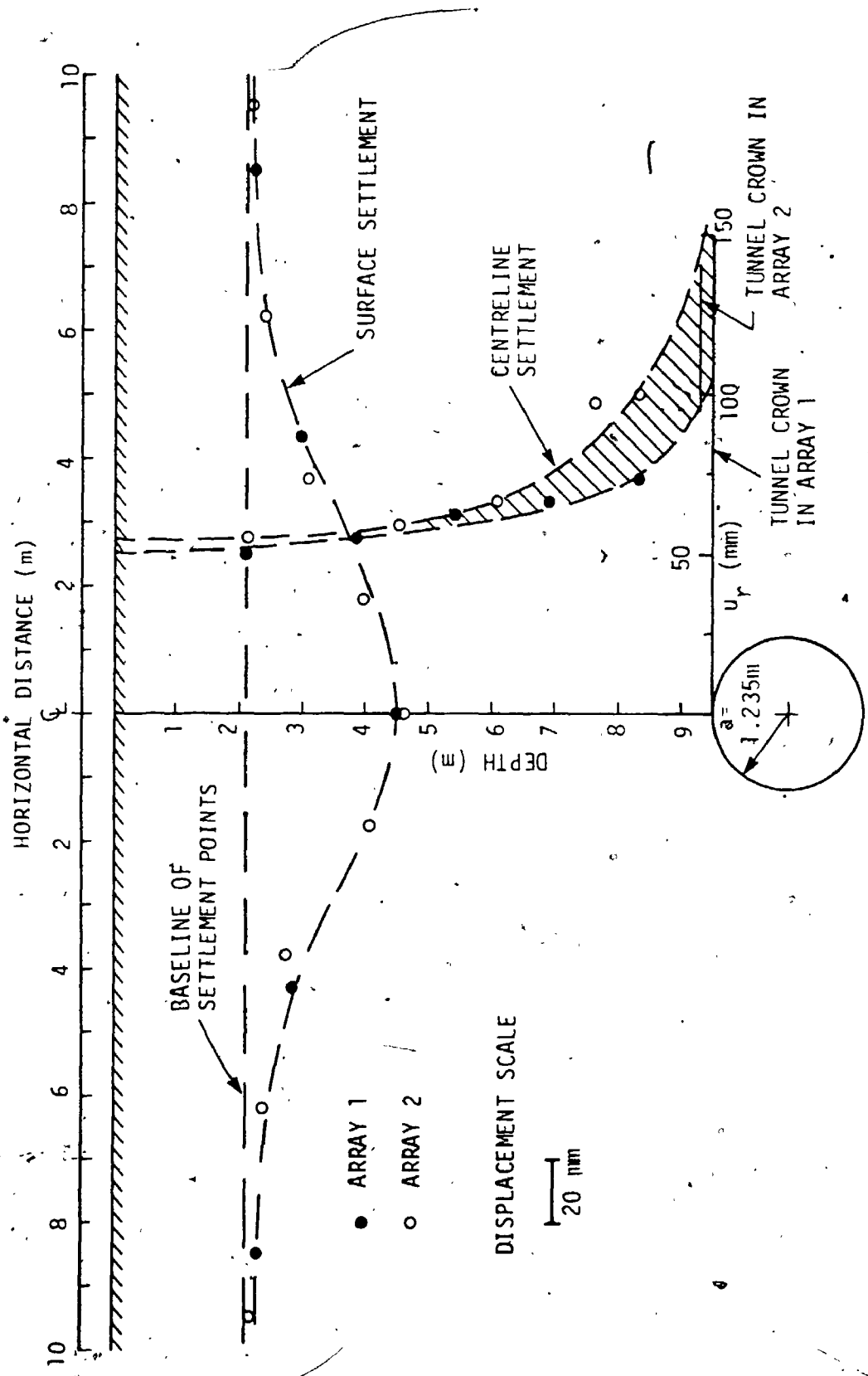


FIGURE 3.10 Measured Displacements at Array 1 and Array 2, Thunder Bay Tunnel

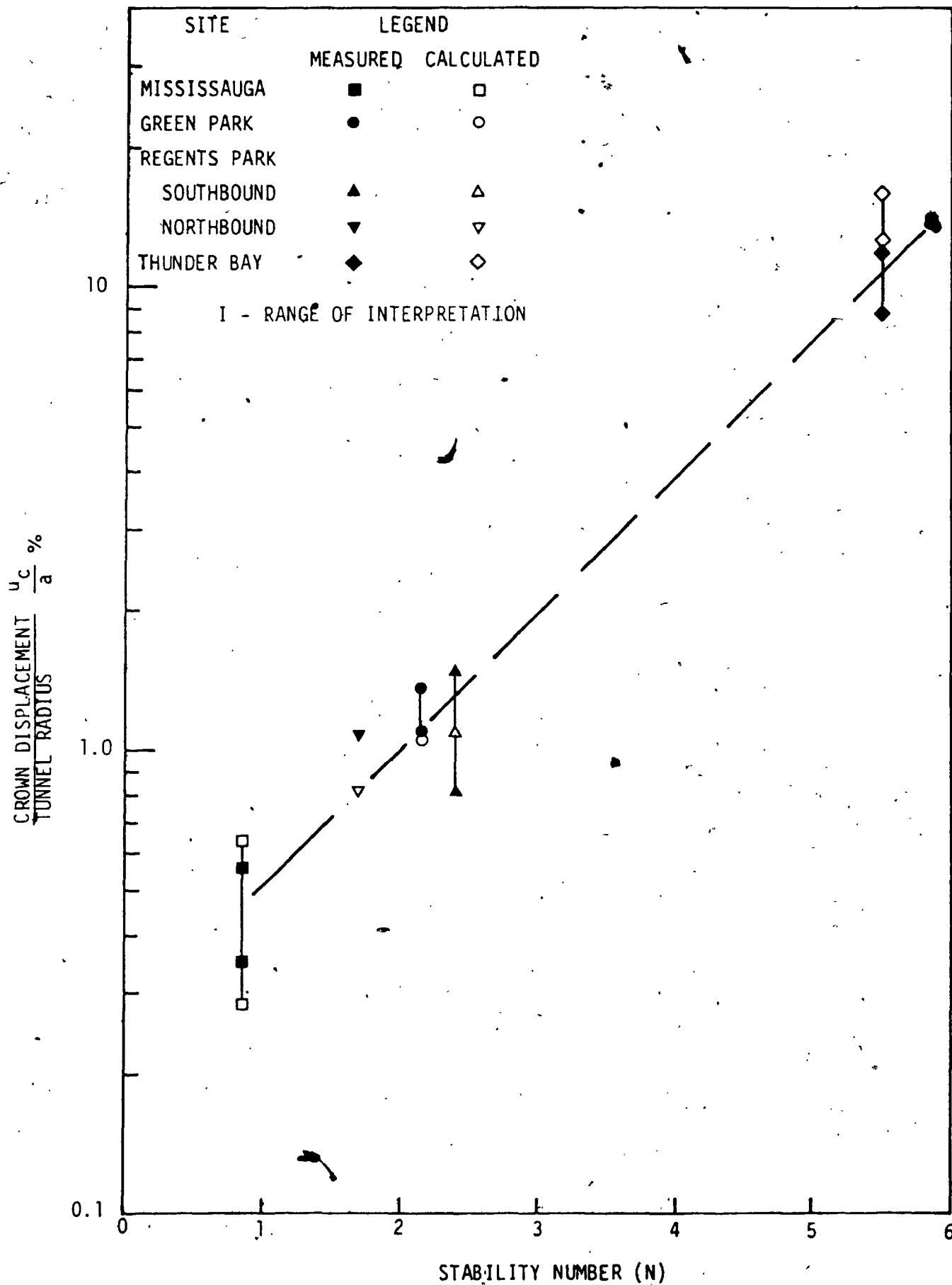


FIGURE 3.11 Comparison of Measured and Calculated Normalized Crown Displacements

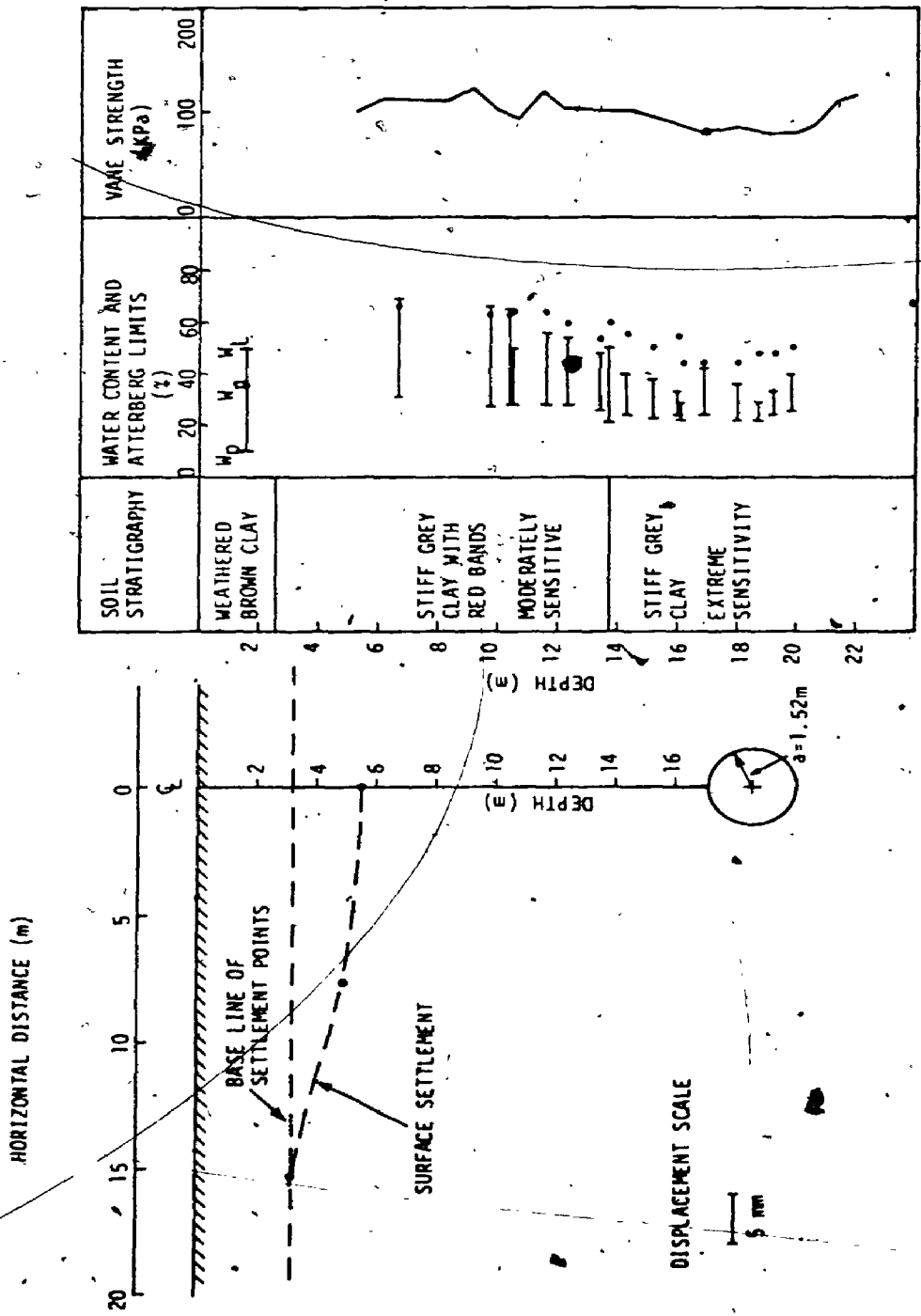


FIGURE 3.12 Soil Properties and Measured Ground Displacements, Ottawa Sewer Tunnel

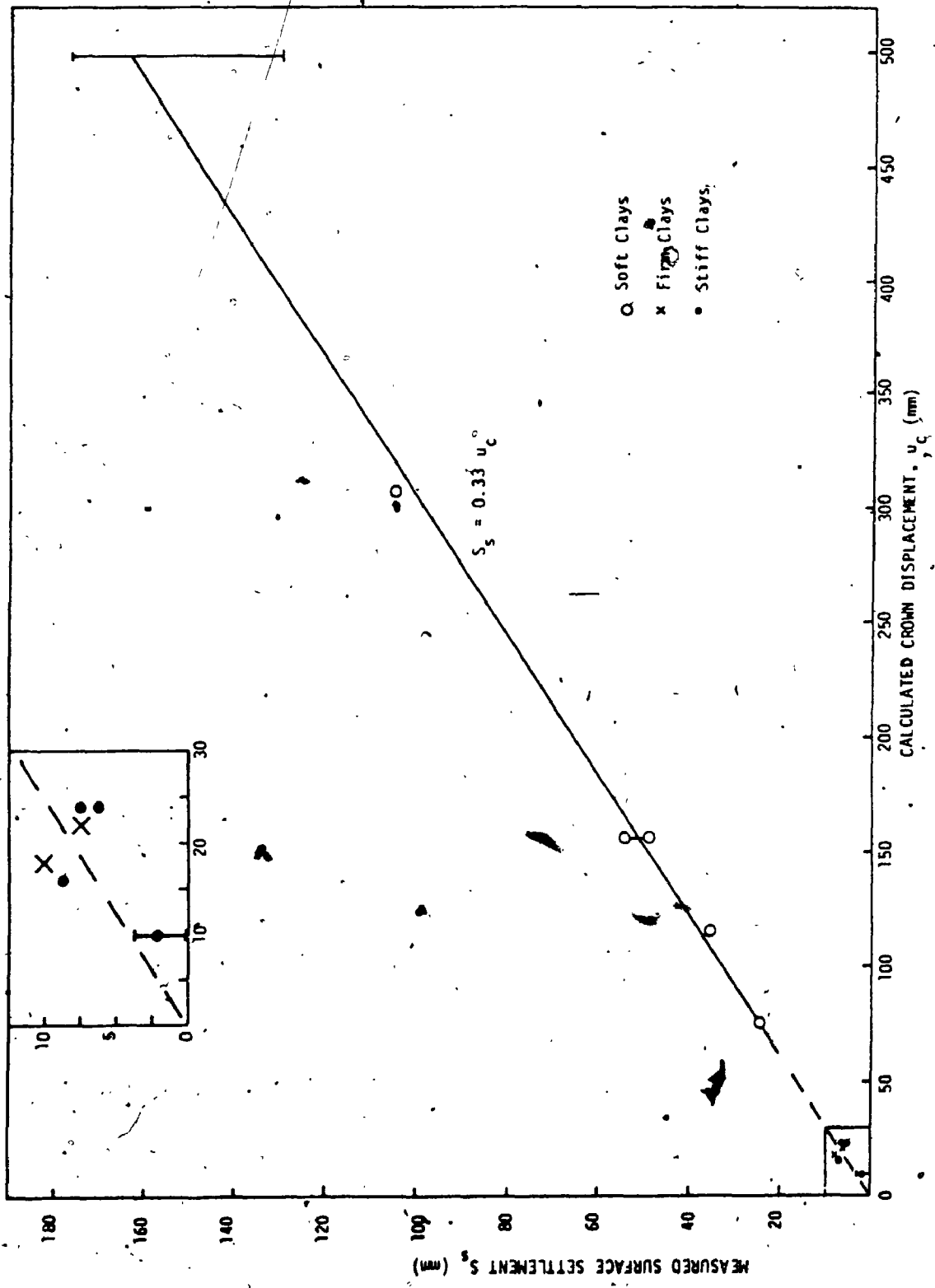


FIGURE 3.13 Relationship between Measured Surface Settlements and Calculated Crown Displacements

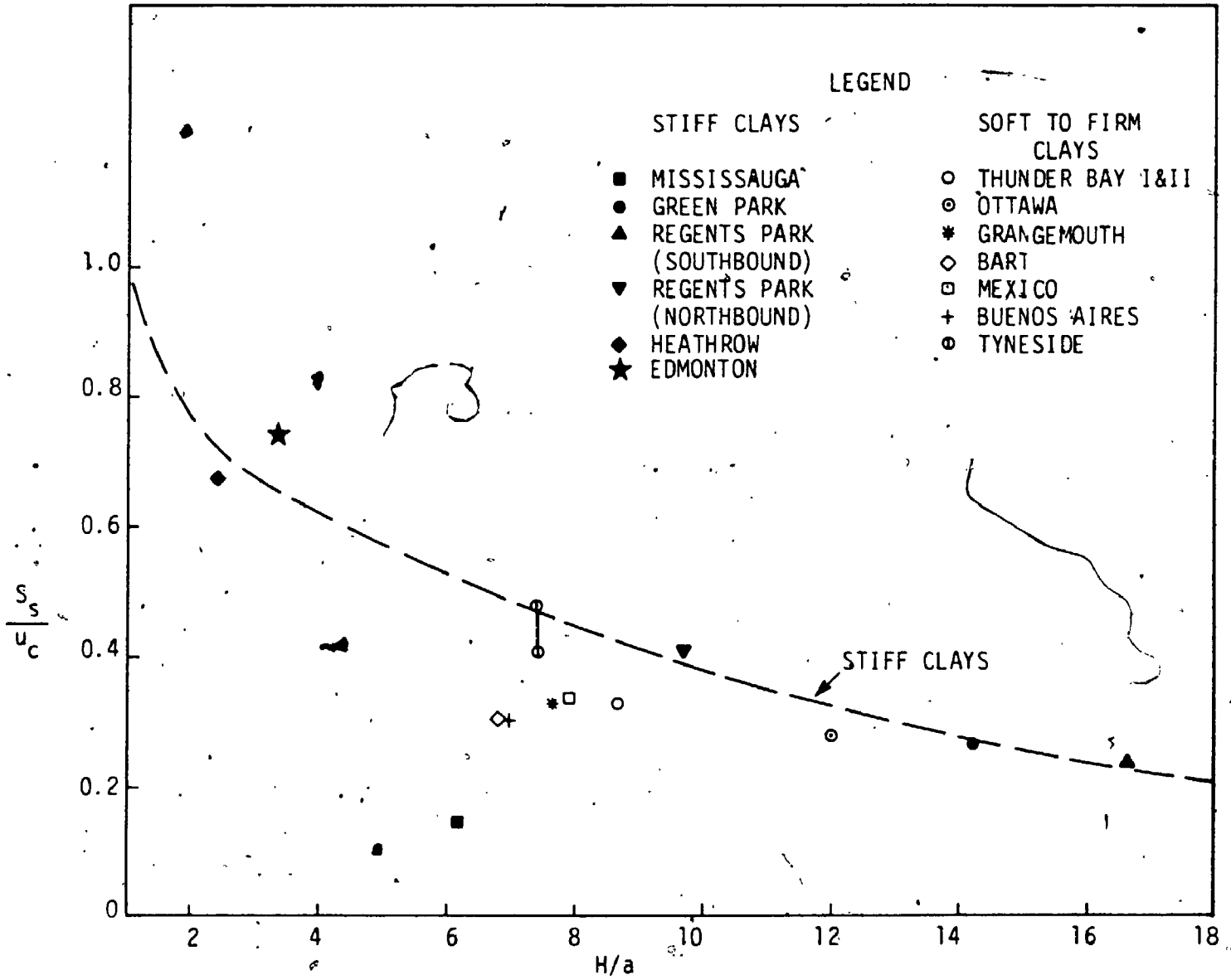


FIGURE 3.14 Influence of Depth to Radius Ratio on Surface Settlement to Crown Displacement Ratio

CHAPTER 4
FUNDAMENTAL CONCEPTS AND METHOD OF SOLUTION
IN A DETAILED ANALYSIS

Surface settlement associated with loss of ground during construction has been discussed in the last chapter. Additional soil deformation may occur due to volume changes in the soil around and above the tunnel. The concept of gap parameter can also be employed to quantify settlement resulting from volumetric change. A method of analysis for the settlement distribution at any depth under undrained and drained conditions will be developed.

Loss of ground and volumetric changes of soil, and hence the magnitude and distribution of settlements are influenced by two classes of factors. The first class is related to construction method such as workmanship, excavation technique and lining geometry. The second class pertained to soil properties such as the stress-strain relationships and insitu stress condition. It is necessary therefore to adopt an appropriate representation of the soil behaviour and a relevant scheme of construction simulation in a settlement analysis. A finite element formulation, together with the description of an elasto-plastic soil model, simulation technique of an advancing tunnel and the theory of soil-structure interaction will be presented in this chapter.

4.1 SOURCES OF GROUND SUBSIDENCE

The sources of ground subsidence arise from (a) loss of ground during construction and (b) volume change with time as a result of effective stress changes in the soil surrounding and above the tunnel.

The components of loss of ground have been discussed in detail in Chapter 3 in the definition of the gap parameter. The additional source of subsidence due to volume change is discussed in detail below.

4.1.1 Changes in Volume Associated With Stress Changes

In addition to settlement due to ground loss in an undrained state, any volume change that occurs within the medium will also induce a resultant settlement or heave variation with depth. The sources contributing to the volume change or consolidation of the soil can be divided into three groups; 1) the stress-redistribution due to tunnel excavation; 2) the change in hydraulic conditions; and 3) the development of a remoulded zone (i.e., change in soil properties) immediately surrounding the tunnel opening.

The stress changes due to tunnel excavation not only will produce immediate deformation, which contributes to ground loss, but also will induce pore water pressure changes. The dissipation of the excess pore pressure with time leads to consolidation of the

soil. Simultaneously, a change in the groundwater flow regime may occur with the tunnel acting as a sink if the lining is not watertight. The phreatic surface may be lowered to a parabolic drawdown surface as shown in Figure 4.1(a) producing additional settlement due to change in effective stresses or, for a strong recharge to a constant phreatic surface with flow characteristics as shown in Figure 4.1(b). In this case, steady-state seepage drag forces will tend to cause settlement above the tunnel.

As the shield is pushed forward by thrusting, a circumferential zone of the soil is mechanically disturbed. The remoulding, particularly in a sensitive clay, will lead to a decrease in compressibility. Further, a wider zone of soil around the tunnel may be overstressed as a result of stress changes with a consequent decrease in compressibility as the soil consolidates leading to an increase in settlement with time.*

Volume change due to the dissipation of pore water pressure may be accounted for by employing effective stress parameters determined from drained tests in the analysis. Change in ground water regime may be treated by imposing the appropriate seepage forces and boundary conditions in the analysis.

The settlements associated with reconsolidation of remoulded or overstressed soil surrounding a tunnel may be analyzed by consolidation theory (eg. Biot, 1941) coupled with appropriate constitutive stress-strain relationships. In a detailed finite element

* The study of the effect of rapid consolidation in the remoulded zone on surface settlement is currently underway.

analysis, the precise knowledge of the geometry of the remoulded area and the properties of the remoulded clay is required. If data on the disturbed zone is not available, the use of a sophisticated analysis which is costly and mathematically complicated will be unjustified. Some investigators have begun to study the quantitative characteristics of the softened zone around the tunnel. Endo and Miyoshi (1978) have investigated the degree of soil disturbance around a shield tunnel through soft silt layer by comparing the measured compressive strengths of the soil before and immediately after shield passage. They suggested that a 50% decrease in strength occurred in most locations studied except near the invert. Thomson and El-Nahhas (1980) have conducted pressuremeter tests to determine the deformation modulus of clay shale around the Whitemud Creek tunnel in Edmonton after placement of ribs in the excavation. Tests were conducted in boreholes drilled within the tunnel in the invert and near the springline. From results of insitu pressuremeter tests, the authors indicated that a softened zone was formed around the tunnel. They also suggested that more extensive insitu measurements are needed to define this softened zone before rational assessment of its influence on deformation behaviour can be made.

While it is inexpedient to analyze settlements due to soil reconsolidation by sophisticated numerical techniques without reliable data on the disturbed zone, simple approximate method may be used to estimate the settlement arising from this source. The additional component of soil movement due to consolidation of the remoulded zone

may be conveniently dealt with by the use of the gap parameter.

4.2 COMPONENT OF GAP DUE TO CONSOLIDATION OF REMOULDED ZONE

It has been shown in Chapter 3 that the gap parameter in the undrained case may be expressed as:

$$G = 2\Delta + \delta + u_{e,p}^* + \omega \quad (3.1)$$

where Δ = thickness of the tailpiece

δ = clearance between the tailpiece and the lining

$u_{e,p}^*$ = three-dimensional elasto-plastic deformation at the face

ω = workmanship term

From the discussion on workmanship in Chapter 3, it is clear that the size of the remoulded zone is directly related to the quality of workmanship. The effect of consolidation of the remoulded zone may therefore be taken into account by increasing ω to $\omega + \omega_1$. The gap parameter for long term cases may therefore be written as

$$G = 2\Delta + \delta + u_{e,p}^* + \omega + \omega_1 \quad (4.1)$$

An example is given in the following paragraphs:

Figure 4.2 shows the settlement-time relationship at various depths along the centreline at Array 1 of the Thunder Bay Tunnel.

The curves are constructed from data contained in a report prepared by Morton, Dodds and Partners (1976) submitted to the National Research

Council. Small heaving of soil was recorded ahead of the face and when the machine was approaching the extensometers*, net downward movement was measured. At $\ell = 4.8$ m, (where ℓ = distance of line of instrumentation from the tunnel face) 22 mm of surface settlement occurred. Construction was terminated for a weekend. During this interval, the settlements remained unchanged indicating settlements occurred essentially in undrained condition at this stage. When work resumed, rapid downward movement occurred after the shield passage until it had advanced to a distance of about 13.8 m from the extensometers and the ratio of ℓ/L_s was 2.5 (where $L_s = 5.6$ m, the length of the shield). Evidently, plane strain undrained condition of the tunnel was attained at this position. Subsequently, the settlement continued with time at a comparatively much slower rate.

An examination of the results showed that there was little relative movement between the extensometer points in Figure 4.2. The ground from 1.2 metres above the tunnel crown (i.e., the location of extensometer E4) to the surface appeared to be settling together as a unit. Such a phenomenon may be explained by considering that a zone of remoulded clay, about 1 m thick, was formed due to poor workmanship. The compressibility of this disturbed zone was lower than the undisturbed clay and time-dependent settlement resulted from consolidation of this remoulded layer.

* The extensometer readings were referred to a benchmark installed into bedrock.

To estimate the parameter ω_1 , the one-dimensional consolidation theory may be used. The remoulded zone may be assumed to be 1 metre thick. Results of consolidation tests on undisturbed samples at locations near the crown showed that the coefficient of volume change m_v is $0.4 \times 10^{-3} \text{ kPa}^{-1}$ (see Chapter 8). The effects of disturbance on consolidation parameters have been investigated by Lo (1972) and a factor of 3 may be used to obtain the approximate value of m_v of the disturbed zone, giving a value of $1.2 \times 10^{-3} \text{ kPa}^{-1}$.

The additional settlement at the centreline due to the consolidation of the remoulded zone may be assessed by an approximate method. The vertical stress after tunnel construction at the centre of the remoulded layer is about 10 kPa, calculated by an elasto-plastic analytical solution. The final stress is not exactly known, but from field observations by Peck (1969) and others, the average radial lining pressure at the crown region eventually approached the original vertical total overburden pressure. The final stress may therefore be taken as approximately 80 kPa. The stress change is therefore about 70 kPa. The value of ω_1 is calculated to be 84 mm.

The accumulated surface settlement over the centreline was measured by Palmer and Belshaw (1979) two years after construction to be 142 mm. Since 1 m of fill was placed on Array 1 one year after construction, the authors suggested that the settlement, excluding the estimated settlement of 35 mm due to surcharge effect, would be 107 mm. The near surface settlement in the undrained condition

(Pin 27) was 49 mm. Therefore, 58 mm of consolidation settlement in the remoulded zone had occurred two years after construction. Since this deduced value of 58 mm is less than the value of w_p of 84 mm, the results are consistent with each other.

4.3 ELASTO-PLASTIC SOIL MODEL ADOPTED IN THE FINITE ELEMENT ANALYSIS

It has been generally recognized that the soil response due to tunnelling in soft ground is generally not elastic (eg. Ward and Pender, 1981). Recent analytical approaches to the problem therefore usually employ elasto-plastic models (eg. Ghaboussi et al., 1978). It has also been found that isotropic elasticity in an elasto-plastic model is inadequate to represent the soil behaviour (Rowe, Lo and Kack, 1983). The soil model adopted in this thesis is an orthotropic elasto-plastic model. The elastic behaviour is represented by cross-anisotropic elasticity with ten independent parameters, five for loading and five for unloading. The plastic response is represented by Mohr-Coulomb failure criterion and a non-associated flow rule proposed by Davis (1968).

By assuming elastic perfectly plastic behaviour, an element of soil will remain elastic until the stress path which it undergoes in the field reaches the yield surface. At this point, indefinite strain occurs unless the element is restrained by surrounding elastic elements (Figure 4.3). The stress-strain relationships of the soft,

normally-consolidated Thunder Bay silty clay under the appropriate stress paths may be closely simulated by this type of material behaviour (see Chapter 8). In the elasto-plastic soil model, the failure surface is taken to be identical with the yield surface in accordance with perfect plasticity (Hill, 1956).

In consideration of an elasto-plastic material, a total increment of strain $\dot{\underline{\epsilon}}$ is composed of an elastic component $\dot{\underline{\epsilon}}_e$ and a plastic component $\dot{\underline{\epsilon}}_p$ such that

$$\dot{\underline{\epsilon}} = \dot{\underline{\epsilon}}_e + \dot{\underline{\epsilon}}_p \quad (4.1)$$

where the dot denotes increment and \sim denotes vector notation.

If the material is elastic, the elastic stress increment $\dot{\underline{\sigma}}$ is related to the elastic strain increment $\dot{\underline{\epsilon}}$ by:

$$\dot{\underline{\sigma}} = -D_e \dot{\underline{\epsilon}} \quad (4.2)$$

in which D_e is a 3 x 3 symmetrical matrix of elastic constants.

When an element becomes plastic, the incremental stress-strain relationship may be written as

$$\dot{\underline{\sigma}} = -D_p \dot{\underline{\epsilon}} \quad (4.3)$$

where D_p is in general, a non-symmetric matrix depending on stress state given by:

$$D_p = D_e - \frac{D_e \underline{a} \underline{b}^T D_e}{\underline{b}^T D_e \underline{a}} \quad (4.4)$$

In equation 4.4, \tilde{a} and \tilde{b} are respectively derivatives of the plastic potential $g(\sigma)$ and the yield function $f(\sigma)$. (The symbol T represents the matrix transpose operation.)

$$\tilde{a} = \frac{\partial g(\sigma)}{\partial \sigma} \quad (4.4a)$$

$$\tilde{b} = \frac{\partial f(\sigma)}{\partial \sigma} \quad (4.4b)$$

The yield function $f(\sigma)$ in equation 4.4b for the material is given by the conventional Mohr-Coulomb relationship,

$$f(\sigma) = \sigma_1 - N_\phi \sigma_3 - 2c\sqrt{N_\phi} \quad (4.5)$$

and

$$N_\phi = \tan^2(45 + \phi/2) \quad (4.5a)$$

where σ_1 , σ_3 are respectively the major and minor principal stresses. The parameters c and ϕ are respectively the cohesion intercept and the friction angle. The plastic potential in equation 4.4a is given by

$$g(\sigma) = \sigma_1 - N_\psi \sigma_3 \quad (4.6)$$

$$\text{where } N_\psi = \tan^2(45 + \psi/2) \quad (4.6a)$$

In the formulation of theory of plasticity, each of the plastic strain increments is found from the partial derivative of the function $g(\sigma)$, i.e.,

$$\dot{\tilde{\epsilon}}_p = \tilde{a} \quad (4.7)$$

where $\dot{\underline{\epsilon}}_p$ is the vector of plastic strain increment and λ is a signed multiplier. Equation 4.7 actually follows from the consideration of flow rule (Davis, 1968) of the material,

$$\frac{\dot{\epsilon}_{3p}}{\dot{\epsilon}_{1p}} = - N_{\psi} \quad (4.8)$$

For a material with a flow rule that depends only on stress state, equation 4.8, the principal axes of stresses and the plastic strain increments will coincide. This is one of the major differences between plasticity theory and incremental elastic theory.

The finite element equations and the stiffness matrix K_p may be readily derived from equation 4.4 by following standard procedures (eg. Zienkiewicz, 1977).

$$K_p \dot{\underline{\delta}} = \dot{\underline{R}} \quad (4.9)$$

in which $\dot{\underline{\delta}}$ and $\dot{\underline{R}}$ are respectively the displacement increment vector and load increment vector in the system. K_p is the incremental tangent stiffness matrix which depends on the current stress states as both \underline{a} and \underline{b} change with stress and K_p is given by

$$K_p = \sum_v \int B^T D_p B dv \quad (4.10)$$

where B = the strain-displacement matrix. The integration in equation 4.10 is carried out over the volume of each element in the finite element mesh and the summation and assembly of the global stiffness

matrix is performed over all the elements within the system. In subsequent sections, a method of lined tunnel analysis which adopts the orthotropic elastic-perfectly plastic behaviour as the constitutive relationships will be presented.

4.4 METHOD OF ANALYSIS

The detailed settlement analysis in this thesis was performed by a finite element formulation which adopted an elasto-plastic constitutive stress-strain relationship. The finite element program is an improved version of EPTUN used by Rowe, Lo and Kack (1983) in a parametric study of settlement prediction due to tunnelling.

The soil-structure interaction theory, with the consideration of lining flexibility has been implemented in the analytical formulation and deformable tunnel liners may be modelled in the analysis to reflect the true interaction behaviour. The construction of an advancing tunnel was simulated as construction sequences by an incremental solution procedure. Modelling of variation of soil strength and deformation behaviour with depth has also been considered in the formulation.

4.4.1 Finite Element Mesh and Beam Elements

Eight-noded isoparametric elements were used in the analysis. These elements have a common description of the element geometry and the unknown displacement. The continuous displacement field is

to the nodal displacements by shape functions mathematically,

$$\underline{u} = N \underline{\delta} \quad (4.11)$$

in an element, where \underline{u} = displacements at any point, $\underline{\delta}$ = nodal displacements, N is the matrix of shape functions and \sim denotes vector notation. In this case N is determined by the geometry of the element. There are relative advantages of the higher order element over the conventional constant strain triangular elements because the former can model curved geometry and complex displacement profiles closely.

The mathematical-formulation of an element-mesh and the integration procedure for obtaining the element stiffnesses may be found in many standard texts (eg. Zienkiewicz, 1977). Typical isoparametric elements arranged in a typical finite element mesh of a shallow tunnel are shown in Figure 4.4. It may also be mentioned that a superelement (Rowe, 1978) was used in the mesh shown in Figure 4.4 down to bedrock. The lateral boundary of the element mesh is sufficiently remote from the tunnel so that the difference in boundary condition, whether smooth or rough, would not lead to a difference in the calculated trough shape. For the purpose of the analysis, a smooth boundary is adopted.

The tunnel lining may be modelled with structural beam elements with parameters appropriate to the structure (eg, E , the Young's modulus, A , the area of the section, and I , the moment of inertia of the section). Segmented flexible lining, such as the segmented unbolted concrete liner used in the Thunder Bay tunnel was not uniform in stiffness because of segment joints and crack inducers. This kind of lining may be modelled by reducing the stiffness at the segment joints and stress raisers by an appropriate factor to provide for

flexibility in the system. This procedure approximately corresponds to the introduction of a 'rusted hinge' at these locations:

4.4.2 Two-Dimensional Simulation of Tunnel Construction

When a tunnel is being constructed, three-dimensional soil movements above and around the tunnel may be anticipated. When the face of a tunnel reaches a point, part of the total settlement at the point has already been developed. Settlements continue to occur as the tunnel advances forward.

For a complete numerical or analytical solution for stresses and displacements in the tunnelling problem, the mathematical model is required to reproduce the effect of advancing face. The three-dimensional finite element method appears to be the most appropriate analysis. The steps in the technique will be the stepwise removal of the elements representing the current tunnel face from the three-dimensional finite element mesh and the removal of tractions equivalent to the insitu stresses from the nodal points in the heading.

Since three-dimensional analysis is difficult to perform and is very costly, a more pragmatic design method is necessary. Examples of two-dimensional analysis which simulate the three-dimensional effects have been given in Chapter 2. It should be emphasized that the 'modified 2-D' approach may be the best alternative to a three-dimensional analysis at the present economy and computing technology for elasto-plastic analysis.

In a modified two-dimensional approach, two important factors are being considered. They are the three-dimensional soil movements ahead of the face and the advancing effect of the tunnel-boring machine or shield. The three-dimensional soil movements ahead of the working face may be accounted for in a two-dimensional approach by the concept of the gap parameter and this approach has been discussed in detail in Chapter 3. The other factor, the advancing effect of the shield, will be discussed.

4.4.2.1 Effect of Advancing Face Modelled As Construction Sequences

The solution scheme for excavation and construction of a tunnel has been described by Lo and Rowe (1982) and Rowe et al. (1983). Excavation of a tunnel can be simulated by removing tractions from the excavated boundary by applying the equivalent nodal forces in the opposite direction to the initial stresses in the soil.

The solution is carried out incrementally by solving for a typical load increment i (or actually a decrement, since loads are being removed),

$$K_p \delta_{i+1} = \dot{R} \quad (4.12)$$

where K_p = elasto-plastic soil stiffness matrix, δ_{i+1} = vector of incremental displacements, \dot{R} = vector of load increments. Since K_p depends on the current stress state, it is reformed in each new load increment i . As tractions are progressively removed from the boundary

in increments, simulating the progress of excavation, the stresses and displacements are obtained by accumulation of the incremental displacements and stresses, i.e.,

$$\tilde{\delta} = \sum_{i=1}^n \tilde{\delta}_i \quad (4.13)$$

The method is considered to provide a reasonable approximation of the stress redistribution that occurs with an advancing tunnel. The approach is also valid for all initial stress states. Construction with compressed air may be simulated by reducing or increasing boundary tractions to correspond with the applied pressure.

Completion of the tunnel construction involves erection of the liner. Soil would invade the tail void, possibly coming in contact with the structural support. The soil-structure interaction theory used in the analysis is given in the next section (see also Rowe, Lo and Kack, 1983). Since the liner is not placed directly at the tunnel head, all the influence coefficients of the lining in the matrix I_e are initially inactive. The excavated diameter of the circular opening in the finite element mesh is larger than the diameter of the liner. Soil displaces into the annular void while the solution is carried out by releasing tractions at the boundary. Once the soil is in contact with the lining, the influence coefficients corresponding to the nodes now in contact will be activated. \tilde{F}_u , the incremental nodal forces due to soil-liner interaction is determined. Soil movements are constrained, depending on the liner stiffness. Construction simulation

is completed when all boundary tractions are removed.

4.4.2.2 Construction Simulation With Consideration of Machine Weight

The presence of the TBM imposes kinematic restraint and loading from its weight on the soil beneath. It is conceivable that complete stress relief initially occurs only above the springline because portions of stress relief below the springline are counterbalanced by the weight of the TBM. The process of stress relief is considered complete after the machine has passed the section under consideration.

The effect of machine weight may be conveniently considered by varying the rate of stress relief at the tunnel boundary in the analysis. The discussion on the scheme of construction simulation and an example is given in Appendix 1. The results indicate that in the case of shield tunnelling in soft clays, the predicted shape of the surface settlement profile is relatively unaffected by this effect.

4.4.3 Consideration of Grouting

This analysis does not explicitly consider the effect of clay grout injected into the tailpiece void. Under short term conditions, consideration of clay grout injection is quite straightforward and can be achieved by applying tractions, equal to the grout pressure, between the soil and lining (eg. see Rowe et al., 1983). If the grout will fill part of the annular void, the physical gap may be reduced.

While this procedure is quite appropriate for predicting deformations shortly after grout injection; there are problems associated with adopting the same procedure for predicting the long term settlement. These problems arise from the fact that the grout pressure will not be sustained over a period of time and stress redistribution will occur. The degree of stress redistribution will depend upon the permeability of the soil and lining as well as the creep characteristics of the soil and it cannot be readily estimated.

Thus, in predicting the long term surface deformation, two approximate approaches may be adopted. Firstly, the gap may be reduced to allow for the effect of clay grout injection upon the net volume of lost ground. This reduction may be quite significant if effective grouting is achieved in construction (eg. see the BART case in Lo and Rowe, 1982; Rowe and Kack, 1983) or may approach zero if problems are encountered in grouting (eg. in the Thunder Bay Tunnel; Palmer and Belshaw, 1979). In this procedure no tractions are applied to simulate the grout pressure. Secondly, the pre-grout gap may be used in the tunnel excavation and then the estimated grout pressure applied as tractions between the soil and lining.

4.4.4 Implementation of Soil-Structure Interaction Theory

Consider a tunnel lining embedded in an elasto-plastic soil mass. The tractions acting upon the soil and lining may be considered to take the form of nodal forces. Within any load increment these forces

will consist of known forces due to applied tractions acting directly on the body, and unknown nodal forces \vec{F}_u acting between the soil and lining.

Supposing for the moment that incremental nodal forces acting between soil and lining were also known, then the initial stress approach (Zienkiewicz et al., 1969) could be used and the vector of nodal displacements at the soil tunnel interface $\vec{\rho}$ may be written in the form

$$\vec{\rho}^{(n)} = \vec{\rho}_K^{(n)} + I_E \vec{F}_u^{(n)} \quad (4.14)$$

where $\vec{\rho}_K$ is the vector of nodal displacements at the soil-tunnel interface due to the known nodal forces acting on the soil (including residual forces arising from the initial stress formulation);

\vec{F}_u is the vector of incremental nodal forces due to the lining acting on the soil;

I_E is the matrix of influence coefficients, which can be determined initially by application of point loads along the excavated surface, and will remain constant for each iteration and load-step;

n (superscript) denotes the "nth" estimate of that variable.

If the tunnel lining is considered as a separate body, subjected to selfweight W and the (unknown) nodal forces \vec{F}_u , it will be free to undergo incremental rigid body motions $\vec{\theta}$. This difficulty is overcome by applying sufficient artificial restraints to remove this indeterminacy.

Thus the nodal displacements at the lining-soil interface $\dot{\rho}_e$ may be written in the form

$$\dot{\rho}_e^{(n)} = \dot{\rho}_{Ke}^{(n)} - I_e \dot{F}_u^{(n)} + A \dot{\theta}^{(n)} \quad (4.15)$$

where the definitions of $\dot{\rho}_{Ke}$ and I_e parallel those of $\dot{\rho}_K$ and I_E and where A is a matrix relating interface deflections to rigid body motions.

If the centreline of the tunnel is also an axis of symmetry, there will be only one rigid body motion (i.e., vertical displacement) and the matrix A reduces to a vector.

Displacement compatibility at all nodes in contact along the interface between the soil and lining may be invoked by combining equations 4.14 and 4.15 giving

$$(I_E + I_e) \dot{F}_u^{(n)} - A \dot{\theta}^{(n)} = \dot{\rho}_{Ke}^{(n)} - \dot{\rho}_K^{(n)} \quad (4.16)$$

If there are m unknown nodal forces and p rigid body motions, then equation 4.16 represents m equations in $(m+p)$ unknowns. The remaining equations may be derived from the observation that the lining must be in a state of equilibrium. Thus the net vertical force acting on the lining must be equal to the tunnel weight and there will be no net horizontal force or moment. These equations of equilibrium may be written in the form

$$A^T (\dot{F}^{(n)} - \dot{W}) = 0 \quad (4.17)$$

where $A^T \dot{W}$ is the weight of the tunnel.

Equations 4.16 and 4.17 may be written in the simple interaction equation

$$\begin{bmatrix} (I_E + I_e) & -A \\ -A^T & 0 \end{bmatrix} \begin{bmatrix} \dot{F}_u^{(n)} \\ \dot{\theta}^{(n)} \end{bmatrix} = \begin{bmatrix} \dot{\rho}_{Ke}^{(n)} & -\dot{\rho}_K^{(n)} \\ & -A^T \dot{W} \end{bmatrix} \quad (4.18)$$

Equation 4.18 may be solved to determine $\dot{F}_u^{(n)}$ and $\dot{\theta}^{(n)}$. Once these quantities are known, the displacements within the soil mass may be directly determined. The process is repeated until convergence is achieved. It is noted that the number of nodes in contact with the lining will generally increase during the loading and the number of unknown forces \dot{F}_u will increase as the distance between the soil and lining closes. For simplicity, the formulation indicated in equation 4.18 is for a perfectly rough lining however problems in which slip occurs at the interface can also be solved using this method (eg. see Rowe et al., 1978).

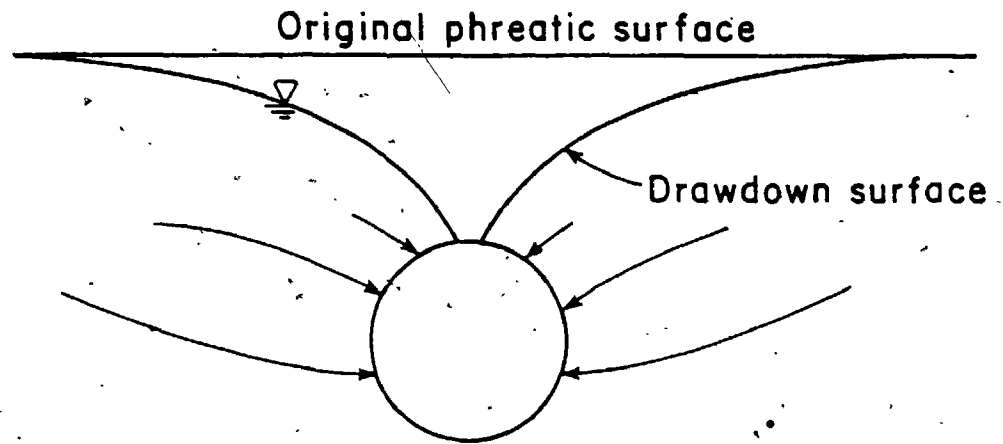
If the tunnel lining is assumed to be rigid, then equation 4.18 reduces to

$$\begin{bmatrix} I_E & -A \\ -A^T & 0 \end{bmatrix} \begin{bmatrix} \dot{F}_u^{(n)} \\ \dot{\theta}^{(n)} \end{bmatrix} = \begin{bmatrix} -\dot{\rho}_K^{(n)} \\ -A^T \dot{W} \end{bmatrix} \quad (4.19)$$

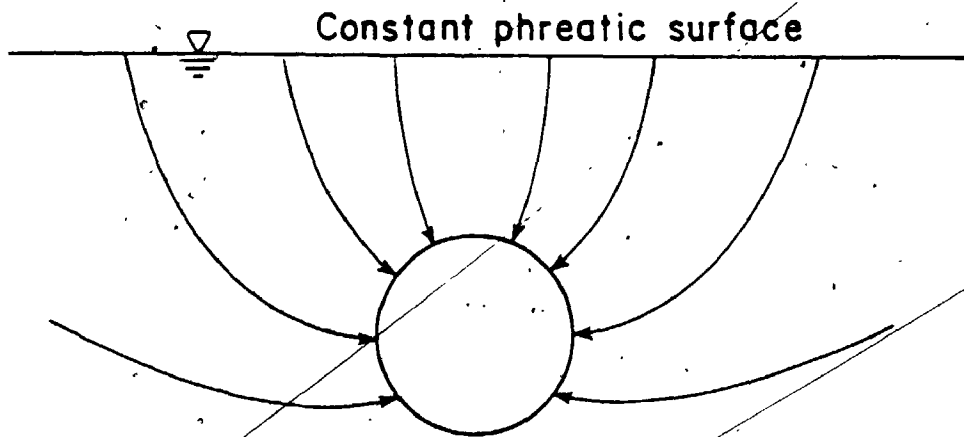
This approach derives its power from the fact that it is only necessary to triangularize the elastic stiffness matrix once for all

iterations and load steps. Furthermore, consideration may be given to a wide range of interface conditions (including gap closure and slip) without the introduction of special joint or contact elements and without reforming the stiffness matrix.

The concepts and theory described in this chapter will be used in conjunction with the results from field and laboratory studies to analyze the behaviour of the Thunder Bay sewer tunnel in Chapter 10.



a) Flow trend with moving free surface



b) Flow trend for recharge condition

FIGURE 4.1 Flow Trends for Drawdown and Recharge Conditions
(after Lo and Rowe(1982))

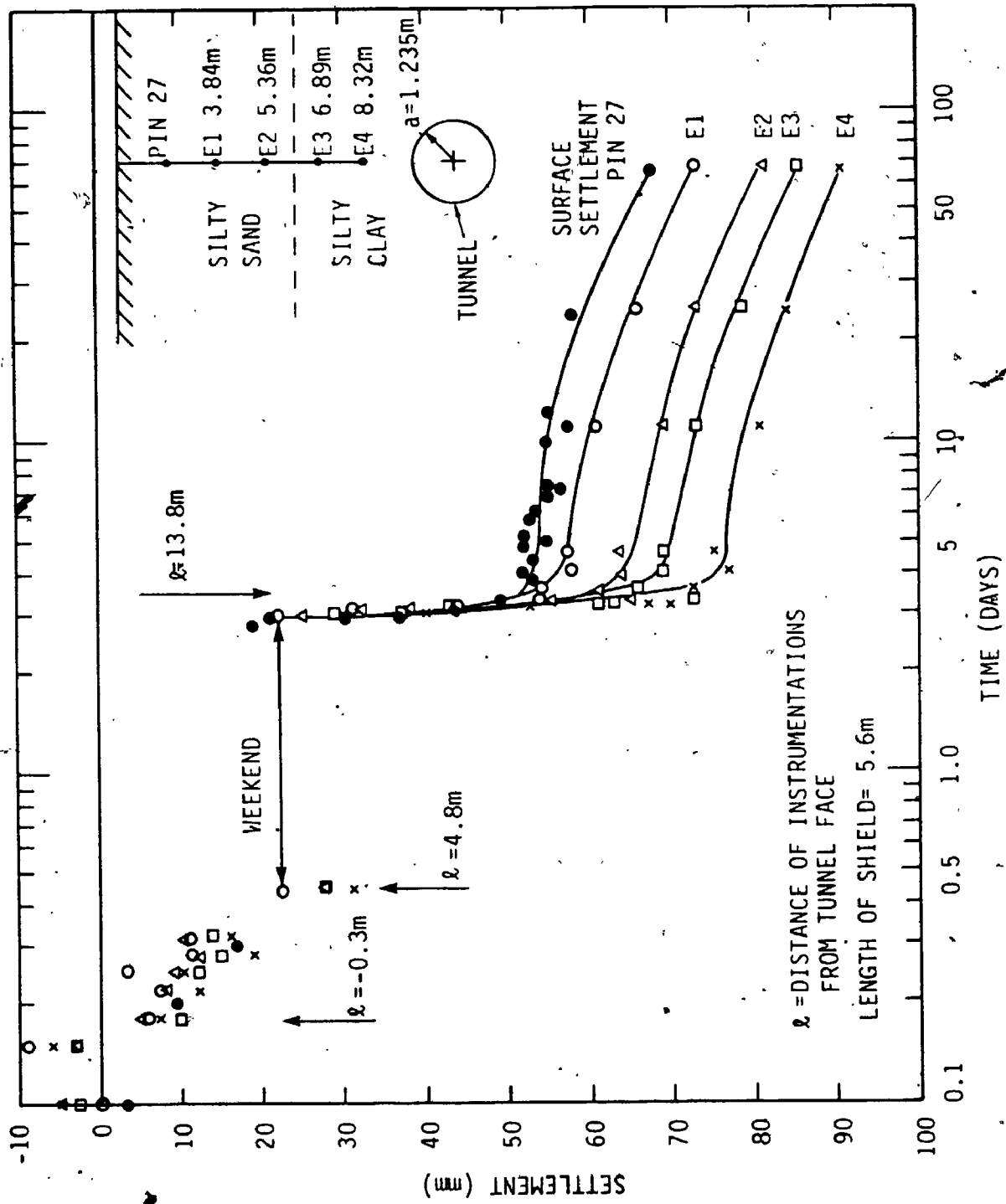


FIGURE 4.2 Plot of Centreline Settlements at Array 1 with Time Showing the Effect of Consolidation of Remoulded Soil

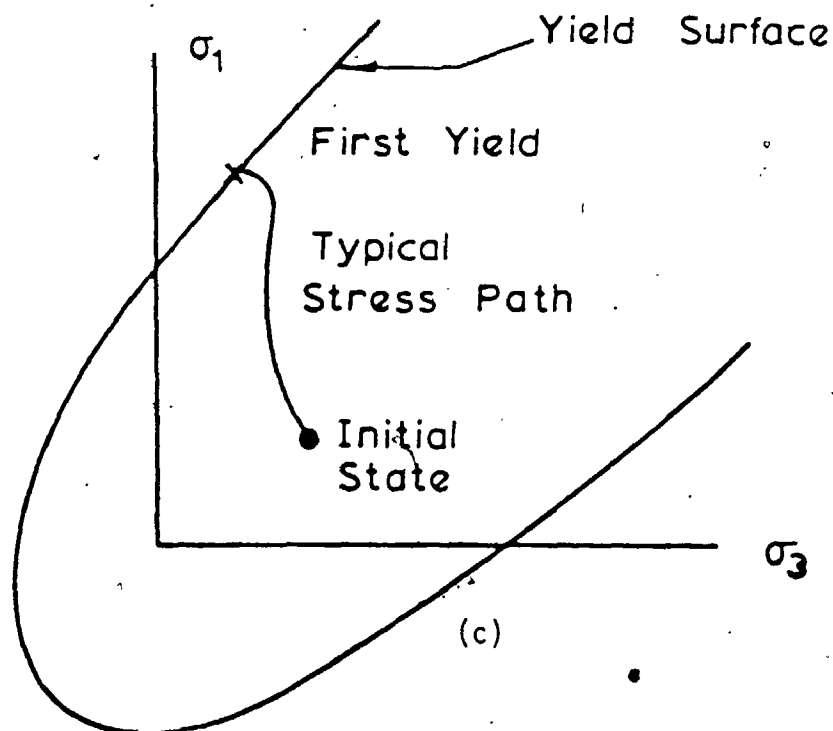
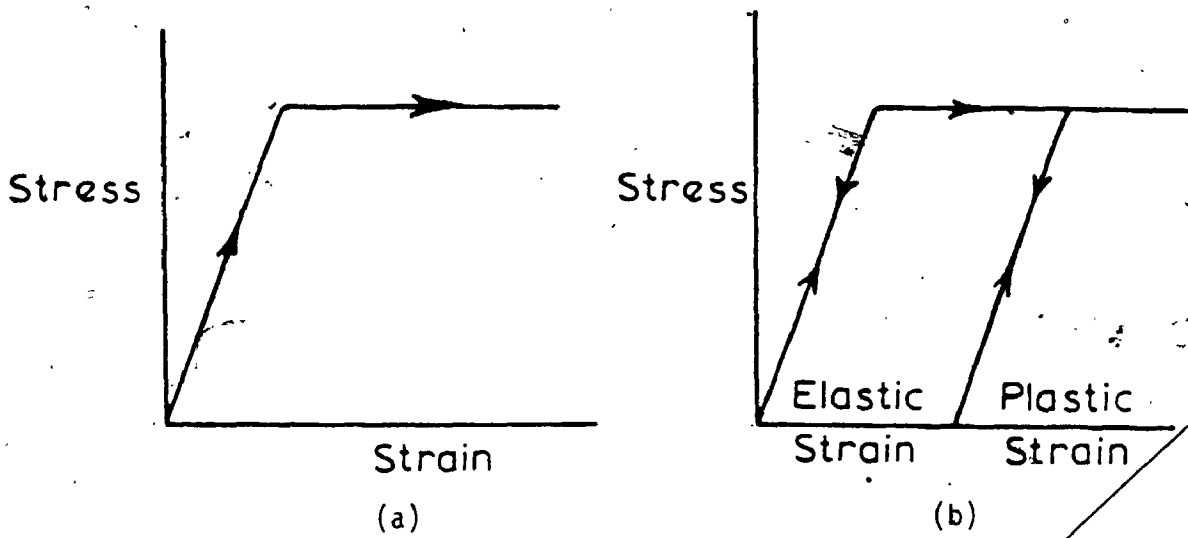
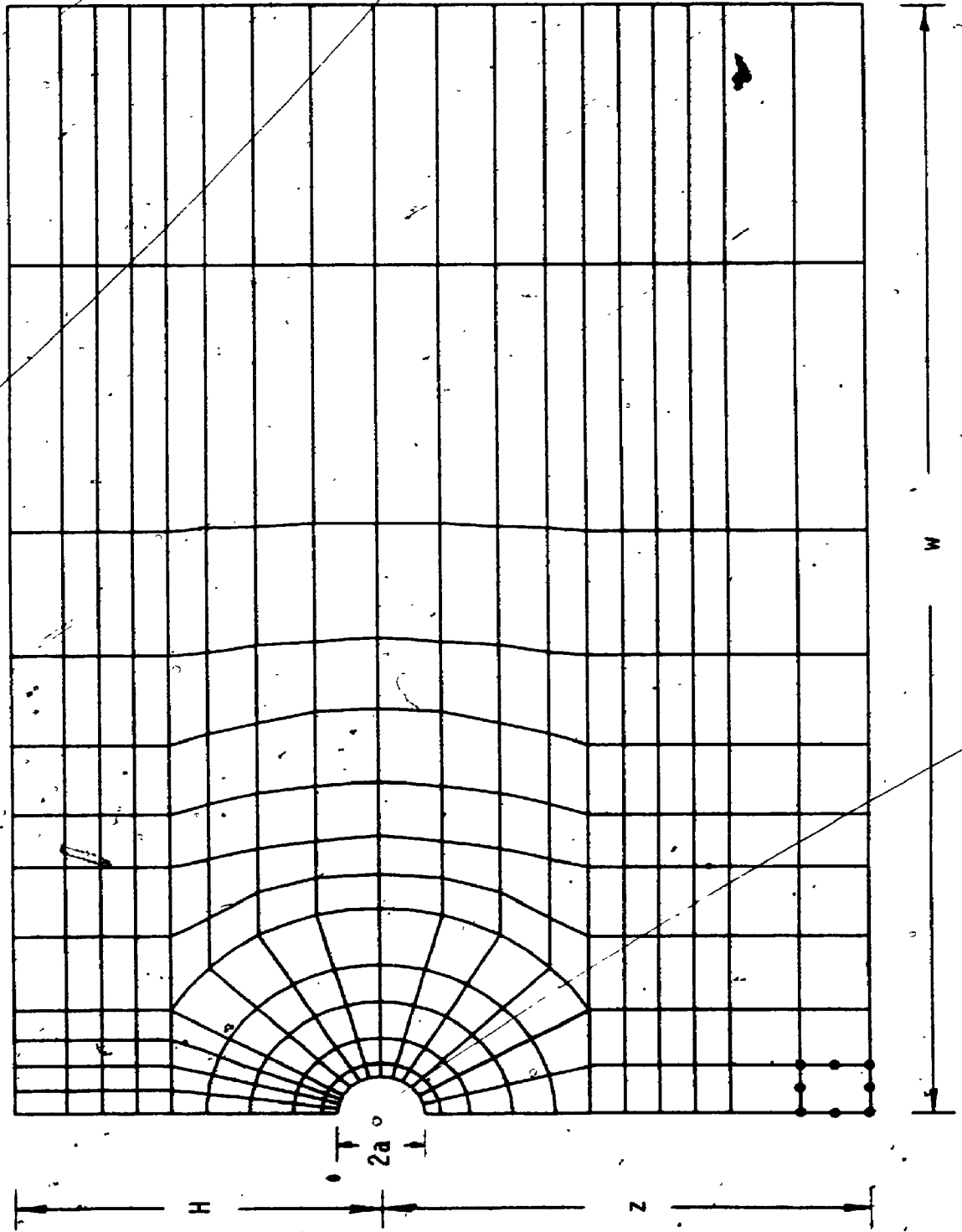


FIGURE 4.3a,b Stress Strain Relationships for a Perfect Elastic Plastic Solid

FIGURE 4.3c Yield Surface for a Perfectly Plastic Material

$a = 1.235 \text{ m}$ $z = 14 \text{ m}$ $w/a = 30$
 $H = 10.5 \text{ m}$ $w = 37 \text{ m}$ $w/H = 3.5$



CHAPTER 5

TEST REQUIREMENTS FOR THE DETERMINATION OF SOIL PARAMETERS IN SOFT GROUND TUNNELLING

5.1 INTRODUCTION

The stress-strain relationships of soils are generally nonlinear, elasto-plastic with strain hardening or softening, and they also exhibit hysteresis on unloading. The response of an element of soil to stress changes in the field or laboratory is dependent on the loading direction and stress level. To study the shear behaviour of soils, these factors should be considered. In addition, with improvements in numerical techniques in the recent decade, the demand for realistic representation of soil behaviour has prompted the use of elasto-plastic constitutive laws in geotechnical analysis. However, the practicality of these soil models is often diminished because of either the lack of appropriate soil parameters or the adoption of parameters obtained from inappropriate testing procedures. Therefore, it becomes necessary to investigate the test requirements for determining soil parameters in soft ground tunnelling for use in an analysis.

The potentially significant factors affecting the prediction of settlements due to tunnelling in soft clay have been investigated by Rowe, Lo and Kack (1982). In this chapter, important considerations in the field behaviour of soil deposits, relevant to a tunnel analysis,

will be discussed. These factors are: 1) the stress path experienced by the soil during construction, 2) the elastic orthotropic anisotropic parameters, 3) the plastic parameters and 4) the insitu stress condition of the soil deposits.

5.2 STRESS PATHS IN TUNNEL EXCAVATION

A stress path is a locus of points in a two-dimensional stress space. Each point defines the current state of stresses and the direction of stress change. The non-elastic response of soils, as discussed previously, renders the deformation behaviour to be stress-path dependent. By subjecting a soil specimen in a laboratory test to a typical field stress path, the deformation and strength parameters may be appropriately determined. Some typical stress paths in the tunnelling problem may be examined.

As a tunnel face is advanced, the initial stresses around the circumference of the tunnel are progressively relieved. The state of stresses at typical locations A (springline), B (crown) and C (45°), as shown in Figure 5.1, will change continuously until a plane strain condition is attained when the face is at a distance of several times the radius of the tunnel past the section under consideration.

The stress paths for different types of conventional triaxial tests (CIDC, CIDE, CK₀DC, CK₀DE, and similarly for undrained tests) are shown in a principal stress plot in Figure 5.2. Starting from a

prescribed mode of consolidation (isotropic-consolidated, I, or consolidated under zero lateral strain, K_0), the effective stress paths of the drained tests and total stress paths in the undrained tests are straight lines meeting the failure envelopes as shown. The effective stress paths for four undrained tests performed are shown in the same figure. All stress paths showed a uniform geometric pattern and apart from K_0 -extension tests in which a sudden principal stress rotation occurs, no principal stress rotation occurs in all these tests.

By using an elasto-plastic finite element analysis in which the excavation process is simulated by reducing the initial stresses in increments, the stress paths at the typical elements A, B and C may be traced and are shown in Figure 5.3. All effective stress paths start from the K_0 -line, their initial positions being governed by the initial effective stress (i.e. the depths at which they are originally located). The short bars on the stress paths indicate the direction of the major principal stress σ_1 .

At the springline (A), excavation induces a reduction in the radial stress (σ_3) and an increase in the tangential stress (σ_1). The stress path rises to the failure line at A' at which the element fails. Further yielding occurs along the failure envelope until the soil surface comes into contact with the lining. Then soil-structure interaction occurs with a slight redistribution of stresses to A". Along the whole process of stress changes, no rotation of principal

stress occurs.

Near the crown (B), excavation produces a reduction of σ_r (σ_1) and a small increase in σ_θ (σ_3) at the early stage. However, the reduction of σ_r is rapid, as is intuitively clear, and a point is quickly reached when $\sigma_r = \sigma_\theta$ at which σ_r becomes σ_3 and σ_θ becomes σ_1 . The principal stresses rotate by 90° and σ_1 (σ_θ) remains nearly horizontal. The stress path meets the failure envelope at B', then yields along the envelope until the soil surface comes into contact with the lining. Soil-structure interaction occurs and the final state of stresses is represented by B". Similar discussion may be made for C (45° point) in which stress rotation of about 45° occurs.

Comparing the conventional stress paths in Figure 5.2 to those representative of field conditions in Figure 5.3, it is clear that none of the conventional triaxial tests approximates the field condition. It is imperative, therefore, to study the effect of stress paths on the deformation properties of the soil and perform stress path tests to delineate the deformation and strength characteristics. Special tests have therefore been performed for this purpose and the results are discussed in Chapter 8. It may also be noted that published results from the analysis of performance records of tunnels in clays should be treated with caution since few, if any, of the published results take into account the effects of stress paths.

5.3 ANISOTROPY OF ELASTIC DEFORMATION IN SOFT CLAY

The deformation behaviour of most natural clay deposits is

anisotropic to varying degrees. It is important that this aspect of behaviour be examined.

It has been discussed in Chapter 4 that the stress and strain vector of an elastic element may be related by the matrix D_e . For an isotropic material under plane-strain condition, D_e is given by:

$$D_e = \frac{-E(1-\nu)}{(1+\nu)(1-2\nu)} \begin{bmatrix} 1 & \nu/(1-\nu) & 0 \\ \nu/(1-\nu) & 1 & 0 \\ 0 & 0 & (1-2\nu)/2(1-\nu) \end{bmatrix} \quad (5.1)$$

For clays that are cross-anisotropic, with an axis of symmetry normal to the plane of the strata, the matrix D_e is different from equation 5.1. The form of D_e suitable for adoption in a plane-strain finite element formulation can be found in several standard texts (eg. Zienkiewicz, 1977). It is given by:

$$D_e = \frac{-E_v}{(1+\nu_{hh})(1-\nu_{hh}-2n\nu_{vh}^2)} \begin{bmatrix} n(1-n\nu_{vh}^2) & n\nu_{vh}(1+\nu_{hh}) & 0 \\ n\nu_{vh}(1+\nu_{hh}) & (1-\nu_{hh}^2) & 0 \\ 0 & 0 & m(1+\nu_{hh})(1-\nu_{hh}-2n\nu_{vh}^2) \end{bmatrix} \quad (5.2)$$

where $n = E_h/E_v$ (ratio of vertical Young's modulus to horizontal Young's modulus)

$m = G_{vh}/E_v$ (ratio of independent shear modulus to vertical Young's modulus)

and ν_{vh} , ν_{hh} are respectively Poisson's ratio for effect of vertical strain on horizontal strain and Poisson's ratio for effect of horizontal strain on horizontal strain in the plane of isotropy.

For a material whose properties are independent of loading directions, five independent parameters are required in equation 5.2, namely, E_v , E_h , G_{vh} , ν_{vh} , ν_{hh} . However, since soil parameters are generally different in the loading and unloading direction, a total of ten independent elastic parameters is needed to define the deformation behaviour completely (Lo et al., 1977).

Conventionally, the deformation moduli and Poisson's ratios are generally evaluated from 'external strain' and 'external volumetric measurements' in triaxial tests. These parameters thus possess inherent inaccuracy because the externally measured displacement quantities are affected by the non-uniformity of strain distribution in the sample due to end-restraints or bulging effects. Further, it is not possible to distinguish clearly the principal strains in different directions through 'external' measurements so that the estimation of anisotropic Poisson's ratios is very difficult. These conventionally determined anisotropic parameters are only useful when they are interpreted with good judgement and experience and the inaccuracy of the parameters is expected to increase with increase in the degree of anisotropy of the clay.

The determination of true anisotropic elastic parameters requires the accurate measurement of the three principal elastic

strains in a soil specimen. Since deformation measurements, especially the lateral deformations, cannot be made with precision in conventional triaxial tests, a special anisotropic parameter apparatus has to be devised. This apparatus and an experimental arrangement designed for anisotropic parameters determination have been described by Lo et al. (1977) and Yuen et al. (1978). In this test apparatus, light gauge points are attached on the soil sample and the displacements during shear are measured directly by sensitive electronic displacement transducers floating in the cell fluid. Since 'internal strain' is being measured, the gauge length can be chosen over the midsection of the specimen where uniformity of strain can be expected during small shear deformation. It is believed that this testing procedure can provide a more accurate evaluation of the true elastic anisotropic parameters compared with other conventional methods.

The independent shear modulus, G_{vh} which relates the elastic shear stress and shear strain in equation 5.2 is an important deformation parameter (Rowe, Lo and Kack, 1983) that influences the shape of a settlement trough. It may be evaluated from the measurements obtained by the anisotropic parameter apparatus as discussed above or alternatively, it may be measured directly from a simple shear test. The NGI simple shear apparatus described by Bjerrum and Landva (1966) uses a circular clay sample surrounded by a reinforced membrane. Horizontal and normal loads are applied to the confined sample so that it is compelled to deform in a 'simple shear' mode. Although

there are researchers (eg. Budhu, 1984; Saada and Townsend, 1981), who have suggested that the simple shear device does not provide uniform stress and strain conditions in the sample; their comments may only apply to large strain measurements. Since it is only the elastic deformation at very low shear strain that is of interest, the NGI apparatus is expected to yield representative stress-strain relationships. The shear modulus G_{vh} determined by the simple shear apparatus and the anisotropic parameter apparatus can be compared so that the validity and consistency of this parameter may be evaluated before it is used in an analysis.

5.4 PLASTIC BEHAVIOUR IN SOFT CLAY

When an element of soil is loaded to the maximum shear stress it can withstand, large deformation takes place and failure occurs. The element is now at the plastic state. In the analytical model described in Chapter 4, the yield function and the plastic potential are assumed to be identical according to theory of perfect plasticity. The complete set of plasticity parameters is therefore the effective stress parameters c' and ϕ' (or the failure envelope if the envelope is curved) and the dilatancy angle ψ .

Many constitutive models have been proposed. For example, the cap model (Baladi and Rohani, 1979), the Cam clay model (Schofield and Wroth, 1968) and Prevost's model (Prevost, 1978) are a few such models. The determination of soil parameters in some models is an

extremely tedious task. The success of such a procedure is strongly dependent on the experience of the researcher. It is not the intent of this thesis to study the procedure of parameter determination in these models or their theoretical limitations. Rather, the conventional strength concept in geomechanics, as appropriate to tunnelling in a soft clay will be examined. These parameters, ϕ' , c' and c_u are applicable to the elastic perfectly-plastic model.

The effective stress parameters c' and ϕ' may be experimentally determined by triaxial tests. Rowe, Lo and Kack (1983) have shown that for the stratigraphy of Thunder Bay soil, where limited, yet notable extent of plasticity occurs, it is incorrect to adopt arbitrary 'conservative' angle of friction. For example, in a finite element study, increases in ϕ' of the clay surrounding the tunnel while keeping other parameters constant have actually resulted in increased centreline settlement. Therefore, these soil parameters should be precisely deduced. Further, it is suggested that the strength envelope should be determined from a study of test results from compression, extension and controlled stress triaxial tests. This procedure will reveal if c' and ϕ' are in fact "intrinsic" parameters of the clay, or subjected to stress path effect.

In the application of the undrained shear strength c_u in a $\phi = 0$ analysis, 'inherent' and 'stress' anisotropy in strength should be noted. A clay may be homogeneous, stratified and possessing joints and fissures.

For inherent anisotropy, the first order structure usually has the most dominant effect on strength. It follows that a macroscopically homogeneous clay will show less directional strength changes than a stratified or fractured clay. Strength variation with orientation has been widely studied (eg. Lo, 1965; Lo and Milligan, 1967). The other aspect of strength anisotropy - the stress anisotropy, is due to the initial stress system. A solution for variation of undrained strength with direction has been presented by Hansen and Gibson (1949).

The critical plasticity parameters for an elasto-plastic analysis of lined tunnels are those for the soft clay adjacent and above the excavation. The parameters in the soil well below the invert are not as important since failure seldom occurs there. In the choice of undrained strength, the variation of c_u (as well as deformation parameters) with depth, especially for soils above the springline must be carefully considered. These soil properties directly influence the extent of plastic behaviour within the soil and the pattern of soil deformation. The variation in undrained strength may be obtained in the field by vane tests or in the laboratory by triaxial tests on good quality samples at different elevations in the ground.

5.5 INSITU STRESS CONDITION

The coefficient of earth pressure at rest K_0 of a cohesive material is not directly related to any fundamental soil property.

It should be evaluated as a basic parameter. The estimation of K'_0 is essential for calculating the insitu stress condition before stress relief occurs and K'_0 is also important in defining the ratio of initial principal stresses in a stress-path test. Due to plasticity in the soil mass adjacent to a tunnel, the soil movements are dominated by the plastic flow characteristics (i.e., the flow rule). There may not be a consistent relationship between K'_0 and the lining closure or the soil displacement pattern in the vicinity of the tunnel. However, the value of K'_0 will influence behaviour in elastic regions or elastic behaviour prior to occurrence of plasticity in soil. Therefore, the determination of K'_0 cannot be omitted.

The hydraulic fracturing test technique (Bjerrum and Anderson, 1972) may be suitably applied for field measurement of the K'_0 condition in soft clay. This method is generally applicable for normally consolidated fine-grained soils which are characterized by a value of K'_0 less than 1.0 and having a low permeability.

5.6 SUMMARY

In the analysis and design of tunnelling in soft ground, it is essential to obtain an accurate conception of the geotechnical behaviour of the subsoil.

To disclose completely the general soil stratigraphy and the detail response of the soil mass to the construction activities, conventional site exploration techniques, laboratory tests, as well

as special testing procedures are required in the testing program.

The main emphases in the special tests are the determination of

- 1) Anisotropic deformation behaviour;
- 2) Stress-strain-strength behaviour of soil under designated stress paths. These stress paths are considerably different from those followed in conventional triaxial compression tests;
- 3) Plasticity parameters.

In addition, the variations of strength and deformation properties with depth and insitu stresses are also important information to be determined.

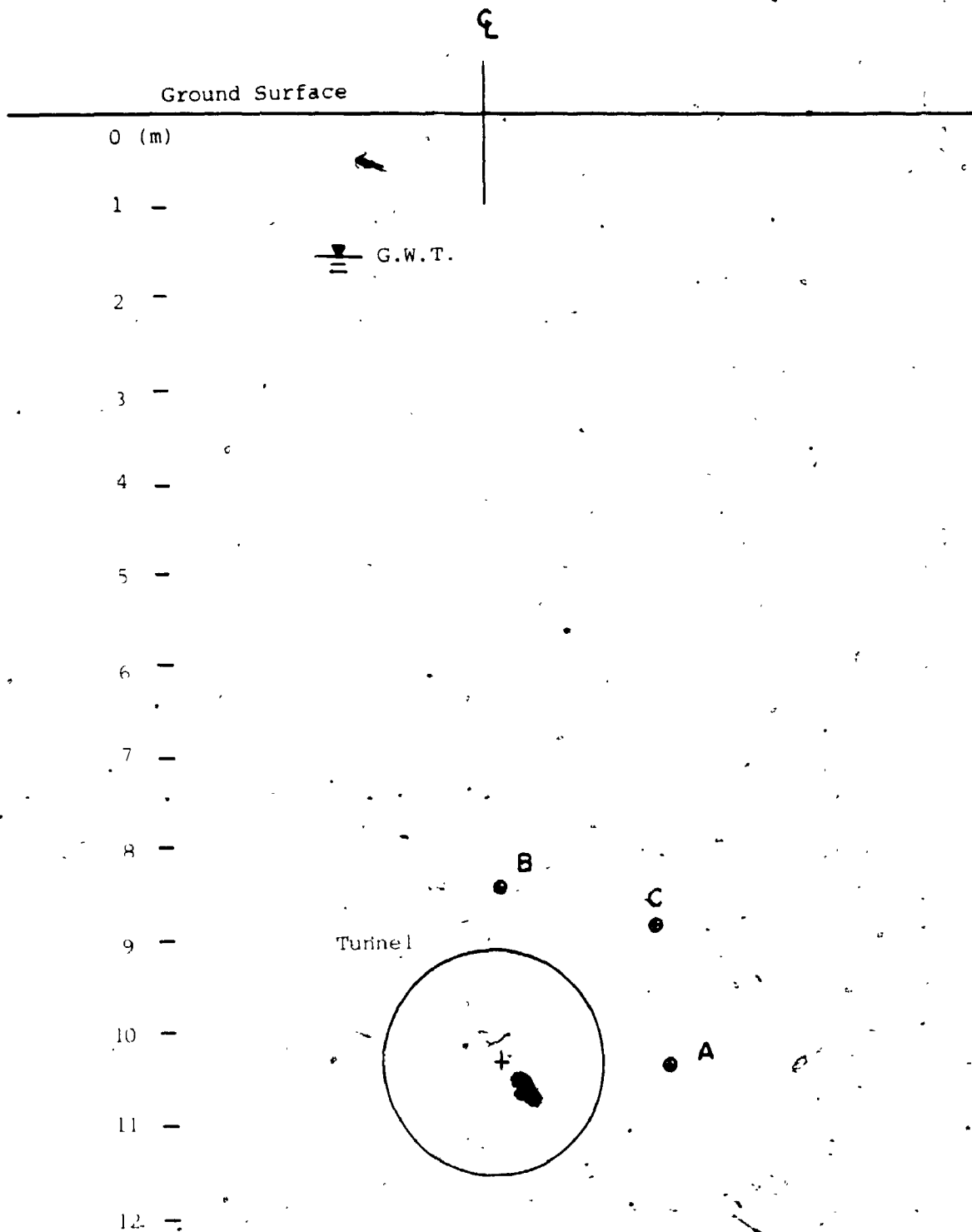


FIGURE 5.1 Location of Typical Points at (B) Crown, (A) Springline and Point (C)

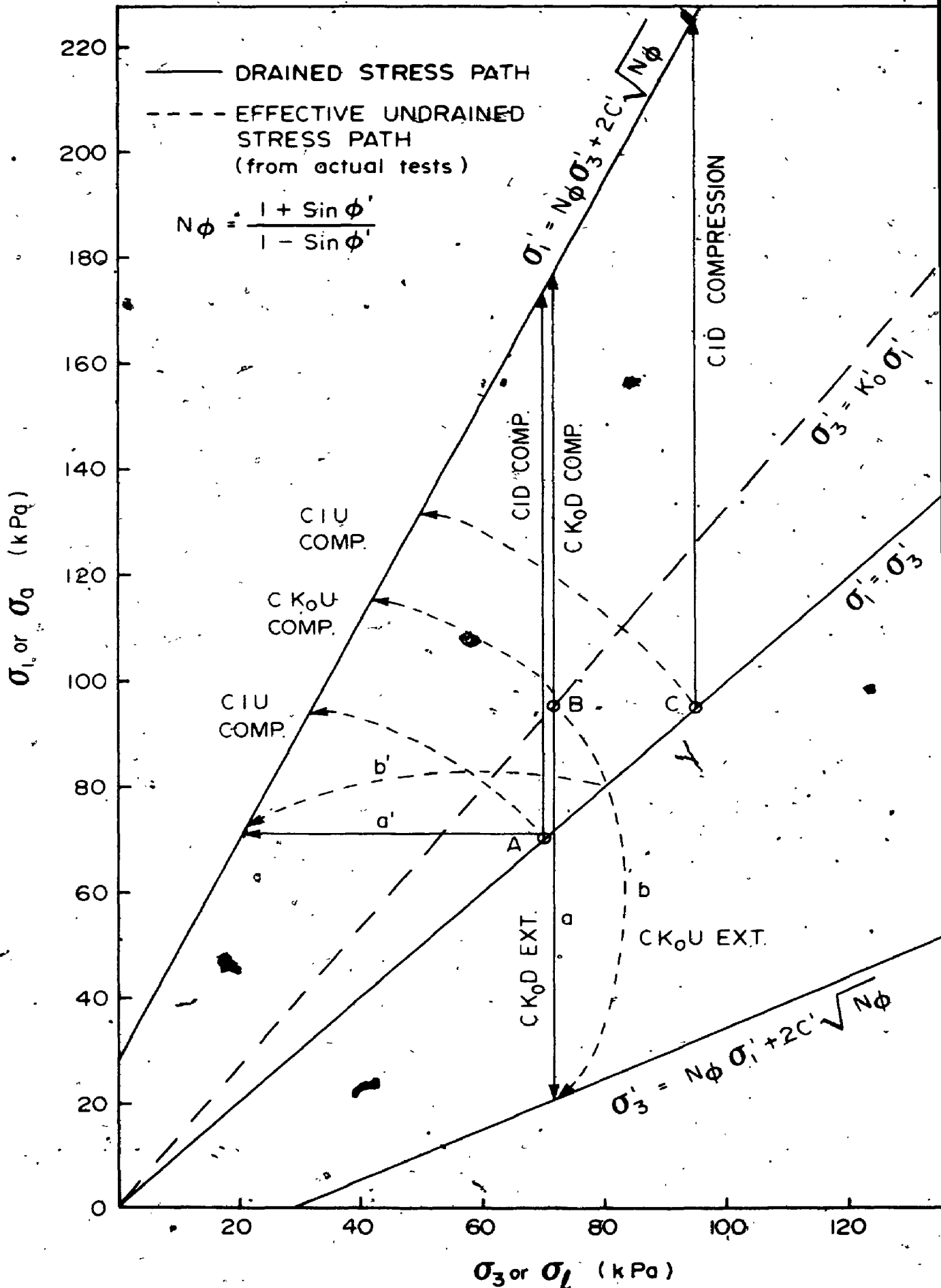


FIGURE 5.2 Stress Paths for Conventional Triaxial Tests

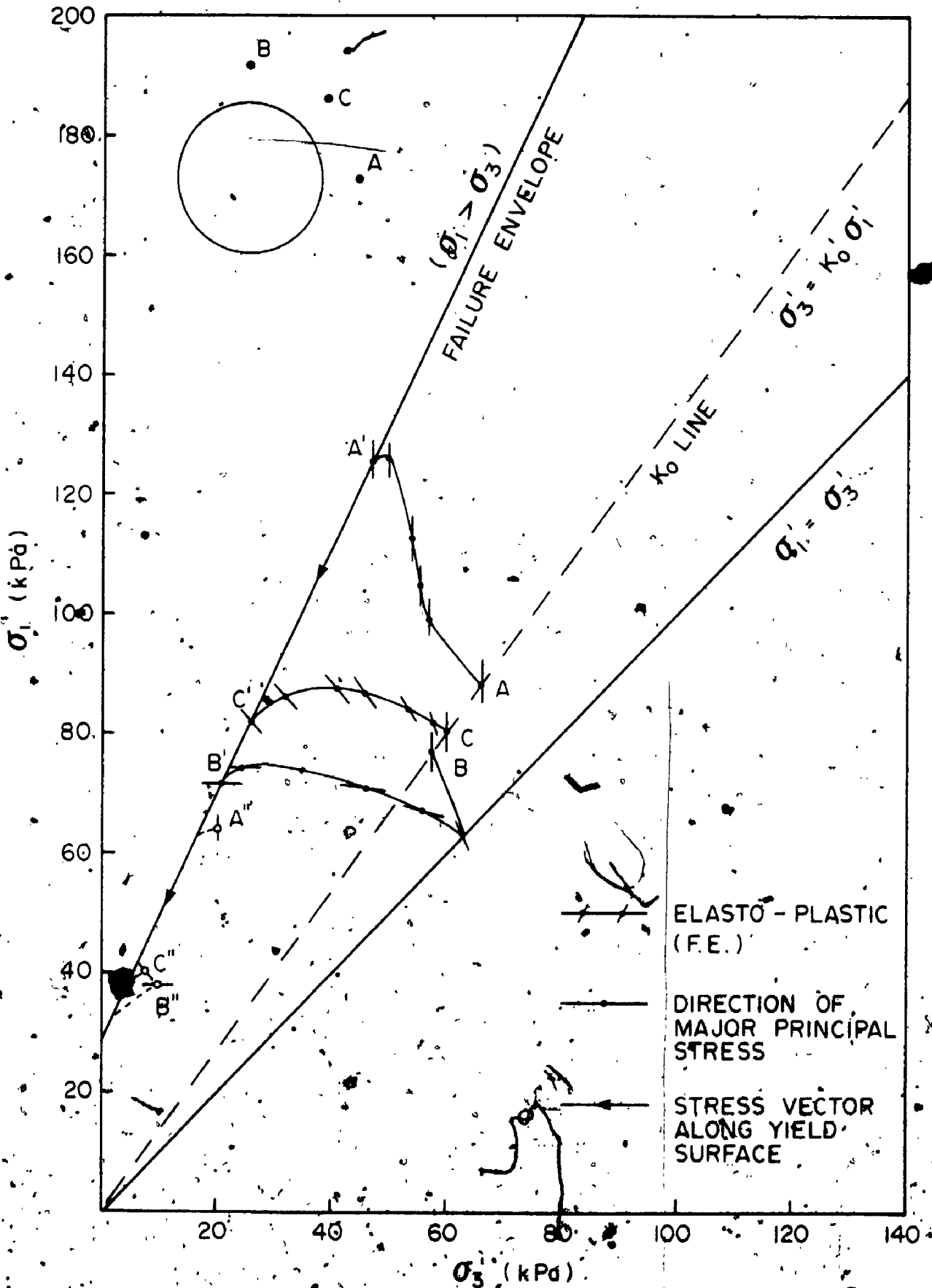


FIGURE 5.3 Stress Paths for Typical Elements in Soil Due to Tunnelling

CHAPTER 6

SITE INVESTIGATION AND GENERAL SOIL PROPERTIES

An extensive field program for the investigation of Thunder Bay Tunnel was carried out to define in detail the stratigraphy and properties of the subsoil in two instrumented locations. The program included:

- 1) the subsurface exploration with standard penetration tests, vane tests and determination of groundwater condition;
- 2) the in-situ measurement of horizontal stress using hydraulic fracturing;
- 3) the recovery of samples with 75 mm large diameter piston sampler for laboratory study.

The results of field investigation together with the general soil properties are presented in this chapter.

6.1 STRATIGRAPHY

6.1.1 Geology of Fort William, Thunder Bay

Fort William, Port Arthur and the surrounding municipalities have been incorporated for administrative purposes into the City of Thunder Bay. Thunder Bay is essentially a drowned lowland, bounded on the north by the unconformity between the Animikie and the Archean, on the east by the Sibley escarpment, and on the west by the deltas of the Kaministikwia, Neebing, and other rivers.

A distinctive feature of Fort William is the extreme evenness of the terrain. Fort William and part of Port Arthur are on the fore-front of an enormous delta occupying lowlands drained by the Kaministikwia River and Neebing and McIntyre Rivers. The delta extends inland to and beyond the village of Stanley over a distance of 26 kilometers and is the largest and most impressive delta flatland found along the north shore of Lake Superior. (Moorehouse, 1970; Pye, 1969)

The study sites are located within the alluvial-deltaic plains formed at the confluence of the Neebing, McIntyre and Kaministikwia Rivers where they flow into Lake Superior.

The surface and subsurface deposits of this deltaic plain are postglacial fine fluvio-deltaic sands overlying deltaic-lacustrine silt and deeper late glacial and postglacial beds of laminated clays and varved clays. These well laminated varved silts and clays are characterized by their regular bedding and they were laid down in an enlarged high water level stage of Lake Superior during the Wisconsin Ice sheet retreat. At maximum development in the centre of the delta, the glacio-lacustrine sediments approached a total thickness of about 30 metres. The glacio-lacustrine deposits also appear to be chemically and mineralogically constant, indicating that the source of the materials was common. Quigley (1980) suggested that the varved clays were derived essentially from rock flour (quartz, feldspar, amphibole) ground off from the Precambrian Rocks of the Canadian Shield and supplemented by

carbonate and smectites from the Hudson Bay lowlands.

The composition of minerals of the soils determined by chemical, mineralogical and x-ray diffraction analyses is given in Tables 6.1 and 6.2. A substantial quantity of mixed-layer illite-chlorite and illite-montmorillonite is present and the major component is illite. Comparison of the proportions of clay minerals in the silty clay and varved clay is shown below. These results are similar to those presented by Soderman and Quigley (1965).

Mineral	Varved Clay (%)	Grey Silty Clay (%)
Illite	44	40
Chlorite	18-30	10-20
Vermiculite	11	7
Montmorillonite	6-10	4-7

Except for chlorite content, the percentages of (illite, vermiculite, montmorillonite) the different clay minerals are very close. The non-clay mineral in the soils contains an abundant amount of carbonate (~20%). Quartz and feldspar are also present.

Beneath the clay stratum is an irregular layer of glacial till which overlies weathered black shale which in turn overlies sound bedrock. The bedrock shales of the Late Precambrian Gunflint Iron Formation are characterized by diabase intrusions. The bedding in shale is essentially horizontal, but with local variations reflecting the deeper basal interface with earlier Precambrian rock surface. (Moorehouse, 1970; Morton and Dodds, 1976)

6.1.2 Tunnel and Borehole Locations

The 2.16 m internal diameter sanitary trunk sewer was constructed in the City of Thunder Bay in the period of 1976. "Array 1" and "Array 2" shown in Figure 6.1 are the location of two sections of the tunnel where instrumentations were installed.

The site investigation program was carried out at the two arrays. Array 1 is situated in the Lakehead Exhibition Ground and Array 2 is in a bushy area with moderate difficulty of access. The boring positions are chosen at positions outside the zone of influence of the tunnel so that the virgin properties of the soil can be obtained. These positions are at least five tunnel diameters (5D) or an embedment depth (z) away from the centreline of the tunnel where movement due to tunnelling was not recorded (Figures 6.2 and 6.3).

A total of five borings were drilled to various depths at each array. Three 80 mm diameter holes were drilled to install geonor piezometers for the purpose of determining the in-situ K_0 value.

Two 200 mm boreholes were advanced for the purpose of recovering 152 mm diameter samples and vane testings. The depths of sampling and vane testing were staggered in order to achieve effectively continuous sampling and vane testing down to 15 m in Array 1 and 16 m in Array 2. These depths are about one to two diameters beneath the invert of the tunnel.

The deep benchmark is taken as the reference elevation for the

boreholes.

6.1.3 Subsoil Conditions

6.1.3.1 Previous Soil Investigation

The stratigraphy at the site of each array presented by Palmer and Belshaw (1979) is shown in Figure 6.4. The tunnel was constructed within a deltaic plain formed at the confluence of the Neebing, McIntyre and Kaministikwia Rivers in the City of Thunder Bay, Ontario. Some 6-7 m of postglacial fluvial silt and sand is underlain by about 17-18 m of late glacial lacustrine deposits of silty clay and varved clay that extend to the black shale bedrock. The granular deposits are generally very loose to loose in relative density, the cohesive deposits are of soft to firm consistency and are lightly overconsolidated.

6.1.3.2 Present Soil Investigation

From the results of the present soil investigation, the pertinent geotechnical data are summarized in Figures 6.5 and 6.6 and Table 6.3. In general, the soil profiles obtained are very similar to those presented by Palmer and Belshaw (1979).

Site Conditions - Array 1

The stratigraphy at the site of Array 1 is shown in Figure 6.5. Approximately 1 m of fill, consisting of mixed granular materials and

slabs of asphalt and concrete was placed over a large area of Array 1. This layer of fill was added one year after the construction of the sewage tunnel.*

The superficial cohesionless deposits consist of 2 m of greyish brown silty sand and then 2.8 m of grey loose silt underlain by 1.4 m of dense to loose silty sand.

The upper portion of the cohesionless deposit is loose to very loose with "N" values decreasing from the order of 8 blows/ft (8 blows/300mm) near the surface to 0 to 2 blows/ft (2 blows/300mm) at 3 to 5.5 m depth beneath the surface of the granular fill. Below the loose layer, a stiff sand layer is encountered and blow counts of 20 to 40 are obtained. However, immediately beneath this relatively thin but dense layer, and at the interface with the clay layer, the sand is again very loose (N ~ 2 to 3 blows/300mm). The natural ground-water table was at 2.4 m below the surface at the time of sampling.

The cohesive deposit from 6.2 to 7.5 m is a firm red-brown layered silty clay with a liquid limit of about 40% and a plasticity index of about 20%. Beneath the layered clay is a soft laminated grey silty clay with a liquid limit of about 70% to 75% and plasticity index of about 45% to 30%. Below a depth of 11.6 m, a layered clay is found.

* The original ground surface, which was considered as the 'zero depth' when the tunnel was being constructed is now at 'one metre depth' below the present surface due to the addition of the fill. In this chapter, all depths are referenced to original ground surface prior to fill placement.

The amount of layering increases with depth and from 12.5 m, alternating grey and reddish brown layers of silt and clay are apparent. The 'layered silt and clay' or varved clay extends to bedrock and the liquid limit and plasticity index are 30% to 40% and 15% to 20% respectively. Occasional sand seams are present in the cohesive soils.

The laminated grey silty clay is homogeneous in appearance in its natural state. On drying, thin dark silt bands of less than 1 mm are revealed (see Figure 6.8). The varved clay is composed of layered sediments deposited in a freshwater lake (see Figure 6.8). A single varve, representing the accumulation of one year of sediments, generally consists of 'summer silt' and 'winter clay'. A sketch showing the structure of a typical section of the distal varved clay is shown in Figure 6.7. Also plotted is the variation in water content. The higher water content of the clay layer probably reflects an open flocculated structure. In one varve, there is silt-rich summer layer, and a graded transition zone which becomes finer towards a clay-rich layer. The transition and fine layers represent settlement of suspended solids during autumn and winter. The average soil properties of the layers are summarized as follows:

	Silty Clay Layers	Clayey Silt Layers
Layer Thickness	2 to 6 mm	6 to 15 mm
Liquid Limit (%)	63.8	29.6
Plasticity Index (%)	41.5	11.9
Natural Water Content (%)	48.6	29.9

The consistency of the cohesive deposit in general increases with depth from soft above the crown of the tunnel to firm below the invert of the tunnel (Figure 6.5). The pattern of vane strength is quite consistent with the pattern of the preconsolidation pressures, and the vane strengths obtained in the present and previous field study show reasonable agreement. An interesting phenomenon is the 'clay crust' found above the grey silty clay. The 'crust' was probably formed by preconsolidation due to dessication of the clay unit during the warmer periods of Wisconsin Glacial stage when these surfaces were exposed.

The soft grey silty clay is slightly overconsolidated with $OCR \sim 1.3$ to 1.4 . Higher preconsolidation pressure is obtained in the upper clay crust ($OCR \sim 2$). The coefficient of earth pressure at rest, K_0 , is measured to be .75 and .59 in the silty clay and varved clay respectively.

Site Conditions - Array 2

Arrays 1 and 2 are 1.25 km apart, but the soil deposits in both arrays are very similar.

The stratigraphy at Array 2 (Figure 6.6) consists of about 1 m of peat underlain by 7.1 m of silt and silty sand, then 16.3 m of silty clay and varved clay extending to bedrock. The water table was at a depth of 1.5 m.

The consistency of the cohesive deposits in both arrays is very much alike and 'N' values obtained in the silty sand deposit from this field investigation are almost identical with the values reported by Palmer and Belshaw (Figure 6.4).

As in Array 1, the sand deposit is generally loose to very loose near the surface. In the upper 3 to 4 m, the grey sand grades to sandy silt with depth and 'N' values decrease from the surface from 10 blows to 1 blow.

The lower 3.6 m to 8.1 m of the cohesionless deposit may be classified as a loose to dense silty sand, occasional clay seams are present and from one split spoon sample taken at 7 m depth, a 50 mm length of layered red-brown layers of clay was obtained. The 'N' values of 20 and 45 blows obtained at 4 to 5 m are consistent with the high value determined from a relatively stiffer layer that also exists in Array 1.

The clay crust is absent in Array 2 and this is the major difference in soil profile between the two arrays. The 'crust' was probably eroded when the cohesionless deposit was laid down and the clay seams might be reminiscent of the 'crust' which was once present. The cohesive deposit consists of two distinct portions. The upper 3.4 m is a laminated grey silty clay and the lower portion is a varved clay. Between the two units, about 1 m of layered clay made up of red-brown and grey layers is found. The appearance, index and strength properties of the clays in Array 2 are virtually identical with the clays

in Array 1. The shear strength, as indicated by Geonor vane tests varies from 28 kPa to 60 kPa and sensitivity varies from 3.4 to 7.5. These values are in good agreement with the results presented by Palmer and Belshaw (1980) in the soft silty clay but the vane strength of the varved clay is slightly lower than the previous results.

The deposit is slightly overconsolidated. OCR for the laminated grey silty clay and varved clay is 1.4 and 1.8 respectively. K_0 is .75 and .58 for the silty clay and varved clay respectively; these values are identical with those in Array 1 indicating that the in-situ stress system in both sites are the same.

Groundwater Conditions

The data taken from 5 Geonor and 12 Solinst piezometers at the time of boring at Array 2 are shown in Table 6.4. These piezometers were installed prior to the construction of the tunnel by the National Research Council of Canada under the supervision of Dr. Palmer. Since this set of readings was taken four years after the construction of the tunnel, the readings may be assumed to indicate the stabilized groundwater conditions.

The average reading of both the Geonor and Solinst piezometers was at elevation 183.76 m. The range of the readings was 183.62 m to 184.07 m and 183.58 m to 183.97 m for the Geonor and the Solinst respectively. The consistent readings indicate that the groundwater regime at Array 2 is hydrostatic and the groundwater table is 1.56 m below

ground surface.

Readings were also taken from two slope indicators in Array 1. The slope indicator casings were filled with water and it functioned as a standpipe. It extends into the clay stratum and the water elevations in both slope indicators were identically 183.59 m so that the water table was at 2.4 m below the ground surface at the time of site investigation.

Although detailed measurements were not performed at Array 1, it can be inferred that the water pressure in Array 1 is also hydrostatic. The water table in Array 1 is almost at the same elevation as in Array 2.

6.2 COEFFICIENT OF LATERAL EARTH PRESSURE, K_0

The ratio of the horizontal to vertical effective stresses in the ground, K_0 , is known as the coefficient of earth pressure at rest. K_0 in a normally consolidated soil is usually assumed to be a constant, depending only on the type of the soil.

The dependence of the predicted surface settlement in soft ground tunnelling upon the value of K_0 has been demonstrated (Rowe et al., 1983). Since K_0 in a cohesive soil is not explicitly related to any fundamental soil property, it must be evaluated independently as a basic parameter.

Bjerrum and Anderson (1972) have proposed a simple method for

in-situ measurement of lateral earth pressure based on the principle of hydraulic fracturing. Only simple and inexpensive equipment is required and the technique has been used successfully by Palmer and Lo (1974) and Becker (1981), among others.

The hydraulic fracturing test suggested by Bjerrum and Anderson (1972) was based on the principle that after a fracture in the soil has been formed by the application of a hydraulic pressure, as the pressure dissipated, the pressure at which the fracture closed is considered to be a reliable measure of the in-situ effective minor principal stresses in the soil. The method has some limitations, but it is applicable to relatively impermeable clays.

Details of the apparatus and field technique are included in Appendix B. A total of six tests of the earth pressure (three at Array 1 and three at Array 2) was made. The results are summarized in Table 6.5. The tests performed within the grey, laminated silty clay showed an average value of K_0 of 0.75. Within the layered clay and the varved clay, the measured K_0 were .74 and .58 respectively.

Though a metre of fill was added to Array 1, the K_0 values at both arrays were very close, showing that the fill had a negligible effect on the in-situ stress ratio at the tested location.

From a collection of K_0 values of some Ontario and Norwegian soils, it is noticed that K_0 appears to be related to the plasticity index of the clay (see Table 6.6).

The K_0 values of the Norwegian soils are in the range 0.4 for the quick clays and 0.5-0.6 for the non-quick clays. The P for the non-quick lean or plastic Norwegian clays ranges from 11 to 16 while the two quick clays assume low $P.I.$ of 5 and 6. The K_0 - P results for the Thunder Bay varved clay ($K_0 = .58$, $P.I. = 16$) appear to be consistent with the K_0 values obtained by Bjerrum and Andersen (1972).

The K_0 values for the silty clay and layered clay have $P.I.$ about 40 and 30. These K_0 values (.73-.76) are close to the K_0 ($K_0 = .7$) of the New Liskeard clay whose $P.I.$ is 30.

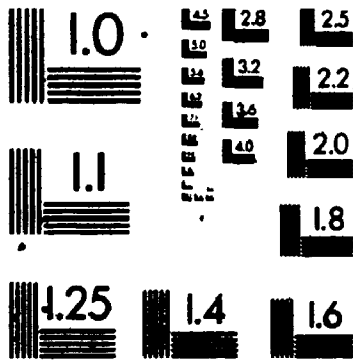
The value of K_0 may also depend on the OCR . Becker (1981) reported higher K_0 values in the crust of the Wallaceburg silty clay (see Table 6.6).

From the above discussion, it is evident that the results obtained at Thunder Bay are generally consistent with those obtained for other normally and slightly overconsolidated soft to firm clays.

6.3 SUMMARY OF FIELD INVESTIGATIONS AT ARRAY 1 AND ARRAY 2

1. The stratigraphy at Arrays 1 and 2 is very similar. The surface conditions generally consist of cohesionless silty sand overlying silty clay which is underlain by varved clay.
2. The tunnel was excavated in the soft, moderately sensitive clay. The varved clay found beneath the invert of the tunnel

3



is a firm, sensitive, layered silt and clay. Both the silty clay and varved clay are slightly overconsolidated.

3. The major difference in the stratigraphy at Arrays 1 and 2 is the amount of clay cover above the crown of the tunnel which varies from 3.3 m at Array 1 to 1.1 m at Array 2. The top of the clay cover in Array 1 appears as a firm 'crust'.
4. The initial stress system in the silty clay and varved clay is anisotropic. The method of hydraulic fracturing was employed to determine the in-situ K_0 condition. It is found that K_0 for the silty clay and varved clay is 0.75 and 0.58 respectively. The K_0 values obtained at Thunder Bay are generally consistent with those reported for other normally and slightly overconsolidated soft to firm clays.
5. The groundwater condition measured four years after construction was found to be essentially hydrostatic.

TABLE 6.1a Composition of Non-Clay Minerals in Whole Soil in Varved Clay (-74 μ)

Mineral	Percentage
Calcite	9.3 Total Carbonate =19.3 (20)
Dolomite	10.0
Quartz	23
Plagioclase-feldspar	10
K-feldspar	Trace

TABLE 6.1b Composition of -2 μ Fraction Soil

Mineral	Percentage
Illite (including illite inter-stratified with montmorillonite and chlorite)	44
Chlorite (including chlorite inter-stratified with illite)	18 - 30
Vermiculite	11
Montmorillonite (including montmorillonite interstratified with illite)	6 - 10
Carbonate	4-10
Quartz	4-10
Plagioclase-feldspar	<3
Potash-feldspar	Trace

*Small quantity of amphibole may be present

TABLE 6.2a Composition of Non-Clay Minerals in Whole Soil
in Silty Clay (-74 μ)

Mineral	Percentage
Calcite	13.5
Dolomite	6.1
Quartz	15
Plagioclase-feldspar	6
K-feldspar	5

Total Carbonate = 19.6 (20)

TABLE 6.2b Composition of -2 μ Fraction Soil

Mineral	Percentage
Illite (including mixed-layer illite-chlorite)	40
Chlorite (including mixed-layer illite-chlorite)	10 - 20
Vermiculite	7
Montmorillonite (including mixed-layer illite-montmorillonite)	5 - 7
Carbonate	20
Quartz	9
Plagioclase-feldspar	4
Potash-feldspar	2

*Small quantity of amphibole may be present

TABLE 6.3 Summary of General Soil Properties

	Silty Clay	Varved Clay
Color	Grey	Reddish brown-grey
Natural Moisture Content (%)	56	34
Plastic Limit (%)	20-25	15-20
Liquid Limit (%)	65-75	30-40
Plastic Index (%)	45.2	16.5
Liquidity Index	.86	.96
Specific Gravity	2.78-2.80	2.80-2.81
Unit Weight (kN/m^3)	16.2	18.7
OCR	1.4	1.8-2.0
K_o	.75	.58
C_c	.79	.24
Vane Strength (kPa)	25-50	>38
Sensitivity	3.4-7.2	4.7-8.6
c' (kPa)	12	14
ϕ' (deg.)	28°	30°

TABLE 6.4 Groundwater Level in Array 2

Geonor Piezometers

Station	Elevation of Water Level (m)
G1	183.62
G2	183.85
G3	183.63
G4	184.07
G5	183.65
	Avg = 183.76

Solinst Piezometers

Station	Elevation of Water Level (m)
S1	183.95
S2	183.95
S3	183.64
S4	183.97
S5	183.66
S6	183.97
S7	183.65
S8	183.59
S9	(probably destroyed)
S10	183.89
S11	183.58
S12	183.62
S13	183.62
	Avg = 183.76

* Ground surface at elev. 185.32 m

** Elevations of piezometers can be found in Palmer & Belshaw (1980)

TABLE 6.5 MEASURED K_0 VALUES

Location	Depth (m)	Description	W_L	W_p	P.I.	OCR	K_0
Array 1	9.75	Silty Clay	69	23	46	1.3	.75
Array 2	10.06	Silty Clay	70	30	40	1.4	.76
Array 1	11.58	Layered Clay	51	19	32	1.6	.73
Array 2	12.50	Layered Clay	50	20	30	1.8	.76
Array 1	13.72	Varved Clay	33	16	17	2.0*	.59
Array 2	14.93	Varved Clay	35**	20*	15*	2.0	.58

* Note, where data are not available at the particular depth; data from the immediate next closest location are reported.

TABLE 6.6 AVERAGE SOIL PROPERTIES AND MEASURED K_o VALUES AT DIFFERENT LOCATIONS

A) Canadian Origin (Ontario)

Location	Soil Description	W_L (%)	W_p (%)	P.I. (%)	OCR	K_o	Reference
Wallaceburg	Soft to firm silty clay	40	20	22	2.2 1.0	0.85 0.68	Becker (1981)
New Liskeard	Soft to firm layered varved clay	55	25	30	1-2.5	0.7 (in-situ) 0.9 (fill-added)	Palmer and Lo (1974)
Thunder Bay	Soft grey (laminated) silty clay	70	27	43	1.3-1.4	.75-.76	
	Red-grey layered clay	51	19	32	1.6-1.8	.73-.76	
	Varved clay	34	18	16	2.0	.58-.59	

B) Norwegian Origin (from Bjerrum and Anderson (1972))

Konnerud	Plastic	61	32	29	1.5	.6	
Konnerud	Lean	33	22	11	1.2	.5	
Drammen	Lean	32	18	14	-	.6	
Sundland	Plastic	52	29	23	1.4	.55	
Sudland	Lean	33	22	11	-	.58	
Studen-terlunden	Lean	35	22	13	-	.6	
Ellingsrud	Quick	26	21	5	-	.45	
Kjelsas	Quick	26	20	6	-	.4-.5	

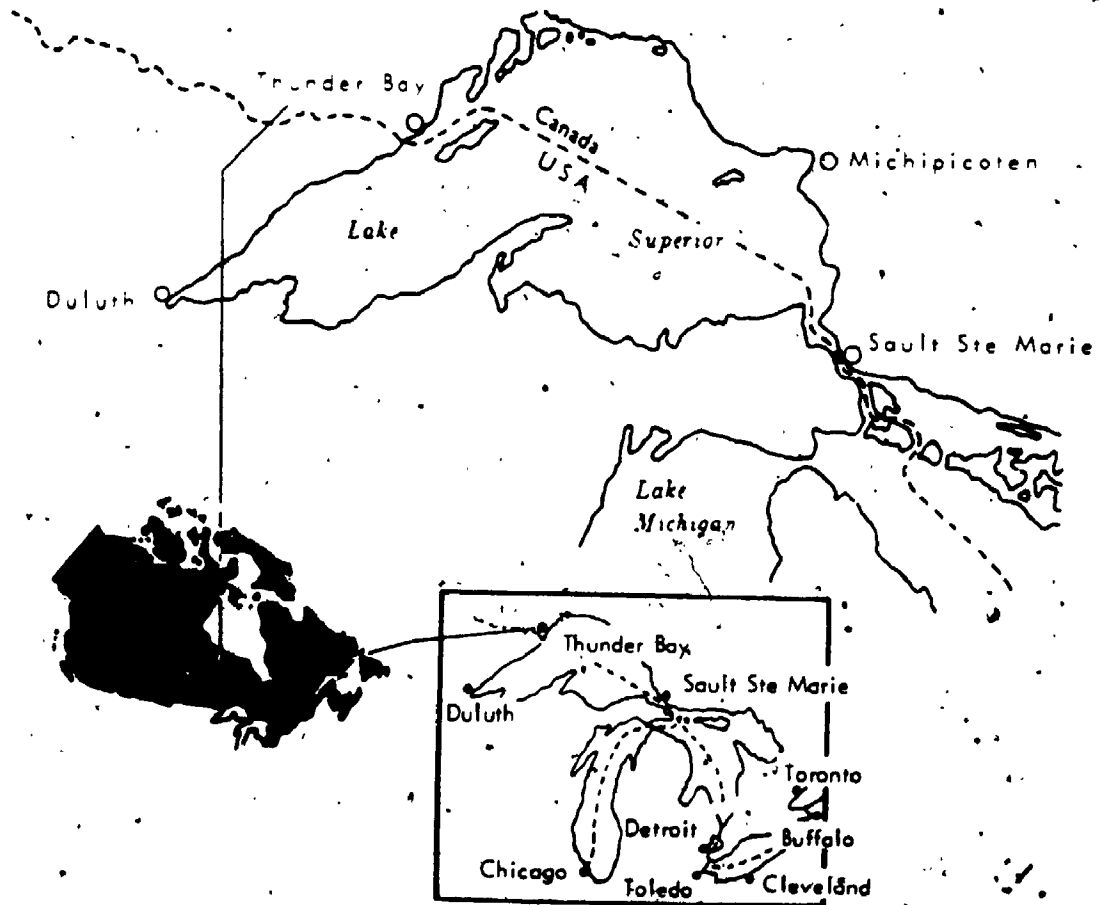
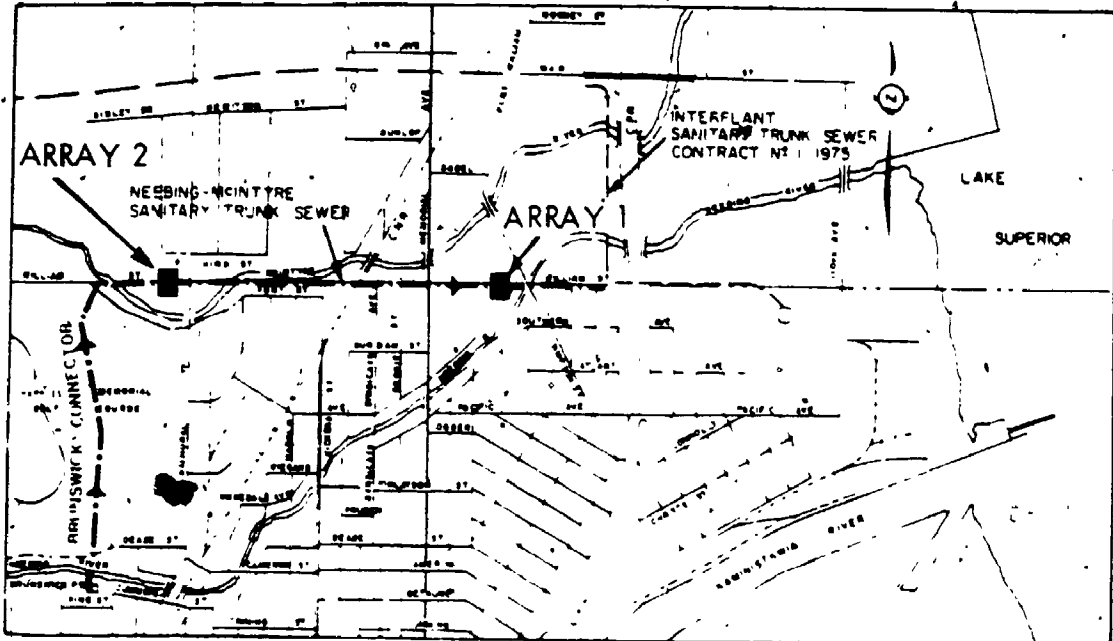


FIGURE 6.1 Tunnel Location (after Palmer and Belshaw, 1980)

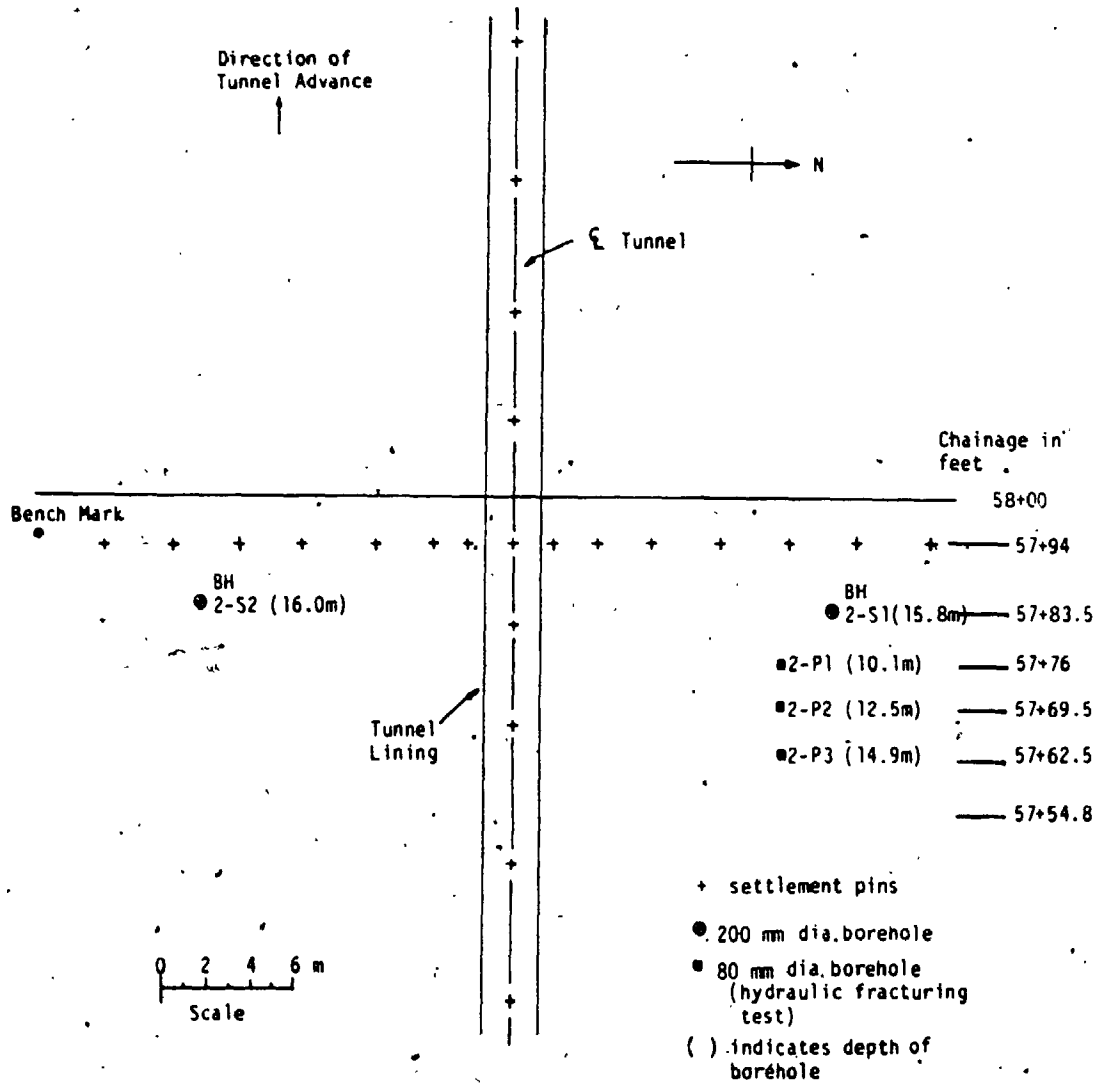


FIGURE 6.3 Plan of Borehole Locations - Array, 2

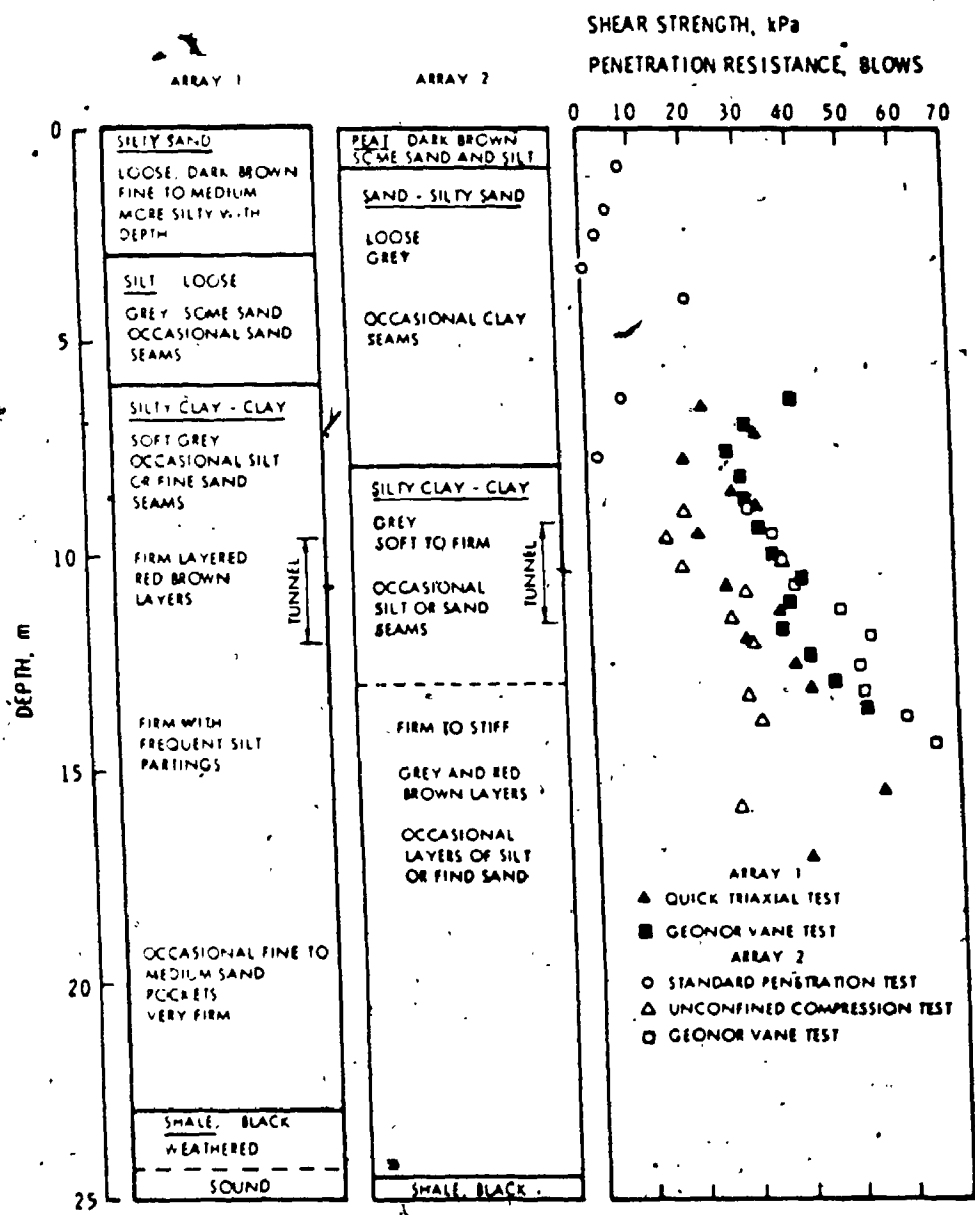


FIGURE 6.4 Soil Section and Summary of Test Results. After Palmer and Belshaw (1979)

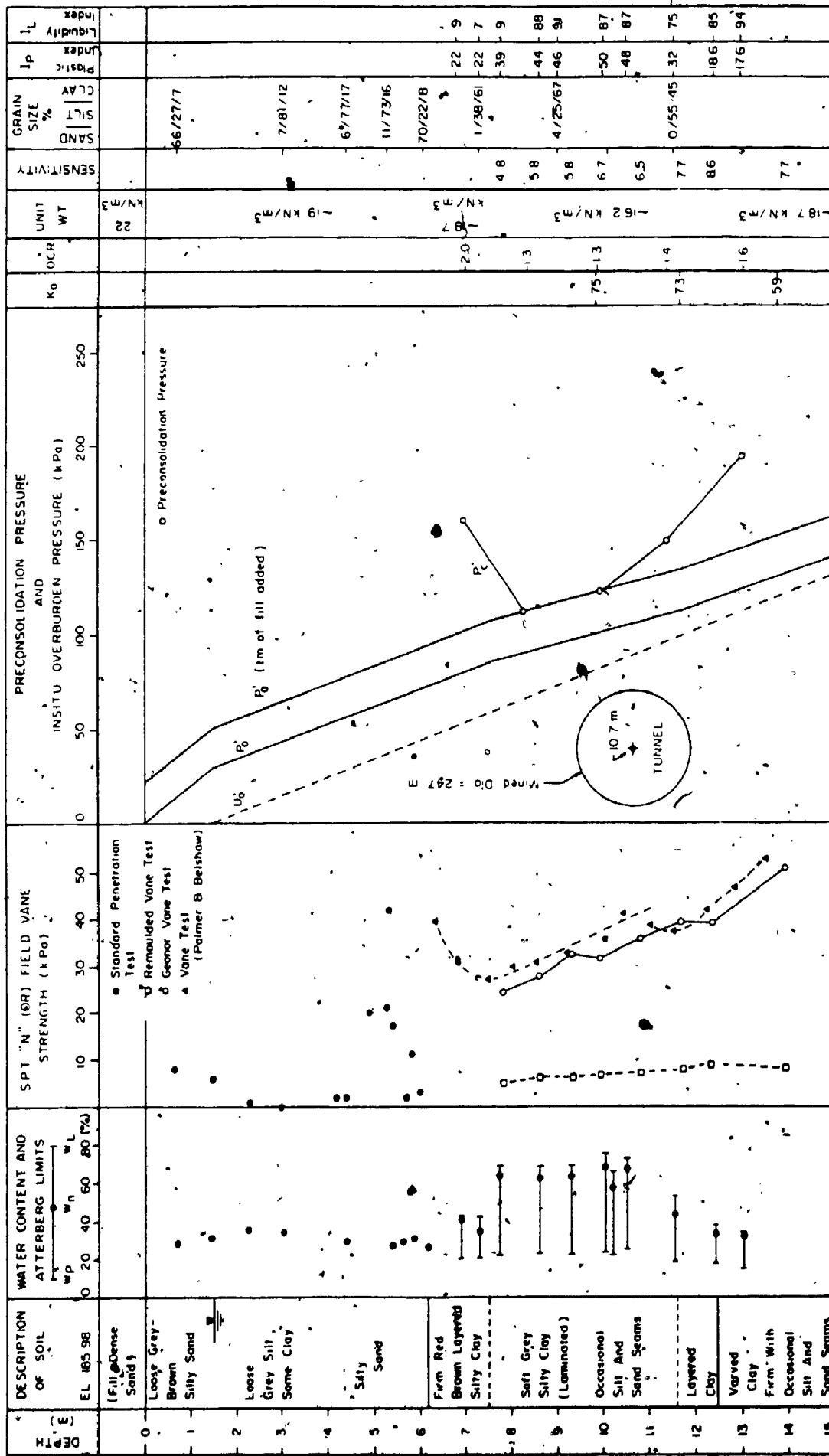


FIGURE 6.5 General Soil Properties - Array 1

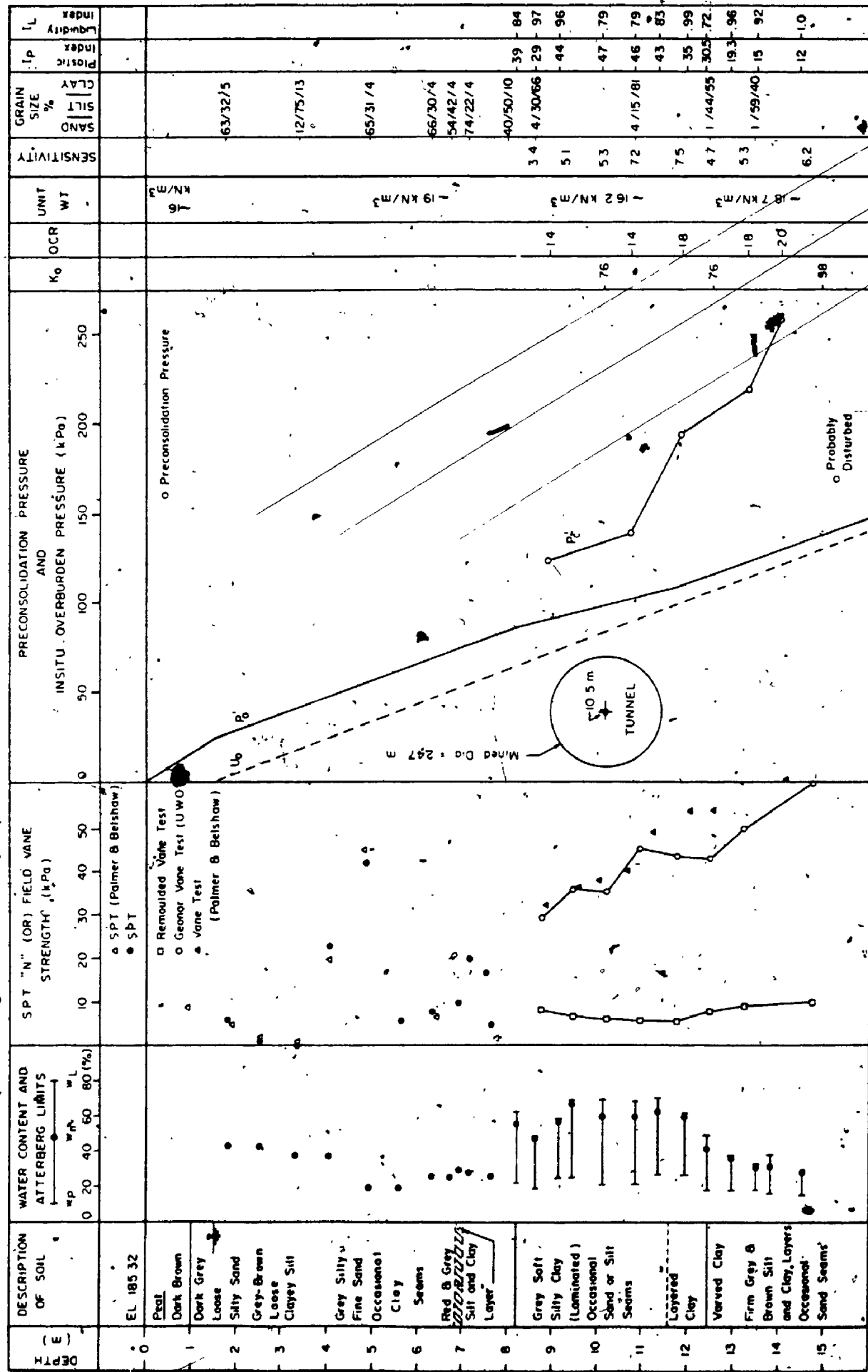





FIGURE.6.6 General Soil Properties — Array 2

-  coarse dark grey silt
-  brown silty clay
-  transition, light grey silt grading to silty clay

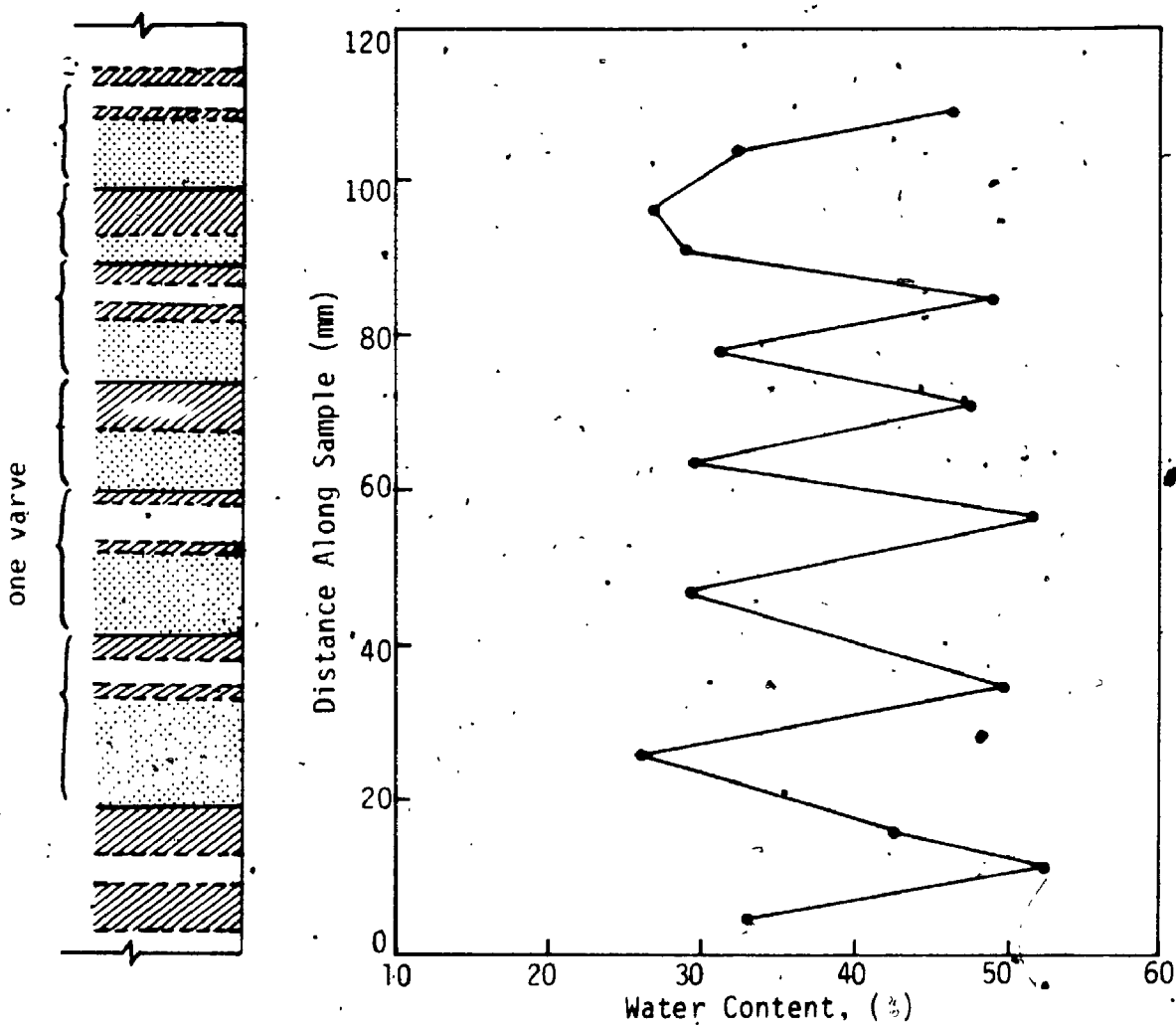


FIGURE 6.7 Variation of Water Content in Varved Clay

*Note: Logging of varved clay sample was performed by visual inspection and only serves as a guide to its appearance.

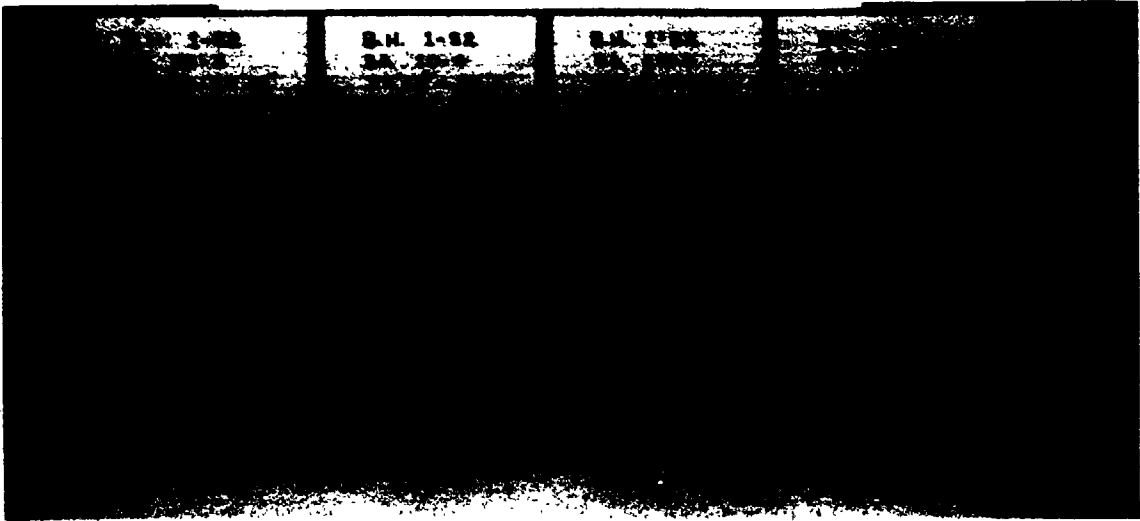


FIGURE 6.8 Silty Clay and Varved Clay Samples

CHAPTER 7

RESULTS OF TRIAXIAL TESTS

In order to have a thorough understanding of the soil behaviour and to determine the appropriate soil parameters, a detailed laboratory testing program which included some special testing techniques was carried out in the Geotechnical Laboratory at The University of Western Ontario.

The laboratory study consisted of the following:

- 1) Standard isotropically-consolidated undrained and drained triaxial compression (CIU and CID) tests on samples at various depths and different orientations to define the strength and modulus profile.
- 2) Anisotropically-consolidated triaxial undrained and drained compression and extension tests to investigate the effect of anisotropic consolidation (CK_0UC , CK_0DC , CK_0UE , CK_0DE).
- 3) Determination of elastic and strength parameters based on the preceding tests.
- 4) Determination of anisotropic deformation parameters using an apparatus developed at The University of Western Ontario (Lo et al., 1977; Yuen et al., 1978).
- 5) Evaluation of the effect of stress paths on the strength and deformation parameters by following the appropriate stress paths.

- 6) Large diameter consolidation tests using the Rowe Cell at appropriate stress levels.
- 7) Measurements of vertical and horizontal permeabilities.
- 8) Simple shear tests using the apparatus developed by the Norwegian Geotechnical Institute (Bjerrum and Landva, 1966).
- 9) CID extension and CID compression triaxial tests on reconstituted samples of sand.

A summary of the type, number and consolidation pressures of all the tests performed on the clay deposit is shown in Table 7.1. The results of conventional triaxial CIU and CID tests are reported in this chapter.

7.1 ISOTROPICALLY-CONSOLIDATED UNDRAINED (CIU) TESTS (WITH PORE WATER PRESSURE MEASUREMENT)

A series of undrained (CIU) strain controlled triaxial tests was performed on cylindrical specimens (50 x 100 mm) carefully hand trimmed vertically and horizontally from 152 mm tube samples. The rate of strain used in the tests was 1% per hour. The applied axial load was measured inside the triaxial cell by an internal electronic load cell. Displacement was monitored externally by a mechanical dial gauge. Continuous monitoring of both load and pore pressure was achieved by a chart recorder. The tests were conducted with the specimens enclosed in thin rubber membrane. Top, bottom and side filter paper drains were used.

A back pressure of 50 kPa was used to ensure saturation of the sample and prompt response of pore water pressure. In all cases, the degree of saturation as measured by Skempton's B value was over 0.96. The initial consolidation pressure used was equal to the effective overburden in most cases to simulate the field confining pressure. Consolidation was allowed to take place overnight to ensure a high degree of consolidation of the sample prior to shear testing. All tests were conducted in accordance with the standard procedure described by Bishop and Henkel (1962).

The undrained behaviour of the silty clay and varved clay tested under triaxial compression is shown in Figures 7.1 to 7.22 inclusive. The comparison of the response of samples tested at vertical and horizontal orientation is shown in Figures C.14 to C.43 in Appendix C. Test data are summarized in Table 7.2.

7.1.1 Undrained Stress-Strain Behaviour

The following observations can be made with reference to Figures 7.1 to 7.22 (tests on vertically ($i = 0^\circ$) and horizontally ($i = 90^\circ$) trimmed samples).

- a) The stress-strain curves of the specimens were fairly linear at low stress or strain level. The secant modulus obtained by either adopting a stress criterion (defined at 1/3 of failure stress, E_{30}) or a strain criterion (modulus taken up to 0.5% strain) would be nearly identical.

- b) The failure strains of the silty clay determined from horizontally or vertically trimmed samples were generally within 2% to 3%. The varved clay failed at larger strains (as indicated by stress ratio) and failure strains up to 8% were recorded.
- c) A post-peak reduction of strength occurred in all silty clay samples. The same phenomenon was not noticed in the varved clay and it behaved as a 'strain hardening' material after yielding (or after passing the 'quasi-elastic' range).
- d) The silty clay samples failed with a shear failure mode while the varved clay failed in a plastic or 'bulging' mode. Since the tests were performed sufficiently slowly (1%/hour) that equalization of pore water pressure was achieved throughout the entire sample, it may be postulated that partial consolidation of the clayey layers of the varved couplets was taking place during undrained shearing. A decrease in water content in the clayey unit accompanied by a corresponding increase in water content in the silt unit occurred as water was squeezed out of the clay and 'continuous strengthening' of the composite sample was produced as a net result of the 'interlayer consolidation' effect. (Equalization of pore pressure in New Liskeard varved clay resulting in consolidation of the fine layer and swelling of the coarse layer was also reported by Townsend (1965).)
- e) Pore water pressure in the silty clay samples continues to rise at peak strength but approaches constant values at about 5% to 8% strain. A small decrease in pore pressure was observed in the varved samples when the stress ratio had reached a constant value.

f). The pore water pressure parameter at failure, A_f , was quite consistent for both clays. A_f ranged only from .57 to .6 for vertically trimmed samples and the average A_f was .58. Higher A_f values were obtained when horizontally trimmed samples were tested. A_f ranged from .65 to .85 and the average was .73 (see Table 7.2). The difference in pore water pressure response could have been one of the factors contributing to the undrained shear strength anisotropy.

g) For two varved samples tested in the horizontal and vertical orientation under a consolidation pressure equal to the preconsolidation load (i.e., $OCR = 1.0$), the A_f values were close to unity (1.02 and .96) (see Figure 7.20).

h) The undrained shear strength for vertical specimens for both clays was between 33 to 76 kPa (with the exception of the two varved clay samples tested under higher consolidation pressure). The strength anisotropy ratio was $c_{uH}/c_{uV} \approx .84 \pm .04$.

i) The p - q plot and the σ'_1 - σ'_3 plot showed two general trends of the effective stress paths in the undrained shearing mode. Initially, the effective stress paths for both clays followed the conventional stress paths of normally consolidated clays. As the stress vectors approached or passed failure, there was divergence in behaviour. Both the mean stress and deviator stress increased in the varved clay sample under further compression loading and vice versa for the silty clay sample.

7.1.2 Effect of Consolidation Pressure on the Modulus of Deformation

For samples tested under CIU conditions at $i = 0$, the modulus of deformation E generally increased with the magnitude of the consolidation pressure. Figures 7.23 and 7.24 show the variation of E_{u30} with consolidation pressure σ'_c (see also Tables 7.3 and 7.4).

E_u of the silty clay was not very sensitive to the effect of consolidation pressure. Except at a relatively low consolidation pressure ($E_{u30} \approx 8.3$ MPa at $\sigma'_c \approx 50$ kPa), E_{u30} only varies between 13.7 and 18.1 MPa for the range of σ'_c from 75 kPa to 390 kPa.

It can be seen from Figure 7.24 that the undrained deformational response of the varved clay was fairly sensitive to the consolidation pressure. Although there was some scatter in the results, it would appear that E_{u30} increased monotonically at low consolidation pressures up to p'_c and then gradually increased to an asymptotic value.

Figures 7.23 and 7.24 suggest the relative importance of initial stress condition on a silty clay and a varved clay found in the same location. In order to clearly delineate the deformational behaviour of a soil, especially a layered soil, the correct field stress conditions must be applied in the test. The magnitude of initial stress and K_0 conditions (to be discussed in a later section) are salient effects to be considered.

7.1.3 Anisotropy in CIU Behaviour

In contrast to the anisotropic strength characteristics, E_{u30} values (or the deformational behaviour under CIU tests) are isotropic. The same phenomenon also occurs in St. Vallier Leda clay (Lo and Morin, 1972). Results of CIU tests on horizontally (H, $i = 90^\circ$) and vertically (V, $i = 0^\circ$) oriented samples at similar depths are shown in Figures 7.17 to 7.22 and Figures C.14 to C.43. An examination of these figures shows:

- a) The deviator stress-strain plots show that the stress-strain curves for CIU tests at $i = 0^\circ$ and $i = 90^\circ$ were almost identical and approximately linear up to ~1% strain. Higher maximum deviatoric stresses were attained by samples at $i = 0^\circ$.
- b) The effective stress ratio or the obliquity of principal stresses developed in the horizontal or vertical samples during the test were, in most cases, very similar until significant yielding of the clay sample had occurred. The vertical samples sustained a higher obliquity of principal stress at failure.
- c) It is interesting to note that the excess pore water pressures developed during the tests on $i = 0^\circ$ and $i = 90^\circ$ samples were very similar and in some cases they could be considered as having identical magnitudes throughout the tests.
- d) Skempton's pore water pressure parameter A_f (at failure) was higher in horizontally trimmed samples than in vertically trimmed samples.

e) The effective stress paths, shown in the p - q plots and σ'_1 - σ'_3 plots, were similar but not identical.

f) From the results of the $i = 0^\circ$ and $i = 90^\circ$ test for varved clay samples initially consolidated to the preconsolidation pressure (Figures 7.17 to 7.22), it may be seen that the effect of higher initial all-round effective stresses was to increase the undrained shear strength, excess pore water pressure, and an increase of the A_f value to approximately 1.0. One notable difference was that the magnitude of consolidation changed the trends in the stress path and the stress-strain curves after yielding in comparison to those previously discussed. The horizontal sample showed a small post-peak drop in strength while the strength in the vertical sample increased steadily with strain. The stress vector for the $i = 0^\circ$ sample bent back to the right, indicating an increase in both mean and deviator stress after the stress ratio had reached a constant value.

7.2 ISOTROPICALLY-CONSOLIDATED DRAINED (CID) TESTS

A series of standard drained triaxial tests was performed. The rate of strain in the tests was 0.1% per hour and continuous recording of pore pressure in the samples confirmed that a drained condition was achieved (i.e., no excess pore pressure during shear). Back pressures equivalent in magnitude to the in-situ pore pressures were used in all tests to ensure saturation of the samples, with B values always over

Silty clay samples and varved clay samples from Arrays 1 and 2 were tested. Horizontal samples were also tested to examine the anisotropy in drained behaviour of the clays.

Samples in Array 2 were tested under consolidation pressures equal to the effective overburden and samples in Array 1 were tested under consolidation pressures of $K'_0 p'$.

7.2.1 Stress-Strain Behaviour in CID Tests

The stress-strain behaviour of the CID drained triaxial tests are plotted in Figures 7.25 to 7.30 inclusive. Results are also summarized in Table 7.5. It may be observed that:

- (1) The drained behaviour of the silty clay and varved clay was quite similar, although the varved clay was significantly stronger and generally exhibited a smaller volumetric strain compared to the silty clay.
- (2) The stress-strain curves of the silty clay increased rapidly up to about 1% strain and yielding occurred as exhibited by pronounced curving of the stress-strain curve. A 'strain-hardening effect' instead of a post-peak drop in strength was observed. This suggested that the post-peak decrease in strength in CIU tests was partly due to pore pressure effects.
- (3) It was difficult to identify an absolute failure stress according to the stress-strain curves shown. However, the effective stress ratio did appear to gradually level off and reach an approximately

constant value at high axial strains ($>10\%$).

7.2.2 Anisotropy of Drained Behaviour

Results of CID tests on vertical ($i = 0^\circ$) and horizontal ($i = 90^\circ$) samples are plotted in Figures 7.31 to 7.36 inclusive. It may be observed that:

- (1) Anisotropic behaviour in drained shearing resistance was apparent. However, in the silty clay sample, shearing resistance of the horizontally oriented sample appeared to approach the shearing resistance of the vertically oriented sample at higher strain ($\geq 7\%$) (Figure 7.31).
- (2) Anisotropy of the low-strain deformational characteristics was also apparent in the drained behaviour of the clays although the same phenomenon was absent in undrained behaviour.
- (3) It is interesting to note that the volumetric strains in samples tested in both orientations were almost identical even up to very large axial strains. This observation is consistent with the pore pressure observed in the CIU test.

7.3 DETERMINATION OF PLASTICITY PARAMETERS USING CONVENTIONAL TRIAXIAL TESTING - CIU

The results from two series of tests performed to define the failure envelopes of both the grey silty clay and the varved clay strata are summarized in Tables 7.3 and 7.4 respectively. An analysis

of the results presented indicates that the parameters determined from the triaxial tests are dependent upon the consolidation pressure. This is particularly obvious for the behaviour of the varved clay. The undrained strength c_u of the material, the pore water pressure at failure, the strain at failure and the change in volume during consolidation were all observed to increase with increasing consolidation pressure. The shearing resistance of the material $(\sigma'_1 - \sigma'_3)_f$ was determined using two failure criteria. One failure criterion occurred when the maximum deviatoric stress was reached, i.e., at $(\sigma'_1 - \sigma'_3)_{\max}$. The other occurred when the effective principal stress ratio σ'_1/σ'_3 was a maximum. For many soils, the shearing resistance determined using either of these two failure criteria was quite similar. However, in tests on normally consolidated, sensitive clays, the pore pressures were generally still increasing when the maximum deviatoric stress $(\sigma'_1 - \sigma'_3)_{\max}$ was reached. In such a case, the maximum value of the stress ratio σ'_1/σ'_3 occurred at a larger strain and for relatively sensitive materials the shearing strength was reduced. In the interpretation of the test results, a choice of failure criterion must be made. Bjerrum and Lo (1961) suggested that the shearing resistance of the soil should be obtained using the maximum deviatoric stress $(\sigma'_1 - \sigma'_3)_{\max}$ as it represents the bulk failure of the soil. On the other hand, for a determination of the ultimate friction angle, ϕ' , the failure criterion σ'_1/σ'_3 was suggested to be used because it represents the ultimate failure of the soil structure.

The undrained strength of the grey, silty clay when isotropically

consolidated to the effective overburden pressure was observed to be approximately 50 kPa. The c_u/σ'_c ratio was slightly less than .3 once the material has entered the normally-consolidated range. The undrained strength of the varved clay was similarly observed to be approximately 75 kPa and the normally-consolidated c_u/σ'_c ratio was slightly in excess of .3.

The effective stress Mohr's circle representation of the tests performed in the grey silty clay and the varved clay is illustrated in Figures 7.37 and 7.38 respectively. These figures indicate that different plasticity parameters are required to describe the material depending on whether the soil is normally-consolidated or over-consolidated. For the grey silty clay the friction angle ϕ' was found to be approximately 28° in the normally-consolidated range. When soil samples were over-consolidated, the failure envelope was found to be slightly curved as is shown in Figure 7.37. For the varved clay the normally-consolidated friction angle ϕ' was found to be approximately 32° while its overconsolidated response was found to be relatively linear with an intercept c' equal to 14 kPa and a friction angle $\phi'_{o/c}$ equal to 30° .

7.4. VARIATION OF UNDRAINED MODULUS AND UNDRAINED SHEAR STRENGTH WITH DEPTH

The undrained shear strengths determined from CIU tests on vertically and horizontally trimmed specimens at different depths are

compared with the field vane strengths in Figure 7.39. From the figure, it may be observed that:

- a) Apart from the 'crust', the undrained strengths of the silty clay deposit and varved clay increase linearly with depth at a rate of approximately 6 kPa/m and 9 kPa/m respectively.
- b) The vane strength in Array 1 is slightly less than that in Array 2. The difference, however, is generally small. The slightly higher shear strengths in Array 2 may be attributed to slightly higher preconsolidation pressure and present effective overburden resulting from a thicker sand deposit in Array 2.
- c) The undrained strength behaviour of both the silty clay and varved clay is anisotropic, as shown by the results of CIU tests. The ratio of horizontal to vertical strength c_{uH}/c_{uV} equals to about 0.84.

The variation of the undrained modulus from CIU tests with depth is shown in Figure 7.40. It may be recalled that in CIU tests, the undrained moduli for vertical and horizontal samples are essentially the same for the clays tested. It may be seen that the modulus profile resembles those of undrained shear strengths in Figure 7.39.

The ratios of the modulus to the undrained shear strength (both from CIU tests) are plotted with depth in Figure 7.41. The modulus E_{u50} follows the conventional definition of taking the secant modulus up to 50% of the failure stress. E_{u30} is the secant modulus taken up to 1/3 of the failure stress. The modulus E_{u30} is more representative

of "elastic" behaviour. It may be seen that both modulus ratios show the same trend of variation with depth. In the silty clay, the ratio E_{u50}/c_u is about 250 in the crust, decreases to about 150 at the mid depth of the layer then increases to about 250 near the bottom. In the varved clay, the modulus ratio also increases with depth. The ratio E_{u50}/c_u at the top of the stratum is about 200.

7.5 VARIATION OF DRAINED MODULUS WITH DEPTH

The variation of the vertical drained modulus with depth determined from CID tests in the range of strain between 0.1% to 0.6% is shown in Figure 7.42. A similar pattern of variation as in undrained modulus is evident. The modulus decreases from about 7.5 MPa in the "crust" to about 2.5 MPa at the middle-third of the silty clay stratum then increases again to 5 MPa near the bottom.

In the varved clay stratum, data from CID tests are insufficient to draw any conclusions. However, from results of CIU tests, it may be expected that the drained modulus also increases with depth.

It may also be noted from a study of the ratio of undrained to drained modulus that the classical relationship from isotropic elastic theory $E_u = \frac{3(1+\nu')}{2} E'$ is not applicable in these soft clay deposits because it implies unrealistic values of Poisson's ratio. One reason for this discrepancy is the anisotropic deformation behaviour in these clay deposits.

The results of the modulus profiles will be compared with the results of the special tests to define in detail the deformation properties in the next chapter so that the appropriate parameters may be chosen for analysis.

7.6 TRIAXIAL TEST ON THUNDER BAY SAND

Triaxial compression tests were performed on saturated reconstituted silty fine sand retrieved from the borehole samples. The grain size distribution curve of the test sample is shown in Figure C.1 in Appendix C, indicating 88% of the sample are sand-sized material. The effective size D_{10} is .006 mm. Using Hansen's formula*, the permeability of the sample is calculated to be of the order of 10^{-5} cm/sec.

Since the SPT values obtained in the field varied considerably, samples were prepared at different densities in order to cover the possible range of variations of in-situ sand porosity.

The average porosity 'n' of the three groups of samples is .37, .42 and .49. These porosities are considered to be representative of dense (saturated density $\gamma = 20.8 \text{ kN/m}^2$), medium ($\gamma = 19.8 \text{ kN/m}^2$) and loose ($\gamma = 18.7 \text{ kN/m}^2$) samples, respectively. Relative densities of the samples were not determined because of the lack of a generally accepted accurate method in the determination of the maximum and minimum density of cohesionless soils.

* Hansen's formula $k = C(D_{10})^2$

where k = permeability in cm/sec

D_{10} = effective grain size (mm) corresponding to 10% on the grain size curve

$C = 1$ to 1.5

All triaxial tests were performed on cylindrical samples with the usual height to diameter ratio of 2 to 1. The advantage of using this ratio is the effect of end restraint on the strength of the sample is small (Bishop & Green, 1965). Lubrication of the end plattens is not necessary.

Samples were initially saturated with B values ranging from 85% to 96%. Difficulties in saturating the samples were encountered in the first few trial tests. The problem was overcome by introducing a thin perforated plate placed between two porous stones at the base of the sample. The perforated plate forced the incoming water from the back-pressure line to flow and spread into the sample in a uniform manner. Consequently, the sample which was initially placed damp was filled with de-aired water. A high back pressure was used to force air into solution. The drained tests were performed at a strain rate of .051% per minute. More detailed description of the test procedure may be found in Appendix C.

7.6.1 Stress-Strain Behaviour in CID Tests

The stress-strain curves and volumetric strain-axial strain curves are plotted in Figures 7.43 to 7.52. From the results, the following observations may be made:

- a) The test results for loose sand ($n \sim 0.49$) are illustrated in Figures 7.43 and 7.44. The samples LC1, LC2, LC3 failed at relatively large strains of about 20% to 30%. They exhibited a considerable

reduction in volume during shear and the volumetric strain ranged from 4.7% to 6.1%.

The sample LC4 was consolidated and sheared at a low confining pressure (52 kPa), it had a smaller failure strain and volume reduction. The volumetric strain gradually reduced after reaching a small peak value of 1.3%.

All the loose samples, consolidated and tested at different confining pressures, did not show any post-peak decrease in strength.

b) The stress-strain behaviour of the medium sands ($n \sim 0.42$) was fairly linear at low strain level. Post-peak decrease in strength was not observed. It may be noted from Figure 7.45 that the stress-strain relationship for sample MC1 and MC3 is typical of elastic-perfectly plastic behaviour.

The volume change behaviour is shown in Figure 7.46. The volumetric strain and axial strain relationship is clearly influenced by the effect of consolidation pressure. At low confining stress, dilatant behaviour at failure was observed. At higher stresses ($\sigma'_c = 101$ kPa), the volumetric strain at failure was negligible, whereas at $\sigma'_c = 201$ kPa, the sample showed a net contraction in volume at failure.

c) The dense sands ($n \sim 0.37$) exhibited a peak strength at a relatively low strain (Figure 7.47) and post-peak reduction in strength was observed. The dense sands also showed a dilatant structure at failure; during shear, the samples increased in volume following a

small contraction upon initial loading (Figure 7.48).

d) The behaviour of loose, medium, dense sands tested under confining pressures of 100 kPa and 200 kPa are shown in Figures 7.49 to 7.52. The comparative behaviour of the material is well illustrated in these figures. The initial tangent modulus of the stress-strain curve in general increases with increasing consolidation pressure and decreasing porosity.

7.6.2 The Effective Friction Angle

The results of CID compression tests on the silty sand are summarized in Table 7.6. The effective angle of internal friction is plotted against initial and final porosities in Figures 7.53a and 7.53b respectively. Each point in the figure represents the result of one triaxial test and the angle ϕ' is calculated from the value of maximum stress ratio at failure, assuming that the cohesion is zero. The figures show that the friction angle gradually decreases as the porosity increases.

The friction angle varies from 30° for loose samples to 38° for dense samples. It is believed that the friction angle for a very loose sample may be lower than 30° . However, due to difficulties in preparing saturated samples in very loose state, the low values of ϕ' had not been demonstrated.

The average angle of friction for loose samples with average

porosities of 0.49 is 32° . Average ϕ' for medium silty sand (average $n = 0.42$) and dense silty sand (average $n = 0.37$) is 36° and 38° respectively.

7.6.3 Poisson's Ratio At Low Strain Level

The Poisson's ratio ν of the silty sand is calculated from the volumetric strain (ϵ_v) and axial strain (ϵ) data from the CID tests with the relationship $\nu = \frac{1}{2} \left(\frac{\epsilon_v}{\epsilon} - 1 \right)$. The values of ν at low axial strain (1%) are tabulated in Table 7.6.

The following observations may be noted from Table 7.6.

- a) The Poisson's ratio indicates a decrease in volume in all tests at low axial strains ($\epsilon < 1\%$).
- b) Poisson's ratio varies with consolidation pressure and under the same pressure, the Poisson's ratio of a dense sand is higher than the value of a loose sand.
- c) The ratio generally increases with decreasing consolidation pressure but the value for dense samples is less sensitive to the effect of confining stresses.
- d) It may be readily seen that the Poisson's ratio is a function of σ'_c (consolidation pressure) and n (porosity), and this quantity is not an intrinsic property of the material.

7.6.4 Determination of the Vertical Drained Modulus

The vertical drained moduli E'_V of the silty sand are summarized in Table 7.7. They are determined as the secant moduli at one-third of the failure stress level. Since the stress-strain behaviour of the sand samples is generally quite linear, the moduli would be representative of the elastic behaviour of the silty sand.

The modulus E'_V may be related to the consolidation on confining pressure by Janbu's equation (Janbu, 1963). The form of the relationship is

$$\left(\frac{E'_V}{p_a}\right) = K \left(\frac{\sigma'}{p_a}\right)^a \quad (7.1)$$

where E'_V is the modulus, σ' is the initial confining stress and p_a is the atmospheric pressure. The parameters K and a can be determined by a plot of E'_V and the (σ'/p_a) ratio on log-log paper as shown in Figure 7.54. The exponent a is given by the slope of the line while the modulus number K is the intercept at $\sigma'/p_a = 1$.

The modulus number K and exponent a for silty sands at three porosities are tabulated in Table 7.8. The K value decreases with an increase in porosity while the exponent a increases with porosity. With reference to Eq. (7.1), the trend of results implies that for a given σ' , the drained modulus E'_V of a denser sample would generally be higher than a looser sample. Since a dense sample has a smaller exponent value a than a loose one, the variation of E'_V is less sensitive to the change in σ' .

The modulus number K and exponent a determined in the experiment are plotted in Figure 7.55. The diagram also shows parameters obtained by Janbu (1963) for many types of soils. Though the parameters obtained for loose Thunder Bay silty sand appear to be on the low side of the plot, all the values determined in the present study are within reasonable limits of the result in sand and silt.

It may also be noted from Figure 7.55 that the parameters K and a for the silty sand at other porosities than those shown in the figures may be readily obtained by interpolation.

7.6.5 CID Extension Tests On Silty Sand

Extension tests on silty sand were also performed to investigate the effect of stress path on the stress-strain behaviour. Typical stress-strain relationship for silty sand under CID extension and compression is shown in Figure 7.56. The samples were tested with a consolidation pressure equal to 100 kPa and the porosities of the samples were 0.32 and 0.37. The dense silty sands exhibited definitely stiffer deformation behaviour in extension than in compression; the ratio of extension to compression modulus in the tests shown were 1.6 and 2.

The stress-strain curves of the dense silty sand in extension test resembled closely elastic-perfectly plastic behaviour.

The observations drawn from the comparison of extension and

compression behaviour from the curves on Figure 7.56 should be treated with caution. It is because the samples may not be exactly identical and they are tested under isotropic conditions. However, qualitatively, the test results suggest stiffer behaviour in extension as in the case of most soils and it may be tentatively concluded that the ratio of extension to compression modulus for the silty sand tested is of the order of two.

7.7 SUMMARY OF RESULTS OF TRIAXIAL TESTS

1. The silty clay and varved clay both exhibit undrained strength anisotropy with a ratio of horizontal to vertical strength of 0.84.
2. The undrained shear strength for the horizontally trimmed samples agreed well with the field vane strength.
3. A post-peak decrease in strength was observed in the silty clay but was absent in the varved clay in the CIU tests.
4. The undrained shear strength decreases with depth within the clay "crust" and then increases with depth within the silty clay and varved clay.
5. The undrained Young's modulus E_u is isotropic for both clays.
6. The value of E_u for the varved clay is quite sensitive to the magnitude of consolidation pressures applied prior to testing, even in the overconsolidated range.
7. The average pore water pressure parameter at failure A_f for both clays in CIU tests at overburden pressure is .58.

8. The general drained stress-strain behaviour and volumetric strain characteristics for both clays are similar.
9. The drained deformation response is anisotropic.
10. The failure envelope for the silty clay in the overconsolidated range is slightly curved. c' and ϕ'_{oc} of the "linearized" envelope are 12 kPa and 28° respectively. For the varved clay, the overconsolidated envelope is relatively linear with $c' = 14$ kPa and $\phi'_{oc} = 30^\circ$.
11. The CID triaxial tests on reconstituted silty sand gave the plasticity parameters $c' = 0$ kPa and $\phi' = 30^\circ$ to 38° for the range of porosities between 0.37 to 0.5. (Lower ϕ' value is possible with higher porosities.)
12. The modulus of deformation of the silty sand varies with consolidation pressure and porosity of the sample and their relationships can be expressed by Janbu's equation.
13. For the reconstituted sand samples, the modulus in extension is about twice the modulus in compression obtained in CID triaxial tests.

TABLE 7.1a SUMMARY OF THE NUMBER OF VARIOUS TRIAXIAL TESTS PERFORMED

Type of Triaxial Test	CIU (0°) [†]	CIU (90°) [†]	CID (0°)	CID (90°)	CK ₀ UC [†]	CK ₀ DC [†]	CK ₀ UE	CK ₀ DE	Anisotropic Parameter Tests	Stress Path Tests
No. of Tests Performed	17	6	8	2	7	4	5	5	2*	4
Range of Consolidation Pressure (kPa)	50 to 600	95 to 135	90 to 100	70 to 80	75 to 140	95 to 140	75 to 140	75 to 140	70 to 75	80 to 85

TABLE 7.1b SUMMARY OF NUMBERS OF VARIOUS LABORATORY TESTS PERFORMED

Type of Test	Direct Simple Shear	Conventional Oedometer	Large [†] Oedometer	Permeability Test k _v	Permeability Test k _H
No. of Tests Performed	8	11	3	2	2
Range of Consolidation Pressure (kPa)	80 to 120	0 to 1600	0 to 200	0	0

[†] with pore water pressure measurement

* triaxial tests performed on samples at i=0°, i=45°, i=90° for each set of tests

TABLE 7.2 CIU TEST RESULTS

Location	Description	Depth (m)	w ₀ (%) Nat. Water Content	ε _f (%)	A _f	POP σ failure (kPa)	c _u (kPa)	(σ ₁ /σ ₃) _f	Δv/v (%) (After consolid.)	σ _c (kPa)	σ _c '/P ₀	c _u /σ _c '	c _{uH} /c _{uV}
Array 1 (1-S2)	Silty clay (V)*	7.12	-	2.30	0.49	38.2	39.1	4.76	-	59	0.75	.66	-
Array 1 (1-S1)	Silty clay (V)	8.02	-	2.92	0.65	42.6	32.8	3.58	-	69.8	0.75	.47	-
Array 2 (2-S1)	Silty clay (V)	9.56	58.7	3.47	0.57	49.0	44	3.06	4	94.2	1	.47	.84
Array 2 (2-S1)	Silty clay (V)	10.78	60.7	2.74	0.59	61.0	52	3.89	4.4	96.7	1	.54	.85
Array 2 (2-S2)	Silty clay (V)	11.55	59.7	2.75	0.60	60.5	60.5	4.10	4.1	110.9	1	.52	.84
Array 2 (2-S2)	Varved clay (V)	13.00	37.8	3.44	0.59	73.0	61.8	3.70	4.6	118.6	1	.52	.79
Array 2 (2-S2)	Varved clay (V)	14.70	33.5	4.36†	0.57	87.1	76.4	3.99	4.7	139.0	1	.55	.85
Array 2 (2-S1)	Silty clay (H)**	9.34	62.9	2.96	0.85	63.0	37	3.42	4.9	93.7	1	.40	-
Array 2 (2-S1)	Silty clay (H)	10.66	62.3	2.48	0.65	57.0	44	3.61	4.9	96.4	1	.46	-
Array 2 (2-S2)	Silty clay (H)	11.60	60.3	2.27	0.67	67.8	51	3.40	3.9	109.8	1	.46	-
Array 2 (2-S2)	Varved clay (H)	12.93	37.2	8.2†	0.83	81.5	49	3.96	4.9	114.3	1	.43	-
Array 2 (2-S2)	Varved clay (H)	14.54	33.7	8.3†	0.67	87.0	65	3.74	3.5	135	1	.48	-
Array 2 (2-S2)	Varved clay (V)	14.54	31.3	6.14†	0.96	181.0	96.5	3.40	7.0	259.7	1.9	.37	.94
Array 2 (2-S2)	Varved clay (H)	14.67	35.8	3.12	1.02	183.5	90.9	3.37	6.8	259.7	1.9	.35	-

† Failure determined by (σ₁/σ₃)_{max} criterion.

* (V) = vertically oriented sample (ψ=0°)

** (H) = horizontally oriented sample (ψ=90°)

TABLE 7.3a ISOTROPICALLY CONSOLIDATED UNDRAINED TEST RESULTS OF SILTY CLAY (ARRAY 2)

Depth of Sample (10.7m - 11.1m); $p'_0 = 100$ kPa; Strain Rate = 1%/hr
 $p'_C = 150$ kPa; Back Pressure = 50 kPa

σ'_c (kPa)	σ'_e/p'_c	$(\sigma'_1 - \sigma'_3)_{f.}$ (kPa)	$(\sigma'_1 - \sigma'_3)_{f.}$ (kPa)	c_u (kPa)	u_f (kPa)	A_f	f (%)	$\Delta V^{(2)}$ (cc)	$(\sigma'_1/\sigma'_3)_f$	c_u/σ'_c
49.5	0.330	77.30	77.3	38.65	34.9	.45	2.7	4.01	5.74	.78
75.0	0.500	90.00	89.4	45.00	51.8	.58	2.7	5.75	4.85	.60
96.7	0.644	100.50	100.2	50.25	61.5	.61	3.0	7.61	3.84	.52
200.0	1.330	124.08	114.0	62.04	115.0	1.01	8.25	23.86	3.20	.31
394.0	2.630	207.86	206.0	103.90	272.0	1.32	8.6	44.66	2.75	.26

* Determined by $(\sigma'_1 - \sigma'_3)_{max}$ failure criterion
 † Determined by $(\sigma'_1/\sigma'_3)_{max}$ failure criterion

(1) Excess pore water pressure
 (2) Changes in volume during consolidation (prior to shearing)

TABLE 7.3b MODULUS DETERMINATION OF GREY SILTY CLAY AT 10.7m - 11.1m

σ'_c (kPa)	E_{u30} (MPa)	E_u/σ'_c	E_u/c_u
49.5	8.28	167	214
75.0	13.7	182	303
96.7	15.0	169	163
200.0	17.3	86.4	303
394.0	18.1	46.0	175

TABLE 7.4a ISOTROPICALLY CONSOLIDATED UNDRAINED TEST RESULTS OF VARVED CLAY (ARRAY 2)

Depth of Sample (14.7m - 15.2m) ; $p'_0 = 133$ kPa ; Strain Rate = 1%/hr
 $p'_c = 293$ kPa ; Back Pressure = 50 kPa

σ'_c (kPa)	σ'_c/p'_c	$(\sigma'_1 - \sigma'_3)_f$ (kPa)	$(\sigma'_1 - \sigma'_3)_f$ (kPa)	c_u (kPa)	u_f (kPa)	A_f	r_f (%)	$\Delta V(2)$ (cc)	$(\sigma'_1/\sigma'_3)_f$	c_u/σ'_c
73	.249	113	113.0	56.5	37.6	.332	3.90	5.858	4.1	.77
139	.475	155	150.0	75.0	85.0	.567	6.50	8.547	3.9	.54
260	.888	180	172.5	86.3	196.0	1.140	8.25	12.212	3.9	.33
298	1.020	188.9	180.0	90.0	227.0	1.260	8.00	15.770	3.5	.30
397.5	1.360	228.5	231.2	115.6	301.5	1.300	9.90	20.800	3.4	.29
599	2.050	408	408.0	204.0	430.0	1.050	12.30	21.310	3.4	.34

* Determined by $(\sigma'_1 - \sigma'_3)_{max}$ failure criterion

† Determined by $(\sigma'_1/\sigma'_3)_{max}$ failure criterion

(1) Excess pore water pressure

(2) Changes in volume during consolidation (prior to shearing)

TABLE 7.4b MODULUS DETERMINATION OF VARVED CLAY AT 14.7m - 15.2m

σ'_c (kPa)	E_{u30} (MPa)	E_u/σ'_c	E_u/c_u
73	9.7	133.0	171
139	18.5	129.0	238
260	24.5	94.3	272
298	19.0	63.8	211
397.5	28.0	70.0	241
599	25.0	35.0	103

TABLE 7.5 CID TEST RESULT ON VERTICALLY TRIMMED SAMPLE

Description	Location	Depth (m)	p'_0 (kPa)	σ'_c (kPa)	E' (MPa)	E'/p'_0	E'/σ'_c
Silty Clay	Array 2 (2-S1)	9.56	95.5	95.5	2.7	28.5	28.5
Silty Clay	Array 2 (2-S1)	11.40	105.2	105.2	5.2	49.4	49.4
Varved Clay	Array 2 (2-S2)	13.00	122.9	122.9	7.7	62.7	62.7
Silty Clay	Array 1 (1-S1)	7.12	87.7	65.8	7.6	86.6	115.5
Silty Clay	Array 1 (1-S1)	8.60	98.7	74	3.1	31.4	41.9
Silty Clay	Array 1 (1-S1)	10.10	109.5	82.1	3.75	34.3	45.7
Layered Clay	Array 1 (1-S1)	11.70	120.2	69.7	3.5	29.1	50.2
Varved Clay	Array 1 (1-S1)	13.1	131.2	76.1	5.7	43.4	74.9

TABLE 7.6 SUMMARY OF CID TRIAXIAL COMPRESSION TEST DATA ON THUNDER BAY SILTY SAND

Test No.	Final Porosity (n)	Initial Porosity (n)	Saturated Density (kN/m ³)	Volumetric Strain at Failure ϵ_{vf} (%)	Axial Strain at Failure ϵ_f (%)	σ'_c (kPa)	$(\sigma'_1 - \sigma'_3)_f$ (kPa)	ϕ' Effective Friction Angle	Poisson's Ratio at 1% Strain
LC4	0.47	0.47	18.9	0.52	12.5	52	106	30.3	.36
LC1	0.47	0.50	18.4	6.10	29.9	101	236	32.6	.27
LC2	0.45	0.48	18.9	4.70	27.9	201	508	33.9	.25
LC3	0.47	0.50	18.5	4.78	28.4	400	890	31.8	.25
MC3	0.42	0.42	19.9	0.25 ^d	7.5	49	145	36.6	.47
MC1	0.42	0.41	20.0	0.27	5.8	101	278	35.4	.37
MC2	0.41	0.44	19.5	3.77	19.4	201	596	36.7	.26
DC2	0.37	0.37	20.7	0.14 ^d	5.8	101	328	38.2	.43
DC1	0.37	0.37	20.8	0.40 ^d	6.3	202	656	38.3	.41

d - indicates dilatancy

TABLE 7.7 SUMMARY OF DRAINED VERTICAL MODULUS OF THUNDER BAY SILTY SAND

Initial Porosity (n)	Consolidation Pressure σ'_c (kPa)	(σ'_c/p_a)	E'_v (MPa)
0.47	52	0.53	2.46
0.47	100	1.03	2.75
0.45	201	2.06	8.38
0.47	400	4.08	12.90
0.42	49	0.50	6.80
0.42	101	1.03	12.00
0.41	201	2.05	14.96
0.37	101	1.03	21.86
0.37	202	2.06	28.00

TABLE 7.8 SUMMARY OF K AND a VALUES OF THUNDER BAY SAND

Description	Average Initial Porosity (n)	Initial Unit Weight (kN/m ³)	K	a	Average ϕ
Loose sand	.49	18.7	42.6	.825	32°
Medium sand	.42	19.8	106	.561	36°
Dense sand	.37	20.8	220	.400	38°

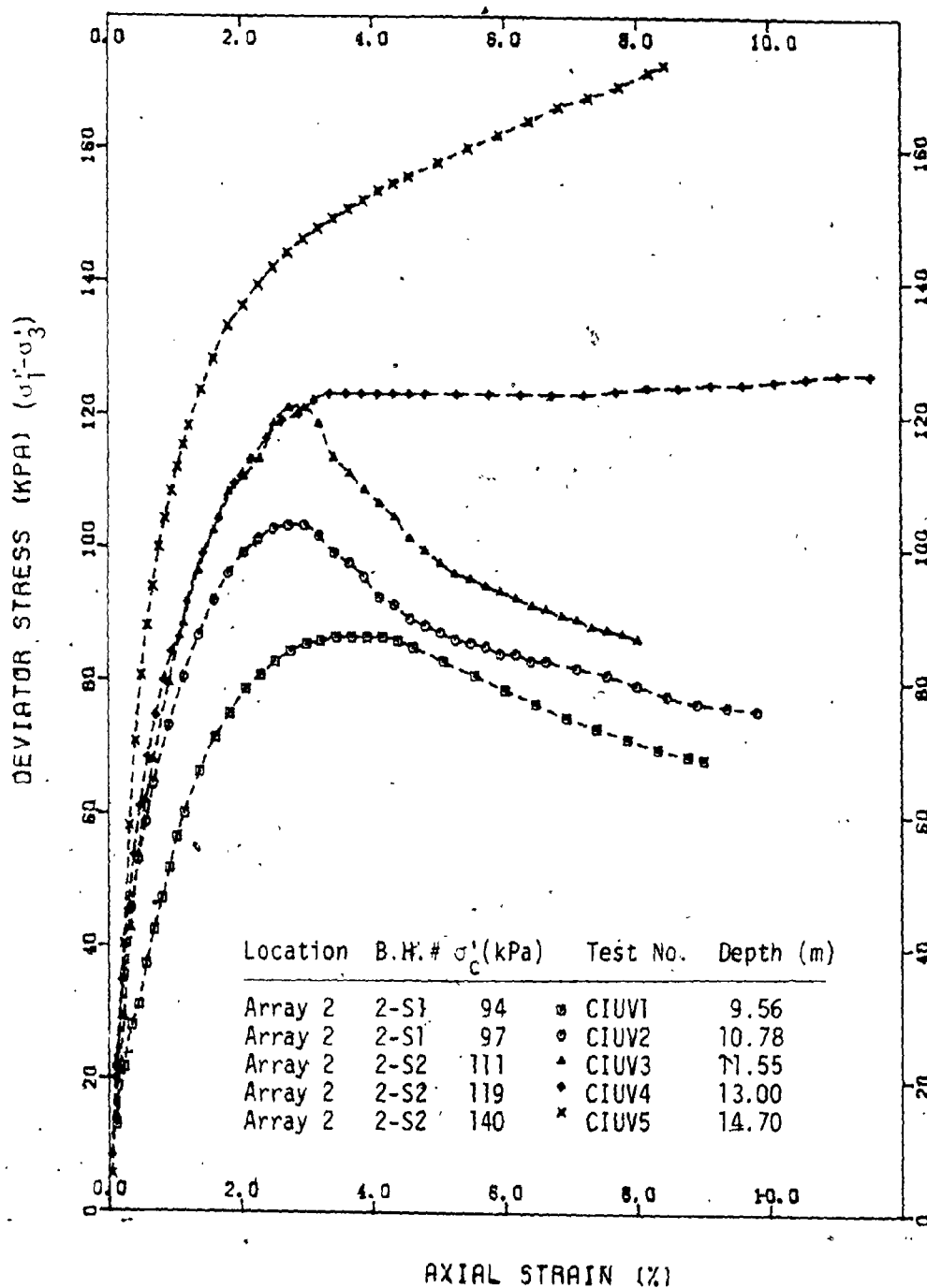


FIGURE 7.1 Stress-Strain Relationship from CIU Tests for Vertically Oriented Silty Clay and Varved Clay Samples

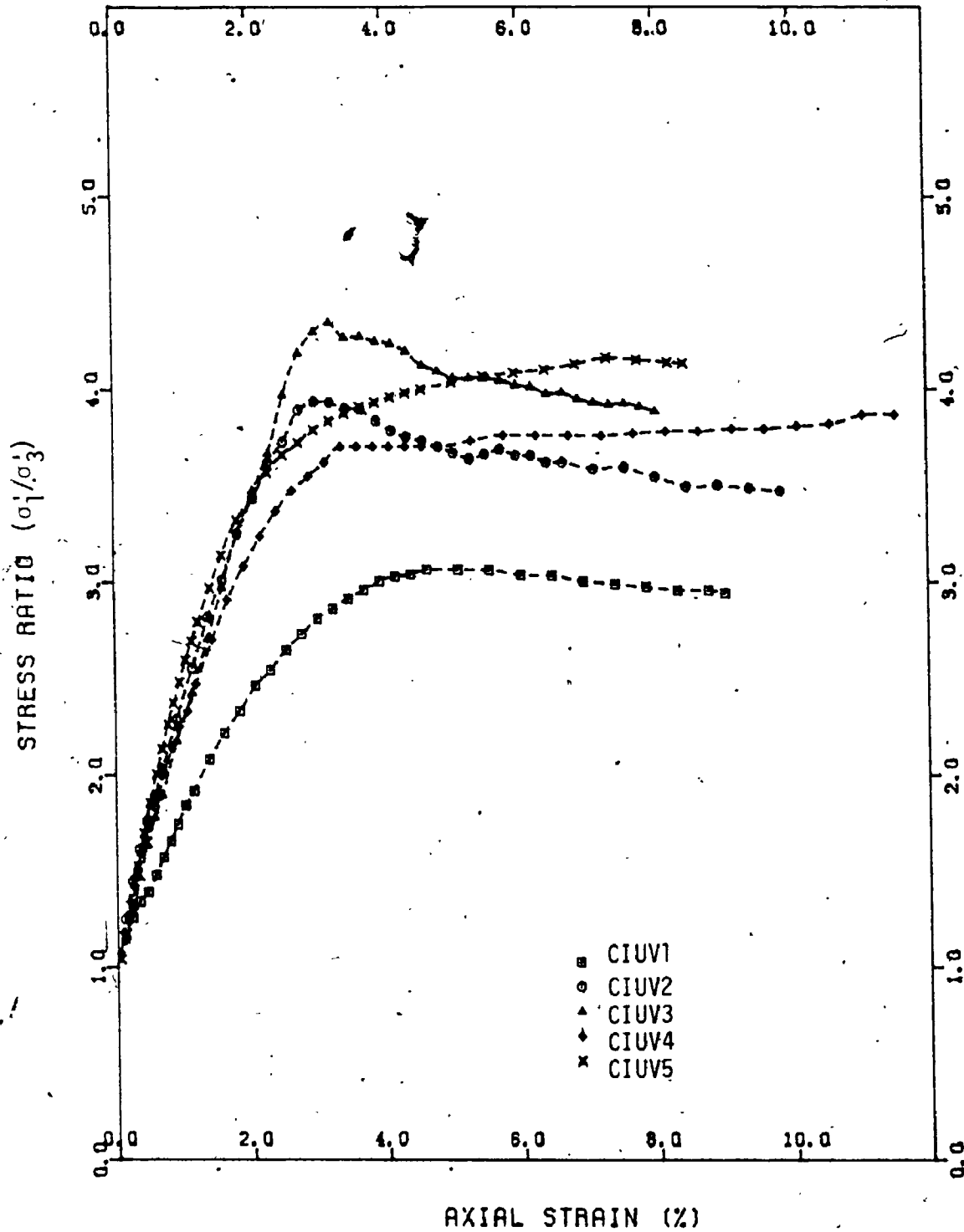


FIGURE 7.2 Stress Ratio-Strain Relationship from CIU Tests for Vertically Oriented Silty Clay and Varved Clay Samples

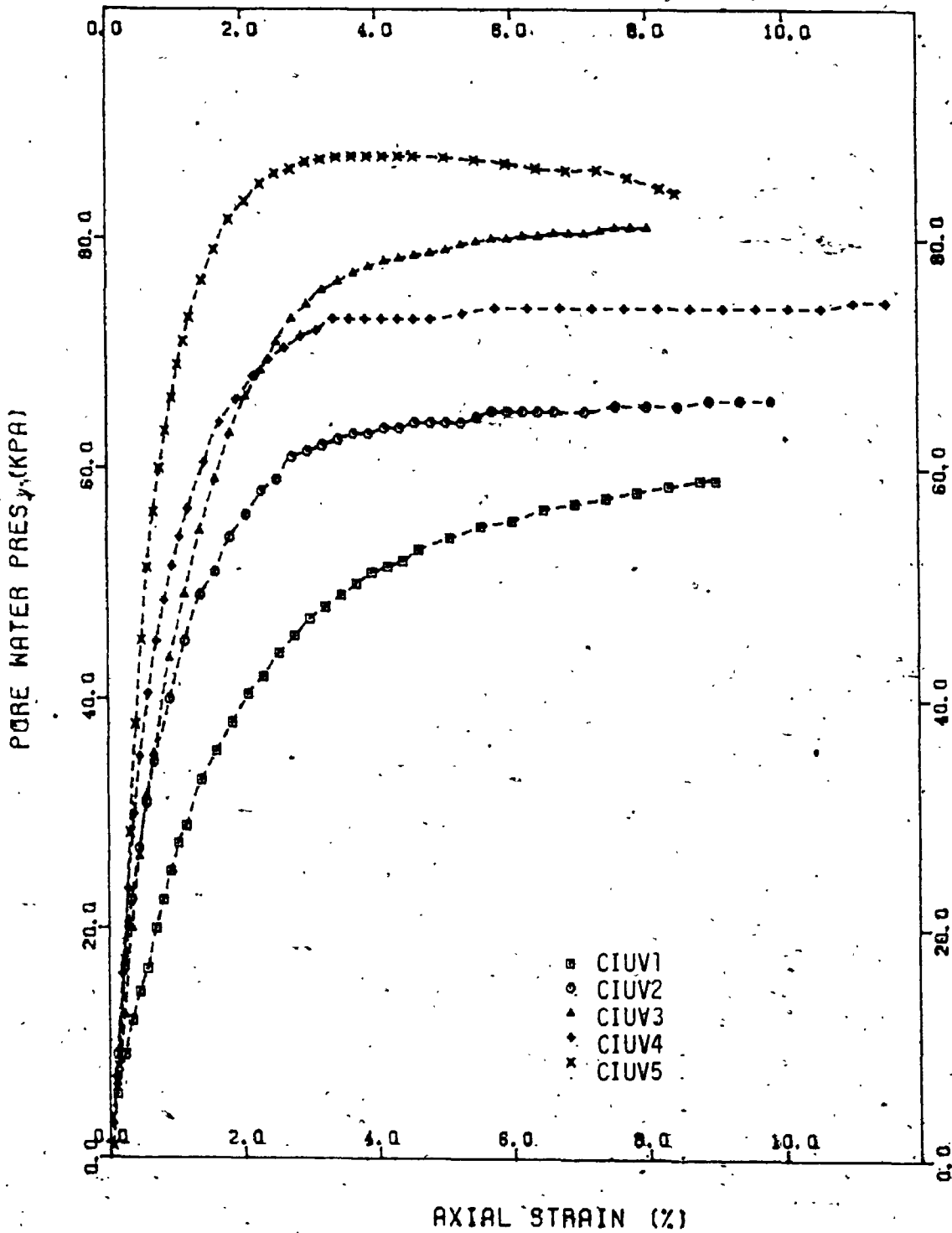


FIGURE 7.3 Excess Pore Water Pressure-Strain Relationship from CIU Tests for Vertically Oriented Silty Clay and Varved Clay Samples

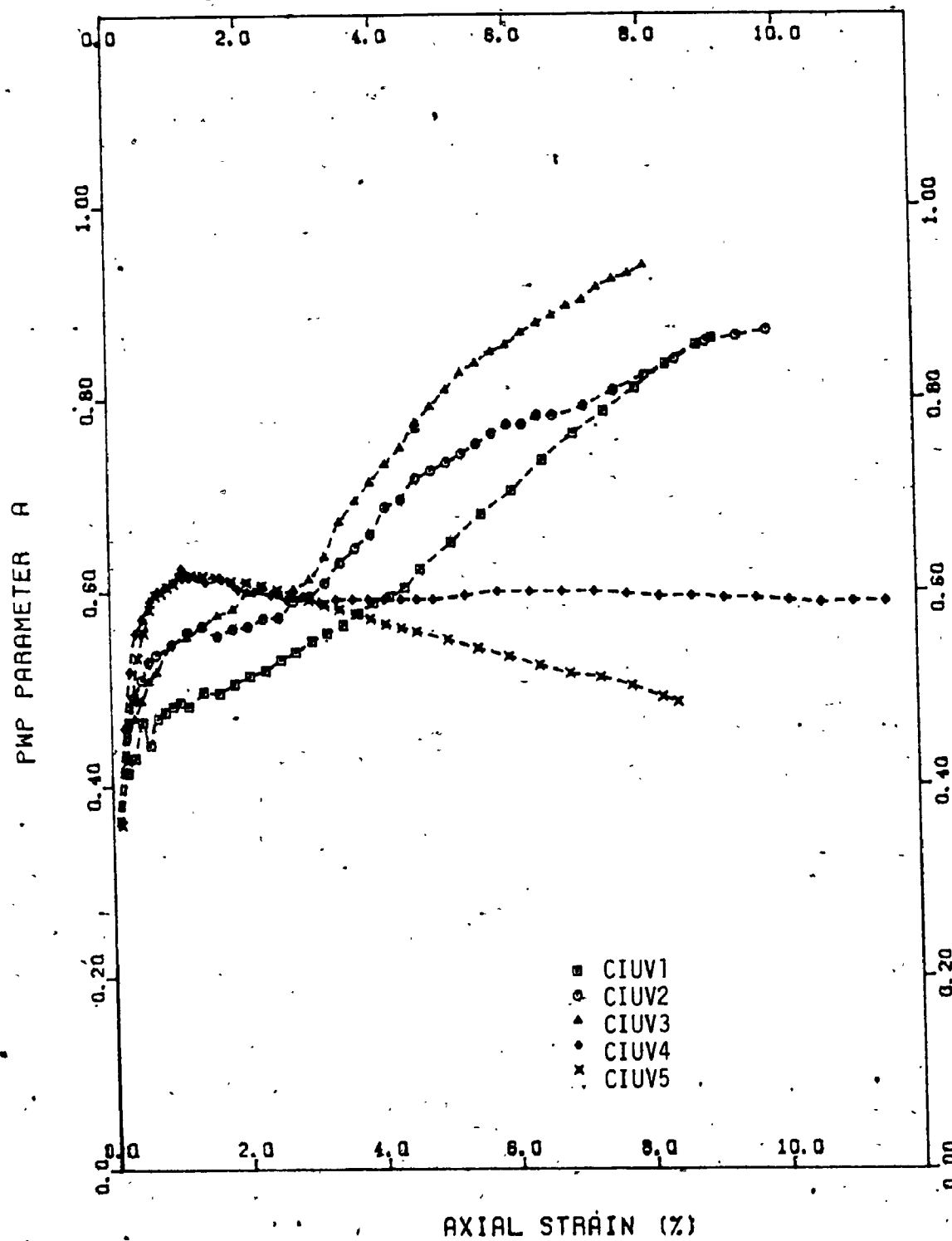


FIGURE 7.4 Pore Pressure Parameter A - Strain Relationship from CIU Tests on Vertically Oriented Silty Clay and Varved Clay Samples

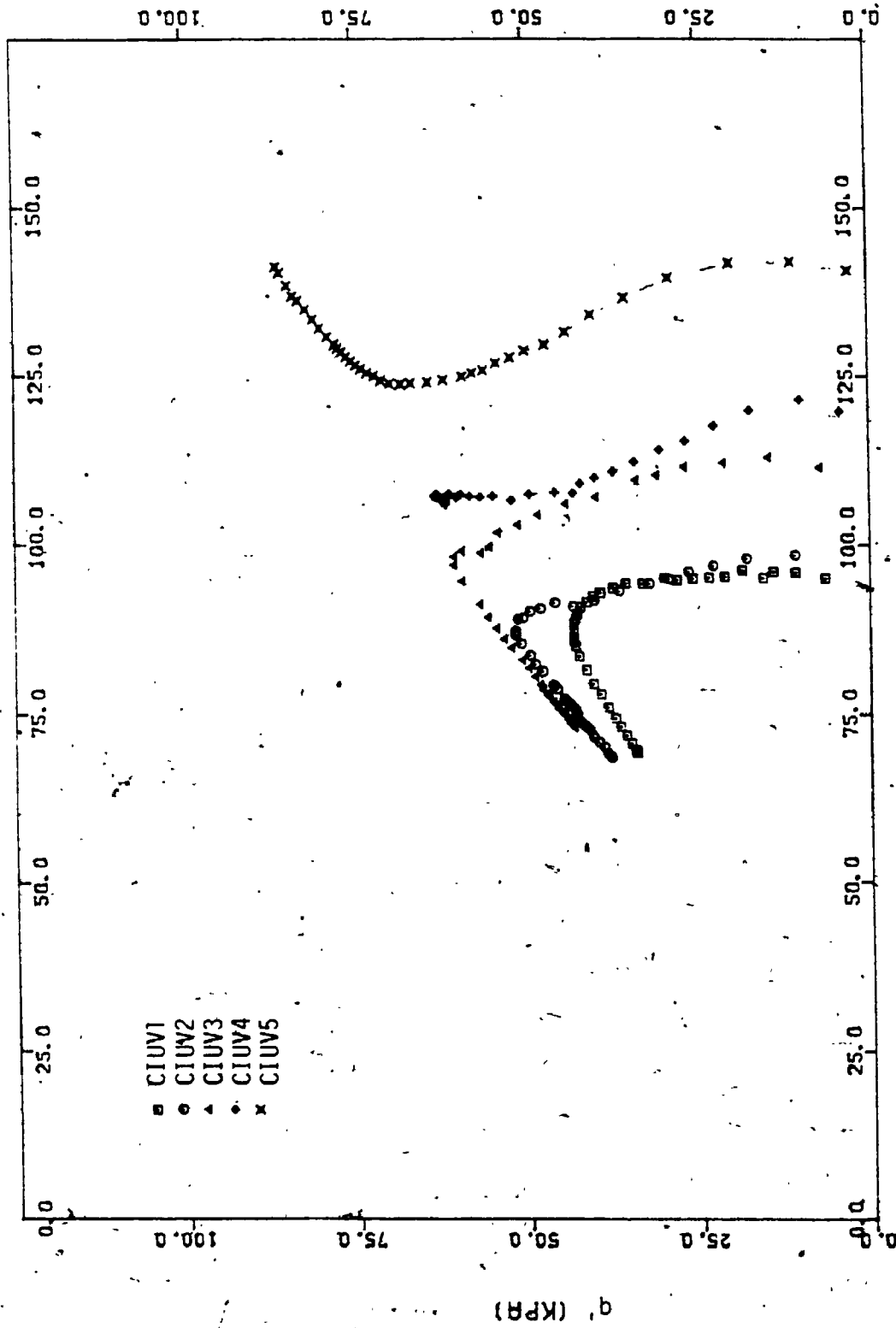


FIGURE 7.5 Effective p-q Stress Path Plot from CIU Tests on Vertically Oriented Silty Clay and Varved Clay Samples.

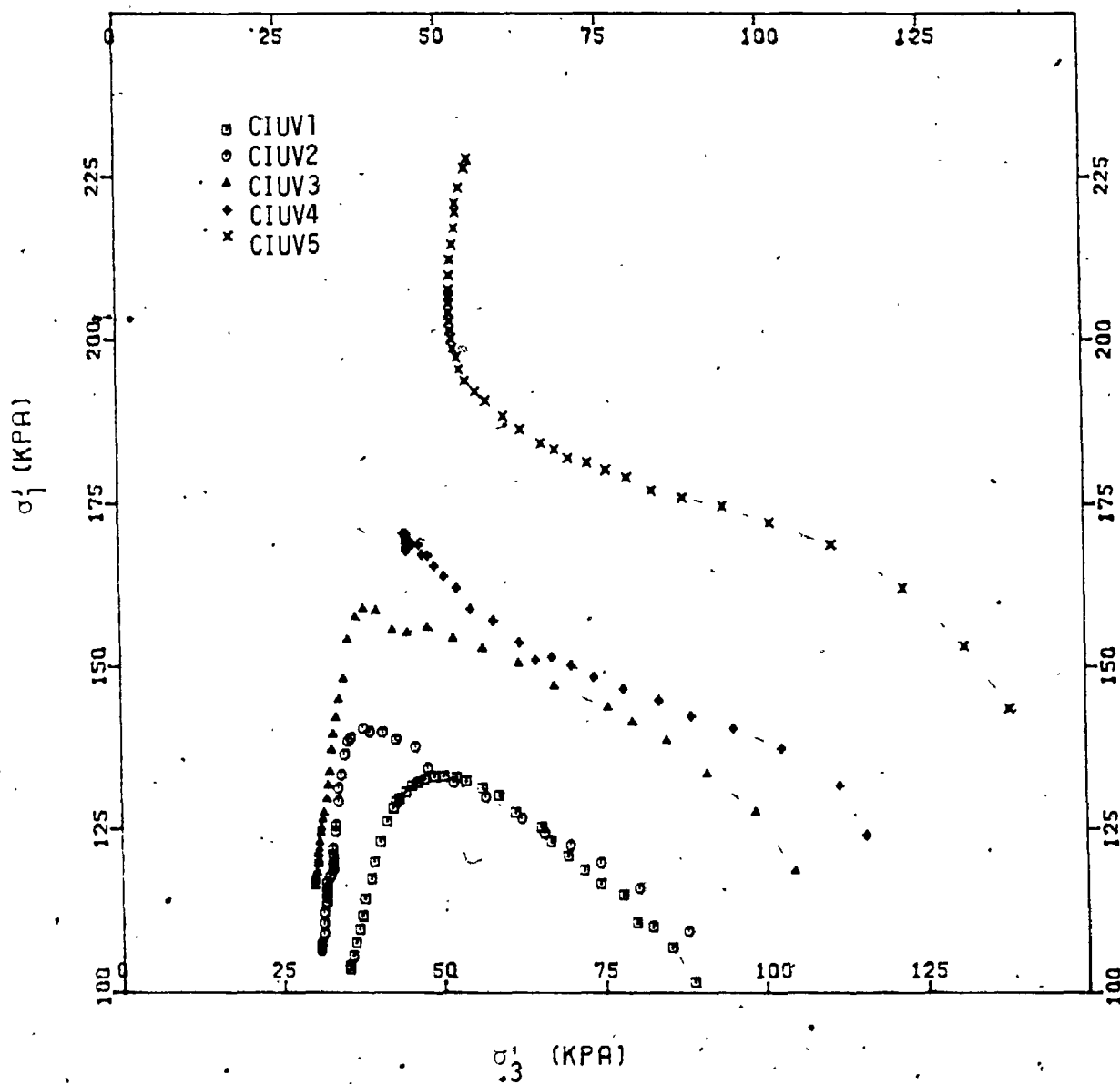


FIGURE 7.6 Effective σ_1' - σ_3' Stress Path Plot from CIU Tests on Vertically Oriented Silty Clay and Varved Clay Samples

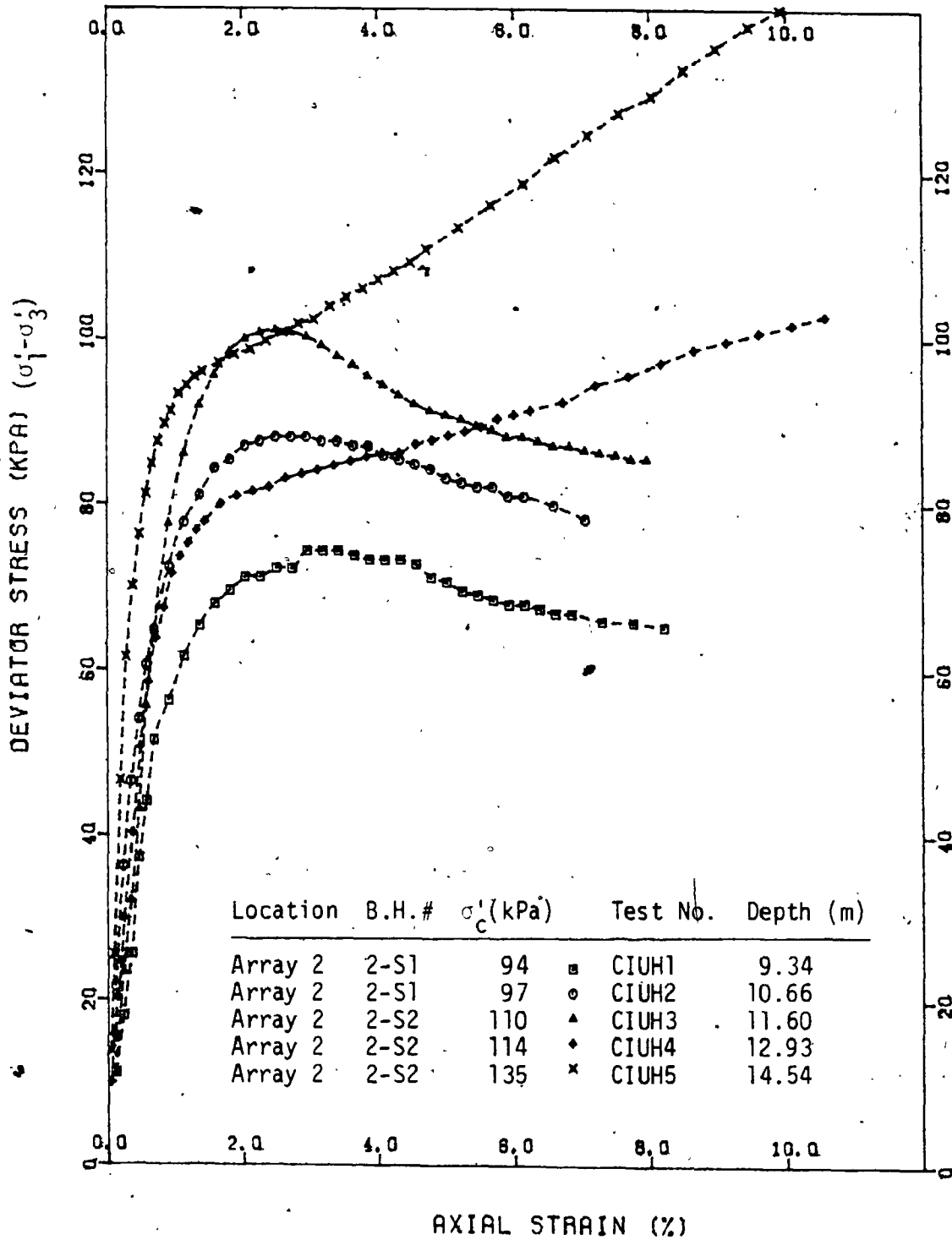


FIGURE 7.7 Stress-Strain Relationship from CIU Tests for Horizontally Oriented Silty Clay and Varved Clay Samples

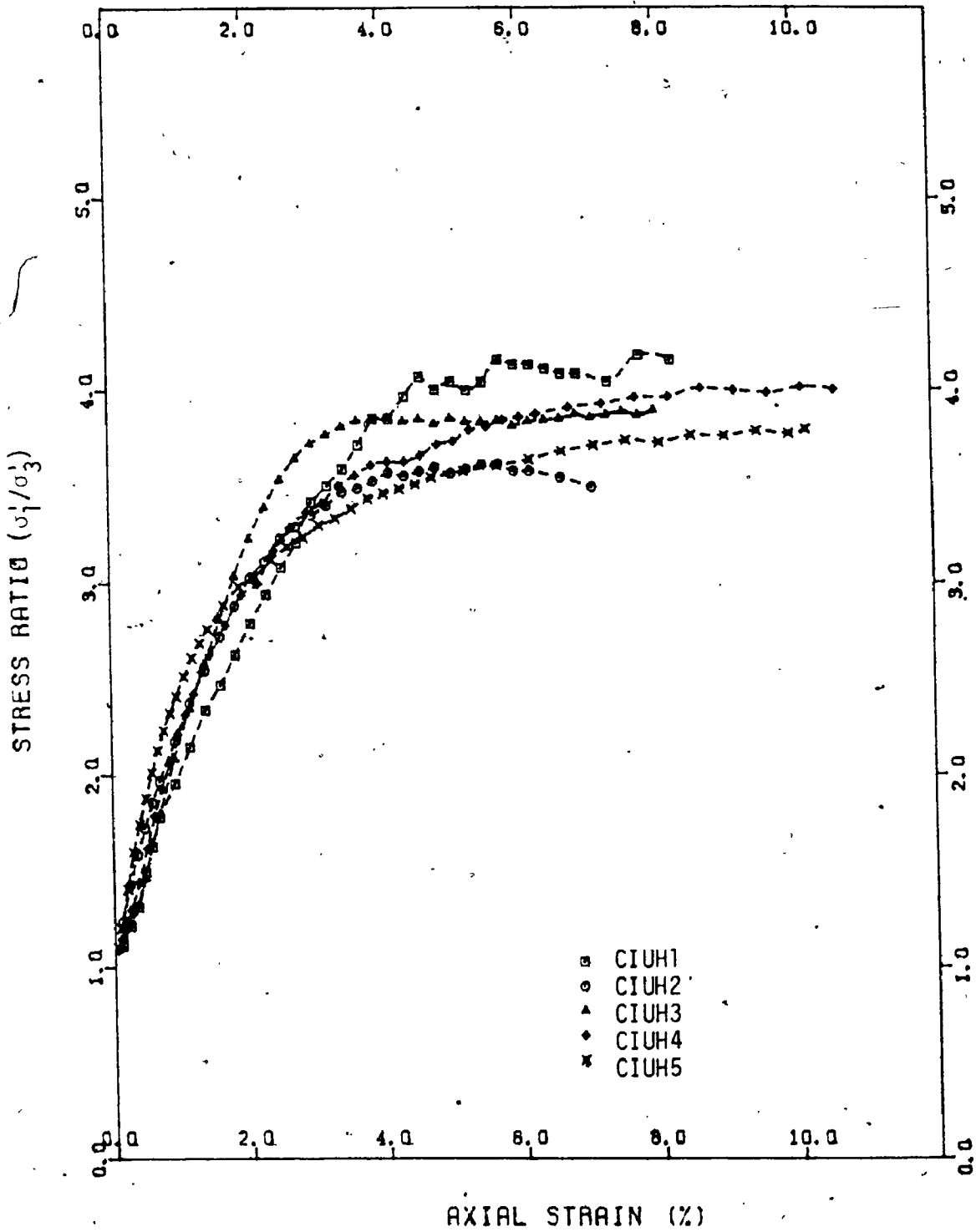


FIGURE 7.8 Stress Ratio-Strain Relationship from CIU Tests for Horizontally Oriented Silty Clay and Varved Clay Samples

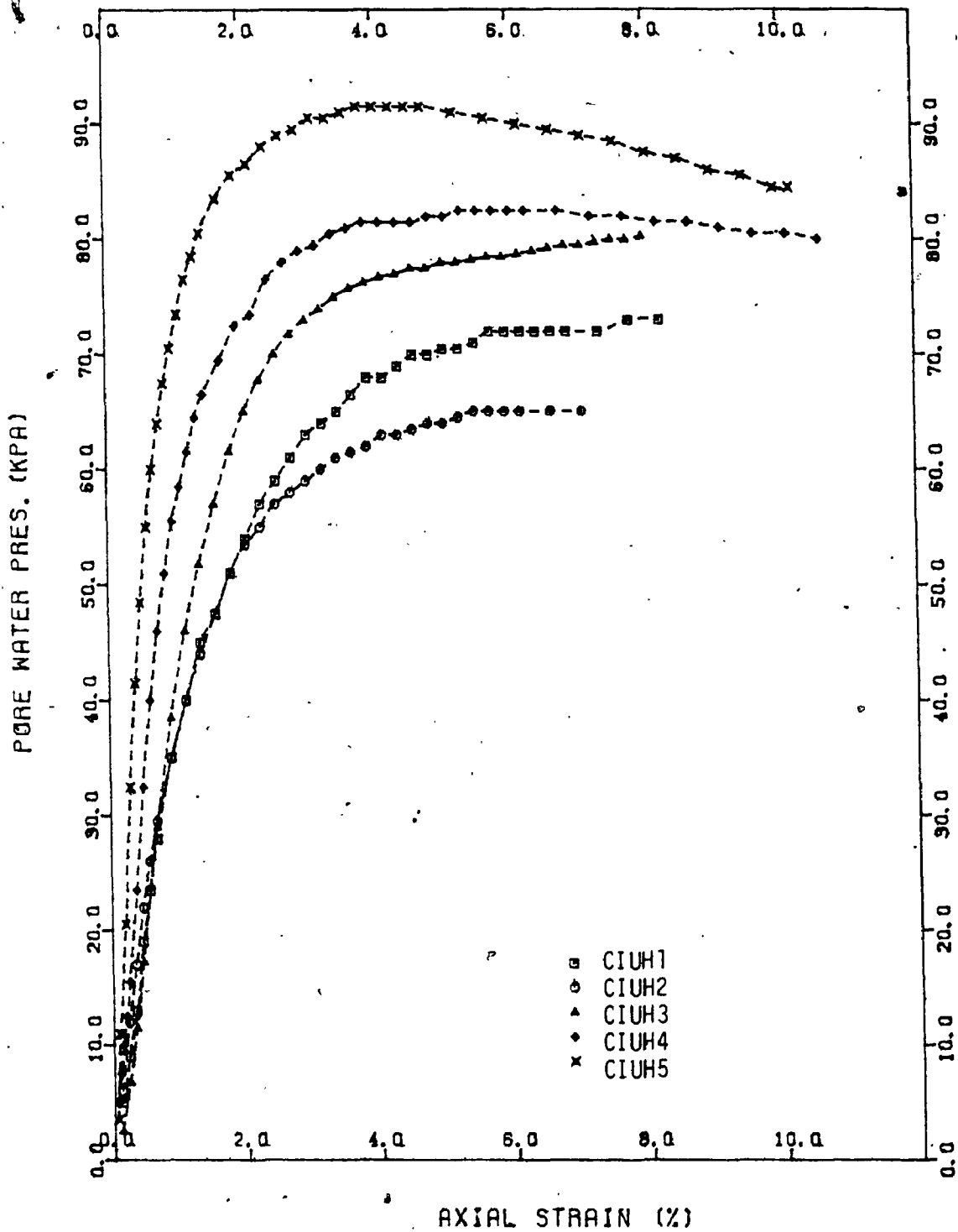


FIGURE 7.9 Excess Pore Water Pressure-Strain Relationship for Horizontally Oriented Silty Clay and Varved Clay Samples

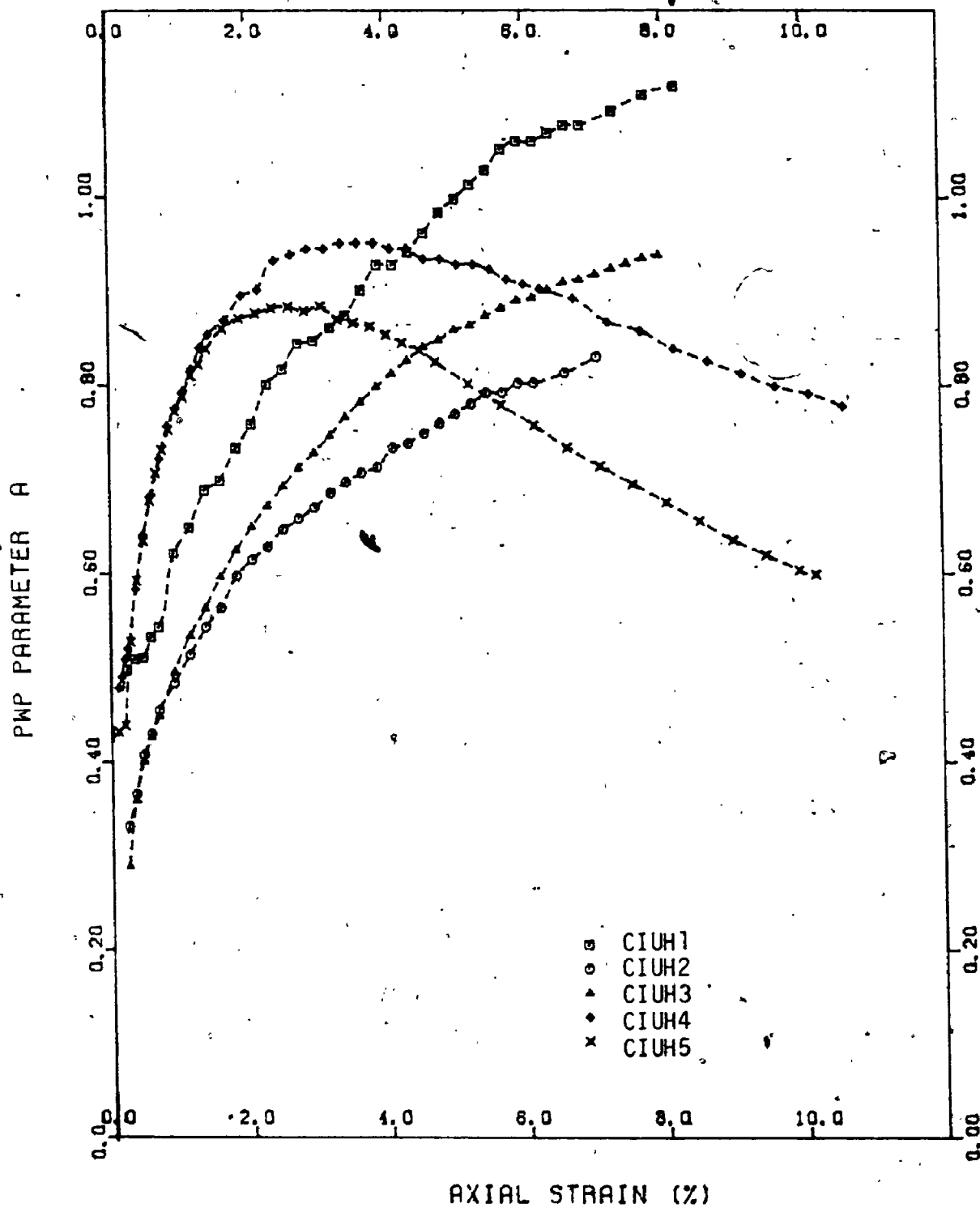


FIGURE 7.10 Pore Pressure Parameter A vs Strain Relationship from CIU Tests on Horizontally Oriented Silty Clay and Varved Clay Samples

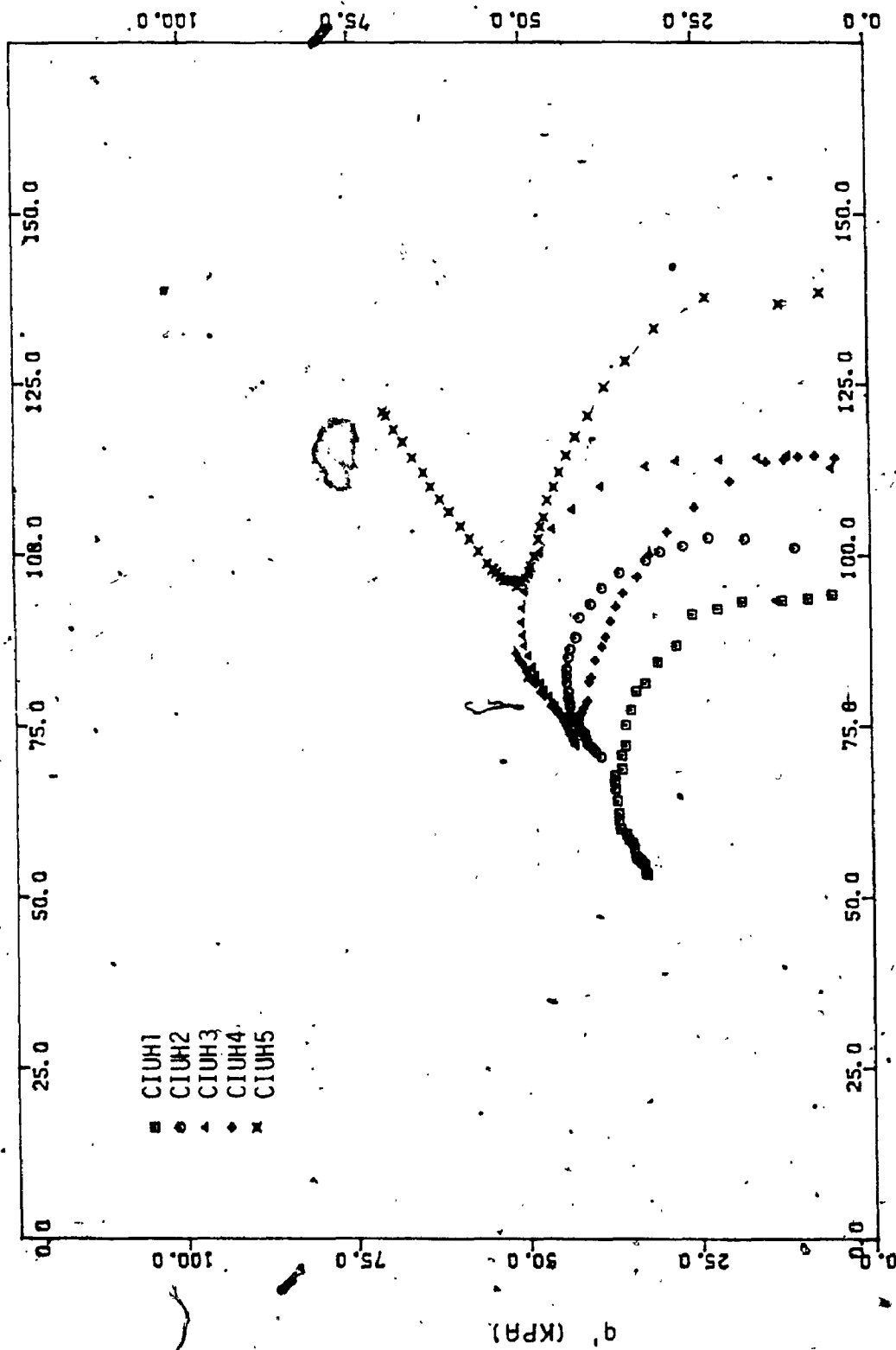


FIGURE 7.11 Effective p-q Stress Path Plot from CIU Tests on Horizontally Oriented Silty Clay and Varved Clay Samples

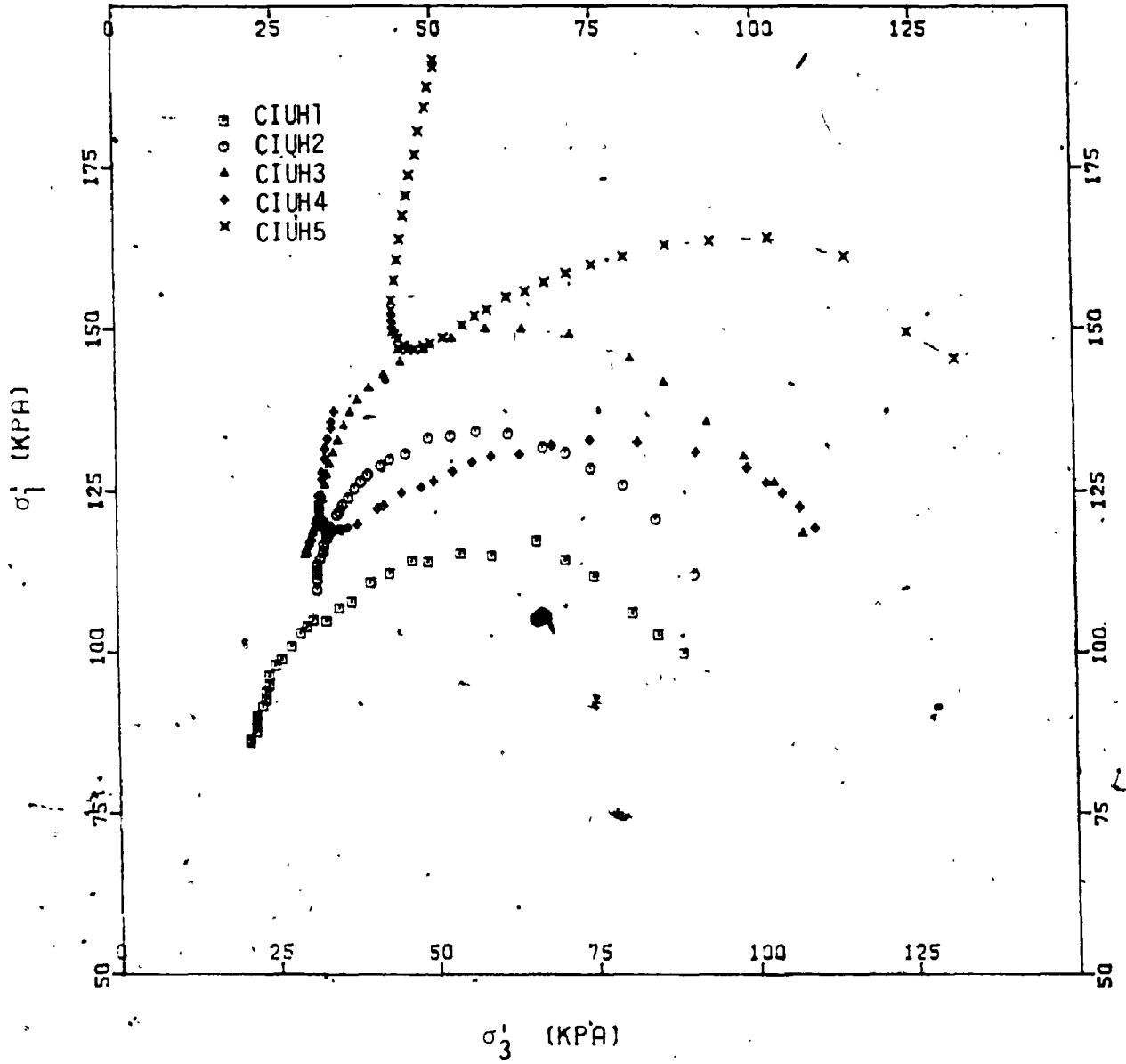


FIGURE 7.12 Effective $\sigma_1 - \sigma_3$ Stress Path Plot from CIU Tests on Horizontally Oriented Silty Clay and Varved Clay Samples

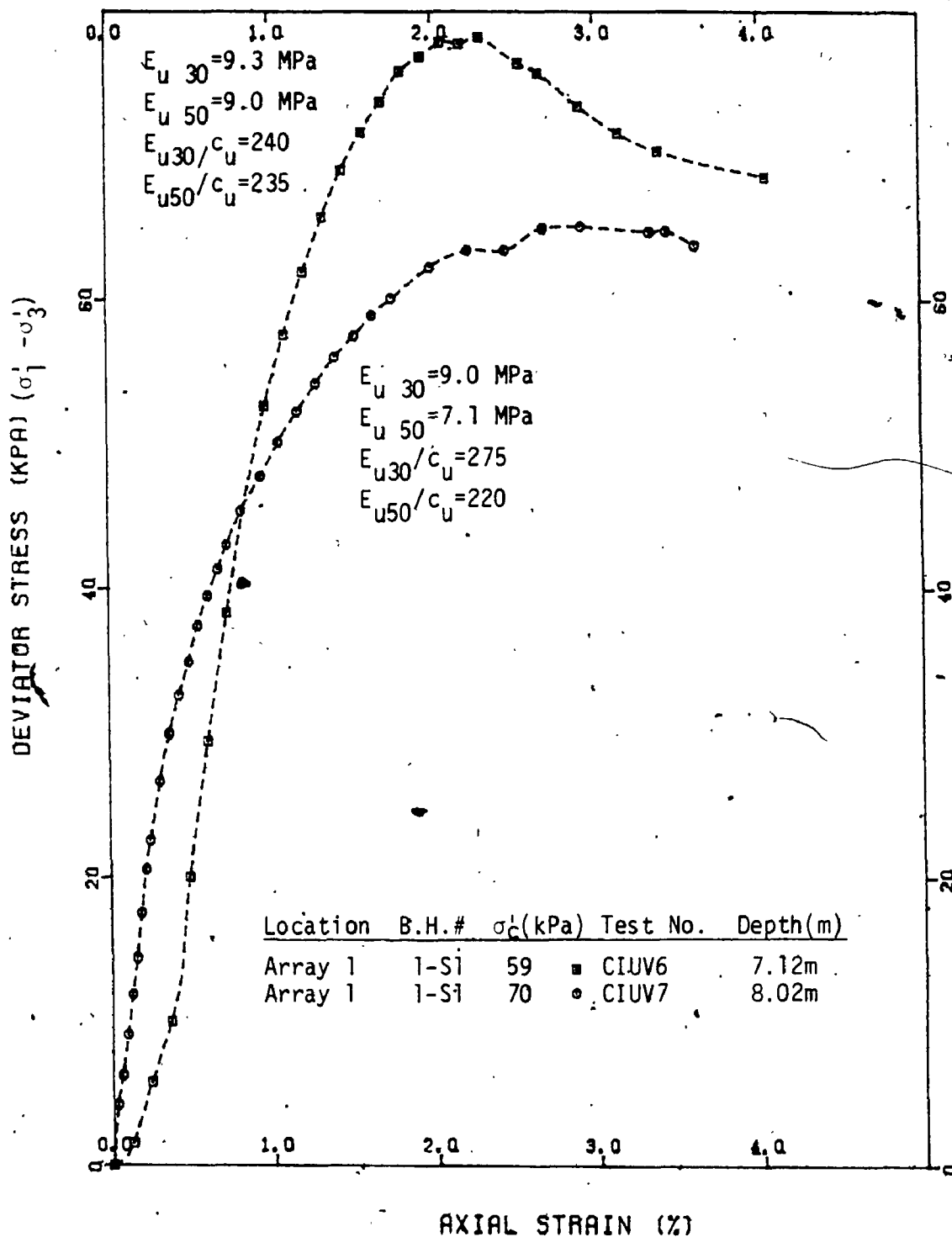


FIGURE 7.13 Stress-Strain Relationship from CIU Tests for Vertically Oriented Silty Clay Samples

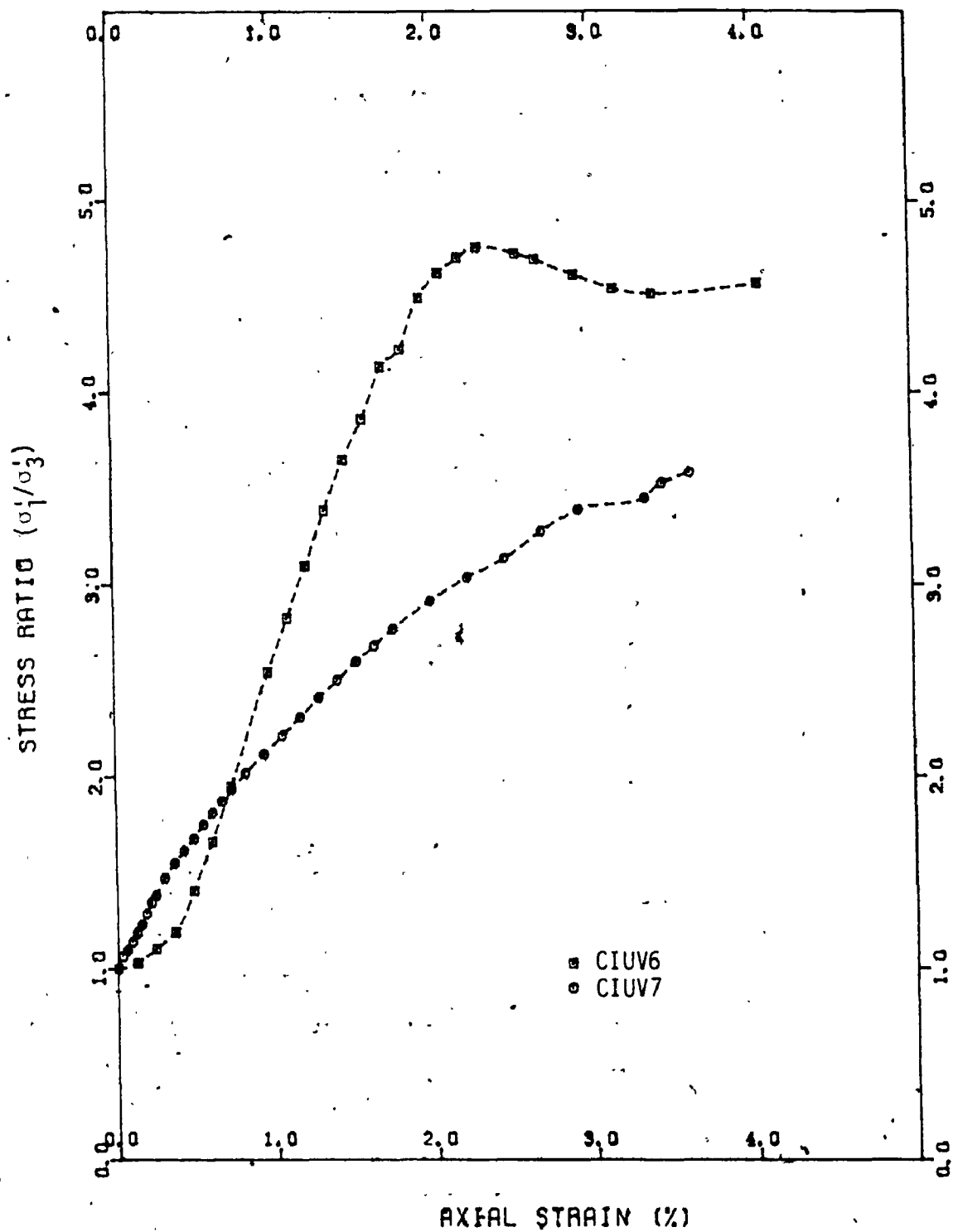


FIGURE 7.14 Stress Ratio-Strain Relationship from CIU Tests for Vertically Oriented Silty Clay Samples

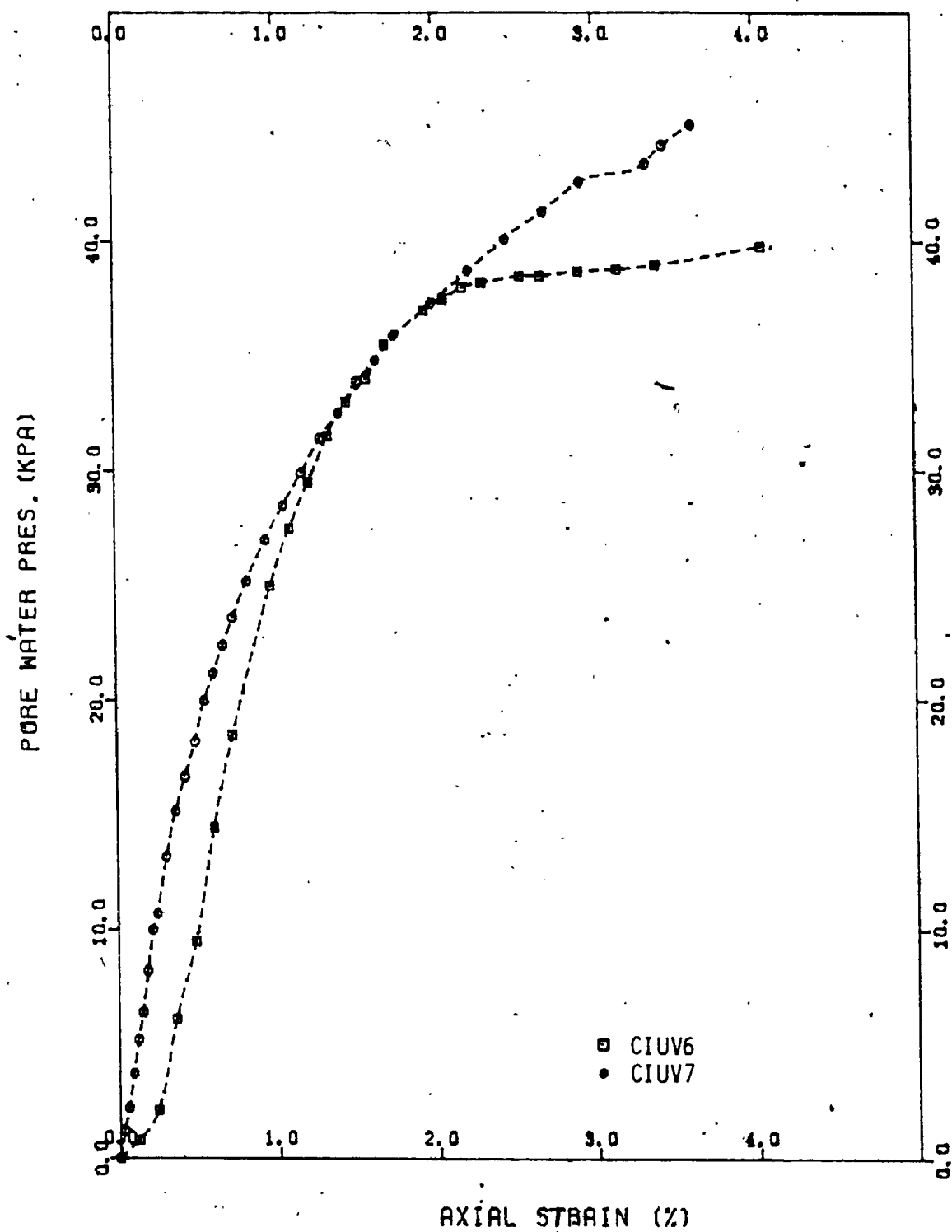


FIGURE 7.15 Excess Pore Water Pressure-Strain Relationship from CIU Tests on Vertically Oriented Silty Clay Samples

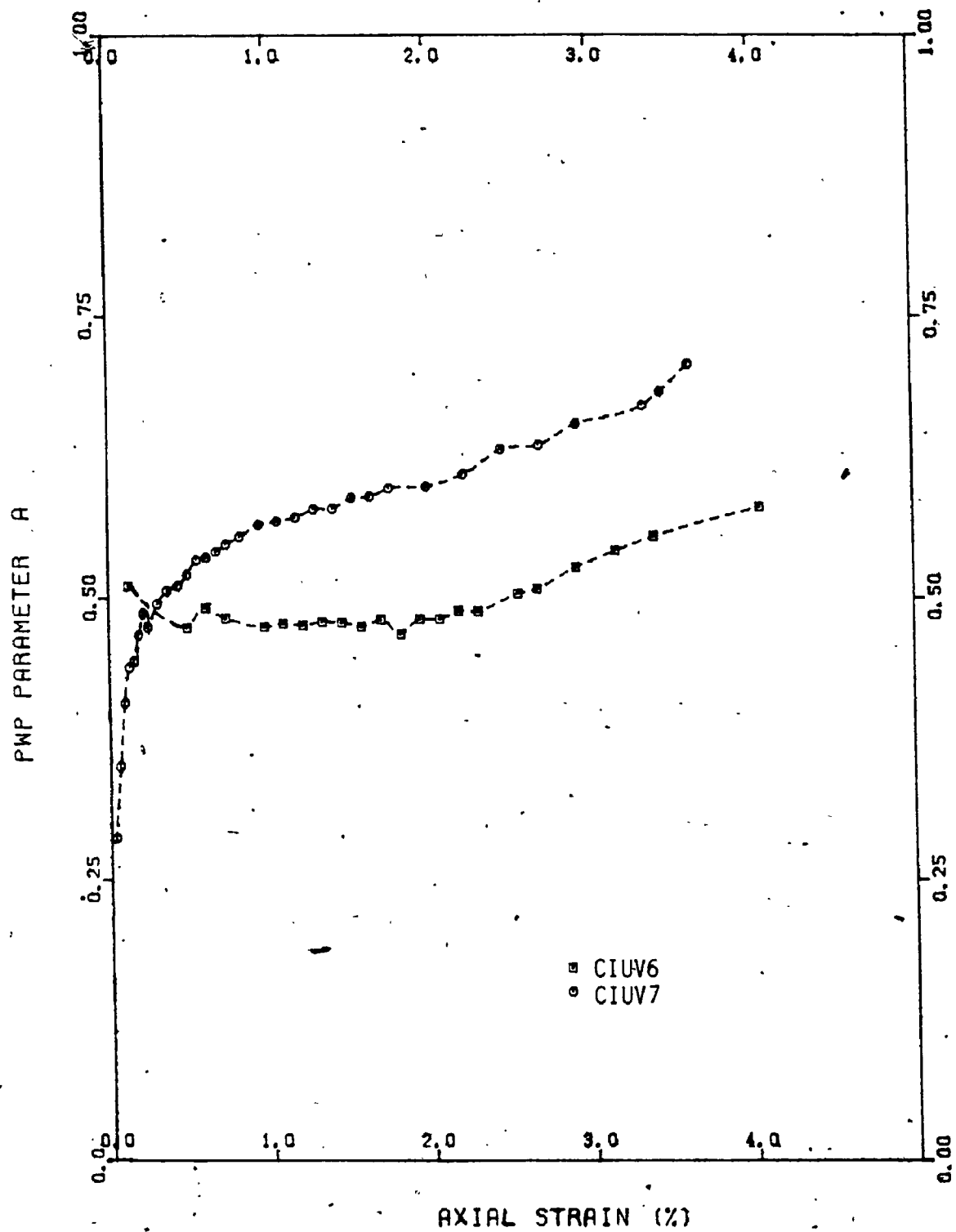


FIGURE 7.16 Pore Pressure Parameter A - Strain Relationship from CIU Tests on Vertically Oriented Silty Clay Samples

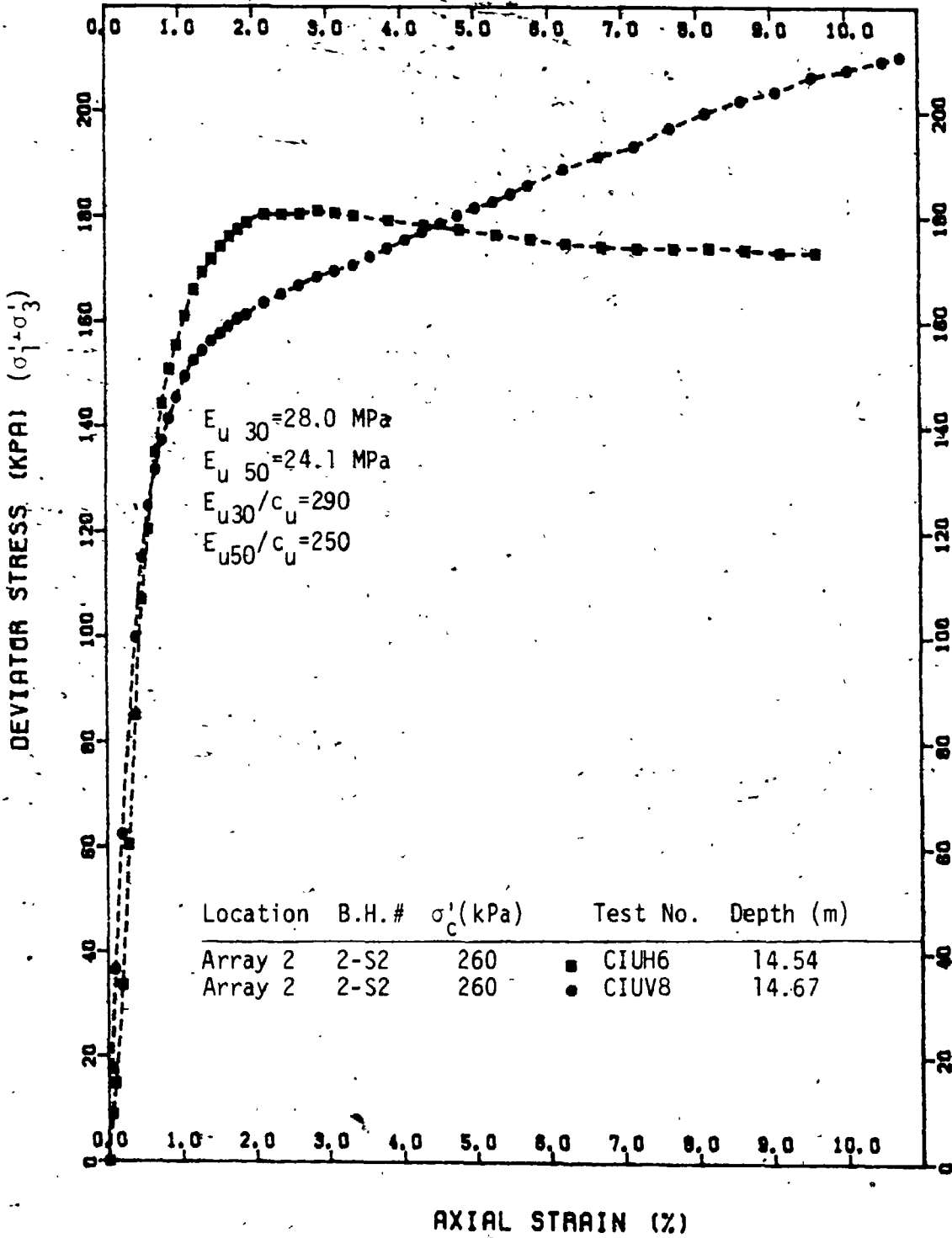


FIGURE 7.17 Stress-Strain Relationship from CIU Tests for Vertically and Horizontally Oriented Varved Clay Samples.

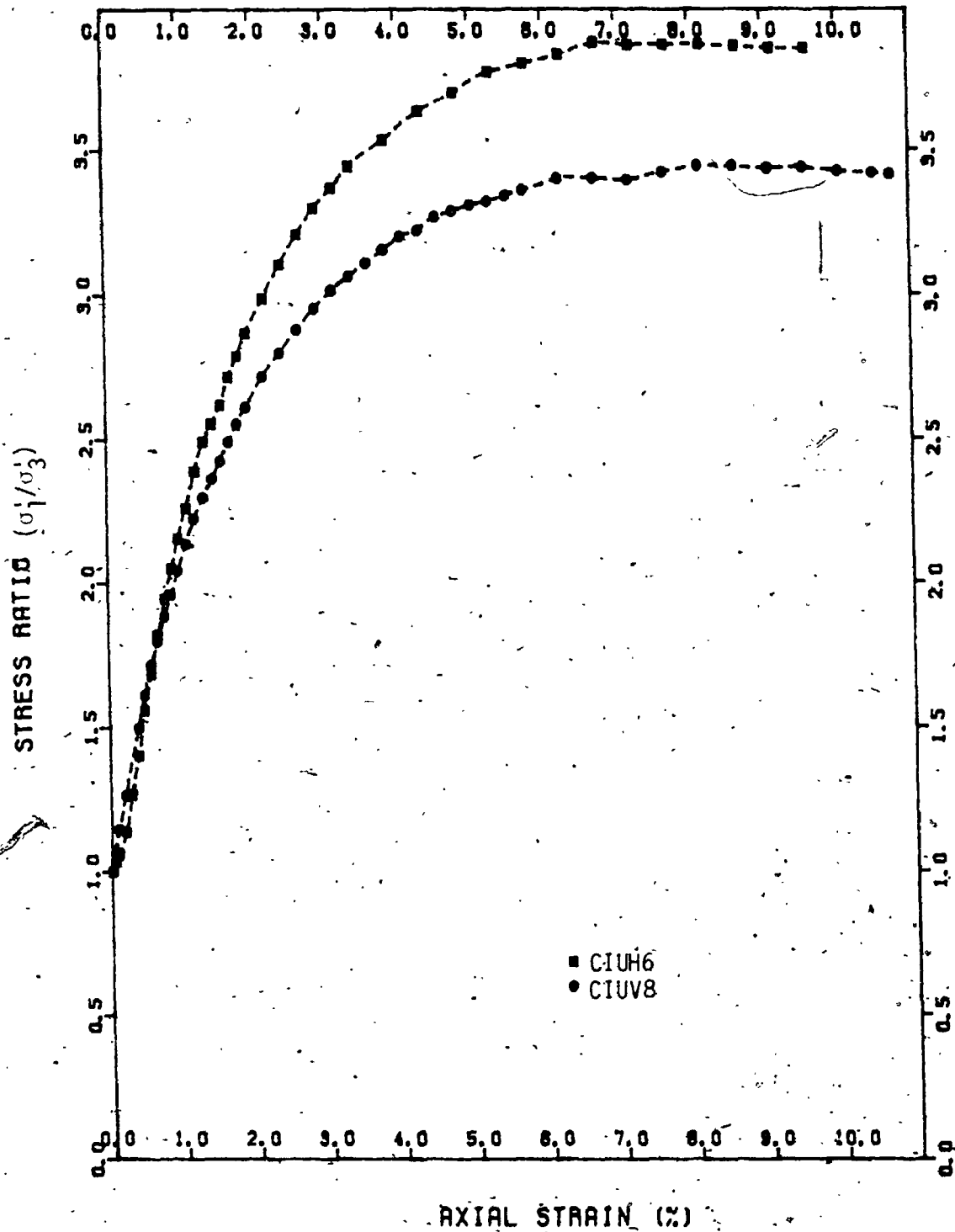


FIGURE 7.18 Stress Ratio-Strain Relationship from CIU Tests for Vertically and Horizontally Oriented Varved Clay Samples

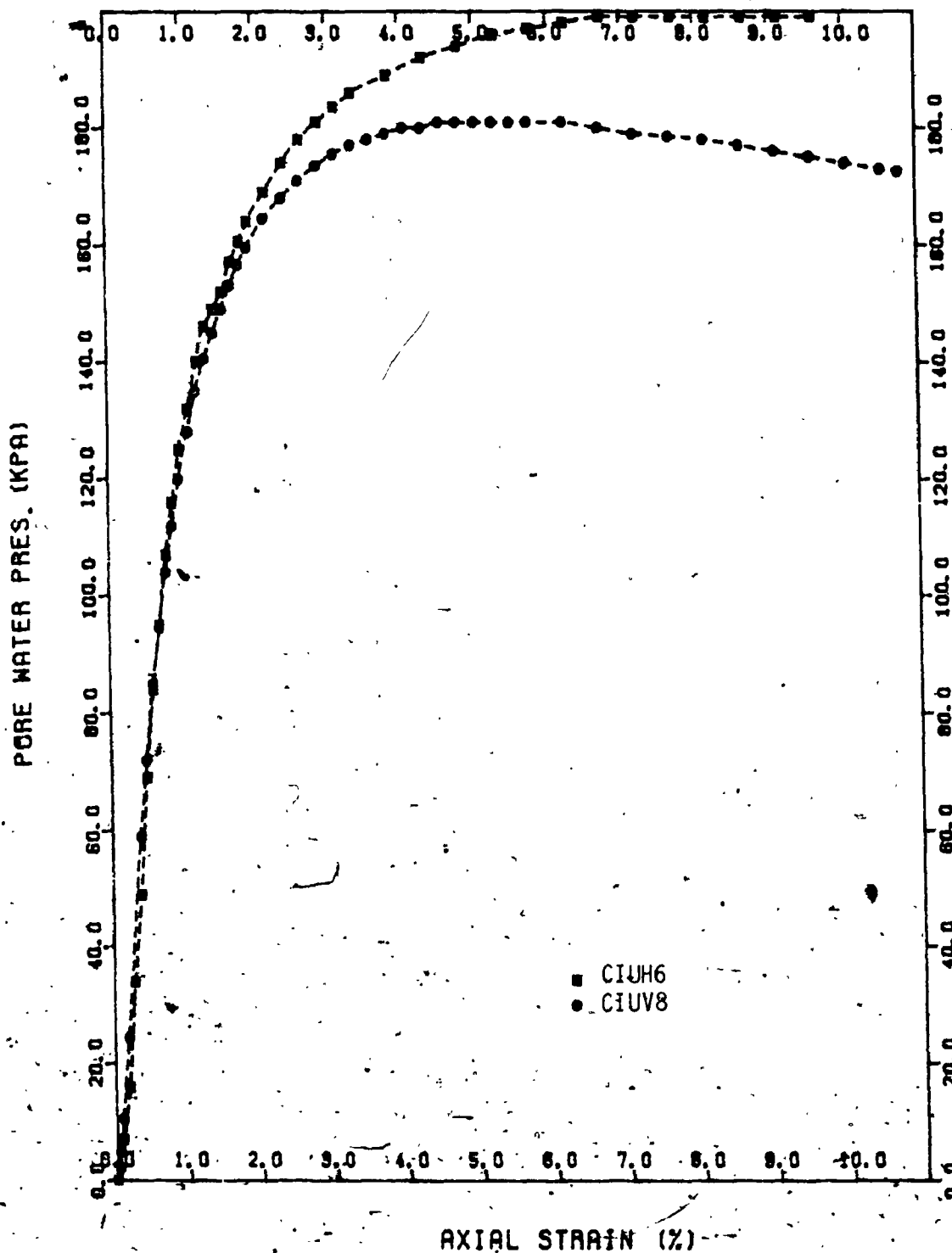


FIGURE 7.19 Excess Pore Water Pressure-Strain Relationship from CIU Tests on Vertically and Horizontally Oriented Varved Clay Samples

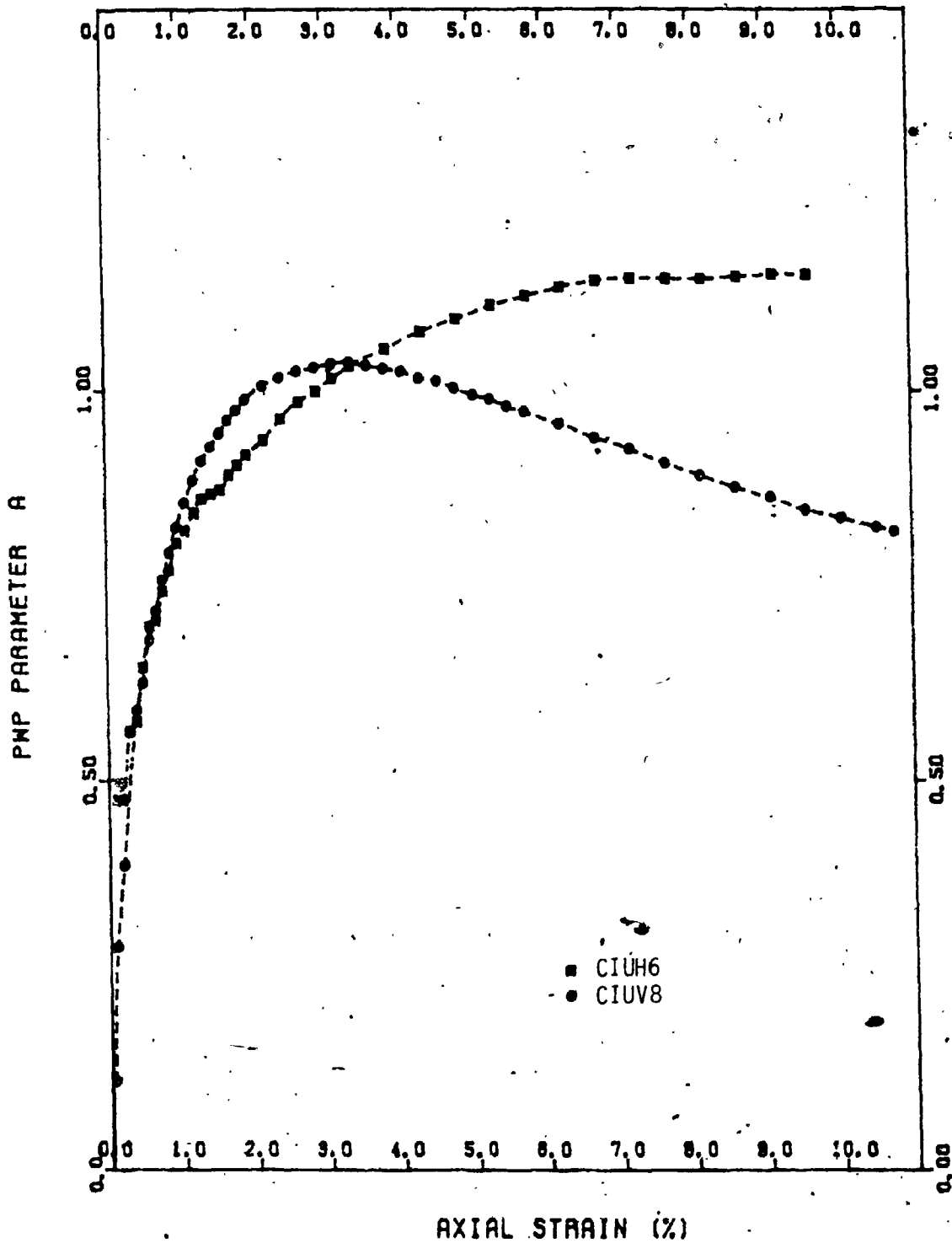


FIGURE 7.20 Pore Water Pressure Parameter A - Strain Relationship from CIU Tests on Vertically and Horizontally Oriented Varved Clay Samples

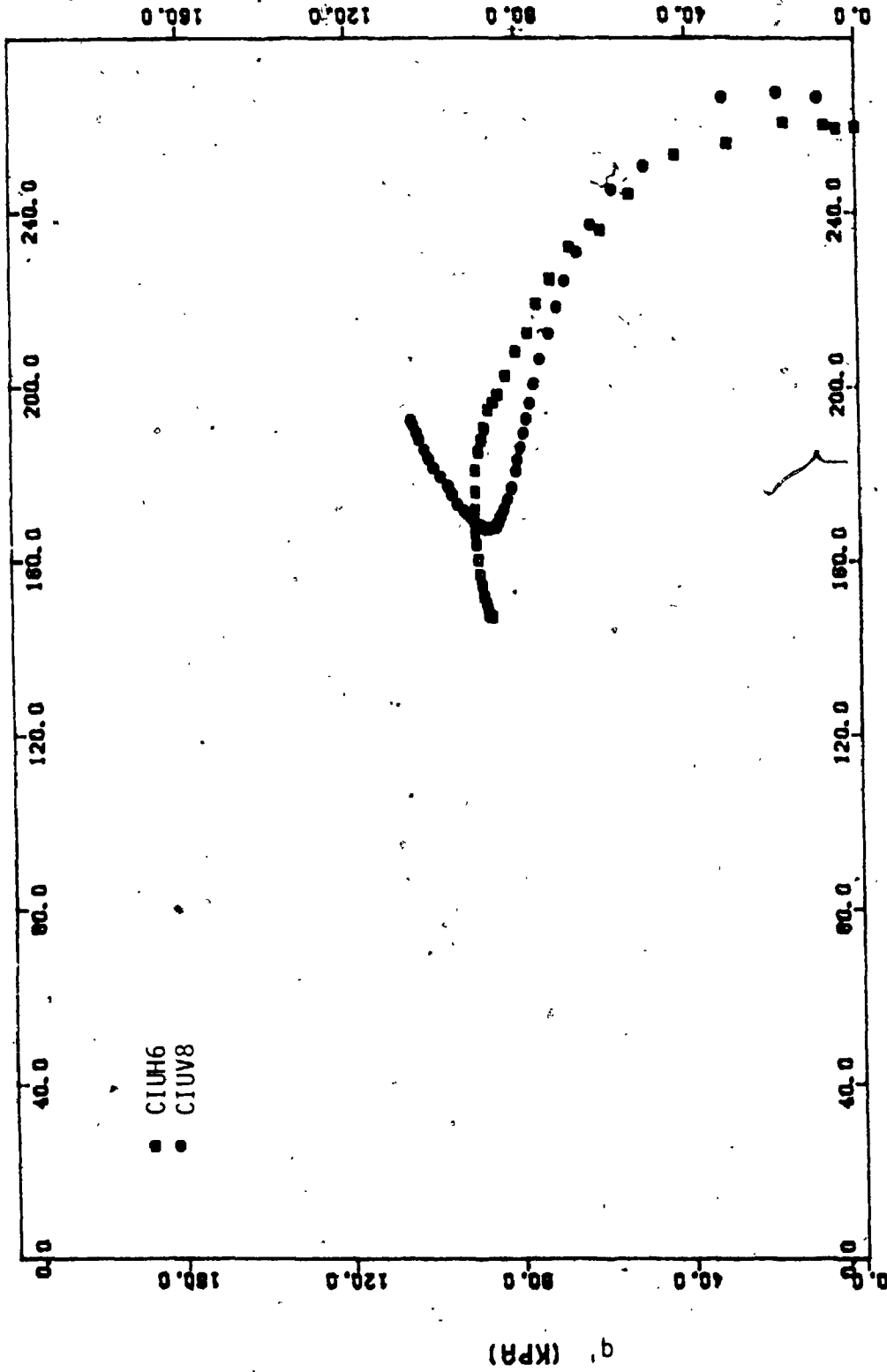


FIGURE 7.21 Effective p-q Stress Path Plot from CIU Tests on Vertically and Horizontally Oriented Varved Clay Samples

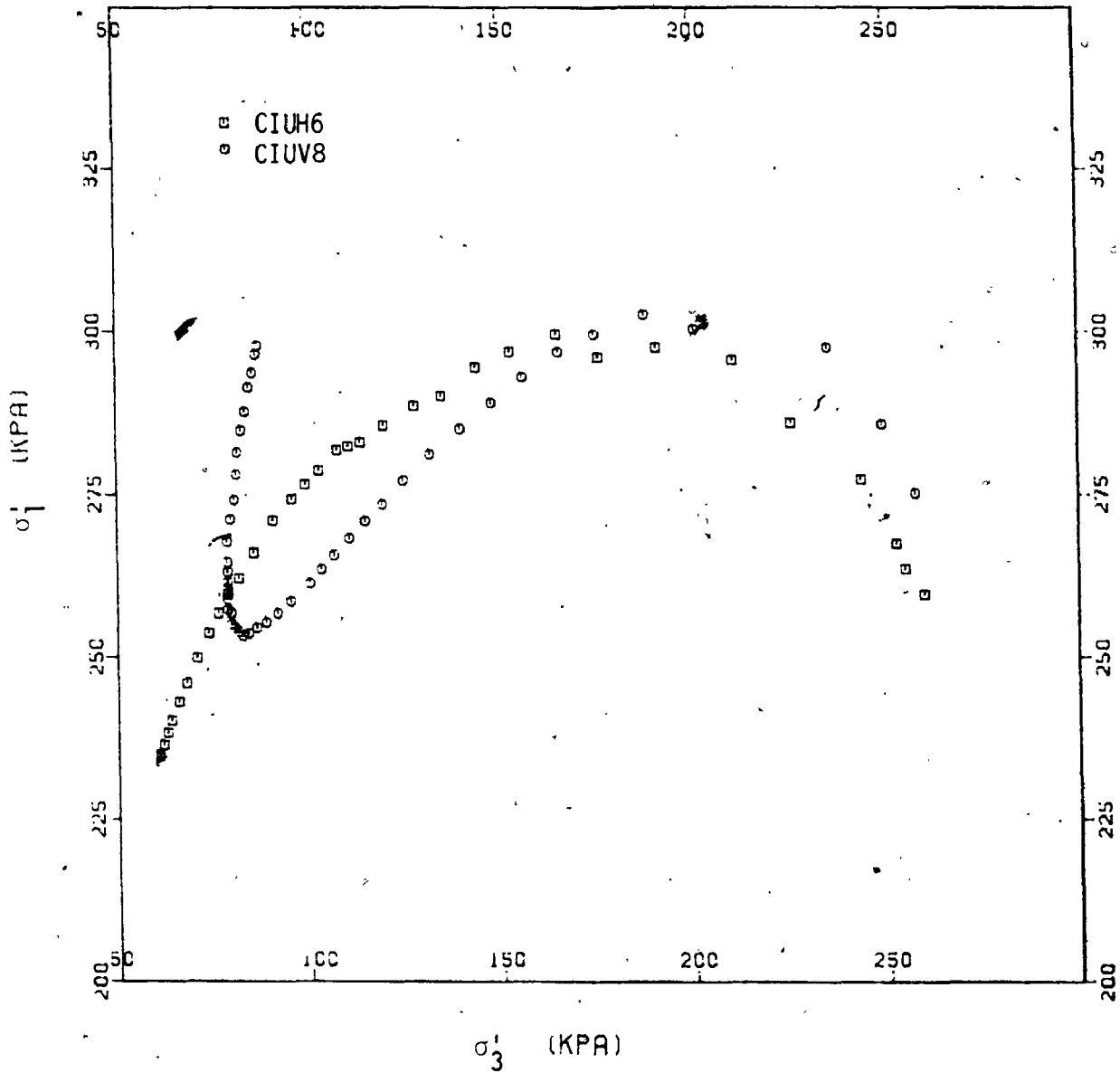


FIGURE 7.22 Effective σ_1' - σ_3' Stress Path Plot from CIU Tests on Vertically and Horizontally Oriented Varved Clay Samples

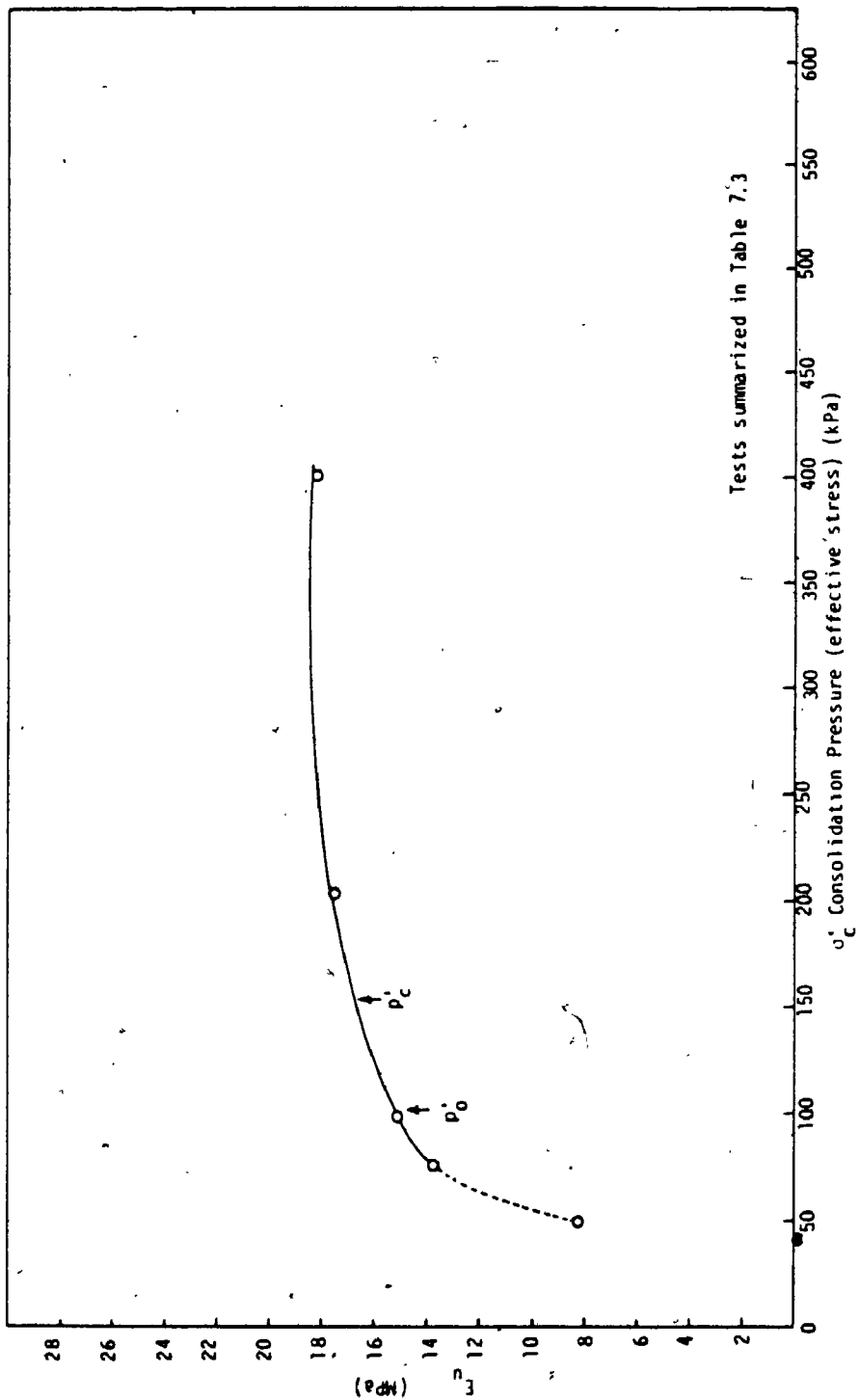


FIGURE 7.23 E_{u30} vs σ'_c for Grey Silty Clay

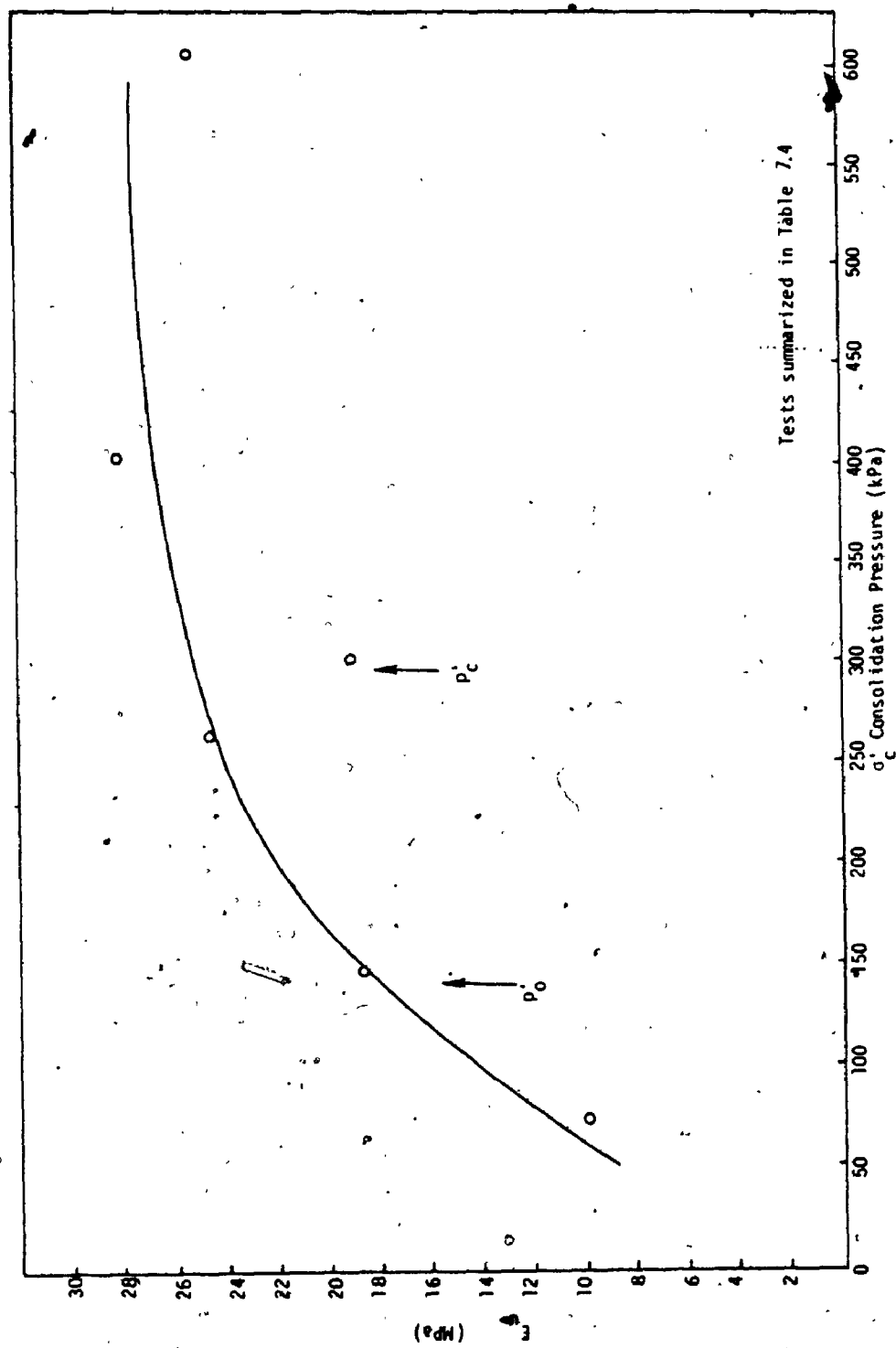


FIGURE 7.24 E_{u30} vs σ'_c for Varved Clay

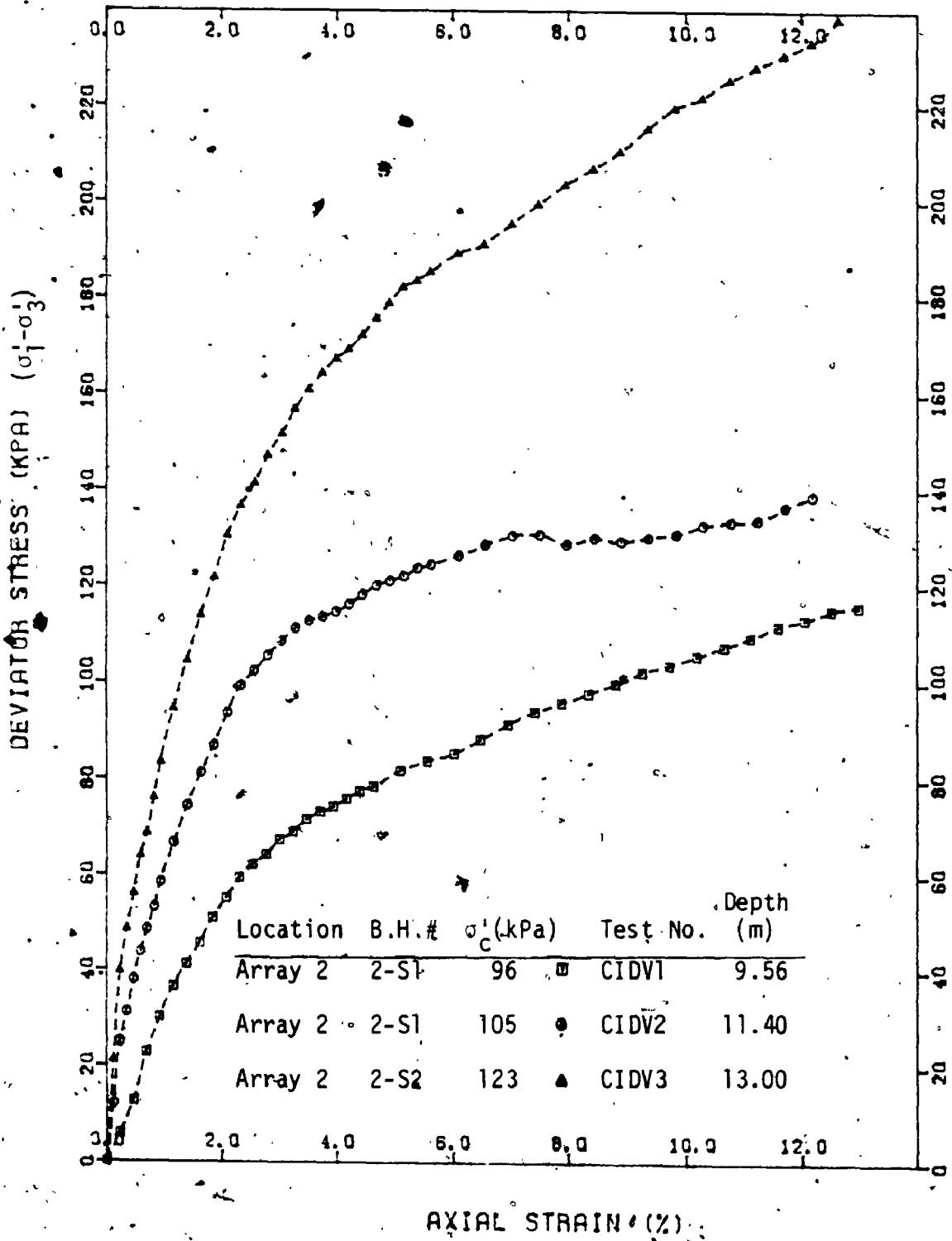


FIGURE 7.25 Stress-Strain Relationship for Silty Clay and Varved Clay from CID Triaxial Tests

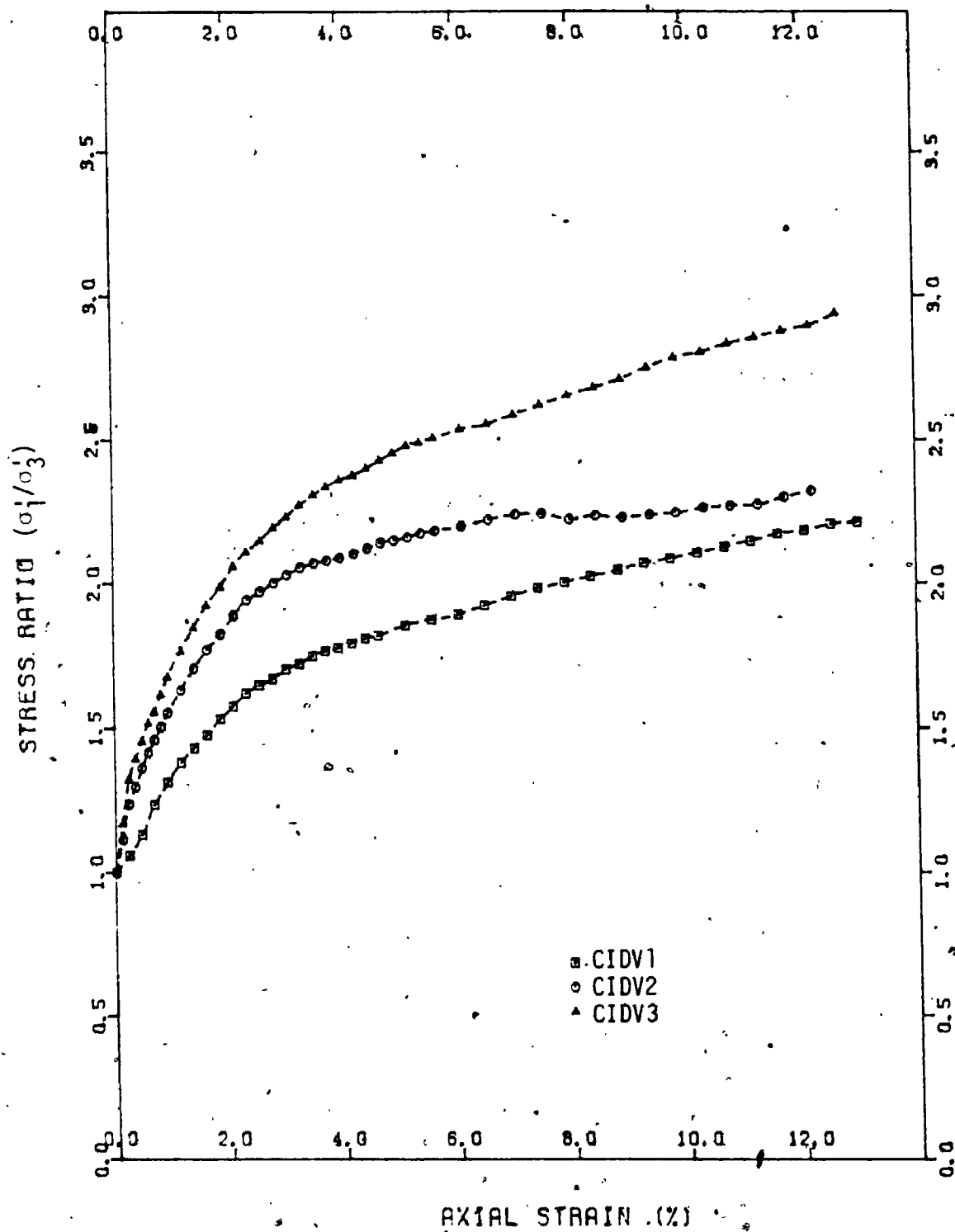


FIGURE 7.26 Stress Ratio-Strain Relationship for Silty Clay and Varved Clay from CID Triaxial Tests

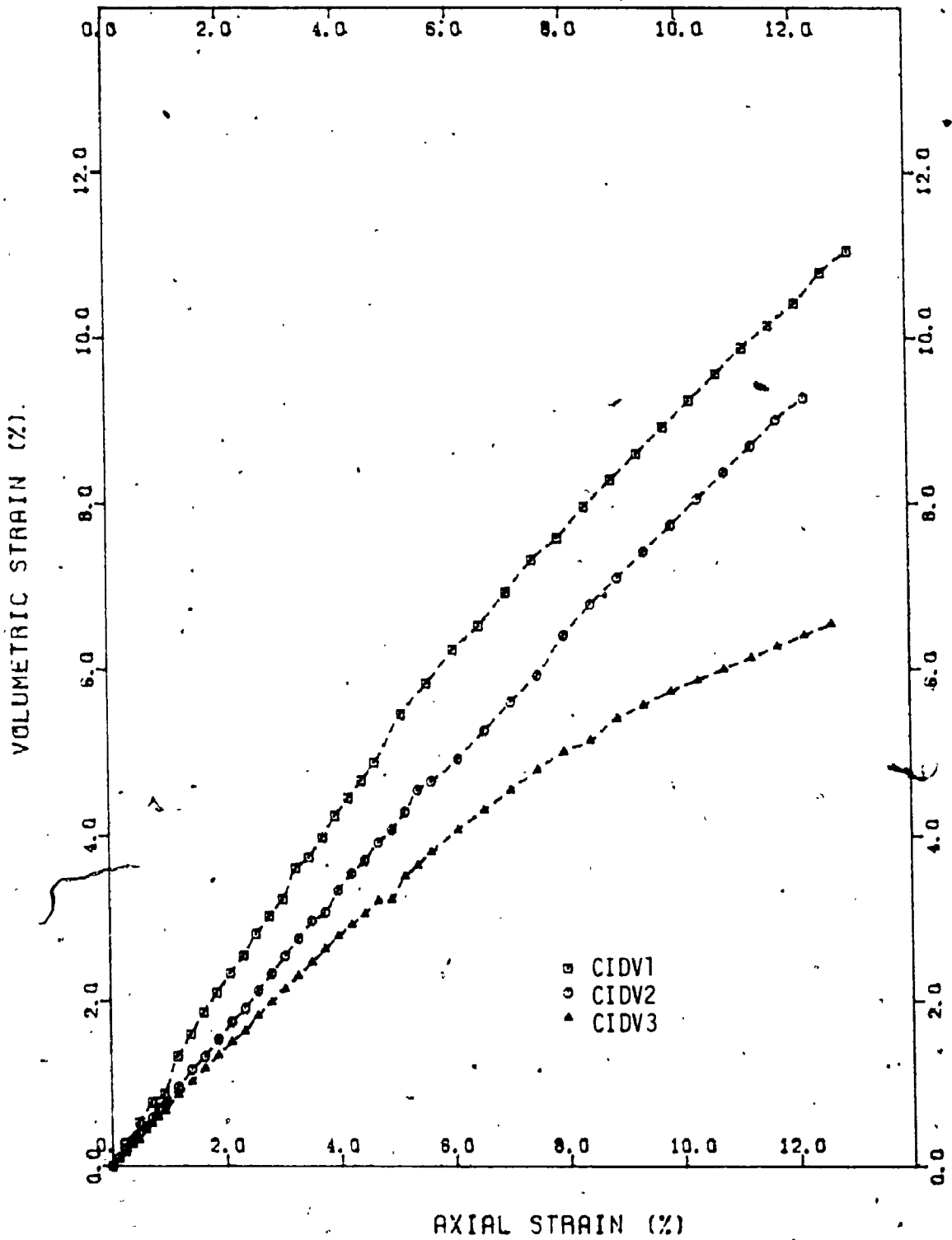


FIGURE 7.27 Volumetric Strain-Axial Strain Relationship for Silty Clay and Varved Clay from CID Triaxial Tests

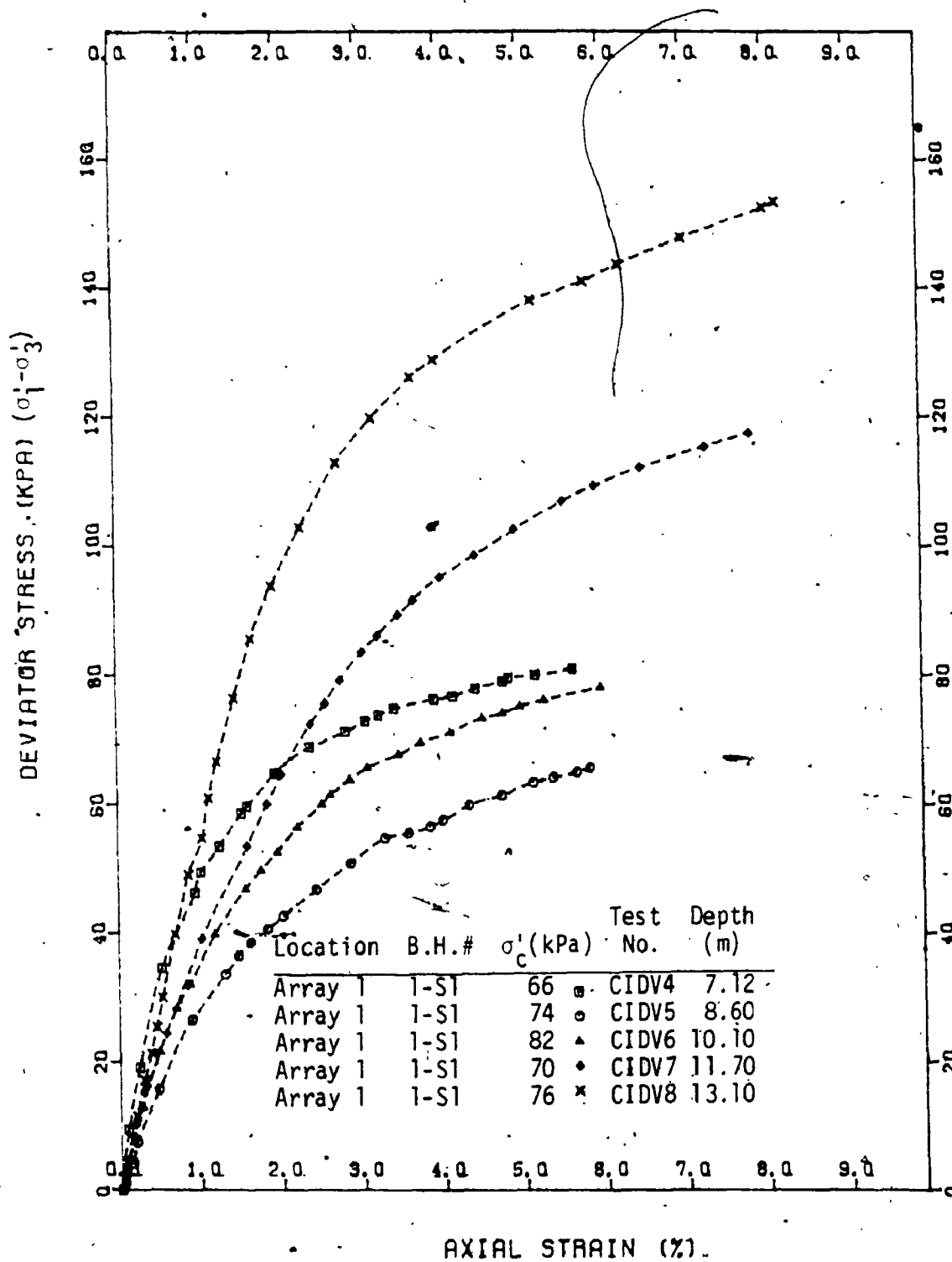


FIGURE 7.28 Stress-Strain Relationship for Silty Clay and Varved Clay from CID Triaxial Tests

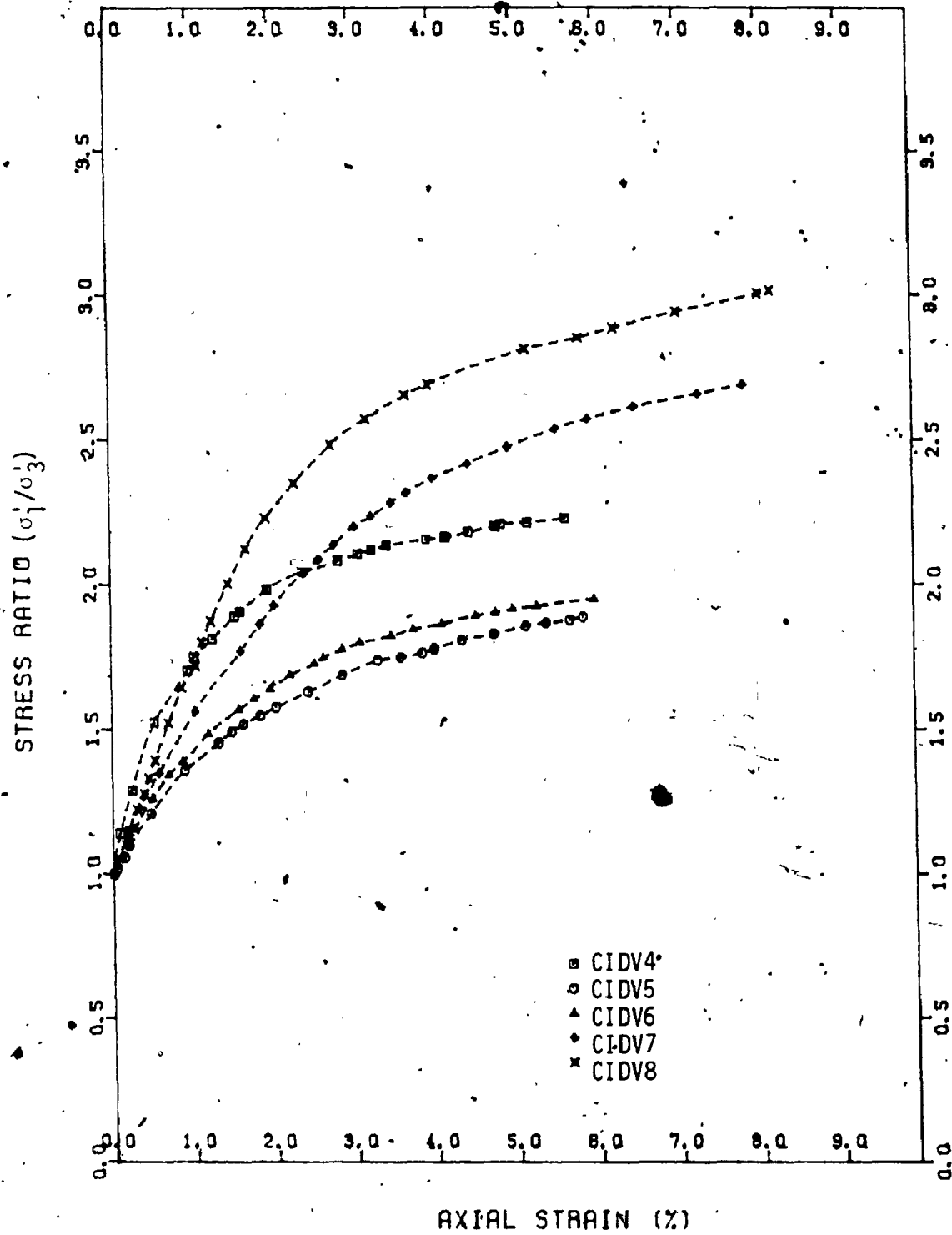


FIGURE 7.29 Stress Ratio-Strain Relationship for Silty Clay and Varved Clay from CID Triaxial Tests

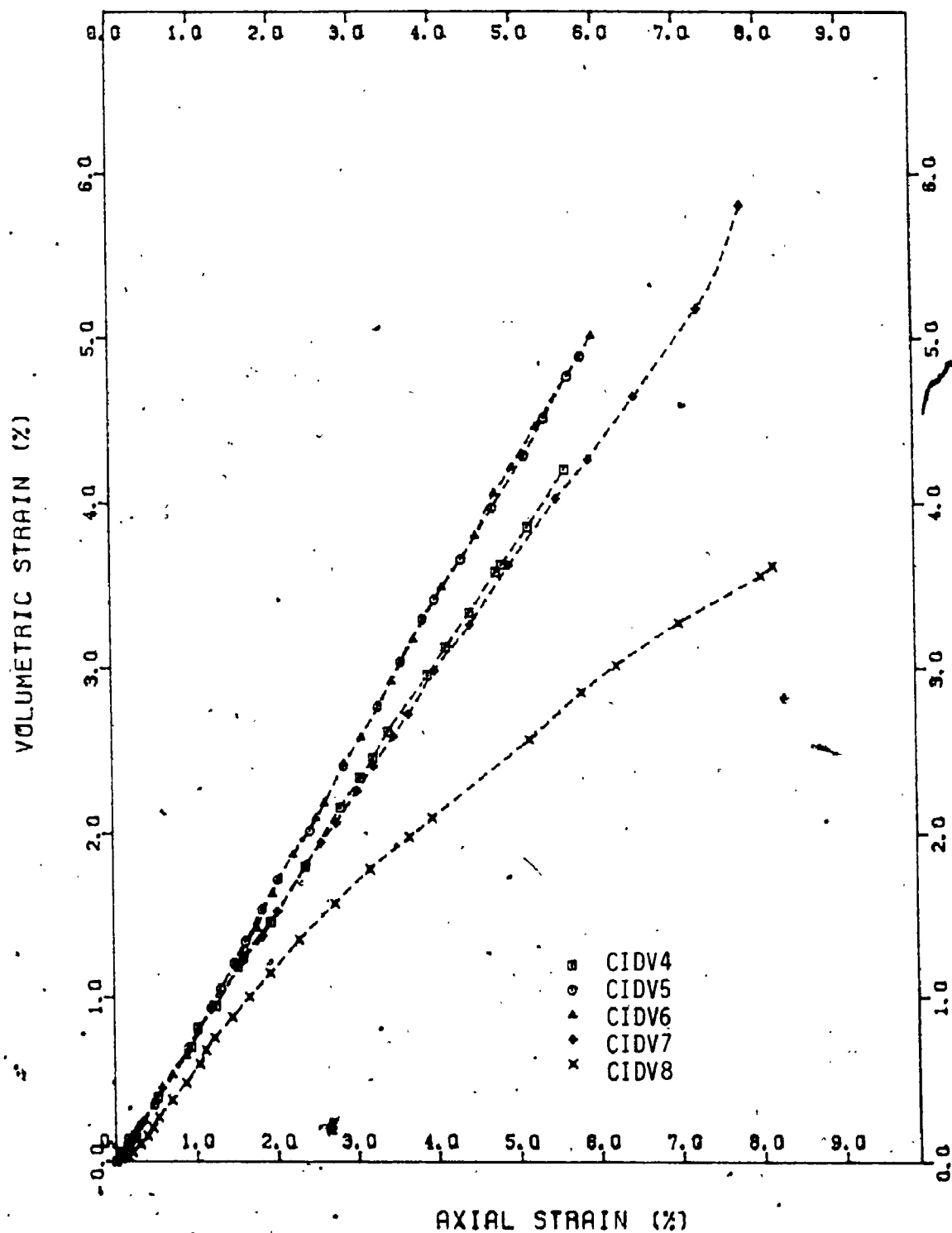


FIGURE 7.30 Volumetric Strain-Axial Strain Relationship for Silty Clay and Varved Clay from CID Triaxial Tests

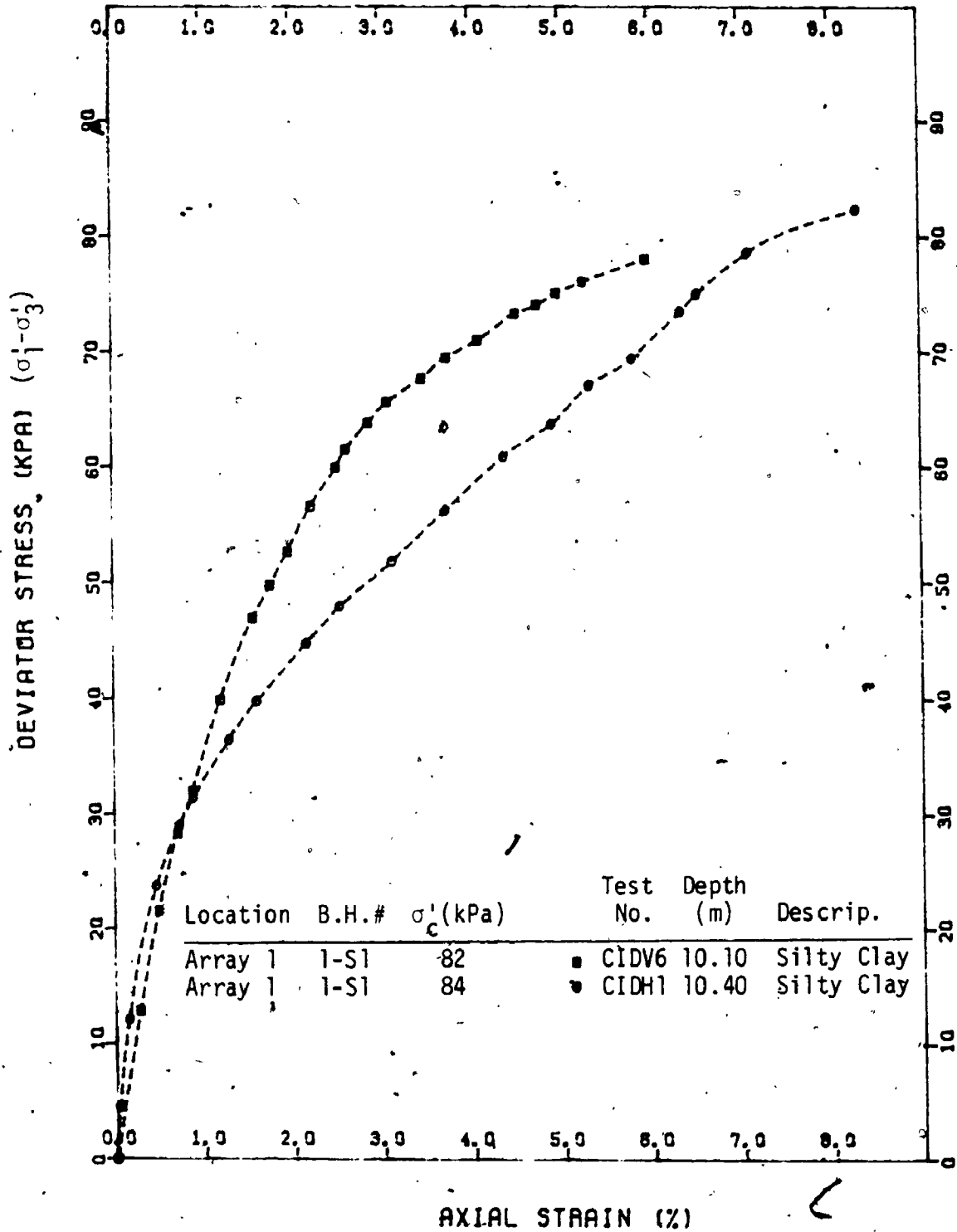


FIGURE 7.31 Stress-Strain Relationship for Silty Clay from CID Tests on Vertically and Horizontally Oriented Samples

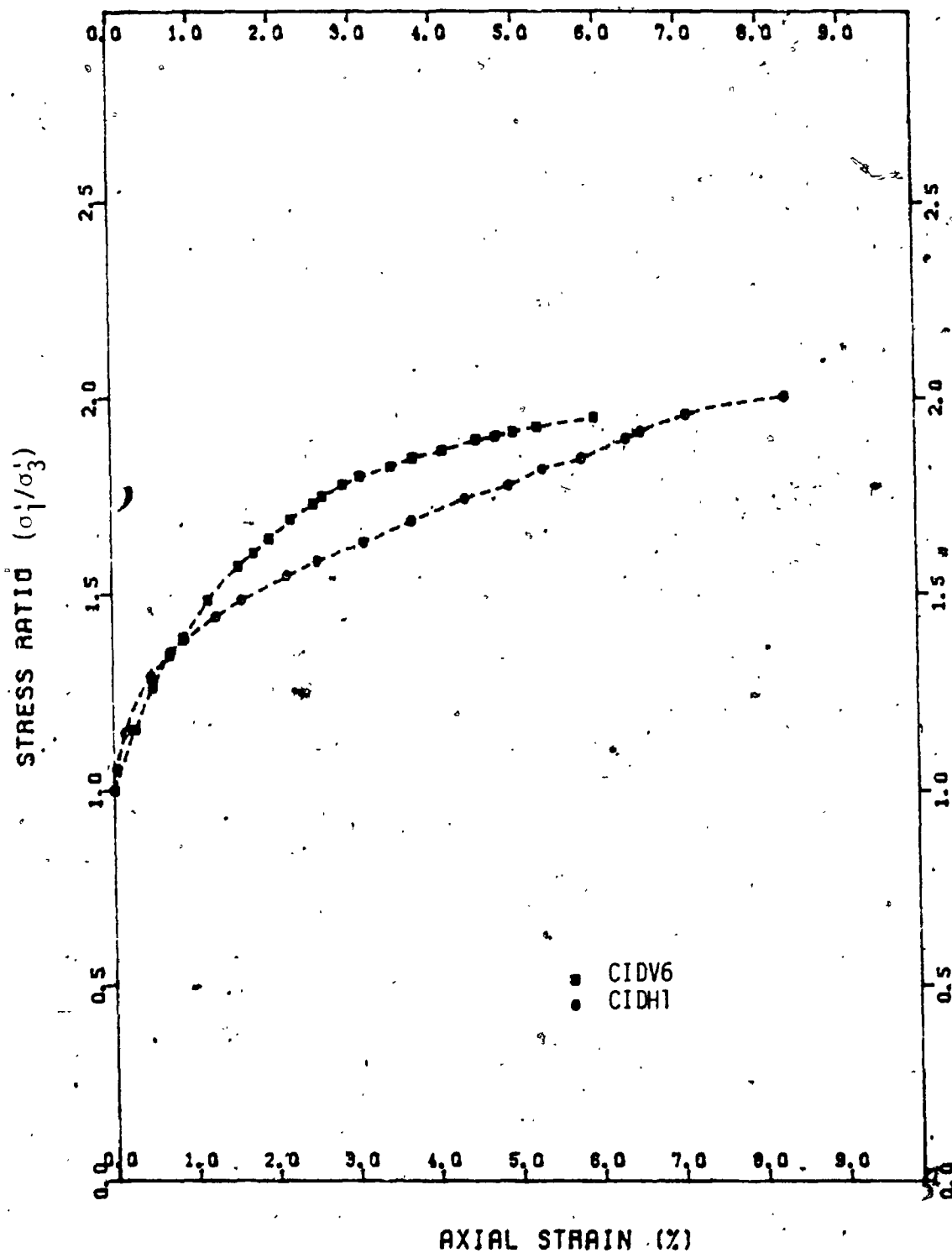


FIGURE 7.32 Stress Ratio-Strain Relationship for Silty Clay from CID Tests on Vertically and Horizontally Oriented Samples

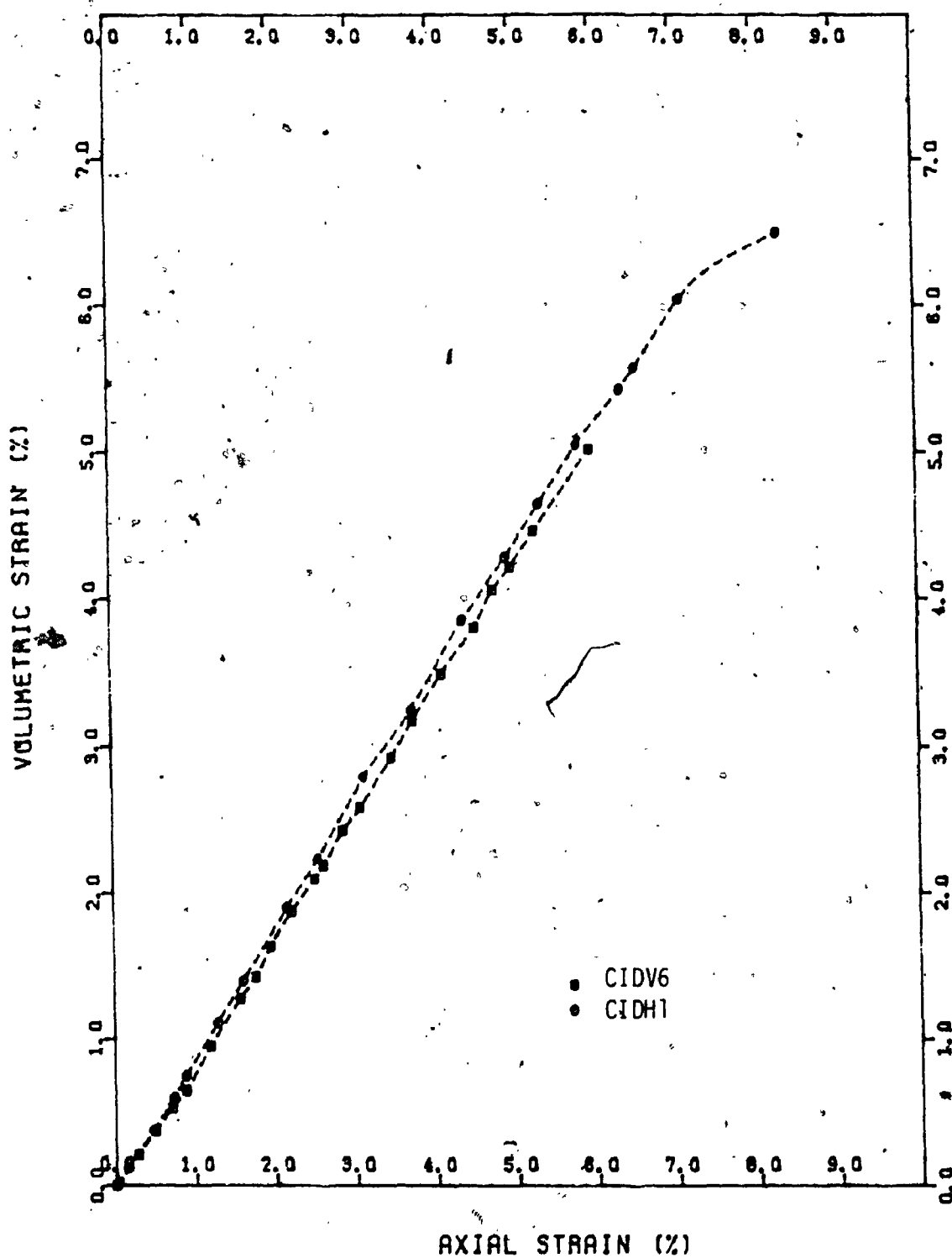


FIGURE 7.33 Volumetric Strain-Axial Strain Relationship from CID Tests on Vertically and Horizontally Oriented Samples

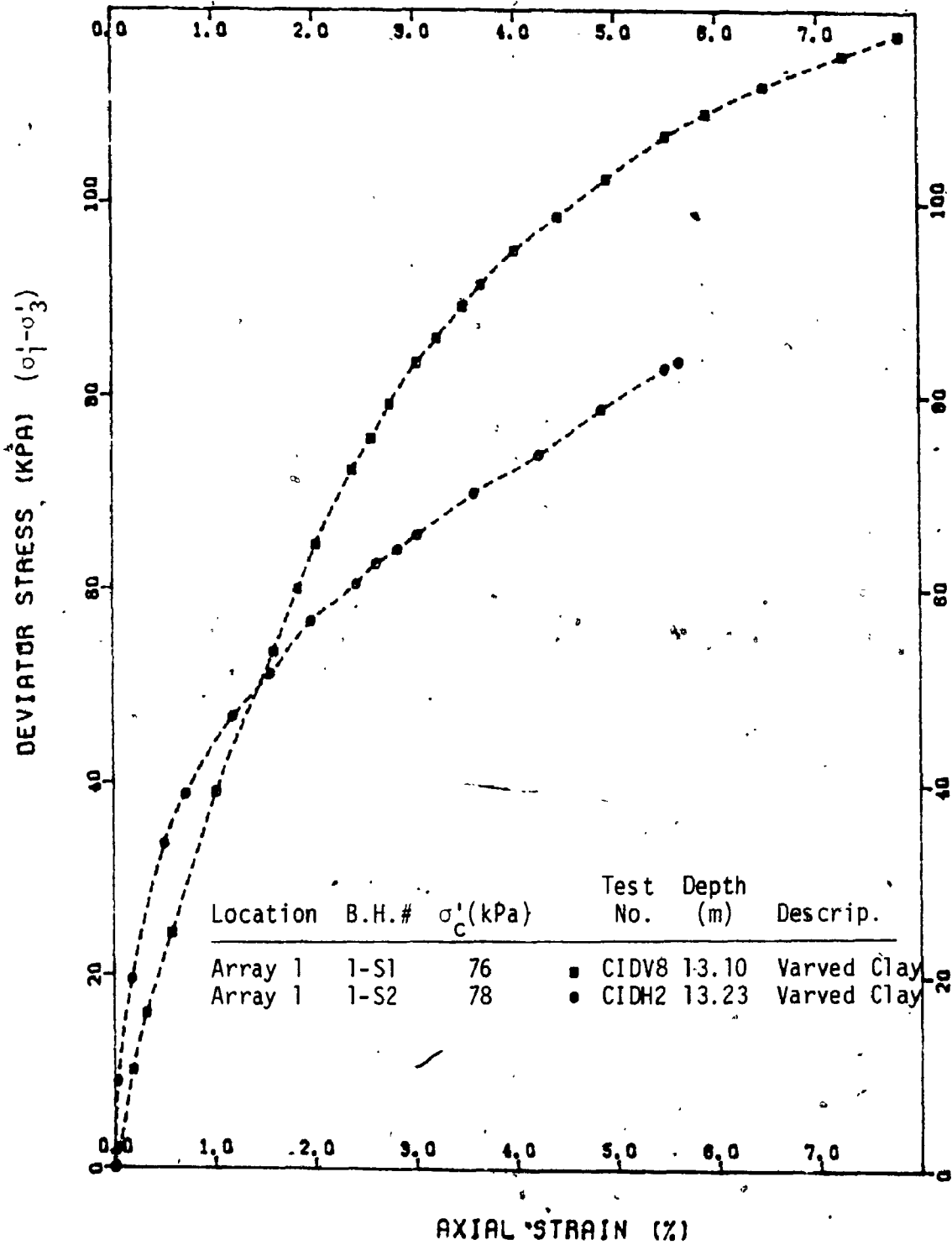


FIGURE 7.34 Stress-Strain Relationship for Varved Clay from CID Tests on Vertically and Horizontally Oriented Samples

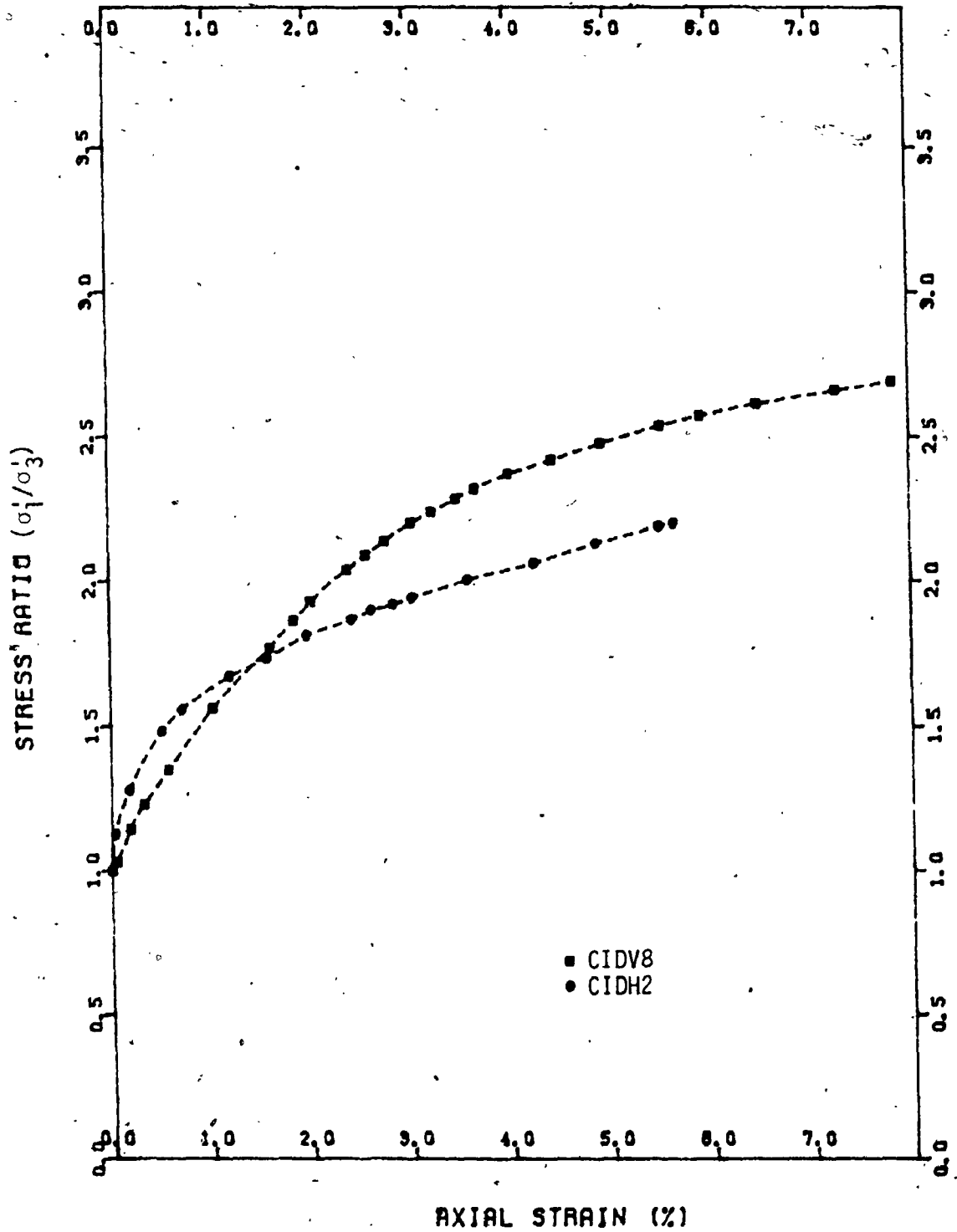


FIGURE 7.35 Stress Ratio-Strain Relationship for Varved Clay from CID Tests on Vertically and Horizontally Oriented Samples

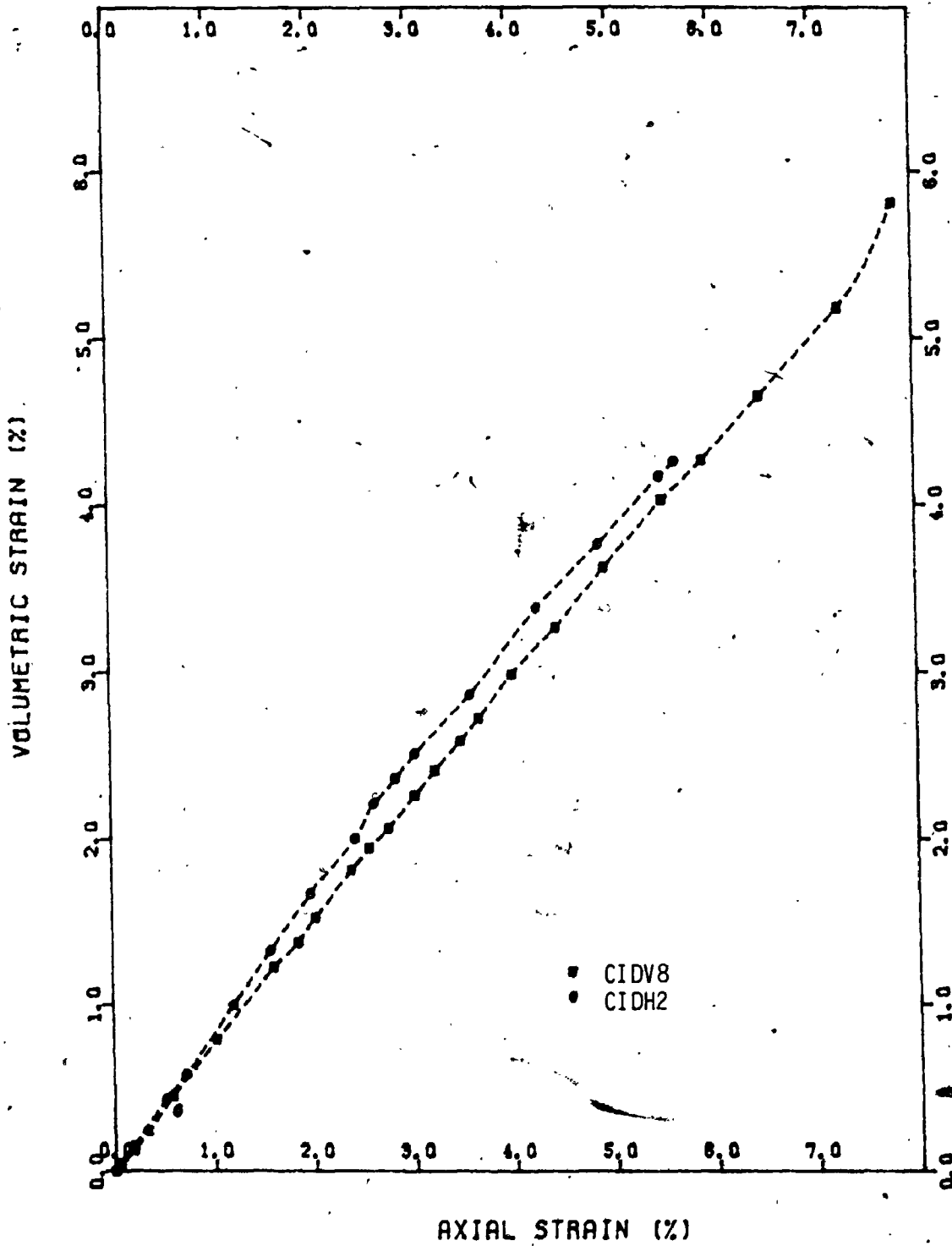


FIGURE 7.36 Volumetric Strain-Axial Strain Relationship for Varved Clay from CID Tests on Vertically and Horizontally Oriented Samples*

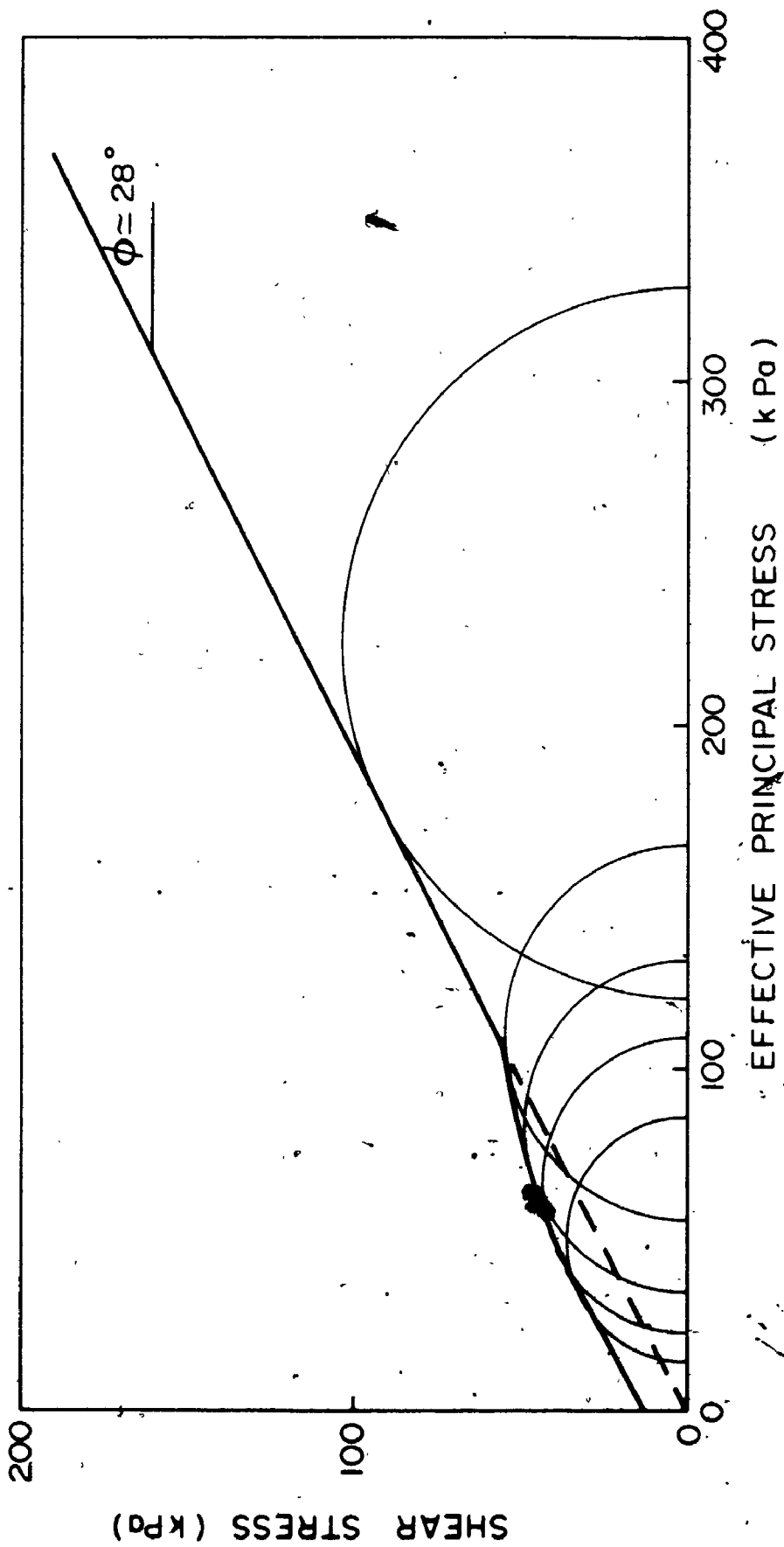


FIGURE 7.37 Strength Envelope - Grey Silty Clay at Thunder Bay (Array 2)

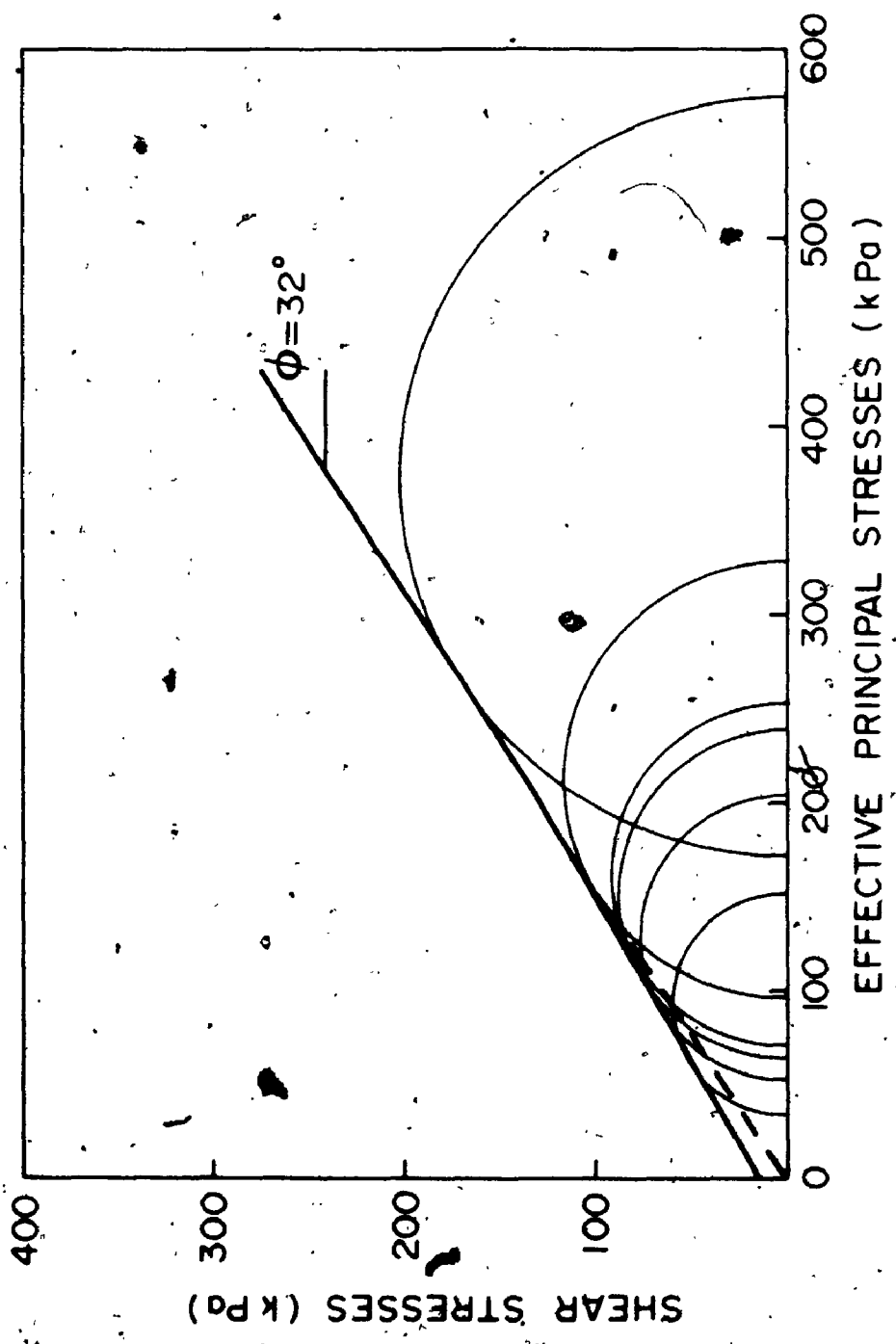


FIGURE 7.38 Strength Envelope - Varved Clay at Thunder Bay (Array 2).

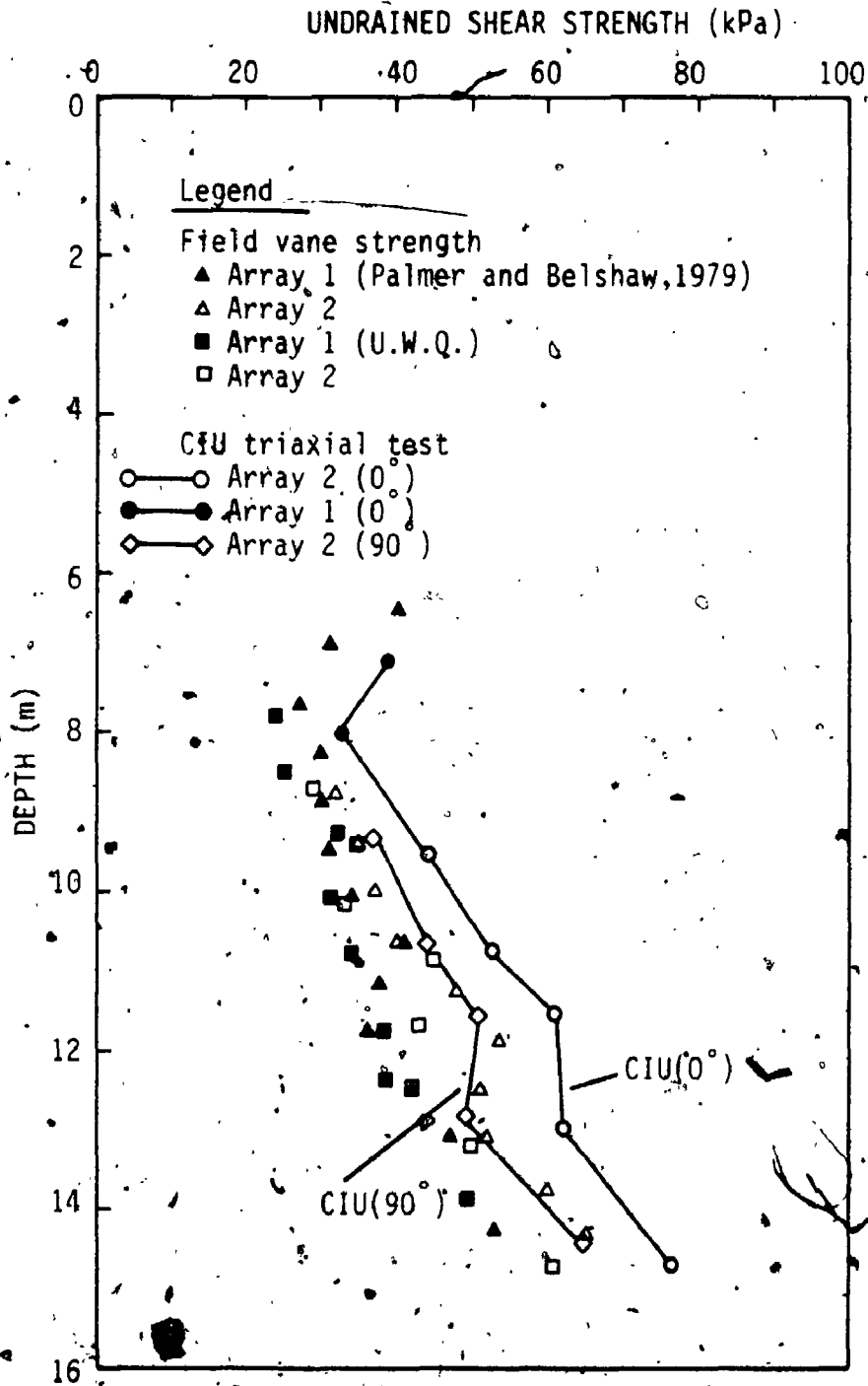


FIGURE 7.39 Variation of Undrained Shear Strength c_u with Depth

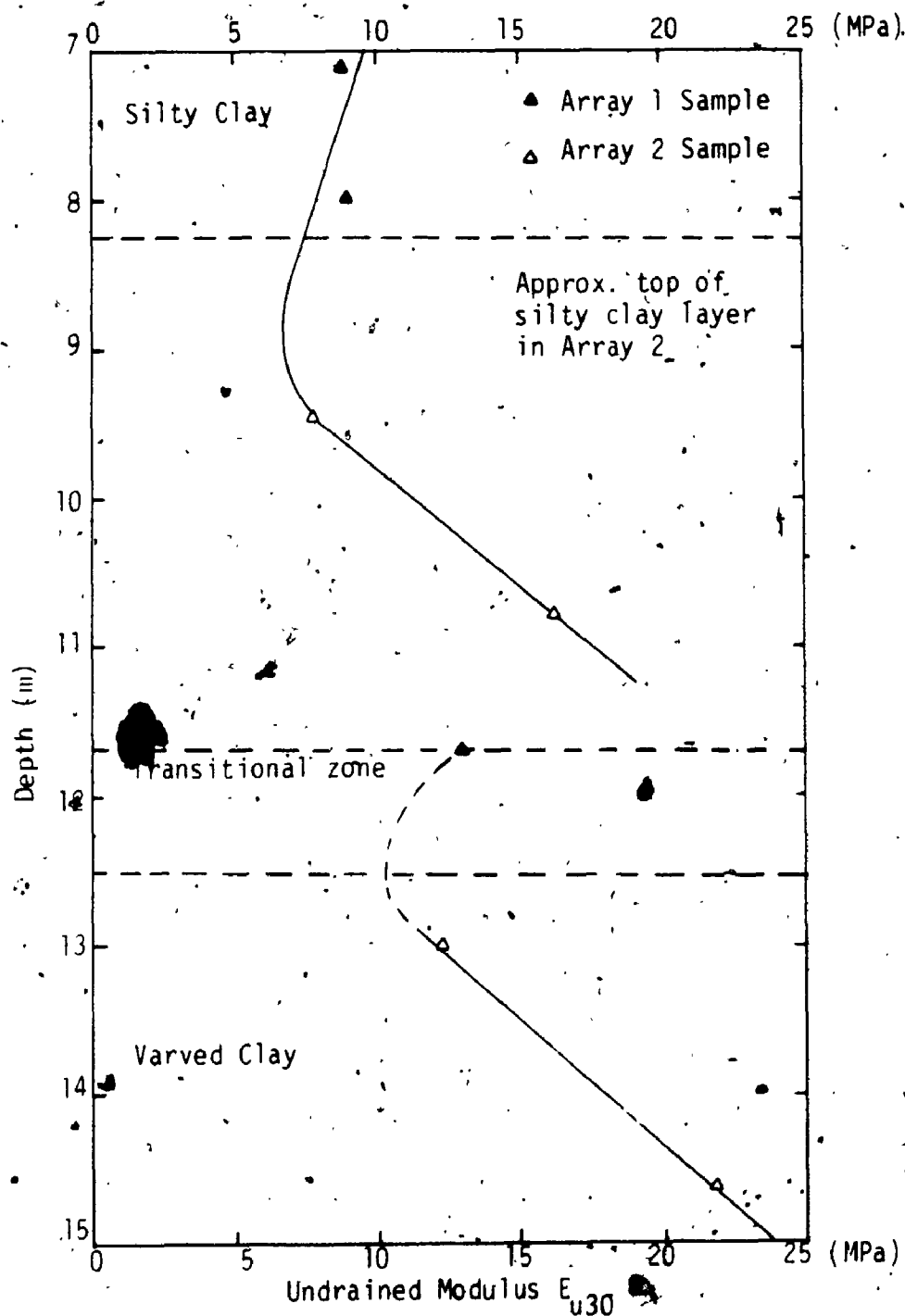


FIGURE 7.40 Variation of Undrained Modulus with Depth

Note: $E_h/E_v = 1.0$ for undrained response

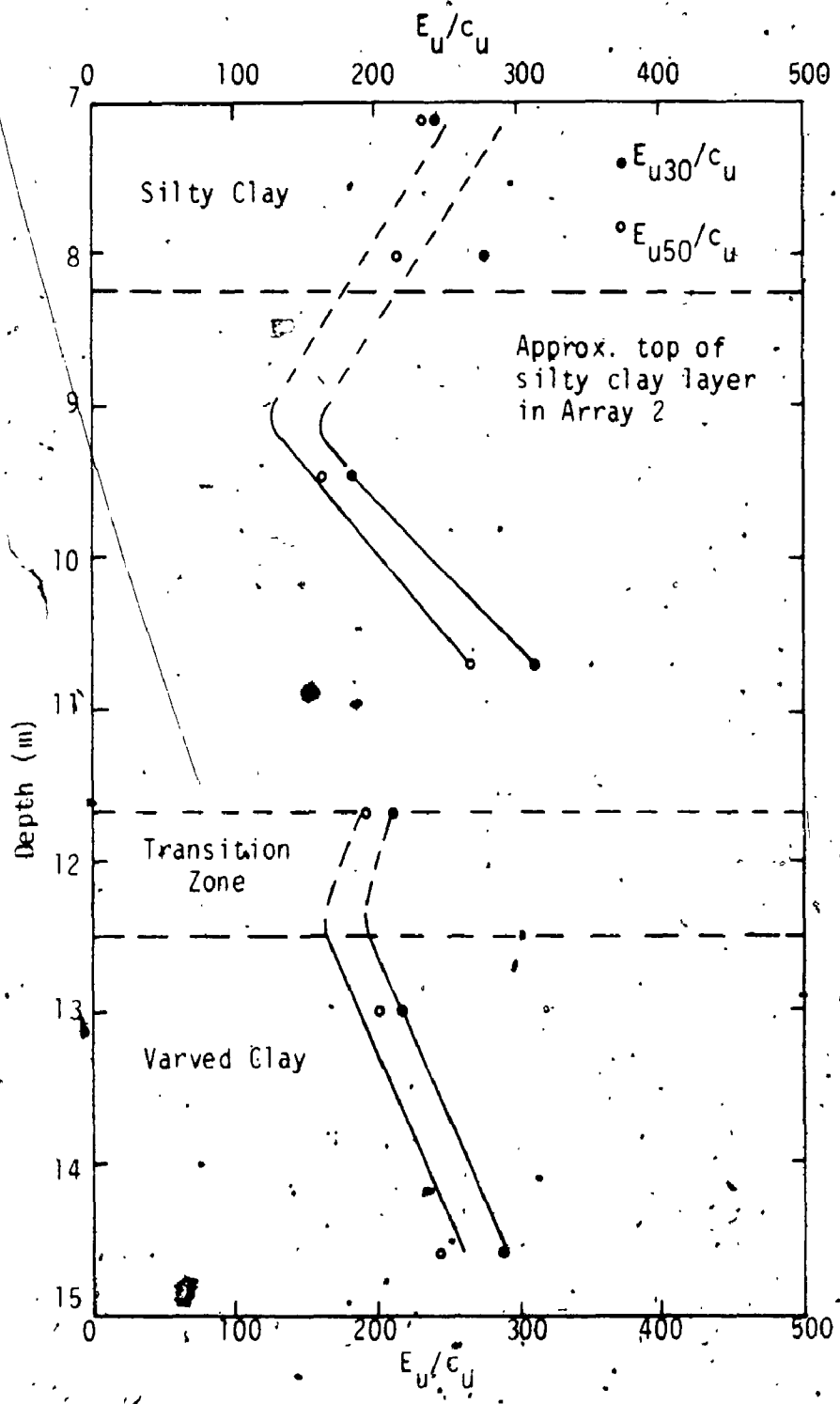


FIGURE 7.41 Variation of E_u/c_u with Depth

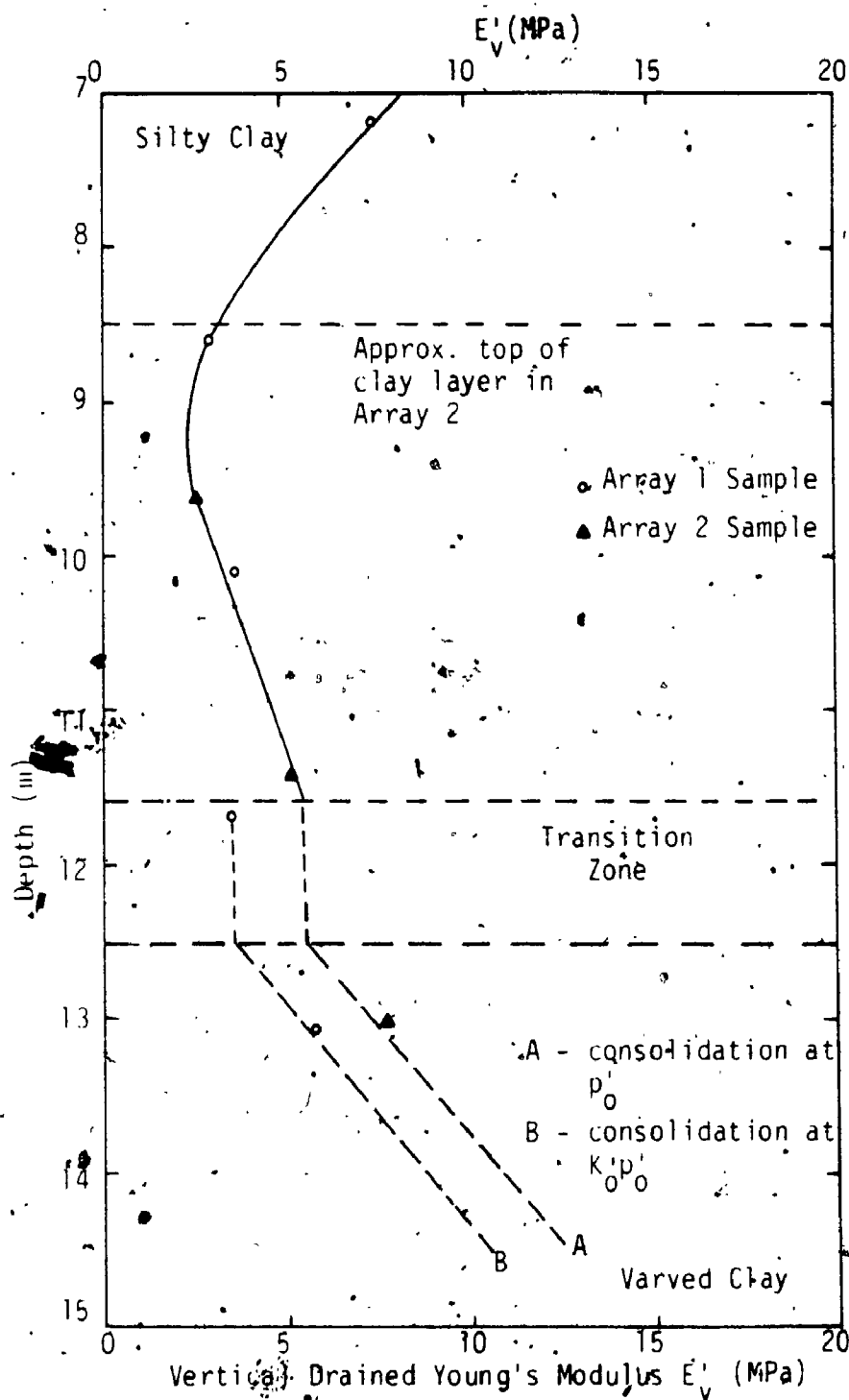


FIGURE 7.42 Variation of Drained Modulus E'_v (from CID Tests) with Depth

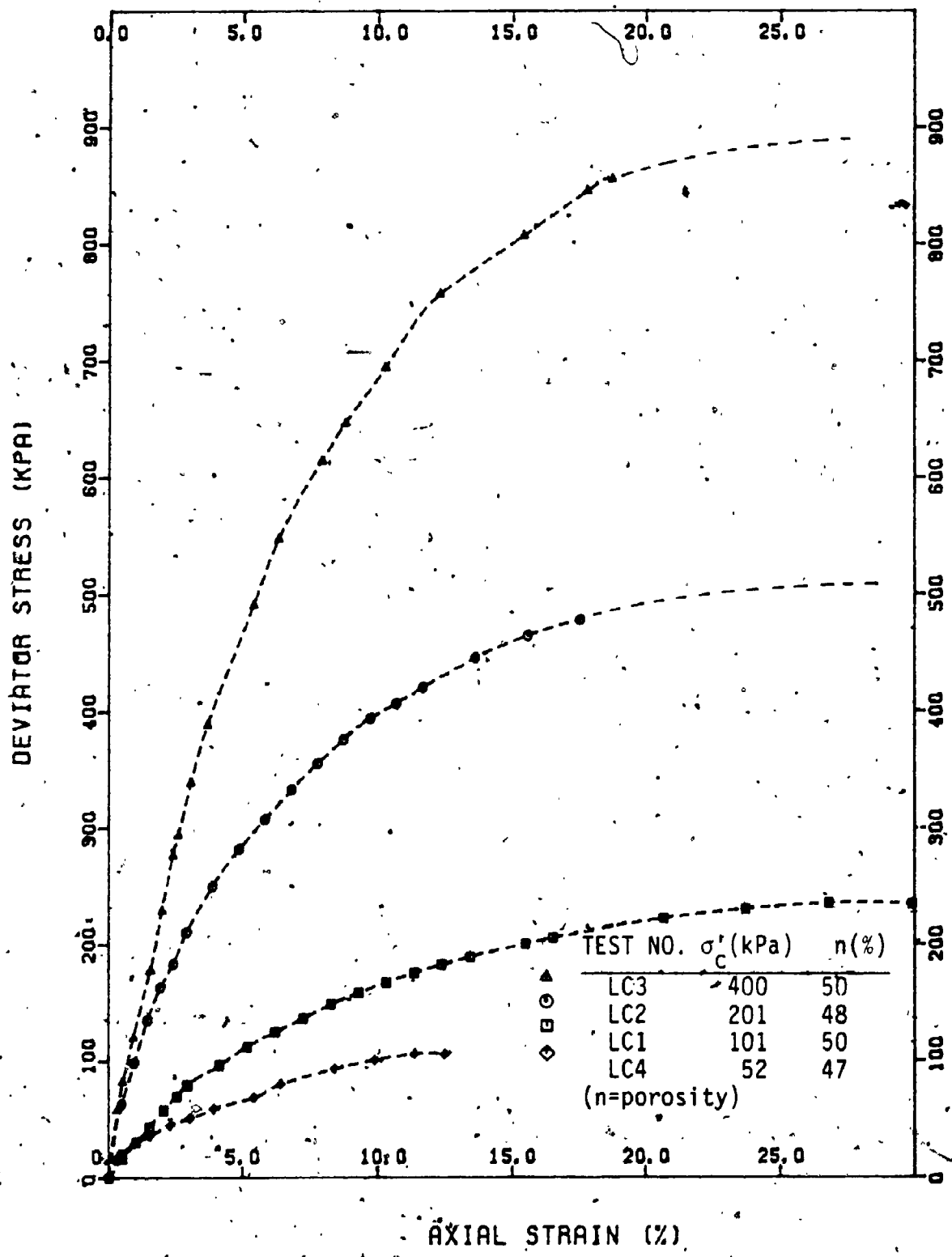


FIGURE 7.43 Stress-Strain Curves from CID Triaxial Compression Tests on Loose Silty Sand

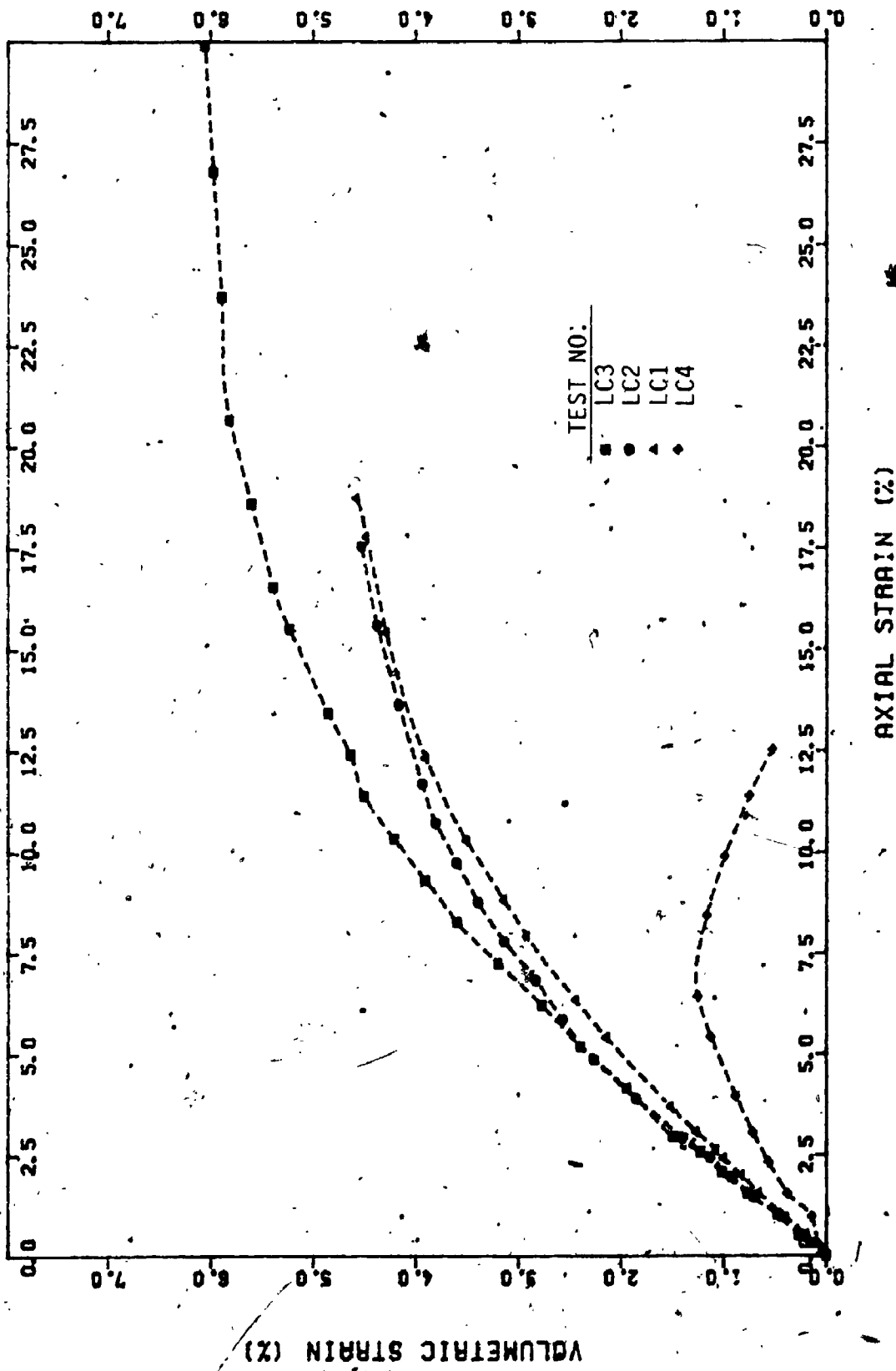


FIGURE 7.44 Volumetric Strain-Axial Strain Curves for Loose Silty Sand from CID Triaxial Tests

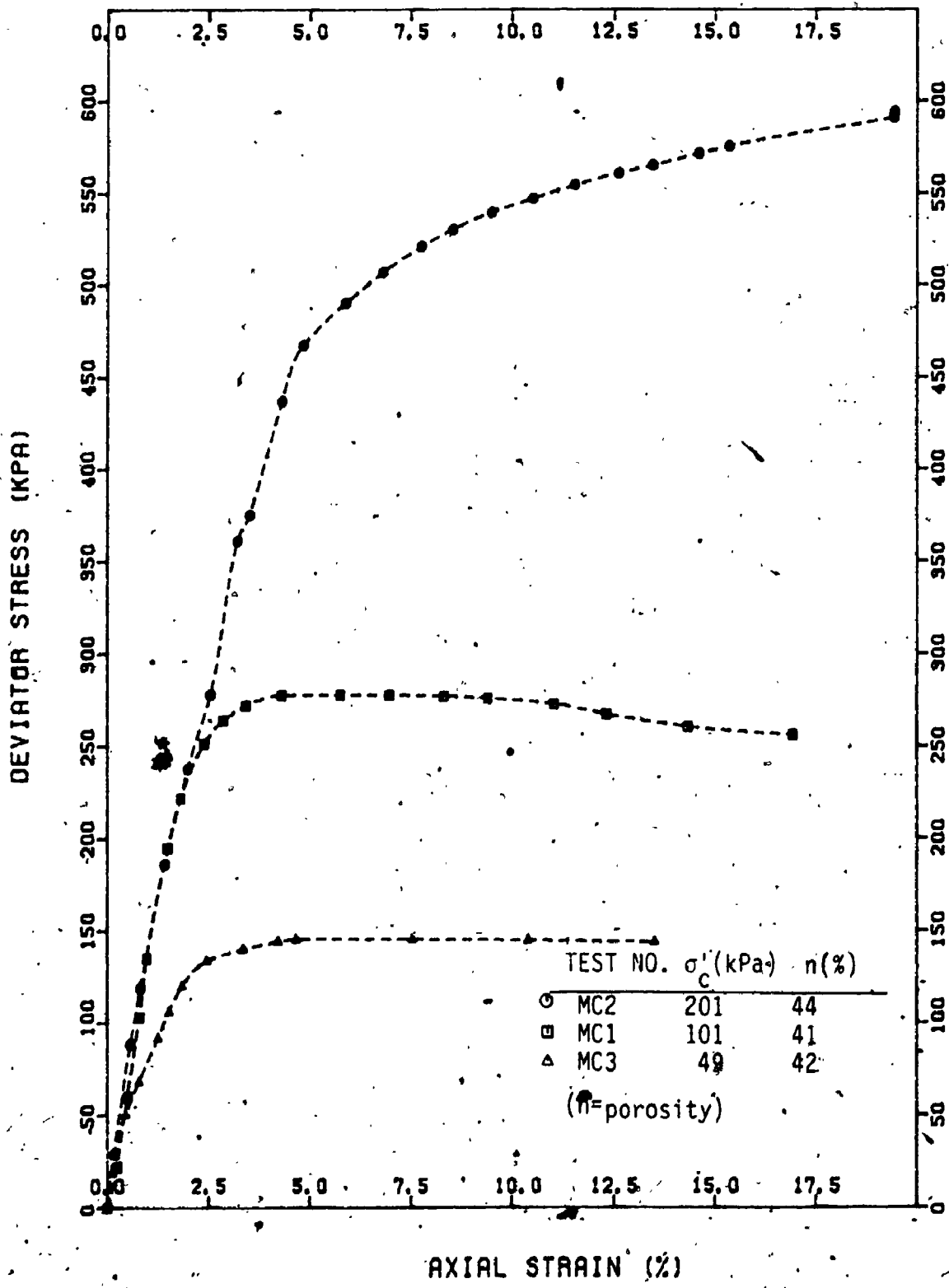


FIGURE 7.45 Stress-Strain Curves from GID Triaxial Compression Tests on Medium Dense Silty Sand

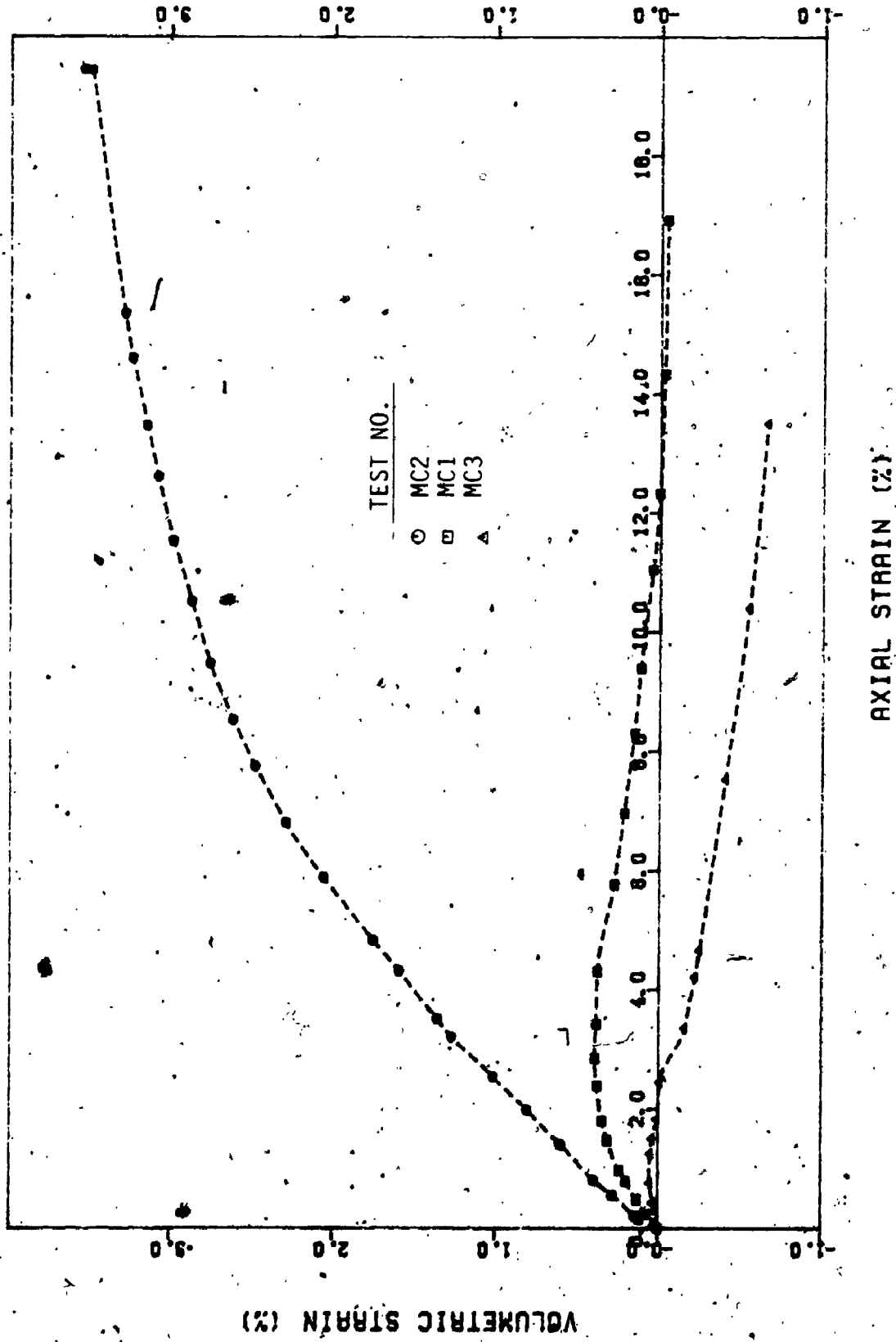


FIGURE 7.46 Volumetric Strain-Axial Strain Curves for Medium Dense Silty Sand from CID Triaxial Tests

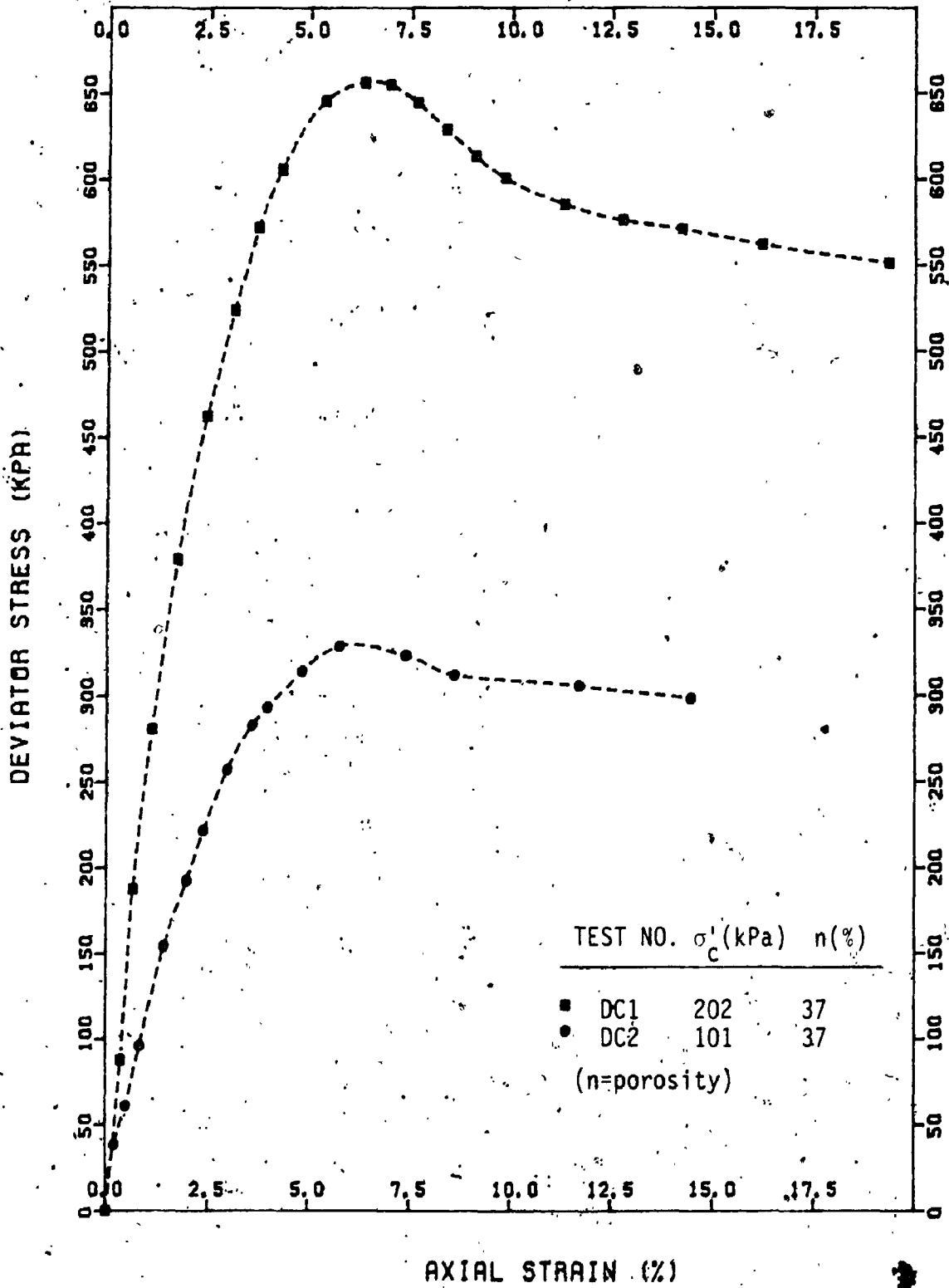


FIGURE 7.47 Stress-Strain Curves from CID Triaxial Compression Tests on Dense Silty Sand

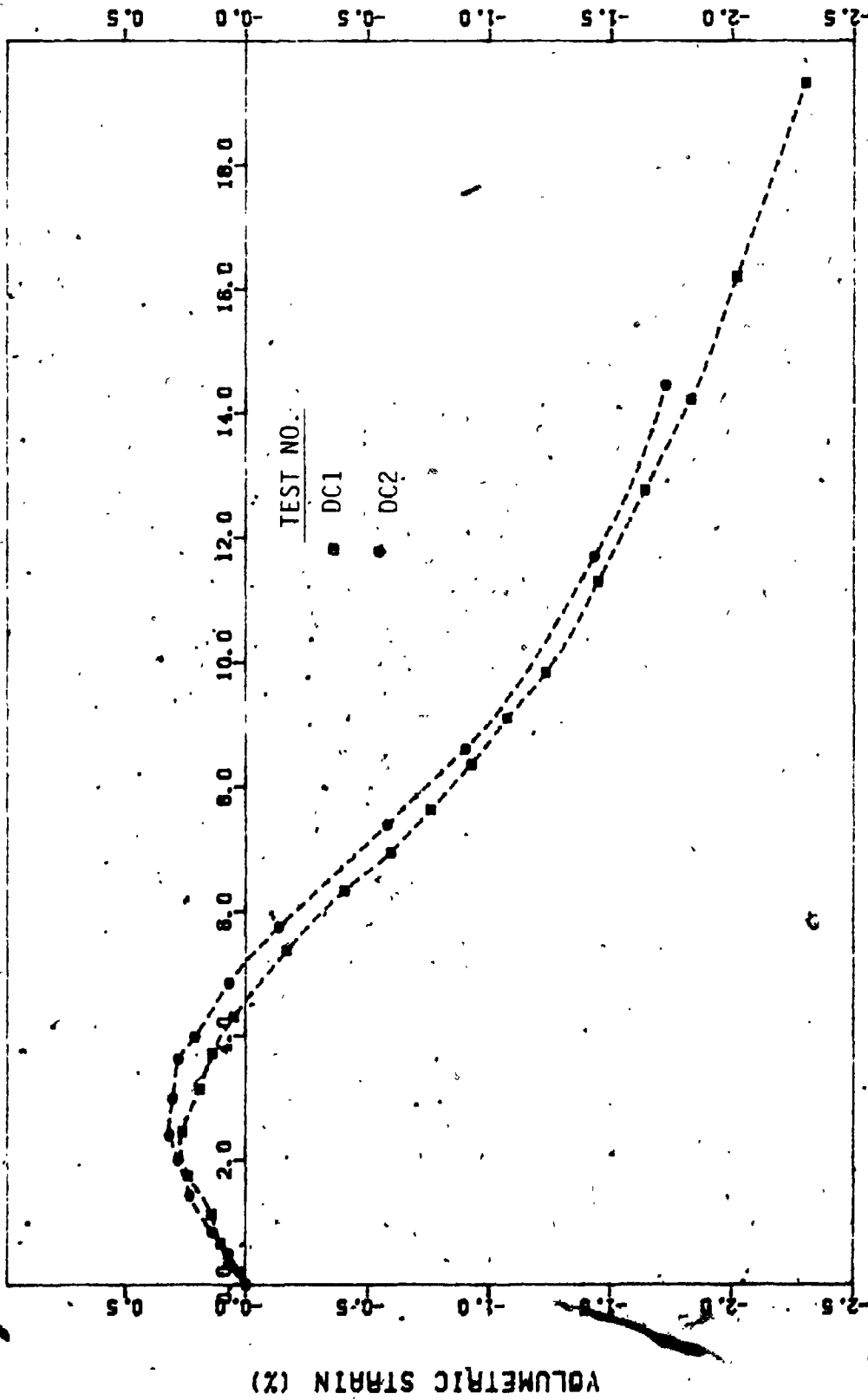


FIGURE 7.48. Volumetric Strain - Axial Strain Curves for Dense Silty Sand from CID Triaxial Tests

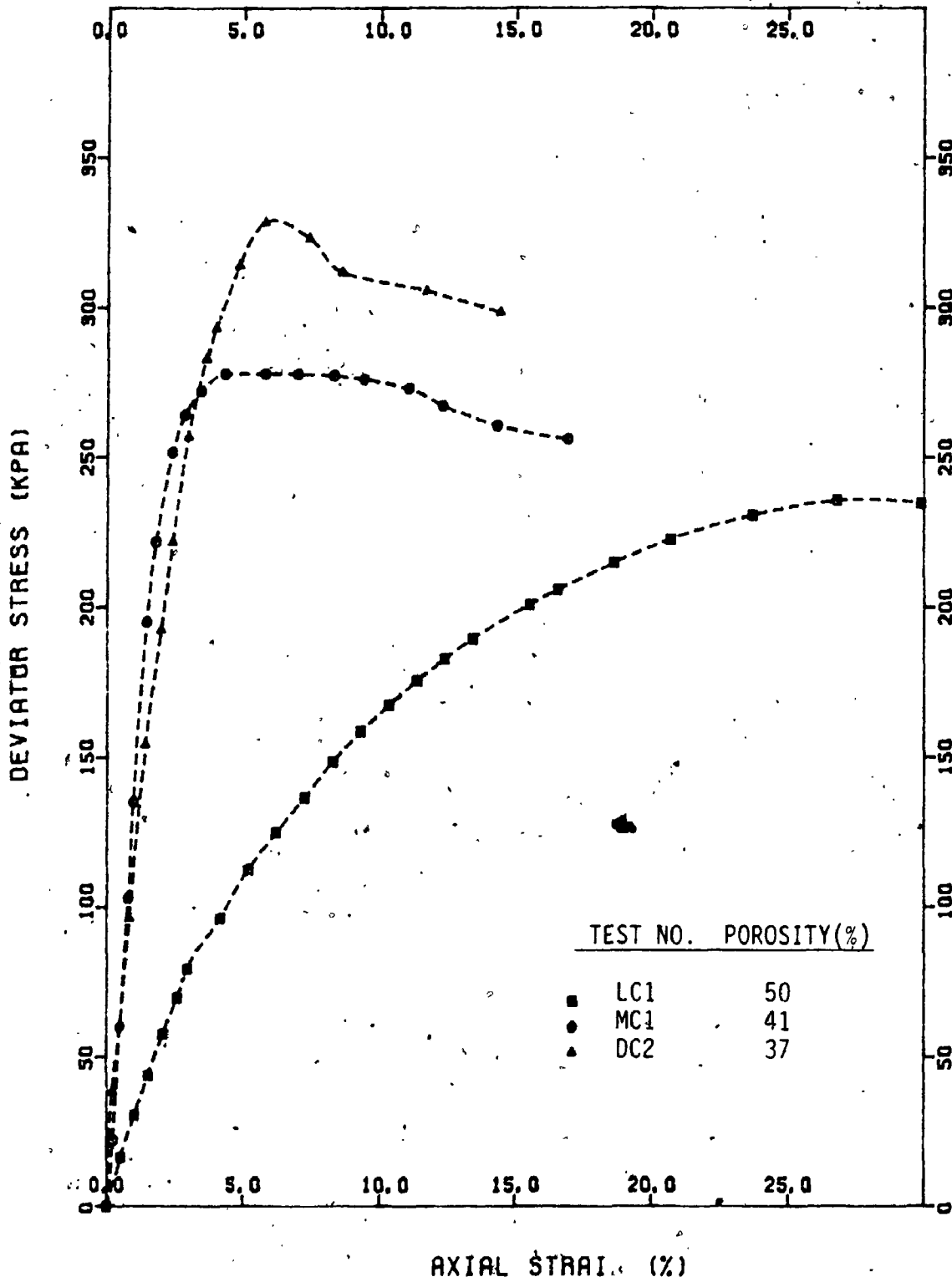


FIGURE 7.49 Stress-Strain Curves for Loose, Medium and Dense Silty Sand (Consolidation Pressure \approx 100 kPa)

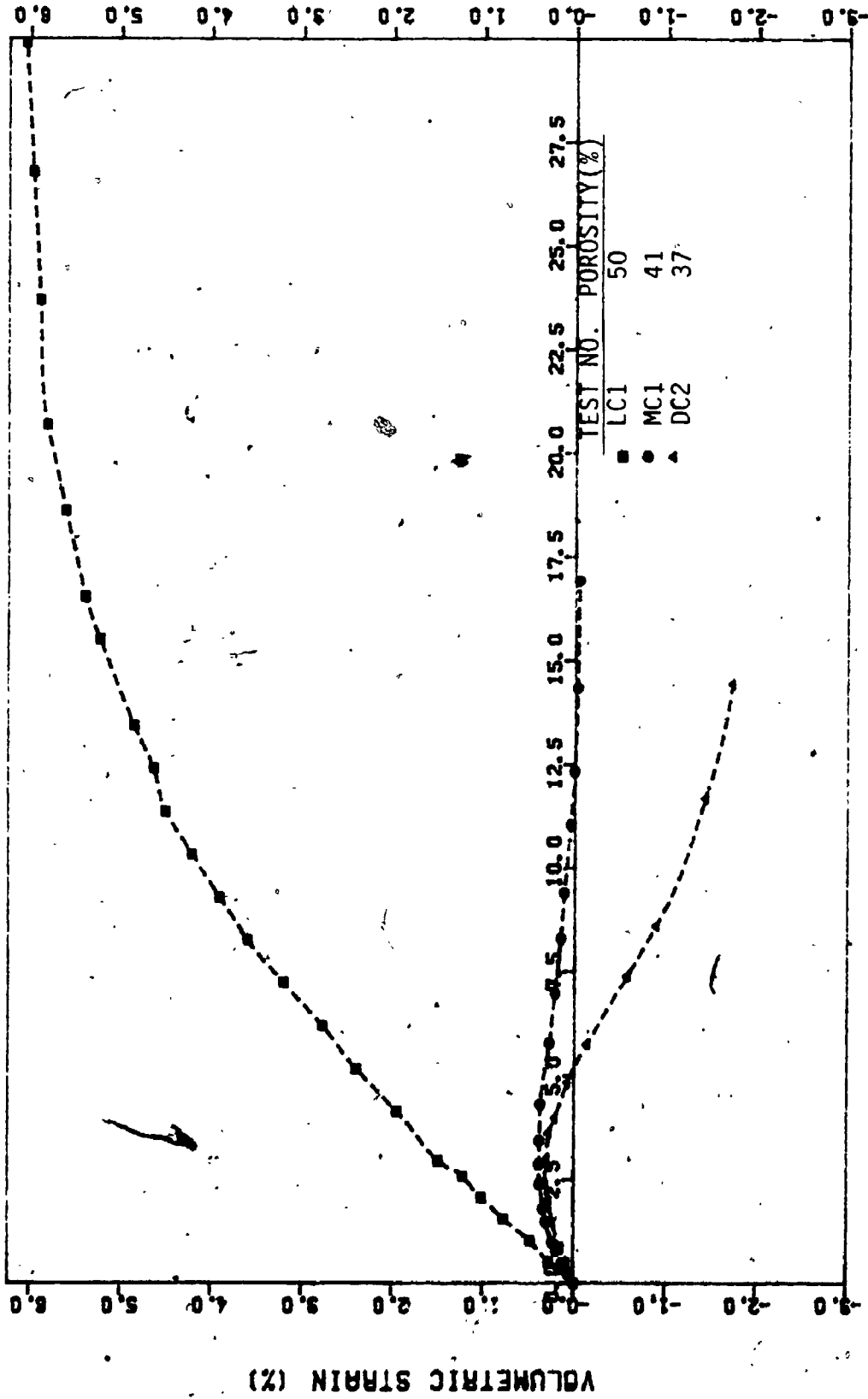


FIGURE 7.50 Volumetric Strain - Axial Strain Curves for Loose, Medium and Dense Sand (Consolidation Pressure = 100kPa)

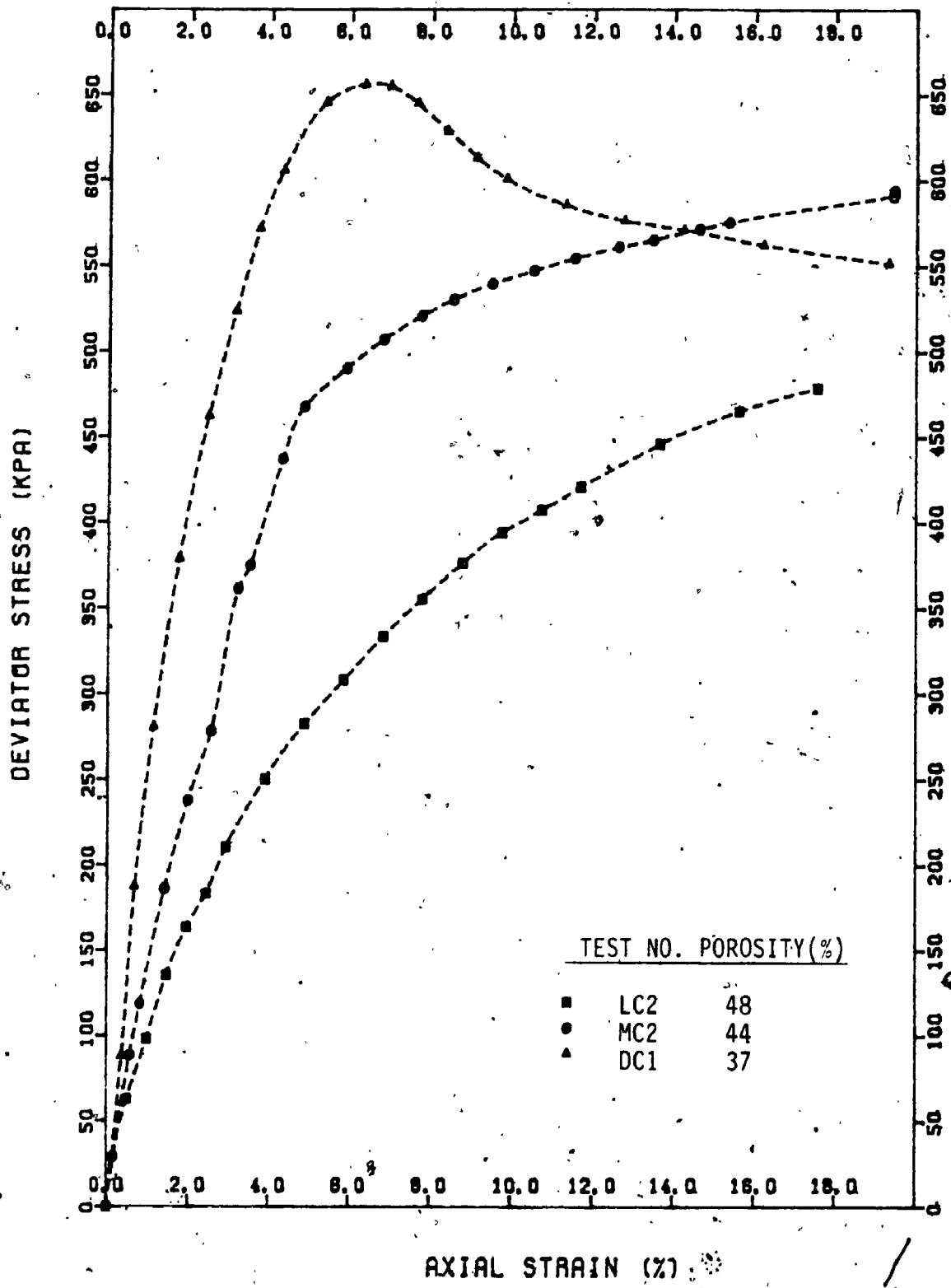


FIGURE 7.51 Stress-Strain Curves for Loose, Medium and Dense Silty Sand (Consolidation Pressure, ~200kPa)

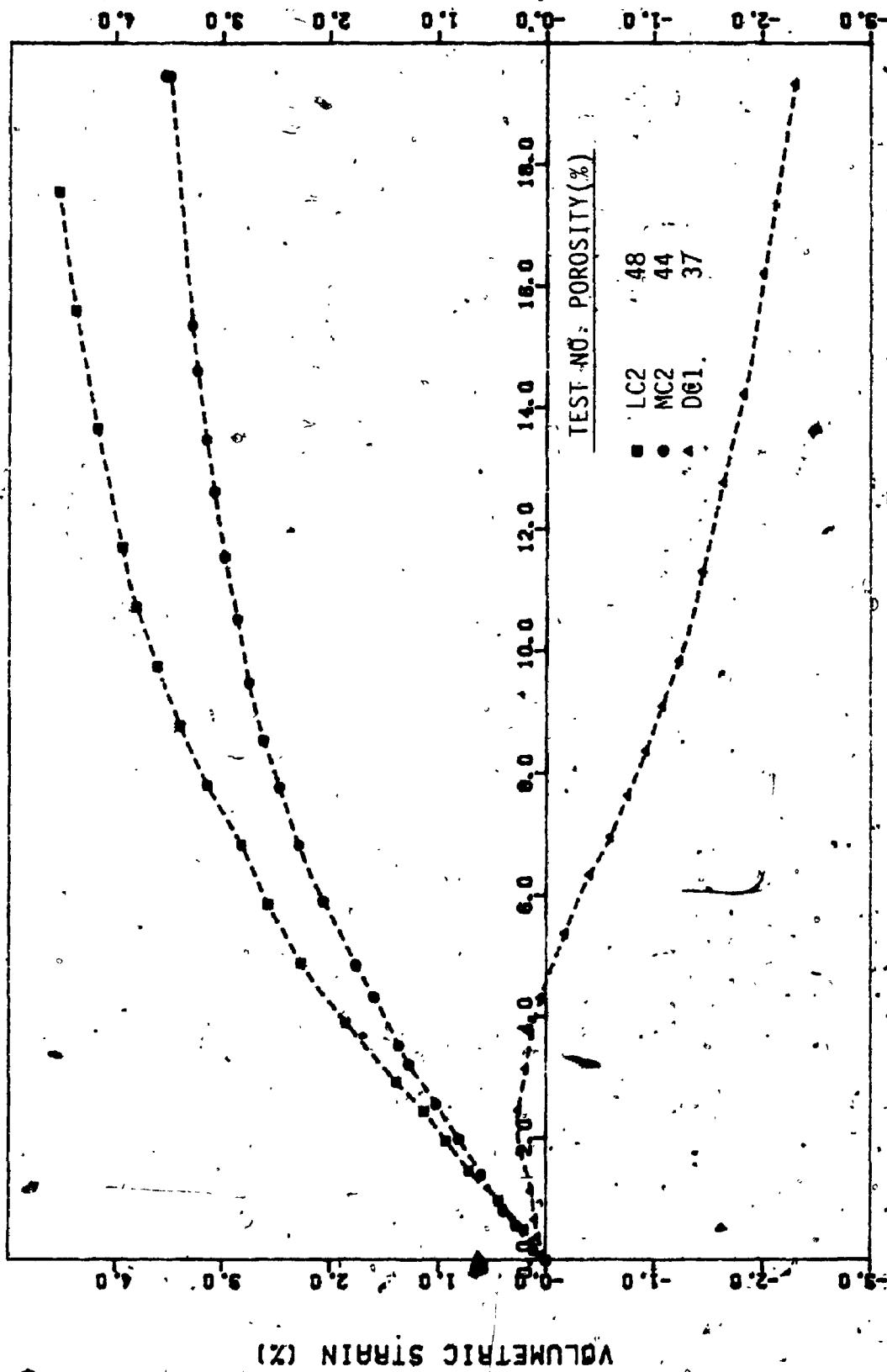
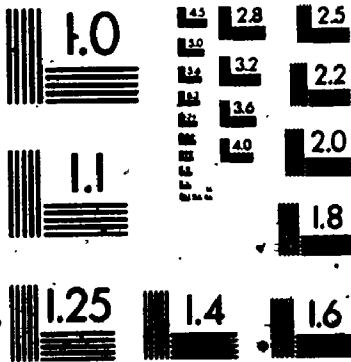


FIGURE 7.52 Volumetric Strain-Axial Strain Curves for Loose, Medium and Dense Silty Sand
 (Consolidation Pressure = 200kPa)

4



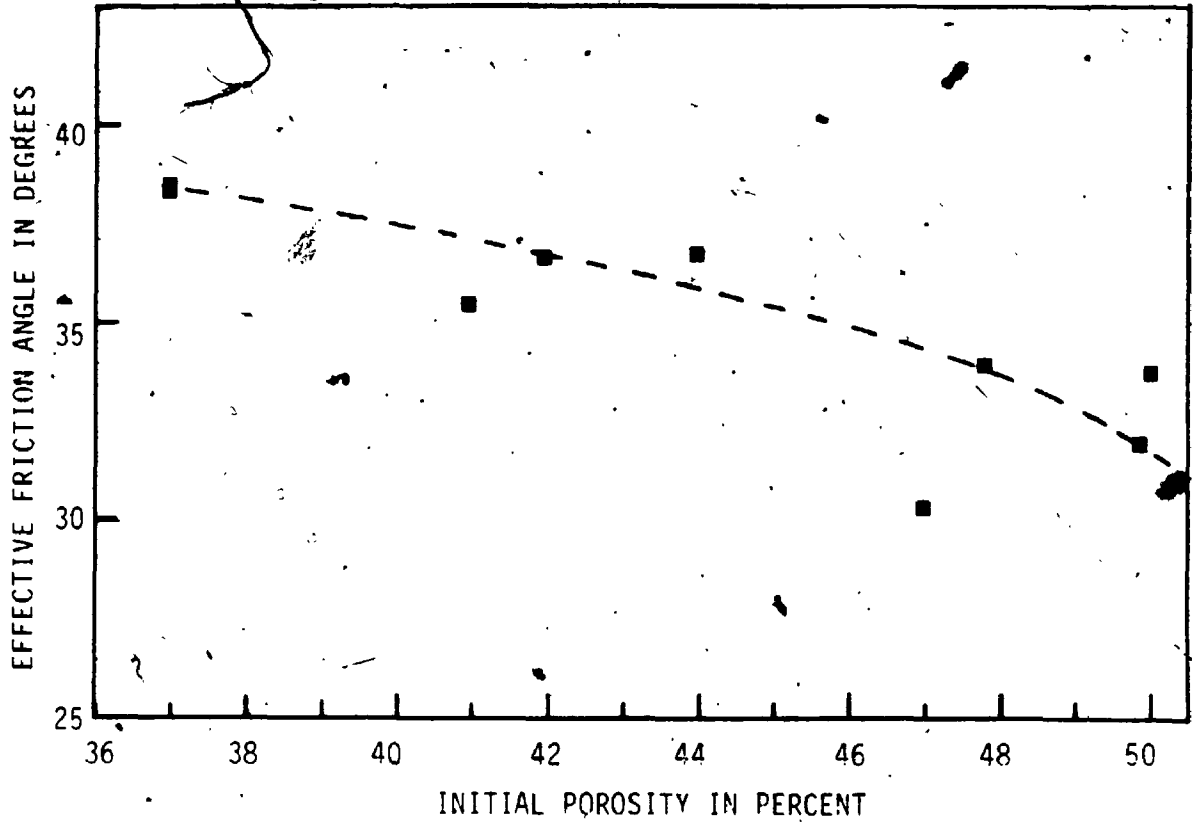


FIGURE 7.53a Variation of Effective Friction Angle with Initial Porosity

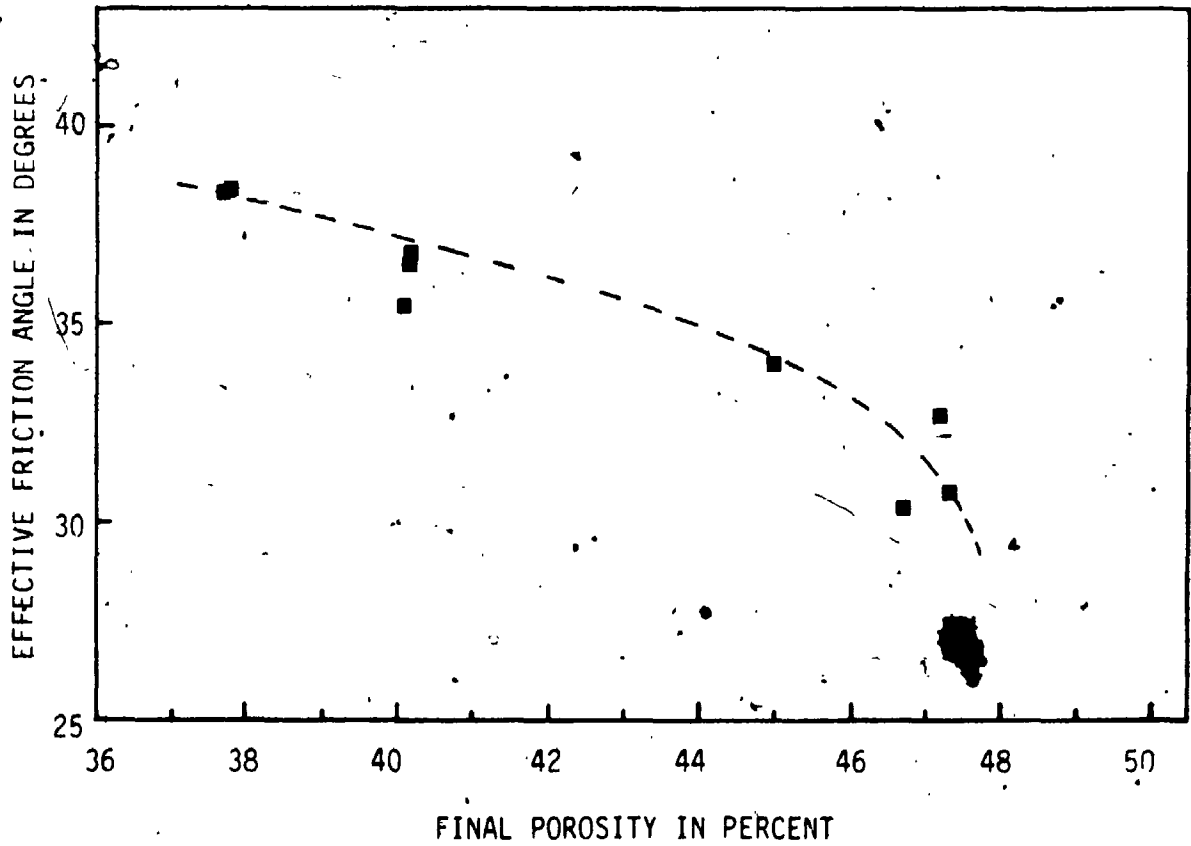


FIGURE 7.53b Variation of Effective Friction Angle with Final Porosity

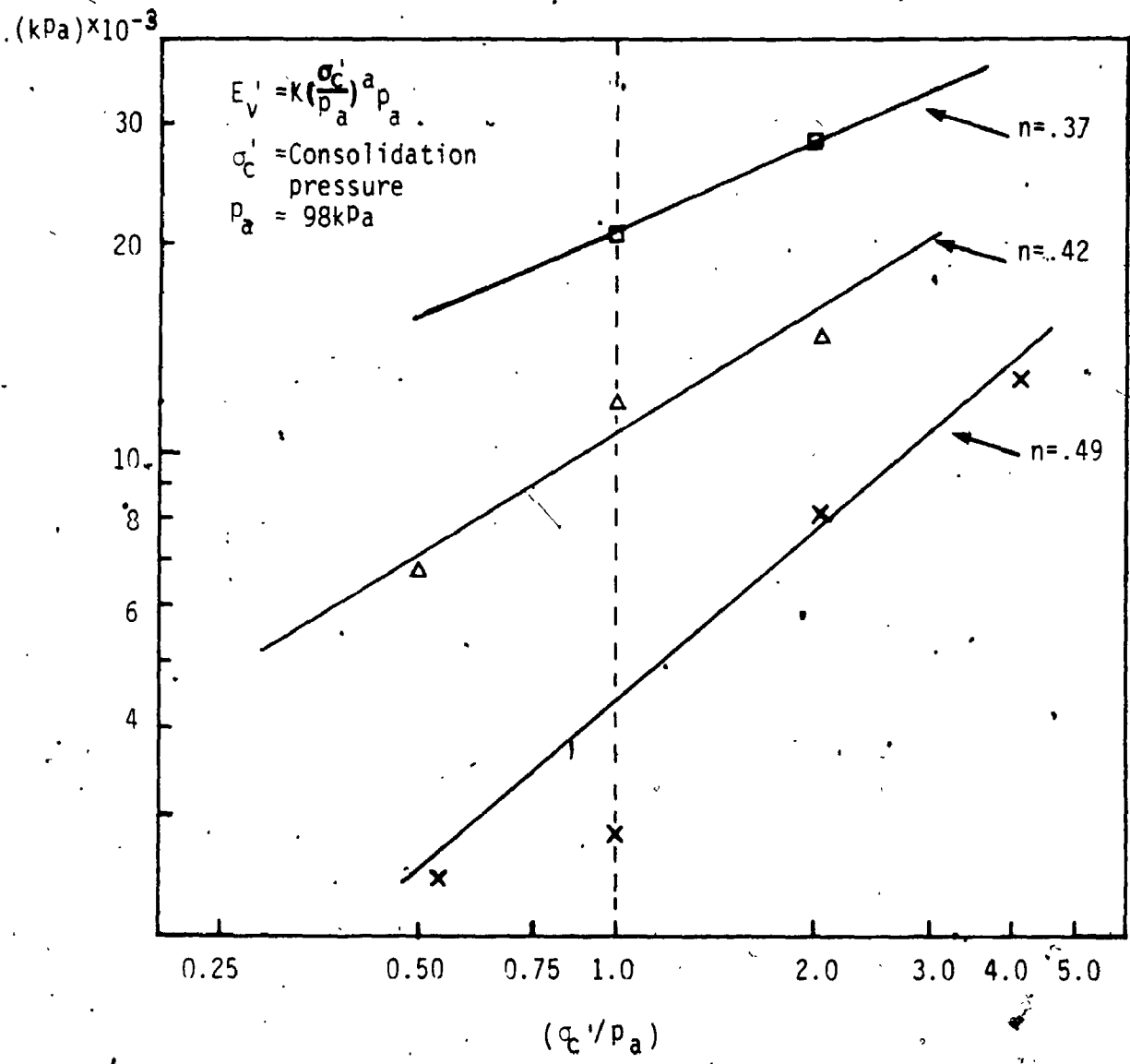


FIGURE 7.54 Relationship between Vertical Drained Modulus, E'_V and (σ'_c/p_a)

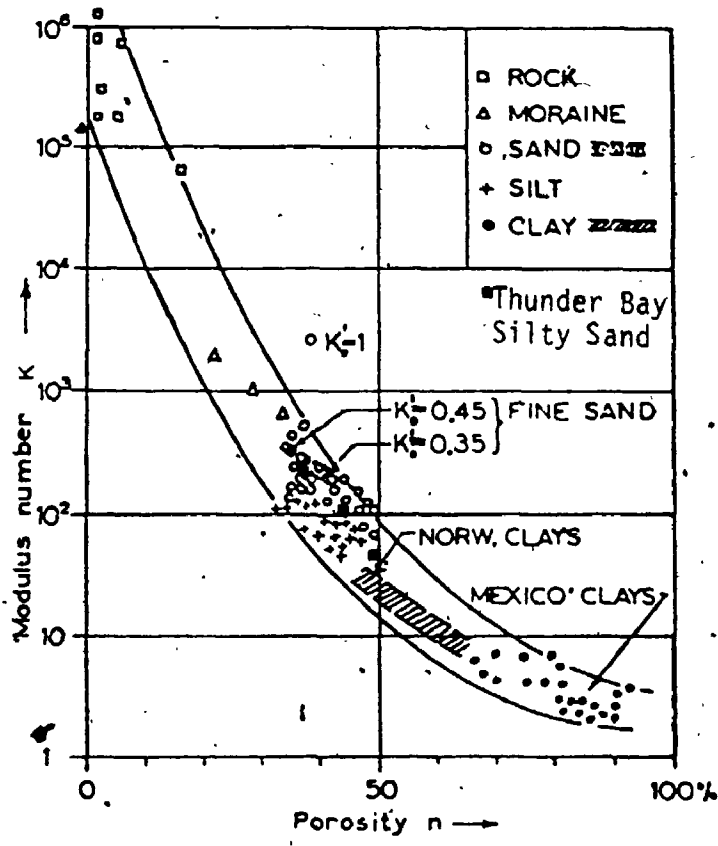
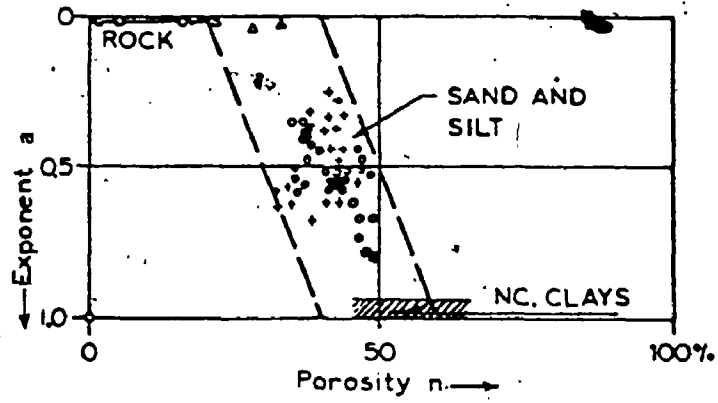


FIGURE 7.55 Typical Range of Variations of Modulus-Number 'K' and Exponent 'a' with Porosity (after Janbu, 1963)

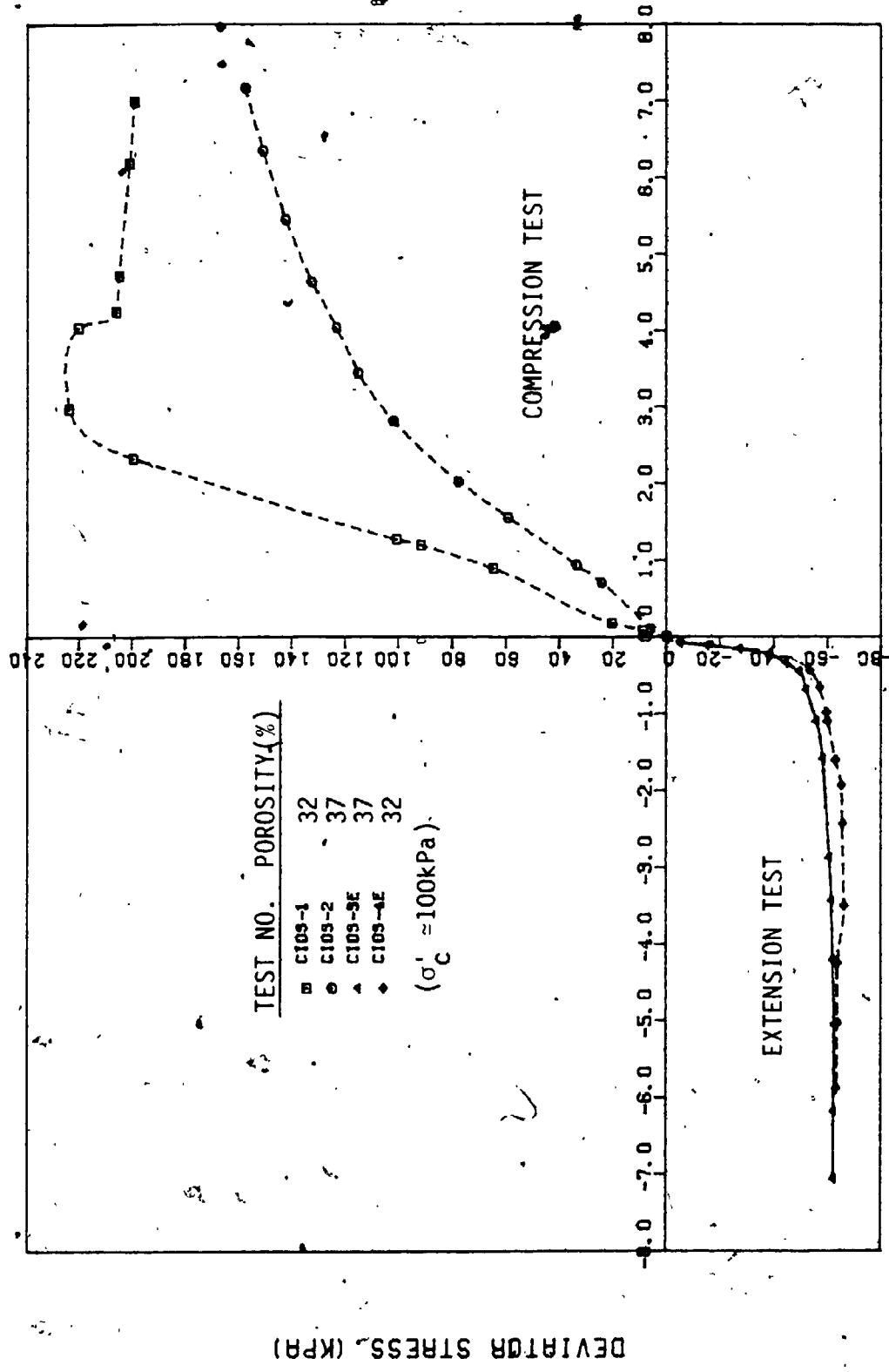


FIGURE 7.56 Stress-Strain Relationships from CID, Compression and Extension Triaxial Tests on Silty Sand

GROUND REACTION AND BEHAVIOUR OF TUNNELS

IN SOFT CLAYS

VOLUME II

by

Robert Man Chiu Ng

Faculty of Engineering Science

Submitted in partial fulfillment
of the requirements for the degree of
Doctor of Philosophy

Faculty of Graduate Studies

The University of Western Ontario

London, Ontario

August, 1984

© Robert Man Chiu Ng 1984

VOLUME II

TABLE OF CONTENTS

	Page
CHAPTER 8 - RESULTS OF SPECIAL TESTS.....	250
8.1 Definition of Deformation Modulus.....	250
8.2 Large Diameter Consolidation Tests Under Loading and Unloading.....	251
8.2.1 Results of Large Diameter Consolidation Tests.....	253
8.2.2 Comparison of Drained Modulus From Consolidation Tests and CID Tests.....	255
8.3 Measurement of Elastic Anisotropic Parameters by the Anisotropic Parameter Apparatus.....	255
8.3.1 Experimental Procedure.....	256
8.3.2 Results of Tests.....	257
8.3.2.1 Stress-Axial Strain Relationship.....	257
8.3.2.2 Volumetric Strain and Axial Strain Relationship.....	258
8.3.3 Evaluation of Anisotropic Elastic Parameters..	259
8.4 Determination of Shear Modulus G_{vh} From Direct Simple Shear Test.....	260
8.4.1 Simple Shear Apparatus.....	261
8.4.2 Constant Volume Test.....	262
8.4.3 Results of Simple Shear Tests.....	264
8.5 Anisotropically Consolidated Triaxial Tests and Controlled Stress Path Tests.....	265
8.5.1 Anisotropically Consolidated, Strain-Controlled Triaxial Tests.....	265
8.5.2 Results of Tests.....	266
8.5.3 Controlled Stress Path Triaxial Tests.....	267
8.5.3.1a Total Stress Controlled Test.....	267
8.5.3.1b Servo-Test.....	268
8.5.3.2 Results of Tests.....	269
8.6 Strength From Anisotropic Consolidated Triaxial Tests and Controlled Stress Path Tests.....	271
8.7 Summary on Special Tests Performed on the Clay at Array 1 and Array 2 on the Thunder Bay Tunnel.....	272
CHAPTER 9 - TUNNELLING PROCEDURE AND FIELD OBSERVATIONS AT THE THUNDER BAY TUNNEL.....	320
9.1 Tunnelling System and Procedure.....	320
9.1.1 Tunnelling Machine and Construction Cycle.....	320
9.1.2 Typical Observations During Tunnelling Operation.....	322
9.1.3 Tunnel Lining.....	322

	Page
9.2 Observed Ground Deformations.....	323
9.2.1 Undrained and Drained Settlements.....	323
9.2.2 Surface Settlements.....	325
9.2.3 Distribution of Subsurface Displacements.....	327
9.2.3.1 Vertical Displacements With Depth On Centreline.....	327
9.2.3.2 Horizontal Displacements.....	328
9.2.3.3 Displacement Vectors in the Vertical Plane..	329
9.3 Pore Water Pressure Due to Tunnelling.....	330
 CHAPTER 10 - ANALYSES OF THE RESULTS OF FIELD INSTRUMENTA- TION IN THE THUNDER BAY TUNNEL.....	 356
10.1 Introduction.....	356
10.2 Details of the Analysis.....	356
10.3 Selection of Drained Parameters for Analysis....	358
10.3.1 Description of Soil Stratigraphy.....	358
10.3.2 Selection of Soil Properties for Analysis of Array 1.....	359
10.3.2.1 Sand and Silt.....	359
10.3.2.2 Silty Clay and Varved Clay.....	362
10.3.3 Selection of Soil Properties for Analysis of Array 2.....	364
10.4 Results of Drained Analysis.....	364
10.4.1 Long Term Surface Settlement.....	365
10.4.1.1 Array 1.....	365
10.4.1.2 Array 2.....	366
10.4.2 Horizontal Displacement Perpendicular to the Tunnel Axis at Array 1.....	366
10.4.3 Distribution of Subsurface Settlement at Array 2.....	367
10.5 Selection of Undrained Parameters for Analysis..	368
10.6 Results of Undrained Analysis.....	370
10.6.1 Centreline Settlement.....	370
10.6.2 Distribution of Surface Settlement.....	372
10.7 Lining Deformation.....	374
10.8 Variation of Centreline Settlement With Depth Above the Tunnel.....	375
10.9 Summary of Comparison Between Results of Field Measurements and Analysis.....	377
 CHAPTER 11 - SUMMARY, CONCLUSIONS AND RECOMMENDATIONS FOR FURTHER RESEARCH.....	 392
11.1 Summary and Conclusions.....	392
11.2 Recommendations for Further Research.....	399

	Page
APPENDIX 1 - SCHEME OF CONSTRUCTION SIMULATION WITH CONSIDERATION OF MACHINE WEIGHT DURING TUNNEL ADVANCE.....	402
APPENDIX 2 - UNDRAINED AND DRAINED SETTLEMENTS DUE TO TUNNELLING.....	411
APPENDIX A - SAMPLING WITH 152 mm DIAMETER PISTON SAMPLER....	416
APPENDIX B - APPARATUS AND FIELD TECHNIQUE USED IN k_0 - DETERMINATION.....	421
APPENDIX C - CONVENTIONAL LABORATORY TEST RESULTS.....	446
C.1 Grain Size Analysis.....	446
C.2 Determination of Unit Weight.....	446
C.3 One-Dimensional Consolidation Tests.....	447
C.4 Results of CIU Tests On Vertically and Horizontally Oriented Clay Samples.....	449
C.5 Drained Triaxial Tests On Silty Fine Sand.....	449
APPENDIX D - CONSOLIDATION TESTS PERFORMED USING THE ROWE CELL.....	476
D.1 Description of Apparatus.....	476
D.2 Specimen Preparation and Test Procedure.....	477
D.3 Coefficient of Consolidation.....	479
APPENDIX E - TESTS FOR DETERMINING ANISOTROPIC ELASTIC PARAMETERS.....	483
E.1 Theoretical Background.....	483
E.2 Formulation of Stress-Strain Relationship for CID Tests.....	484
E.3 Description of the Apparatus and Method of Measurement.....	488
APPENDIX F - DETERMINATION OF PERMEABILITY.....	493
F.1 Program of Testing and Procedure.....	493
F.2 Results of Permeability Test.....	494
REFERENCES.....	497
VITA.....	508

CHAPTER 8

RESULTS OF SPECIAL TESTS

In this chapter, the stress-strain and strength behaviour measured in different types of tests are presented. These tests include:

- (a) Consolidation tests using a large diameter cell with pore pressure measurements;
- (b) Measurement of elastic anisotropic parameters both in loading and unloading;
- (c) Simple shear tests for the measurement of shear modulus;
- (d) Anisotropically-consolidated, compression/extension, undrained/drained as well as controlled stress path tests.

The results of these tests are compared with one another and with results of CIU and CID tests so that an appropriate modulus profile obeying the soil conditions, the boundary conditions and the stress conditions in tunnelling may be developed.

8.1 DEFINITION OF DEFORMATION MODULUS

The stress-strain relationships for clays are usually nonlinear. The degree of nonlinearity increases as the failure stress is approached. The definition of a deformation modulus for the purpose of comparison between different types of tests and for finite element analysis is a matter of some difficulty. A detailed study has been

carried out by defining the modulus at different ranges of stresses and strains within small ranges of strains within which elastic deformation dominates. It was found that the secant modulus defined at 0.1% strain yields results that are self-consistent within one type of test (e.g. CK_{0UC} , CK_{0UE} etc.) and between different types of tests. In CIU tests, this definition would correspond to modulus defined at a stress level about 1/3 the failure stress, E_{30} . In CID tests, some test error occurred at very small strains (below 0.1%) and the modulus was therefore defined in the strain range of 0.1% to 0.6%. The modulus so defined should also be appropriate for the analytical model described in Chapter 4:

8.2 LARGE DIAMETER CONSOLIDATION TESTS UNDER LOADING AND UNLOADING

The one dimensional consolidation and swelling behaviour of the clay subsoil was studied by a series of large oedometer tests (Rowe Cell) with pore water pressure measurement on vertical specimens 149.2 mm in diameter and 49.2 mm in height.

The procedure for performing the tests in the Rowe Cell was described by Rowe and Barden (1966). The improved version of the Rowe Cell used at The University of Western Ontario and the procedure of testing is briefly described in Appendix D.

The Rowe Cell possesses several advantages over the conventional oedometer test such as:

- 1) The use of larger specimens so that effects of structural features such as layering may be included.
- 2) Complete drainage control is achieved as in the triaxial test. A sample may be loaded initially without drainage to allow a full development of the induced initial excess pore water pressure. The dissipation stage can then be started from an equilibrium pore pressure condition.
- 3) The sample can be saturated with a back pressure and errors due to cavitation are reduced.
- 4) The sample is not subjected to vibration effects magnified by the lever system as is the case in conventional tests. The error associated with compression of the loading system is also reduced.

Three samples were tested. These were taken from 7.24 m, 9.78 m and 13.1 m in Array 1 located respectively in the "crust", silty clay layer and varved clay layer so that the typical consolidation behaviour of the soil profile may be studied.

The specimens were trimmed from 152 mm diameter samples by pushing the sample through the modified oedometer ring with a cutting edge. In this process, the edge of the original sample smeared during sampling was removed. A 50 mm diameter filter paper was placed between the sample in the ring and the sensing element (porous stone) connected to a pore pressure transducer. By increasing the sensing area, the response time for the development of induced excess pore pressure was improved. The whole system was assembled under de-aired water to

prevent entrapment of air.

The samples were saturated under a back pressure of 150 kPa. Applied pressure was increased in increments and then was decreased by the same procedure during unloading. For the clay sample at 7.24 m, it was loaded up to 200 kPa at multiple increments of 50 kPa (i.e. 50, 100, 200) and substantial volume change occurred at the 100-200 kPa increment when p'_c was exceeded. Subsequently, the loading increments were reduced in the other tests and stress levels were limited to pressures below preconsolidation pressure.

In both loading and unloading, the applied pressure was held constant for about 24 hours or until the initial excess pore water pressure induced had been completely dissipated. Continuous monitoring of pore pressure and displacement was achieved by the use of electronic pressure transducer, LVDT and chart recorder.

8.2.1 Results of Large Diameter Consolidation Tests

The settlement-time relationships for loading and unloading are shown in Figures 8.1 to 8.7 and the dissipation of excess pore water pressure with time are shown in Figures 8.8 to 8.10. It is generally observed that:

- (a) The initial excess pore pressure u_0 relative to the applied load increment is generally close to unity for all three specimens in the silty clay and varved clay deposits.

- (b) With few exceptions, the excess pore pressure dissipated within a period of 24 hours. The rate of dissipation appears to be faster in unloading than in loading.

From the experimental data, the compressibilities in loading m_V and the expansibilities in unloading m_R have been computed and are shown in Table 8.1. The coefficients of consolidation c_V in loading and c_R in unloading were computed from two curve fitting procedures, one from the settlement curves for an average degree of consolidation of 50% and one from the pore pressure dissipation curves, at 50% dissipation at the base. These values are also shown in Table 8.1, from which the following observations may be made:

- (a) The consolidation parameters are strongly nonlinear both in loading and in unloading. This emphasizes the requirement that the parameters used in analysis must be determined at the appropriate stress levels.
- (b) Both c_V and c_R determined from pore water pressure dissipation are higher than those determined from the settlement-time curves.
- (c) At the same stress level, the values of c_V and c_R for the varved clay are considerably higher than those of the silty clay.
- (d) For the varved clay, c_R in unloading is considerably higher than c_V in loading. The coefficients, however, are similar in magnitude for the silty clay deposit.

8.2.2 Comparison of Drained Modulus From Consolidation Tests and CID Tests

The drained modulus E' may be derived from results of consolidation tests by using the theoretical relationship

$$E' = \frac{(1-2\nu')(1+\nu')}{m_v(1-\nu')} \quad (8.1)$$

where m_v is the compressibility from consolidation test and ν' is the Poisson's Ratio. Results of triaxial tests (see section 8.3) showed that for loading case ν' is small for both the silty clay and varved clay, being of the order of 0.1 to 0.15. It may also be noted from the above equation that E' is not sensitive to ν' provided ν' is small.

Choosing the values of m_v in the stress range of 50-100 kPa for silty clay and 100-200 kPa for varved clay to correspond to the consolidation pressures used in CID tests, E' computed from Eq. 8.1 is compared to the drained modulus profile from CID tests in Figure 8.11. Data from the conventional consolidation tests described in Appendix C are also shown. It may be seen that the results of the two types of tests show reasonable agreement. The variation of modulus with depth from the two sets of data also indicate the same general trend.

8.3 MEASUREMENT OF ELASTIC ANISOTROPIC PARAMETERS BY THE ANISOTROPIC PARAMETER APPARATUS

Experimental determination of the anisotropic deformation parameters are seldom reported in the literature because the experimental requirements are exacting. Yet, it is well known that the deformation

properties of many clay deposits are anisotropic. Lo et al. (1977) developed an apparatus to provide accurate measurements of the axial and lateral deformation of soft sensitive clays. The details of this apparatus were described by Yuen et al. (1978). The experimental arrangement contained gauge points and electronic displacement transducer LVDT floated in a cell fluid in a manner such that small strains of the soil sample can be measured directly with a minimal amount of disturbance.

The complete set of ten elastic parameters, five for loading and five for unloading, is determined by drained triaxial tests on samples trimmed with their long axes oriented at 0° , 45° , 90° from the vertical. Brief discussions on the theoretical background and testing procedures may be found in Appendix E.

8.3.1. Experimental Procedure

In the experiment, square-sectioned specimens (35.6 mm by 71.1 mm high) were trimmed from samples at 10.15 m (silty clay) and 13.4 m (varved clay) from Array 2. The use of a parallel-sided specimen eliminates the ambiguity of the direction of principal stresses in a cylindrical specimen and at the same time facilitates instrumentation for lateral strain measurement. The samples were saturated under a back pressure equal to the geostatic hydrostatic pressure, and the B values were always over 0.96. The consolidation pressures for the tests were 74 kPa and 68 kPa respectively for the silty clay and varved

clay and these pressures correspond to the $K'_0 p'_0$ condition of the natural soil so that the initial stresses were within the preconsolidation pressure. The volume change during consolidation was small (<1.5%).

The tests were performed at a strain rate of 0.1% per hour. In the loading stage, the specimens were tested to axial strains of about 0.6% and were unloaded to zero axial stress. The axial strains were measured by rigidly supported LVDTs over a gauge length equal to half the height of the sample wherein the strain distribution was uniform. The lateral strain at the mid-point was measured also by LVDTs, floated by an assembly of styrofoam and aluminum bracket. The outputs from the displacement transducer, pressure transducer and volume-change device were monitored and recorded by a data-logger (see Figure 8.41a and Figure 8.41b).

8.3.2 Results of Tests

8.3.2.1 Stress-Axial Strain Relationship

The stress-strain curves for the vertical, horizontal and inclined specimens ($i = 0^\circ, 45^\circ, 90^\circ$) are given in Figures 8.12 to 8.17 for silty clay sample and varved clay sample. The stress-strain curves are quite linear up to about 0.3% strain. The unloading curves are generally nonlinear at the initial and final stages and these are probably the effects of stress relaxation and a more spontaneous recovery of the elastic strain components at low stress level. Within

this small strain level, elastic theory would therefore apply, provided different sets of parameters are used for loading and unloading.

The lateral strains vary linearly with axial strain and this indicates that Poisson's ratio is constant within the stress level reached in the test. During unloading, substantial compressive strain in the lateral direction results from axial extension but a linear relationship is still retained. This indicates that the Poisson's ratio is also a constant during unloading.

The large difference in slopes of the lateral and axial strain relationship in loading and unloading indicates that the Poisson's ratio in unloading will be considerably higher than that in loading. For the silty clay, $v_{vh}^* = 0.46$, $v_{hv}^* = 0.41$ and $v_{hh}^* = 0.45$ as compared to $v_{vh} = 0.15$, $v_{hv} = 0.12$ and $v_{hh} = 0.17$. Similar observations may be made for the varved clay (see Table 8.3). These high Poisson ratios (approaching 0.5) in the silty clay imply that its drained volumetric behaviour in unloading would not be considerably different from its undrained behaviour.

8.3.2.2 Volumetric Strain and Axial Strain Relationship

For the silty clay, the volumetric strain developed for samples at $i = 0^\circ, 45^\circ, 90^\circ$ inclination are quite similar and the volumetric strains in unloading are very small with high Poisson's ratio in unloading.

In the varved clay, volumetric strains in the $i = 0^\circ$ and $i = 45^\circ$ samples are very similar but are moderately less than the volumetric strains in the $i = 90^\circ$ sample. Volumetric strains in unloading are also much smaller than those obtained in the loading.

8.3.3 Evaluation of Anisotropic Elastic Parameters

With the principal stress and strain measured in both clays, the set of 'elastic anisotropic parameters' may be evaluated in terms of effective stresses. Deformation moduli and Poisson's ratios are obtained from the initial 'linear' portion of the curves which are typically between 0.1% to 0.35% strains and from the linear portion of the unloading curve. Since the stress level is approximately below one-third of the failure stress, it may be assumed that the soils show little yielding so that it is essentially 'elastic'. The parameters were obtained by using the equations listed in Appendix E and they are summarized in Tables 8.2 and 8.3. Several observations may be made regarding these parameters in the two main clay deposits:

- (a) The modulus ratio E_h/E_v is lower in the varved clay ($E_h/E_v = E_h^*/E_v^* = .67$) than in the silty clay ($E_h/E_v = .81$, $E_h^*/E_v^* = .90$). This indicates that the deformation behaviour of the varved clay is more anisotropic.
- (b) The ratio of the shear modulus to vertical modulus G_{vh}/E_v ratios are about the same for both clays (the values are 0.42 and 0.43 for the silty clay and varved clay respectively). In unloading,

the G_{vh}^*/E_v^* ratios are .28 and .20 for the silty clay and varved clay respectively.

- (c) The Poisson's ratios are low in loading but significantly higher in unloading for both clays.
- (d) The ratio of unloading to loading modulus both in the horizontal and vertical direction and for both clays is about 2. Thus the modulus in unloading is approximately double the modulus in loading.

The shear modulus G_{vh} for the silty clay and varved clay agrees very well with the results of simple shear tests described in section 8.4. This is encouraging since G_{vh} is found to be one of the sensitive parameters involved in the analysis of tunnel behaviour (Rowe et al., 1983).

The complete set of anisotropic elastic parameters for the silty clay and varved clay will be utilized for the analysis of the results of field instrumentation in Arrays 1 and 2 in Chapter 10.

8.4 DETERMINATION OF SHEAR MODULUS G_{vh} FROM DIRECT SIMPLE SHEAR TEST

To complement the evaluation of G_{vh} from the results of the inclined specimens in the triaxial test and to obtain a more direct measurement, several simple-shear tests were conducted on samples of the silty clay and varved clay using the Norwegian Geotechnical Institute (NGI) Simple-Shear Apparatus.

8.4.1 Simple Shear Apparatus

A detailed description of the simple shear apparatus and the equipment for mounting and trimming undisturbed specimens can be found in Bjerrum and Landva (1966) and Landva (1964).

The apparatus was built to perform drained and constant volume tests on specimens which are strained in simple-shear and plane strain. By having the specimen confined in a reinforced rubber membrane and using relatively thin specimens (14 mm thick), a uniform straining of the specimen is obtained, at least within the small range of deformations of interest. Two loading caps are provided on the top and bottom of the sample for application of a shearing stress (Figure 8.18). The base cap is fixed to a loading frame and the top cap is attached to a specimen carriage that permits both horizontal and vertical movement but prevents the sample from tilting. The shear stress is applied to the specimen by moving the top cap horizontally while the base cap remains fixed, resulting in a sample deformed during shear as shown in Figure 8.18.

The shear modulus may be calculated from $G_{vh} = \tau/\gamma$ where τ is the shear stress on the horizontal plane and γ is the shear strain. In contrast to the triaxial test, which is based on controlling the principal stresses, the NGI simple-shear apparatus controls the strain conditions. During the consolidation phase of the test the major principal stress is equal to the vertical consolidation pressure p'_0 whereas the minor principal stress is equal to $K'_0 p'_0$. The increase in

shear stress on the horizontal plane will cause a rotation of the principal stresses and a change of their magnitude. Since the principal stress conditions are unknown, the interpretation of the test results is limited to a consideration of the shear stress and normal stress on the horizontal plane. The specimen is considered to have failed when the shear stress on the horizontal plane shows a peak value. This assumption may affect the interpretation of the shearing strength of the material (Hoeg and Prevost, 1976). However, it does not present a problem with respect to the determination of the shear modulus, G_{vh} , which is evaluated at small deformations.

8.4.2 Constant Volume Test

The undrained conditions of the tests were simulated using the constant-volume test described by Bjerrum and Landva (1966). Constant volume is maintained by keeping the specimen height the same by varying the vertical load on the specimen using a screw-controlled loading device and regulating the load in such a way that the height of the sample remains constant. Since the soil maintains a constant volume, the undrained condition is modelled and the change in vertical stress is equal to the change in pore water pressure Δu that would occur in a normal undrained test. The rate of feed used by the machine was .1 mm per 45 minutes.

Dimensionless stress-strain relationships of five typical samples are presented in Figures 8.19 to 8.23. Three curves are plotted in

each figure. The (τ/p) curve represents the horizontal applied shear stress (τ) normalized by dividing by the vertical consolidation pressure (p). (τ/σ') is the ratio of applied shear stress to the effective normal stress on the sample. The (σ'/p) curve represents the ratio of effective normal stress to the consolidation pressure.

From these results, the following observations can be made:

- (i) The tests on samples from the upper "crust" and silty clay show a fairly well-defined peak followed by a slight post-peak drop in strength. For the layered clay and the varved clay, the stress-strain relationship resembles a plastic material. The strain at failure was found to vary between 2.8 and 4.9%. These trends are consistent with those obtained in CIU triaxial compression tests.
- (ii) The soil exhibited a general tendency to decrease in volume when sheared and it was necessary to steadily decrease the normal stress during the test so as to maintain a constant volume. The rate of shearing was sufficiently slow to prevent the development of pore pressures and hence the effective stress is equal to the applied total stress. Thus the changes in effective stress shown by $(1-\sigma'/p)$ in Figures 8.19 to 8.23 are equivalent to the pore pressures u/p that would be set up in a corresponding undrained test.
- (iii) The computed value of stress ratio (τ/σ') increases with strain in every test and it appears that an ultimate value would only

be reached at large strains (>10%).

This (τ/σ') stress ratio plot is probably not as useful as the σ_1'/σ_3' plot employed in the triaxial test results. The (τ/σ') stress ratio does not show any indication of failure even when the bulk shear strength (τ) is fully mobilized.

The shear modulus, G_{vh} , obtained from the simple shear tests is representative of the soil behaviour during tunnel excavation. The test specimen underwent a decrease in mean stress in order to maintain a constant volume during the test and this gradual decrease in mean stress is consistent with the unloading stress path in the soil which is caused by tunnelling.

8.4.3 Results of Simple Shear Tests

The relevant parameters obtained from eight simple shear tests are summarized in Table 8.4. It may be noted that the shear modulus obtained was very consistent and repeated tests at the same depth yielded almost identical results.

The variation of shear modulus with depth is shown in Figure 8.24. The shear modulus at two depths in the silty clay and varved clay determined from "anisotropic parameter tests" are also shown in Figure 8.24. It may be seen that the results agree reasonably well. The shear modulus increases linearly with depth at a rate of about 0.3 MPa/m.

8.5 ANISOTROPICALLY CONSOLIDATED TRIAXIAL TESTS AND CONTROLLED STRESS PATH TESTS

In this section, the effects of anisotropic consolidation as pertaining to the field initial stress condition and the effects of stress path on the deformation and strength behaviour are studied. Three principal types of tests were performed including

- (a) Strain controlled, undrained and drained compression and extension tests;
- (b) Stress-path tests in which the applied axial and lateral stress increments were varied in such a way as to conform to the stress changes in the field during tunnelling;
- (c) As in (b), but the tests were performed using the NRC servo-system.

8.5.1 Anisotropically Consolidated, Strain-Controlled Triaxial Tests

The following strain-controlled triaxial tests were performed, after the specimens were consolidated under the condition of zero lateral strain, to the in-situ stresses in the field:

- (a) undrained compression, σ_1 increasing (CK_0UC)
- (b) drained compression, σ_1 increasing (CK_0DC)
- (c) undrained extension, σ_1 decreasing (CK_0UE)
- (d) drained extension, σ_1 decreasing (CK_0DE).

The initial effective stress ratio, K'_0 , was determined in the

field by hydraulic fracturing tests to be 0.75 and 0.58 for the silty clay and varved clay, respectively. A total of four series (16 tests) were performed.

The tests were performed in a K_0 -cell in which the loading piston has a diameter equal to that of the specimen (50 mm). The K_0 -cell was manufactured by Wykeham Farrance Engineering Ltd. For extension tests, a loading device was fabricated and used as shown in Figure 8.25. The undrained tests were performed at a strain rate of 1% per hour while the drained tests were performed at 0.1% per hour. A back pressure equal to the in-situ hydrostatic pressure was employed and the B values obtained were greater than 0.98 in all tests.

8.5.2 Results of Tests

A typical set of results for the silty clay is shown in Figures 8.26 to 8.29. From these figures, the following observations may be made:

- (a). The stress-strain curves for the undrained and drained tests in the extension mode are virtually identical. The observation is consistent with the high Poisson's ratio obtained in unloading in "anisotropic parameter tests" (see section 8.3).
- (b) In compression, the specimen is stiffer in undrained behaviour, and the failure strain is about 2.5% compared to about 5% in the other tests.

- (c) The undrained strength in extension is about 75% of that in compression.
- (d) The pore pressure in the undrained compression tests increases with axial strain yielding the pore pressure parameter $A_f = 0.5$. The pore pressure in extension tests decreases with strain, reaches a maximum negative value of -15 kPa at a strain of 0.7%, then increases with larger strains.
- (e) The volumetric strains in compression in the drained tests are consistent with the pore pressure behaviour in undrained tests.

A typical set of results for varved clay is shown in Figures 8.30 to 8.33. The trend of these test results, particularly at small strains is similar to that of the silty clay. The moduli determined from these tests will be compared to those obtained in stress path tests in the next section.

8.5.3 Controlled Stress Path Triaxial Tests

Controlled stress path triaxial tests (Davis and Poulos, 1963) were performed on samples at depths approximately corresponding to the locations of the crown and springline of the tunnel. The samples were tested along the stress path predicted by the finite element method to simulate tunnel excavation, as shown in Figure 5.3 in Chapter 5.

8.5.3.1a Total Stress Controlled Test

A number of 'total stress controlled' triaxial tests were carried

out on the silty clay. These samples were first anisotropically consolidated to the in-situ K_0 condition of the soil. When consolidation is completed, the 'stress path test' was started by varying the stress conditions according to the desired stress path. Dead weights were added on or taken away from the load hanger and the cell pressure was adjusted so that the axial and lateral pressure would conform with the postulated stress path. Since the axial stress (σ'_v) and cell pressure (σ'_h) were changed in a stepwise fashion, the actual stress path reproduced in the laboratory would have a 'zig-zag' like pattern. However, the general trend of the stress conditions was faithfully reproduced.

Drainage was kept closed initially during the experiment so that the undrained modulus can be determined from the stress-strain relationship. Before the stresses had reached the failure stage, the drainage was opened and the corresponding deformation was recorded. Thus, the drained modulus can be determined from the slope of the secant drawn between the initial and final points of the stress-strain curve.

8.5.3.1b Servo-Test

Two samples of silty clay were tested by Dr. K.T. Law of the National Research Council in a servo system (Law, 1981). Stress-controlled tests following the stress paths for the crown and spring-line region were performed. These two tests which will be referred to as 'Servo Tests' were performed so as to provide some comparison with

the results of total stress control tests in (a) above.

8.5.3.2 Results of Tests

The results of the "total stress controlled tests" and "servo tests" as well as the results of CK_0U extension and compression tests are compared in Figures 8.34 to 8.37. The results of the undrained strain controlled tests are included since their stress paths do not depart widely from those of controlled stress path tests in the $p'-q'$ plot... (See Muckle, 1984.)

(a) Tests Simulating Stress Conditions At the Crown Region

The stress paths of the different tests together with the prescribed stress path determined from the finite element analysis are shown in Figure 8.34. It may be seen that starting from the in-situ stress condition, there is a general decrease in mean stress p' and an increase in deviator stress q . Principal stress rotation occurs at $q = 0$.

The stress-strain curves shown in Figure 8.35 indicate that for an initial portion of the curves up to a strain of 0.25%, the results of the different types of tests are very similar. The modulus at small strains for the extension mode corresponding to stress conditions at the crown region are summarized in Table 8.5. It may be noted that in computing the E values in controlled stress path tests the generalized Hooke's Law has to be used since the principal stresses

are changing. It may be seen that the results agree well. This result suggests that the modulus is not unduly sensitive to the exact stress paths followed, provided the stress paths do not depart widely from one another. In addition, the modulus in drained and undrained conditions are identical and Poisson's ratio approaches 0.5, a result that has been noted previously.

(b) Tests Simulating Stress Conditions at the Springline Region

The stress paths for the different types of tests performed, together with the prescribed stress path determined from finite element analysis at the springline region are shown in Figure 9.36. It may be seen that both the deviator and mean stress increase at this location and that the CK_0U compression test stress path departs somewhat from the prescribed stress path.

The stress-strain curves for the different tests are shown in Figure 8.37. The two total stress controlled tests yielded repeatable results. The servo test showed rather unusual stress-strain behaviour. It is suspected that the sample might be disturbed and the result is questionable.

The moduli computed from the test results are shown in Table 8.5. It may be seen that the results from CK_0UC are only slightly different from those obtained from "total stress-controlled tests". There is a significant difference in the results obtained from undrained tests and the different drained tests. This may be attributed to the

significant difference between the stress paths followed in these tests.

The modulus values determined from the CK_0UC , CK_0UE , CK_0DE , CK_0DE and controlled stress path tests are shown in Figure 8.38. Modulus profiles deduced from these results are given in Chapter 10:

8.6 STRENGTH FROM ANISOTROPIC CONSOLIDATED TRIAXIAL TESTS AND CONTROLLED STRESS PATH TESTS

The shear strength of the silty clay obtained from anisotropic consolidated triaxial tests (CK_0U compression and extension, CK_0D extension) and controlled stress path test are plotted on the $p'-q'$ space in Figure 8.39. The effective Mohr-Coulomb envelope determined from conventional CIU triaxial compression tests as discussed in Chapter 7 is also shown in the same figure. The envelope on the negative deviator stress region in the $p'-q'$ space is a mirror image of the same envelope.

There is very good agreement between the shear strengths determined from conventional triaxial tests and the anisotropic consolidated triaxial tests and controlled stress path tests. Also, it can be seen that the absolute magnitude of cohesion and internal friction angle are the same for compression and extension failure.

The strength of the varved clay determined from CK_0U and CK_0D triaxial compression tests is also in good agreement with the strength envelope obtained from conventional CIU triaxial tests (Figure 8.40).

From the conventional and anisotropic consolidated triaxial test results on the silty clay and varved clay, it appears that the effective stress parameters c' and ϕ' (or \bar{c}' and α' in the p' - q' stress space) are intrinsic properties of the soils which are independent of the method of testing. The failure envelopes for the silty clay and varved clay may therefore be employed with adequate experimental support for the analysis of tunnel performance discussed in Chapter 10.

8.7 SUMMARY OF SPECIAL TESTS PERFORMED ON THE CLAY AT ARRAYS 1 AND 2 ON THE THUNDER BAY TUNNEL

1. The modulus of deformation was defined as a secant modulus at 0.1% strain for undrained tests since this yielded results which were self consistent within one type of test and between different tests. In CIU tests this definition would correspond to a modulus defined at a stress level about 1/3 of the failure stress. In CID tests, some test error occurred at very small strains (below 0.1%) and the modulus was therefore defined in the strain range of 0.1 to 0.6%. The modulus defined above is consistent with the use of the "elastic" modulus in the Finite Element Analysis.

2. One dimensional consolidation tests performed using the large diameter Rowe Cell indicated that

- a) The consolidation parameters are strongly nonlinear both in loading and in unloading. This emphasizes the requirement that the parameters used in analysis must be determined at the appropriate stress levels.

- b) The coefficient of consolidation in loading (c_V) and unloading (c_R) determined from pore water pressure dissipation is higher than those determined from the settlement-time curves.
- c) At the same stress level, the values of c_V and c_R for the varved clay are considerably higher than those of the silty clay.
- d) For the varved clay, c_R in unloading is considerably higher than c_V in loading. The coefficients, however, are similar in magnitude for the silty clay deposit.

3. The drained modulus profile deduced from the results of the one dimensional consolidation tests, assuming Poisson's ratio in the range 0.1-0.15, is in reasonable agreement with that obtained from isotropically consolidated drained triaxial tests (CID).

4. Poisson's ratio in unloading is considerably higher than that in loading. For the silty clay, Poisson's ratios in loading and unloading are approximately 0.15 and 0.45 respectively. For the varved clay the loading and unloading Poisson's ratios are approximately 0.1 and 0.3. The high unloading Poisson's ratio in the silty clay suggests that its drained volumetric behaviour, in unloading, would not be considerably different from its undrained behaviour.

5. The ratio of horizontal to vertical modulus E_h/E_v is lower in the varved clay ($E_h/E_v = E_h^*/E_v^* = 0.67$) than in the silty clay ($E_h/E_v = 0.81$, $E_h^*/E_v^* = 0.9$). This indicates that the deformation behaviour of the varved clay is more anisotropic than the silty clay.

6. The vertical and horizontal moduli in unloading are approximately double the corresponding values in loading for both clays.

7. The ratio of independent shear modulus to vertical modulus G_{vh}/E_v varied slightly with depth but is typically approximately 0.43 for both the silty and varved clay in loading. In unloading, G_{vh}^*/E_v^* ratios are typically 0.28 and 0.2 for the silty clay and varved clay respectively. The ratio G_{vh}/E_v in loading approximately corresponds to the isotropic value for both clays, however the unloading ratio G_{vh}^*/E_v^* is highly anisotropic. Again, the varved clay is more anisotropic than the silty clay.

8. The shear modulus G_{vh} determined from the special "anisotropic parameter triaxial apparatus" agrees well with the results obtained using the NGI Simple-Shear apparatus.

9. The stress-strain curves obtained from simple-shear tests on the silty clay indicated a well defined peak followed by a slight post-peak drop in strength. For the layered clay and varved clay the stress-strain relationship resembles a plastic material. These trends are consistent with those observed in the CIU triaxial compression tests.

10. The shear modulus, G_{vh} , obtained from the simple-shear apparatus is considered to be representative of soil behaviour during tunnel excavation. The test specimen underwent a decrease in mean stress in order to maintain constant volume during the test. This is consistent

with the unloading stress path in the soil which is caused by tunnelling.

11. The shear modulus obtained from the simple-shear test was very consistent and repeated tests at the same depth yielded almost identical results.

12. The shear modulus gradually increased with depth.

13. The stress-strain curves, and hence the modulus, obtained in K_0 consolidated undrained and drained extension tests were virtually identical. (This is consistent with the high Poisson's ratio observed in unloading in the anisotropic parameter tests.)

14. The modulus obtained in K_0 consolidated drained compression is much lower than that obtained in undrained compression.

15. The undrained strength in extension is lower than that in compression.

16. The volumetric strains in compression in the drained tests are consistent with the pore pressure behaviour in undrained tests.

17. Controlled stress path tests performed to follow the anticipated stress path above the tunnel crown involved a general decrease in mean stress and a 90° principal stress rotation. This stress path is similar to that observed in the strain controlled CK_0U extension tests. The drained and undrained elastic moduli obtained from the controlled stress path tests and the CK_0U and CK_0D extension tests are all very similar and consistent. This result suggests that the modulus

is not unduly sensitive to the exact stress path followed, provided the stress paths do not depart widely from one another. Furthermore, it is implied that the results of strain controlled extension tests would provide a reasonable estimate of the appropriate elastic modulus above and below the tunnel.

18. Controlled stress path tests performed to follow the anticipated stress path at the springline involved an increase in both the mean and deviator stress. This stress path is different from that followed in drained (CK_0DC) and undrained (CK_0UC) compression tests. The undrained modulus deduced from controlled stress and CK_0UC tests are only slightly different. However, there is a significant difference in the drained modulus deduced from the controlled stress path test and that deduced from conventional CK_0DE tests. The drained modulus at the springline obtained from the controlled stress path test lies between the values deduced from CK_0DE and CK_0DC tests.

19. There is good agreement between the shear strengths determined from conventional triaxial tests and the anisotropic consolidated triaxial tests and controlled stress path tests. Also, the absolute magnitude of cohesion and internal friction angle are the same for compression and extension failure. From the conventional and anisotropic consolidated triaxial test results on the silty clay and varved clay, it appears that the effective stress parameters c' and ϕ' are intrinsic properties of the soils which are independent of the stress path followed.

TABLE 8.1(a) RESULTS OBTAINED FROM THE LARGE OEDOMETER FOR SILTY CLAY ("CRUST") (7.24 m)

	Load (kPa) Increment	c_v or c_R (m^2/yr) (a)	c_v or c_R (m^2/yr) (b)	m_v or m_R (1/kPa)
	0 - 50	14	8	1.7×10^{-4}
Loading	50 - 100	6	4	3.5×10^{-4}
	100 - 200	2	1	9.6×10^{-4}
	200 - 100	10	5	0.86×10^{-4}
Unloading	100 - 50	4	2	2.3×10^{-4}
	50 - 0	2	1	5.0×10^{-4}

TABLE 8.1(b) RESULTS OBTAINED FROM THE LARGE OEDOMETER FOR SILTY CLAY (9.78 m)

	Load (kPa) Increment	c_v or c_R (m^2/yr) (a)	c_v or c_R (m^2/yr) (b)	m_v or m_R (1/kPa)
	0 - 36	10	7	2.0×10^{-4}
Loading	36 - 71	4	3	3.3×10^{-4}
	71 - 142	3	2	4.3×10^{-4}
	142 - 71	20	12	0.68×10^{-4}
Unloading	71 - 36	10	4	1.8×10^{-4}
	36 - 0	3	1	5.8×10^{-4}

TABLE 8.1(c) RESULT OBTAINED FROM THE LARGE OEDOMETER FOR
VARVED CLAY (13.1 m)

	Load (kPa) Increment	c_v or c_R (m^2/yr) (a)	c_v or c_R (m^2/yr) (b)	m_v or m_R ($1/kPa$)
	0 - 41	16	16	2.4×10^{-4}
Loading	41 - 81	34	18	4.0×10^{-4}
	81 - 161	33	11	2.6×10^{-4}
	161 - 81	224	111	0.22×10^{-4}
Unloading	81 - 41	231	98	0.95×10^{-4}
	41 - 0	36	8	2.95×10^{-4}

Note:

(a) Based on pore pressure dissipation.

(b) Based on settlement.

TABLE 8.2 ANISOTROPIC ELASTIC PARAMETERS FROM CID TESTS
ON SILTY CLAY (ARRAY 2, DEPTH 10.15 m)

Anisotropic Elastic Parameters	Results From CID Tests (MPa)
E_v	6.5
E_v^*	12.1
E_h	5.3
E_h^*	10.9
G_{xx}	2.3
G_{xx}^*	3.8
G_{zx} (G_{vh})	2.7
G_{zx}^* (G_{vh}^*)	3.3
μ_{xx}	.17
μ_{xz}	.12
μ_{zx}	.15
μ_{xx}^*	.45
μ_{xz}^*	.41
μ_{zx}^*	.46
E_h/E_v	.81
E_h^*/E_v^*	.90
G_{zx}/E_v	.42
G_{zx}^*/E_v^*	.27
E_v^*/E_v	1.9
E_h^*/E_h	2.1

Note: * denotes unloading

TABLE 8.3 ANISOTROPIC ELASTIC PARAMETERS FROM CID TESTS
ON VARVED CLAY (ARRAY 2, DEPTH 13.4 m)

Anisotropic Elastic Parameters	Results From CID Tests (MPa)
E_v	10.1
E_v^*	23.4
E_h	6.8
E_h^*	15.8
G_{xx}	3.0
G_{xx}^*	5.9
G_{zx} (G_{vh})	4.3
G_{zx}^* (G_{yh}^*)	4.7
μ_{xx}	.13
μ_{xz}	.07
μ_{zx}	.11
μ_{xx}^*	.33
μ_{xz}^*	.20
μ_{zx}^*	.30
E_h/E_v	.67
E_h^*/E_v^*	.68
G_{zx}/E_v	.43
G_{zx}^*/E_v^*	.20
E_v^*/E_v	2.3
E_h^*/E_h	2.3

Note: * denotes unloading

TABLE 8.4 RESULTS FROM SIMPLE-SHEAR TESTS ON THE THUNDER BAY SOIL (CONSTANT VOLUME TEST)

Location	Material Type	Sample Depth (m)	Water Content (%)	p (kPa)	(1/p) _f	(γ _f) (%)	(Δu/p) _f	G _{vh} (MPa)	G _{vh} /p
Array 1	'Crust' Silty Clay	7.5	62.5	80	0.40	4.5	0.18	2.6	33
Array 2	Silty Clay	(1) 8.8	62.3	86	0.37	2.8	0.22	3.3	38
		(2) 8.8	59.3	86	0.46	4.9	-	3.0	35
Array 2	Silty Clay	(1) 10.4	57.6	94	0.33	4.0	0.30	3.0	32
		(2) 10.4	58.3	99	0.35	3.6	0.27	3.0	30
Array 1	Layered Clay	11.7	41.3	110	0.59	4.9	0.19	4.0	36
Array 2	Varved Clay	(1) 12.6	40.7	115	0.28	2.5	0.21	4.5	39
		(2) 12.6	35.7	115	0.34	3.8	0.30	4.3	37

P = Initial vertical consolidation pressure P₀'

TABLE 8.5 COMPARISON OF MODULI FROM DIFFERENT TYPES OF TESTS

Type of Test	Modulus			
	Extension Mode		Compression Mode	
	E _{undrained}	E _{drained}	E _{undrained}	E _{drained}
Servo	11.6	11.6	-	-
Total Stress Controlled	11.8	11.8	16.4*	9.5*
CK ₀ E or CK ₀ C	11.3	11.3	16	6.1*

*Note: There is a significant difference between the stress paths followed in these tests

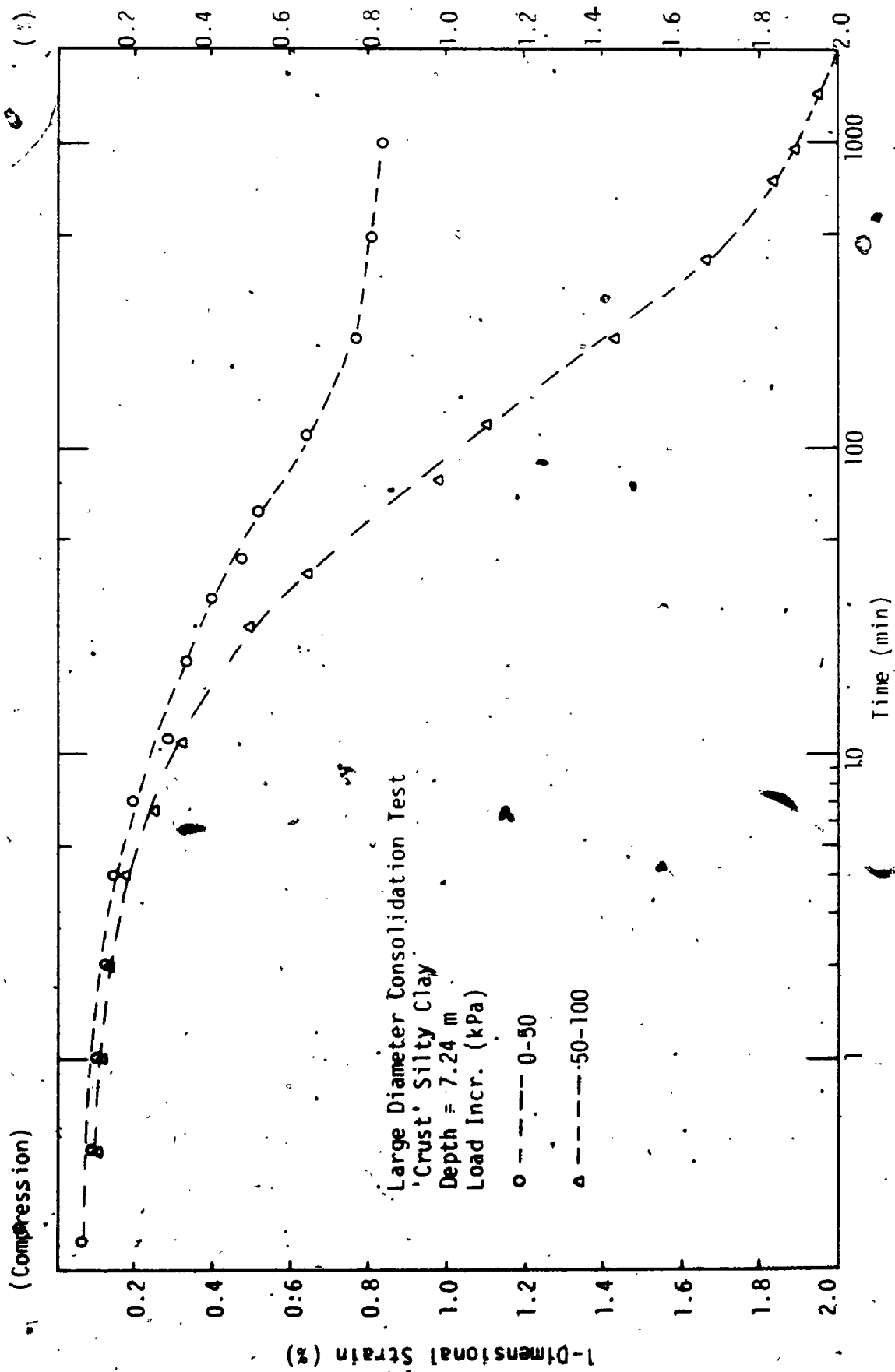


FIGURE 8.1 1-Dimensional Compressive Strain vs Time for Loading Stage in Large Oedometer Test.

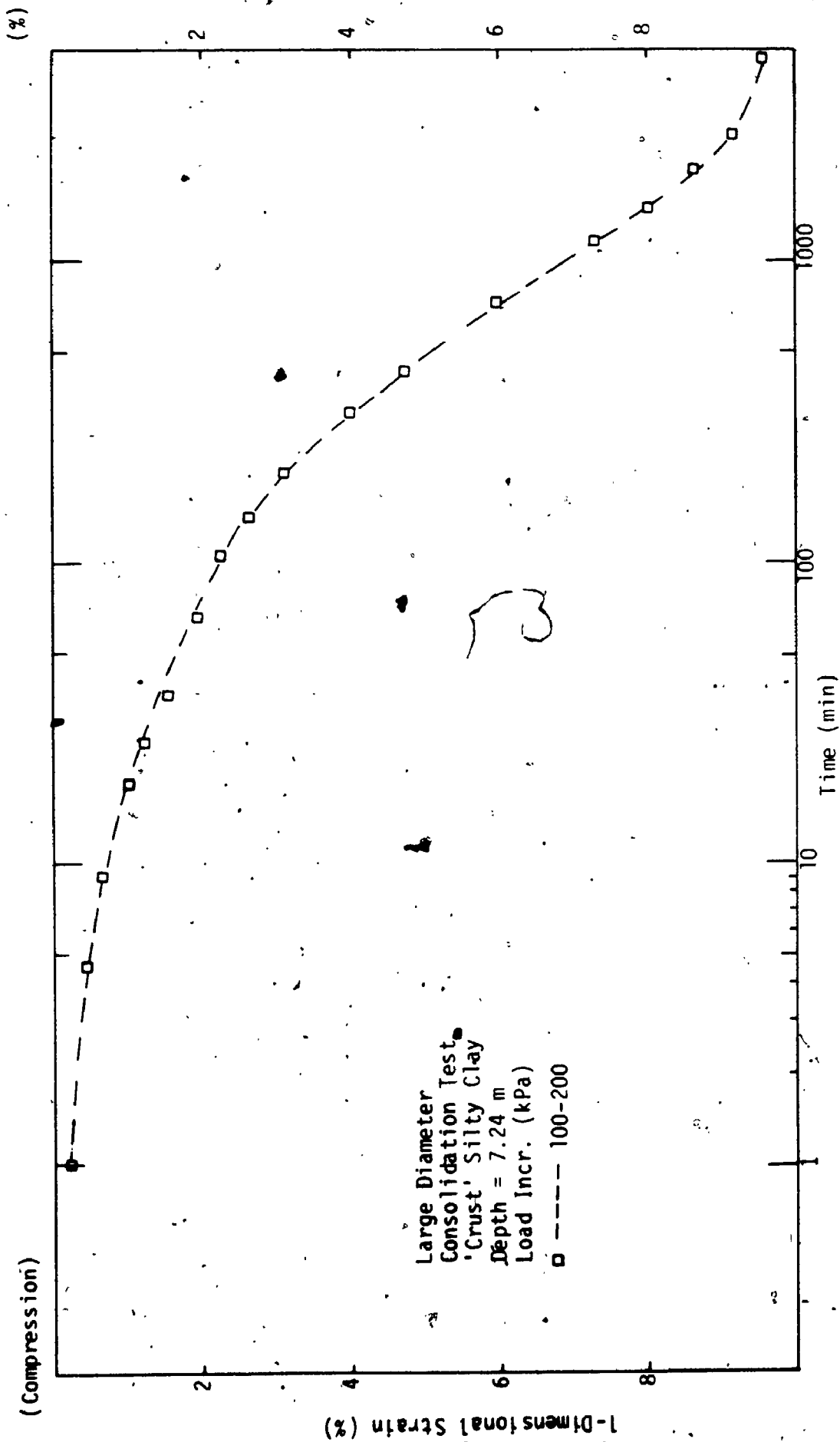


FIGURE 8.2 1-Dimensional Compressive Strain vs Time for Loading Stage - in Large Oedometer Test

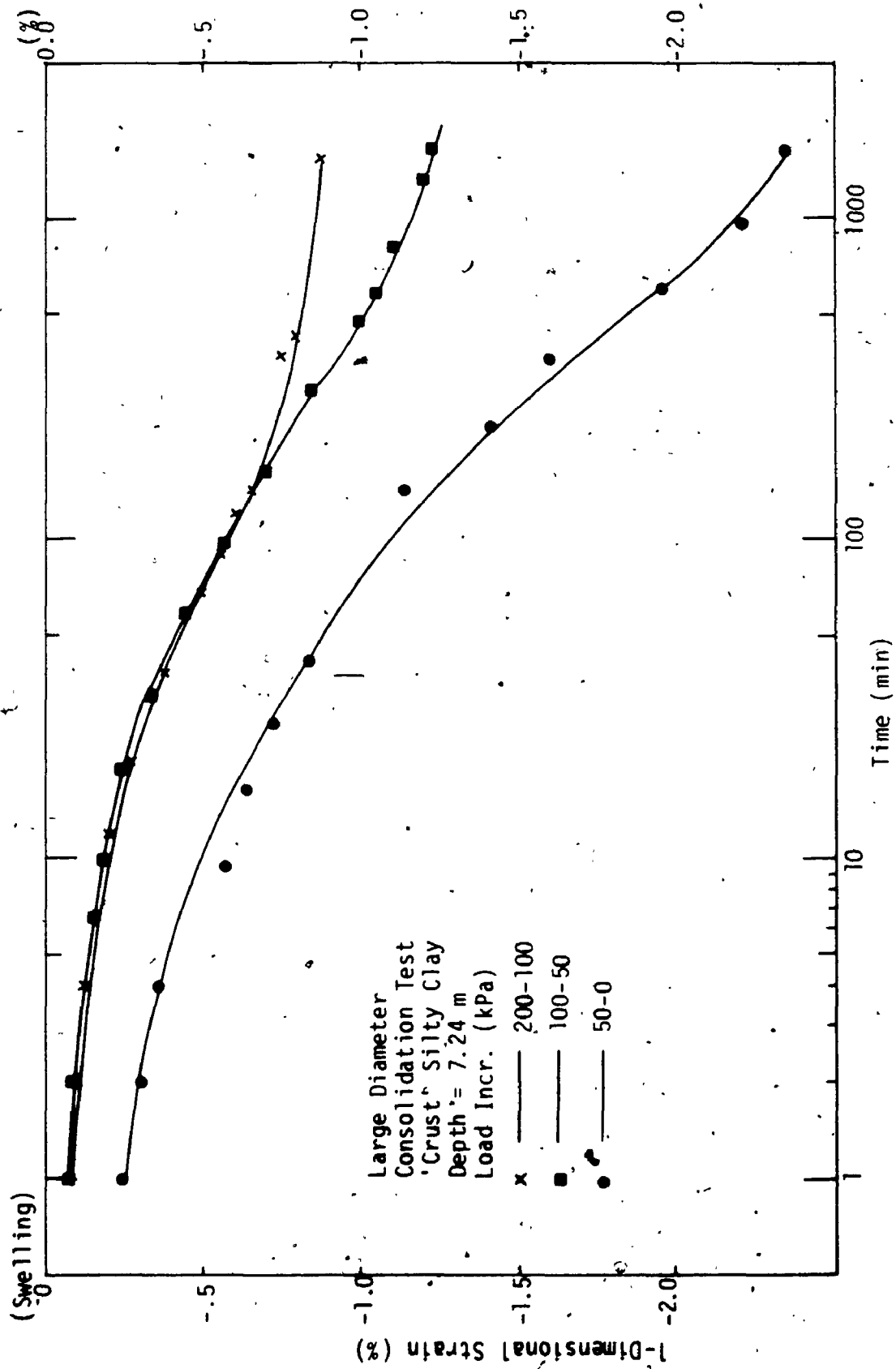


FIGURE 8.3 1-Dimensional Swelling Strain vs Time for Unloading Stage in Large Oedometer Test

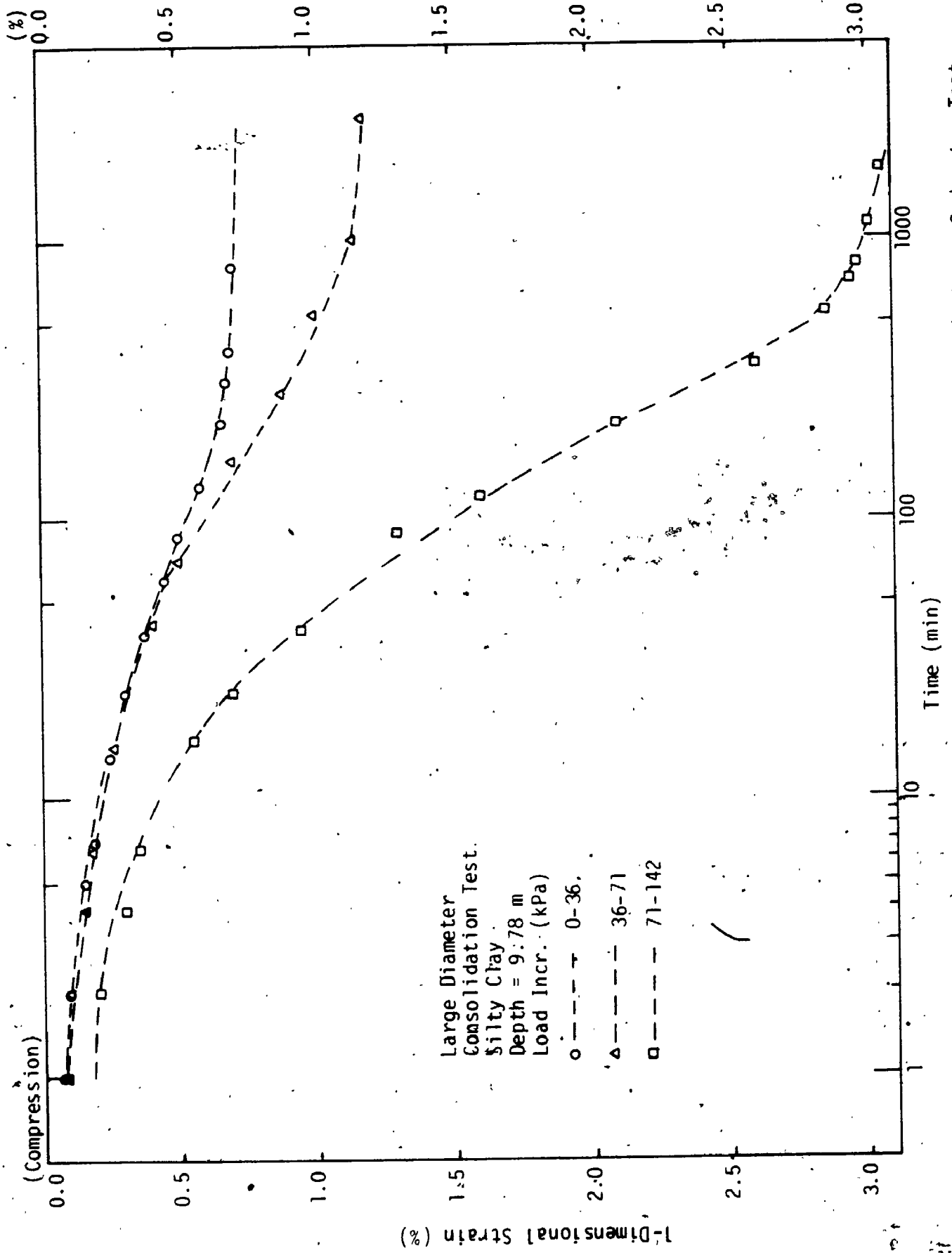


FIGURE 8.4 1-Dimensional Compressive Strain vs Time for Loading Stage in Large Oedometer Test

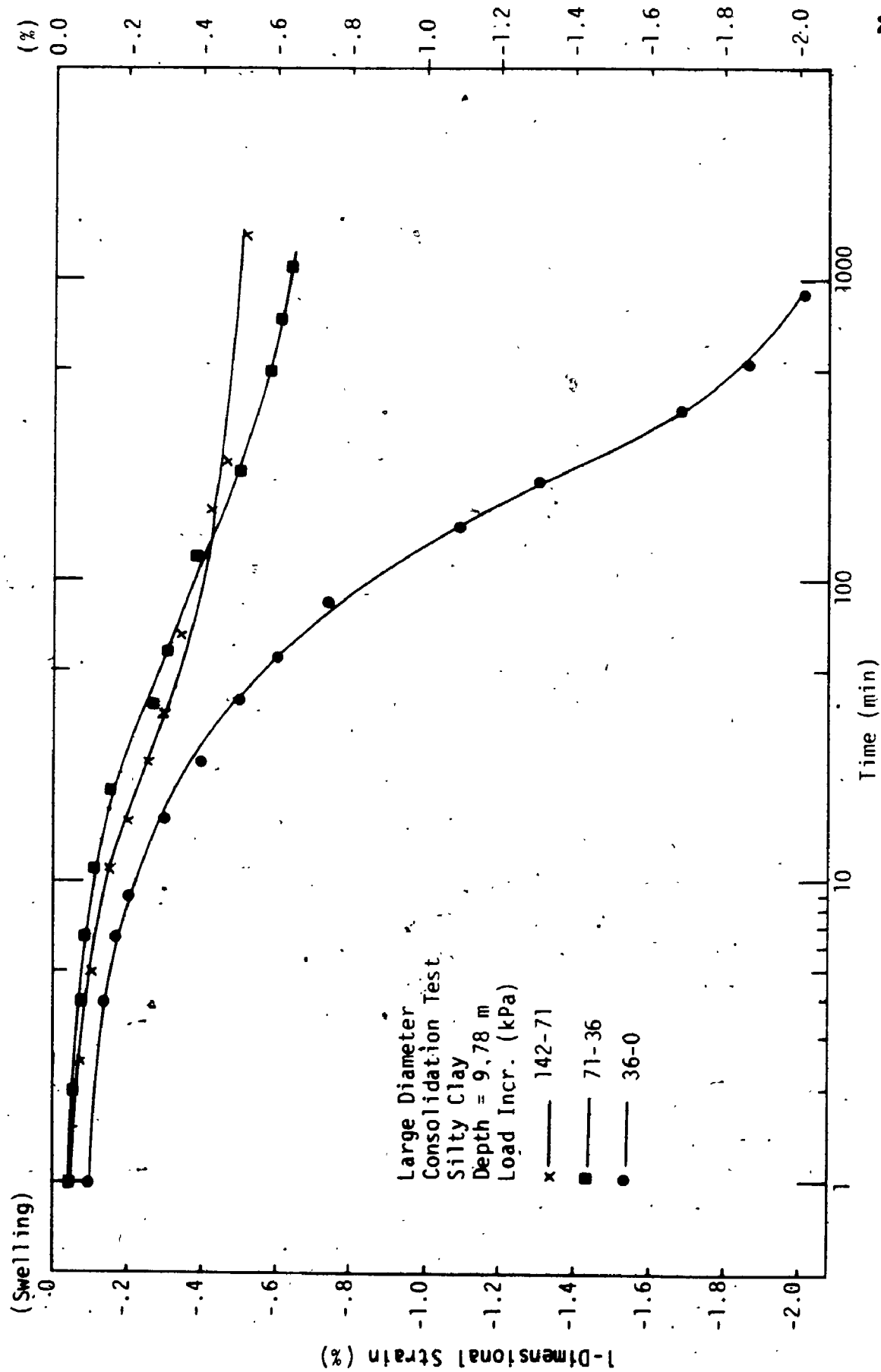


FIGURE 8.5 1-Dimensional Swelling Strain vs Time for Unloading Stage in Large Oedometer Test

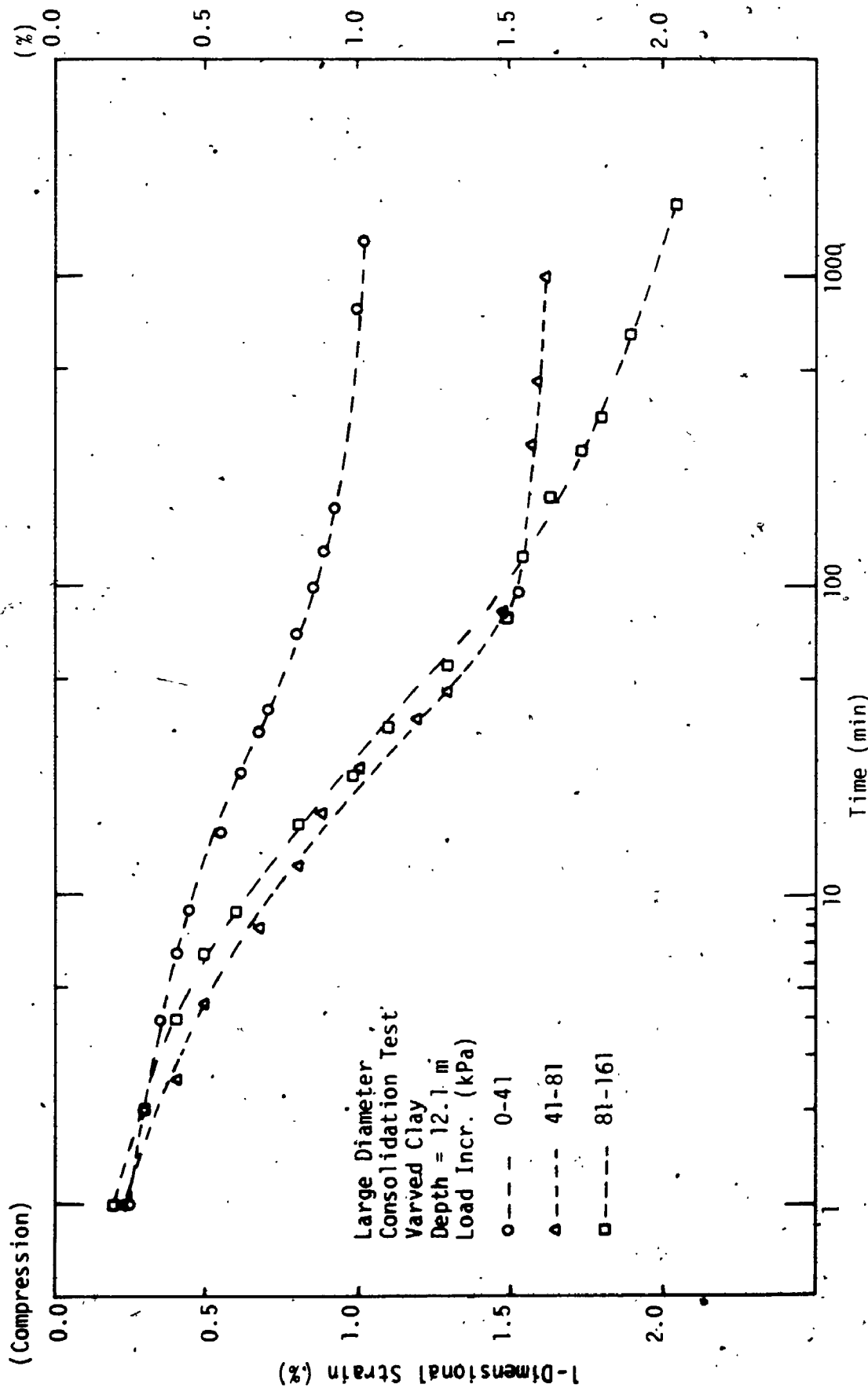


FIGURE 8.6 1-Dimensional Compressive Strain vs Time for Loading Stage in Large Oedometer Test

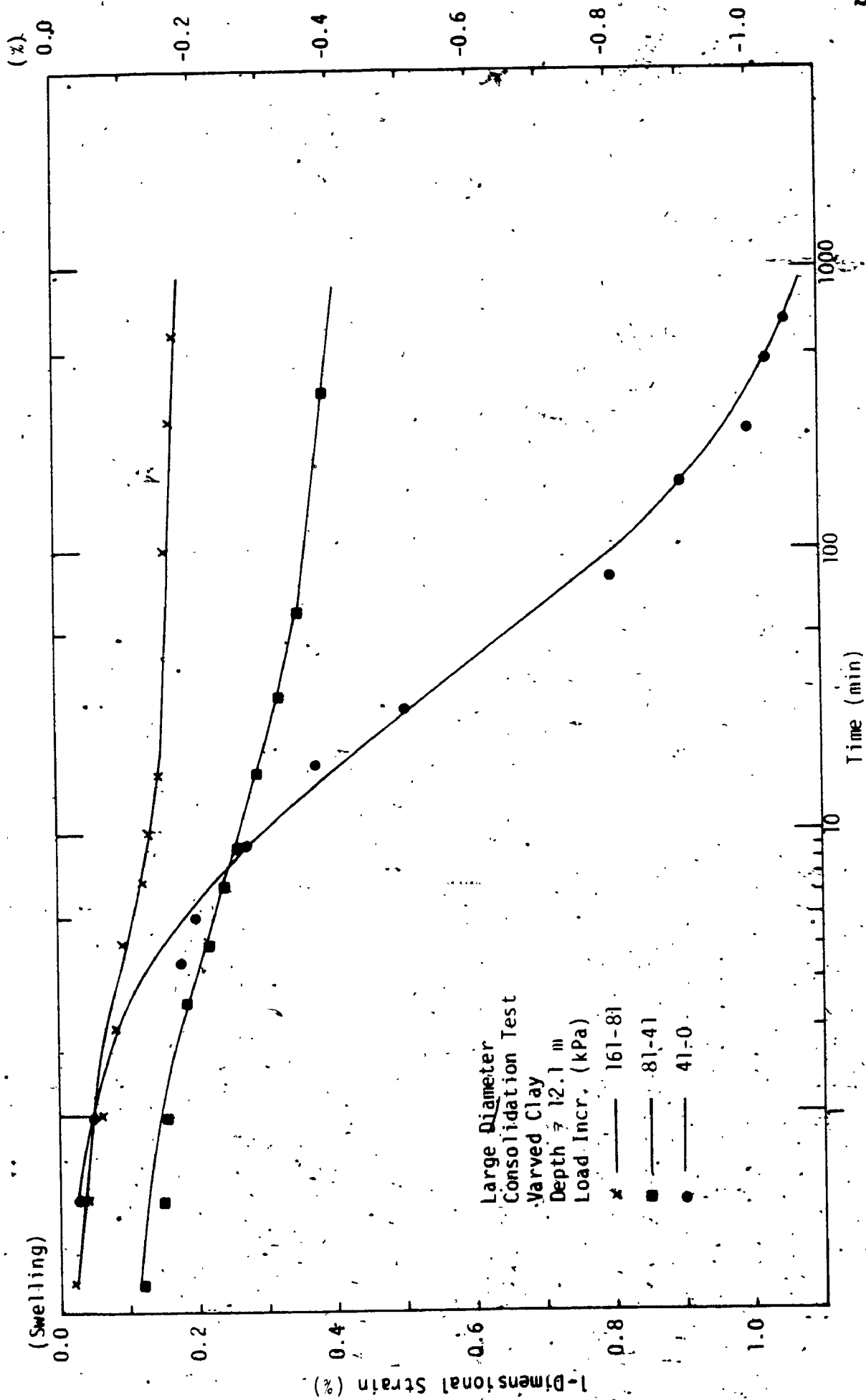


FIGURE 8.7 1-Dimensional Swelling Strain vs Time for Unloading Stage in Large Oedometer Test

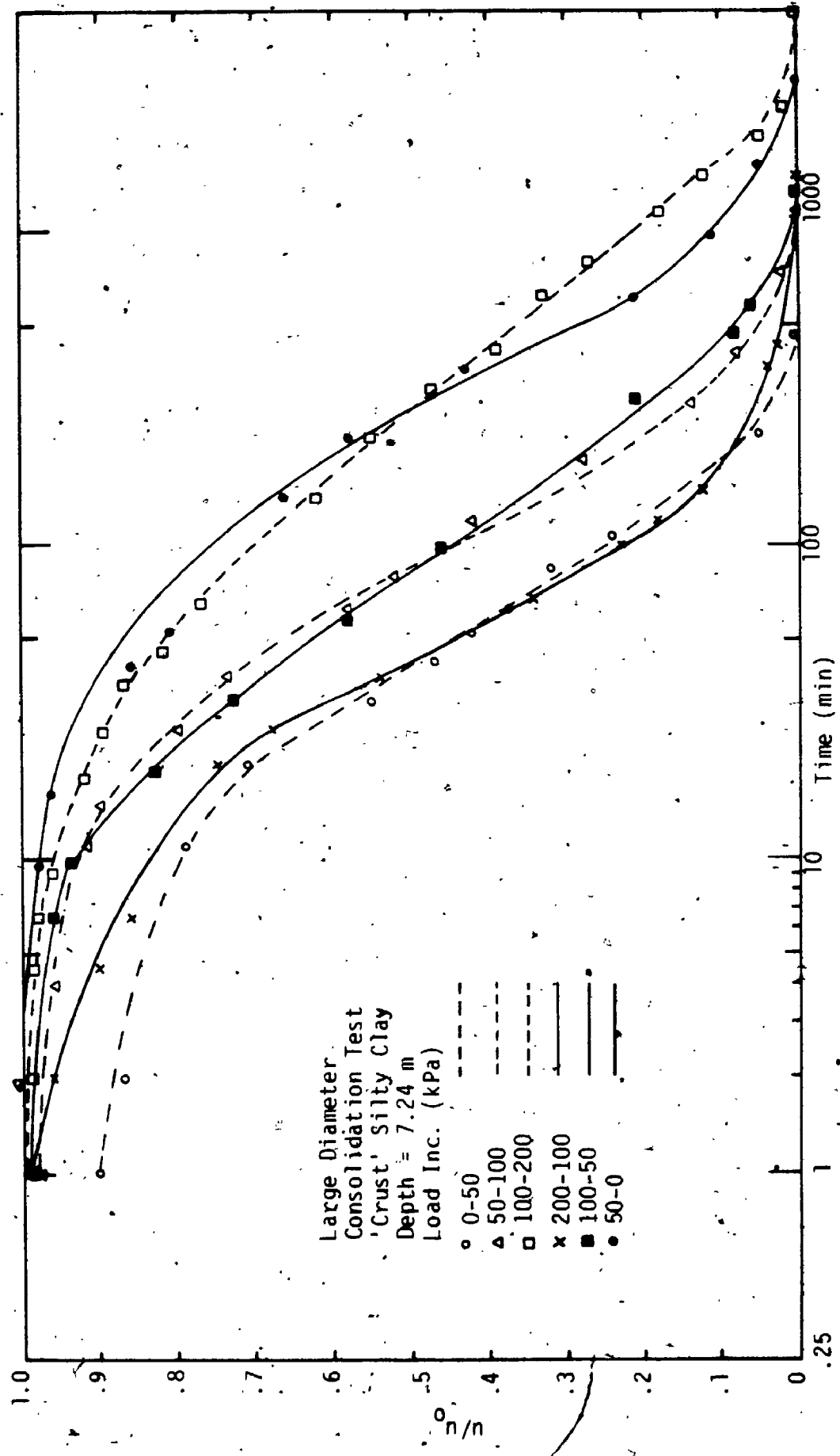


FIGURE 8.8 Relationship Between Pore Pressure Dissipation With Time

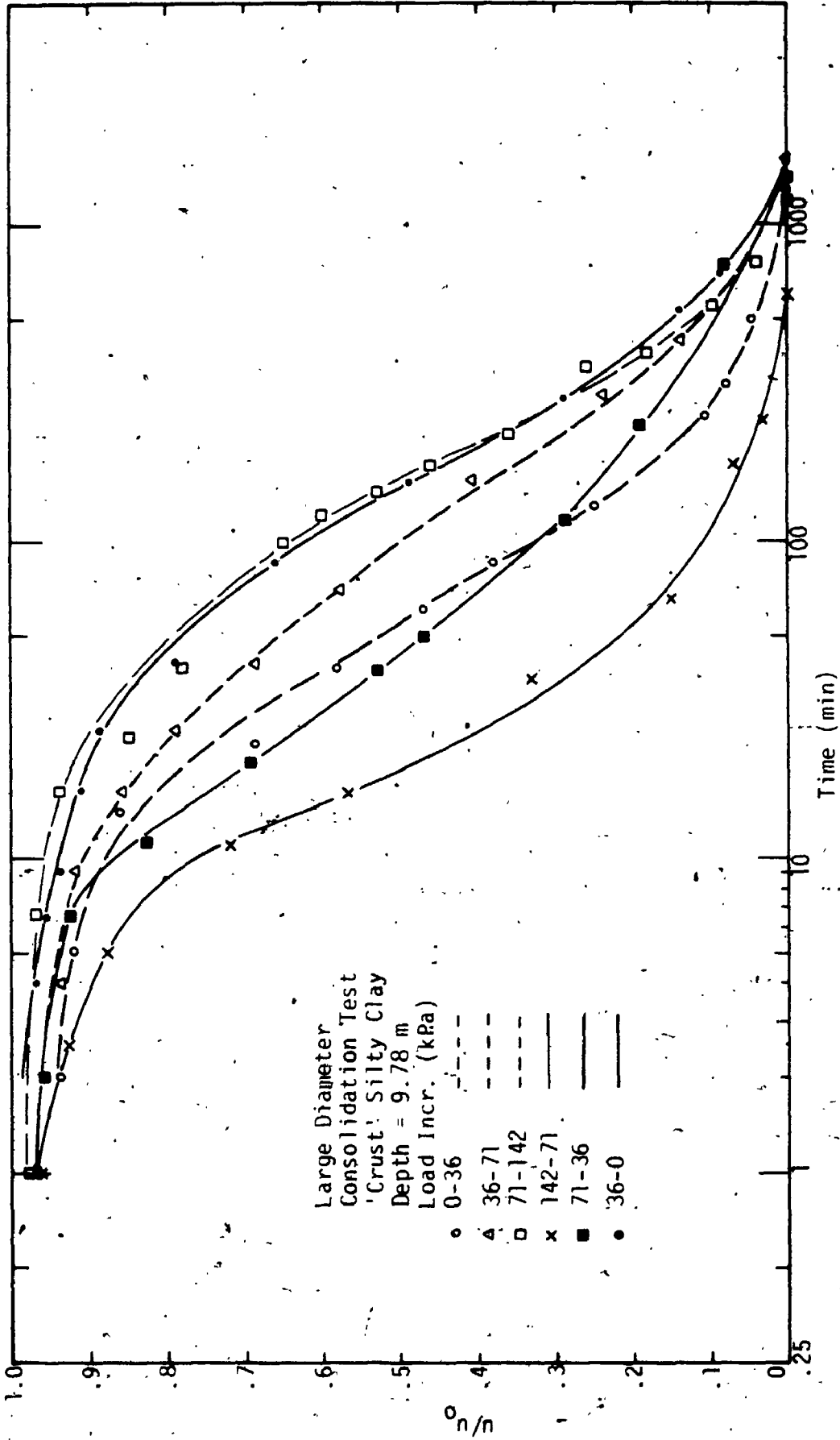


FIGURE 8.9 Relationship Between Pore Pressure Dissipation With Time

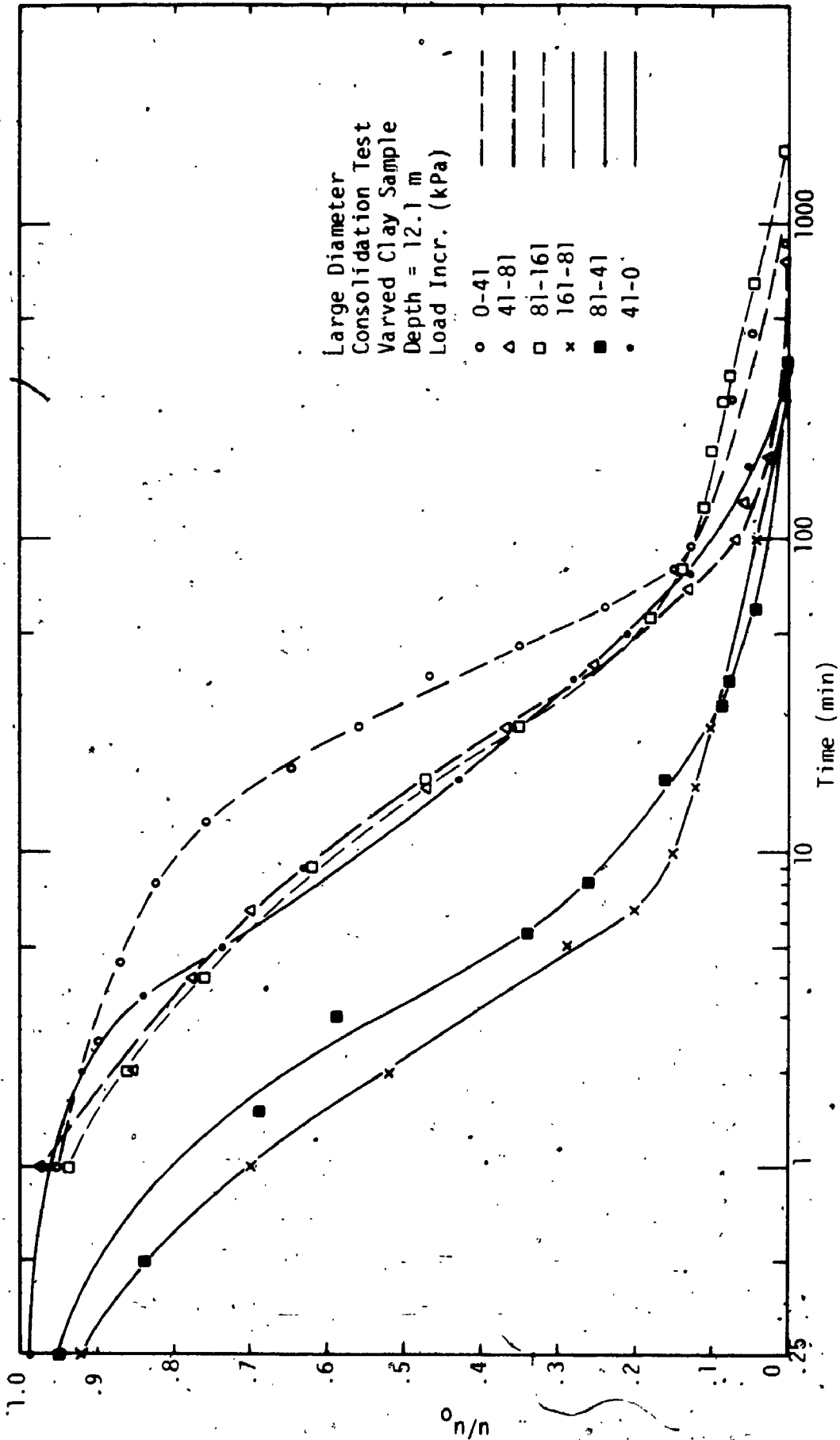


FIGURE 8.10 Relationship Between Pore Pressure Dissipation With Time

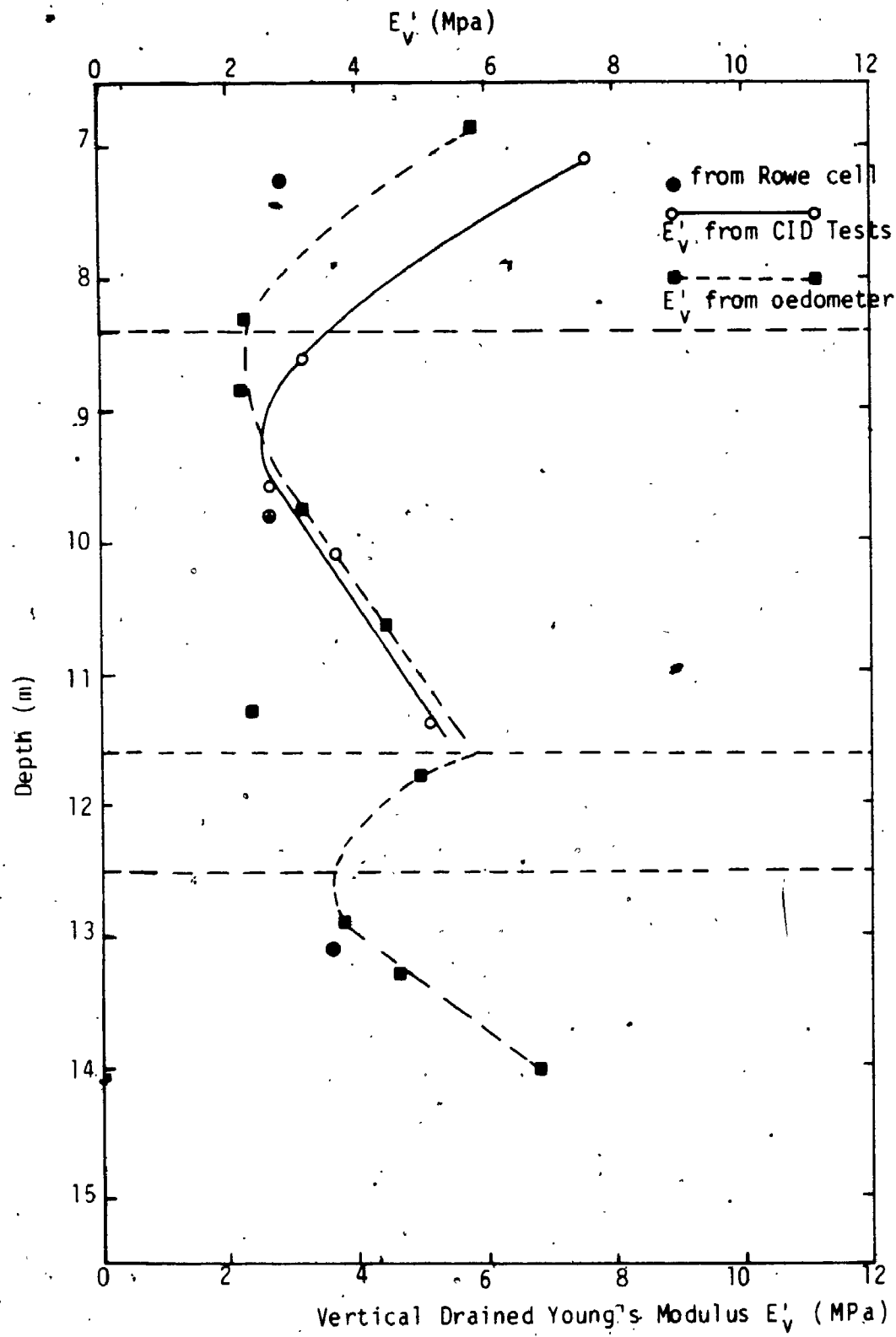
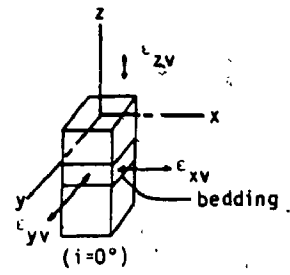
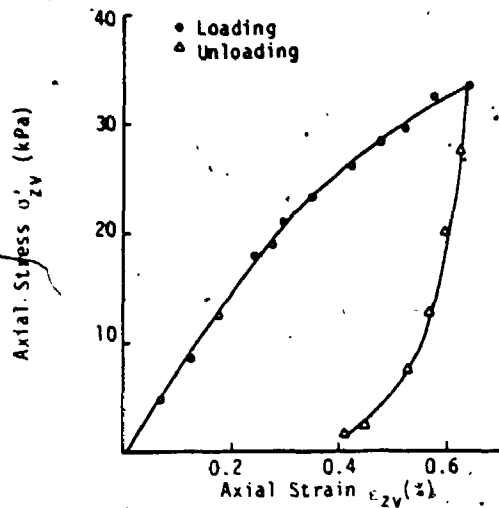
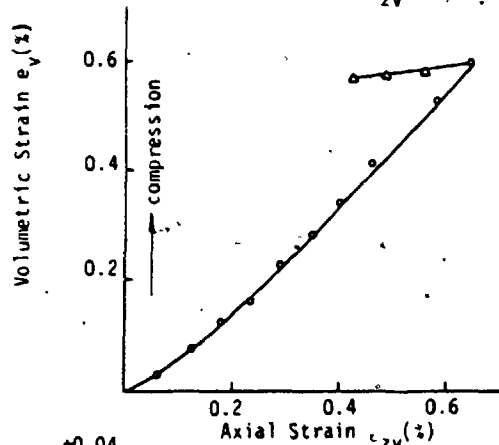


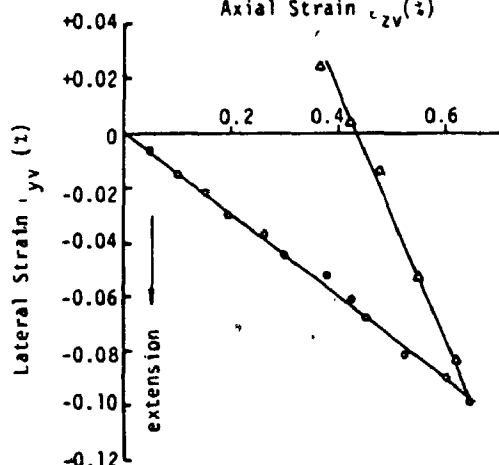
FIGURE 8.11 Variation of Drained Modulus E'_v With Depth



a) Axial Stress vs Axial Strain
 Array 2
 B.H. #2-52
 $\sigma'_c = 75 \text{ kPa}$
 σ_c
 Depth=10.15m
 Silty Clay

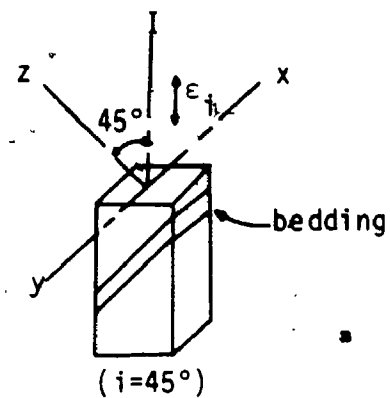
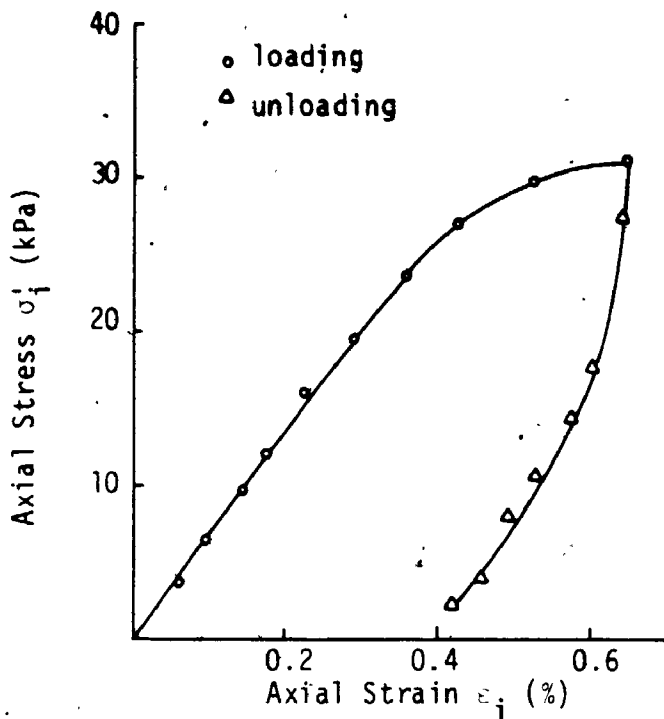


b) Volumetric Strain vs Axial Strain

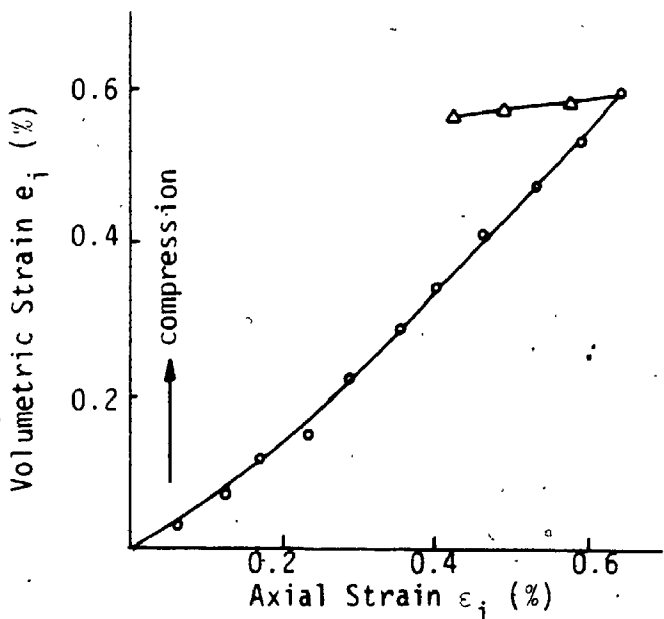


c) Lateral Strain vs Axial Strain

FIGURE 8.12 Results of CID Test on a Vertically Oriented Specimen of Silty Clay ($i=0^\circ$)

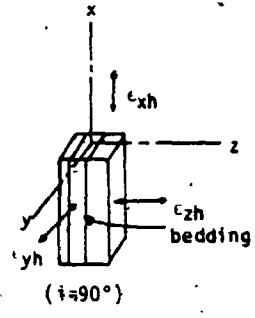
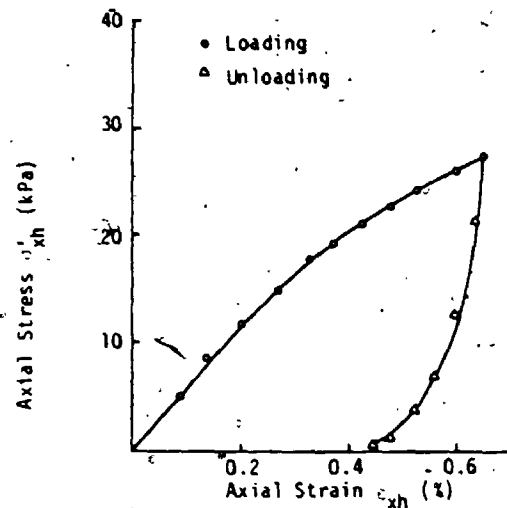


a) Axial Stress vs Axial Strain.

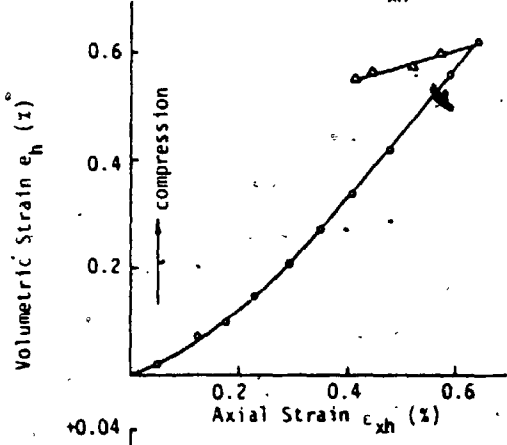


b) Volumetric Strain vs Axial Strain

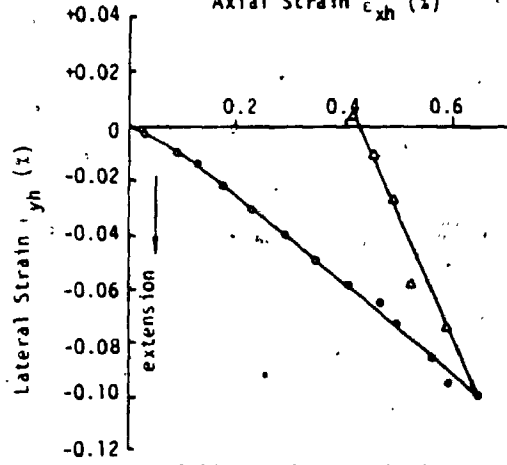
FIGURE 8.13 Results of CID Test on an Inclined Specimen ($i=45^\circ$) of Silty Clay



a) Axial Stress vs Axial Strain

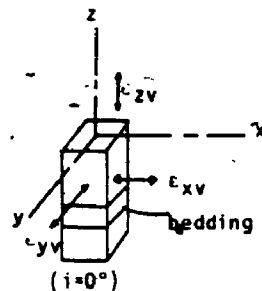
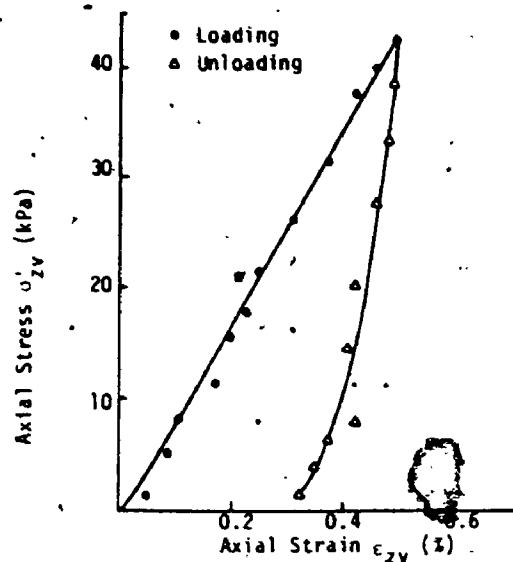


b) Volumetric Strain vs Axial Strain

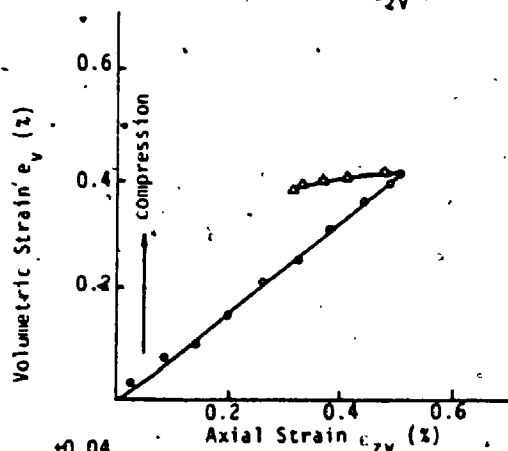


c) Lateral Strain vs Axial Strain

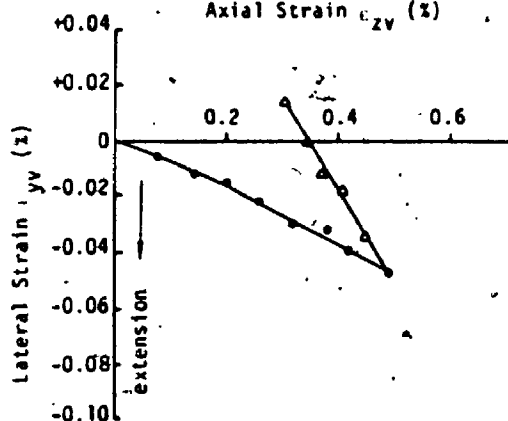
FIGURE 8.14 Results of CID Test on Horizontally Oriented Specimen of Silty Clay ($i=90^\circ$)



a) Axial Stress vs Axial Strain
 Array 2
 B.H. # 2-S1
 $\sigma'_c = 70$ kPa
 Depth=13.4 m
 Varved Clay

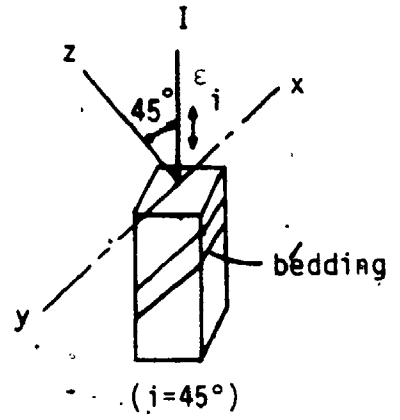
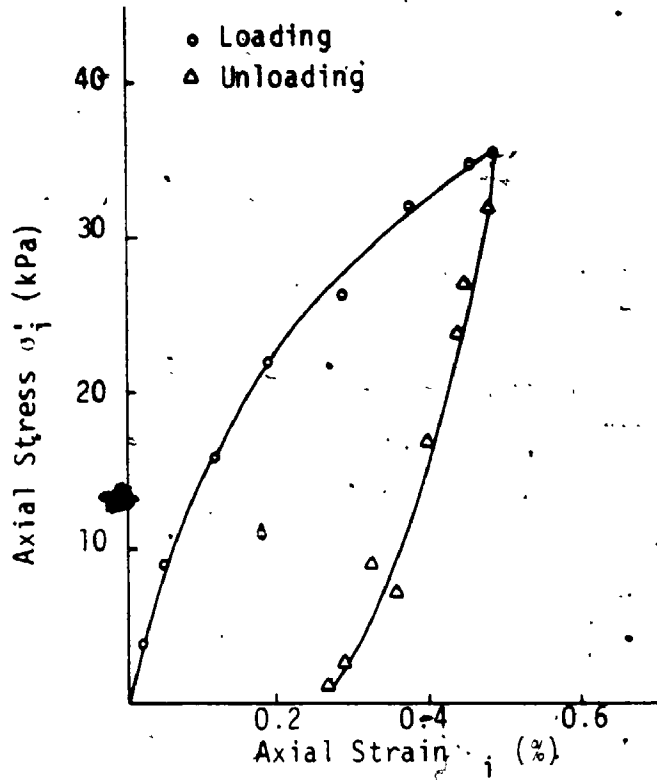


b) Volumetric Strain vs Axial Strain

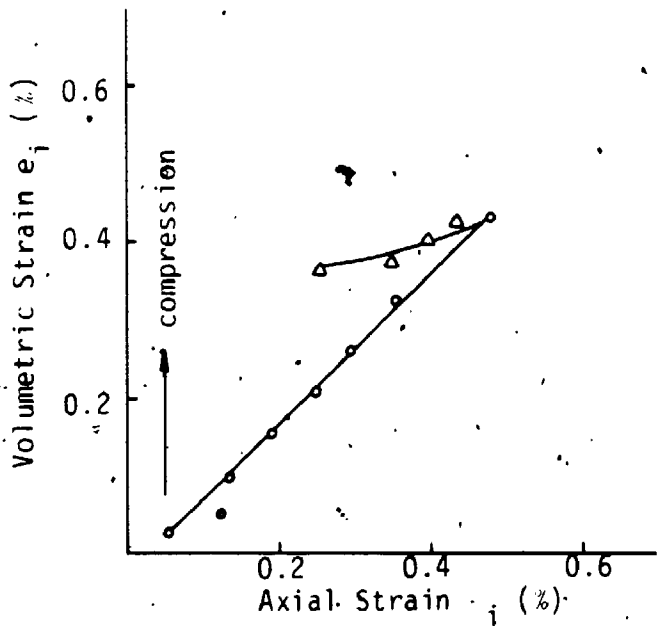


c) Lateral Strain vs Axial Strain

FIGURE 8.15 Results of CIDeTest on a Vertically Oriented Specimen of Varved Clay ($i=0^\circ$)

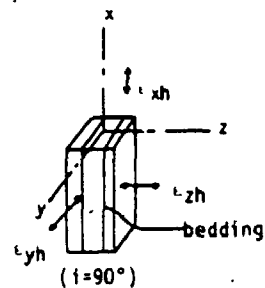
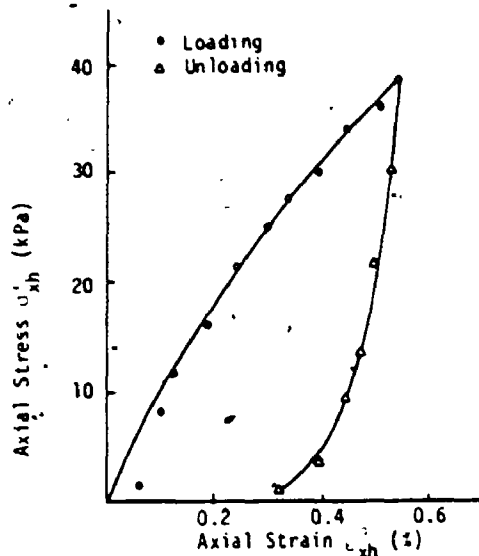


a) Axial Stress vs Axial Strain

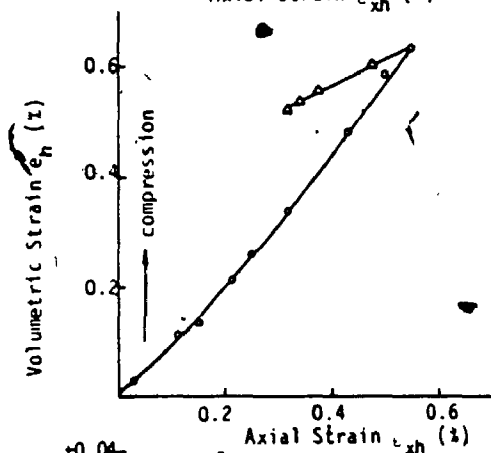


b) Volumetric Strain vs Axial Strain

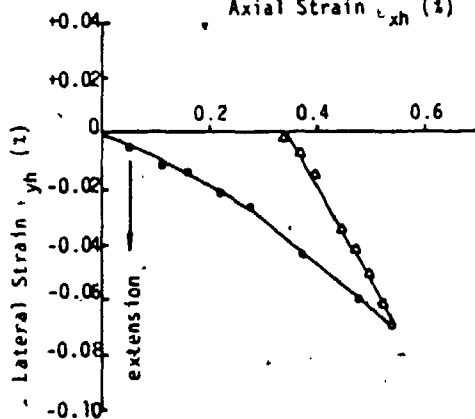
FIGURE 8.16 Results of CID Test on an Inclined Specimen of Varved Clay ($i=45^\circ$)



a) Axial Stress vs Axial Strain



b) Volumetric Strain vs Axial Strain



c) Lateral Strain vs Axial Strain

FIGURE 8.17 Results of CID Test on a Horizontally Oriented Sample of Varved Clay ($i=90^\circ$)

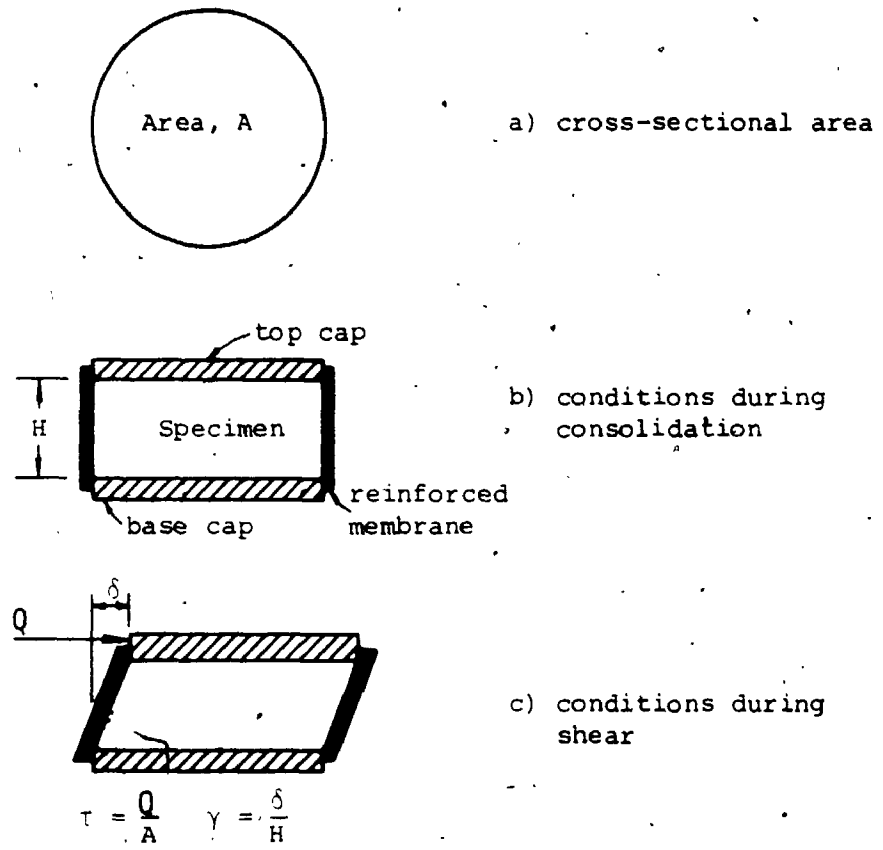


FIGURE 8.18 Simple Shear Test Apparatus

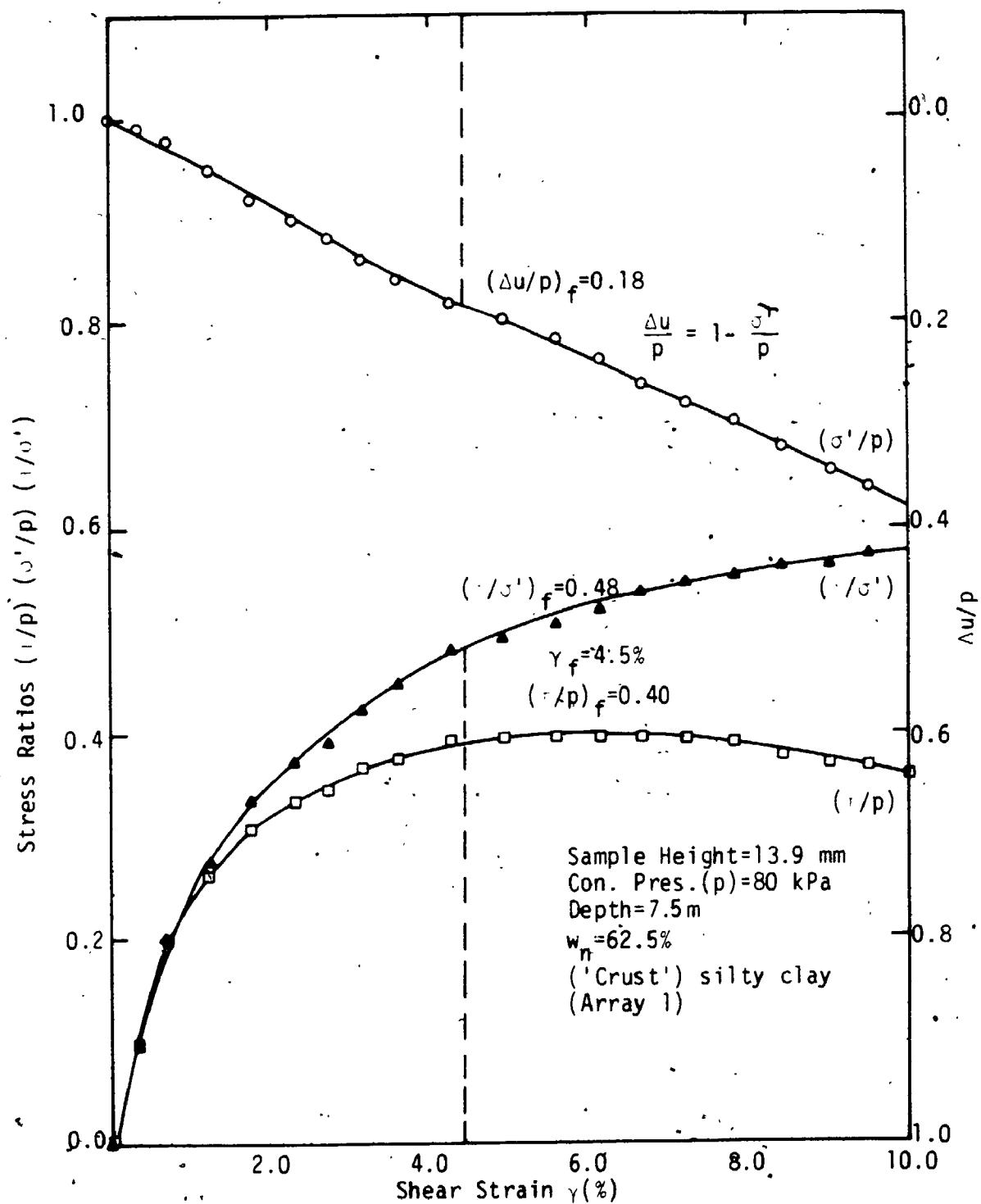


FIGURE 8.19 Result of Constant-Volume Simple Shear Test on Silty Clay

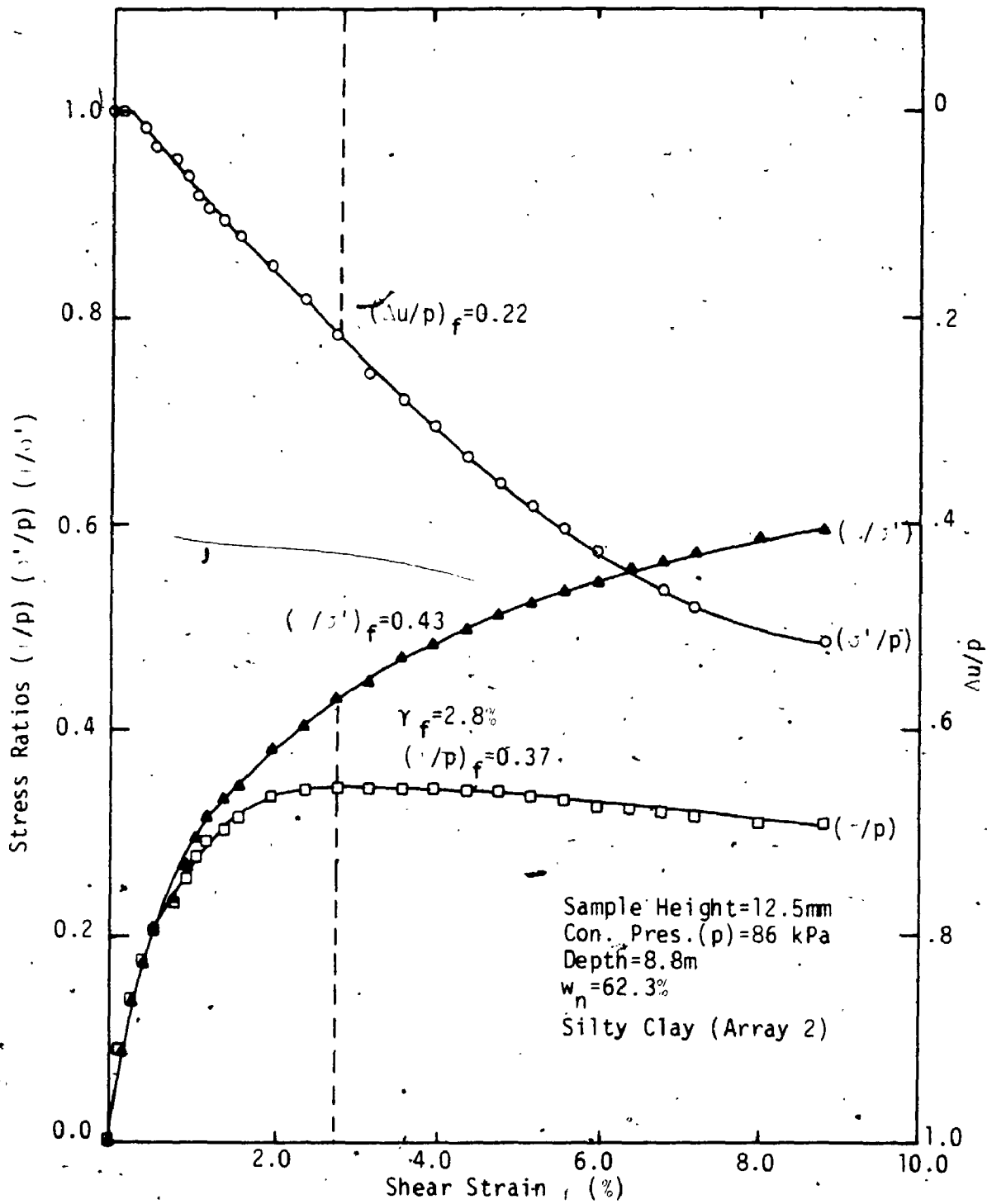


FIGURE 8.20 Result of Constant-Volume Simple Shear Test on Silty Clay

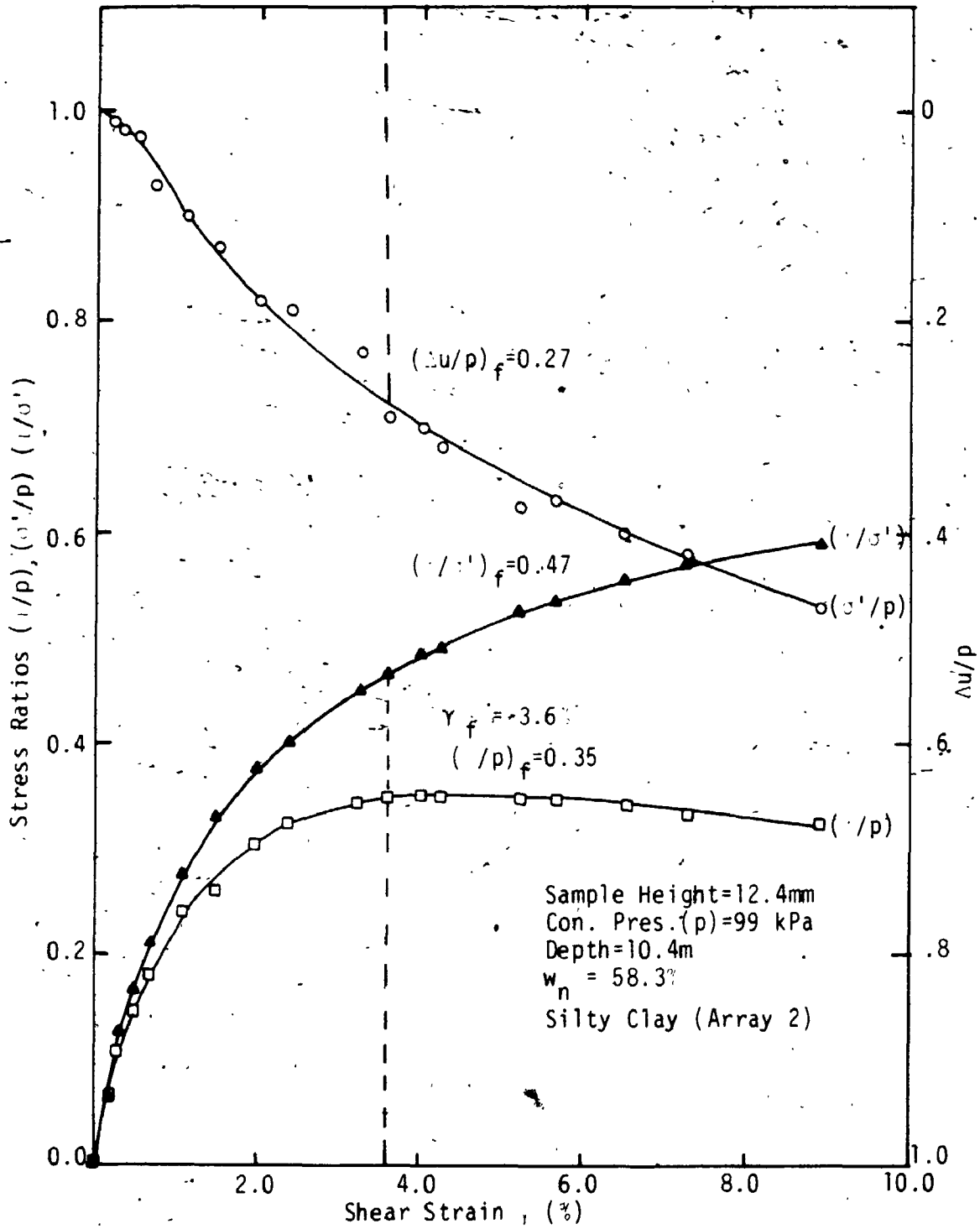


FIGURE 8.21 Result of Constant-Volume Simple Shear Test on Silty Clay

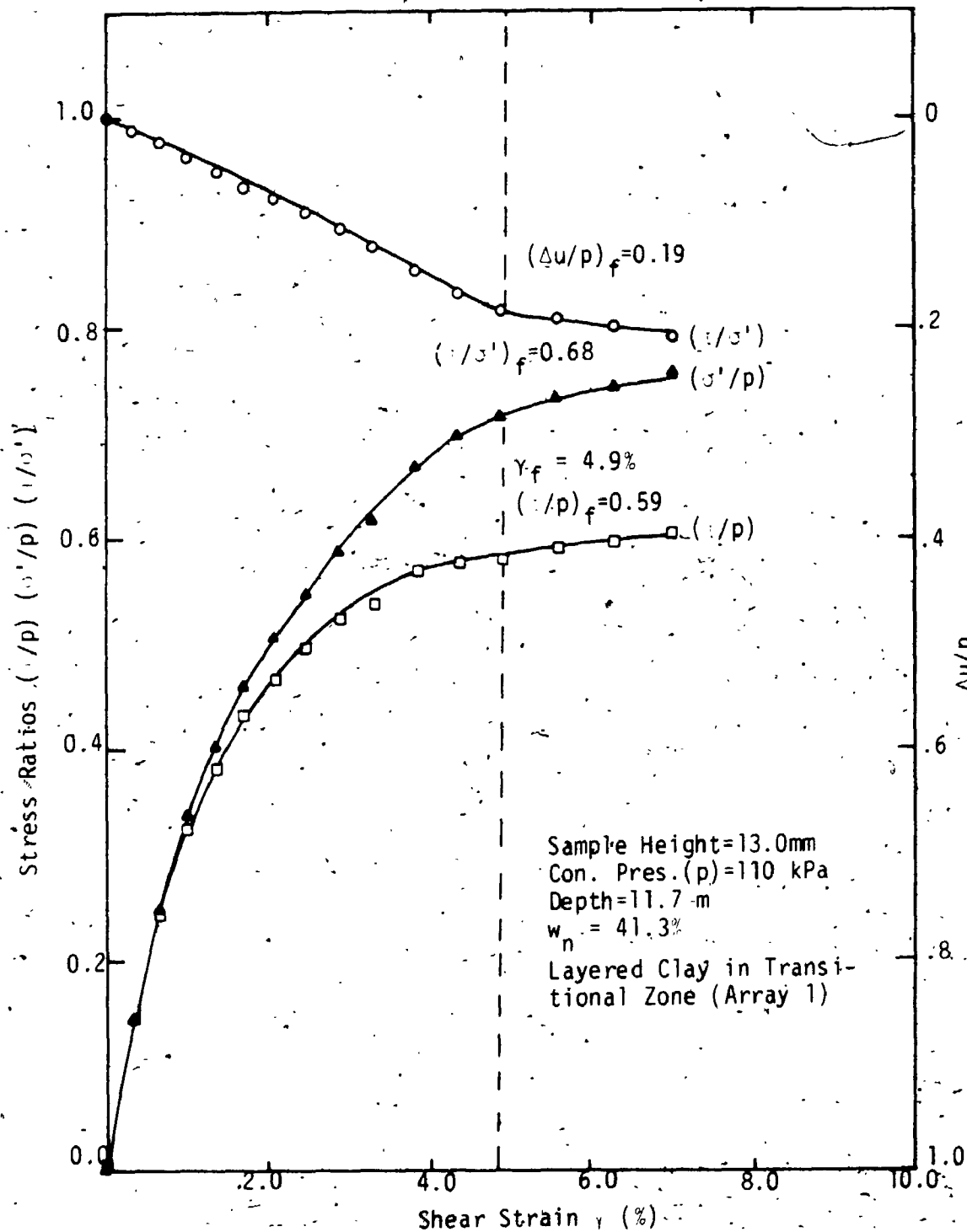


FIGURE 8.22 Result of Constant-Volume Simple Shear Test on Layered Clay in 'Transitional Zone'

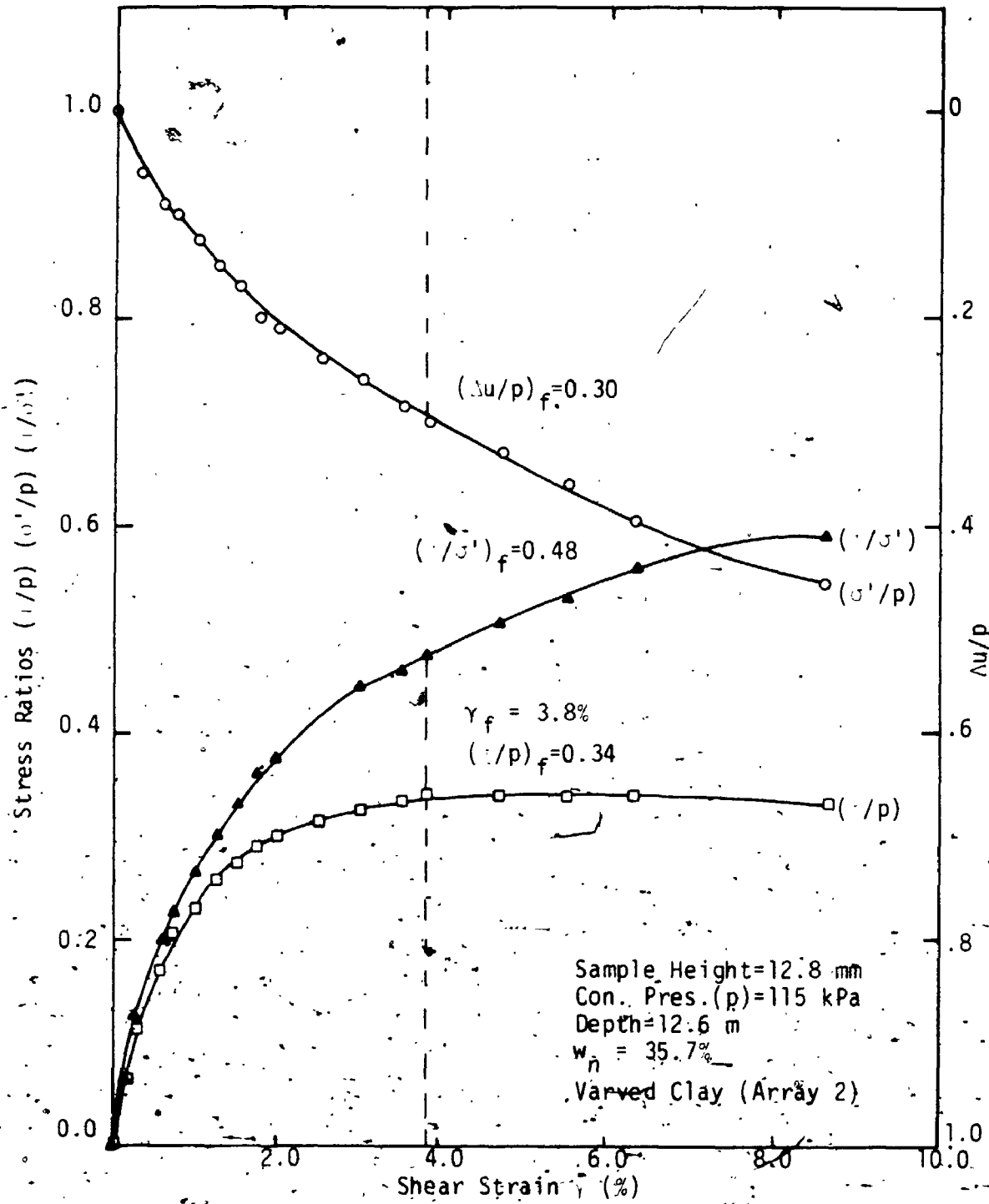


FIGURE 8.23 Result of Constant-Volume Simple Shear Test on Varved Clay

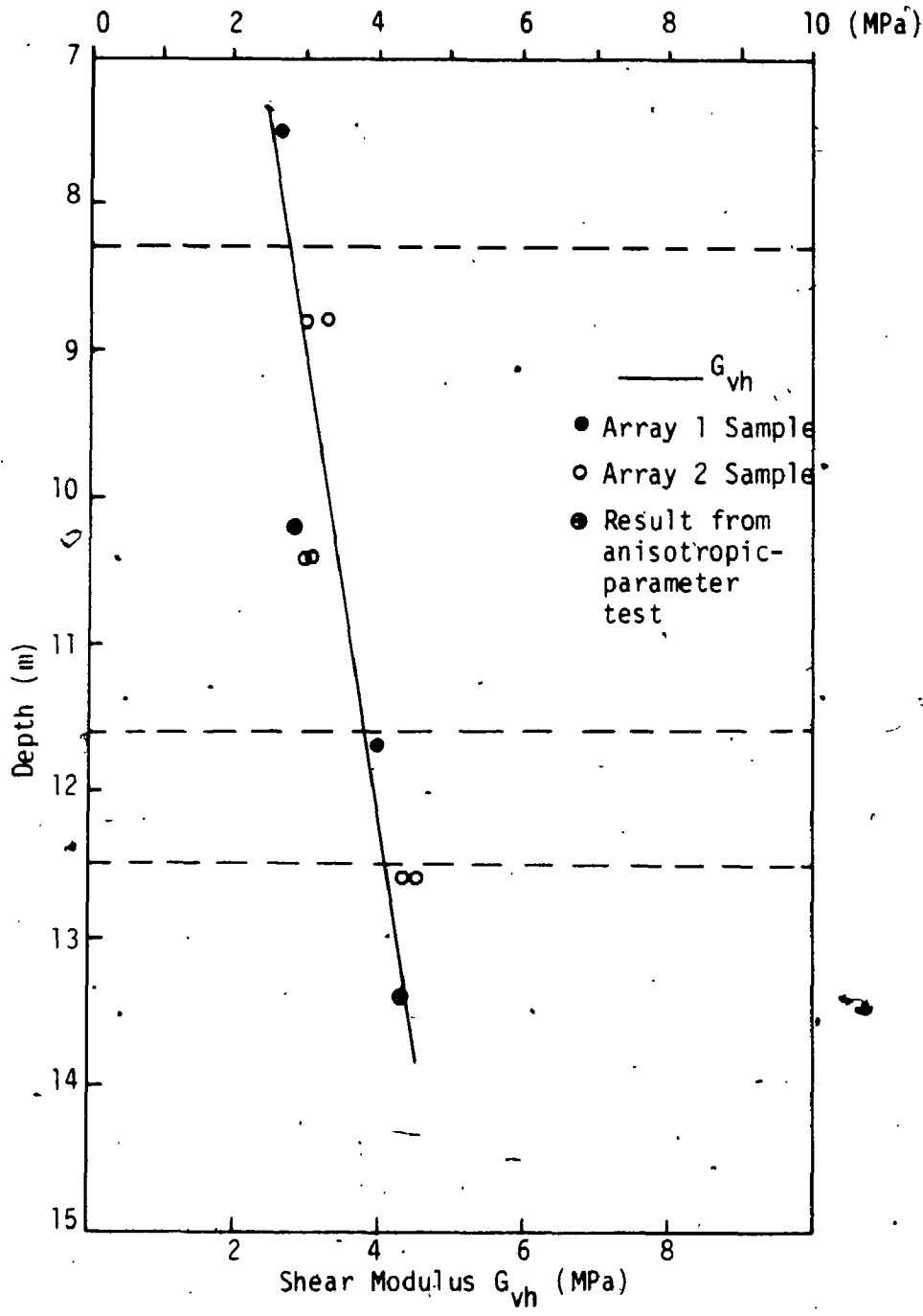


FIGURE 8.24 Variation of G_{vh} with Depth

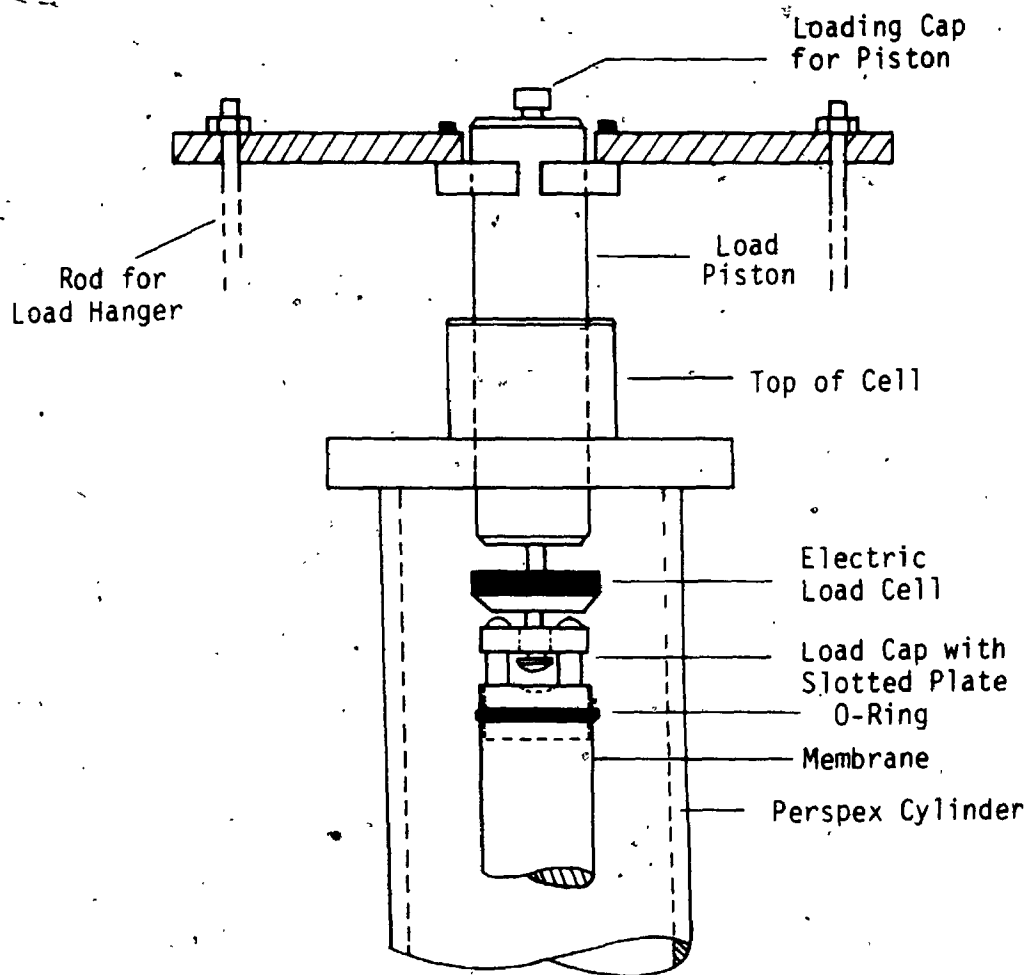


FIGURE 8.25 Sketch of K_0 -Cell Set Up for Extension Test

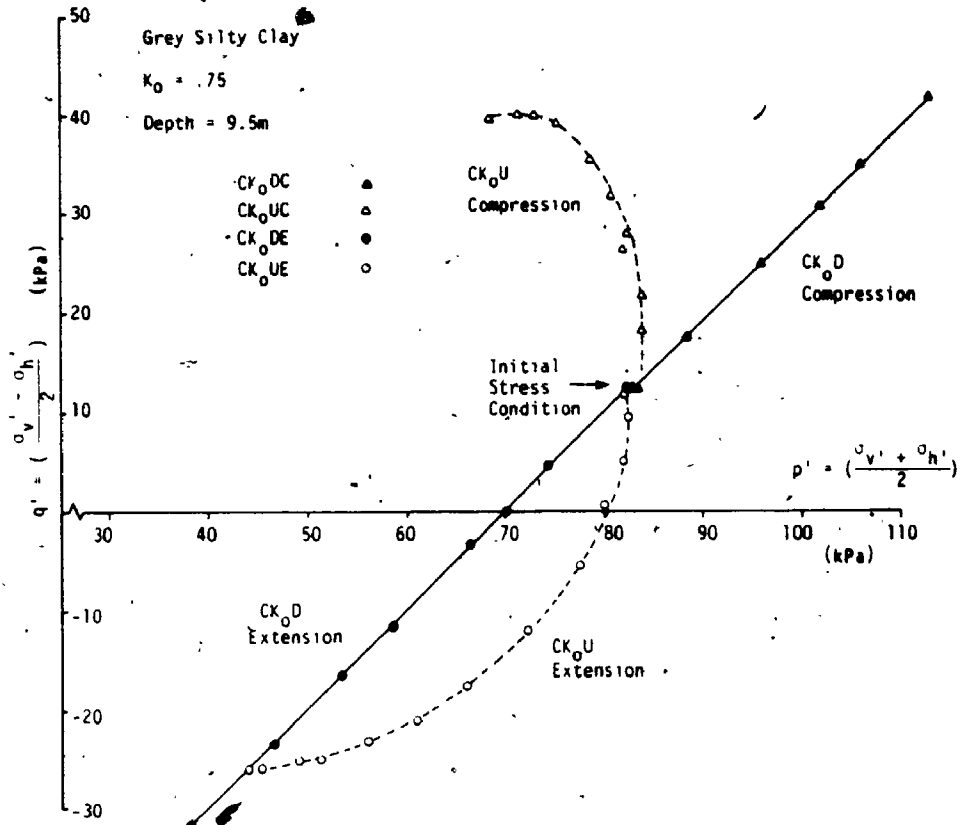


FIGURE 8.26 Stress Paths on p' - q' Space for Four Modes of Triaxial Tests on Silty Clay

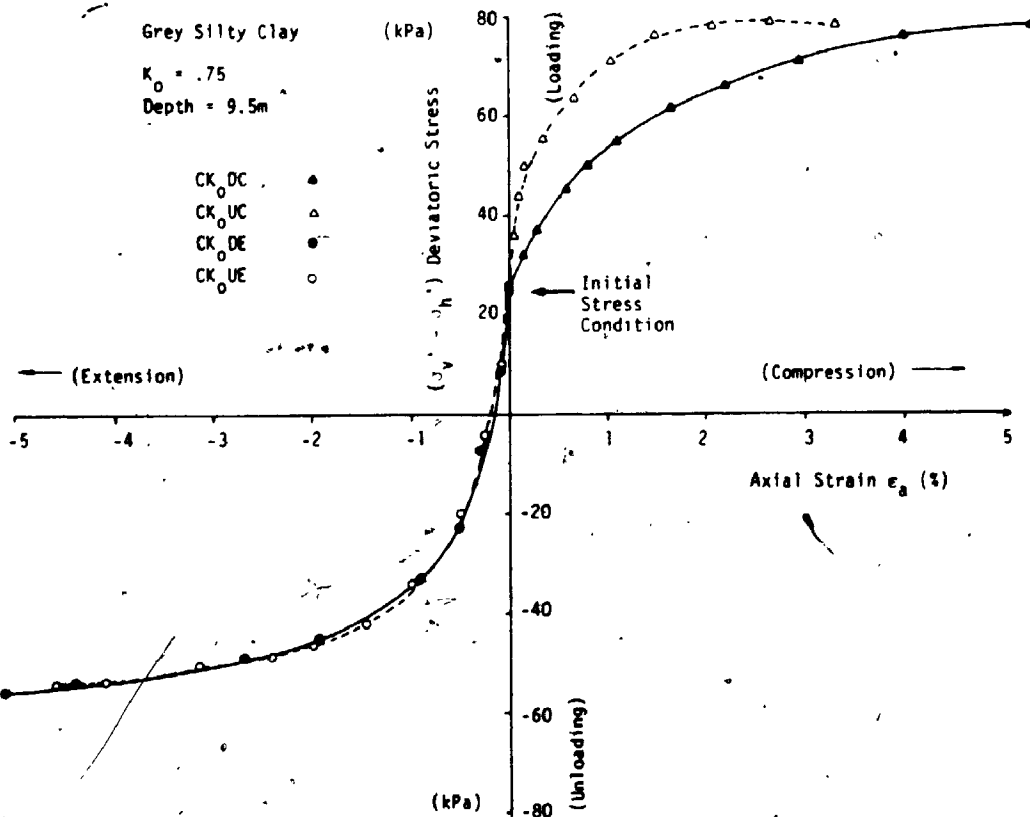


FIGURE 8.27 Stress-Strain Relationships for Four Modes of Triaxial Tests on Silty clay

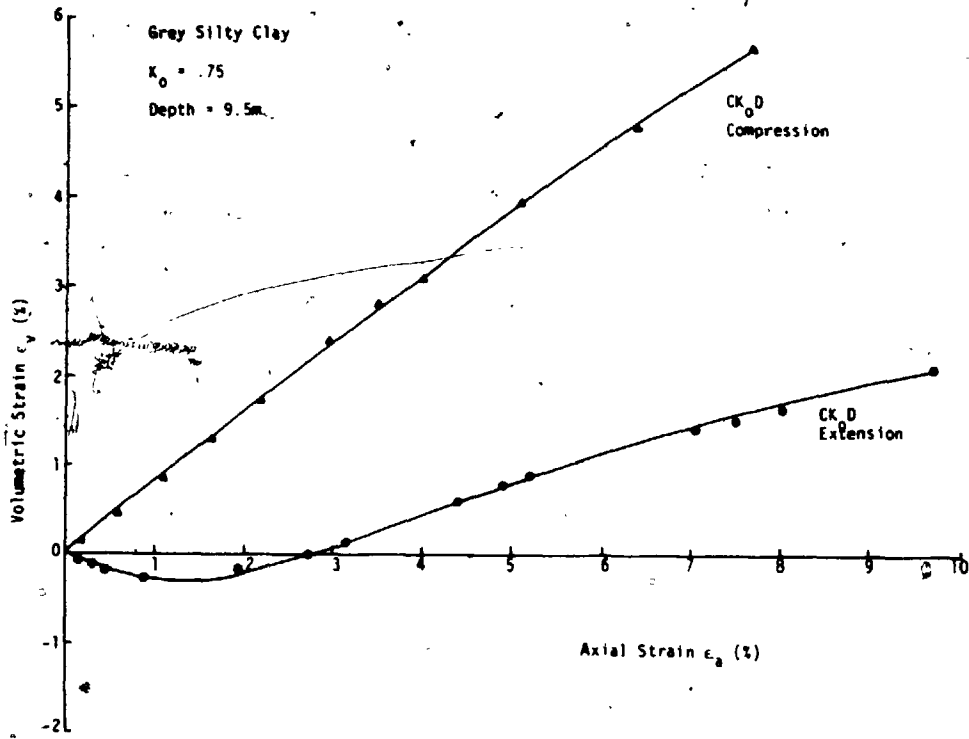


FIGURE 8.28 Volumetric Strain-Axial Strain Relationships from CK₀D Compression and Extension Tests on Silty Clay

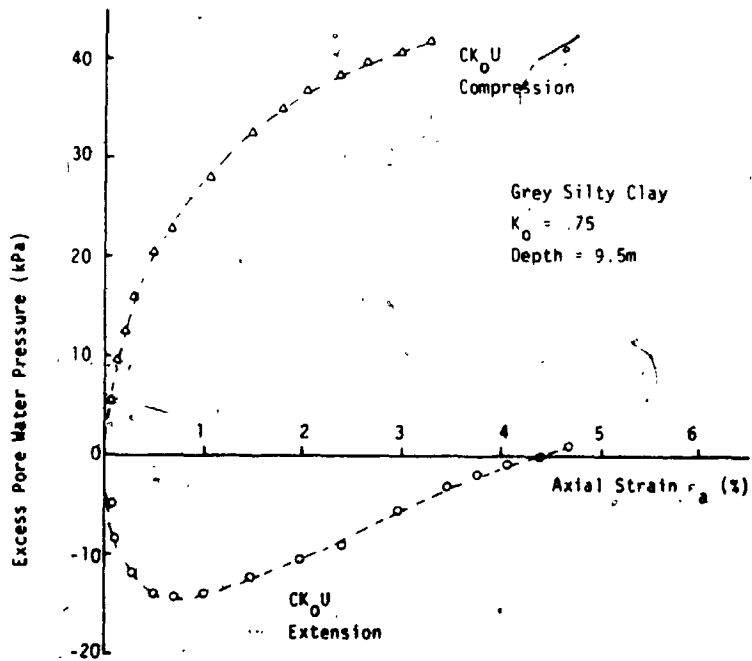


FIGURE 8.29 Excess Pore Water Pressure-Strain Relationships from CK₀U Compression and Extension Tests on Silty Clay

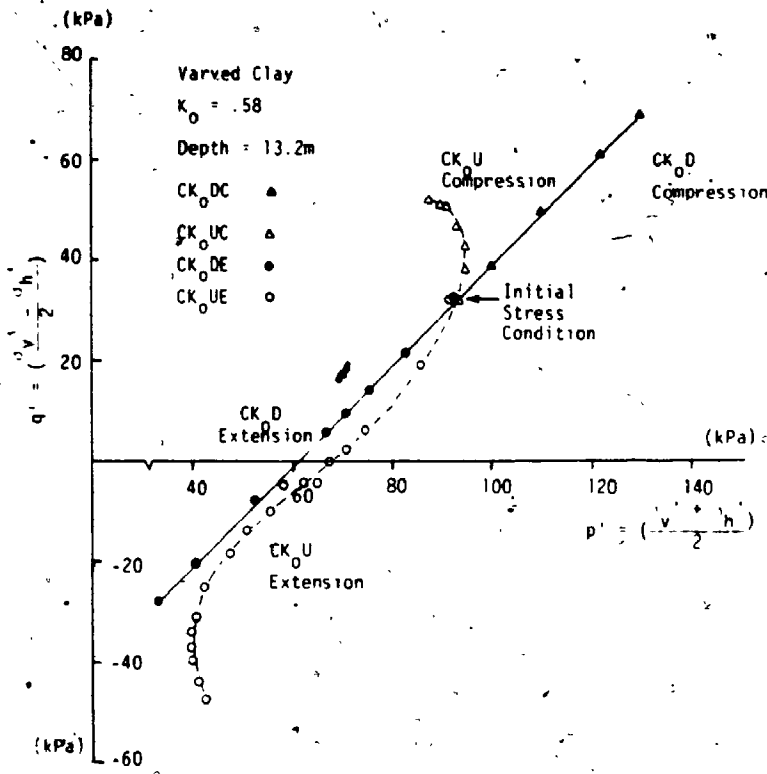


FIGURE 8.30 Stress Paths on p' - q' Space for Four Modes of Triaxial Tests on Varved Clay

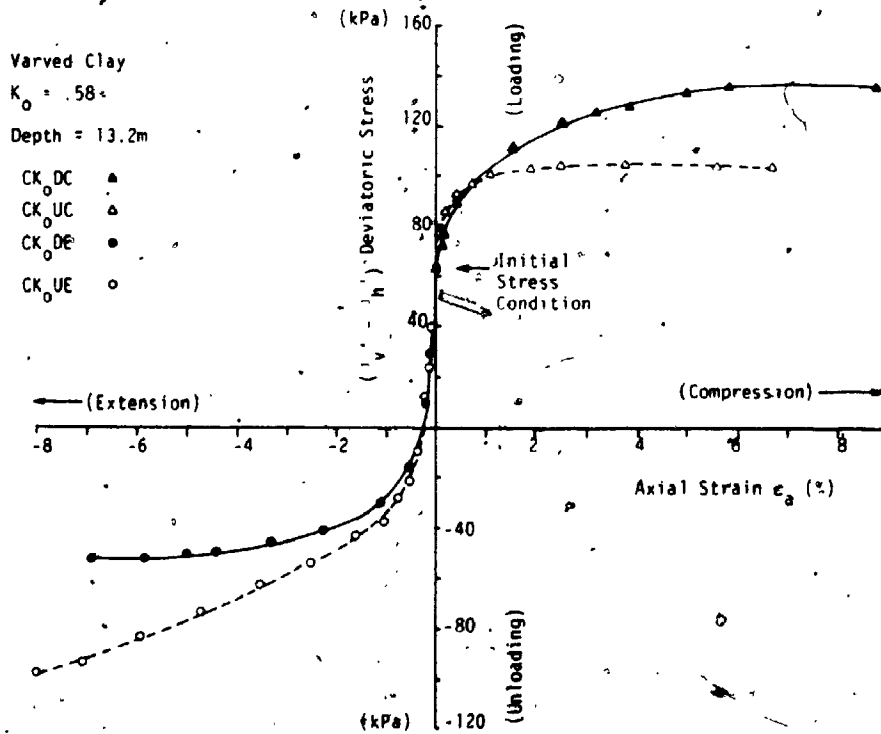


FIGURE 8.31 Stress-Strain Relationships for Four Modes of Triaxial Tests on Varved Clay

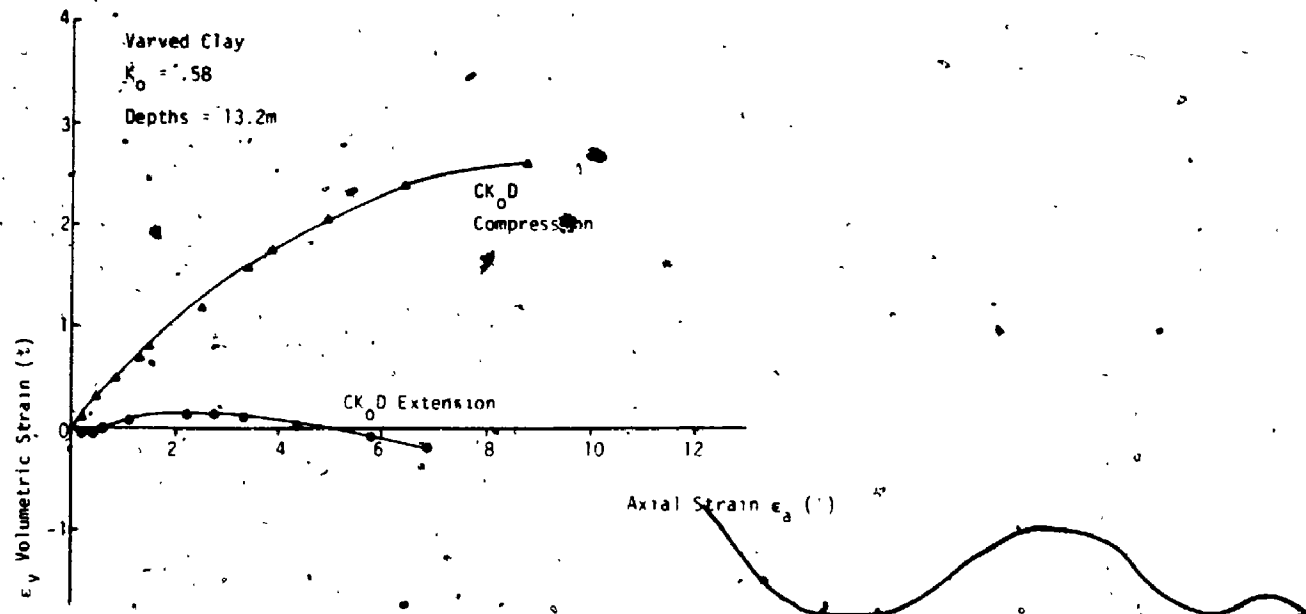


FIGURE 8.32 Volumetric Strain-Axial Strain Relationships from CK₀D Compression and Extension Tests on Varved Clay

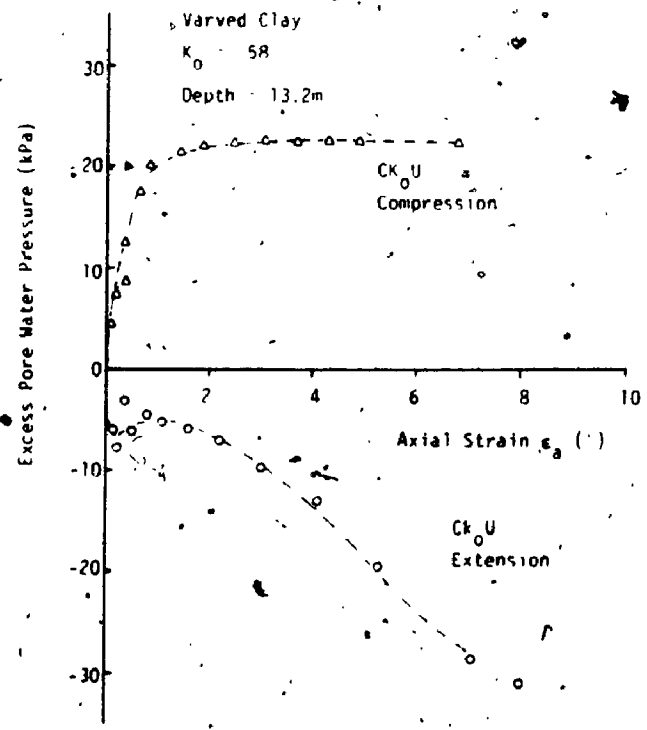


FIGURE 8.33 Excess Pore Water Pressure-Strain Relationships from CK_U Compression and Extension Tests on Varved Clay

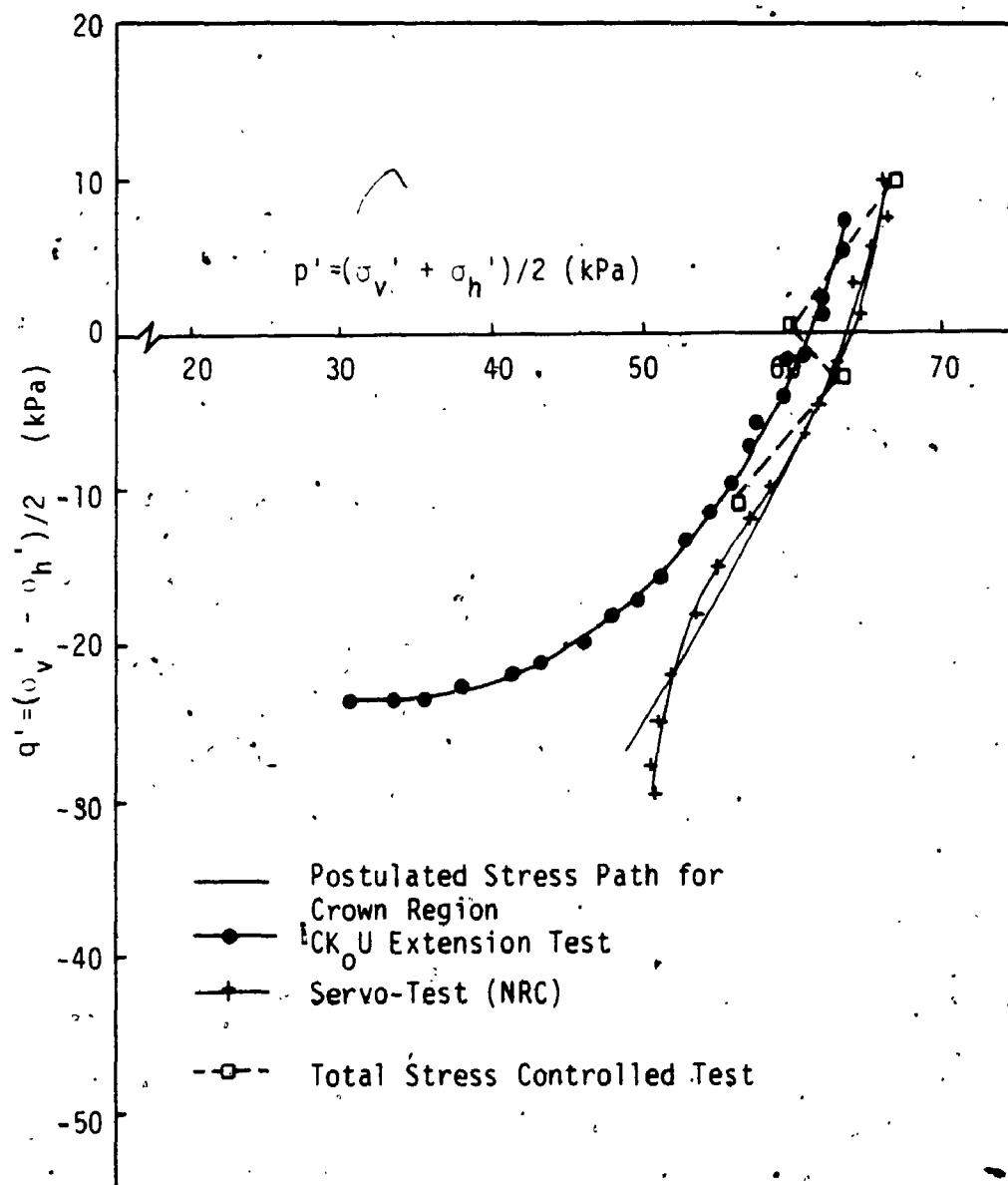


FIGURE 8.34 Stress Path Tests in p' - q' Space for the Crown Region.

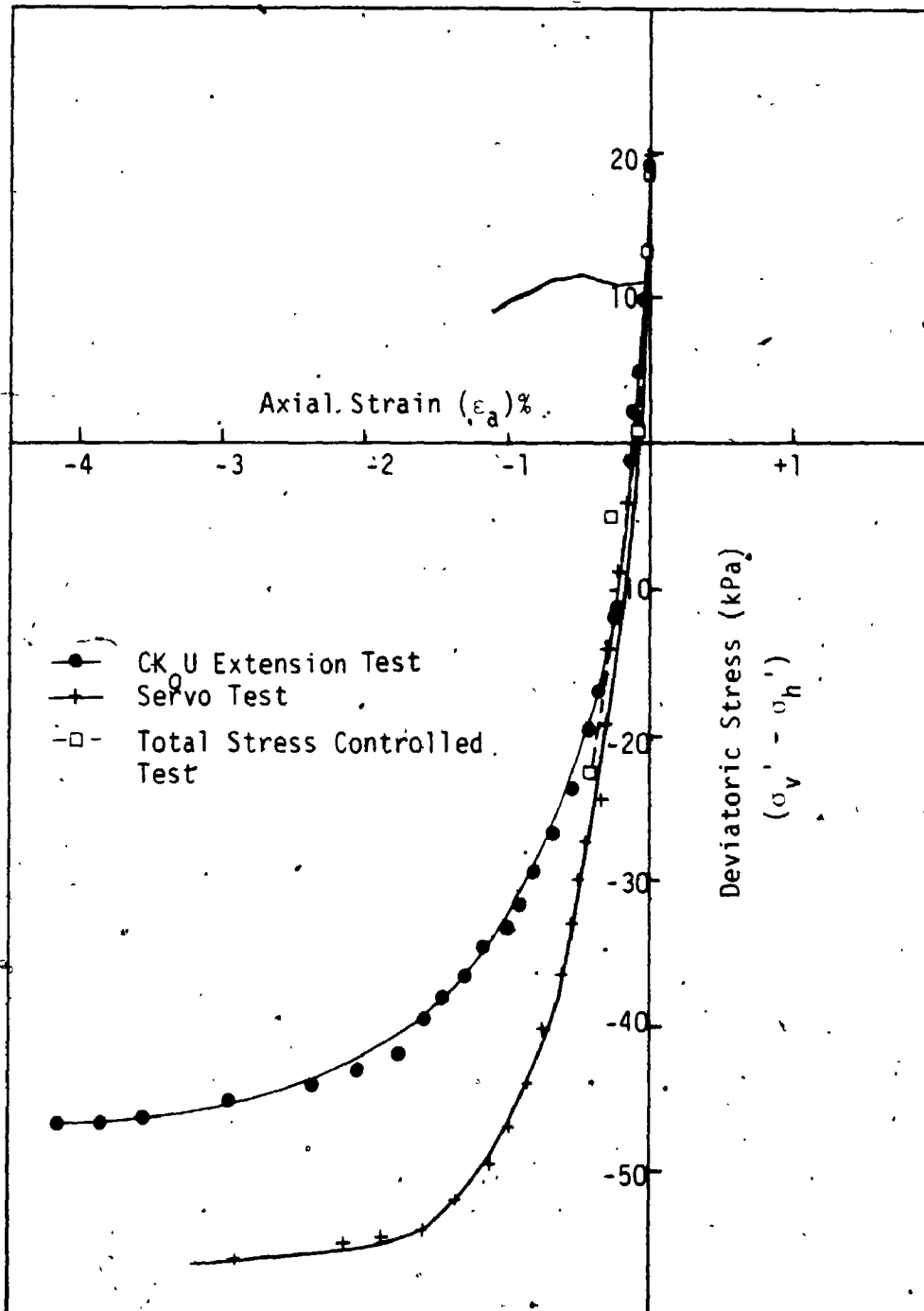


FIGURE 8.35 Stress-Strain Relationships from Triaxial Tests for the Crown Region

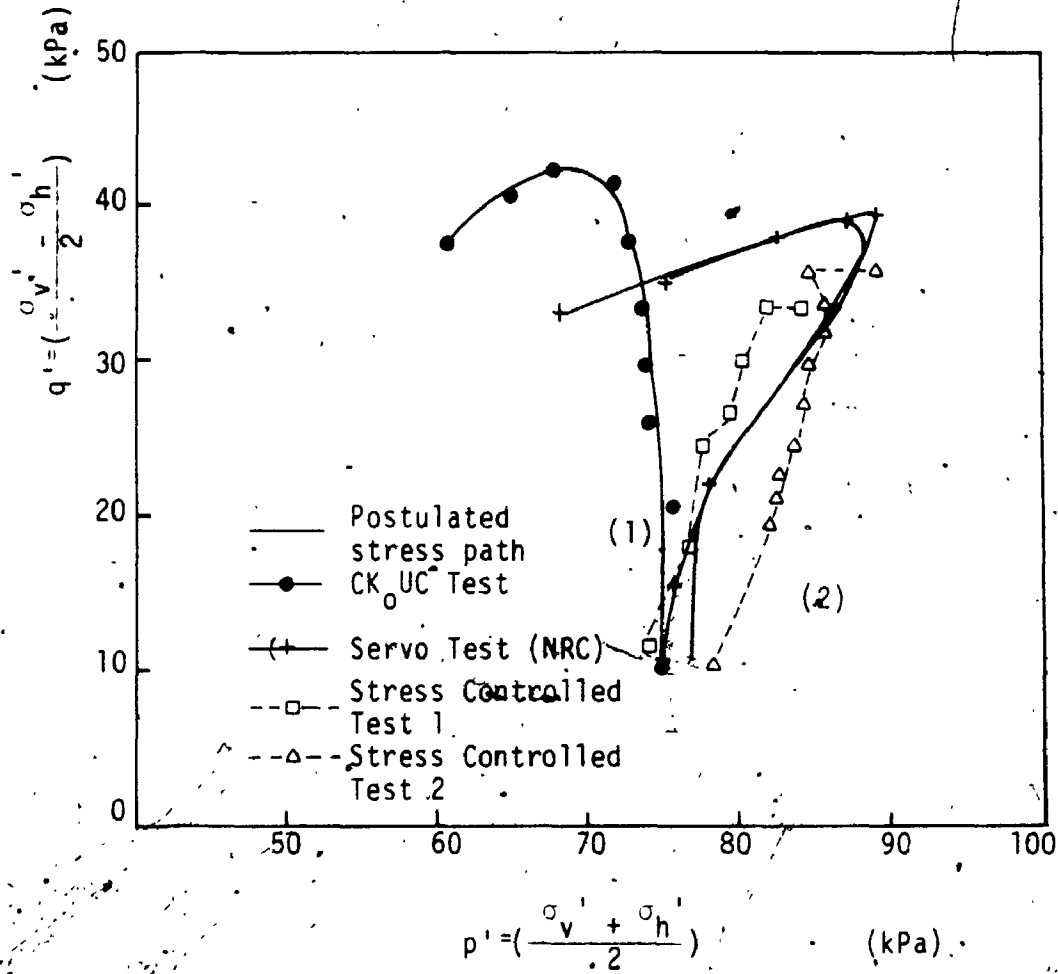


FIGURE 8.36 Stress Path Tests in $p'-q'$ Space for the Springline Region

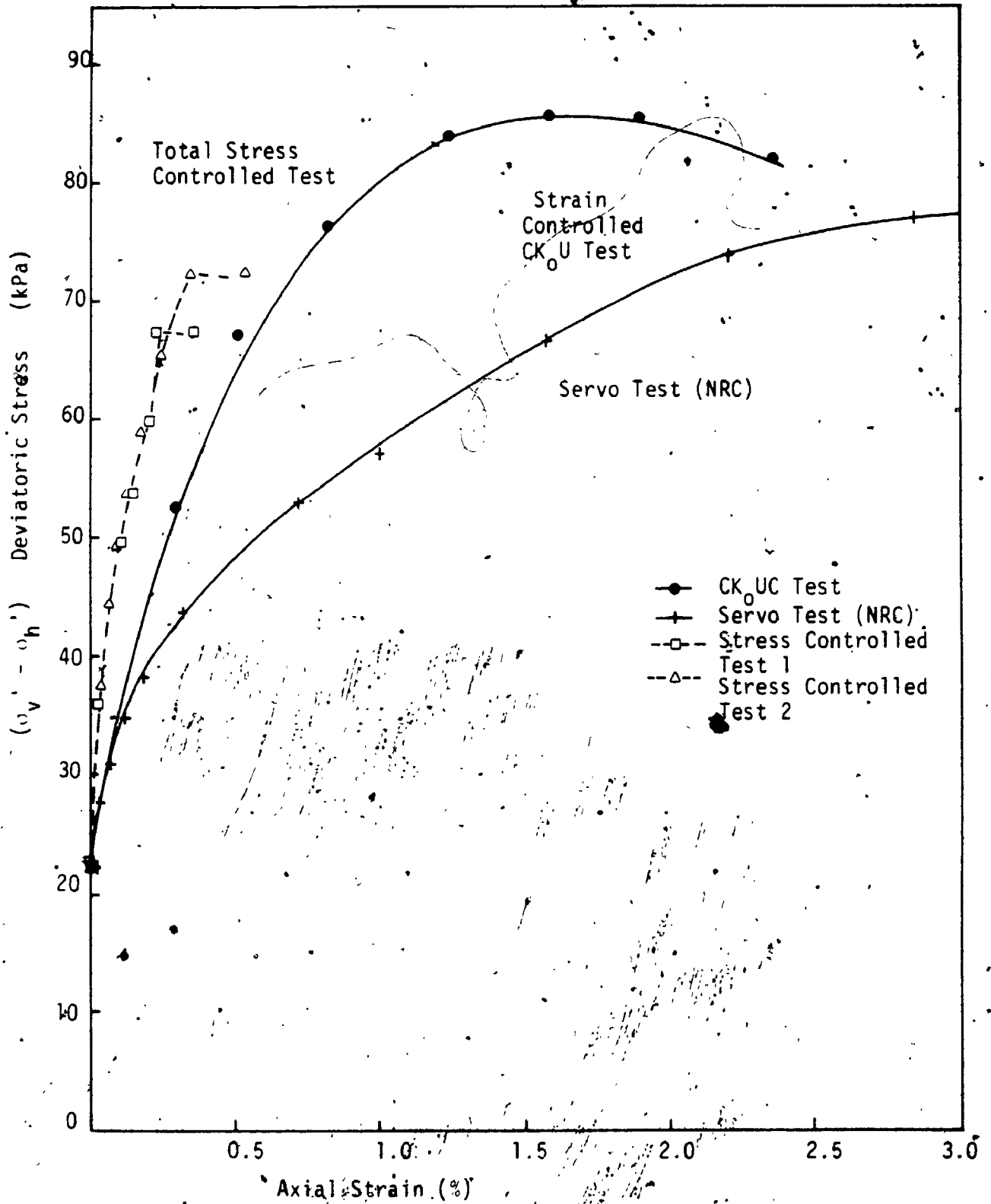


FIGURE 8.37 Stress-Strain Relationships from Triaxial Tests for the Springline Region

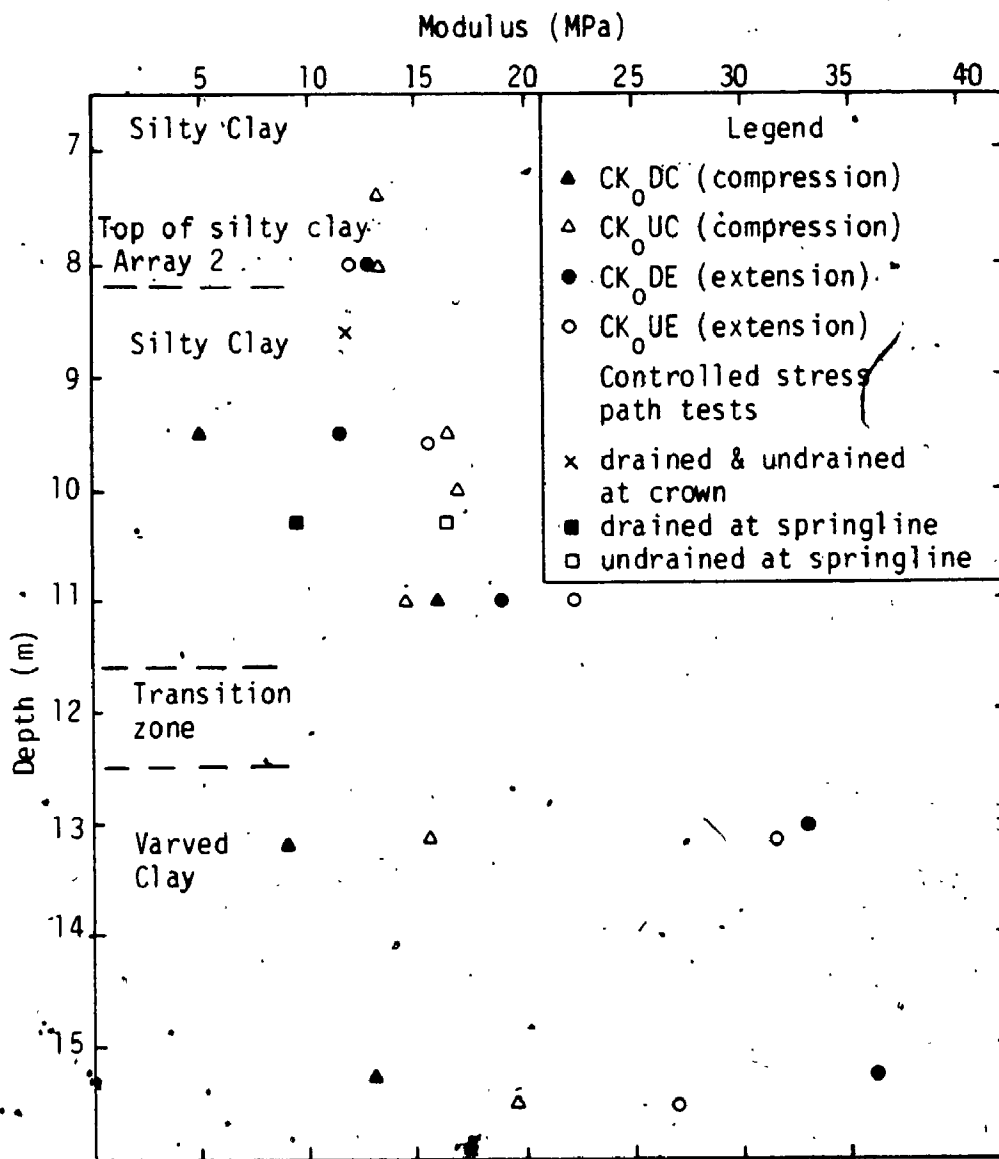


FIGURE 8.38 Modulus Values Deduced from K₀ Consolidated Tests

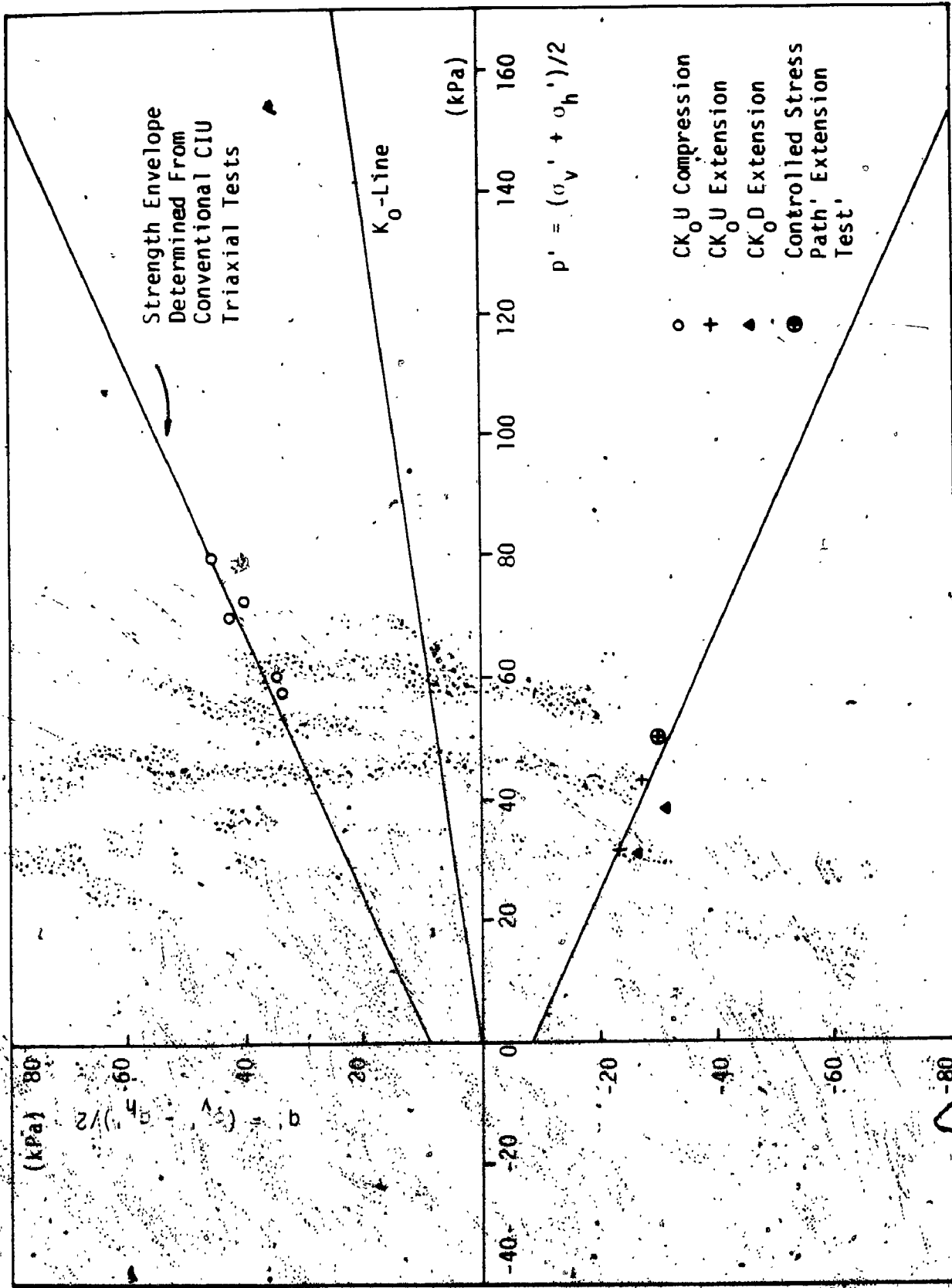


FIGURE 8.39 p'-q Plot of Shear Strength from Anisotropic Consolidated Triaxial Tests and Controlled Stress Path Test (Silty Clay).

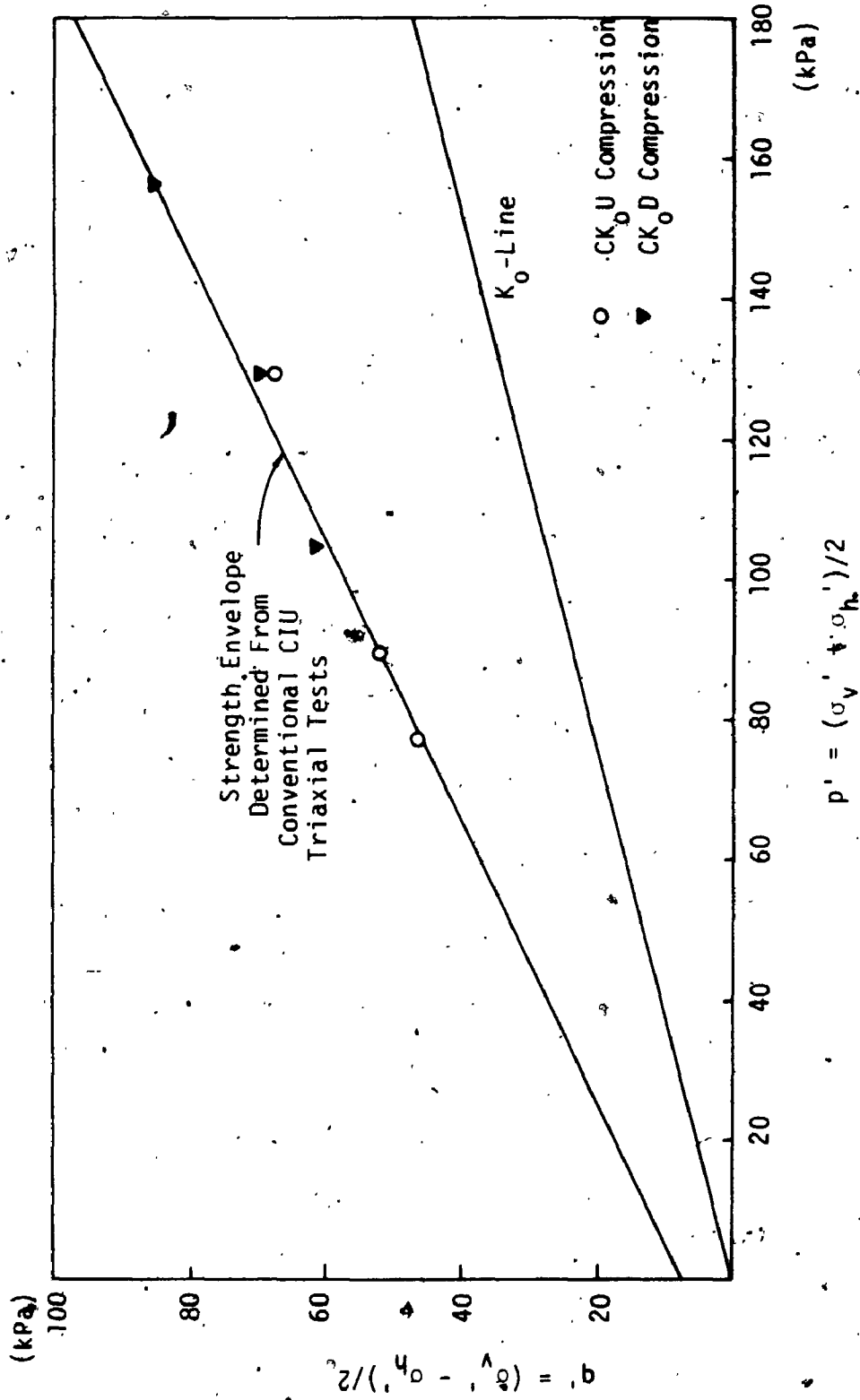


FIGURE 8.40 p' - q' Plot of Shear Strength from Anisotropic Consolidated Triaxial Tests (Varved Clay).

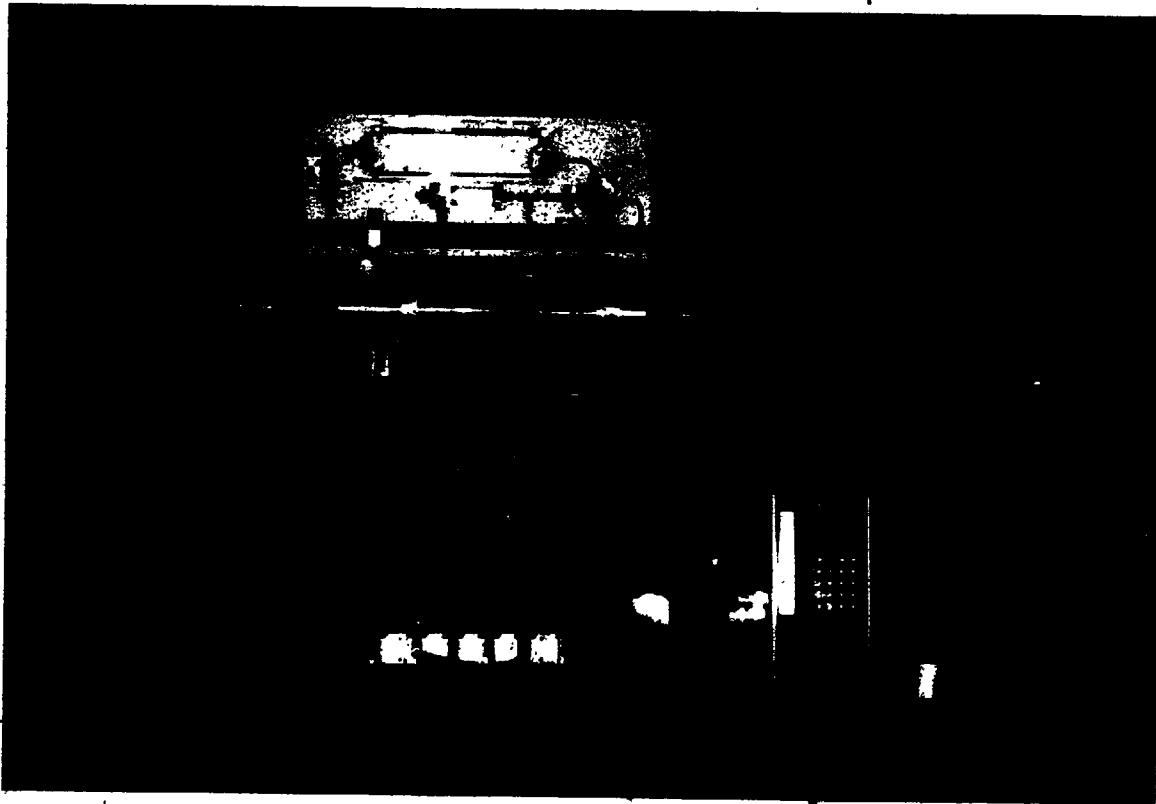


FIGURE 8.41a Anisotropic Parameter Apparatus and Data-Acquisition System.

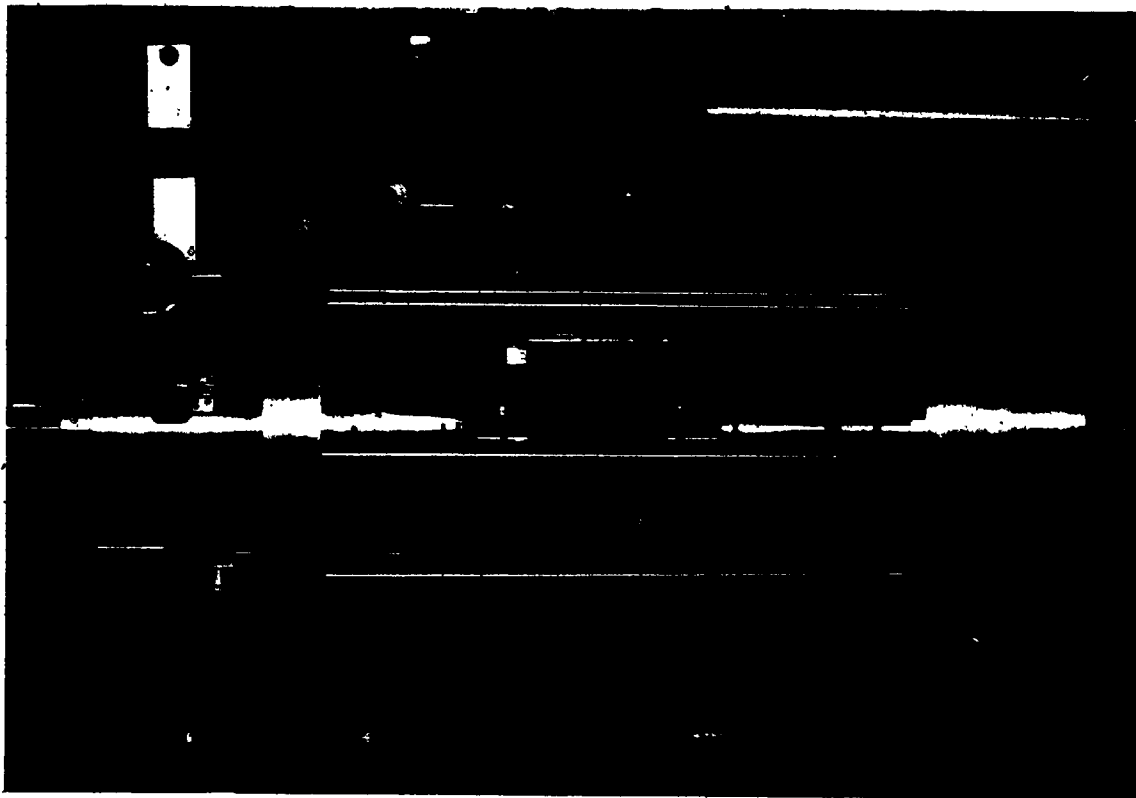


FIGURE 8.41b

Test Sample and Floating Transducer Units Within Triaxial Cell

CHAPTER 9

TUNNELLING PROCEDURE AND FIELD OBSERVATIONS

AT THE THUNDER BAY TUNNEL

The case history of the Thunder Bay Tunnel is presented in this chapter. This tunnel is 3.3 km in length, with a finished external diameter of 2.38 m. It was constructed in soft to firm silty clay by a 2.47 m diameter tunnel boring machine. The liner consisted of a precast, unbolted, segmental concrete lining assembled in the shield tailpiece. Two sections of the tunnel were instrumented and details of the instrumentation and monitoring program of the project have been presented by Belshaw and Palmer (1978) and Palmer and Belshaw (1980). The plans of the instrumentations at Array 1 and Array 2 are shown respectively in Figures 9.1 and 9.2.

9.1 TUNNELLING SYSTEM AND PROCEDURE

The tunnelling system employed a full face tunnel boring machine (TBM) together with an unbolted precast segmented concrete lining.

9.1.1 Tunnelling Machine and Construction Cycle

The oblique views of the TBM are shown in Figures 9.19a and 9.19b; its dimensions are shown in Figure 9.3. The TBM was equipped with a rotary excavator that supported the face during excavation. The rate of intrusion of spoil through the machine head could be

controlled by the size of the opening at the face. The opening was kept small most of the time during operation. This design enabled the rate of advance of the machine to be consistent with the volume of soil excavated. Since the TBM was advanced essentially 'closed-face', the exposed tunnel face could be 'breasted' through the thrusting force provided by thrust jacks. The 'face pressure' created would consequently reduce ground loss. The tunnel at the instrumented sections was excavated in free-air.

A schematic section of the tunnelling operation is shown in Figure 9.4a. As the cutting head (1) is rotating, the excavated soil intrudes from the face directly onto a conveyor belt (8) and it is transported rearwards and is deposited into muck cars. The machine advances by thrusting on the last completed lining ring (12). Grout injection into the tail void* is applied simultaneously as the lining (12) leaves the tailpiece. While excavation is proceeding, the lining segments are removed from the segment carriage (6) by a small crane (5). When the advance and grouting are completed, the thrust jacks (3) are retracted to allow the assembly of another lining ring by an erector arm (4). Once the liner is completed, axial thrust is re-applied. The machine is ready for the next advance and this completes one excavation cycle.

* The tail void or tailpiece void is the space between the outer diameter of the shield and the lining. The clearance at the crown is equal to $2\Delta+6$ with reference to Chapter 3.

9.1.2 Typical Observations During Tunnelling Operation

An engineer was stationed in the machine as an observer of the tunnelling operation during the construction at Arrays 1 and 2. Typical observations of the excavation cycles at Array 2 beneath the locations of settlement pins 2 and 5 are shown in Table 9.1. As inferred from the 'level bubble', the machine was slightly pitched and rotated during each 'shove' and it also tended to lean sideways. During mining of the tunnel beneath pin 5 (i.e., the nominal centre of Array 2), some construction difficulties were encountered. Slight 'blind-shoving' and grout-leak were recorded.

9.1.3 Tunnel Lining

Detailed descriptions of the lining and sealant were presented by Morton et al. (1977) and the ACI committee 504 (1982). Figure 9.4b shows the liner segment and joint details. Each liner ring was composed of four unreinforced concrete segments which were 1 m in length and 110 mm in thickness. The segments were designed to crack along stress raisers and the liner system was made flexible in this way. Observation of lining performance indicated that the liners cracked as planned. Closure of the lining rings was also observed. The joints of the liner segment were factory coated with sealant and designed to be compressed during assembly to form a watertight seal. The sealant also protected the edges of the segment from damage during handling.

9.2 OBSERVED GROUND DEFORMATIONS

The tunnelling procedure at Array 1 and Array 2 was technically identical but Array 1 was only 60 m away from the first shaft. Since the crew members were not yet familiar with the construction technique, advance was slow and intermittent. As shown in Figure 9.5, the section of the tunnel where pin 27 (at Line 5) was located was completed in more than one workshift. By the time construction was started at Array 2, the crews had become experienced. Twenty-one metres of tunnel were completed in one 8-hour shift at this array. It is interesting to note for both arrays that the surface settlement developed as the shield advanced and stress changes due to excavation or jacking were taking place, but little movement occurred during work stoppage. The same observations in soft clay have also been noted by Peck (1969).

9.2.1 Undrained and Drained Settlements

In the development of ground displacements, two phases of settlements may be distinguished. The first phase, or short term settlement, is caused by changes in ground geometry and stress conditions associated with the tunnelling process itself. The second phase, or long term settlement, is associated with volume changes in the ground due to soil consolidation or creep and seepage flow into the tunnel. Though the soil movement due to tunnelling is a kinematic and time-dependent process, the distinction between 'undrained' and 'drained' settlement behaviours is generally of engineering interest. Since these terms

are not well defined in tunnelling, it becomes necessary that the terminology be explained before proceeding with further discussion.

It may be seen from Figures 9.6 and 9.7 that the rapid rate of vertical soil displacement decreased abruptly when the tunnel face was at 10 m to 15 m or at $\lambda_1/a \doteq 6$ from the instrumented section (i.e., $\lambda/a = 8$ to 12, or $\lambda_1/a = 4$ to 8, where λ = distance of the instrumented section to the tunnel face, λ_1 = distance of the instrumented section to rear of the shield tail). At this stage, the lined tunnel section attained plane strain condition with the crown coming into contact with the lining. The settlement measured was termed the immediate or undrained settlement.

The observed settlement which was taken after the entire length of the instrumented array had been completed may be referred to as the 'settlement at the end of construction (of array)'. This settlement was only slightly larger than the undrained settlement and the measurement data were taken within a week after the face had passed. Some dissipation of induced pore pressure might have occurred but no significant volume change had taken place.

The long term settlement was the total accumulated settlement that has occurred when soil consolidation was completed. At this stage, all the excess pore pressure would have dissipated and the volumetric changes in soil would have been completed. The soil mass also reached a final drained equilibrium.

The surface settlements observed at different stages at Array 1 and Array 2 are summarized in Tables 9.2a and 9.2b.

9.2.2 Surface Settlements

The "end of construction" surface settlements along the alignment of the tunnel at the two arrays are shown in Figure 9.8. At Array 1, the centreline settlements varied from 51 mm to 64 mm except for the measurement at pin 40 where 76 mm was recorded. The anomaly was caused by a combination of steering problems with the machine and a blockage in the grouting system (Belshaw and Palmer, 1978). The average of the settlements* at Array 1 was 59 mm. At Array 2, the maximum centreline settlement was recorded at pin 5 and it was 54 mm measured three days after shield passage. The other measurements varied from 37 mm to 47 mm, with an average of 44 mm. The centreline settlements at Array 1 were generally larger than those observed at Array 2. In terms of the average of measurements at the end of construction, the magnitude of the settlement at Array 1 was 1.34 times the settlement at Array 2.

The long term behaviours of the two sites shown in Figure 9.9 were dramatically different. Whereas at Array 2, the settlement after almost one year showed only minor changes, the settlement at Array 1 after one year had almost doubled. Palmer and Belshaw (1979) attributed this anomalous behaviour to the result of poor workmanship during tunnel operation at Array 1. The clay in the vicinity of the excavated

* The abnormally large settlement of 76 mm at Array 1 has been excluded in the calculation of average settlement.

circumference was significantly remoulded and settlement occurred with time due to soil reconsolidation. A fill of about 1 m was later placed over a large portion of Array 1 and the magnitude of surface settlement increased further.

The larger or more variable settlements observed at the initial phase of a tunnel project is not an uncommon phenomenon. For example, Kuesel (1969) observed invariably greater settlements at the start of all tunnel drives in the Bart project. Clough et al. (1983) reported that the surface settlements measured at the early part of the EPB shield tunnel in Bay mud were more variable and it was also suggested that this phenomenon was due to the inexperience of the tunnel-crews at the early stages of excavation.

The surface settlement profile at Array 2 (measured at the end of construction) was narrower in width than the profile at Array 1 (see Figures 9.10b and 9.11b). Two years after construction, no significant change occurred at Array 2 but the trough width at Array 1 had increased substantially. The transverse surface settlement profile at Array 1 was very similar from cross-section to cross-section (Belshaw and Palmer, 1978). The same comparison cannot be made for Array 2 because there was only one line of transverse surface settlement pins. However, it may be assumed that the measured settlements at this section are representative of the shape of the settlement profile at Array 2. The distribution of surface settlements may be constructed from the data in Figures 9.11a and 9.11b. A conceptual, approximate

plan view of the displacement contours is illustrated in Figure 9.11c.

9.2.3 Distribution of Subsurface Displacements

9.2.3.1 Vertical Displacements With Depth On Centreline

The settlements over the centreline of the tunnel at Array 1 and Array 2 have been shown respectively in Figures 9.6 and 9.7.

Three stages of movement may be identified during tunnelling before a plane strain condition was reached. In the first stage, little to slight heaving of the settlement points was observed before the face reached the line of extensometers. In the second stage, some amount of settlement occurred as the shield passed the instrumentation station (i.e., x between 0 to 5.6 m). However, after the tailpiece cleared the section (i.e., $x > 5.6$ m), the third stage of settlement occurred rapidly as the soil invaded the space between the circular tunnel boundary and the lining. (This suggested that the soil was able to fill the tail void in spite of the grouting process.) As evidenced in the figures, the movement due to tunnelling appeared to be approaching completion as the plane strain condition was reached.

A similar pattern of soil movement associated with shield tunnelling was also reported by Peck (1969). Figure 9.18 shows the displacements due to tunnelling in San Francisco Clay. Peck observed that on approach of the shield, the clay moved slightly away from the tunnel, but the clay was drawn sharply towards the tail void as the shield passed (Figure 9.18a). The rate of increase of surface settlement

was greatest as the rear of the shield passed beneath the measurement point (Figure 9.18b).

The pattern of soil movement suggests that the displacements were influenced by stress changes due to excavation as well as the kinematic restraint of the shield and lining. The rapid soil movement that had occurred as the rear of the shield passed reduced the effectiveness of grouting.

9.2.3.2 Horizontal Displacements

The lateral displacements in a plane perpendicular to the tunnel axis at Array 1 when the tunnel face was at -5 m, 4 m and 20 m from the line of slope indicators are shown in Figure 9.12. The readings taken 138 days after the tunnel face had passed the section were very similar to the data obtained at 20 m from the section and they are not shown in the figure. The maximum reading was 32 mm, recorded at the springline level. Since time-dependent lateral movement appeared insignificant, it may be suggested that soil deformation due to reconsolidation of remoulded soil took place mainly in the vertical direction.

The displacement vectors in Array 1 measured by slope indicators A, C, D at the springline level and slope indicator B, 0.96 m above the crown are shown in Figure 9.13. A similar plot for Array 2 is shown in Figure 9.14. (These data are obtained from Morton and Dodds

Report, 1976.) It may be seen from Figure 9.13 that the magnitude of the displacement vectors increased by about three times between $\ell = 4$ m to $\ell = 12$ m. Clearly, this was the effect of tailpiece clearance which has been discussed previously. The annular space was filled rapidly so that the difference in observed horizontal movements between ℓ of 12 m to 28 m behind the face was very small. There were insufficient data to reconstruct a clear pattern of displacements at Array 2 but the occurrence of similar phenomena may be expected. With reference to slope indicator D at Array 2 (1.2 m above the crown), movement towards the face was initially recorded in front of the shield (negative values of ℓ). Measured movements became progressively smaller as the machine approached the section. It may be noted from Figures 9.14 and 9.7 that only little face deformation occurred during excavation.

9.2.3.3 Displacement Vectors in the Vertical Plane

The magnitude and distribution of displacement in a plane perpendicular to the tunnel axis at Arrays 1 and 2 are shown respectively in Figures 9.15 and 9.16. These two plots are constructed from extensometer and slope indicator data. Since the instrumentations were about 1 m apart, the combined vertical and horizontal displacements may only be considered as apparent vectors. The movements above the springline were larger than those beneath it. Very little deformation was observed beneath the depth of the tunnel invert; displacements

occurred mainly above the springline with maximum displacement occurring above the crown.

9.3 PORE WATER PRESSURE DUE TO TUNNELLING

The changes in pore pressure due to tunnelling are shown in Figure 9.17. The Thor piezometers T1 to T7 were not co-planar (see Figure 9.2), but the distance was only 3.75 m apart. As the shield approached, all the piezometers registered increase in pore pressure. As the shield passed, the pressure decreased rapidly. Maximum decrease of pressure was recorded by piezometer T4 at the level of springline. The piezometric readings of T1 above the tunnel seemed to be erratic and were probably influenced by the effect of shield pitching during construction. All the piezometric readings reached a minimum after the face had passed about 9 to 10 m beyond the piezometers. At this point, the 'restricted undrained plane strain condition' has probably been approached. Subsequently, the trend of pressure changes reversed and began to increase. This remarkable phenomenon probably reflected the effect of tail-grouting and soil-liner interaction. The excess pore pressure eventually decreased and became close to the initial hydrostatic condition though the pre-tunnelling pressure was not re-established even after ten months.

Palmer and Belshaw (1980) suggested that the tunnel acted as a drain. However, the drawdown was small and piezometric readings taken one year after construction indicated the tunnel had little effect on

water pressure except in the immediate vicinity of the tunnel, i.e., within 1 m. This minimal effect was interpreted as an indication that the grout and disturbed soil, with a lower permeability than the surrounding undisturbed soil, was acting as a seal for the tunnel.

In fact, measurement of pore pressure conducted four years after construction showed that the overall ground water regime was essentially hydrostatic (see Chapter 6). The seepage forces deduced from the flow net constructed by Palmer and Belshaw (1980) and from a preliminary finite element seepage analysis were small. Long term settlements associated with drawdown were not significant in the Thunder Bay Tunnel.

The theoretical excess pore pressure arising from tunnelling may be calculated approximately by Skempton's pore water pressure equation. The final principal stresses at the positions of the piezometers, determined by a finite element analysis (to be discussed in Chapter 10) are shown in Table 9.3. It may be seen that a reduction of minor principal stress occurred at all the seven positions of the piezometers.

The general pattern of calculated excess pore pressure is in reasonable agreement with the observed maximum negative pore pressure. Both the theoretical and observed excess pore pressure indicated large decreases of pore pressure at piezometers T1 and T4, located near the crown and springline respectively. Moderate decreases in pore pressure were observed and predicted at piezometers T2 and T3, which were

located at approximately the same elevation as piezometer T1 but were further away from the tunnel. A minor change in pore pressure was observed and predicted at piezometer T5. However, agreement was not obtained between the calculated and observed pore pressure at piezometers T6 and T7 which were installed in varved clay. Due to the complex silt and clay layering structure of the soil, it is believed that the field pore pressure may not be accurately measured. Alternately, the pore pressure condition may be complicated and could not be easily estimated by simple calculations without taking into account anisotropic behaviour.

TABLE 9.1 TUNNEL OBSERVATIONS AT ARRAY 2 (Extracted from Morton and Dodds Report, 1976)

1). Two excavation cycles beneath settlement pin 2 (near the start of Array 2)

<u>TIME</u>	<u>CHAINAGE</u>	<u>REMARKS</u>
Aug. 19, 1976		
7:33 p.m.	57+47'4"	Start mining clockwise, grouting pressure 22 psi
		Level 2 mm west, 3 mm north
7:35	57+47'8"	Stop pushing on jacks 1 and 2
7:37	57+48'11"	Reverse heady counterclockwise
7:40	57+49'11"	
7:42	57+50'6"	Stop grouting
7:42:30	57+50'7"	Stop mining, empty cars, install ring 1299
8:10 p.m.	57+50'7"	Start mining counterclockwise, not grouting
		Level bubble 6 mm north, level west
		Using jacks 5 to 8 only, machine possibly being pushed up
8:13	57+51'7"	
8:15	57+52'3"	Stop mining
8:15:30	57+52'3"	Start mining counterclockwise
		Start grouting 34 psi
8:17	57+53'0"	
8:18	57+53'9"	Stop grouting
8:18:30	57+53'10"	Stop mining, empty cars, install ring 1300

One excavation cycle
 One excavation cycle

TABLE 9.1 (cont'd)

2) Two excavation cycles beneath settlement pin 5 (nominal centre of Array 2)

<u>TIME</u>	<u>CHAINAGE</u>		<u>REMARKS</u>
Aug. 20, 1976			
8:18:30	57+89'9"	↑ One excavation cycle	Start mining counterclockwise, grouting
			Not using jacks 1 and 2, 7 and 8
			Level 7 mm west, 3 mm south
			Laser 2 1/2" low, 1/2" south from target
8:22	57+91'2"		Stop mining for 20 sec, reverse head
8:23	57+92'6"		Stop grouting
8:24	57+93'0"		Stop mining, empty cars, install ring 1312
8:30	57+93'0"		Set jacks, slight blind shove
8:32			Slight push ahead, 1/2"
			Level 9 mm west, 3 mm south
9:02	57+93'0"	↑ One excavation cycle	Start mining counterclockwise
			Not using jacks 1 and 2, 5 and 6
9:04	57+93'4"		Start grouting
9:06			Grout coming through one instrument hole, stop grouting
9:07	57+94'2"		
9:07:30	57+94'2"		Pull head back 1/2", reverse to clockwise
9:11	57+95'5"		Stop mining, empty cars, install ring 1313
9:13:5	57+96'3"		Set jacks, push machine ahead 1/2"
9:21:5	57+96'3"		Level 8 mm west, level north-south

TABLE 9.2a OBSERVED CENTRELINE SURFACE SETTLEMENTS AT DIFFERENT STAGES OF DEVELOPMENT (ARRAY 1)

Array 1	Average (mm)	Range (mm)	At Nominal Central Section (mm)	Remarks
Undrained Settlement	-	-	49	Face at 12.8 m. t = 4 days
End of* Construction at Array 1	59	51 to 64 (76)	56	() implies excep- tionally large settlement
After 1 Year (Drained)	-	-	94	Settlement due to consolidation of remoulded soil was nearly completed
After 2 Years and With Sur- charge Added	147	131 to 162	142	Consolidation near completion

TABLE 9.2b OBSERVED CENTRELINE SURFACE SETTLEMENTS AT DIFFERENT STAGES OF DEVELOPMENT (ARRAY 2)

Array 2	Average (mm)	Range (mm)	At Nominal Central Section (mm)	Remarks
Undrained Settlements	-	-	50	Face at 15.2 m t = 1 day
End of* Construction at Array 2	44	37 to 47 [54]	54	[] implies compara- tively larger settlement
After 2 Years (Drained)	-	-	54	Little to no con- solidation settlement

* see Figure 9.8

TABLE 9.3 COMPARISON BETWEEN OBSERVED¹ MAXIMUM NEGATIVE EXCESS PORE PRESSURE AND THEORETICAL² EXCESS PORE PRESSURE

Piezo-meter No.	Observed Maximum Negative Excess PWP (kPa)		Initial Principal Stress (kPa)		Final Principal Stress (kPa)		$\Delta\sigma_3$ (kPa)	$\Delta\sigma_1 - \Delta\sigma_3$ (kPa)	Δu Calculated Excess PWP (kPa)	Adopted Value of A
	σ_v	σ_h	σ_1	σ_3	σ_1	σ_3				
T1	153.0	131.1	131.9	74.9	131.9	74.9	-56.2	35.1 ³	-36.5	.56
T2	149.9	128.3	149.5	90.7	149.5	90.7	-37.6	37.2 ³	-16.8	.56
T3	150.9	129.0	165.0	84.9	165.0	84.9	-44.1	58.2	-24.9	.33
T4	186.3	161.6	150.3	99.6	150.3	99.6	-62.0	26.0	-53.4	.33
T5	184.6	160.0	242.4	137.3	242.4	137.3	-22.7	80.5	3.9	.33
T6	220.0	191.7	244.0	166.5	244.0	166.5	-25.2	49.3	-8.9	.33
T7	204.9	178.5	248.8	157.2	248.8	157.2	-21.3	65.2	0.2	.33

¹ Data obtained from Palmer (1982)

² Stresses are obtained from Gauss points closest to the piezometer locations.

³ Plastic stress state

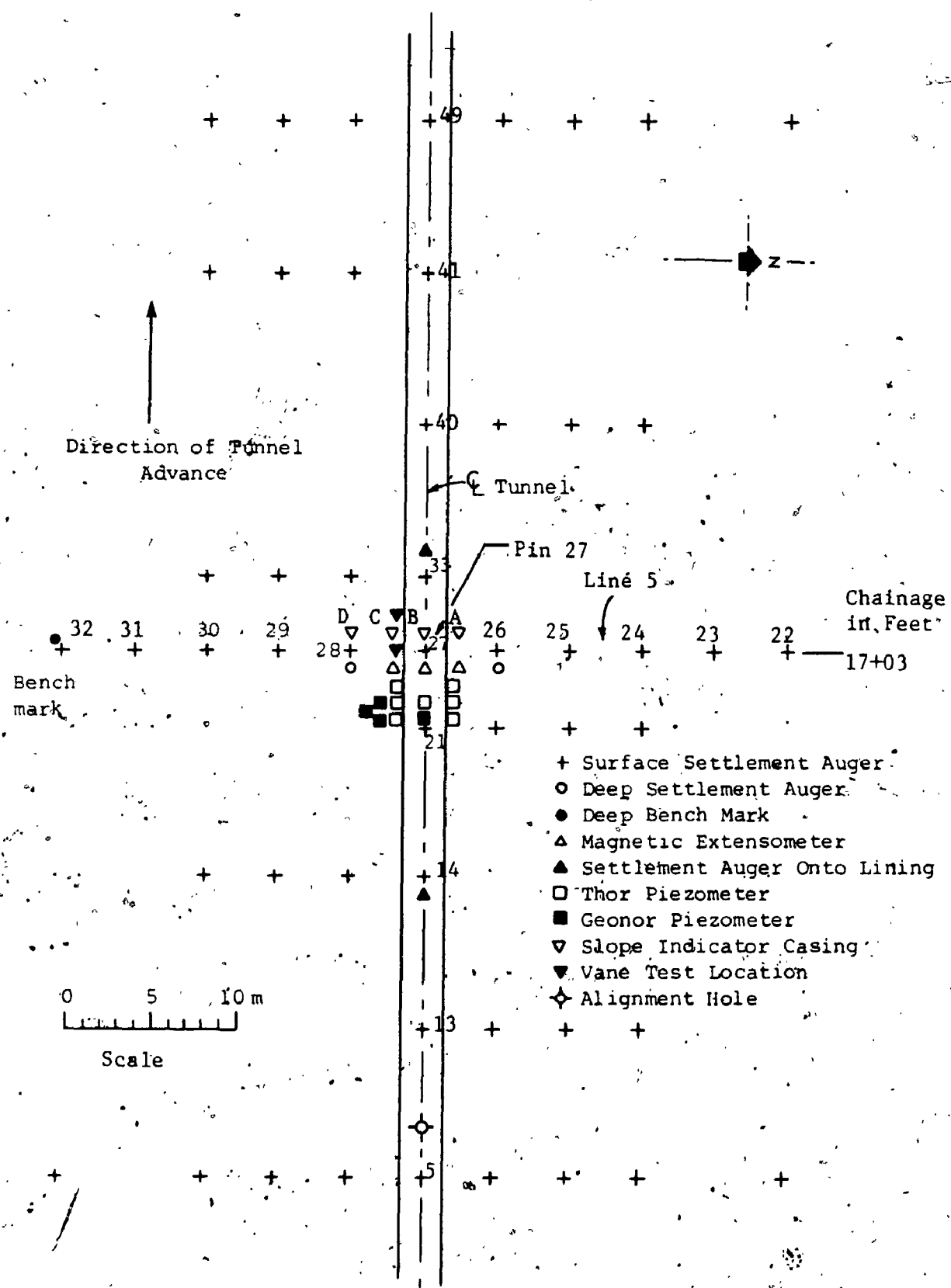


FIGURE 9.1 Plan of Instrumentation at Array-1 (after Belshaw and Palmer, 1978)

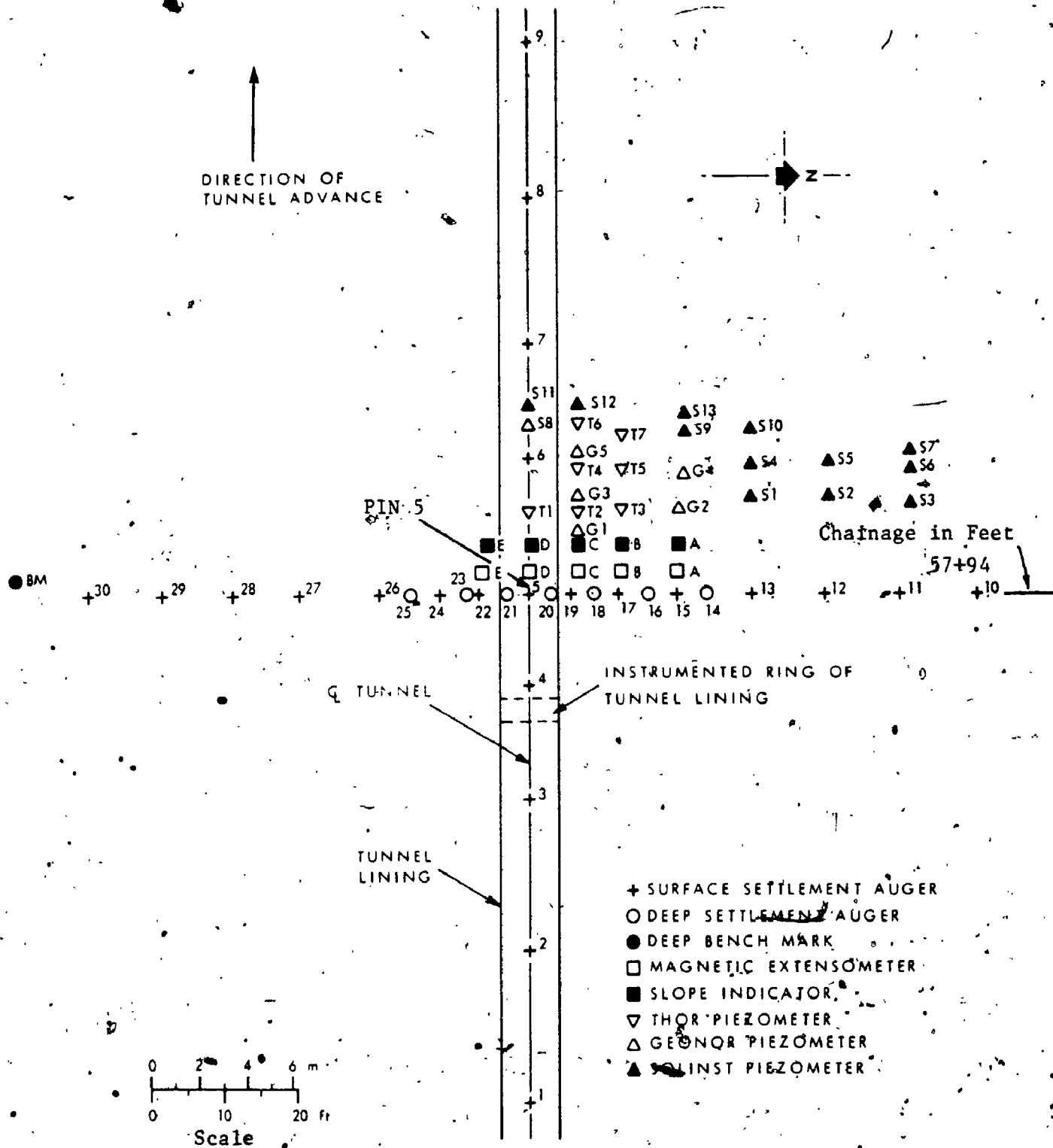
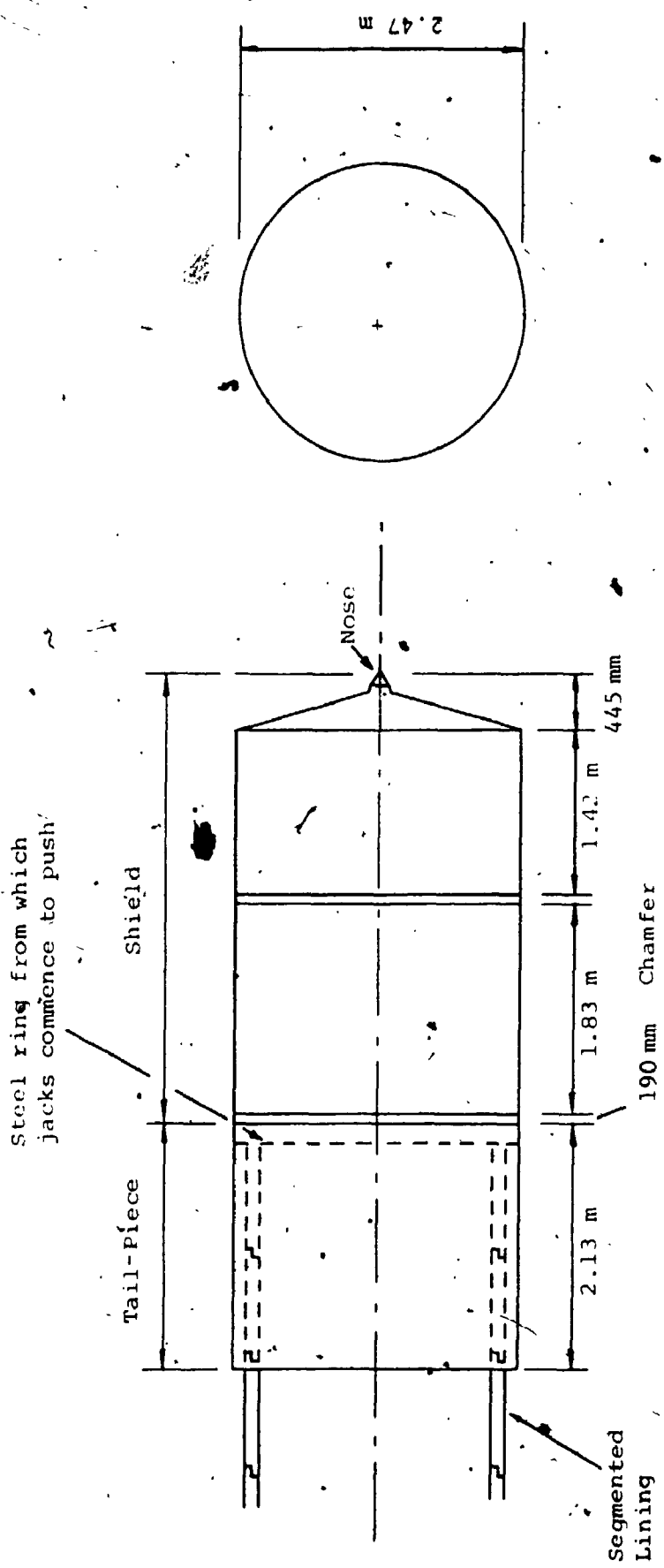


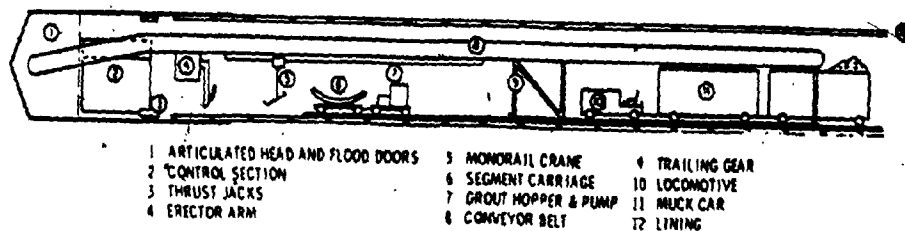
FIGURE 9.2 Plan of Instrumentation at Array 2 (after Palmer and Beishaw, 1980)



(a) Side Elevation

(b) End Elevation

FIGURE 9.3 Dimensions of Tunneling Machine (Morton Dodds and Partners, 1976)



- | | | |
|------------------------------------|-----------------------|-----------------|
| 1 ARTICULATED HEAD AND FLOOD DOORS | 5 MONORAIL CRANE | 8 TRAILING GEAR |
| 2 CONTROL SECTION | 6 SEGMENT CARRIAGE | 10 LOCOMOTIVE |
| 3 THRUST JACKS | 7 GROUT HOPPER & PUMP | 11 MUCK CAR |
| 4 ERECTOR ARM | 8 CONVEYOR BELT | 12 LINING |

(Not to Scale)

FIGURE 9.4a Schematic Section of Tunneling Operation (after Morton et al., 1977)

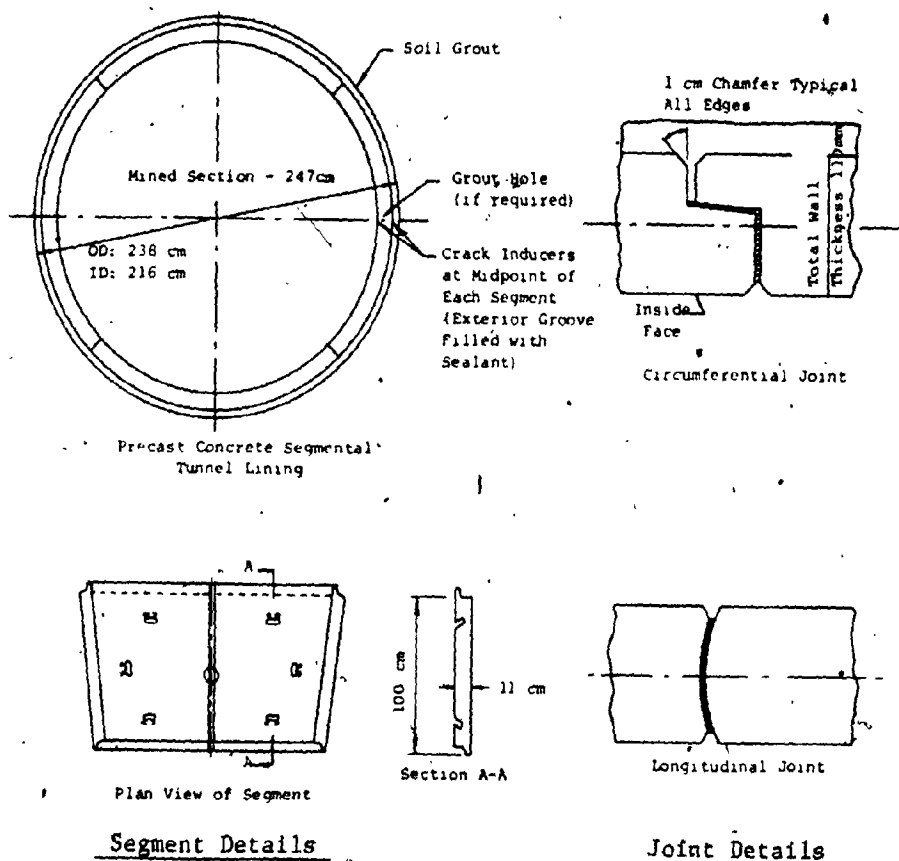


FIGURE 9.4b Details of Tunnel Liner (after Morton et al., 1977)

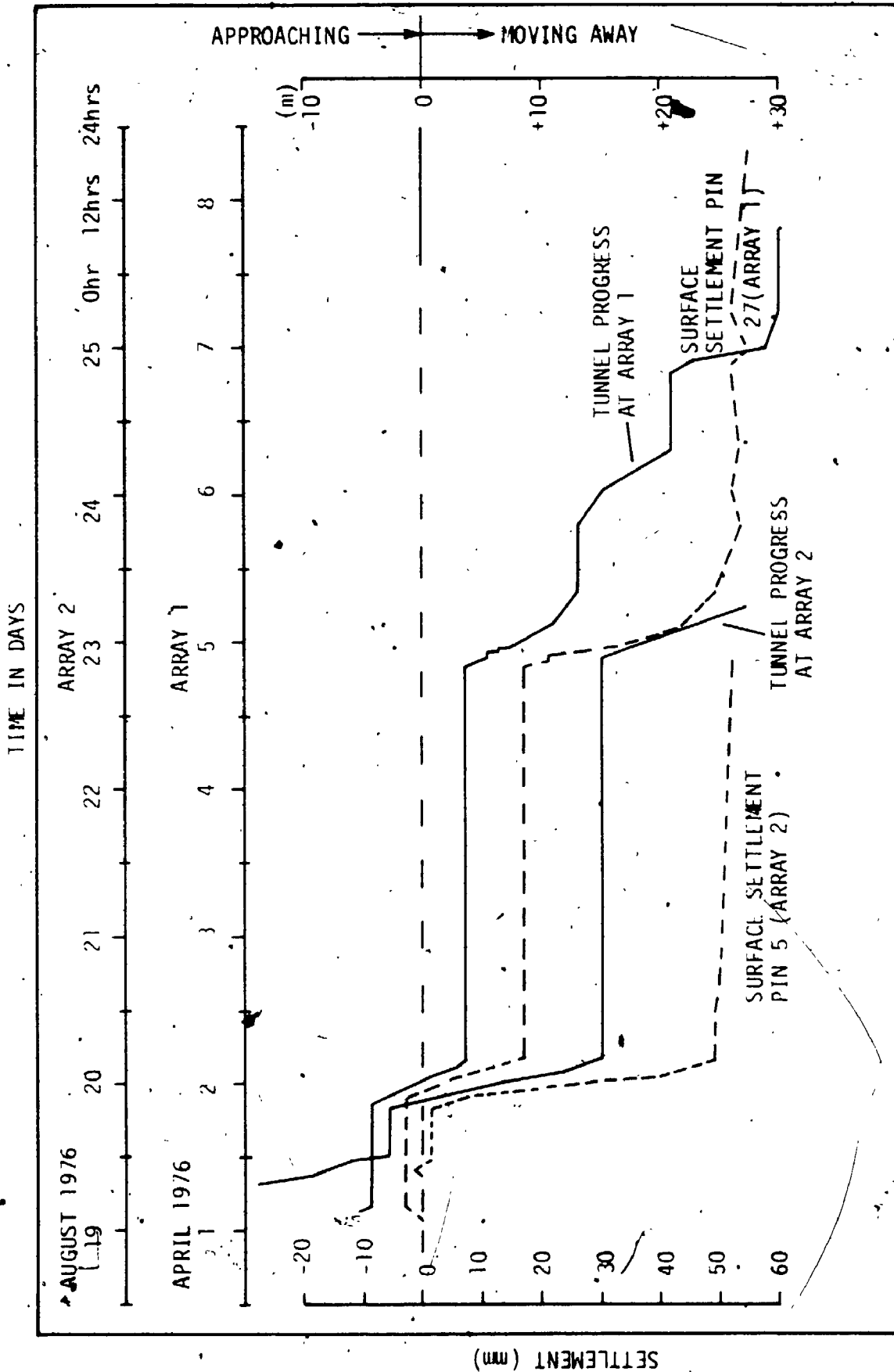


FIGURE 9.5 Time, Settlement, Tunnel-Progress Relationships

DISTANCE OF TUNNEL FACE FROM LINE OF INSTRUMENTATION AT CH 17+03 (ARRAY 1) AND CH 57+94 (ARRAY 2)

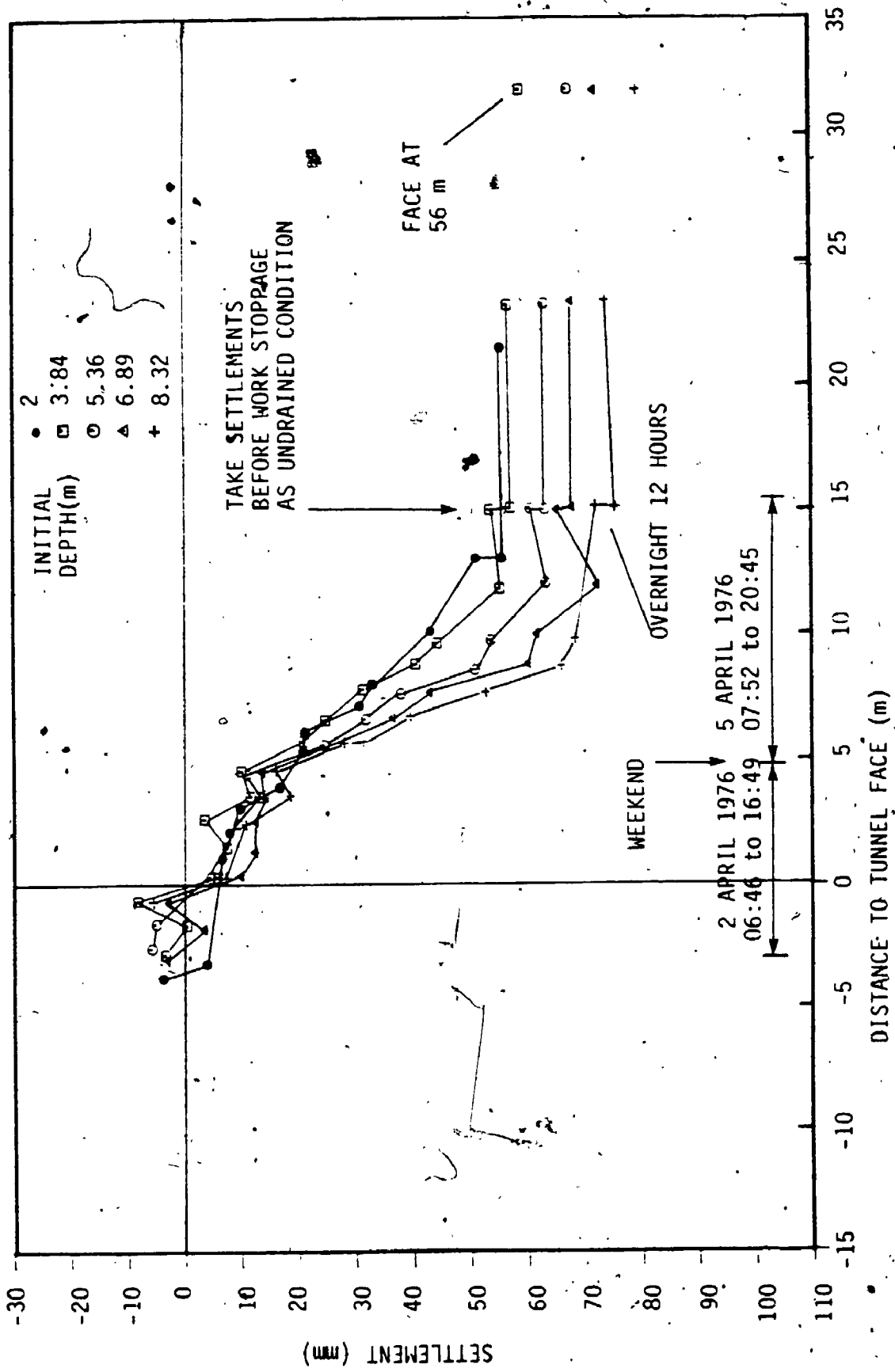


FIGURE 9.6 Vertical Soil Displacement Over Centreline of Tunnel at Array 1 (after Belshaw and Palmer, 1978)

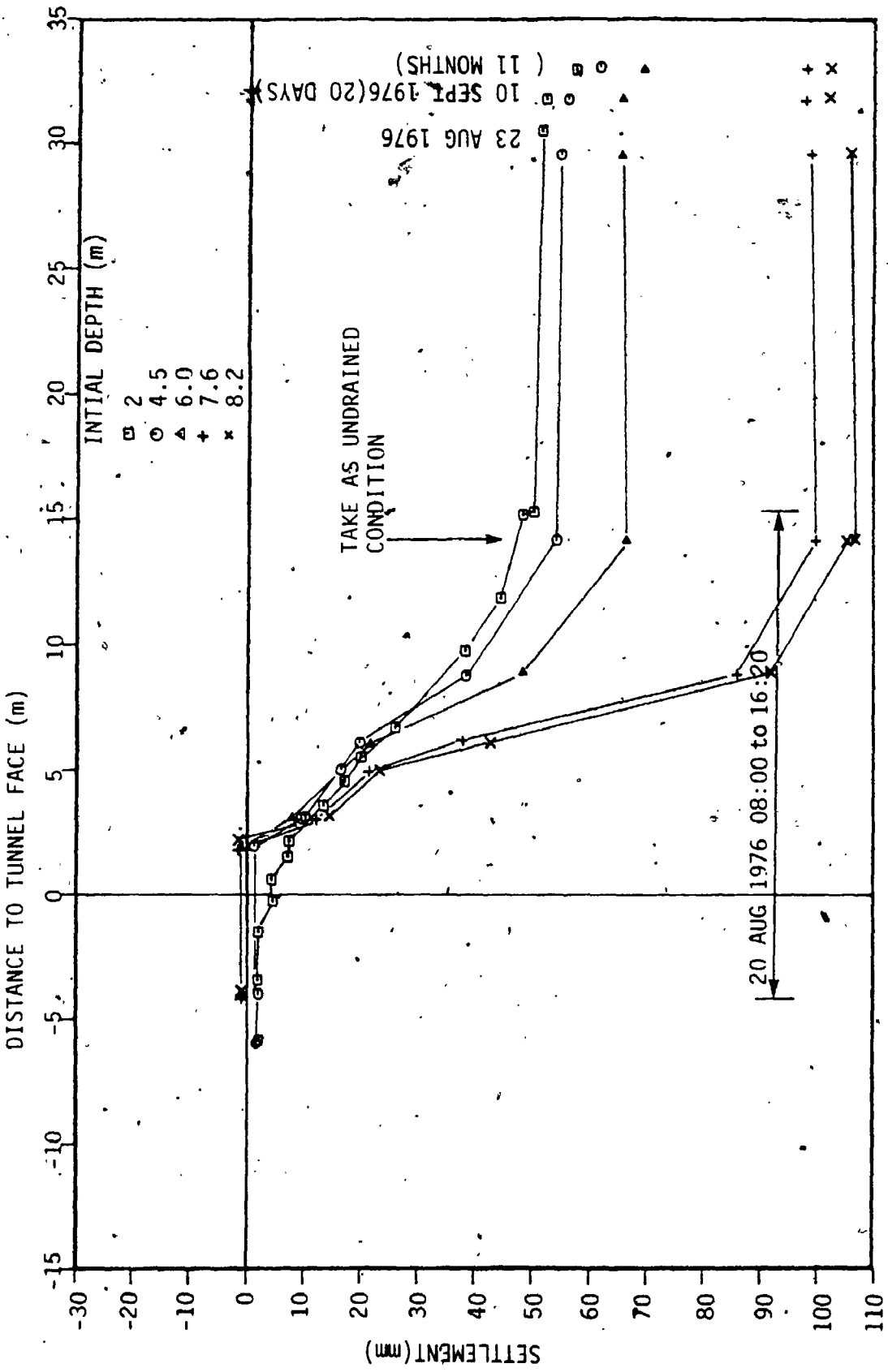
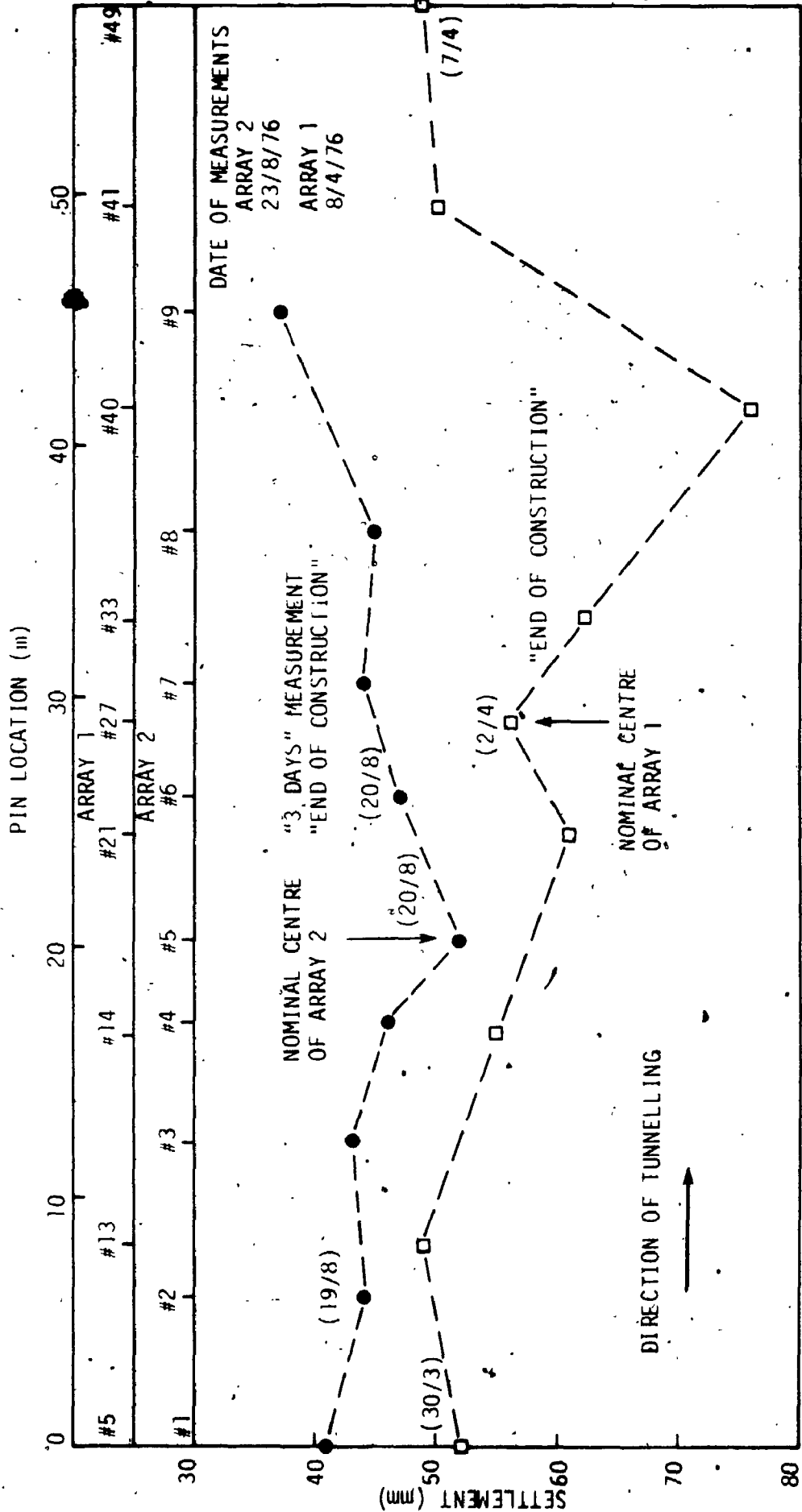


FIGURE 9.7 Vertical Soil Displacement Over Centreline of Tunnel at Array 2 (after Palmer and Belshaw, 1980)



1) (Date/Month) indicates time when the face passed the section

FIGURE 9.8 Surface Settlement Over Tunnel Centreline at Array 1 and Array 2

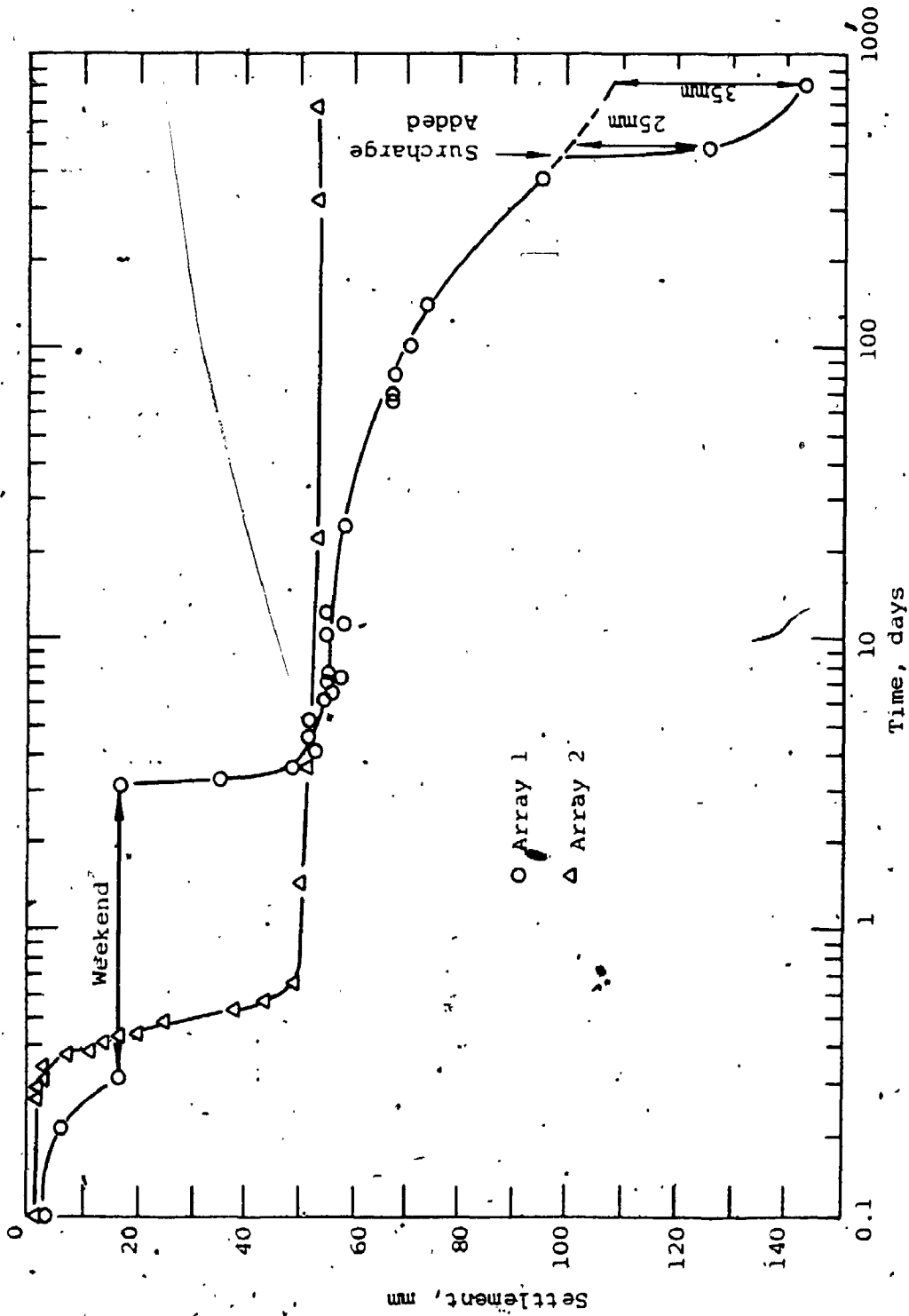


FIGURE 9.9 Settlement Over Centreline (after Palmer and Belshaw, 1979)

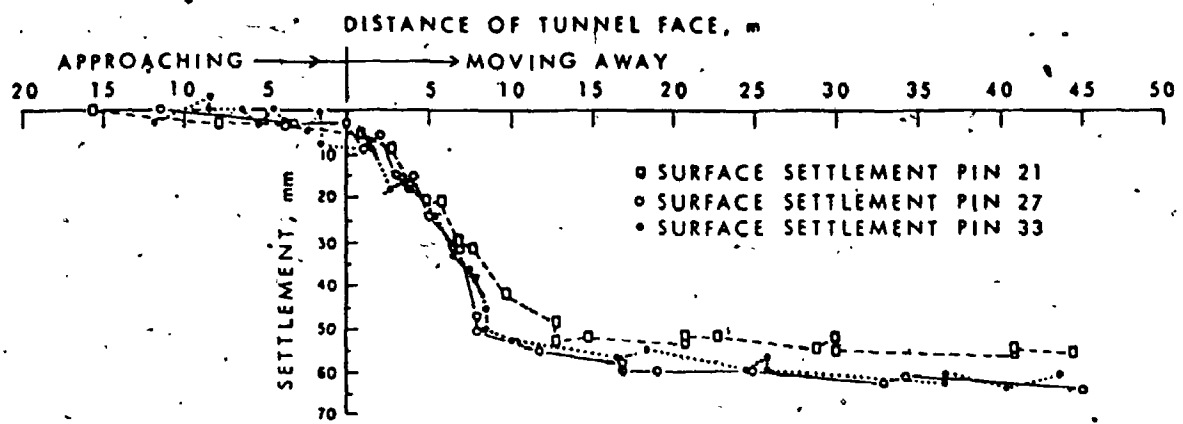


FIGURE 9.10a Surface Settlement Over Centreline of Tunnel at Array 1 (after Belshaw and Palmer, 1978)

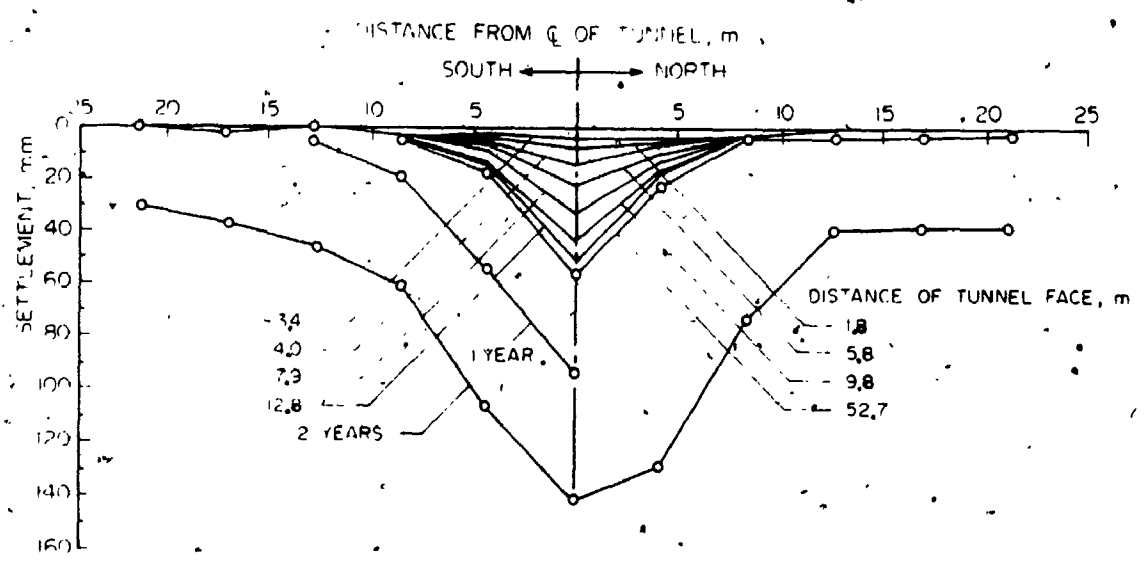


FIGURE 9.10b Surface Settlement Along Line Through Pin 27 at Array 1 (after Belshaw and Palmer, 1978)

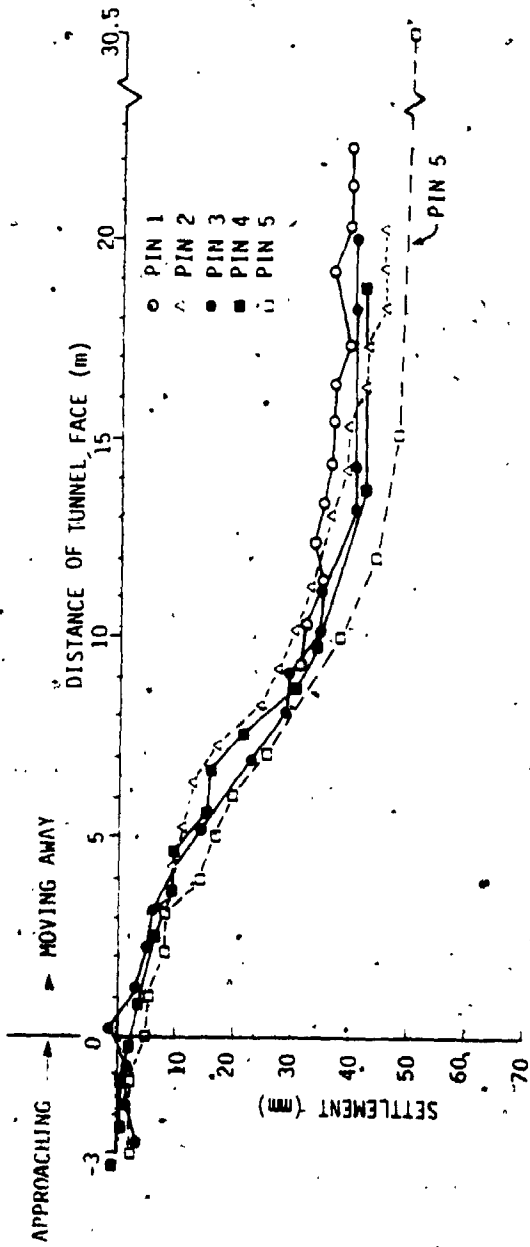


FIGURE 9.11a Surface Settlement Over Centreline of Tunnel at Array 2

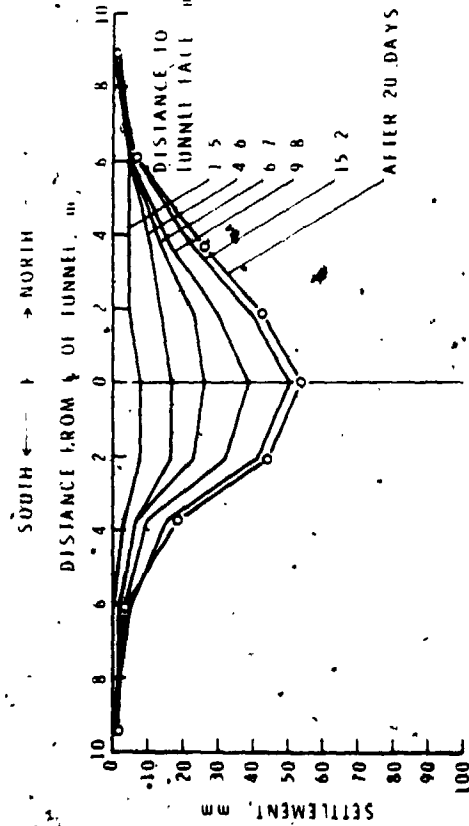


FIGURE 9.11b Surface Settlement Along Line Through Settlement Pin 5 at Array 2 (after Palmer and Belshaw, 1980)

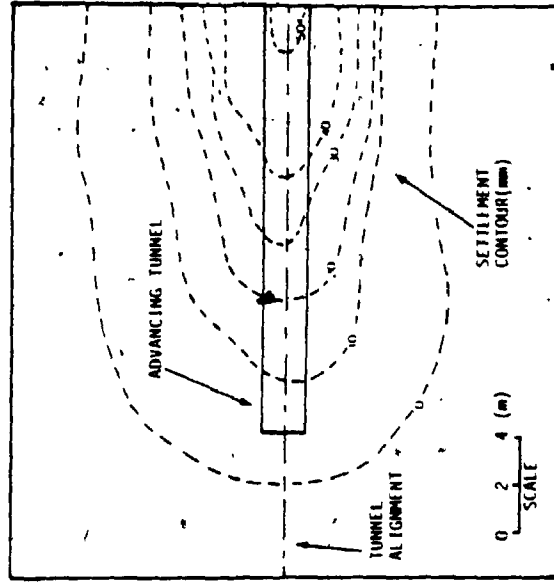


FIGURE 9.11c Plan View of Conceptual 'Bowl' of Settlement Trough Above the Advancing Tunnel at Array 2

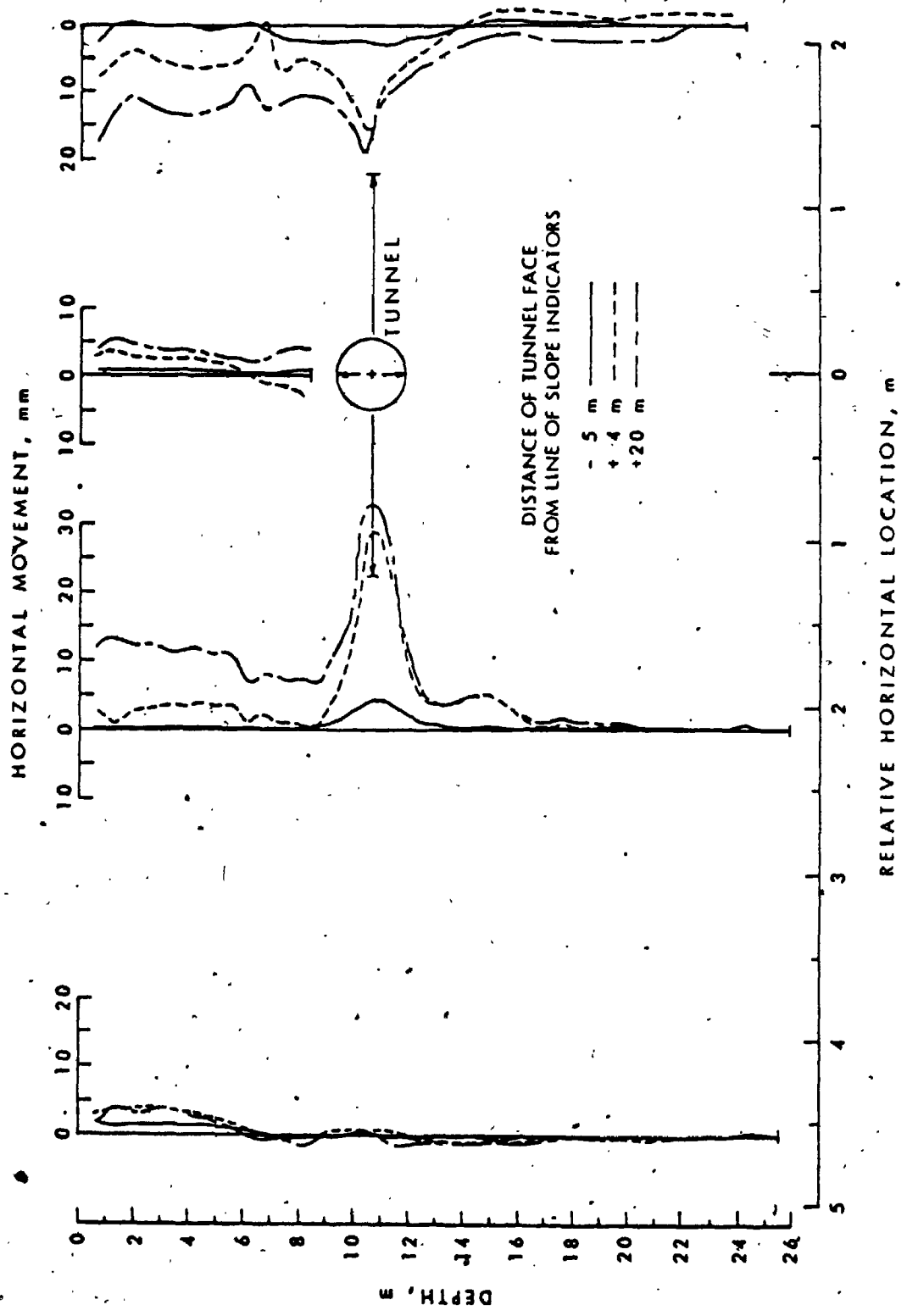


FIGURE 9.12 Slope Indicator Data Perpendicular to Tunnel Axis at Array I (Belshaw and Palmer, 1978).

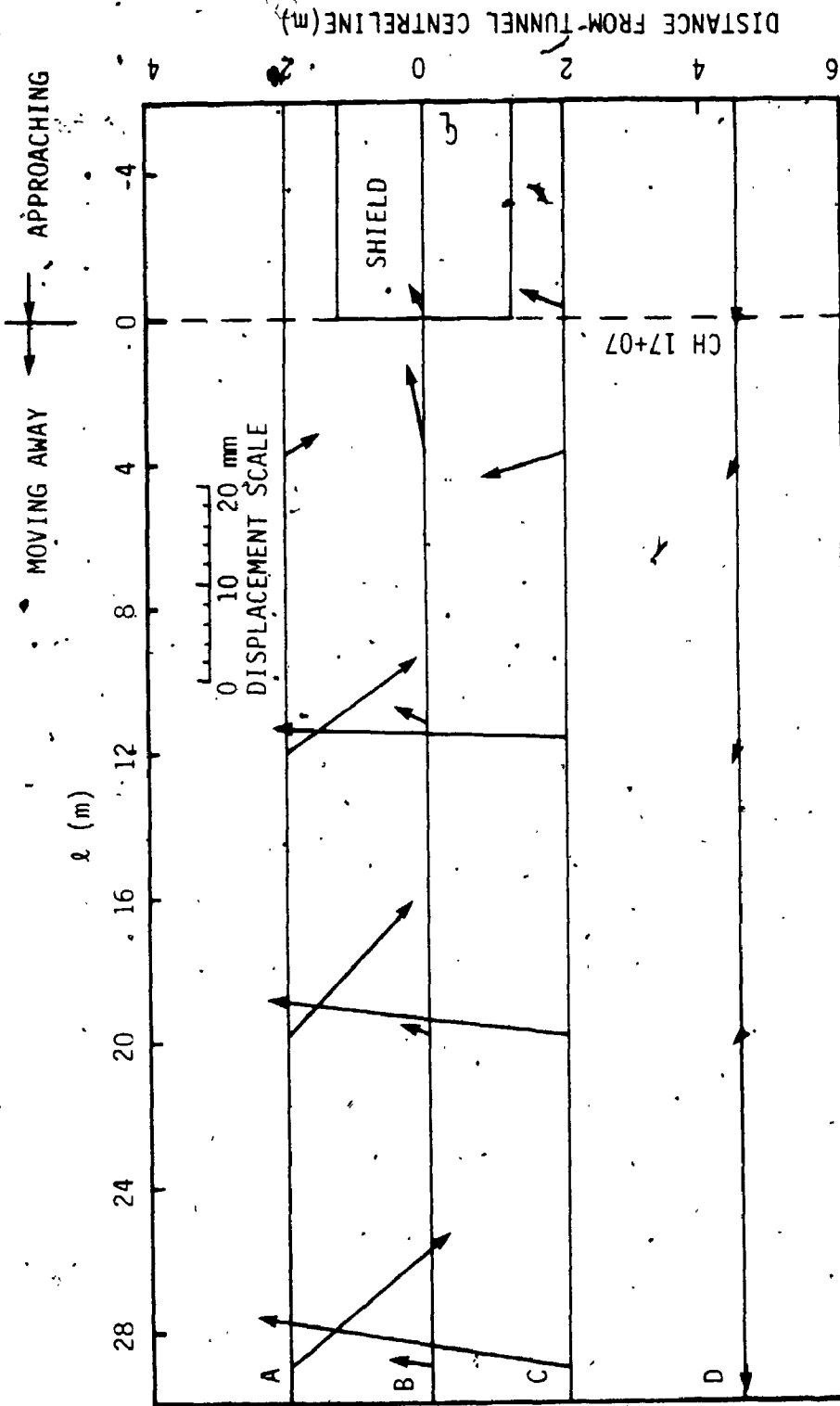


FIGURE 9.13 Horizontal Displacement Vectors at Springline (A,C,D) and 0.96m above Crown (B) During Shield Advance (Array 1)

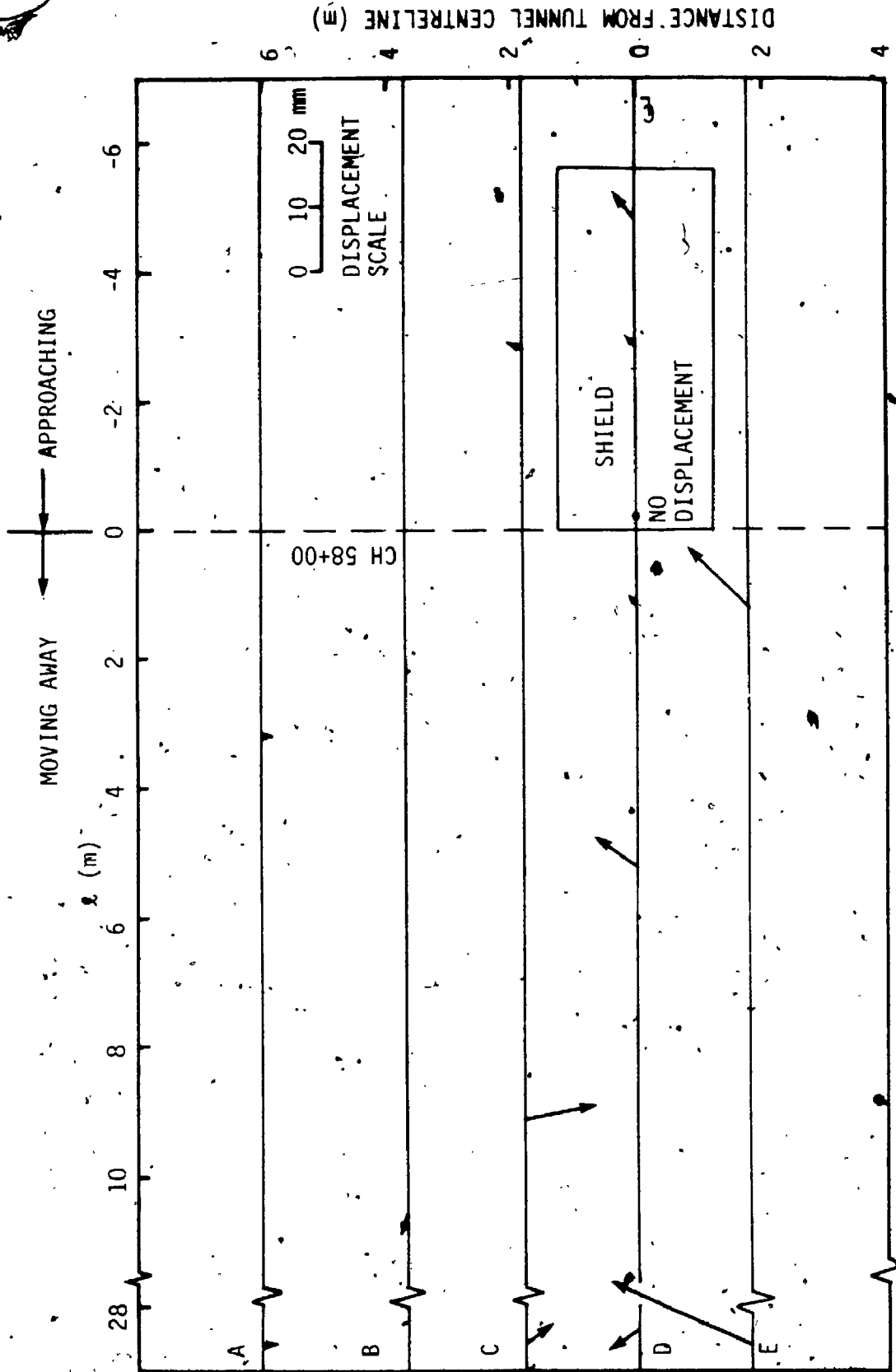


FIGURE 9.14 Horizontal Displacement Vectors at Springline (A,B,C,E) and 1.2m above Crown (D) During Shield Advance (Array 2)

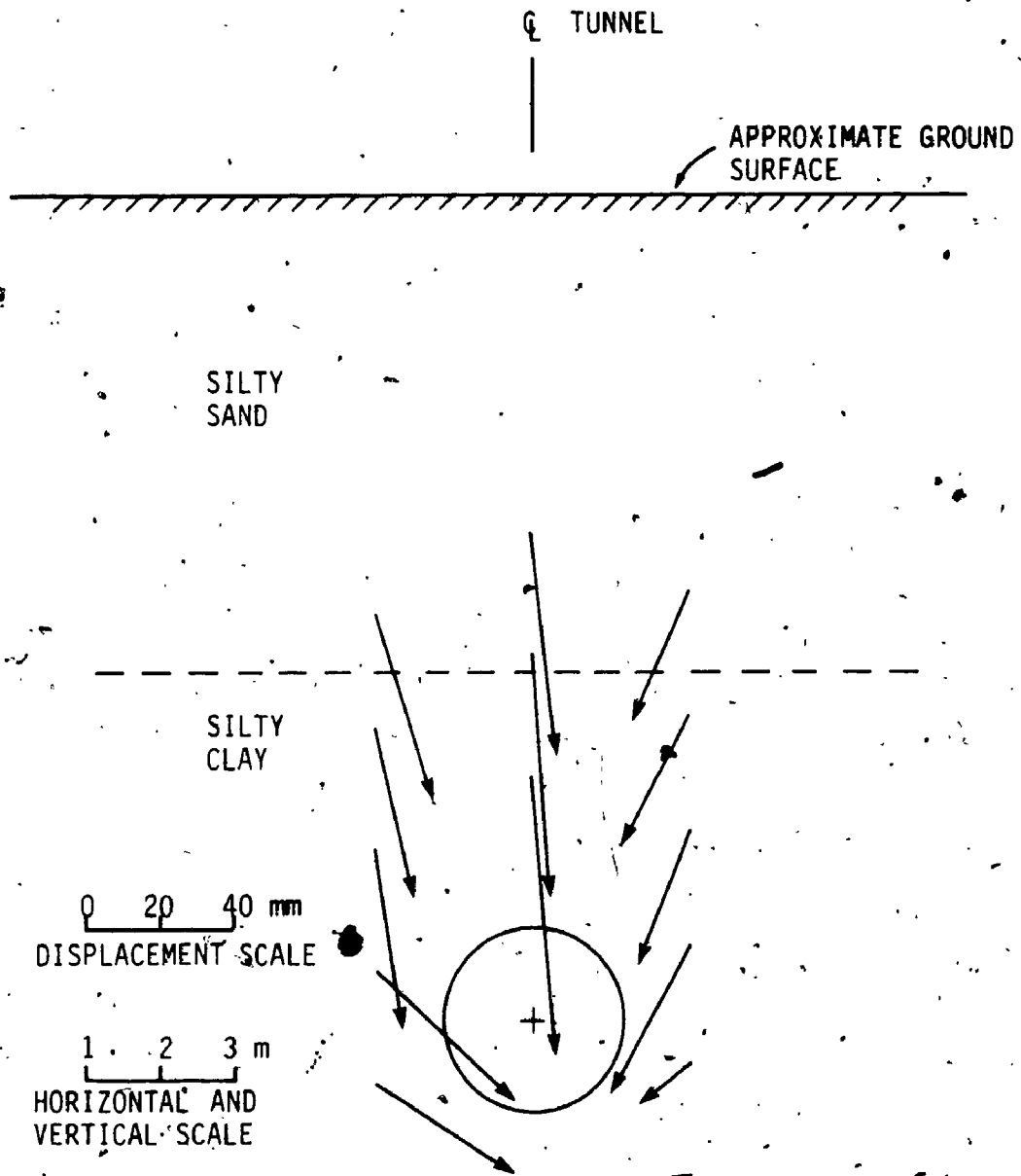


FIGURE 9.15 Displacement Vectors in Vertical Plane at Array 1 Perpendicular to Tunnel Axis (Face at 10.8 m)

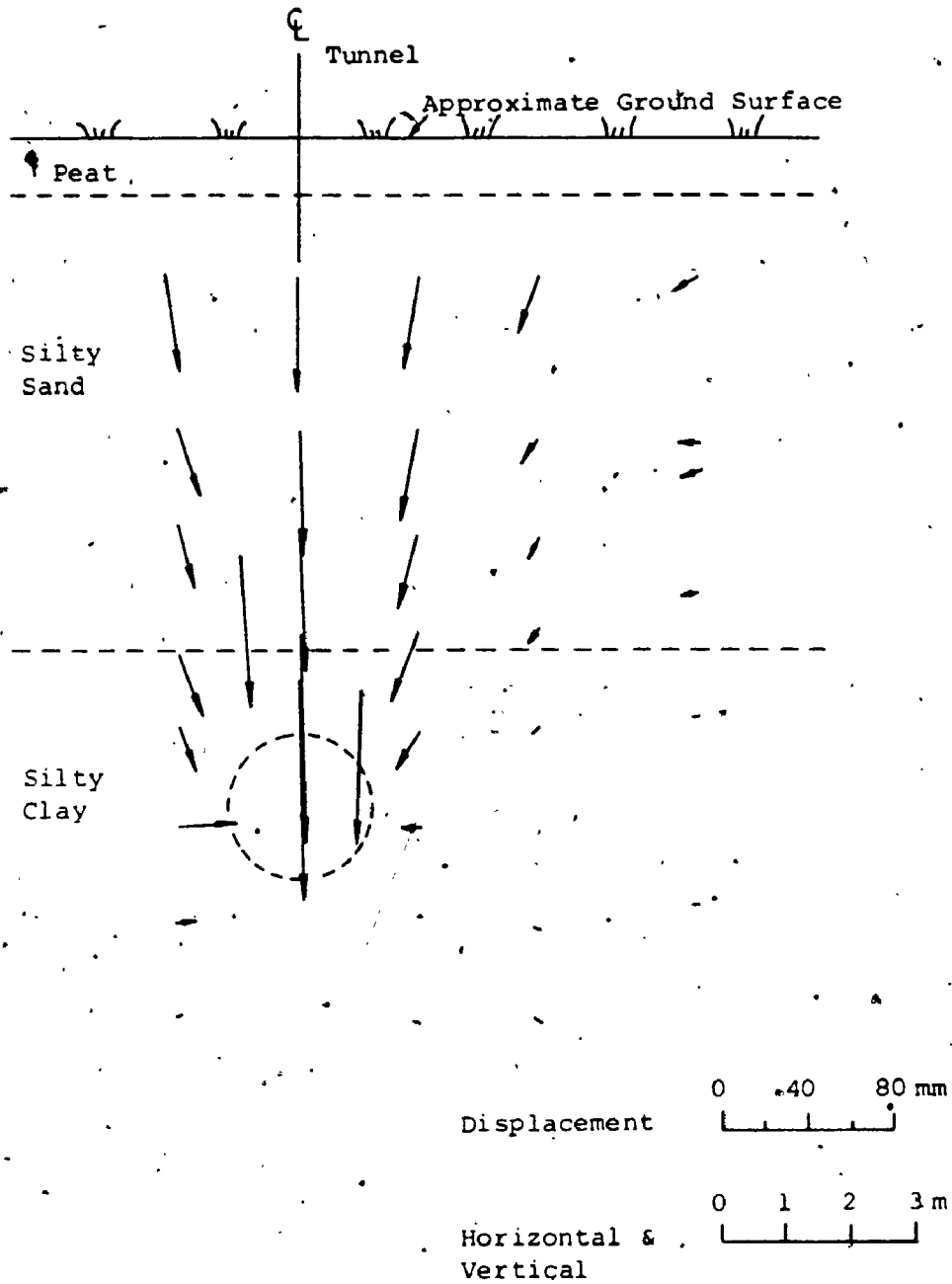


FIGURE 9.16 Displacement Vectors in Vertical Plane at Array 2 Perpendicular to Tunnel Axis (after 20 Days) (Palmer and Belshaw, 1980)

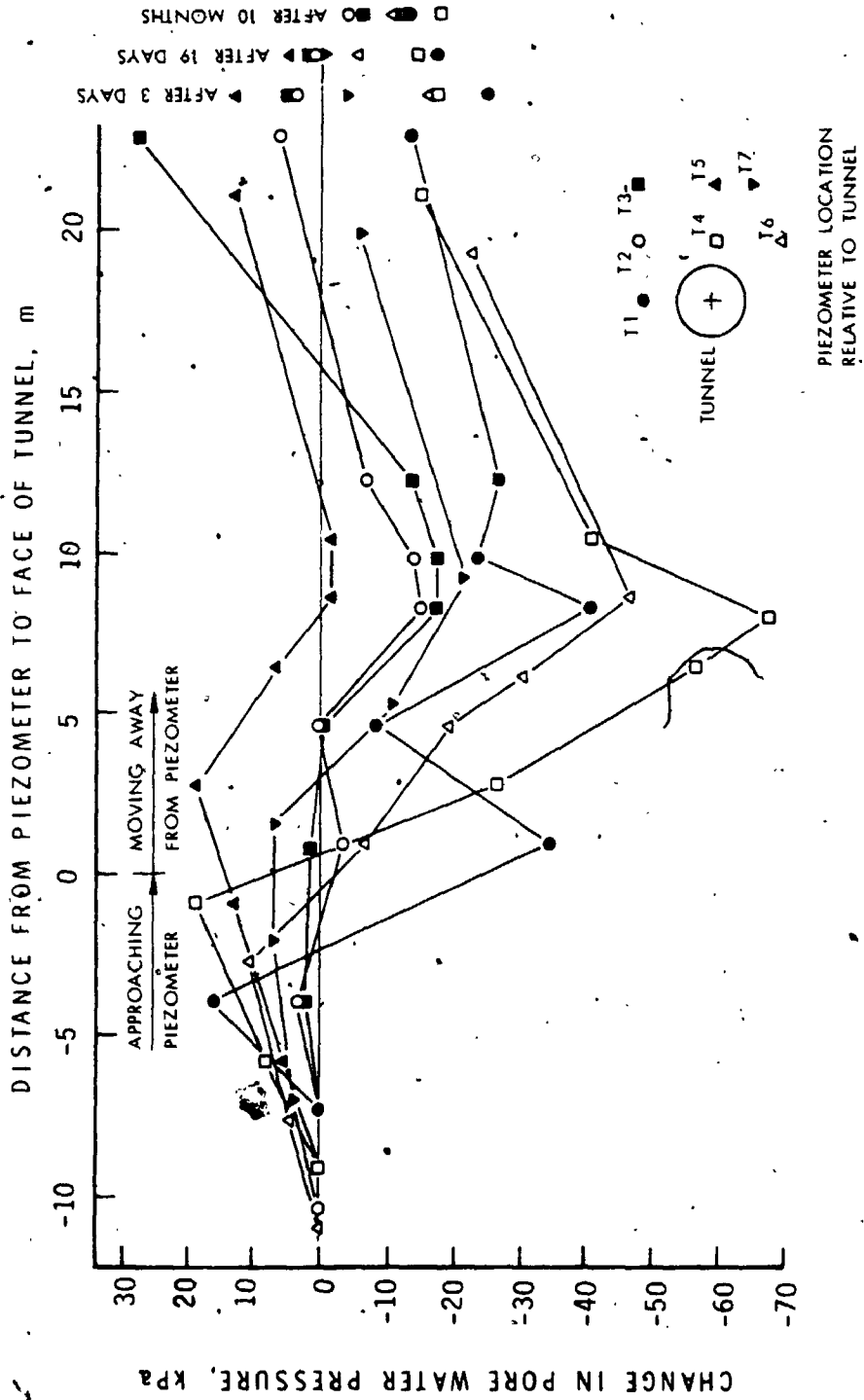


FIGURE 9.17 Changes in Pore Pressure at Array 2 (after Palmer and Belshaw, 1980, corrected)

Handwritten scribble or signature.

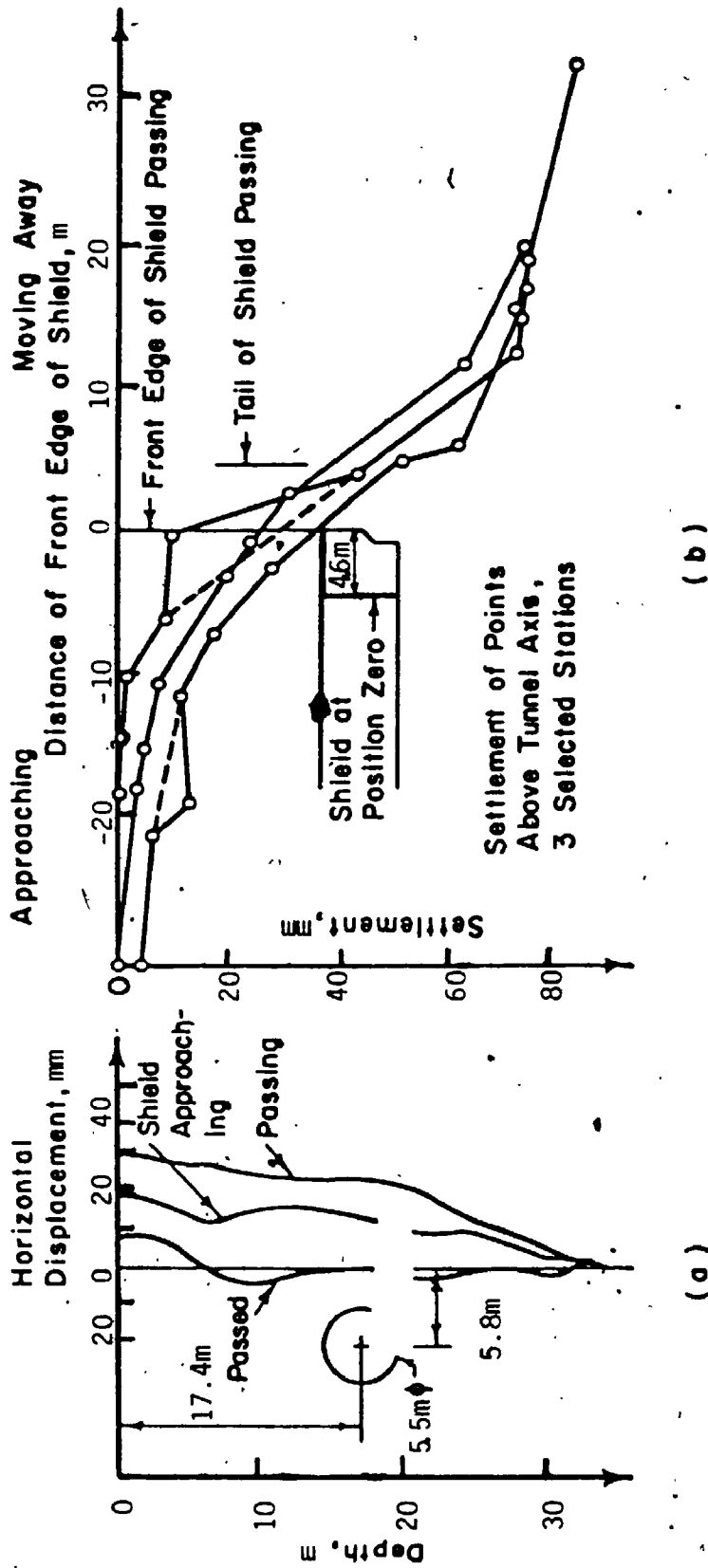


FIGURE 9.18 Shield Tunnel in Plastic Clay:
 (a) Successive Positions of Originally Vertical Line in Soil Beside Tunnel as Shield Approached and Passed;
 (b) Settlement of Reference Points above Tunnel as Shield Approached, Passed Beneath, and Continued Beyond the Points
 (after Peck, 1969)

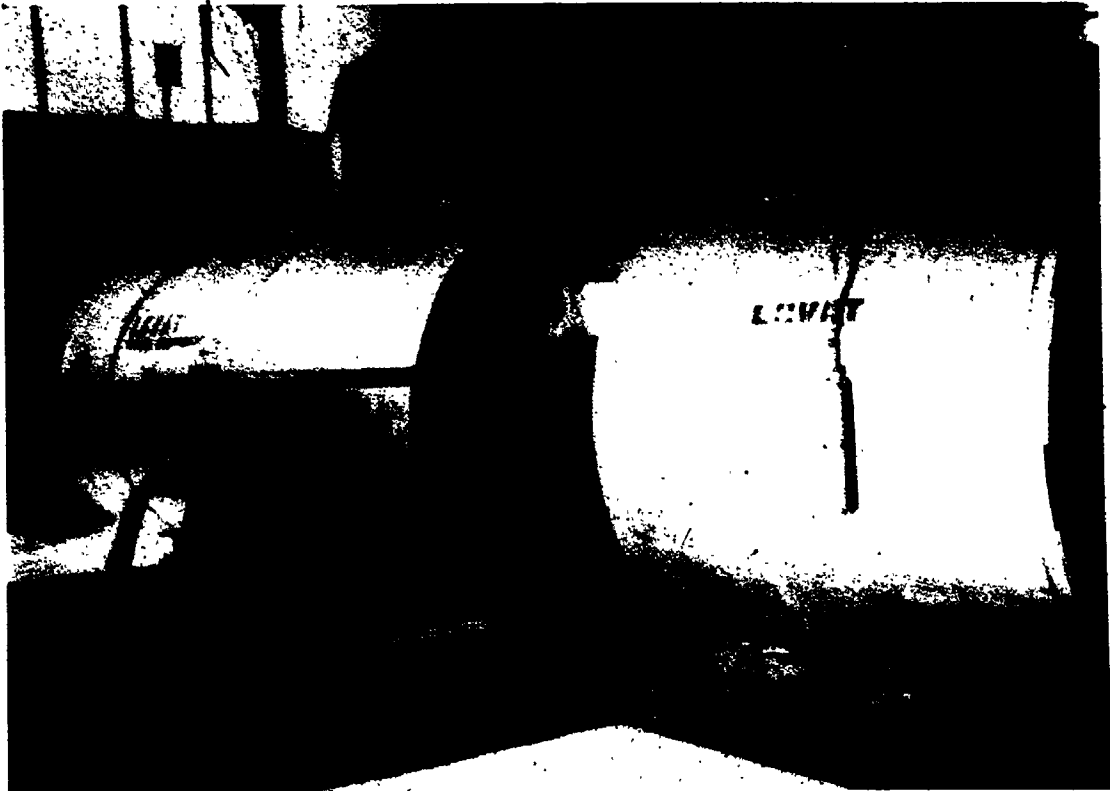


FIGURE 9.19a Oblique Rear View of Tunnel Machine Assembly

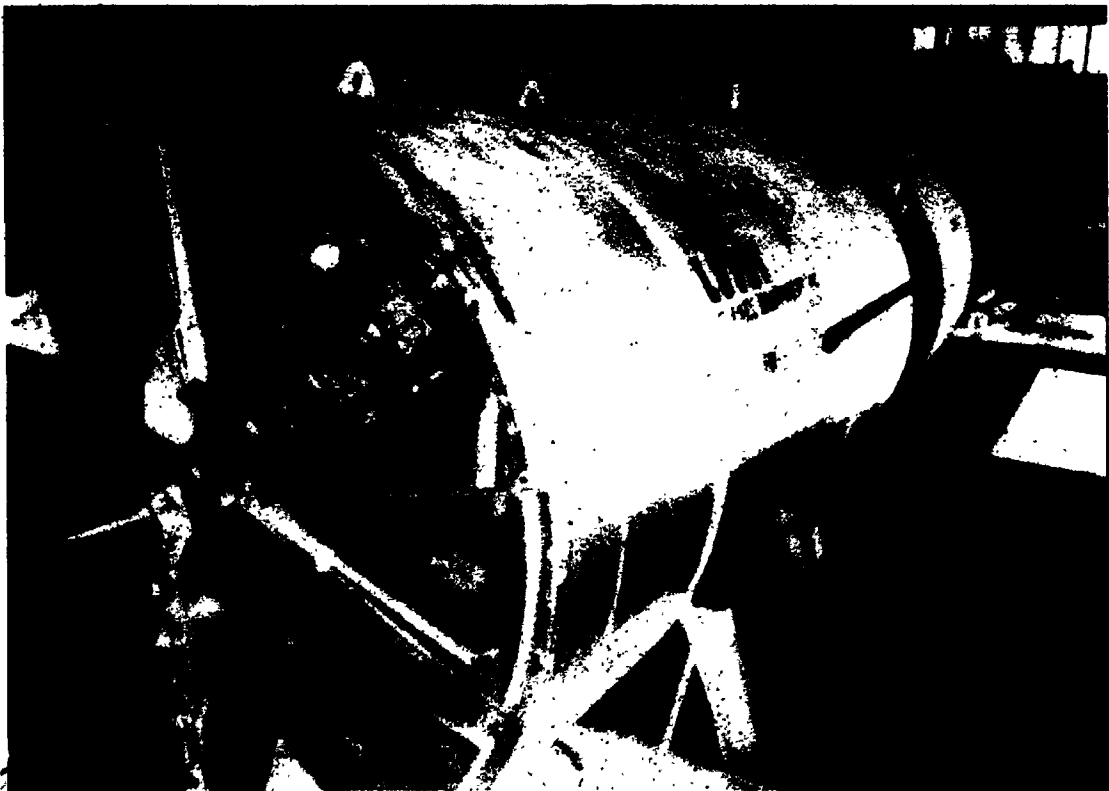


FIGURE 9.19b Oblique Front View of Tunnel Machine Assembly
(Courtesy of Morton and Partners)

CHAPTER 10
ANALYSES OF RESULTS OF FIELD INSTRUMENTATION
IN THUNDER BAY TUNNEL

10.1 INTRODUCTION

In this chapter, the finite element analysis of a tunnel constructed in the City of Thunder Bay is presented. The study sites, Array 1 and Array 2, were located respectively in the Lakehead Exhibition Ground and a bushy area. Array 1 was close to the start of the tunnel drive and there was only a small clay cover beneath sand layers over the tunnel at Array 2 so that these locations may be considered as critical sections for tunnelling. The calculated surface settlement profiles as well as the distributions of subsurface soil displacements will be compared with the results of field measurements. As the program of field instrumentations is relatively comprehensive, the study provides a unique opportunity for demonstrating the usefulness and practicality of the present method of analysis.

10.2 DETAILS OF THE ANALYSIS

The finite element analysis was performed using the soil parameters shown in Figures 10.1 and 10.2. The method of analysis was described in Chapter 4. Eight noded isoparametric elements, arranged as shown previously in Figure 4.4 in Chapter 4 were used to discretize the soil. The tunnel lining was modelled using structural beam element

with parameters appropriate to the concrete lining ($E = 20$ GPa, $A = .11 \text{ m}^2/\text{m}$, $I = 1.11 \times 10^{-4} \text{ m}^4/\text{m}$). Since there were segment joints, and crack inducers at the crown, springline and invert, the moment of inertia in these regions was reduced by a factor of 100 to provide the appropriate flexibility for the lining.

The mined diameter of the tunnel was 2.47 m while the external lining diameter was 2.38 m. This corresponds to a theoretical physical gap, defined in Chapter 3, of 90 mm. However, construction activities and three-dimensional movement at the face invariably gave rise to a larger gap. With reference to Chapter 3, the conservative estimate of the undrained crown displacement was 197 mm. The more probable situation was that three-dimensional deformation occurred at the face, with residual deformation limited by the lining constraint. In this case, the gap parameter would be 156 mm. Because of the variation in construction and soil conditions, a range of gap parameters will be employed for this study.

Belshaw and Palmer (1978) hypothesized that the alignment and construction problems at Array 1 resulted in significant remoulding of the clay. The effect of this process on settlement has been discussed in Chapter 4 and it was shown that additional settlement due to re-consolidation of the remoulded zone may be represented by introducing an additional term, ω_j , to the gap parameter. It was calculated that $\omega_j = 84$ mm in Chapter 4. For the present analysis for long term condition, it is sufficient to take ω_j to be 100 mm.

The effect of grouting was not modelled in this analysis since the procedure was considered ineffective (Belshaw and Palmer, 1978; Palmer and Belshaw, 1980). Ladanyi (1981) has also shown by simple elasto-plastic solution (De Beer, 1964) of a cylindrical cavity that the tail void might be nearly instantaneously closed after the passage of the shield.

Since the surface settlement pins were located at 2 m beneath the surface, the theoretical predictions in this chapter are given at the same depth as the field observations for a direct comparison.

10.3 SELECTION OF DRAINED PARAMETERS FOR ANALYSIS

The soil properties and tables of parameters adopted for the drained analysis of Array 1 and Array 2 are shown in Figures 10.1 and 10.2, based on the data obtained from comprehensive laboratory and field testing programs. Since the test requirements and results of experimental testing have already been described in Chapters 5 to 8, only the important points concerning the selection of parameters will be included in the following discussions.

10.3.1 Description of Soil Stratigraphy

The stratigraphy at Array 1 (Figure 10.1) consists of about 2 m of loose silty sand underlain by 2.8 m of very loose silt, 0.7 m of medium silty sand, 0.7 m of loose silty sand, a 1.3 m clay crust,

4.1 m of silty clay, 0.9 m of a layered clay, and 10.4 m of varved clay extending to bedrock. The clay 'crust' over the tunnel is a stronger clay layer with an OCR of 2 compared with 1.4 of the underlying silty clay. The water table was at a depth of 1.5 m. The tunnel is located in the silty clay and the depth from surface to the centreline of the tunnel is 10.7 m.

The stratigraphy at Array 2 (Figure 10.2) consists of about 1.0 m of peat underlain by 7.2 m of silt and silty sand, then 3.4 m of silty clay, 0.9 m of a layered clay, and 12.0 m of varved clay extending to bedrock. The water table was at a depth of 1.5 m. The tunnel is also located in the silty clay layer. The depth to the centreline of the tunnel is 10.5 m.

10.3.2 Selection of Soil Properties for Analysis of Array 1

10.3.2.1 Sand and Silt

The stratum of silt and silty sand was divided into four sub-layers on the basis of SPT data and soil densities. The uppermost layer with blow counts 'N' of less than 10 blows/300 mm (10 blows/foot) is considered as loose to medium sand. The next layer is a very loose material, 'N' was as low as 0 to 1. Underlying this layer is a medium to dense silty sand, the upper part of this layer may be assumed to be very dense ('N' = 20 to 40).

The friction angle ϕ' adopted for the layers was chosen according to their estimated soil densities and laboratory test results on

reconstituted samples. The lowest friction angle determined was 30° but $\phi' = 25^\circ$ was assumed for the very loose silt because of the difficulties in preparing a very loose sample corresponding to the insitu state. The coefficient of earth pressure at rest K'_0 of these layers was assumed to be given by the equation $K'_0 = (1 - \sin\phi')$.

The vertical modulus in the sublayers was determined from Janbu's Equation (equation 7.1). The parameters required in equation (7.1) were determined from laboratory triaxial test results as discussed in Chapter 7. The moduli given in Figure 10.1 are higher than the moduli normally obtained from conventional triaxial compression tests on sand by a factor of 2. This reflects the effect of stress path in the soil, being closer to triaxial extension than compression. The ratio of 2 was affirmed by CID extension tests on the same sand.

Most natural deposits possess inherent anisotropic structure causing directional variations in deformation and strength characteristics. For natural sands, there is clear evidence (Oda, 1972, 1981; Oda et al., 1978; Arthur and Menzies, 1972) that the modulus ratios E_h/E_v and G_{vh}/E_v are not governed by the isotropic relationships. Therefore, the ratio E_h/E_v for the Thunder Bay Sand is assumed to be 0.8. A previous study reported by Rowe, Lo and Kack (1983) has shown that modest changes in E_h/E_v ratio do not affect the surface settlements so that the uncertainty in E_h/E_v is not of practical significance. However, the ratio of G_{vh}/E_v is of significance to the predicted shape of surface settlement profile and considerable care should be exercised

in its choice. Oda (1981) has examined the anisotropic behaviour of sands by conventional and plane strain shear testing of sands deposited in various orientations. From the stress-strain relationships of uniform, anisotropic Toyoura Sand (with void ratio ranging from 0.65 to 0.69) in loading, the elastic modulus ratio of a typical natural uniform sand can be evaluated as follows:

E_h/E_v	G_{vh}/E_v	(Assumed ν'_{hh})
	0.36	0.1
0.84	0.34	0.2
	0.31	0.3

Based on the above results, it is assumed that the ratio of G_{vh}/E_v of the Thunder Bay silty sand in loading also varies from 0.3 to 0.4. Since the shear modulus G_{vh} of most soils is essentially independent of direction of shear while the unloading modulus is generally higher than the loading modulus for the Thunder Bay sand (see Chapters 7 and 8), the ratio of G_{vh}/E_v was taken to be 0.2 to 0.25 for the analysis. The values adopted in the analysis are consistent with the G_{vh}/E_v ratio of the clay beneath the sand stratum and it is believed that the ratios are representative of the field behaviour.

The values of Poisson's ratio are also shown in Figure 10.1. While ν'_{hh} is an assumed value, ν'_{vh} was determined from drained triaxial compression tests described in Chapter 7. For the soil conditions and geometry of the tunnel in the Thunder Bay case, the maximum settlement is not very sensitive to the Poisson's ratio of the sand

(Rowe, Lo and Kack, 1983).

10.3.2.2 Silty Clay and Varved Clay

The parameters adopted for the silty clay and varved clay were determined from an extensive laboratory testing program including stress path testing as described in Chapters 7 and 8.

The modulus profile in the regions above and below the tunnel is represented by data obtained from CK_0DE triaxial tests. These moduli are consistent with the values obtained from controlled stress path tests. The CK_0DE tests have stress paths approximately corresponding to the actual stress path experienced by the soil in these areas. Near the springline of the tunnel, the stress path is intermediate between triaxial compression and extension and the modulus lies between the compression and extension values. A smooth transition in modulus was adopted between the modulus at the springline region and the modulus at the invert and crown as indicated in Figure 10.1.

The anisotropic parameters and ratios ν_{hh} , ν_{vh} and E_h/E_v above and below the tunnel correspond to the values obtained, under unloading conditions, from special anisotropic parameter tests. These values are consistent with the results from the CK_0DE tests. It should be noted that the Poisson's ratios obtained in unloading and extension for the silty clay are close to 0.45, which is in marked contrast to

the Poisson's ratios obtained in compression ($\nu \sim 0.15$). The ratios ν_{hh} , ν_{vh} and E_h/E_v near the springline correspond to the average of the values obtained in loading and unloading.

The variation of independent shear modulus G_{vh} with depth is shown in Figure 8.24 in Chapter 8. This quantity is not as depth dependent as E_v and consequently the ratio G_{vh}/E_v varies with depth, as indicated in Figure 10.1.

Further consideration of stress paths indicates that it is appropriate to select the drained strength parameters c , ϕ' from the over-consolidated envelopes of the silty clay and varved clay in Chapter 7. The values of K'_0 for the silty clay and varved clay were based on the hydraulic fracturing tests reported in Chapter 6.

One year after tunnel construction, approximately 1 m of fill was placed over Array 1 and the surrounding area. This resulted in at least 35 mm of additional settlement. The stress path within the soil due to the addition of the fill is clearly one of compression. Therefore, in the analysis, the modulus profile and other elastic parameters were selected on the basis of their compressive behaviour (see Chapters 7 and 8). The modulus of the clay was assumed to correspond to the compression profile in Figure 10.1. The shear modulus G_{vh} was as given by Figure 8.24. For the silty clay, E_h/E_v was taken to be 0.8 and $\nu_{vh} = 0.15$. As indicated in Chapter 8, the strength parameters are identical in compression and extension for stress levels below the preconsolidation pressure.

10.3.3 Selection of Soil Properties For Analysis of Array 2

The stratigraphy at Array 1 and Array 2 are related. The sands, silts and clay layers have very similar properties. The silt and silty sand stratum was divided into three sublayers as shown in Figure 10.2. The layers were assigned parameters on the basis of soil densities, laboratory testing and empirical correlations with SPT data. These parameters are consistent with the values adopted in the analysis of Array 1. The properties of the peat were only estimated from empirical correlations and are relatively uncertain. Fortunately, the surface settlement points were located beneath the bottom of the peat layer and the properties of the peat practically have no effect on the results of analysis. The clay layers were assigned extension modulus variation with the appropriate anisotropic parameters consistent with those of Array 1.

10.4 RESULTS OF DRAINED ANALYSIS

In the following discussions, the finite element analytical predictions will be compared with the field observations reported by Belshaw and Palmer (1978); Palmer and Belshaw (1979, 1980). When evaluating the comparisons, the practical limitations of field measurement should be noted. Since all the settlement readings of a cross-section were not taken simultaneously, they were not absolutely consistent in terms of time and distance from the face. Moreover, errors in measurements were possible. Therefore, the synoptic view of the

entire study should be considered rather than making point to point comparisons.

10.4.1 Long Term Surface Settlement

10.4.1.1 Array 1

It has been discussed in Chapter 4 that a portion of the long term settlement at Array 1 was associated with soil volume change due to reconsolidation of remoulded clay. This effect is taken into account by using an additional gap parameter of 100 mm with a total gap parameter of 220 mm. It may be recalled that the estimated deep settlement above the crown due to long term reconsolidation of the remoulded zone is estimated to be 84 mm. For the purpose of analysis, a gap parameter of 100 mm is used.

The computed results are shown in Figure 10.3 together with the results of field measurements taken one year after construction.* Reasonable agreement is obtained between predicted and observed settlement. The observed and predicted trough width to radius ratio (i/a) was 3.4 and 3.1 respectively. It is interesting to note that the volume of surface settlement trough shown in Figure 10.3a is similar to the volume of ground loss calculated geometrically with a gap of 220 mm. The result of this study also indicates that the long term settlements at Array 1 cannot be explained by the dissipation of pore pressure induced by stress relief at the tunnel boundary alone, but the effect of reconsolidation of the remoulded zone should also be taken into account.

* In this and subsequent similar figures, the settlements measured on the two sides of the centreline are shown as two dots connected by a vertical line.

The surface settlement profile after the addition of surcharge was also analyzed. Compressive modulus profile was adopted in this stage of the analysis and a new stiffness matrix was compiled for the soil medium. It may be seen from Figure 10.3 that the agreement between calculated and measured settlement is not unreasonable and the effect of the fill was to increase the surface settlement uniformly.

10.4.1.2 Array 2

The observed long term settlement at Array 2 is shown in Figure 10.4a and the normalized settlement curve is shown in Figure 10.4b. The long term settlement at Array 2 increased only by less than 15% during the first year following construction. The drained analysis predicted a maximum settlement of 58 mm with a gap parameter of 120 mm.* Both the magnitude and shape of the predicted settlement profile are in good agreement with the field observations. The ratio of $i_{\text{predicted}}/i_{\text{observed}}$ is 1.1. A predicted settlement curve with gap parameter = 90 mm (physical gap) is also shown in Figure 10.4a.

10.4.2 Horizontal Displacement Perpendicular to the Tunnel Axis at Array 1

The observed lateral deformations recorded when the tunnel face

* The maximum settlement shown in Figure 7 of Palmer and Belshaw (1980) was 58 mm measured at 11 months after construction. A larger gap parameter of 130 mm would be needed to predict this magnitude of displacement.

was 20 m away from the slope indicators are shown in Figure 10.5. Readings obtained about 138 days later were similar. The maximum movement was 32 mm. The predicted lateral displacement profiles are also shown on the same figure. These calculated results closely followed the trend of the measured displacements though the magnitude of movement was overestimated. Nevertheless, the results should be considered compatible. Both the observed and predicted displacements indicate that maximum lateral soil deformation occurred close to the springline. Below the springline, soil displacement decreases very rapidly.

10.4.3 Distribution of Subsurface Settlements at Array 2

Studies on subsidence due to tunnelling have mainly concentrated on the surface settlements. However, soil movements below the surface are also important because they affect subsurface structures such as pile foundations, existing sewers and subways. Since the finite element analysis can be used to calculate the displacement at any nodal points in the element mesh, both the surface and subsurface displacement vectors can be obtained in the same analysis. Measured displacement vectors in a vertical plane perpendicular to the tunnel axis reported by Palmer and Belshaw (1980) are shown as solid arrows in Figure 10.6. The predicted displacement vectors, calculated by the drained analysis, were superimposed on the figure as dotted-line arrows. Since the displacements below the springline were small, they were

omitted from the figure for the sake of clarity. The pattern of soil movements suggests that the soil displaced towards the tunnel as if it was a source of ground loss. It may be seen that both the magnitude and direction of the calculated and measured displacements generally agree fairly well. Better comparison is obtained between predicted and observed displacement in areas away from the tunnel. This could be attributed to the effect of construction such as liner-wedging on the soil, grouting, or machine motion etc. However, these disturbances were apparently localized without affecting the overall pattern.

10.5 SELECTION OF UNDRAINED PARAMETERS FOR ANALYSIS

The definition of 'undrained analysis' is rather ambiguous when applied to the case of Thunder Bay soil stratigraphy. While the clay layer may remain undrained, the overlying sand was in a drained condition. Nevertheless, the settlement behaviour was mainly influenced by the clay layer where the tunnel was located. Thus, the term 'undrained settlement' may still be used to describe the short term movements since the clay was 'undrained'. When drained and undrained responses are considered simultaneously in an analysis, the total stress approach is appropriate. (It may be recalled that the incremental effective stresses in a sand element equal the incremental total stresses.) The parameters adopted for sand in the previous discussions can also be used in the 'undrained' settlement prediction.

In the undrained condition, the plasticity parameter for clays

used is $\phi = 0$ and the undrained shear strength c_u . From results of CIU tests on vertical and horizontal samples, the ratio of $c_{u,H}/c_{u,V}$ is 0.84. The field vane strengths corresponded to the horizontal shear strengths $c_{u,H}$ (Lo, 1965). For the purpose of constructing a simplified undrained strength variation with depth, the vertical undrained strength in CIU compression was adopted. The effect of undrained strength anisotropy exhibited by the clay is then examined by performing analysis using the vertical and horizontal strengths.

Since the extension drained and undrained elastic vertical moduli obtained in the triaxial tests are similar (see Chapter 8), the undrained modulus profile adopted in the undrained analysis is similar to that shown in Figure 10.1 with the exception of the modulus at the springline region. In this area, compressive behaviour dominates and the undrained modulus determined from stress path test is greater than the drained modulus. An interesting phenomenon displayed by the clay was the apparent isotropy in undrained deformation response in CIU compression test so that the E_v/E_h ratio was taken to be one. The shear modulus, G_{vh} is similar in drained and undrained condition of the clay and the shear modulus values used in the drained analysis are also appropriate for the undrained analysis. The Poisson's ratio of 0.48 was used instead of the theoretical ratio of 0.5 to avoid the problem of numerical instability in computation.

10.6 RESULTS OF UNDRAINED ANALYSIS

10.6.1 Centreline Settlement

The observed centreline surface settlements along the arrays were not constant. The magnitude of the average of settlements at Array 1 was 1.34 times the average of settlements at Array 2 at the end of construction. The reported data of Palmer and Belshaw (1979) are summarized in the following table:

OBSERVED MAXIMUM SETTLEMENT (IN mm) AT THE END OF CONSTRUCTION*

Location	Average	Range	At Nominal Centre (Mid-Section)	Exceptionally Large Measurement
Array 1	59	51 to 64	56	76
Array 2	44	37 to 47	54	54

The relationship between the maximum surface settlement and the gap parameter adopted in the finite element prediction is shown in Figure 10.8. It is evident that the maximum settlement increases with increasing gap parameter. The results for Array 1 and Array 2 were combined in the same plot because relatively little difference is obtained when the identical gap parameter is adopted.

* These measurements are slightly larger than the undrained settlements.

The relationship between S_s^* and G , as shown in Figure 10.8 is linear (or only very weakly nonlinear) for the range of gap parameters investigated. This is a clear indication that, at moderate or acceptable level of ground loss during tunnelling, in which the soil deformations are controlled by the construction procedures, the ratio of S_s/G is a constant for a particular tunnelling situation. The ratio of S_s/G , calculated from the slope of the line in Figure 10.8, is 0.42. The gap parameter shown in the figure has excluded the component of crown displacement due to lining deformation. When this additional component of gap is considered, the ratio of S_s/G will be slightly modified.

It has been discussed in Chapter 3 that the upper bound gap parameter was calculated to be 197 mm. This value of gap will give rise to 85 mm of surface settlement and it is clearly a reasonable and yet not overly-conservative calculation when compared to the largest settlement of 76 mm recorded. In Chapter 3, the likely gap is 156 mm and this value is calculated from a consideration of three-dimensional movement and closure of the physical gap. The calculated settlement associated with this gap parameter is 65 mm and it is consistent with the range of settlements at Array 1 (51 to 64 mm).

* S_s is given at 2 m below the ground surface in this study; therefore, S_s/G ratio calculated in this chapter will be slightly higher than the true S_s/G ratio.

The comparison with Array 2 data (37 mm to 47 mm) is also reasonable but represents a slight overestimate of the field measurements. The overestimation of the gap at Array 2 is possibly due to the relatively small three-dimensional face movement as indicated in Figures 9.7 and 9.14 of Chapter 9. It is interesting to note that the smallest settlement (37 mm) may be obtained with a minimum gap parameter equal to the physical gap of 90 mm (see Figure 10.8.)

10.6.2 Distribution of Surface Settlement

The predicted surface settlement profiles at Array 1 and Array 2 are shown together with the observed settlements in Figures 10.9a and 10.10a respectively. The normalized shape of the curves, obtained by dividing the settlements by the centreline settlement, are shown in Figures 10.9b and 10.10b.

It may be seen from Figures 10.9a and 10.10a that the maximum settlements at these two sections are underestimated by adopting a gap parameter of 90 mm. The settlement curves with the correct centreline settlements are in good agreement with the observed settlements and they have the appearance of an error function. The shape of the surface settlement profiles are rather narrow, with Array 2 having a slightly narrower trough shape than Array 1. Using the terminology of Peck (1969), the observed and predicted data may be tabulated as follows:

OBSERVED AND PREDICTED TROUGH WIDTHS

Location	Observed i/a	Predicted i/a	$\frac{i_{pred.}}{i_{obs.}}$
Array 1	2.7*	3.0	1.1
Array 2	2.4	2.7	1.1

The above results of undrained settlement prediction have been based on the use of the vertical shear strength profile. With the adoption of the vane strength, or horizontal shear strength in the analysis, the predicted width of settlement trough would be wider by 15%. However, the change in predicted maximum settlement is minor. It is observed that an increase in plastic zone near the springline occurred when the vane strength profile is adopted and this led to a wider surface settlement trough.

The plots of normalized settlements (Figures 10.9b and 10.10b) are of particular interest because the shape of curves associated with moderate ground loss does not vary significantly with the gap parameter. The normalized curves determined by assuming gap parameters of 90 mm and 120 mm in Figures 10.9a and 10.9b respectively are almost identical, as in the case of drained analysis.

* Belshaw and Palmer reported that $i/a = 3.4$. However, by fitting a Gaussian curve to the data in Figure 10.9b, i/a is found to be 2.7.

A comparison of Figure 10.4 and Figure 10.10 shows that only a 4 mm increase in maximum settlement in the drained analysis is obtained in the analysis with gap parameter of 120 mm. Both the shape of the drained and undrained surface settlement profiles are very similar. The theoretical predictions clearly indicate that the drained (long term) and undrained settlement behaviour due to tunnelling are similar, which is consistent with the observations at Array 2 as well as other case histories of tunnelling in clays, unless significant remoulding of soil leading to large reconsolidation deformation has occurred.

10.7 LINING DEFORMATION

Although the study of lining behaviour is beyond the scope of this thesis, it is an interesting topic to be included in the discussions.

At Array 1, the observed lining closure was initially -1.4% laterally and -0.4% vertically. The tunnel had 'tended to squat somewhat' with the vertical diameter decreased by 3 mm one year after construction (Belshaw and Palmer, 1978). The record of lining deformation at Array 2 was neither clear nor complete. From data obtained in the Dodds and Morton Report (1976), it was estimated that the vertical diameter might have decreased by 10 to 20 mm within a month after construction.

The 'flexible' segmented concrete liner used in the Thunder Bay Project was equipped with joints and crack inducers. The exact

stiffnesses at these locations were not known precisely but it is apparent that they were capable of sustaining some residual moments. The analysis modelled the lining by reducing the stiffness of the appropriate beam elements by a factor of 100. From the undrained analysis of Array 1, the predicted lining closures were -0.6% in both vertical and horizontal directions. (The observed and predicted lining closure in both the vertical and horizontal directions is an interesting and uncommon phenomenon.) At Array 2, an increase of (+)1.4% in horizontal diameter and a decrease of (-)1.4% in the vertical diameter was predicted. The trend of predicted deformations is consistent with the field observations. However, the predicted liner behaviour may depend on the lining stiffness given a fixed soil profile. The uncertainty of the assumed 'hinge' stiffness could be a source of error in calculating the lining deformations and soil displacements near the tunnel. In reality, the stiffness of the 'hinges' was not constant and may increase with time as the liner ring was being loaded and the cracks and joints were put into compression.

It is interesting to note from the predicted and observed lining behaviour at Array 1 that the mode of deformation is not the expected character of a uniform circular tunnel in elastic ground with $K_0 < 1$. This phenomenon suggests that plasticity within the soil mass also plays an important role in determining liner deformations.

10.8 VARIATION OF CENTRELINE SETTLEMENT WITH DEPTH ABOVE THE TUNNEL

The observed and predicted centreline settlements with depth above the tunnel at Array 1 are plotted in Figure 10.11a. The observed long term distribution of settlement is not shown because the

data were not reported. From the figure, it may be seen that the predicted and observed results are in good agreement. A comparison of the undrained distribution of settlement with the predicted long term settlement distribution indicates that a large increase in settlement occurred near the crown. The additional long term settlement became progressively smaller towards the surface and it would appear that the sand layer and the upper part of the clay layer have settled due to the large consolidation settlement above the crown.

In Figure 10.11b, the observed and predicted drained and undrained settlement distributions at Array 2 are shown. The trend of the measured variation of settlements with depth was correctly predicted but perfect agreement was not obtained between the observed and predicted settlements measured within a length of two tunnel-radius from the crown. The discrepancy may be due to an overestimation of the strength of sand immediately above the clay cover adopted in the analysis. Lowering the friction angle of the sand would lead to increased plastic deformation in this region. It should be noted that the clay above the crown has already become plastic, therefore decreasing the shear strength of clay above the crown would not necessarily result in significant increase in displacement. Alternatively, there could be inaccuracy in the extensometer readings since the measured settlements are nearly the same at 7.6 m and 8.2 m depths.

From Figures 10.11a and 10.11b, it may be seen that the variations of settlement with depth in the two arrays were not identical.

At Array 1, the settlement distribution was approximately linear from the surface down to about 7 m to 8 m below the surface before the settlement increased rapidly towards the tunnel crown. On the other hand, the relatively linear settlement distribution at Array 2 was sustained only to 5 m or 6 m below the surface. The rapid rate of increase of settlements reveals plastic soil response. The difference in behaviour of settlement variations near the crown of the tunnel at the arrays was probably due to the difference in stratigraphy as a thicker clay cover exists at Array 1 in place of loose sands at Array 2. It may be noted that the change in the settlement-depth relationship from approximately linear to rapid increase of settlement near the crown corresponds to the plastic radius at the crown for both Array 1 and Array 2.

10.9 SUMMARY OF COMPARISON BETWEEN RESULTS OF FIELD MEASUREMENTS AND ANALYSIS

In this chapter, the results of calculated displacements are compared with the results of field observations for Array 1 and Array 2 of the Thunder Bay Tunnel. In this case record, the soil stratigraphy, as well as the geometry of the machine-lining system are well defined. This method of analysis takes into account the simulation of construction activities and the elasto-plastic soil response. In the selection of soil parameters for the analysis, careful consideration was given to the important effects of anisotropy in elastic deformation and the stress paths followed by the soil. Since the

soil parameters were appropriately determined by a comprehensive testing program, the input data for the analysis is believed to be representative of the field soil behaviour. From the results of this study, the following conclusions can be made:

1. The calculated maximum surface settlement was found to be increasing almost linearly with increasing gap parameter for the range of values from 90 mm to 200 mm. The minimum and maximum values of gap parameter represent respectively the physical gap size and the displacement associated with exceptionally poor workmanship. Since the values of surface settlement computed with this range of gap parameters agree with the magnitudes of settlement observed along the two arrays, the longitudinal variation of surface settlements may be attributed, at least in part, to the variation of gap resulting from the difference in construction conditions at various locations.
2. The effect of reconsolidation of the remoulded zone around the tunnel at Array 1 was modelled approximately by an increase in the magnitude of the gap parameter in the drained analysis. This additional component of gap, determined from the consideration of one-dimensional consolidation theory, was taken to be 100 mm. Using this approximation, reasonable agreement was obtained between observed and predicted magnitude and distribution of long term surface settlements.
3. The calculated shape of the surface settlement profile resembles

a Gaussian distribution curve and is relatively independent of the range of values of gap used in the analysis performed. The calculated drained and undrained trough shapes and hence trough widths (for gap of 120 mm) are in good agreement with the corresponding field measurements at both arrays.

4. The comparison of the calculated distributions of centreline settlements with depth with the field observed settlements gives good agreement for both Array 1 and Array 2. The centreline settlement curve is characterized by two recognizable trends of soil behaviour. The slope of the curve is approximately linear, showing moderate increase in settlement from the surface towards the crown in elastic ground. In the region above the crown, the rate of settlement increase becomes very rapid, corresponding approximately to the plastic zone determined in the analysis for each array.
5. Both the observed slope indicator data and calculated horizontal displacements for Array 1 indicate that maximum lateral displacement occurs at the springline level. The calculated profile of horizontal displacements compares reasonably well with the observed data.
6. Apart from minor differences in details, the calculated pattern of soil displacement vectors in a plane perpendicular to the tunnel is in good agreement with the observed soil displacements. All the displacement vectors were directed towards the tunnel

as if it were a source of ground loss, and displacements above the springline were considerably larger than those beneath it.

It is evident, therefore, that reasonable agreement has been obtained between the overall pattern of observed and calculated soil displacements in terms of the magnitude and distribution of surface settlement, variations of vertical and horizontal displacement with depth, as well as the distribution of subsurface displacement vectors. The study has therefore demonstrated the applicability and capability of the method developed in determining the overall pattern and magnitude of soil movements due to tunnelling. The results of such detailed analysis are clearly of value to the Engineer in the design of a tunnel, particularly for the critical sections in a project.

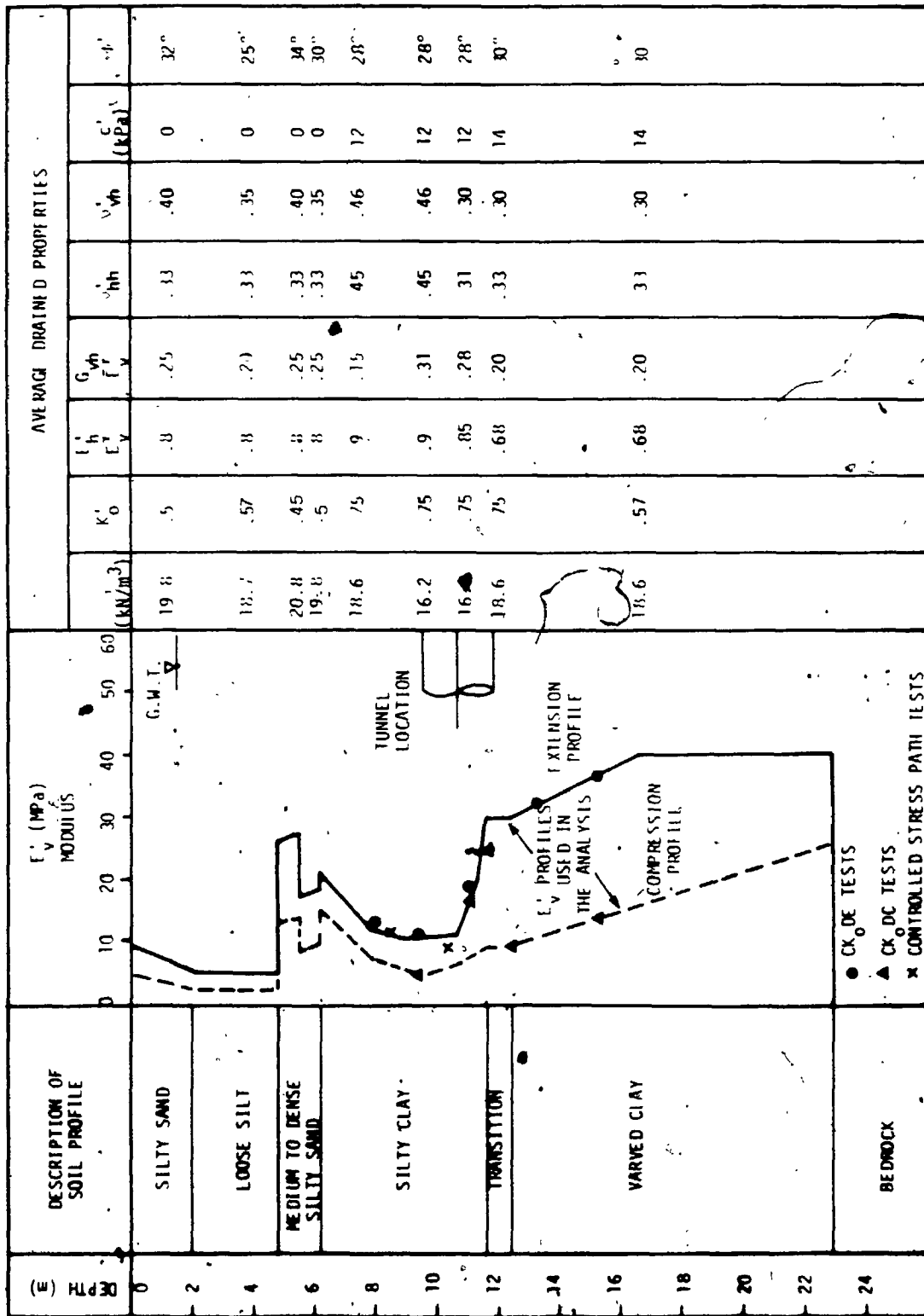


FIGURE 10.1 SOIL PROFILE ADOPTED IN THE ANALYSIS OF ARRAY 1

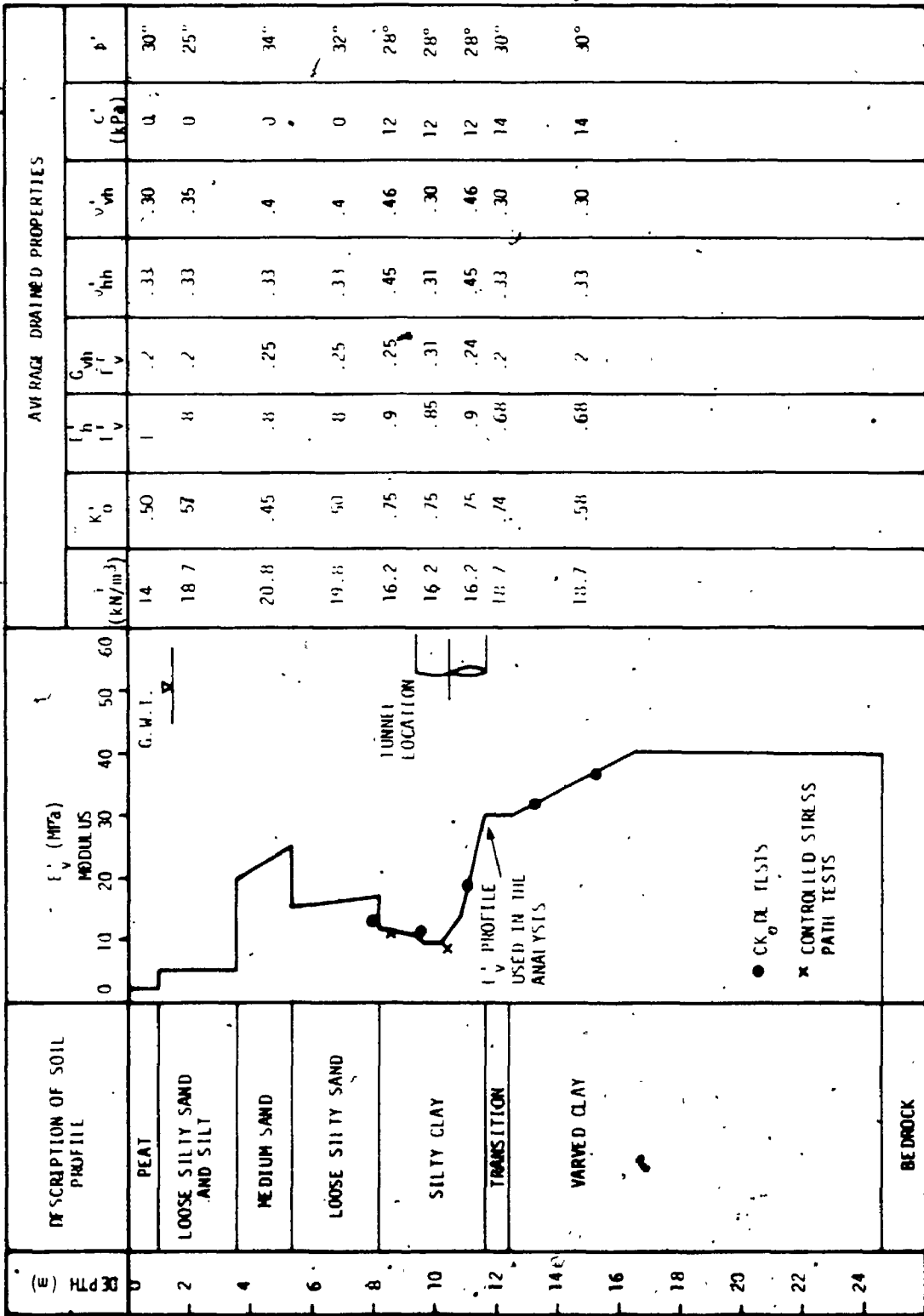


FIGURE 10.2 SOIL PROFILE ADOPTED IN THE ANALYSIS OF ARRAY 2

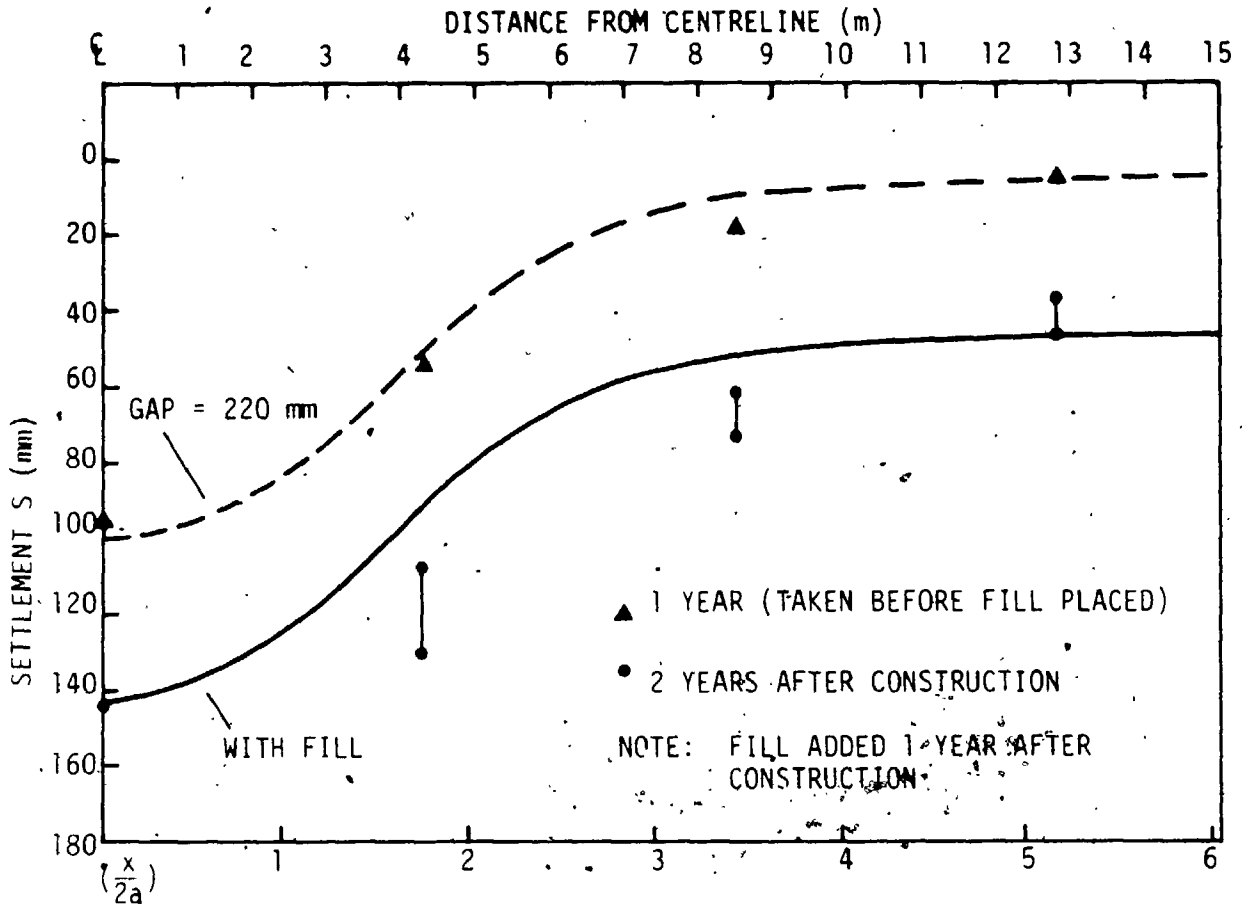


FIGURE 10.3a OBSERVED AND CALCULATED LONG TERM SURFACE SETTLEMENT PROFILE AT ARRAY 1

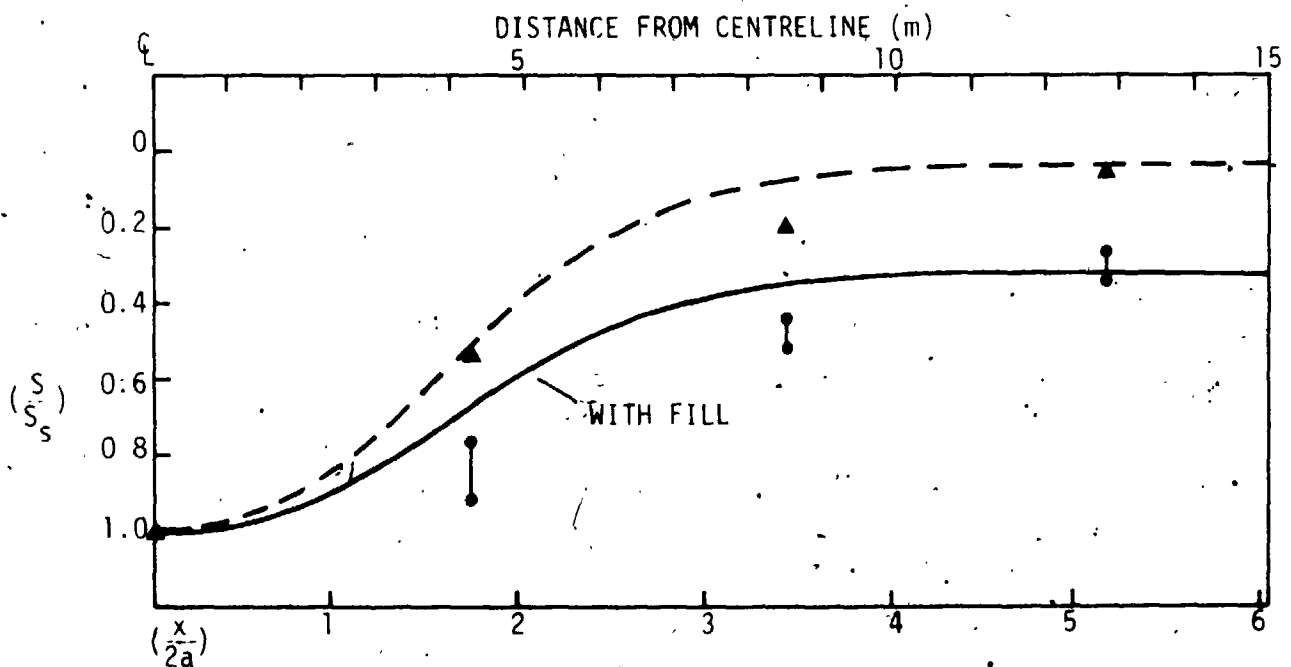


FIGURE 10.3b OBSERVED AND CALCULATED LONG TERM NORMALIZED SURFACE SETTLEMENT PROFILE AT ARRAY 1

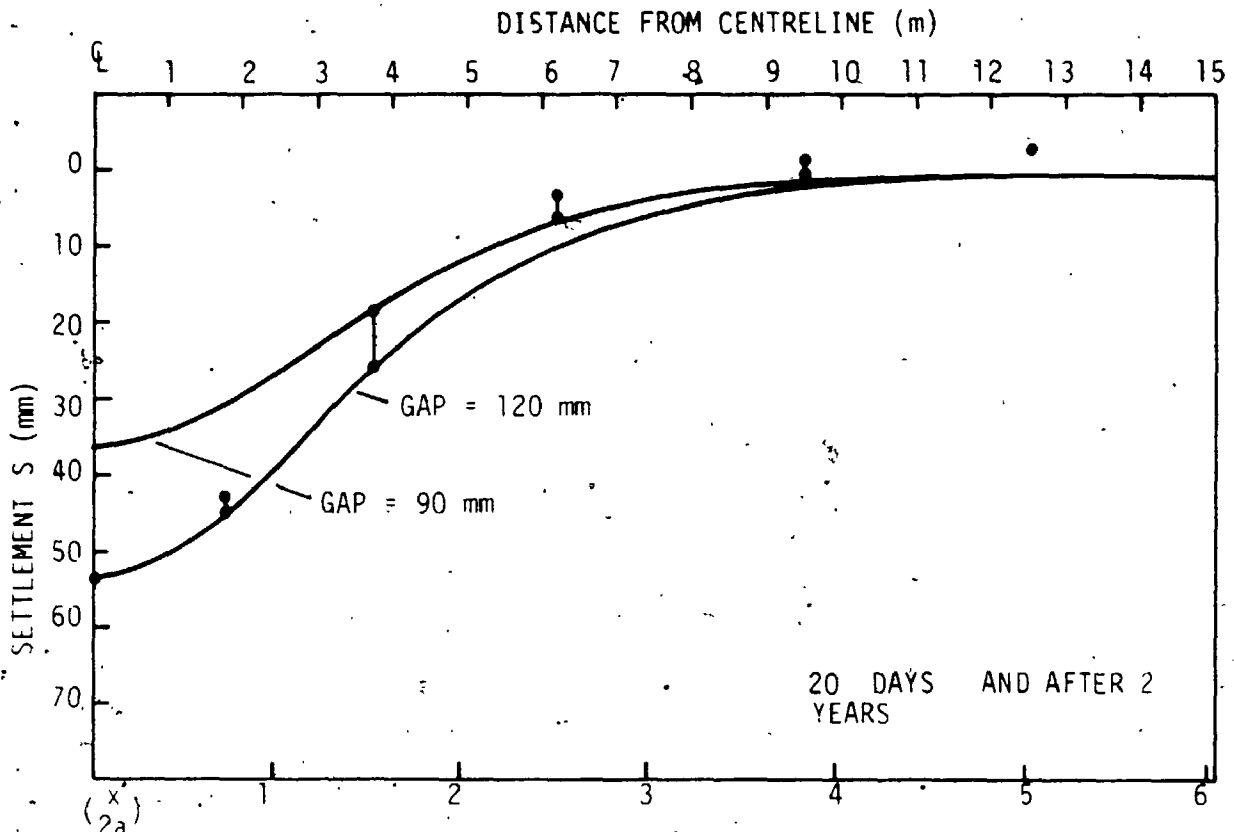


FIGURE 10.4a OBSERVED AND CALCULATED LONG TERM SURFACE SETTLEMENT PROFILE AT ARRAY 2

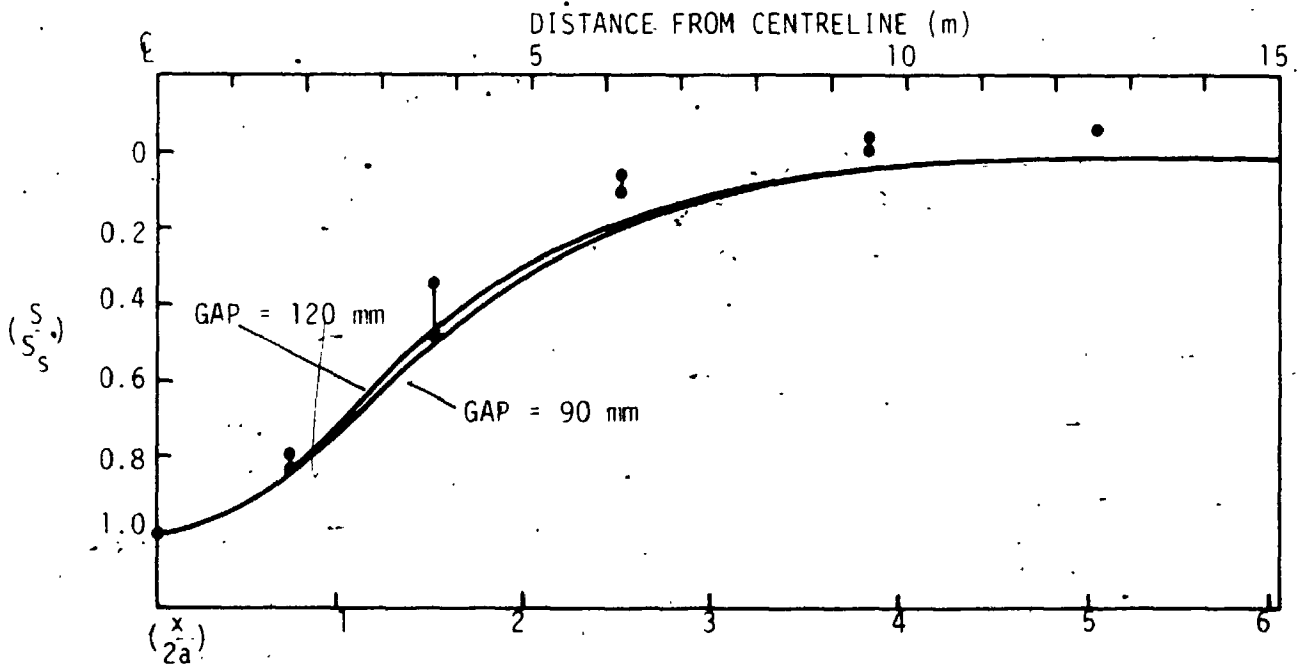


FIGURE 10.4b OBSERVED AND CALCULATED LONG TERM NORMALIZED SURFACE SETTLEMENT PROFILE AT ARRAY 2

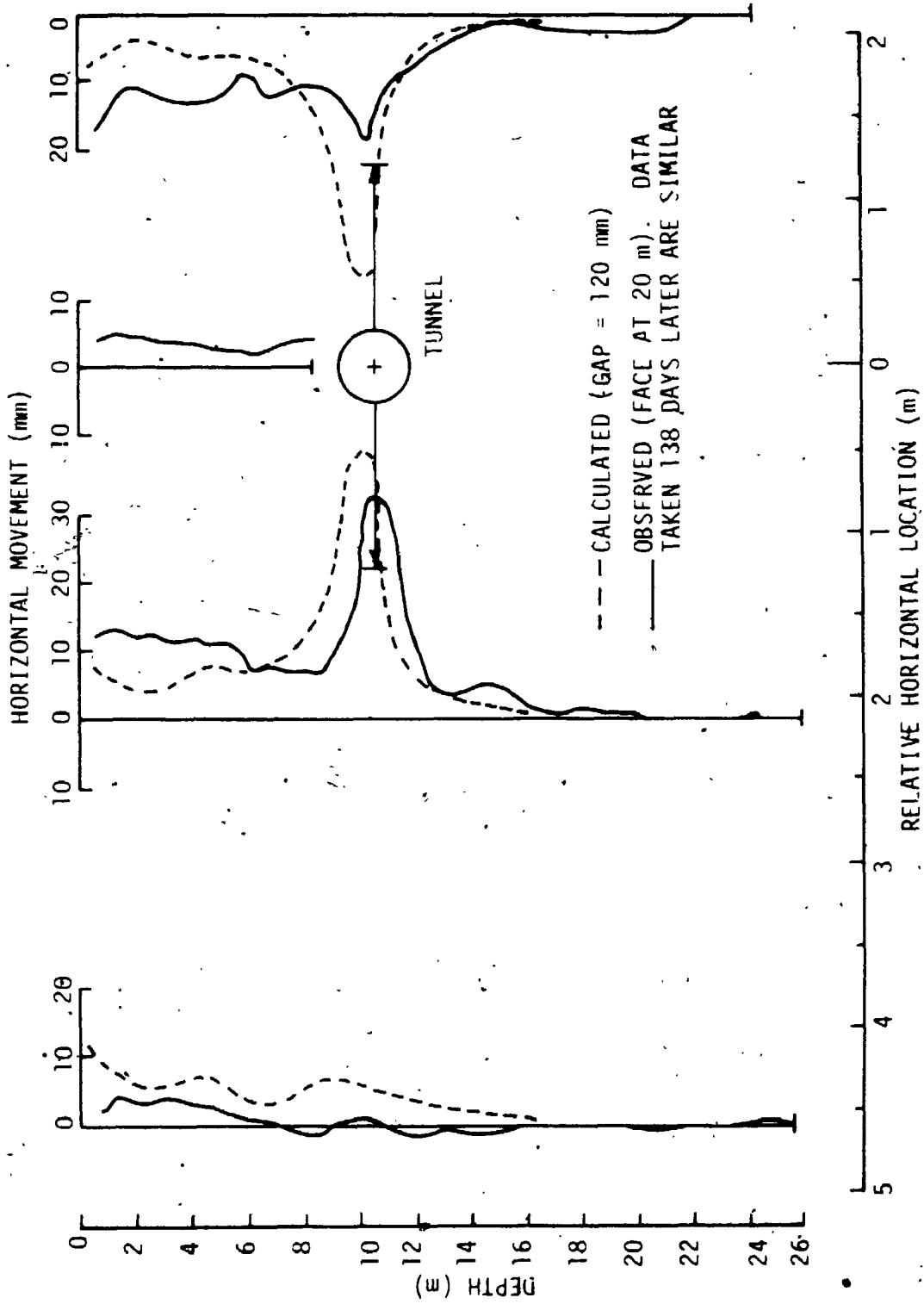
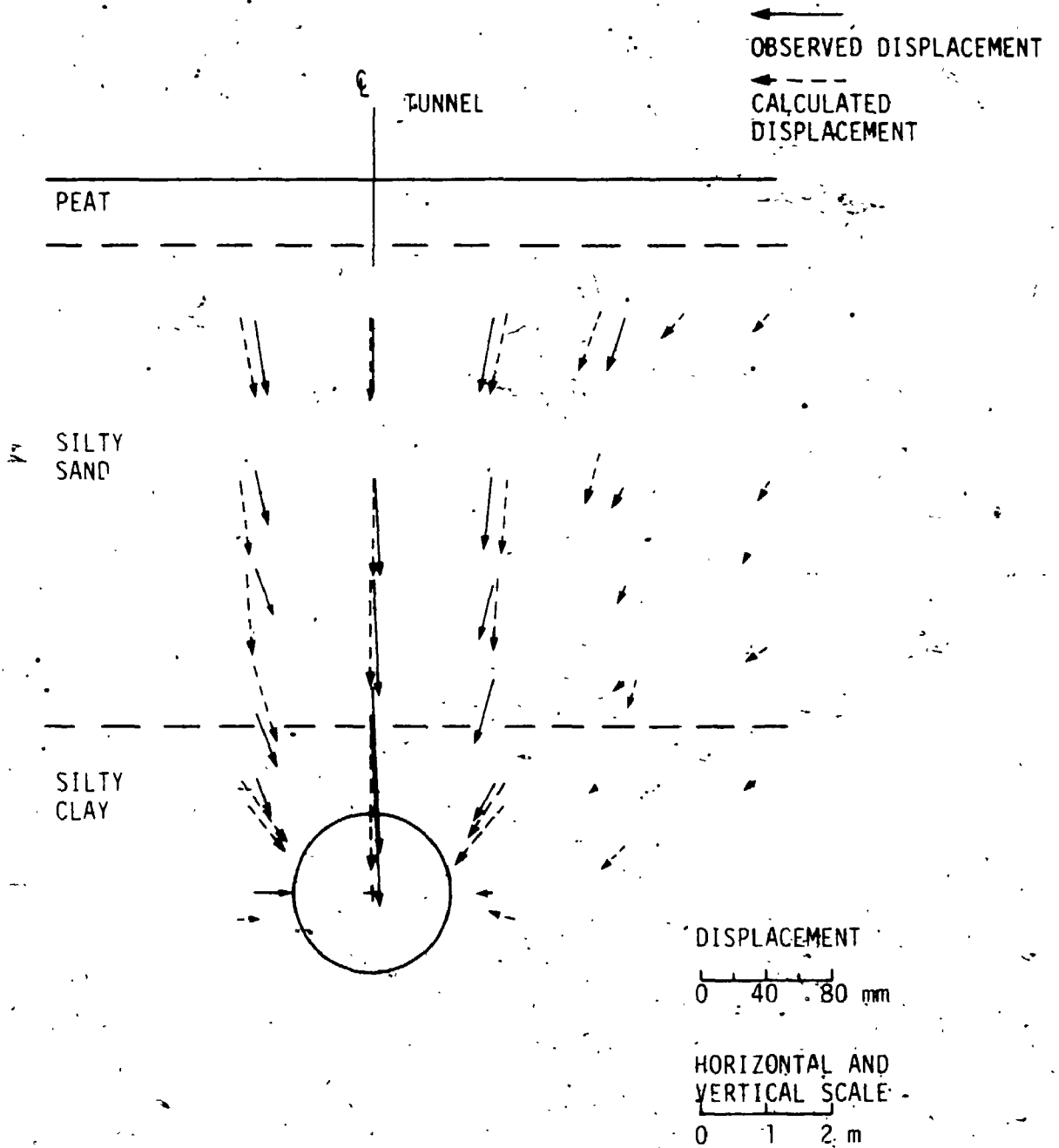


FIGURE 10.5 COMPARISON OF OBSERVED SLOPE INDICATOR DATA PERPENDICULAR TO TUNNEL AXIS WITH CALCULATED DATA (ARRAY 1)



NOTE: DISPLACEMENTS BELOW SPRINGLINE ARE NOT SHOWN

FIGURE 10.6 DISPLACEMENT VECTORS IN VERTICAL PLANE PERPENDICULAR TO TUNNEL AXIS (20 DAYS) AT ARRAY 2

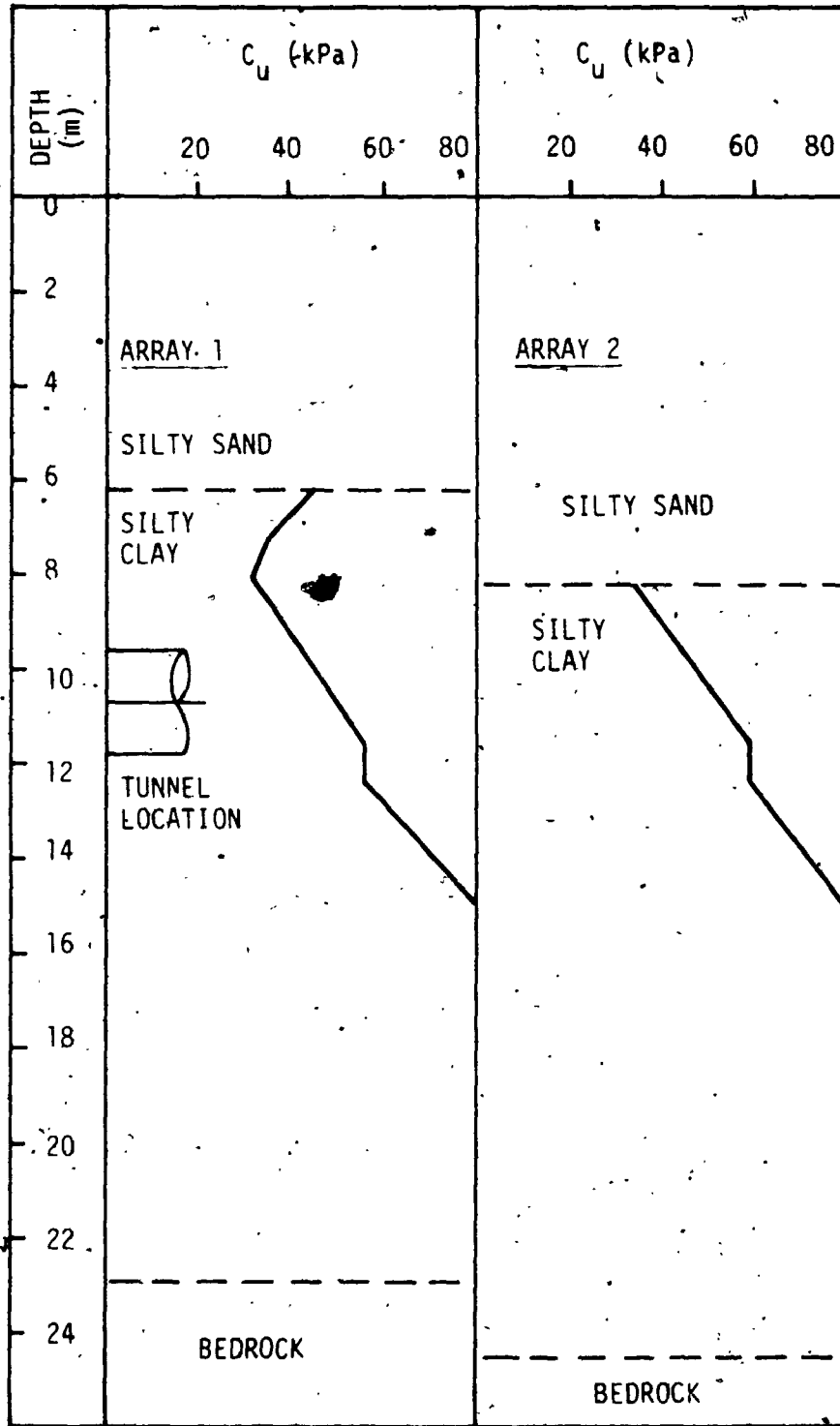


FIGURE 10.7. UNDRAINED STRENGTH PROFILE FOR UNDRAINED ANALYSIS

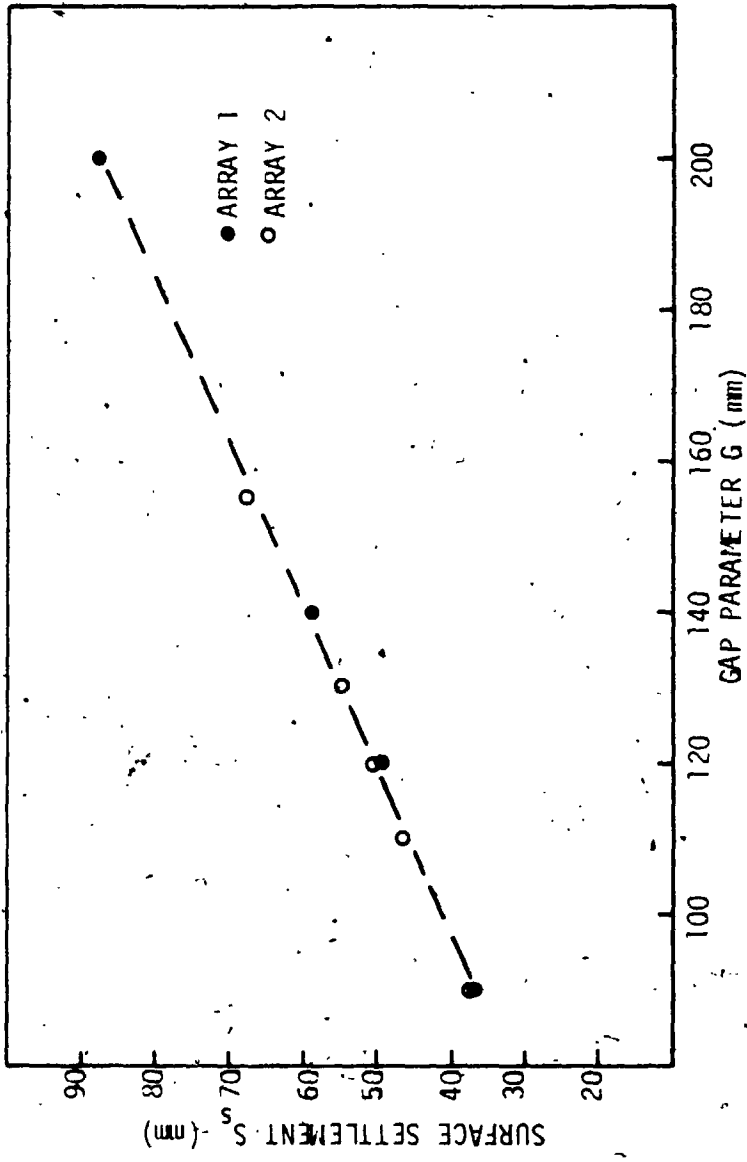


FIGURE 10.8 RELATIONSHIP BETWEEN S_s AND G CALCULATED BY THE FINITE FILAMENT ANALYSIS

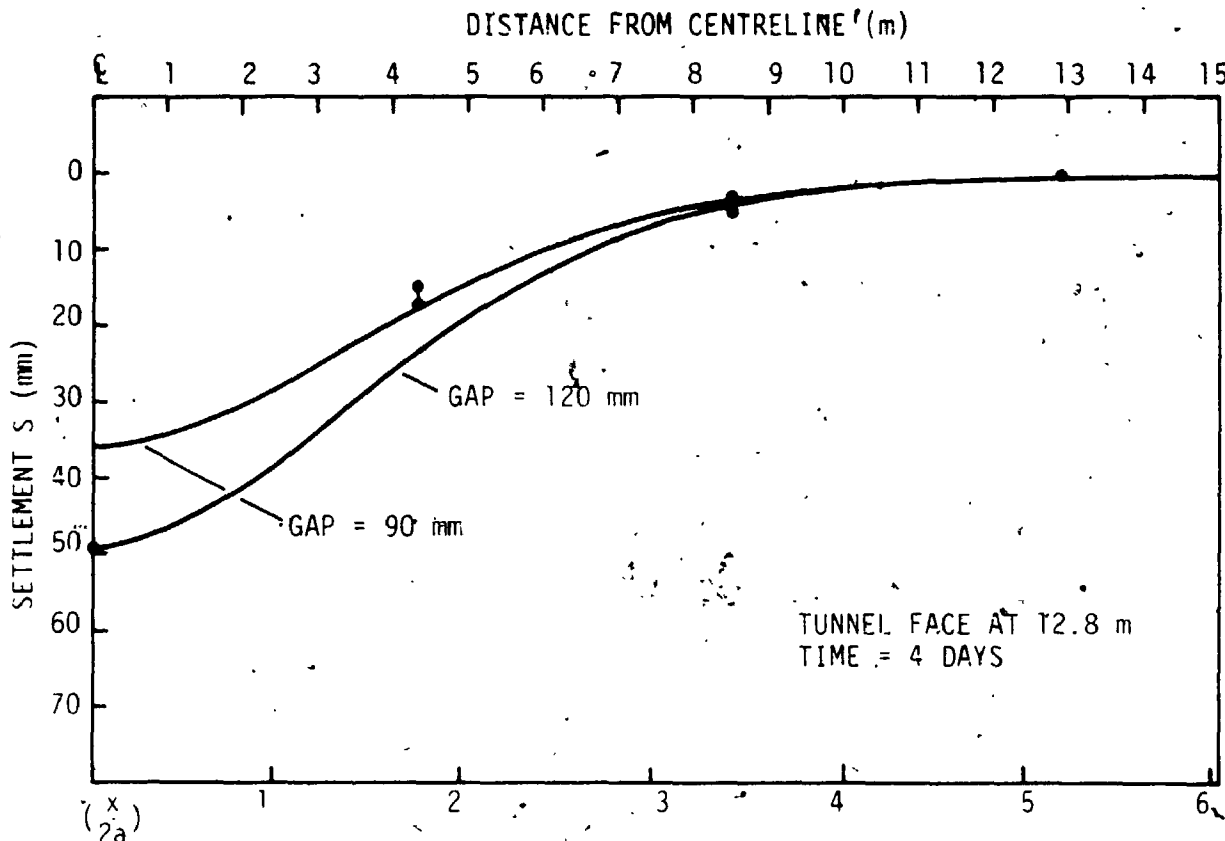


FIGURE 10.9a OBSERVED AND CALCULATED SURFACE SETTLEMENT PROFILE AT ARRAY 1 - UNDRAINED CONDITION

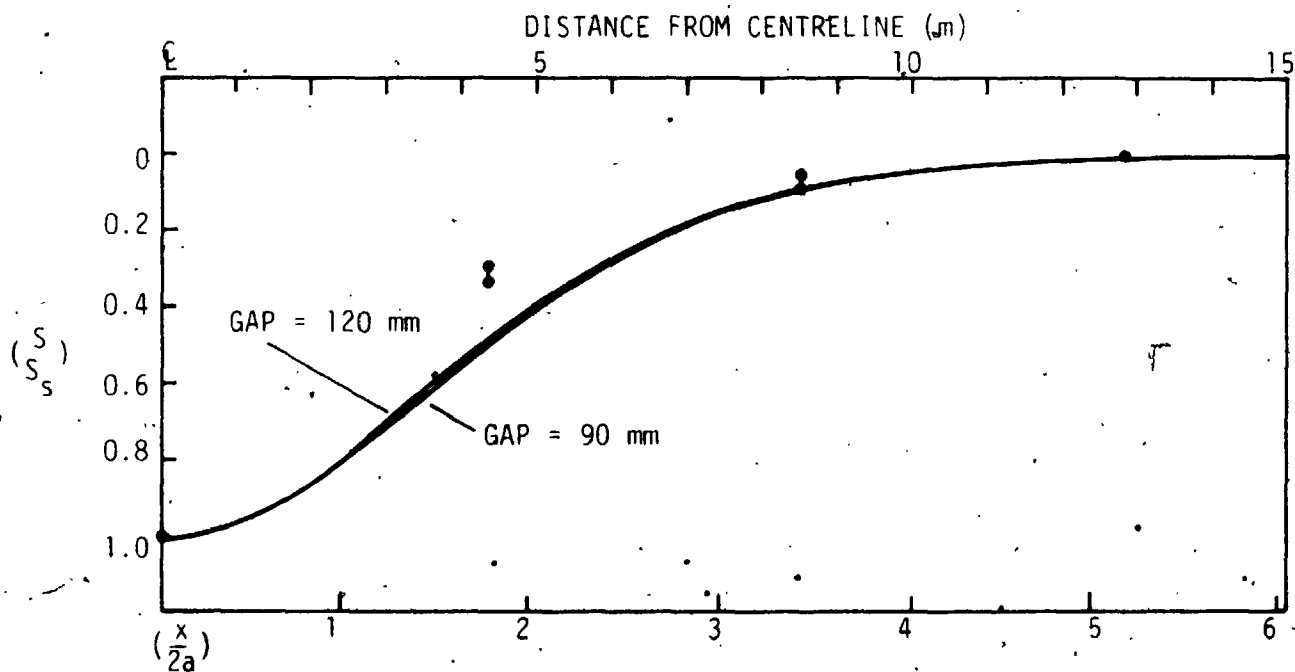


FIGURE 10.9b OBSERVED AND CALCULATED NORMALIZED SURFACE SETTLEMENT PROFILE AT ARRAY 1 - UNDRAINED CONDITION

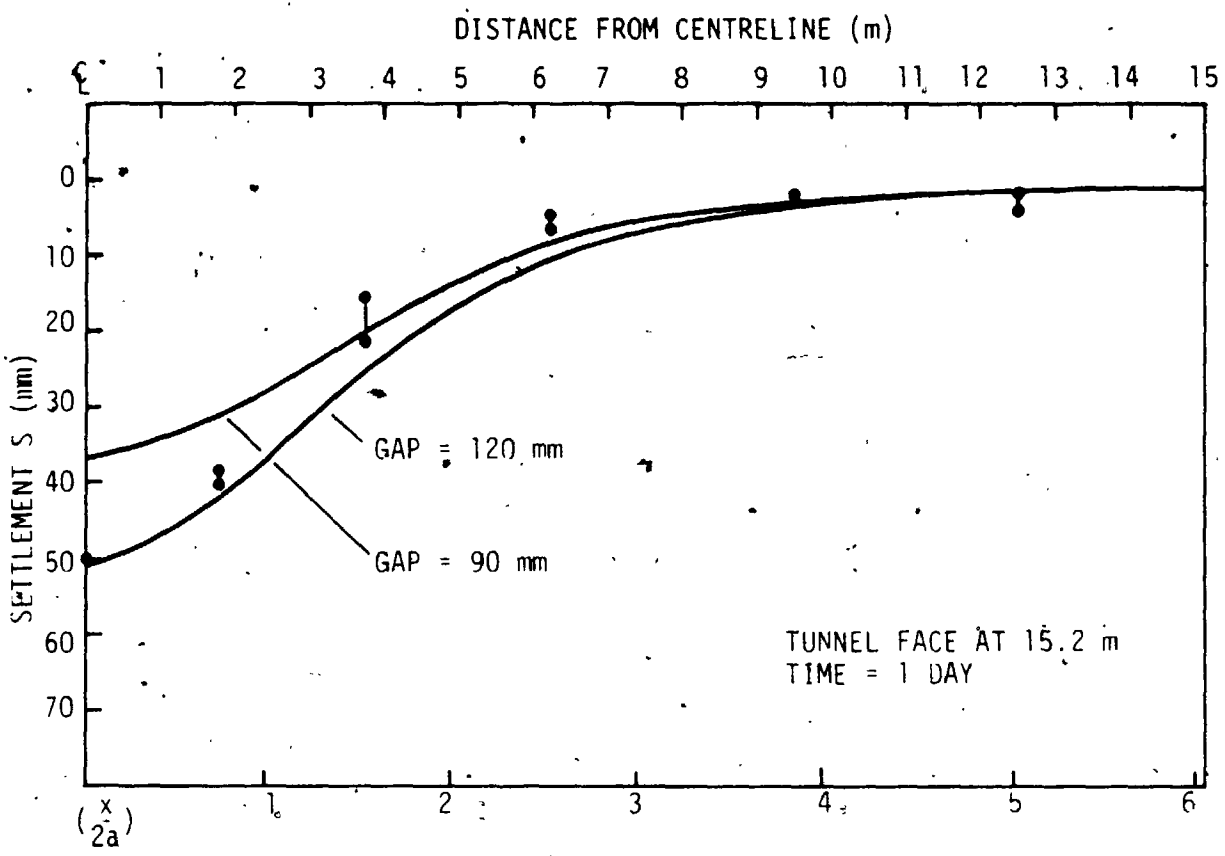


FIGURE 10.10a OBSERVED AND CALCULATED SURFACE SETTLEMENT PROFILE AT ARRAY 2 - UNDRAINED CONDITION

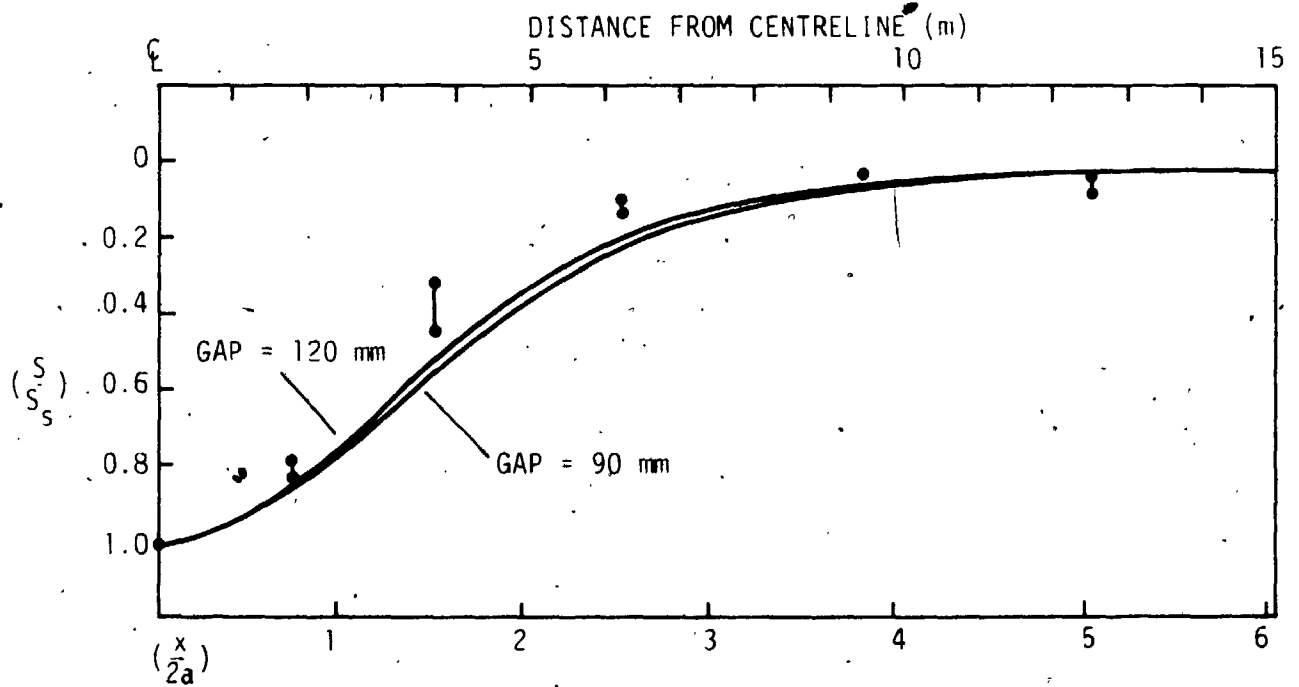


FIGURE 10.10b OBSERVED AND CALCULATED NORMALIZED SURFACE SETTLEMENT PROFILE AT ARRAY 2 - UNDRAINED CONDITION

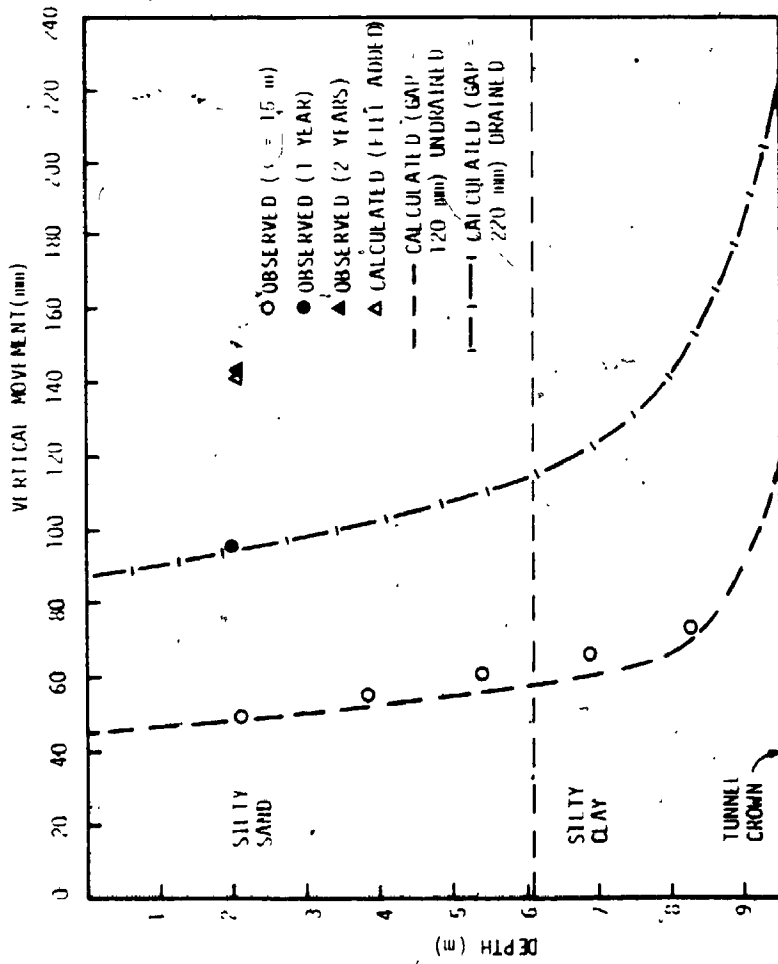


FIGURE 10.11a COMPARISON OF CALCULATED AND OBSERVED SETTLEMENT VARIATION WITH DEPTH ABOVE THE TUNNEL AXIS AT ARRAY 1

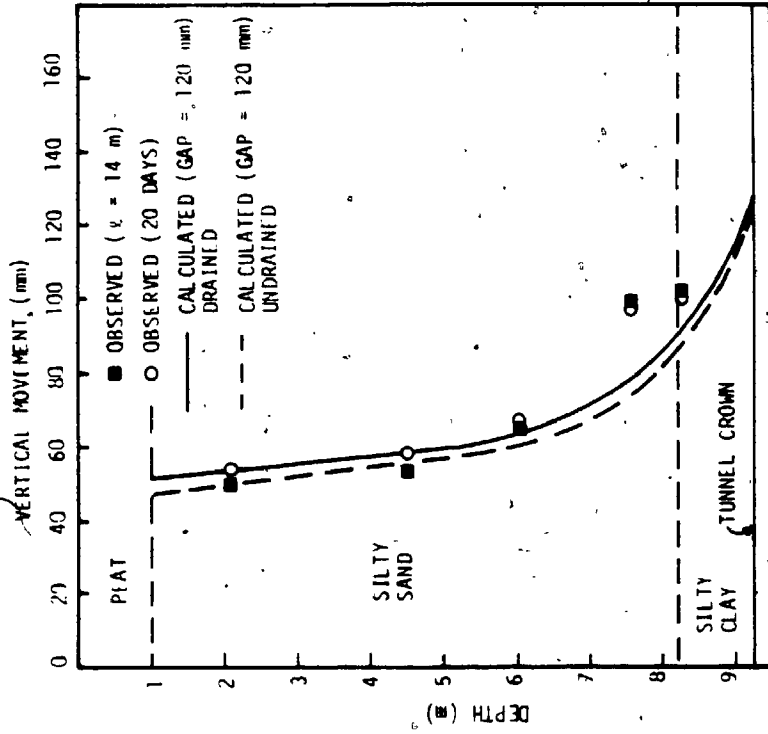


FIGURE 10.11b COMPARISON OF CALCULATED AND OBSERVED SETTLEMENT VARIATION WITH DEPTH ABOVE THE TUNNEL AXIS AT ARRAY 2

CHAPTER 11
SUMMARY, CONCLUSIONS AND RECOMMENDATIONS FOR
FURTHER RESEARCH

11.1 SUMMARY AND CONCLUSIONS

An extensive study on the prediction of ground response and soil displacement induced by tunnelling in soft clays has been performed. The research performed is centred around three main areas: fundamental concepts and methodology for analysis, results of experimental study, and detailed analysis of the comprehensive case record of the Thunder Bay Tunnel.

In the first part of the thesis, the methods of predicting ground movements are reviewed together with an assessment of the reliability of different approaches of prediction. By identifying the mechanisms governing settlement above tunnels, a consistent method of estimating the 'gap parameter' and surface settlement is developed for preliminary design purposes. The methodology for a detailed analysis, particularly suitable for design of critical sections of a tunnel is established. This method employs a finite element formulation which adopts an anisotropic elasto-plastic soil model, with consideration of the effect of excavation procedure, machine-liner geometry and soil-liner interaction. The significant difference between stress paths employed in conventional testing and those followed by the soil in the excavation process is pointed out. This part of the thesis, therefore, constitutes

the fundamental theoretical framework for analyses and test requirements for determining soil behaviour in tunnelling.

In the second part of the thesis, the procedure and results of a comprehensive program of laboratory and field investigation of soil properties are described. The field measurements include the determination of vane strength, groundwater and insitu stress condition. For the laboratory testing, particular attention is paid to the effects of anisotropy in elastic deformation and the stress paths followed by the soil in the field. The conventional and special tests carried out are described. The oedometer tests, simple shear tests, conventional triaxial tests, and anisotropic parameter tests are some of the soil testing performed to evaluate the appropriate soil properties. The experimental results obtained and the soil stratigraphy defined are then employed in the analytical procedure for displacement prediction.

The displacement behaviour of the Thunder Bay Tunnel is presented in the final part of the thesis. The comprehensive program of field instrumentation has been monitored over a two year period. It provides, therefore, a rather detailed source of undrained and drained settlement data for a comparative study of calculated and observed settlements. The analysis is performed using the method developed, and careful consideration is given to the selection of input soil data to the analysis. The results of the analysis are compared with the field observations to ascertain the validity and usefulness of the proposed method of predicting settlement.

The main conclusions obtained from this study are summarized below.

I) Conclusions obtained from the approximate elastic-plastic solution and analysis of case histories:

a) Loss of ground which controls the magnitude and distribution of settlements can be quantified by a gap parameter. The components of the gap parameter are i) the three-dimensional crown displacement at the advancing face of the tunnel, ii) the physical gap defined by the shield and lining geometry, and iii) displacement due to workmanship which includes the effect of grouting.

The effect of volume change in clay caused by reconsolidation of the remoulded zone can also be modelled as an additional component of the gap parameter.

b) A method for determining the gap parameter for tunnels in clays has been developed. The theoretically computed gap is shown to be reasonably consistent with the observed crown displacement in five case histories encompassing a range of soil conditions from soft to stiff clays. Both the measured and calculated displacements also show a trend for the crown displacement to be increasing logarithmically with increasing stability number.

c) From a study of thirteen case histories, the crown displacements associated with the soil conditions and construction procedures were determined and compared with the observed maximum surface settlements. It has been found that,

- i) for stiff clays, the ratio of surface settlement to crown settlement decreases with the depth to radius ratio;
- ii) for soft clays, the surface settlement increases approximately linearly with increasing crown settlement.

The results, therefore, form a clear basis for a simple semi-theoretical approach for settlement prediction.

II) Conclusions obtained from experimental study of soil behaviour:

a) From the results of the anisotropic parameter tests on the Thunder Bay Clay, it has been found that,

- i). The vertical and horizontal drained moduli in unloading are approximately twice the corresponding values in loading,
- ii) The Poisson's ratio in unloading is about three times that in loading,
- iii) The shear modulus G_{vh} , determined during loading and unloading phases of the test is similar; since the modulus E_v is higher in unloading, the ratio of G_{vh}/E_v becomes lower in the unloading stage.
- iv) The ratio of horizontal to vertical drained modulus E_h/E_v remains relatively unchanged in loading and unloading.

b) The elastic independent shear modulus G_{vh} obtained from the N.G.I. simple shear apparatus agrees well with the result determined by the anisotropic parameter test apparatus. This

indicates that the shear modulus may be relatively independent of the mode of testing.

c) From the results of K_0 consolidated triaxial tests and stress path tests, it has been found that

- i) The stress-strain curves, and hence the modulus obtained in K_0 consolidated undrained and drained extension tests are virtually identical (this being consistent with the high Poisson's ratio observed in unloading).
- ii) The modulus obtained in K_0 consolidated drained compression is much lower than that obtained in undrained compression.
- iii) The stress path followed by the soil in CK_0U and CK_0D extension tests, and the controlled stress path tests for the crown region do not depart widely from each other. The elastic drained and undrained moduli obtained from these tests are also quite similar, suggesting that the results of extension tests would provide a reasonable estimate of the appropriate elastic soil modulus at the regions of the crown and invert of the tunnel.
- iv) The stress path followed by the soil at the springline is different from those in the CK_0D or CK_0U compression tests. While the undrained modulus deduced from the controlled stress and CK_0UC tests are only slightly different, the drained modulus for the springline region

appears to lie between the values deduced from CK_{0DE} and CK_{0DC} tests.

Since the stress-strain behaviour of soils is dependent on the stress path it follows, employing conventional triaxial compression modulus data in settlement computation may lead to erroneous results.

d) There is good agreement between the strength envelope determined from conventional triaxial tests, anisotropic consolidated triaxial tests and controlled stress path tests. Furthermore, the absolute magnitudes of cohesion and internal friction angle are the same for compression and extension failure. Therefore, it appears that the effective stress parameters are "intrinsic" soil properties of the clays which are independent of the stress path followed, from a phenomenological point of view.

III) Conclusions obtained from the detailed analysis of the Thunder Bay Tunnel:

a) The results of the analysis indicate that the calculated centreline surface settlement increases linearly with increasing gap parameters of 90 mm to 200 mm. The maximum and minimum gap parameters used represent respectively the condition of large ground loss (poor workmanship) and the size of physical gap (good workmanship). These calculated values of undrained surface settlement encompass the observed range of settlements at the end of construction. The analysis, using the most probable gap of

156 mm (determined in Chapter 3) also yields conservative yet reasonable settlement compared with the average settlements at the arrays.

b) The analysis which adopts an additional gap of 100 mm to take into account the effect of reconsolidation in the remoulded zone gives settlements that are comparable with the observed settlements at Array 1 taken about one year after construction. This suggests that this source of volume change in soil may be approximately accounted for in the analysis.

c) The shape of the predicted surface settlement profiles follows the shape of the Gaussian distribution curve, as usually found.

d) For the soil condition and tunnelling activities at Array 2, both the calculated and observed undrained and drained behaviours are similar.

e) A comparison of the results of the detailed analysis with the results of a two year field observation for the Thunder Bay Tunnel indicates reasonable agreement with respect to the magnitude and distribution of surface settlements, variation of vertical and horizontal displacements with depth, as well as the distribution of subsurface displacements.

Since the calculated overall pattern of soil behaviour is in agreement with the field observations, it is evident that the proposed method of analysis is a useful and valid means of predicting ground

behaviour due to tunnelling.

11.2 RECOMMENDATIONS FOR FURTHER RESEARCH

Based on the study performed, a brief summary of suggested further research pertinent to the areas of field measurements, laboratory testing and analysis is given as follows:

1) Field Measurements

There exists the need for further field investigation of behaviours of tunnels for varying soil and construction conditions so that more appropriate assumptions may be made in an analysis. In addition to monitoring soil movements and changes in pore pressure, the remoulded zone and the face pressure caused by tunnelling should be investigated in detail.

Soil disturbances associated with shield tunnelling are attributed to pitching and yawing of the machine and the friction drag between the shield skin and surrounding soil during tunnel advance. The geometry and soil properties of the remoulded zone which can only be determined in the field are considered important factors for detailed numerical analysis to investigate the reconsolidation behaviour influencing the surface settlement.

Three-dimensional movements towards the face are influenced by the face pressure generated by "closed type" shields when the shield face is thrust against the tunnel face. From the relationship between

measured face pressure and soil displacement at the face for different soil conditions and machine characteristics, an appropriate method for calculating the displacements ahead of the face may be developed, hence improving the reliability and accuracy of settlement predictions.

2) Laboratory Testing

The selection of soil parameters for use in the analysis requires the consideration of stress path and anisotropy. It is suggested that these parameters may be estimated from conventional field and limited amount of special laboratory testing together with results of conventional tests modified by empirical factors. Therefore, further laboratory tests are necessary for determining the appropriate empirical factors for various soils.

Model studies of tunnels can be performed to obtain a better understanding of the ideal overall pattern of soil movements and stability. These studies are especially rewarding for examining the displacement behaviour for tunnels with geometry and soil conditions that are not available from case histories. The relationship between the ratio of surface to crown settlement and the ratio of depth to radius for tunnels in stiff clays, as described in this thesis, may be more clearly defined by results of model tests if the soil and tunnelling conditions are properly simulated.

3) Analysis

The phenomenon of reconsolidation of the remoulded zone has been

considered by a gap parameter in this thesis but quite approximately using one-dimensional consolidation theory. However, once the geometry and properties of the remoulded zone are better defined, an appropriate consolidation theory may be included in the finite element analysis.

Two-dimensional elasto-plastic finite element analysis has been used in this study to examine the tunnelling problem which is generally three-dimensional in nature; however, it is considered that the results provided by this analysis are sufficiently accurate as evidenced by the agreement obtained between calculated and observed settlements. However, three-dimensional elasto-plastic analysis should be performed to investigate the soil behaviour at the heading, the results also being useful for comparing with those obtained by two-dimensional analysis.

Finally, it should be mentioned that the time for preparing the data and the cost of obtaining a computer solution which involves all the tunnelling variables and soil properties could be prohibitive. Therefore, the relative importance of the input parameters for an analysis must be considered and further parametric studies on the settlement behaviour due to tunnelling should be performed for developing practical guidelines for design and analysis, thus simplifying the procedure for predicting displacement behaviour at critical sections.

APPENDIX 1

SCHEME OF CONSTRUCTION SIMULATION WITH CONSIDERATION OF MACHINE WEIGHT DURING TUNNEL ADVANCE

To simulate the actual construction sequence as closely as possible, the rate of stress relief is varied around the tunnel, being initially greater near the crown than near the invert. At the end of construction, the tractions removed from the excavated surface correspond to the magnitude of initial stress at the point prior to construction.

A diagrammatical representation of the "sequential unloading" procedure is illustrated in Figure A1.1. Three simulated construction sequences are involved. The first stage is the removal of a portion of the insitu total stress from nodal points above the springline, and this proportion is taken to be 30% of the insitu stress for the purpose of discussion. In the second stage, 70% of the initial stresses are removed from all nodal points. The remaining initial stresses are taken away in the final stage.

The portion of stress relief in each stage of unloading is chosen from a consideration of elastic solution for stresses and displacements around the advancing tunnel face and the influence of the weight of the machine.

In an elastic medium, depending on the insitu K_0 condition, between 20% to 40% of the inward radial displacement associated with release or unloading of the insitu stresses has already occurred at the tunnel face (Lo et al., 1984). As an illustration, Figure A1.2 shows the development of inward radial displacements near the face when an

unlined circular opening is being advanced in elastic ground.

Relief of 30% of the initial stresses in a plane strain section may give the equivalent three-dimensional displacement at the face of the advancing tunnel. However, due to the effect of the weight of the TBM, the sequence of stress relief may be modified. 'Sequential unloading stages' are adopted in the analysis. In these sequences of unloading, it is assumed that stress relief initially occurs above the springline. The pattern of stress relief is discussed below and the relative importance of the variations in unloading sequences will be examined by a comparative study.

Figures A1.3a to A1.3d show the physical meaning of the 'sequential unloading stages'. The example represents tunnelling of the Thunder Bay Tunnel. When the TBM is approaching a location under consideration, three-dimensional movements occur ahead of the face (Figure A1.3a). The shield rests on the soil beneath it and its weight is transferred to the soil. The weight of the soil removed by the cylindrical volume of the TBM is 440 kN. Effect of the weight of soil removed is temporarily counteracted by the weight of the TBM (270 kN). Since the TBM is advancing, its average effect on the section should be considered. Assuming that the stress distribution is similar to that of a rigid embedded rectangular loaded area, it can be shown (Figure A1.3b) that the soil at a particular section would be subjected to an average pressure equal to half of the moving load. The overall equivalent effect is the momentary suppression of about 30% of the

unloading below the springline. Thus, in the first stage of construction simulation, 30% of the insitu loading is released above the springline. In other words, the machine weight effectively delays the stress relief below springline.

As the machine advances as the soil invades the tail void (Figure A1.3c) further stress relief occurred. In all probability, the soil would come into contact with the lining. The influence of the machine weight is minimal when it has cleared the section and the rate of stress relief must be the same all around the tunnel surface. In the second stage of construction simulation, 70% of the full release is applied on all nodal points.

The displacement of the excavated surface is also monitored in the analysis. Once the soil nodes come onto the lining, interaction is modelled by activating the influence coefficients of the appropriate structure nodes where contact occurred. Deformation of the soil nodes would be limited by the soil-liner interaction pressure provided by the stiffness of the liner. Detailed description of the interaction influence matrix and soil-structure interaction theory is given in Chapter 4.

Finally, the remaining stresses are removed from below the springline in the third stage of construction simulation (Figure A1.3d). This represents the completion of the tunnel. Additional settlement is small in the third stage of analysis but some modification of the

trough shape occurs. The final construction stage simulates the idealization of any further stress redistribution when all soil nodes have been in contact with the liner.

Evaluation of effect of the TBM weight by comparative study shows that it is not a major factor which affects the result of the solution. The results of four analyses, in which all parameters are kept identical except for the construction sequence are shown in Figure A1.4 and Table A1.1.

Case A represents the simulation of tunnelling neglecting the weight of the TBM with all stress relief removed in one step. Case B to C represents 40%, 50% and 70% differential unloading in the excavation sequence respectively and they simulate varying degrees of the influence of the machine. In the particular case of TBM tunnelling in Thunder Bay, only 6% difference in the magnitude of the predicted settlement is obtained between case A (no machine weight) and case B (machine weight approximately considered). Increase in machine weight, in cases C and D again only lead to small difference in the solution compared to case A. The approach in B is adopted in the present analysis for the Thunder Bay Tunnel since case B would represent a more realistic solution than case A even if the difference is negligible.

TABLE A1.1 EFFECTS OF SIMULATION OF EXCAVATION PROCEDURE ON THEORETICAL RESULTS

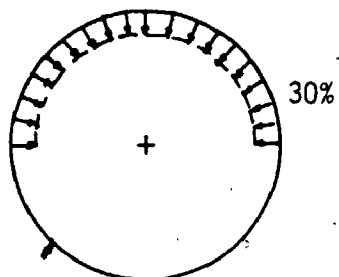
No.	Method of Analysis	S_{\max} (mm)	$\frac{S_{\max}}{G}$	$\frac{2i}{D}$	Procedure of Stress Relief
A	modified. 2-D no machine wt.	33.9	0.38	2.83	all found stress release
B	m. 2-D machine wt. considered	36.0	0.40	2.71	stage 1: 30% above springline stage 2: 70% all around stage 3: 30% below springline
C	m. 2-D arbitrary heavier machine wt.	37.6	0.42	2.63	# 1: 50% above springline # 2: 50% all around # 3: 50% below springline
D	m. 2-D arbitrary heavier machine wt.	39.7	0.44	2.53	# 1: 70% above springline # 2: 30% all around # 3: 70% below springline

S_{\max} = maximum or centreline surface settlement

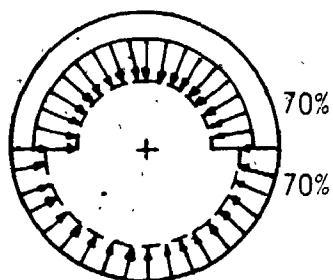
G = gap parameter

i = distance from centreline where $0.61 S_{\max}$ occurred

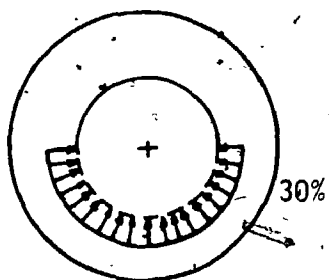
D = 2.47 m, the mined diameter



STAGE 1
UPPER HALF
30% STRESS RELIEF

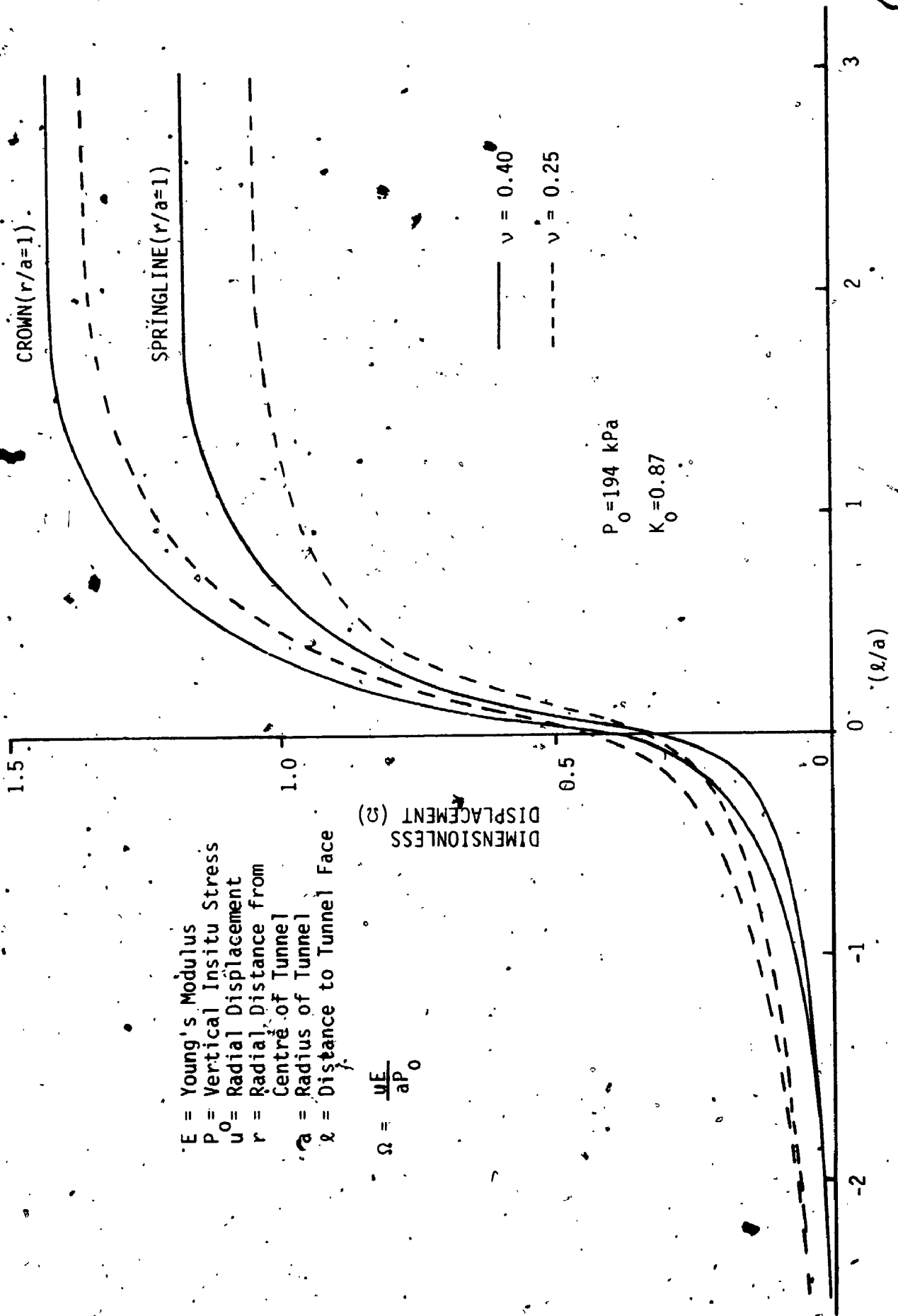


STAGE 2
OVERALL
70% STRESS RELIEF



STAGE 3
LOWER HALF
30% STRESS RELIEF

FIGURE A1.1 Simulation of 3-D Effect in 2-D Analysis by Means of Unloading Sequences



E = Young's Modulus
 P = Vertical Insitu Stress
 u_0 = Radial Displacement
 r = Radial Distance from Centre of Tunnel
 a = Radius of Tunnel
 x = Distance to Tunnel Face

$$\Omega = \frac{uE}{aP_0}$$

FIGURE A1.2 Variation of Dimensionless Radial Displacement with Normalized Distance to the Advancing Face — Elastic Solution (Niwa et al., 1979)

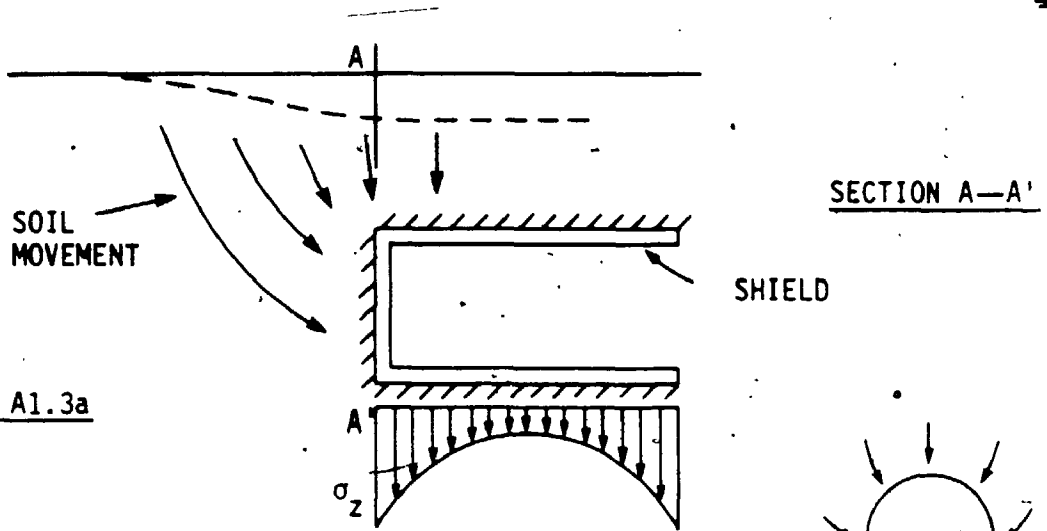


FIGURE A1.3a

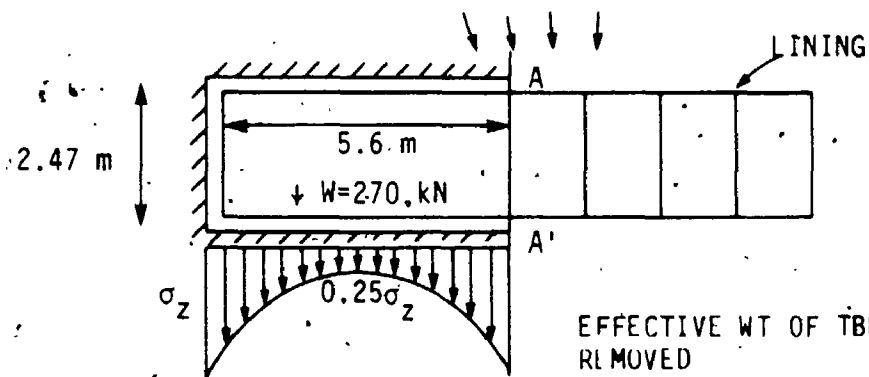


FIGURE A1.3b

EFFECTIVE WT OF TBM \approx 0.3 OF WT OF SOIL REMOVED

NET EFFECT IS 30% OF THE INITIAL STRESS RELIEF SUPPRESSED BENEATH SPRINGLINE

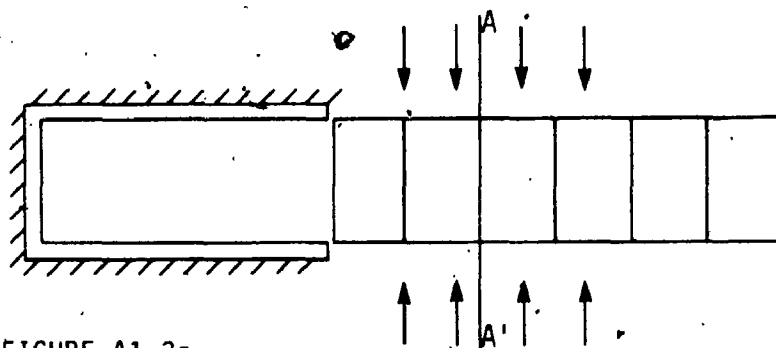


FIGURE A1.3c

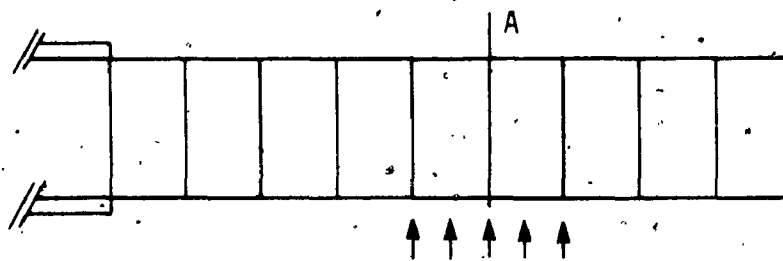


FIGURE A1.3d

FIGURE A1.3 Physical Interpretation of Sequential Unloading Procedure

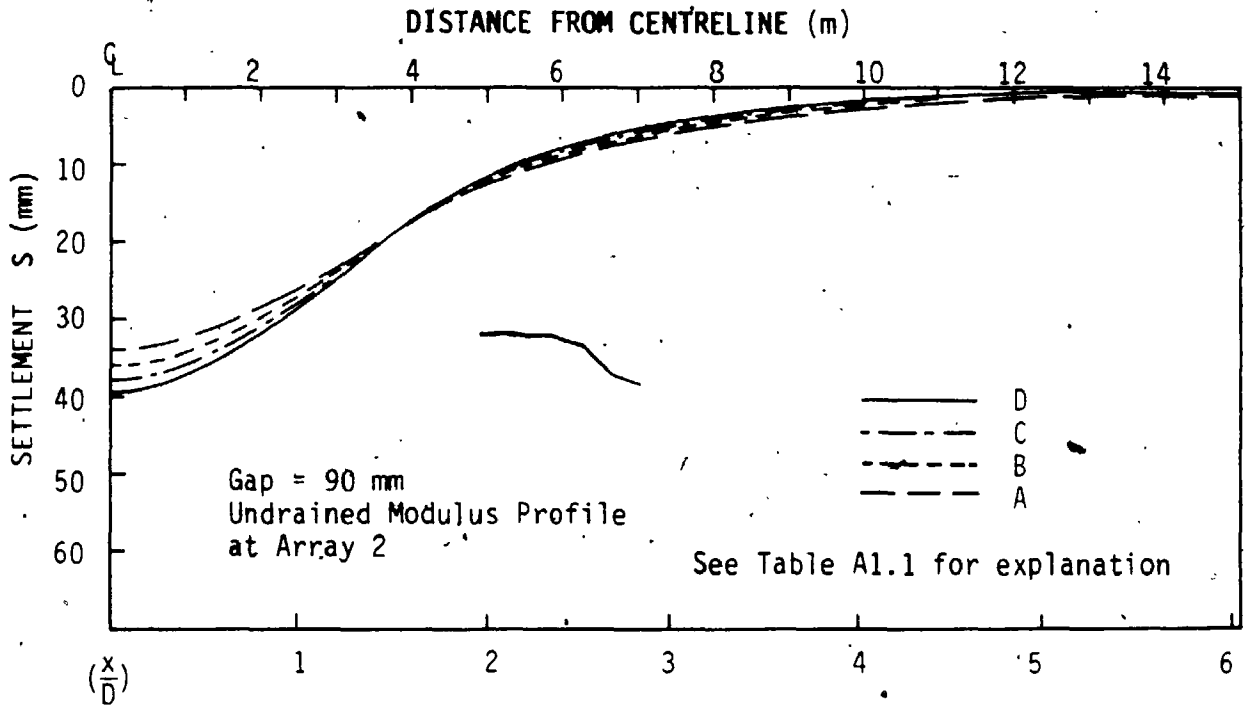


FIGURE A1.4a Surface Settlement Profile for Modified '2-D' Approach

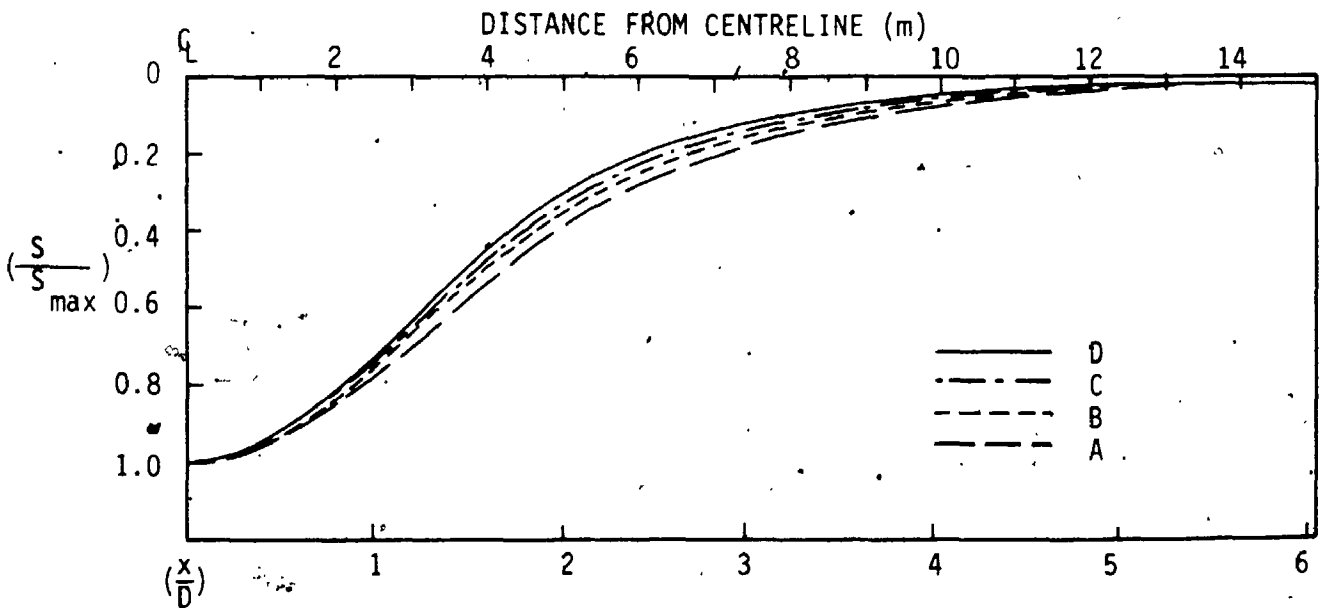


FIGURE A1.4b Normalized Surface Settlement Profile for Modified '2-D' Approach
 (A - Effect of Machine Ignored,
 B to D - Effect of Machine Considered)

APPENDIX 2
UNDRAINED AND DRAINED SETTLEMENTS
DUE TO TUNNELLING

The soil displacements discussed in the case histories in Chapter 3 are short term displacements. Calculation of the gap parameter is based on the total stress concept. The proposed method is strictly appropriate for determining the undrained soil behaviour. However, the soil mass will eventually reach a drained equilibrium. It is therefore of interest to investigate the development of settlement with time and the difference in magnitude between undrained and drained settlement.

The subsoil conditions of the case histories analyzed may be divided into three categories, namely; 1) hard till, 2) firm to stiff clay, and 3) soft clay. Although detailed long term settlement observations have not been reported in all the case records, it is possible to include examples in each category of clay medium. The development of settlements will be briefly discussed in the following paragraphs.

1) Hard Till

In the case of the Mississauga Sewer, Delory et al. (1979) have summarized that the soil displacements in response to tunnelling were reasonably rapid. Relatively little additional movement was recorded

after the shield had passed the measuring points. Most of the movement occurred within one or two days and the final displacement was attained within a few weeks after excavation.

The settlement observations for an experimental tunnel (section 2, section 3) in Edmonton were reported by Eisenstein et al. (1979, 1981). The tunnel is 2.5 m in diameter and it is located in stiff dense till. The experimental tunnel was lined with precast segmented concrete liner expanded radially to the excavated surface of the tunnel. The plot of centreline settlements with depth vs. tunnel advance in section 2 was presented by the authors. The settlements developed as the shield passed and after the tailpiece cleared the line of extensometer. Movement started to stabilize after the lining was expanded in place when the cross-section was about 10 m from the face. Little increase in settlement was recorded as the face advanced from 30 m to 90 m from the cross-section. The same tunnel passed through section 3 which is 60 m in length and 300 m away from section 2 during an eight day period. From the time history record of settlement at section 3, the authors indicated that the soil movement was stabilized and reached their final values at 50 m behind the tunnel face.

It appears from the above two case histories that the undrained and drained settlements in hard till do not differ appreciably.

2) Firm to Stiff Clay (London Clay)

The soil movement due to construction of the Northbound and Southbound London Underground in Regents Park was monitored over a two month period by Barratt and Tyler (1976). The undrained centreline settlements at various depths taken at the point where the rapid rate of settlement decreased abruptly (within 10 days of shield passage) and the settlements observed two months later have been shown in Figure 3.8. The two sets of settlements representing undrained and partially drained condition were nearly identical.

Similar phenomenon is also evident from the recorded settlements over the London Underground Tunnel in Green Park. Attewell and Farmer (1974) have reported the centreline settlements at various depths. From the settlement data at borehole Z1, the rapid progress of soil deformation was observed to decrease abruptly at about 15 m from the face. The rate of settlement approached zero at 30 m from the face, about 9 days after the face had passed. No significant change in settlement was observed even when the face had advanced to 80 m away from the cross-section.

The settlement observations in stiff clay are consistent with the experimental data of Atkinson and Potts (1977b). From results of centrifuge model tunnel tests in overconsolidated kaolin, they have suggested that there is little distinction between undrained and drained deformation in overconsolidated clays.

3) Soft Clay

The observed displacements of the Thunder Bay Tunnel (Belshaw and Palmer, 1978; Palmer and Belshaw, 1980) have been shown in Figure 3.10. These displacements are representative of 'restricted' undrained plane strain deformation behaviour. The undrained settlements can be recognized from the progress of centreline settlements, as the tunnel advanced. Though the undrained settlements at the two arrays were similar, the surface centreline settlement at Array 1 was doubled in a year. The surface centreline settlement at Array 2 remained essentially unchanged.

Large time-dependent soil displacement in the Mexico Siphon was reported by Tinajero and Vieitez (1971). The time-dependent movement was more gradual and considerably smaller than the rate of settlement associated with tunnel excavation. The settlement increased from 105 mm taken at 11 days (when the settlement rate was observed to change significantly) to 150 mm at the end of 28 days.

The time-dependent settlement in soft clay may be attributed to reconsolidation of remoulded or overstressed soil around the excavation. The disturbed zone is created by construction activities; it may be especially significant in shield driven tunnels (Terzaghi, 1942; Peck, 1969). The settlement behaviour at Array 2 suggested that under good workmanship, favourable field situation and soil condition, the drained and undrained settlement behaviour may be rather similar.

From the case study of settlement development due to tunnelling, the following comments may be made:

- 1) A plane strain condition of the tunnel may be recognized from the settlement-tunnel progress curve. This may be representative of the undrained soil behaviour if the condition is attained in a short time (say, 10 days).
- 2) In stiff to hard clay, the undrained and long term drained displacements are essentially the same.
- 3) The difference in ideal drained and undrained settlement behaviour in soft clay may not be very significant. Large time-dependent settlement is more likely associated with reconsolidation of remoulded soil around the tunnel and other factors rather than volumetric change in the soil due to pore pressure dissipation.

APPENDIX A

SAMPLING WITH 152 mm DIAMETER PISTON SAMPLER

A detailed experimental program was planned to delineate the strength and deformation behaviour of the soil. Since it was necessary to obtain undisturbed soil at a depth of at least one diameter below the invert of the tunnel, a large diameter (152 mm ID) piston Shelby sampler was employed.

Piston samplers with small area ratios are capable of furnishing excellent samples of cohesive soils even for very soft and sensitive clays (Terzaghi and Peck, 1948). For samplers of a given diameter forced into the soil, the degree of disturbance depends on the area ratio,

$$A_r(\%) = 100 \frac{D_e^2 - D_i^2}{D_i^2} \quad (A.1)$$

where D_e is the external diameter and D_i is the internal diameter of the sampler (Hvorslev, 1949). It was suggested that the value of A_r should not exceed 20% if disturbance is to be minimized and in the case of the 152 mm diameter Shelby sampler used at Thunder Bay, A_r is equal to 8%.

An advantage of the thin-walled tube sampler of this size is the provision of ample specimens for soil tests in which sizable test samples are required (e.g. large oedometer and permeability tests). For a 152 mm dia. x 150 mm high soil sample, three 50 mm diameter

triaxial test samples can be obtained and the side of the 152 mm tube sample, which might have been remoulded during sampling, would be trimmed off as excess during preparation for testing.

The disturbance associated with tube sampling is shown in Figures A.1 and A.2 (Hvorslev, 1949). Virgin soils might be disturbed by failing and flowing into the shelly tube or by being displaced by a soil plug in the tube. These conditions could be improved by providing the sampling tube with a piston as shown in Figure A.3. At the start of sampling, the piston is at the tube bottom, in contact with the soil surface. The piston is fixed in this position by its actuating rod, which extends to the ground surface and which is clamped to a rigid support. The sampling tube is driven ahead of the piston into the soil below. The fixed piston prevents soil from squeezing upward. The tendency of the sample to slip out of the tube is prevented by a vacuum created between the piston and the soil, which helps to hold it in place.

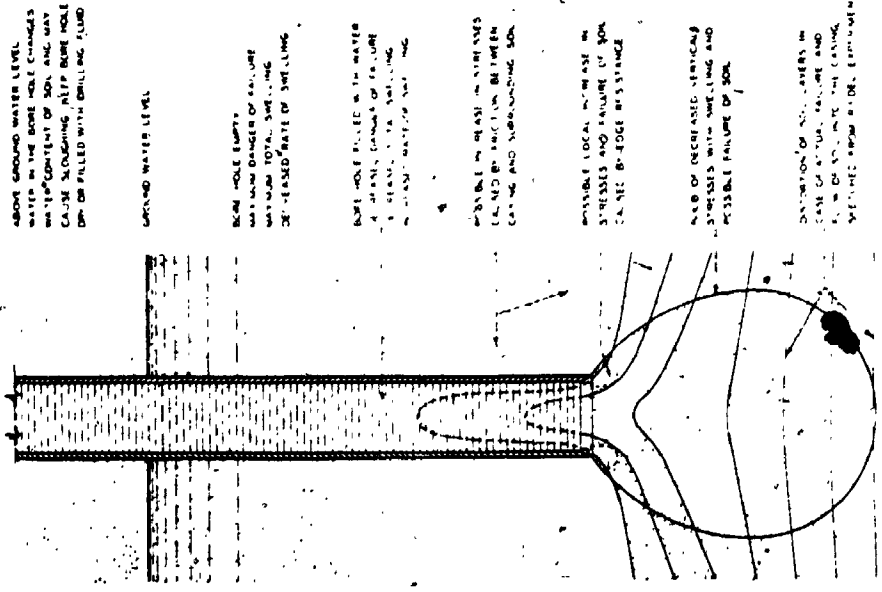
The samples recovered by the 152 mm diameter piston sampler are of excellent quality. From a visual inspection of the samples, it was believed that these specimens were relatively undisturbed. The layering and structure of the soils were very well preserved and the behaviour of the samples tested in the laboratory should closely resemble the field behaviour.

The field procedure of obtaining the thin walled tube samples is described below:

The boreholes for the retrieval of tube samples were initially advanced by washboring in the upper cohesionless deposits together with the placement of a 200 mm outside diameter protective casing. Upon reaching the clay layer, the borehole was drilled using 160 mm diameter hollow stem augers. The casing was seated approximately one metre into the clay stratum and any additional augering was performed unsupported. The staggered method of sampling discussed in Chapter 6 began at the sand-clay interface. Soil samples were taken every 1.5 m using 152 mm ID shelly tubes capable of retrieving over 700 mm of material. Prior to sampling, the bottom of the borehole was carefully cleaned to minimize the remoulded material left at the end of the drill hole. After extraction of a soil sample, the augers were reconnected and the borehole was increased to approximately 350 mm. A strength test with a standard 67 mm diameter Geonor vane was then performed. Following the vane test, the augers were again employed to increase the depth of the borehole to the elevation of the next sample to be taken. Once the sampler was recovered from the ground, the tube was disconnected from the sampler head and remoulded material from the upper part of the sample was removed. About 20 mm of soil from the cutting edge near the bottom of the sampler was trimmed to allow room for the sealing plug. Molten wax was poured in at one end and after the wax had solidified, the tube was inverted and a 20 mm to 30 mm wax plug was made in the other end of the tube.

A total of nineteen 152 mm tube samples were taken.

All of the fieldwork described above was performed using a CME 750 drilling unit, by Dominion Soils Ltd. of Thunder Bay under the direction of The University of Western Ontario. The equipment that was used for the 152 mm shelby tube sampling was manufactured by Dominion Soils.



ABOVE GROUND WATER LEVEL
WATER IN THE BORE HOLE CHANGES
WATER CONTENT OF SOIL AND MAY
CAUSE SWELLING. AFTER BORE HOLE
IS FULL WITH DRILLING FLUID

GROUND WATER LEVEL

BORE HOLE EMPTY
WITHOUT DANGER OF FAILURE
WATER TOTAL SWELLING
DECREASED RATE OF SWELLING

BORE HOLE FILLED WITH WATER
DECREASED RISK OF FAILURE
DUE TO TOTAL SWELLING
WATER TOTAL SWELLING

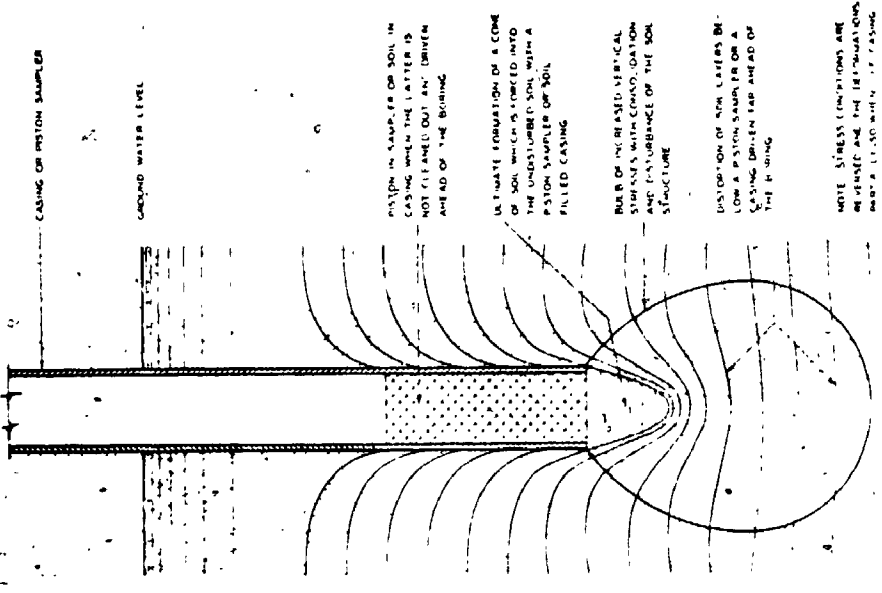
POSSIBLE INCREASE IN STRAINS
DUE TO FRICTION BETWEEN
CASING AND SURROUNDING SOIL

POSSIBLE LOCAL INCREASE IN
STRESSES AND FAILURE OF SOIL
DUE TO EDGE RESISTANCE

AREA OF DECREASED VERTICAL
STRESSES WITH SWELLING AND
POSSIBLE FAILURE OF SOIL

DISTRIBUTION OF SOIL LAYERS IN
CASE OF TOTAL FAILURE AND
CASE OF PARTIAL FAILURE
WITH DRILLING FLUID

FIGURE A.1 Boring by Removal of Soil
Stress Changes and Deformations of Soil Layers Below Bottom of Borehole
(after Hyorslev, 1949)



CASING OF PISTON SAMPLER

GROUND WATER LEVEL

INFLUENCE OF SOIL IN
CASING WHEN THE LATTER IS
NOT CLEANED OUT AND DRIVEN
AHEAD OF THE BORING

INFLUENCE OF SOIL IN
CASING WHEN THE LATTER IS
NOT CLEANED OUT AND DRIVEN
AHEAD OF THE BORING

RISK OF INCREASED VERTICAL
STRESSES WITH COMPACTION
AND DISTURBANCE OF THE SOIL
STRUCTURE

DISTRIBUTION OF SOIL LAYERS IN
LOW A PISTON SAMPLER OR A
CASING DRIVEN FAR AHEAD OF
THE BORING

NOTE: STRESS CONDITIONS ARE
REPRESENTED BY THE DISTRIBUTION
OF SOIL LAYERS IN THE CASING
AND NOT BY THE POSITION
OF THE PISTON

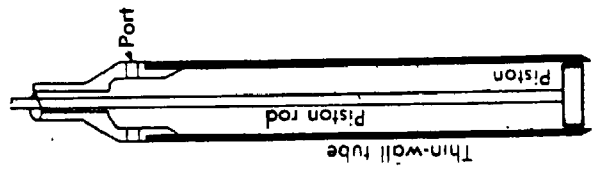


FIGURE A.3 Schematic Sketch of a Piston Sampler

APPENDIX B
APPARATUS AND FIELD TECHNIQUE USED
IN K_0 -DETERMINATION

A sketch of the hydraulic fracturing test apparatus is shown in Figure B.1. The apparatus consists of the following components:

1. A Geonor piezometer with a conical tip and plastic tube.
2. Motor driven screw pump with two speed reducers.
3. Electronic pressure transducer and associated read-out devices.
4. Water reservoir for removing trapped air bubbles.

The apparatus is similar to the one described by Palmer and Lo (1974). The system can supply a rate of water injection from 0.036 litre/hr (0.6 cc/min) to 1.5 litres/hr (25 cc/min). Since power supply outlets were remote from the work sites, a portable AC generator and a constant voltage transformer were used to provide power to the motor pump.

Six insitu stress measurements were made at the two arrays. Three Geonor piezometers were first installed at Array 2 and after testing was completed they were retrieved and reused at Array 1.

The centres of the piezometers were installed at the following depths:

Location	Depth (m)	Piezometer No.
Array 1	9.75	1-P1
Array 2	10.06	2-P1
Array 1	11.58	1-P2
Array 2	12.50	2-P2
Array 1	13.70	1-P3
Array 2	14.93	2-P3

These piezometers were positioned outside the zone of influence of the tunnel so that the undisturbed insitu ground stresses could be measured.

Locations of the piezometers are shown in Figures 6.2 and 6.3. The depths were referenced to a fixed point about 1 m above the ground. (The elevation of this point was at 186 m at Array 1.)

The field technique in general followed the procedure outlined by Palmer and Lo (1974). This method was found to be successful and practical.

Three boreholes were drilled to the clay-sand interface while the apparatus was being assembled. Special care was taken to ensure that the system was completely saturated with deaired water. The piezometer was dismantled and the sintered bronze filter was deaired by boiling in water before the piezometer was reassembled under water. The flexible tubing was filled with deaired water, sealed with wooden plugs, threaded through all of the required drilling A-rods, before it was connected to the piezometer.

The piezometer was inserted into the casing of the predrilled borehole, lowered and pushed 0.33 m (one foot) into the clay. The

piezometer tubing was then connected to the previously desired apparatus. Subsequently, the piezometers were driven to the desired depth at a rate of approximately 5 mm/sec (1 foot/min). The peak excess pore water pressure developed during the driving of the Geonor piezometers at Array 2 is shown in Figure B.2. The stress changes occurring in the soil close to the piezometer during its installation would result in some soil disturbance. However, the technique employed by Bjerrum and Anderson (1972) would avoid this problem since the water pressure at which the crack closes is measured instead of the water pressure required to fracture the soil. (Thus, the critical pressure is not dependent on the tensile strength of the soil which might have been affected.)

The high peak value of excess pore pressure and soil remoulding appeared to be a localized phenomenon since the excess pore water pressure dissipated quickly. For the deepest driven piezometer, nearly all the excess pore pressure was dissipated within two hours. The actual tests were not performed until a minimum of four days had passed after the date of installation in order to ensure an equalization of the geostatic water pressure conditions.

In the test, water was forced into the soil through the piezometer by the screw pump producing a pressure so that a crack was formed. When there was an indication of cracking, pumping of water was stopped. All the test results were monitored continuously by a chart recorder which provided a graph of water pressure versus time. From the chart

recorder traces, a curve of average pressure versus rate of dissipation of pressure over a given time increment was plotted. The horizontal effective stress corresponding to the pressure at which an abrupt reduction in the rate of pressure dissipation occurred is shown in the figure. The results for Arrays 1 and 2 are shown in Figures B.3 to B.5 and Figures B.6 to B.8 respectively.

Three cycles of hydraulic fracturing were performed at each location. At Array 1, the rate of water injection was kept at a constant rate of 0.96 litre/hr (16 cc/min) for all three cycles. The rate was varied in the tests at Array 2 and the rate of water injection was 0.96 litre/hr (16 cc/min) for the first two cycles and 2.58 litres/hr (43 cc/min) for the third cycle. The variations in water injection rate enabled the study of the effect of rate of pumping water on the value of K'_0 obtained. It can be seen from Table B.1 that the value of K'_0 was independent of the number of cycles of fracturing when the rate of 0.96 litre/hr (16 cc/min) was used. The K'_0 values were virtually the same in all three cycles of each test at Array 1 and the first two cycles of each test at Array 2. K'_0 values also appeared to be similar at both arrays at the corresponding depths. When the injection rate was increased to 2.58 litres/hr (43 cc/min), the K'_0 obtained was significantly higher by about 25% to 40%. This appeared to indicate that the rate of pumping had caused a volume of water greater than that required to propagate the crack to be injected.

It was believed that accurate K'_0 values could be obtained in

tests employing the injection rate of 0.96 litre/hr (16 cc/min). This rate corresponded to the rate of injection which Bjerrum (1972), Bozozuk (1973), Palmer and Lo (1974) and Becker (1981) had used in the hydraulic fracturing tests.

TABLE B.1 EFFECT OF RATE OF WATER INJECTION ON RESULTS OF K_0 TEST

Location	Depth (m)	Elevation (m)	K_0			Average K_0 for First Two Cycles
			First Fracture	Second Fracture	Third Fracture	
Array 1	9.75	175.25	.75	.76	**	.76
Array 2	10.06	175.3	.76	.77	1.10*	.77
Array 1	11.58	173.4	.73	.76	.75	.75
Array 2	12.50	172.8	.76	.79	.96*	.77
Array 1	13.72	171.22	.59	.57	.6	.58
Array 2	14.93	170.4	.58	.58	.76*	.58

Note:

Rate of injection of water = 16 cc/min unless specified by *

* Rate of injection of water = 43 cc/min

** Recorder tracing destroyed

(1 cc/min = 0.06 litre/hr)

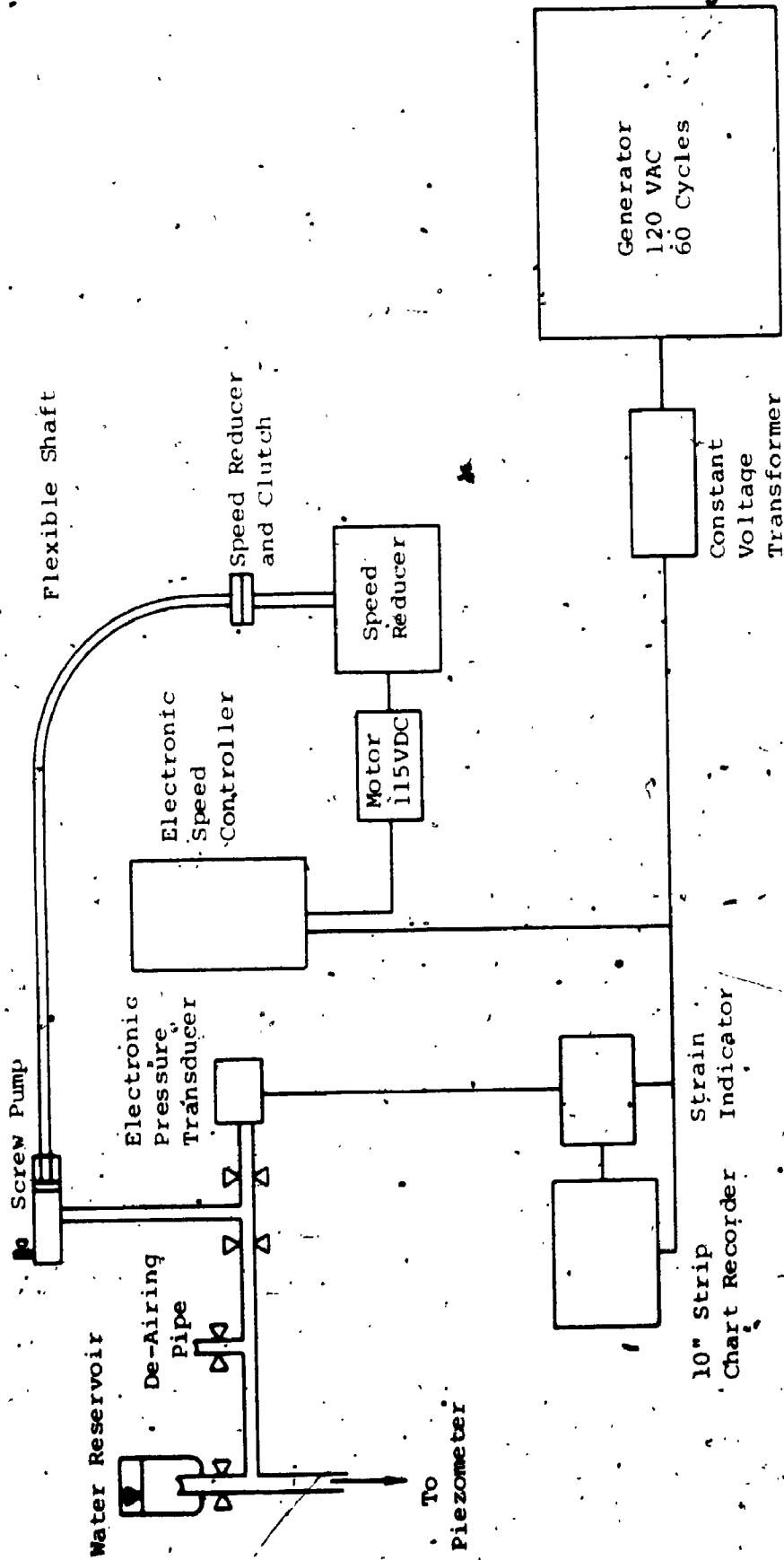


FIGURE B.1 Sketch of Hydraulic Fracturing Apparatus (after Palmer and Lo, 1974)

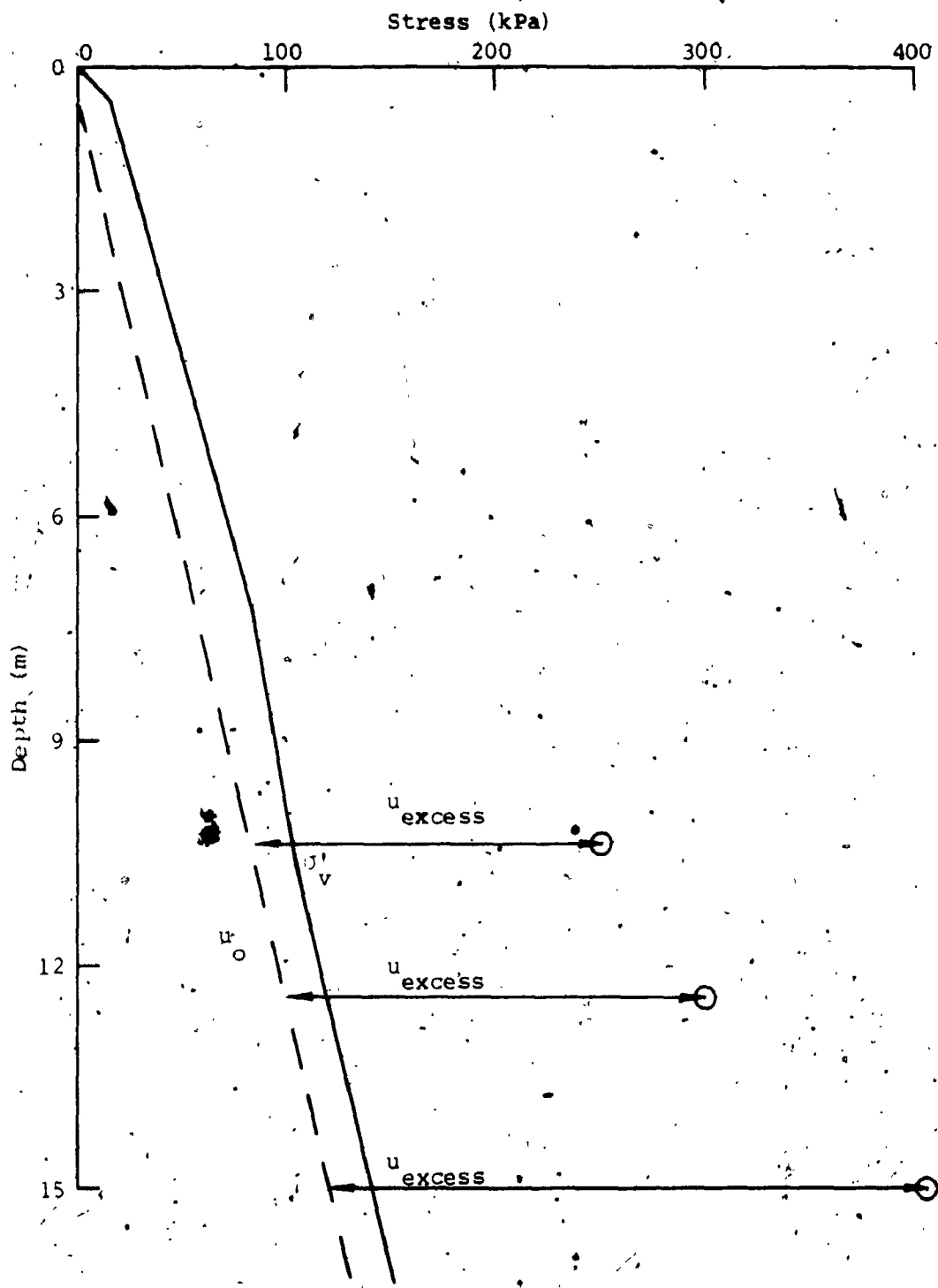


FIGURE B.2 Excess Pore Pressure Developed During Piezometer Driving at Array 2

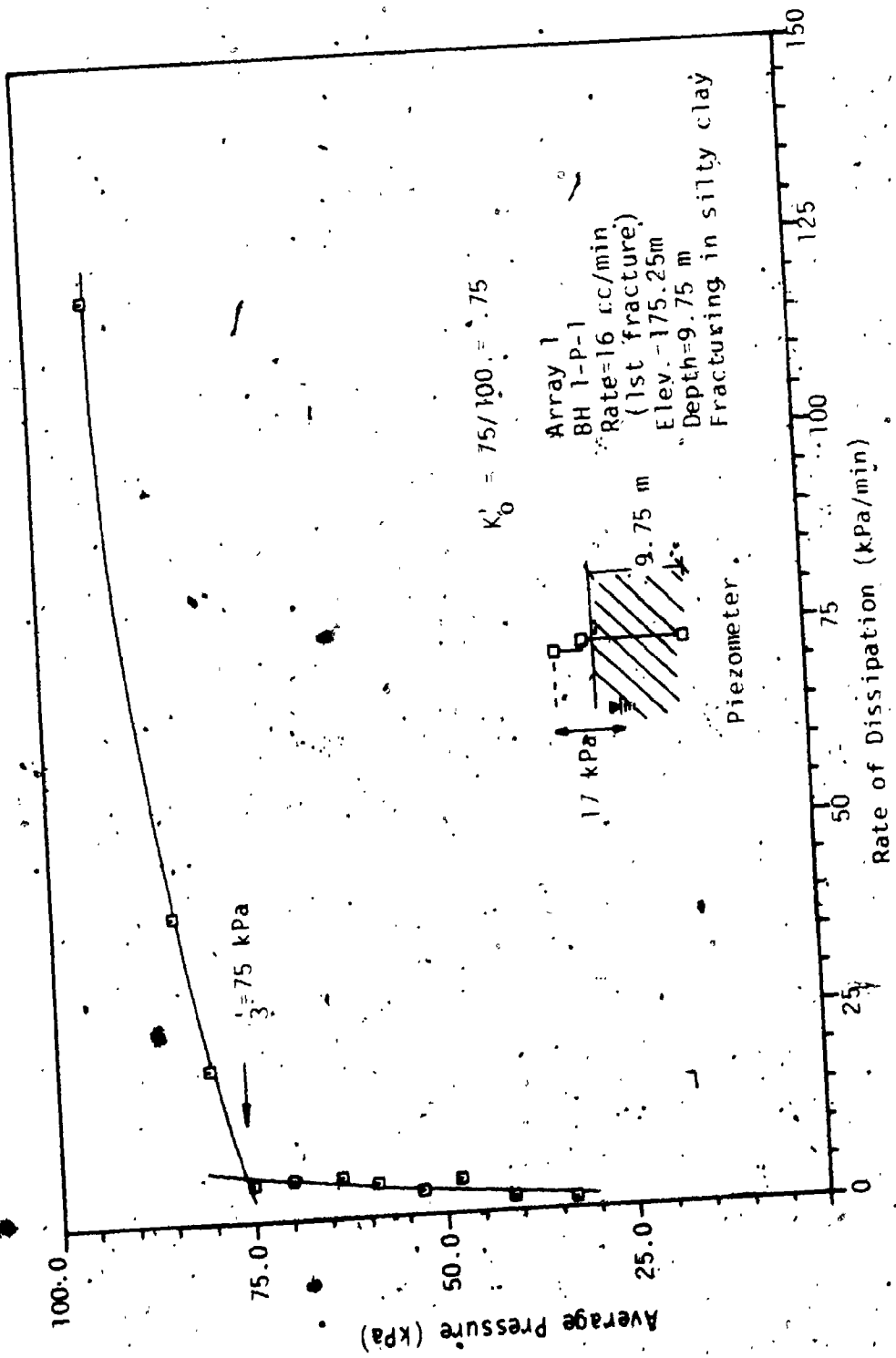


FIGURE B.3a Dissipation Curve for Hydraulic Fracturing Test 1-P1 (1st fracture)

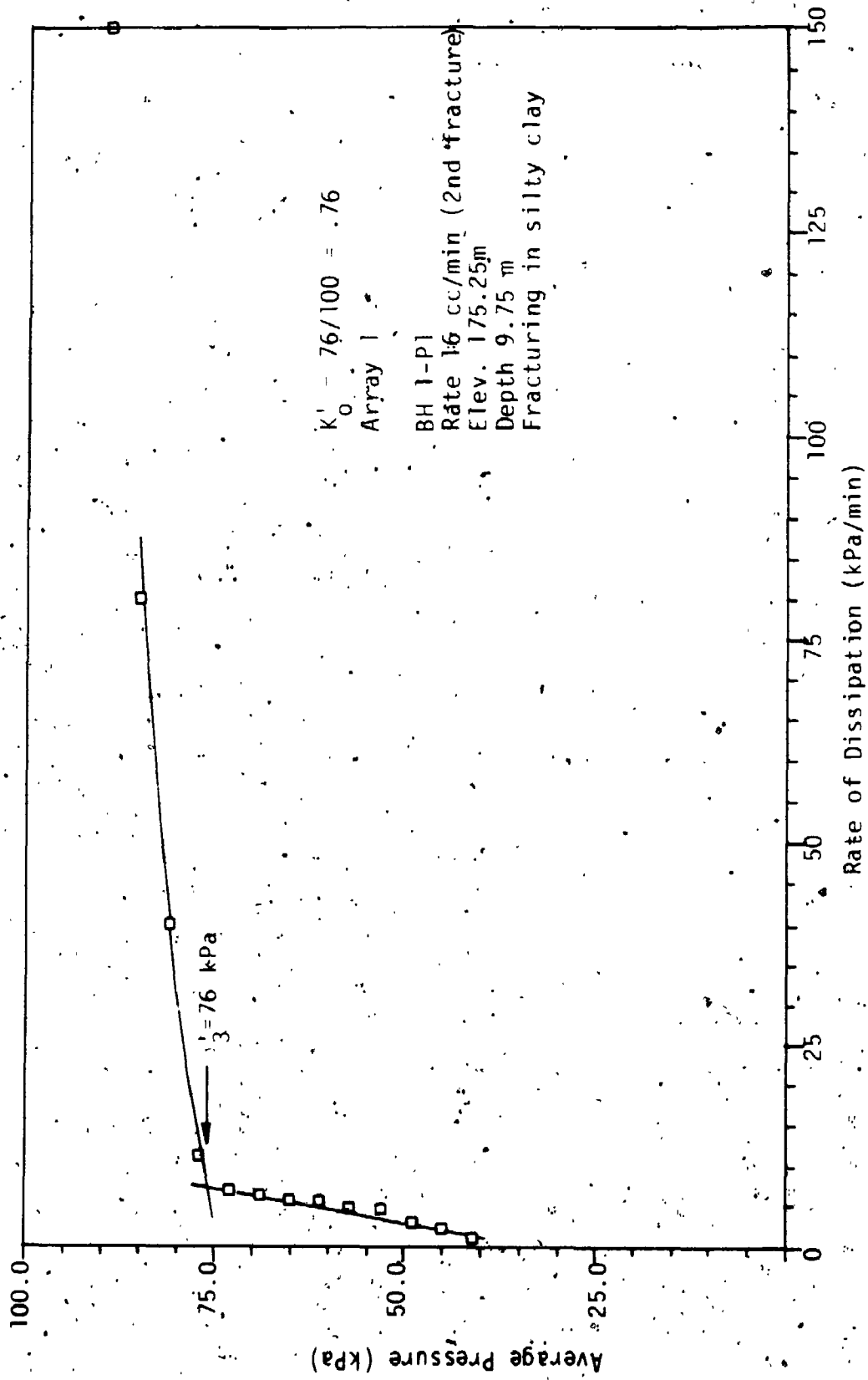


FIGURE B. 3b Dissipation Curve for Hydraulic Fracturing Test 1-P1 (2nd fracture).

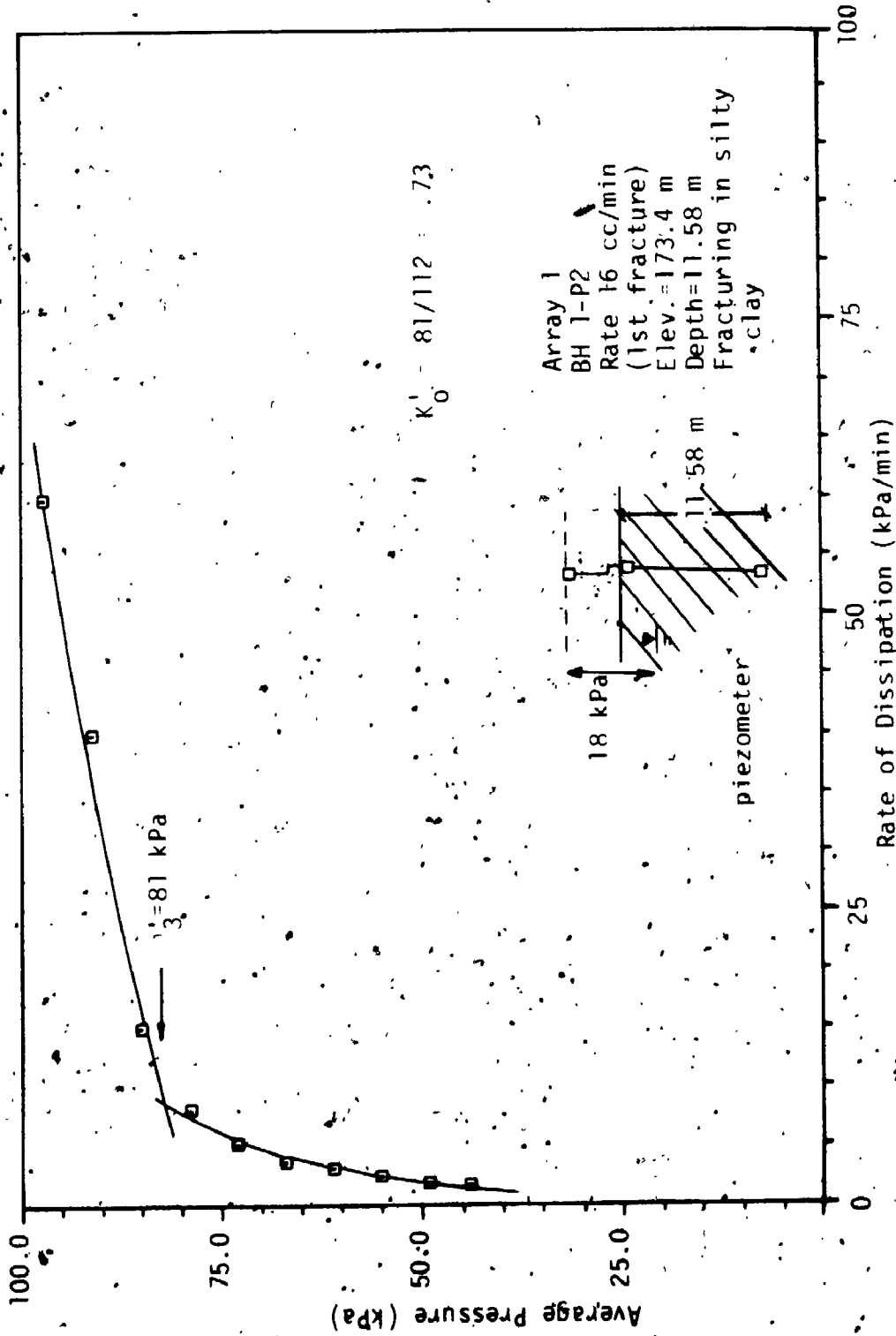


FIGURE B.4a Dissipation Curve for Hydraulic Fracturing Test 1-P2 (1st fracture)

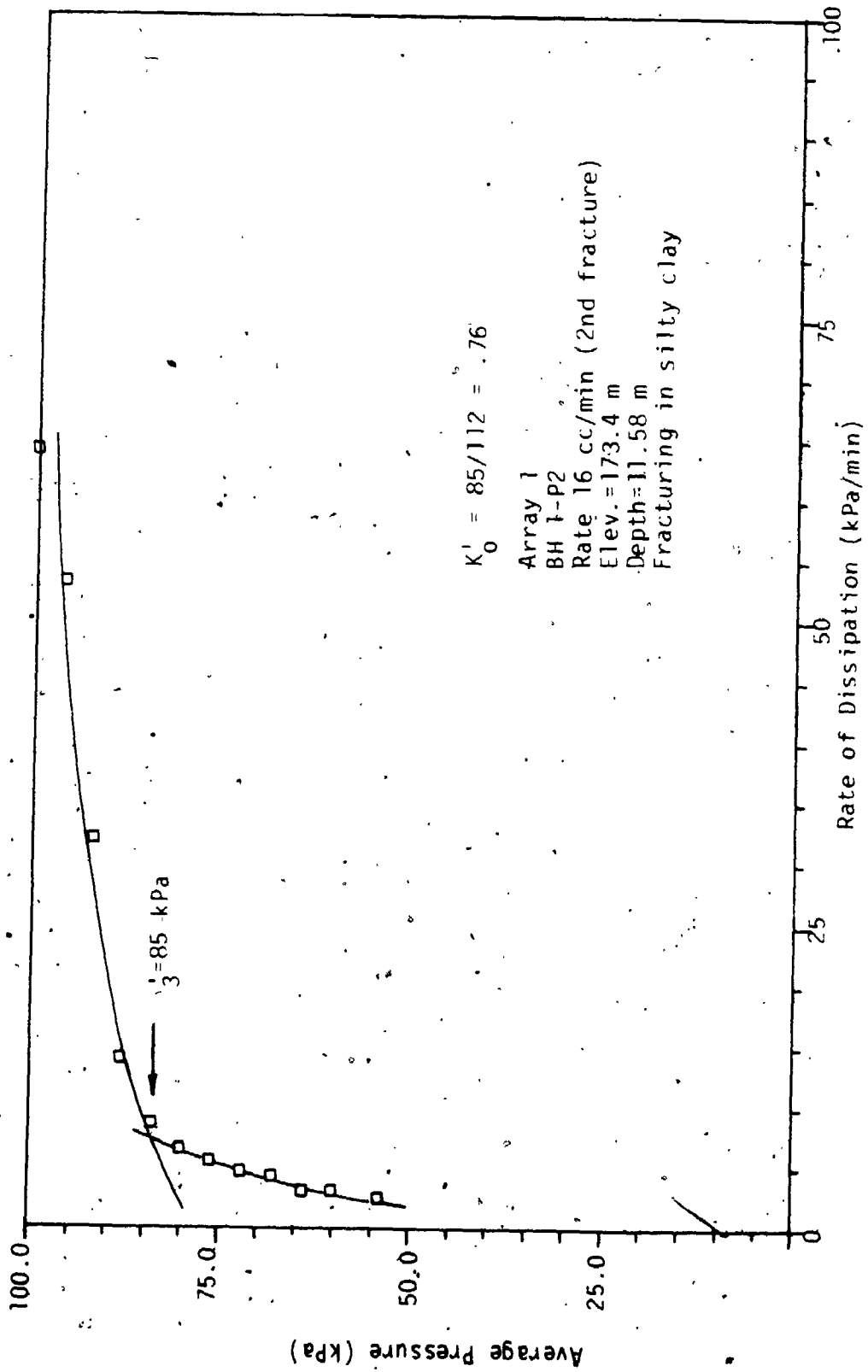


FIGURE B.4b Dissipation Curve for Hydraulic Fracturing Test 1-P2 (2nd fracture)

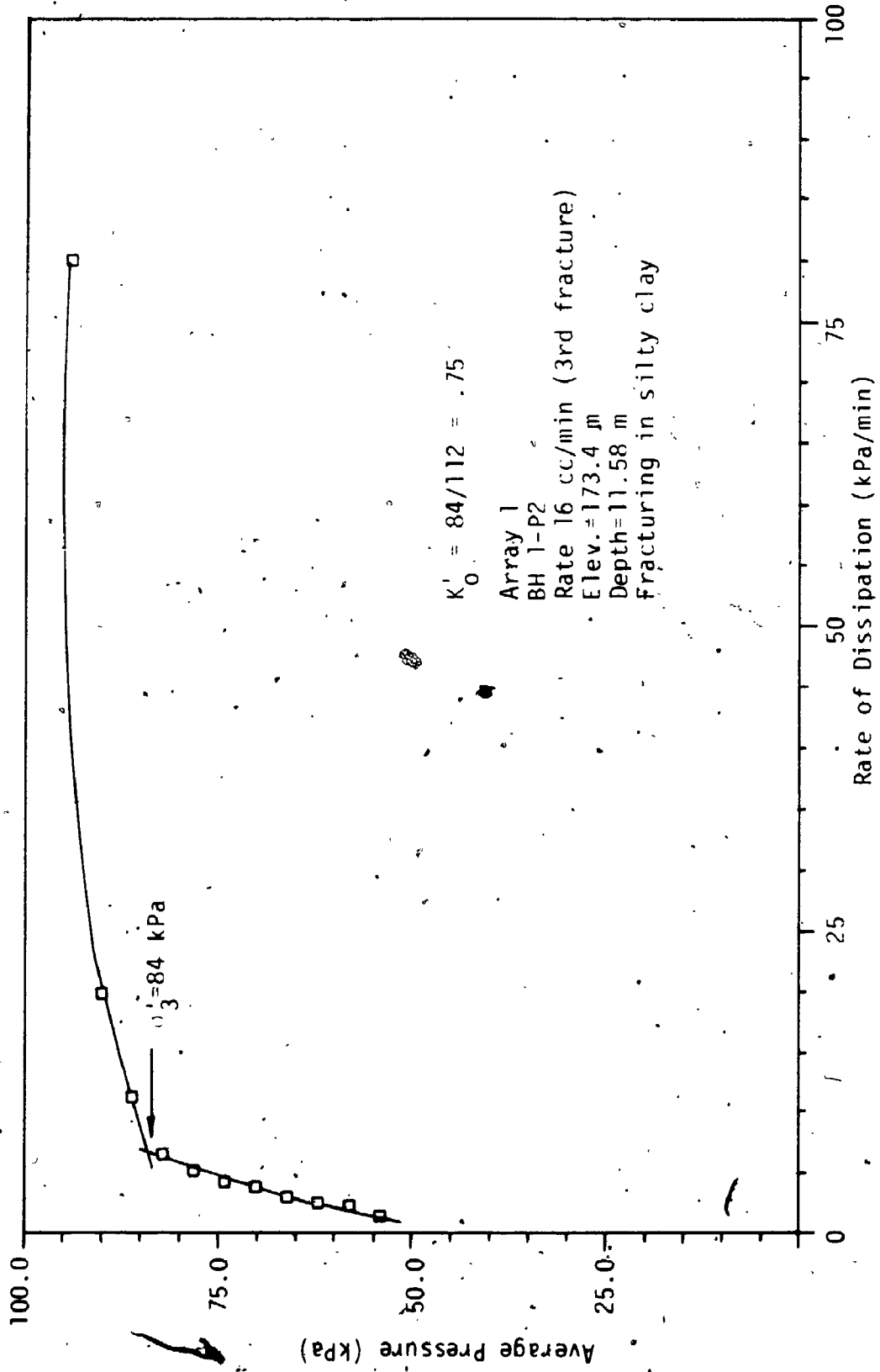


FIGURE B.4c Dissipation Curve for Hydraulic Fracturing Test 1-P2 (3rd fracture)

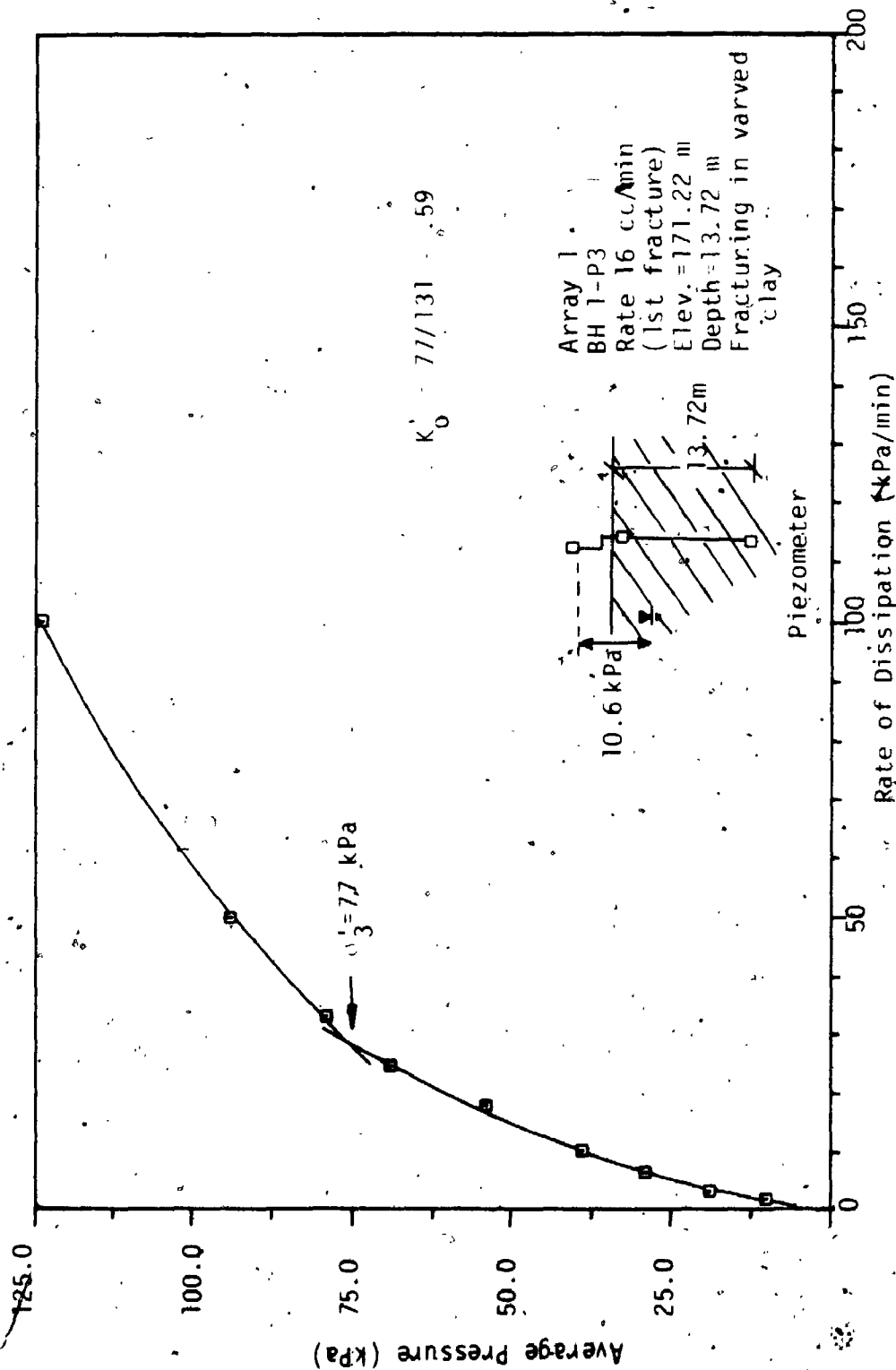


FIGURE B.5a Dissipation Curve for Hydraulic Fracturing Test 1-P3 (1st fracture)

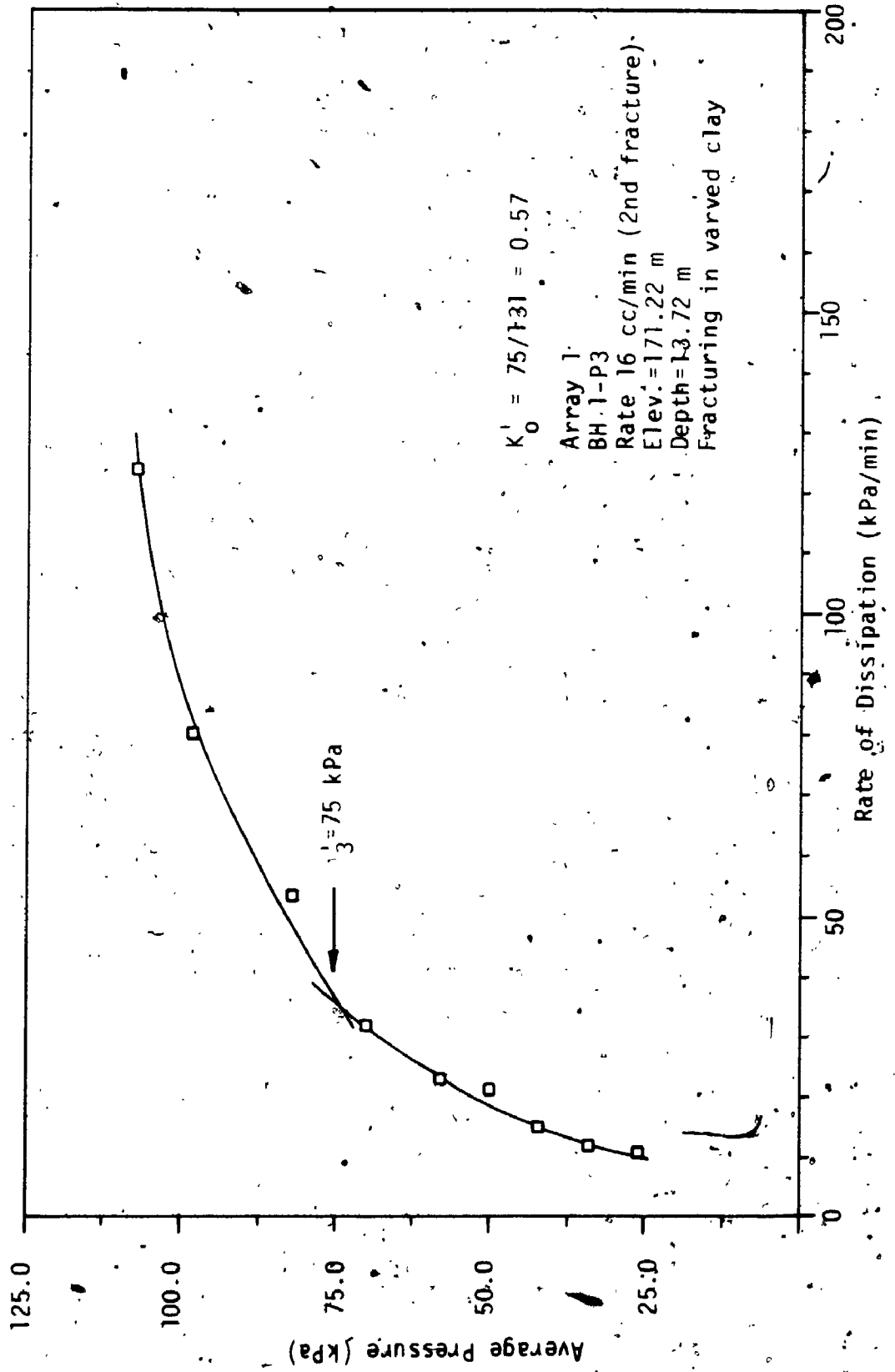
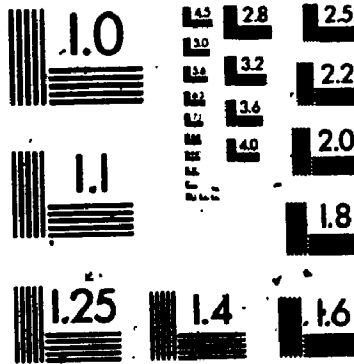


FIGURE B5.b Dissipation Curve for Hydraulic Fracturing Test 1-P3 (2nd fracture)

6

6

OF / DE



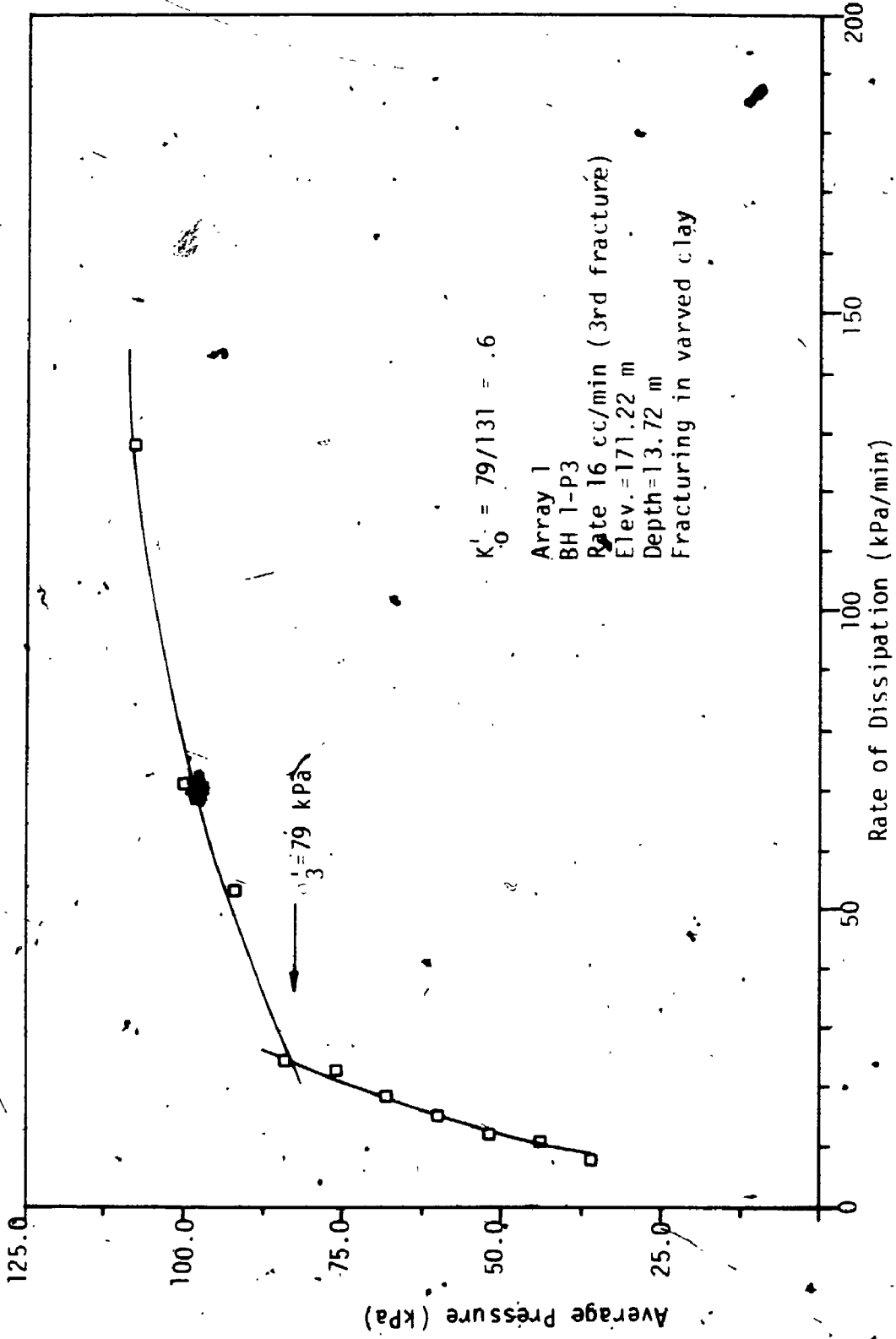


FIGURE B.5c Dissipation Curve for Hydraulic Fracturing Test 1-P3 (3rd fracture)

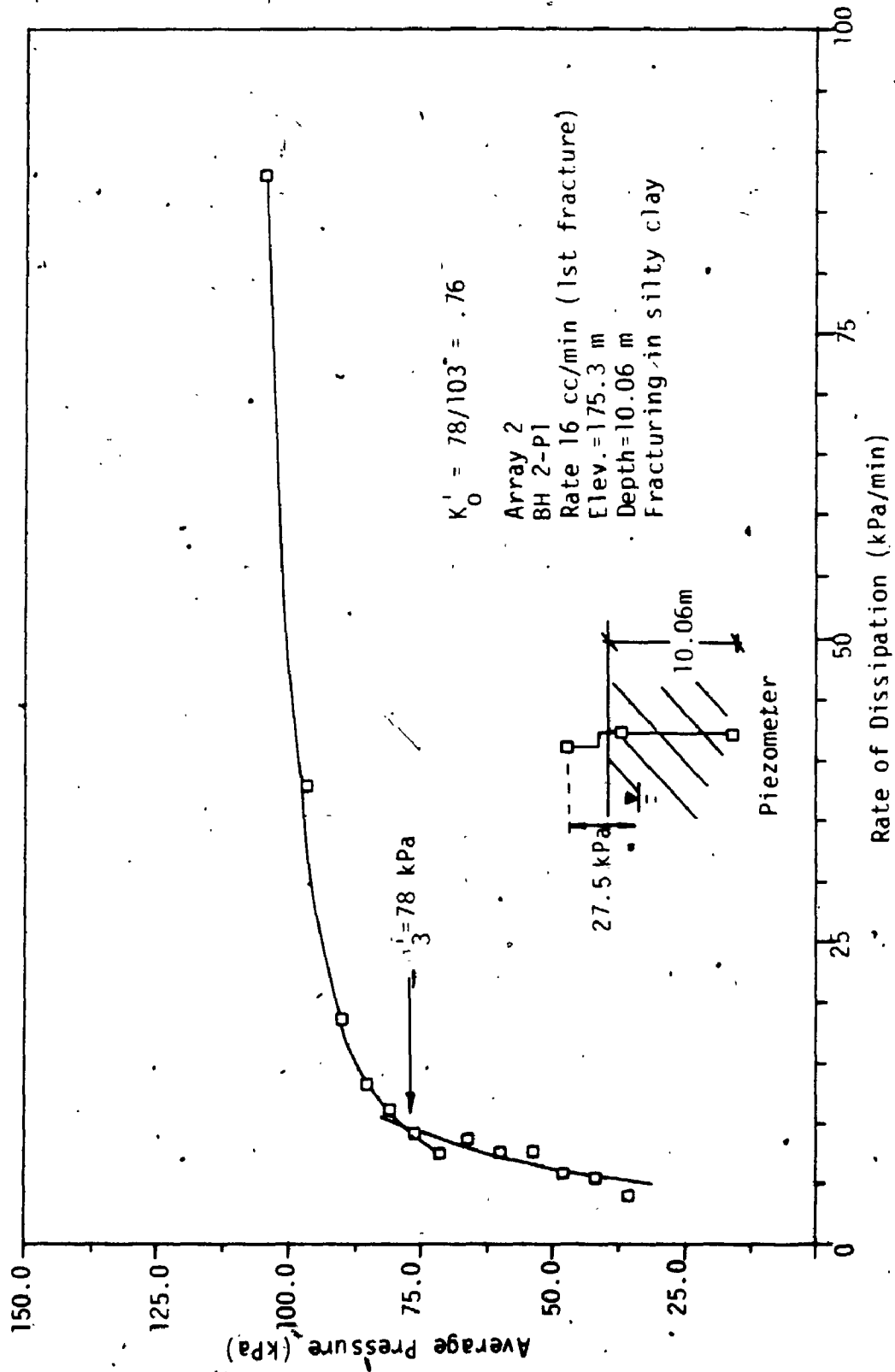


FIGURE B.6a Dissipation Curve for Hydraulic Fracturing Test 2-P1 (1st fracture)

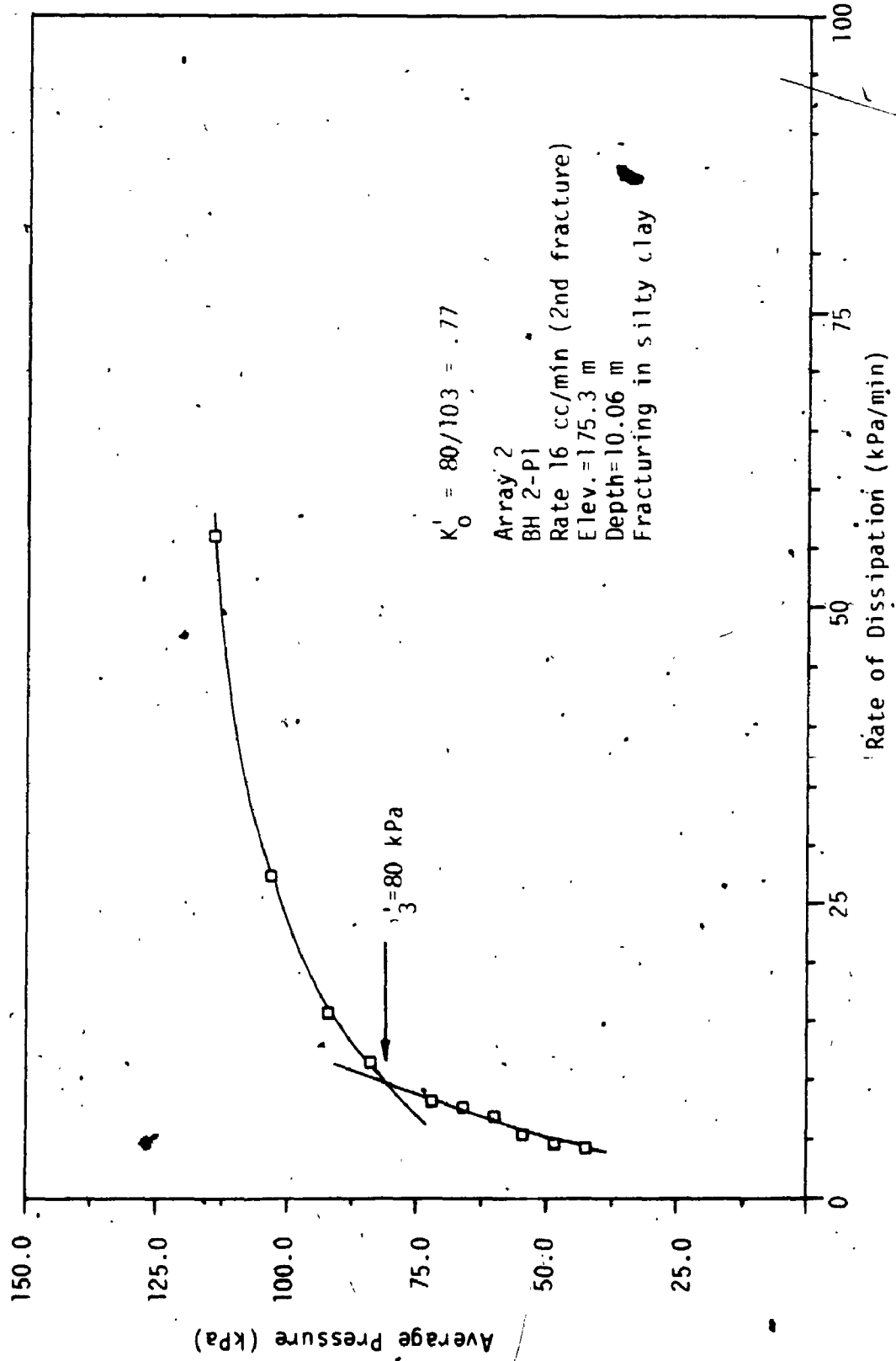


FIGURE B.6b Dissipation Curve for Hydraulic Fracturing Test 2-P1 (2nd fracture)

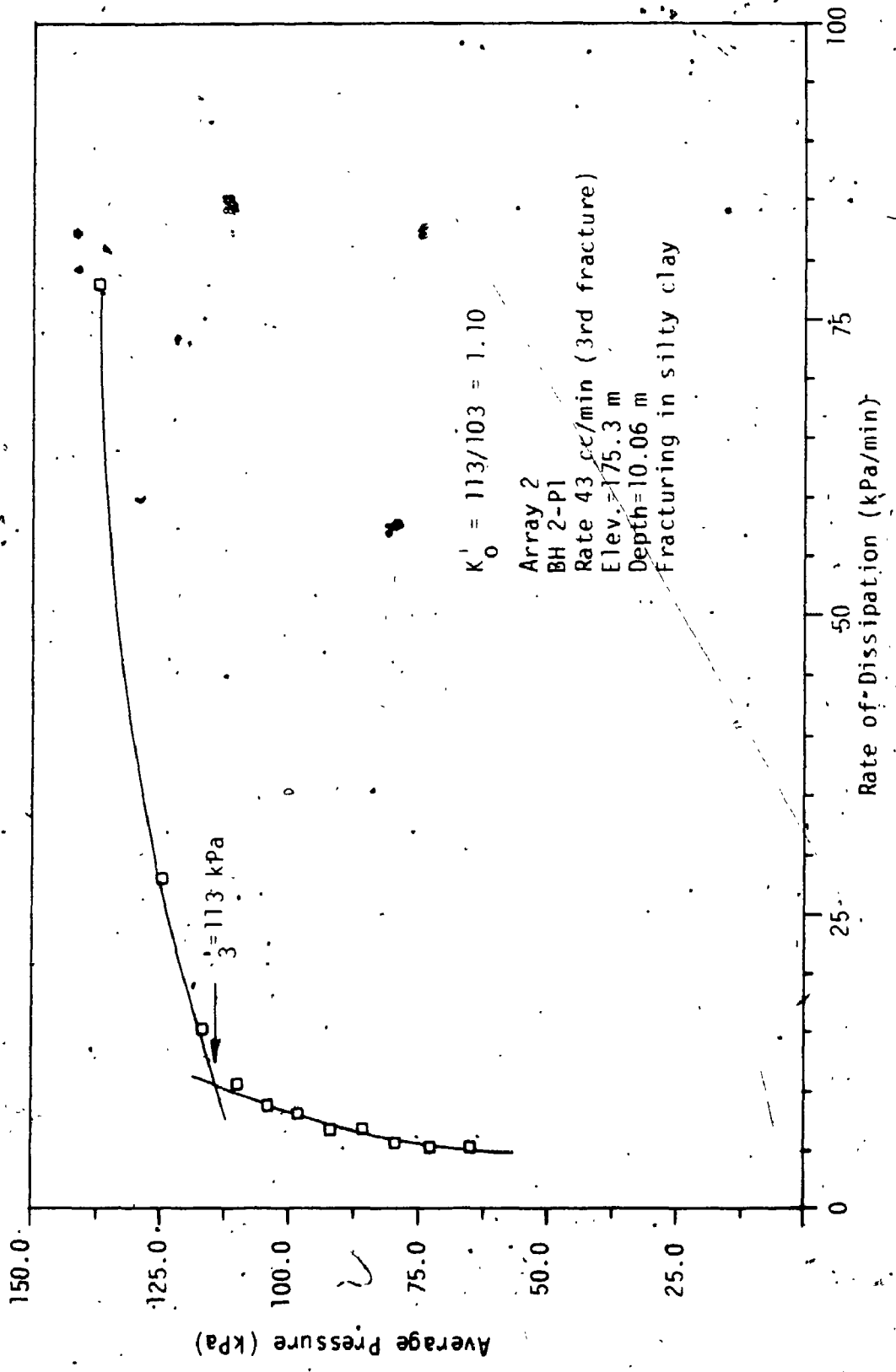


FIGURE B.6c Dissipation Curve for Hydraulic Fracturing Test 2-P1 (3rd fracture)

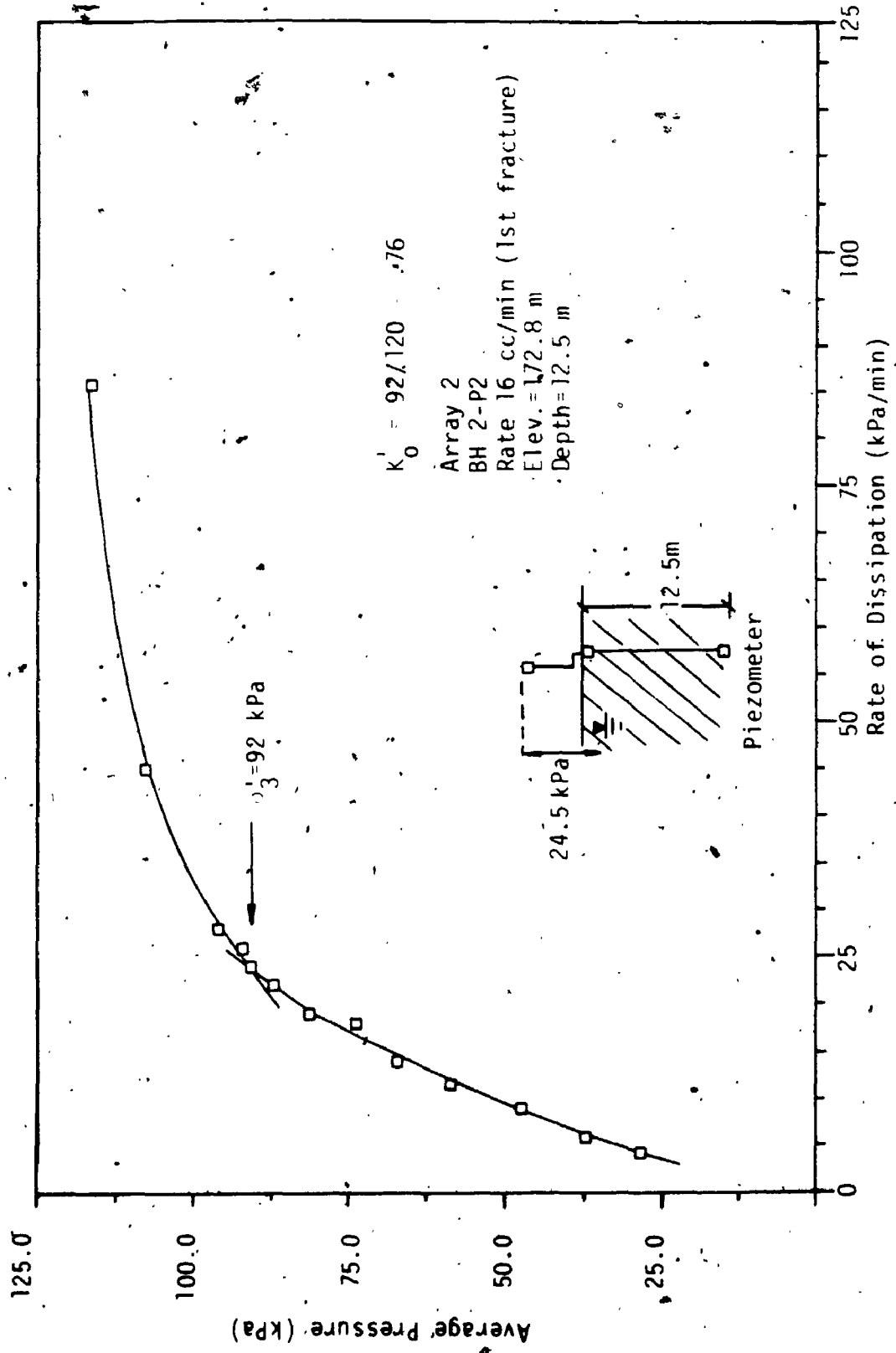
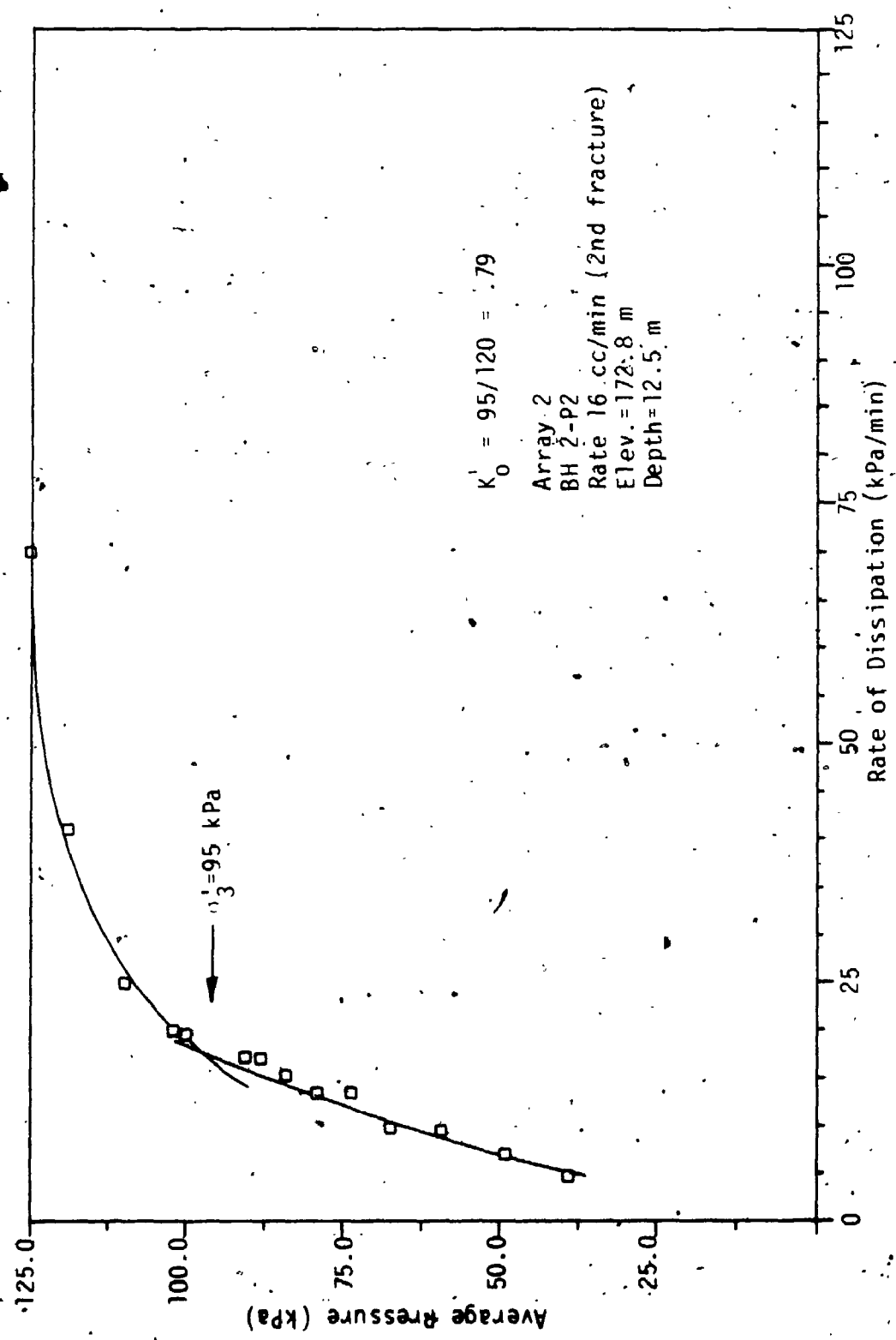


FIGURE B.7a Dissipation Curve for Hydraulic Fracturing Test 2-P2 (1st fracture)



$K_0^i = 95/120 = .79$

Array 2
BH 2-P2
Rate 16 cc/min (2nd fracture)
Elev. = 172.8 m
Depth = 12.5 m

FIGURE B.7b Dissipation Curve for Hydraulic Fracturing Test 2-P2 (2nd fracture)

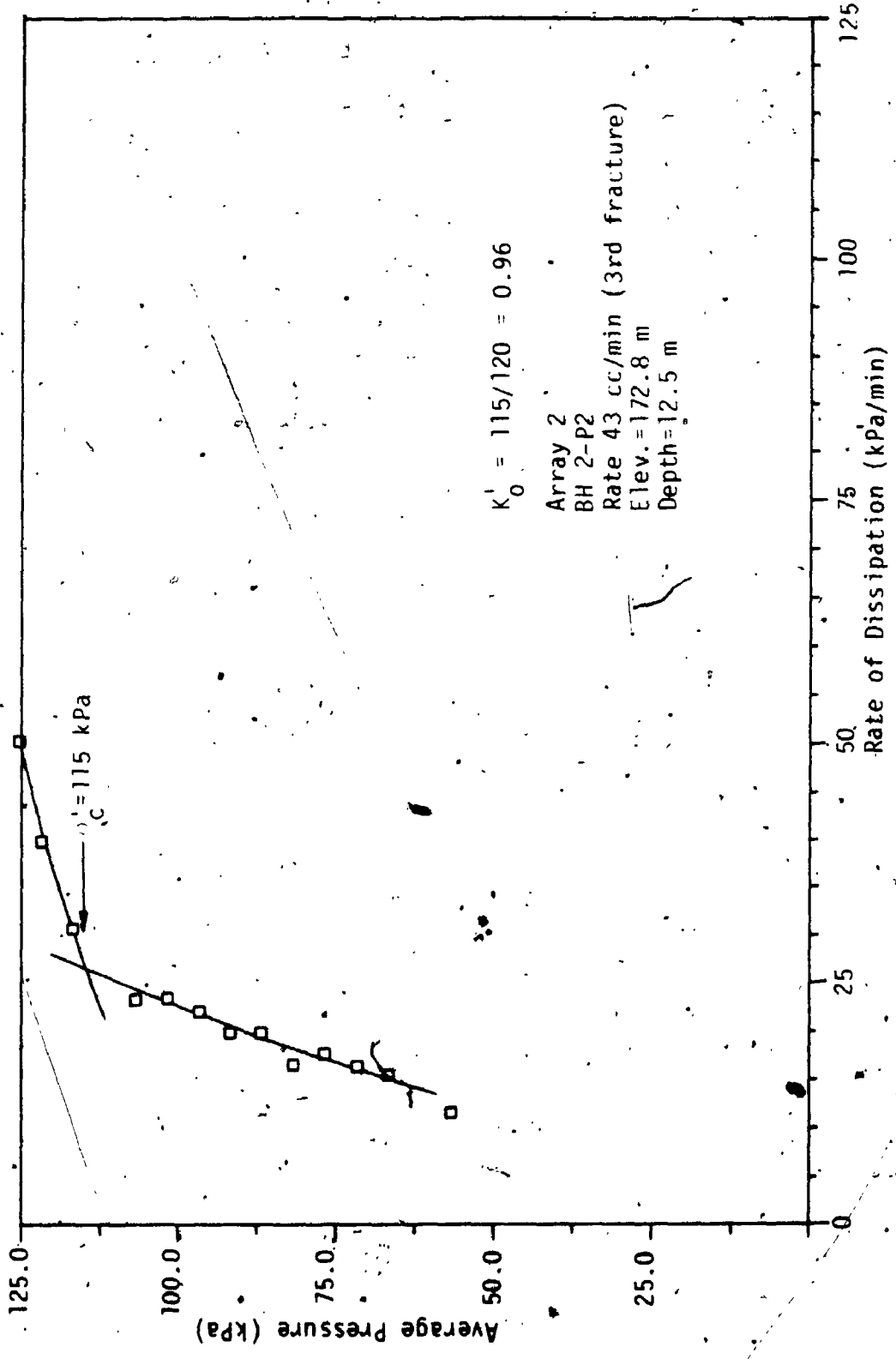


FIGURE B.7c Dissipation Curve for Hydraulic Fracturing Test 2-P2 (3rd fracture)

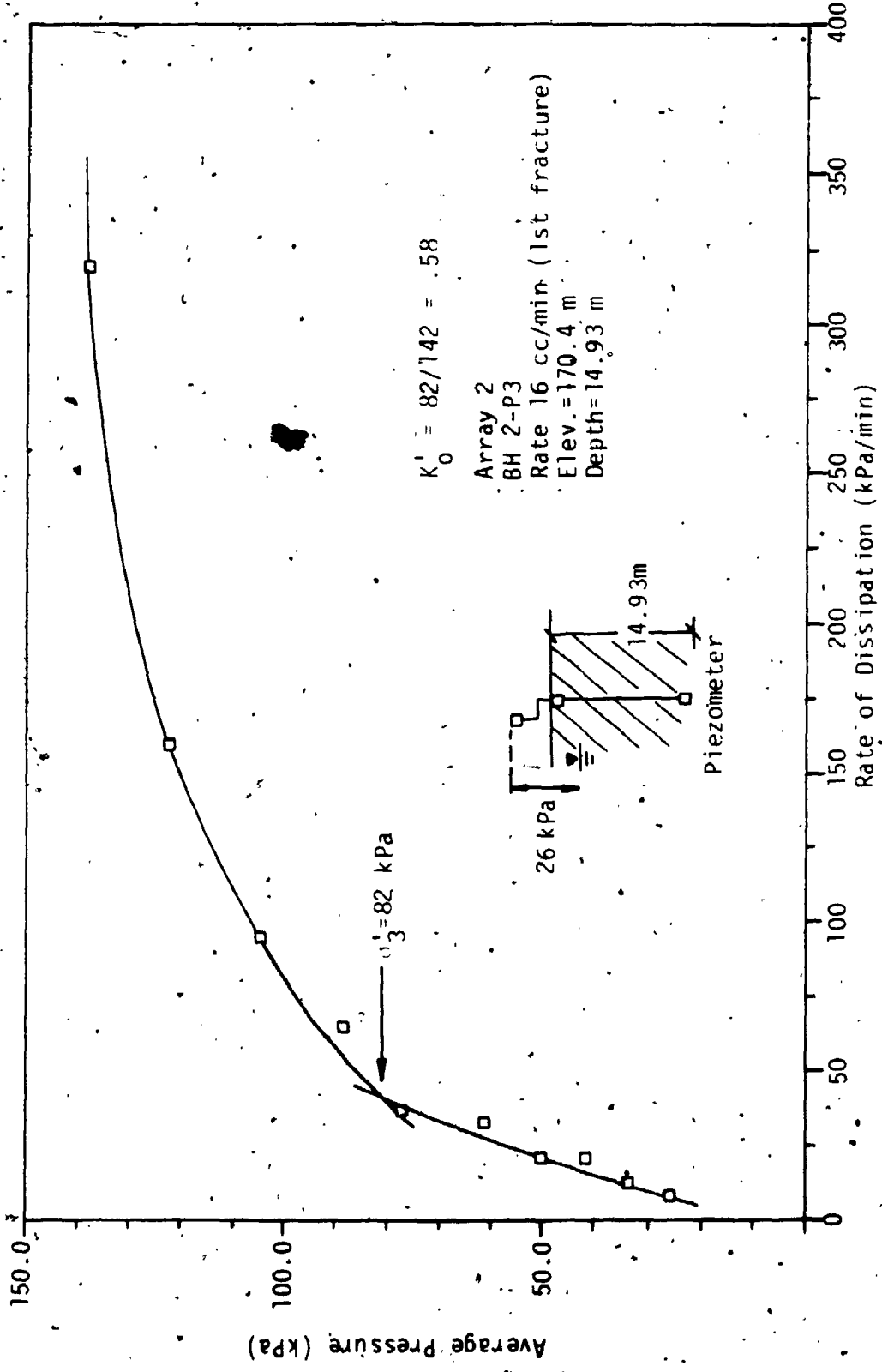


FIGURE B.8a Dissipation Curve for Hydraulic Fracturing Test 2-P3 (1st fracture)

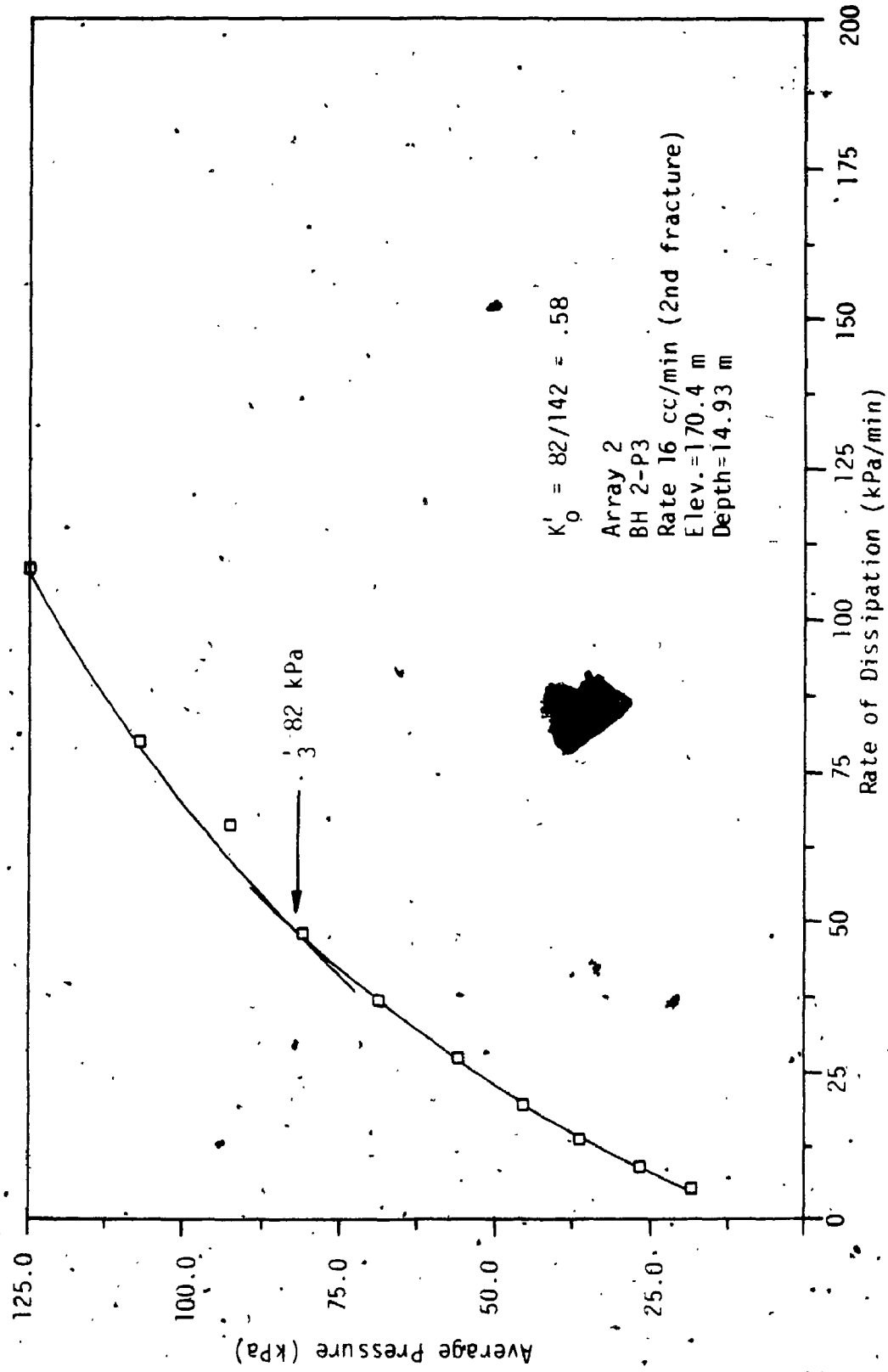


FIGURE B.8b Dissipation Curve for Hydraulic Fracturing Test (2nd fracture)

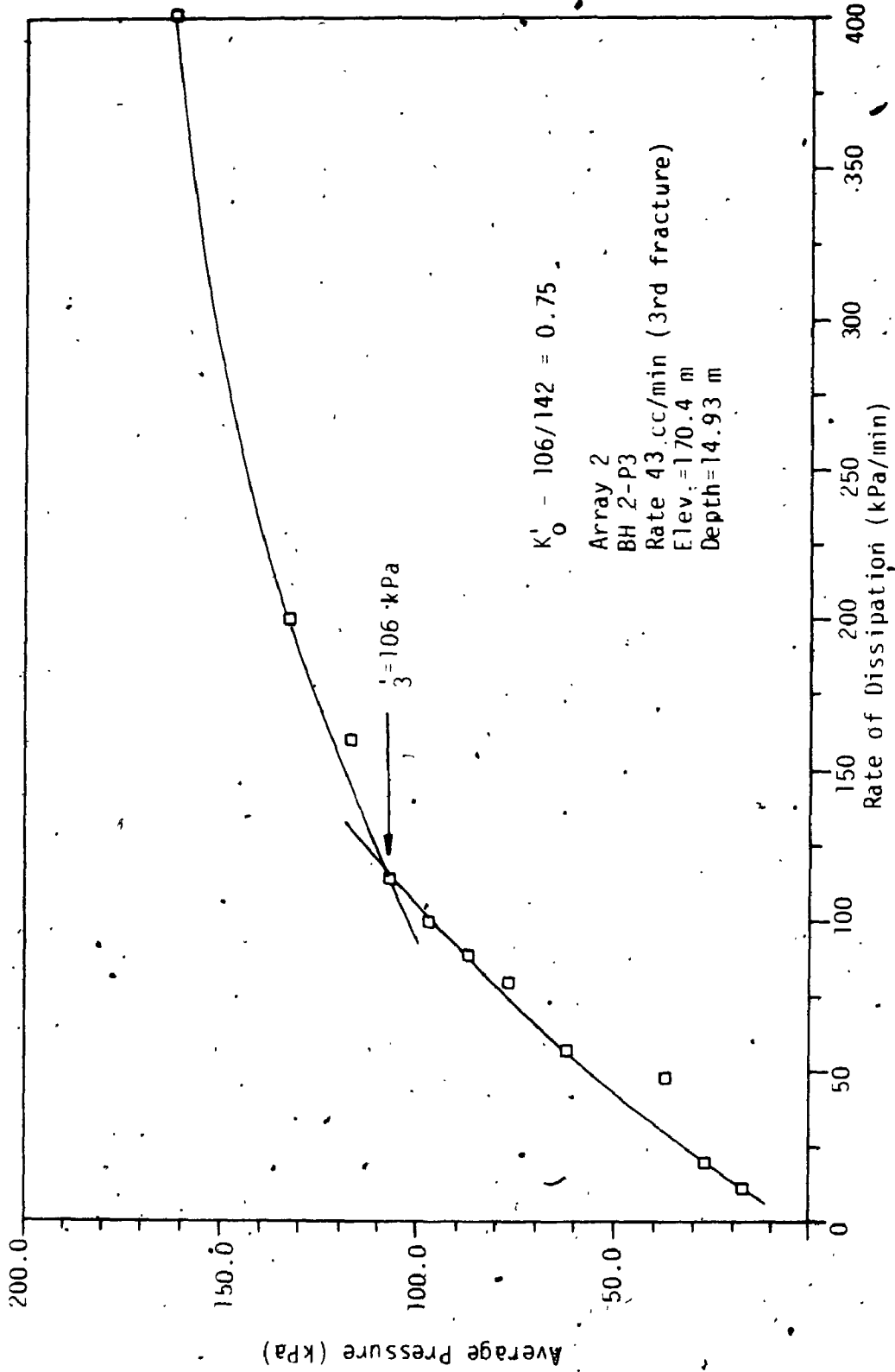


FIGURE B.8c Dissipation Curve for Hydraulic Fracturing Test (3rd fracture)

APPENDIX C

CONVENTIONAL LABORATORY TEST RESULTS

The following sections outline and discuss some of the laboratory testing included in this project. The results of grain size analysis, on the cohesionless deposit, unit weight determination and conventional oedometer tests are presented.

C.1 GRAIN SIZE ANALYSIS

The grain size curves for the cohesionless deposits at Arrays 1 and 2 are shown in Figures C.1 and C.2. The proportions of sand, silt and clay for the samples at various depths are shown in Figures 6.5 and 6.6. The material in the upper cohesionless deposit is predominantly sand, with a moderate amount of silt-sized particles. However, at depths of 2 m to 3.5 m at Array 2, and 2 m to 5 m at Array 1, the material is predominantly a loose sandy silt. The percentage of silt increases towards the sand and clay interface.

C.2 DETERMINATION OF UNIT WEIGHT

Specific gravity and water content determinations were performed on the sand and clay. The saturated unit weights (γ_s) of the materials were found using the following formula,

$$\gamma_s = \left(\frac{G_s + e}{1 + e} \right) \gamma_w \quad (C.1)$$

where G_s = specific gravity
 γ_w = unit weight of water
 e = void ratio

The void ratio was obtained, assuming full saturation of the soil, using the formula,

$$e = G_s w \quad (C.2)$$

where w is the natural moisture content.

Representative moisture contents were obtained for every 1.5 m of the silty-sand deposit, so that an average unit weight could be obtained. The values of γ_s calculated using equations C.1 and C.2 were found to vary between 17.6 and 20.9 kN/m³, with an average value slightly less than 19 kN/m³. Similar methods were applied to both the grey silty clay and the varved clay, yielding average γ_s values of 16 kN/m³ and 18.5 kN/m³ respectively. These values of unit weight in the clays were later verified by weighing clay samples of known dimensions.

C.3 ONE-DIMENSIONAL CONSOLIDATION TESTS

To study the consolidation characteristics, 11 conventional oedometer tests were carried out at various depths in the clay deposits at Array 1 and Array 2 down to about 13 m. The samples were either 48.8 mm in diameter, 12.7 mm in height or 70.7 mm in diameter, 24.8 mm in height. These samples were carefully trimmed from 152 mm tube samples. Table C.1 shows a summary of the consolidation test results. The consolidation curves (Figures C.3 to C.13) exhibit the typical characteristics of sensitive clays. The void ratio remains relatively

unchanged up to the preconsolidation pressure before it decreases sharply with increasing pressure. However, the slope of the e -log p curve gradually decreases with further increase in consolidation pressure. There is no significant difference in results obtained from samples of either size.

The 'crust' at Array 1 is in an overconsolidated condition with an OCR of 2.0 and a compression index, C_c , of 0.86. The grey silty clay is slightly overconsolidated with an OCR of 1.3 to 1.4. This OCR value is consistent with the value of 1.4 reported by Palmer and Belshaw (1979). The compression index, C_c , varies from 0.45 to 1.40, with an average of 0.79. The value of C_c seems to be increasing with depth within the silty clay soil layer. It also appears that the C_c values obtained for Array 1 are, in general, slightly higher than those for Array 2. The varved clay is overconsolidated with OCR of 1.8 to 2.0, and C_c ranges from 0.18 to 0.35. The average C_c value for the varved clay is 0.24, and comparing with the average C_c value for the silty clay, the varved clay is less compressible.

The preconsolidation pressure, p'_c , and the present effective vertical stress, p'_o , of the clay deposits at Arrays 1 and 2 are shown in Figures 6.5 and 6.6. The preconsolidation pressures at both arrays are rather similar. It is noteworthy to indicate that the calculated effective vertical pressure, in the silty clay at Array 1, including the surface traction provided by one metre of fill, is very close to the preconsolidation pressure.

C.4 RESULTS OF CIU TESTS ON VERTICALLY AND HORIZONTALLY ORIENTED CLAY SAMPLES

Figures C.14 to C.43 show the combined plots of the results of CIU tests on horizontally ($i = 90^\circ$) and vertically ($i = 0^\circ$) oriented samples at comparative depths. The descriptions of the stress-strain behaviours, excess pore pressure conditions and stress paths for these tests at $i = 0^\circ$ and $i = 90^\circ$ have been given in Chapter 7.

C.5 DRAINED TRIAXIAL TESTS ON SILTY FINE SAND

The procedure for the drained triaxial tests on silty sand discussed in Chapter 7 is outlined in the following paragraphs. The equipment used for these tests is the standard triaxial test apparatus used in Soils Laboratories.

The tests were carried out on cylindrical samples with diameters of 50.8 mm and heights of 101.6 mm. The specimen was contained in a membrane and sealed with 'O' rings, two at each end. During the placement of the sample, a split mould (manufactured by Soiltest, Chicago) was used for supporting the specimen. An assembly of a thin perforated plate inserted between two porous stones was placed on the pedestal of the triaxial cell. This plate is 48 mm in diameter with 1 mm holes arranged in concentric rings. During the 'saturation phase' water permeated uniformly through the sample by this perforated plate. The use of this plate was found to have facilitated the process of saturation.

Loose, medium and dense sand samples were prepared. The lowest range of porosities was obtained by tamping single layers of wet sand with a brass rod (diameter = 220 mm, weight = 506 g). The placement moisture content was about 18% and the resulting porosity was around 37%. Medium dense packing of sand was prepared by light tamping of the sample at a placement moisture content of 12%. The porosities which resulted from this procedure varied from 41% to 44%. For higher porosities, sand with 10% moisture content was placed carefully in the split mould and the sample was lightly tamped with a hollow brass rod (weight = 393 g). The porosities obtained in this way varied from 47% to 50%.

Filter paper, porous stone and a top cap were placed on the sample. A small level was used when levelling the top cap which was supplied with a drainage line connected to a vacuum. A suction pressure was applied (-25 kPa to -50 kPa) after 'O' rings were placed over the membrane and top cap. The strength of the sample acquired at this 'consolidation pressure' was sufficient to permit removal of the mould. For extension tests, the top cap or loading cap was provided with a slotted plate which allowed the modified load cell to 'extend' the sample. This loading cap is shown in Figure 8.25. At this stage, the triaxial cell was assembled and it was filled with deaired water. Cell pressure was applied as soon as the vacuum was disconnected.

Deaired water was allowed to permeate through the sample under a small hydrostatic head and the residual vacuum suction pressure in the

sample. Both cell pressure and back pressure were increased to facilitate saturation of the sample. A slightly larger cell pressure than the back pressure was used to avoid collapse of the sample during saturation. Under a back pressure of 450 kPa, B values of 85% to 95% were obtained. The sample was consolidated to the desired pressure and it was subsequently sheared at a strain rate of 3.1% per hour. (It was shown in pilot tests that excess pore pressure was not recorded even when the tests were conducted at 12% per hour. Volumetric change, deformation and axial load were monitored throughout the test.

TABLE C.1 CONVENTIONAL ONE DIMENSIONAL OEDOMETER CONSOLIDATION TEST RESULTS

Location	Description	Depth (m)	p_c (kPa)	OCR	Sample Diameter (mm)	C_c
Array 1	silty clay 'crust'	6.86	151	2.0	50	.86
Array 1	silty clay	8.28	111	1.3	50	1.21
Array 1	silty clay	9.78	120	1.3	50	1.41
Array 1	layered clay	11.33	150	1.4	50	.91
Array 1	varved clay	12.9	195	1.6	50	.35
=====						
Array 2	silty clay	8.85	125	1.4	70.66	.45
Array 2	silty clay	10.66	140	1.4	70.66	.76
Array 2	silty clay	11.78	195	1.8	70.66	.88
Array 2	varved clay	13.30	220	1.8	70.66	.47
Array 2	varved clay	14.0	260	2.0	50	.18
Array 2	varved clay	15.2	170 (probably disturbed)	-	70.66	.20

Note: OCR for silty clay (1.3-1.4)
 OCR for varved clay (1.8-2.0)

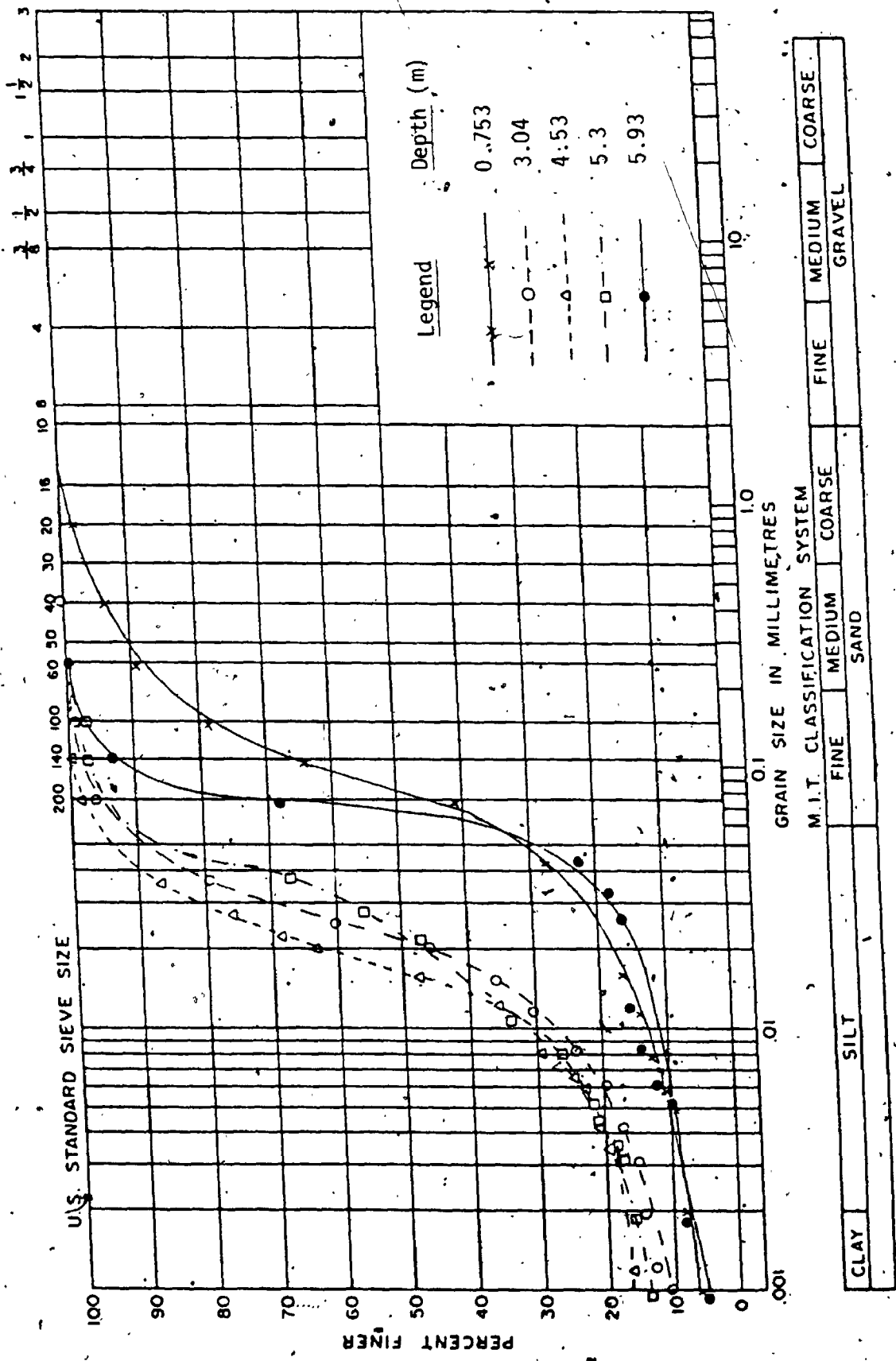


FIGURE C.1 Hydrometer Analysis - Array 1

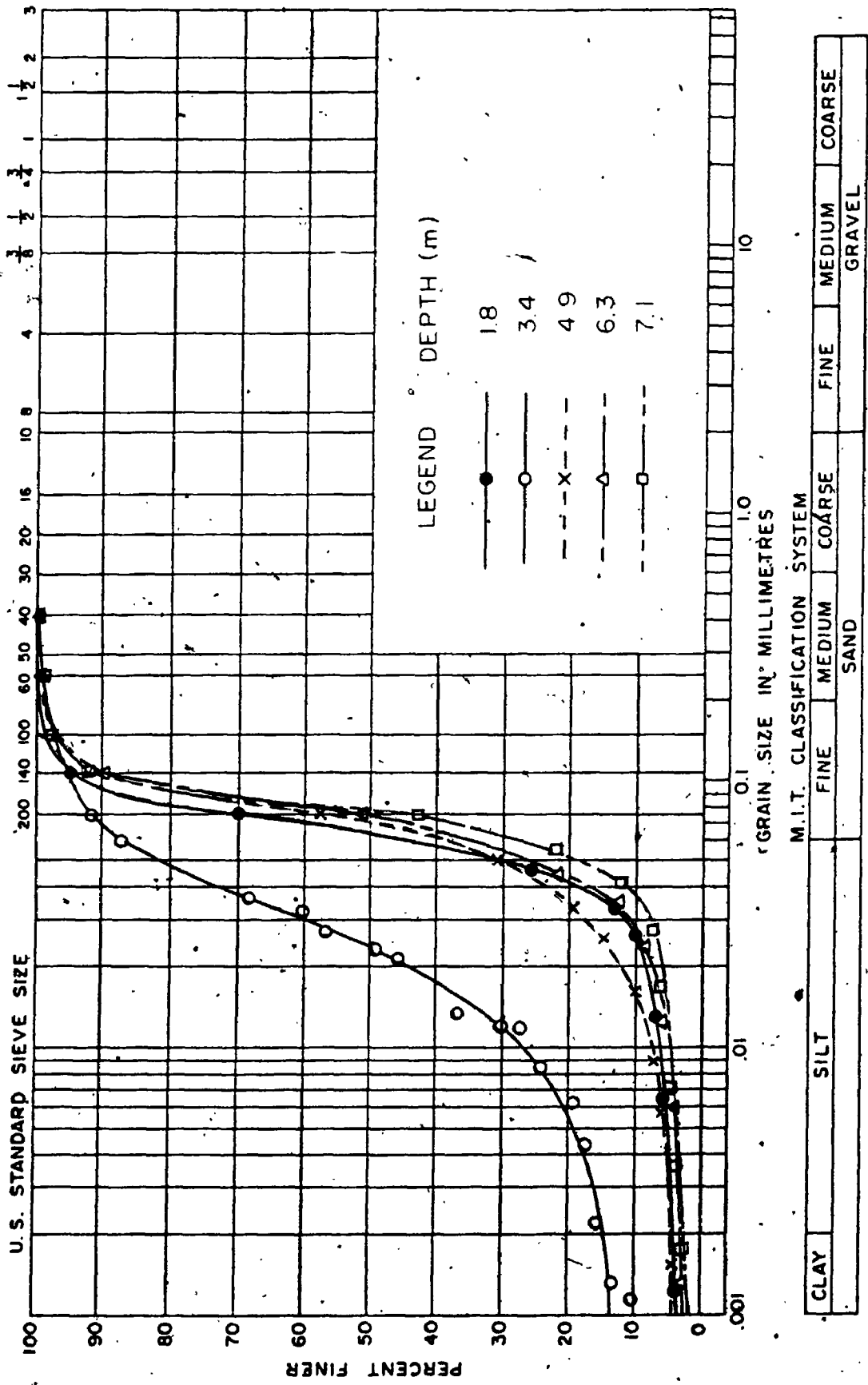


FIGURE C.2 Hydrometer Analysis - Array 2

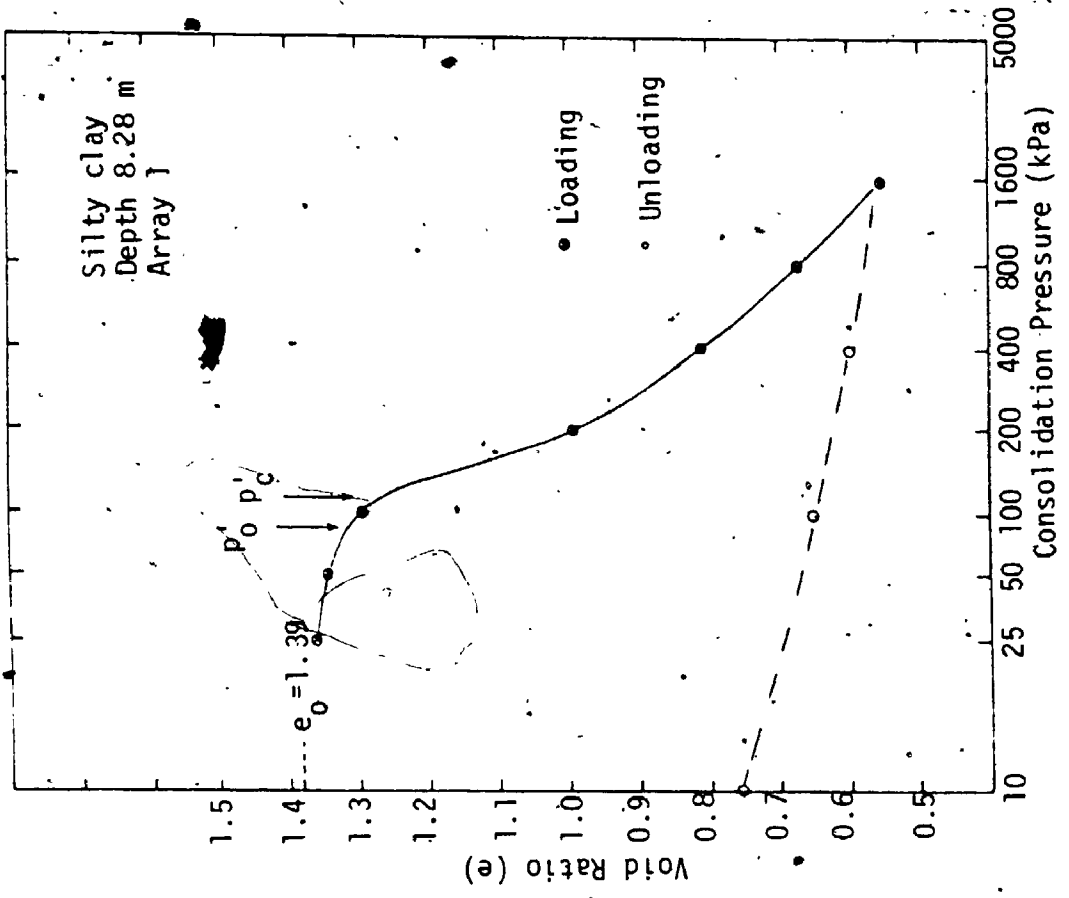


FIGURE C.4 Consolidation Curve for One Dimensional Conventional Oedometer Test.

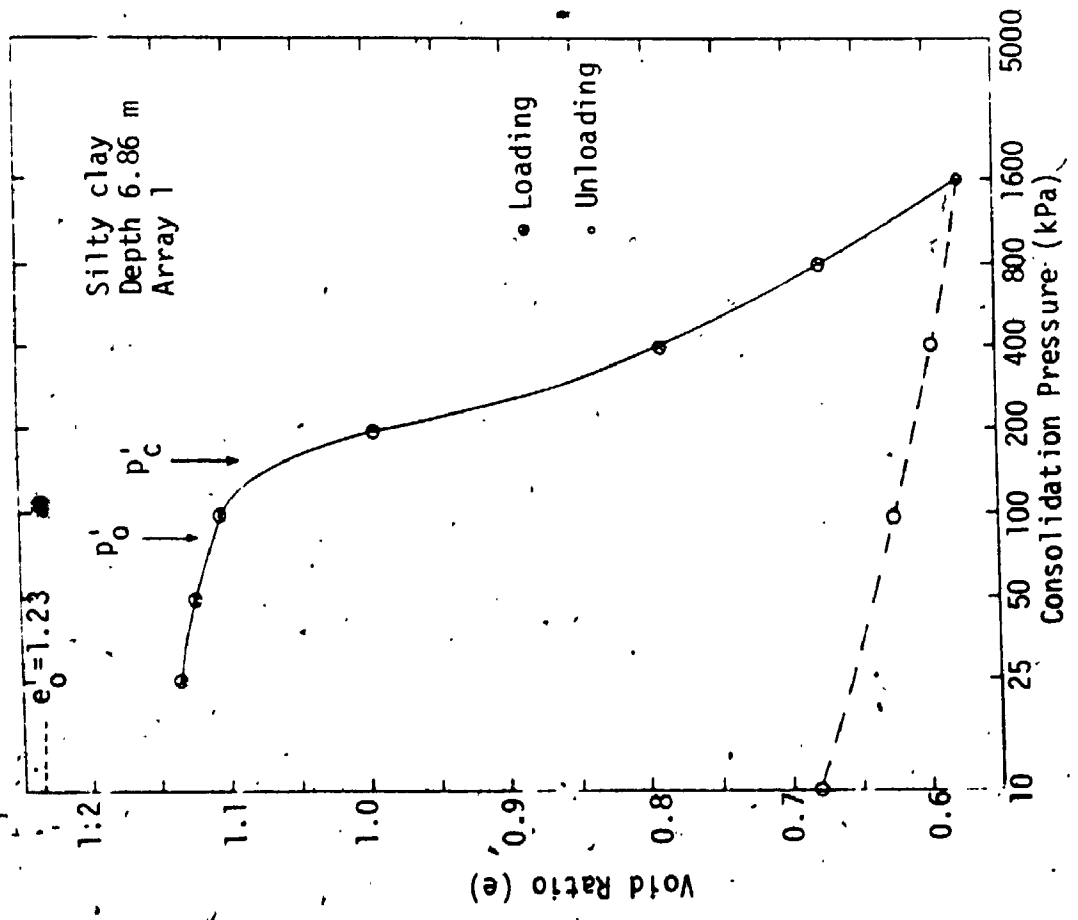


FIGURE C.3 Consolidation Curve for One Dimensional Conventional Oedometer Test.

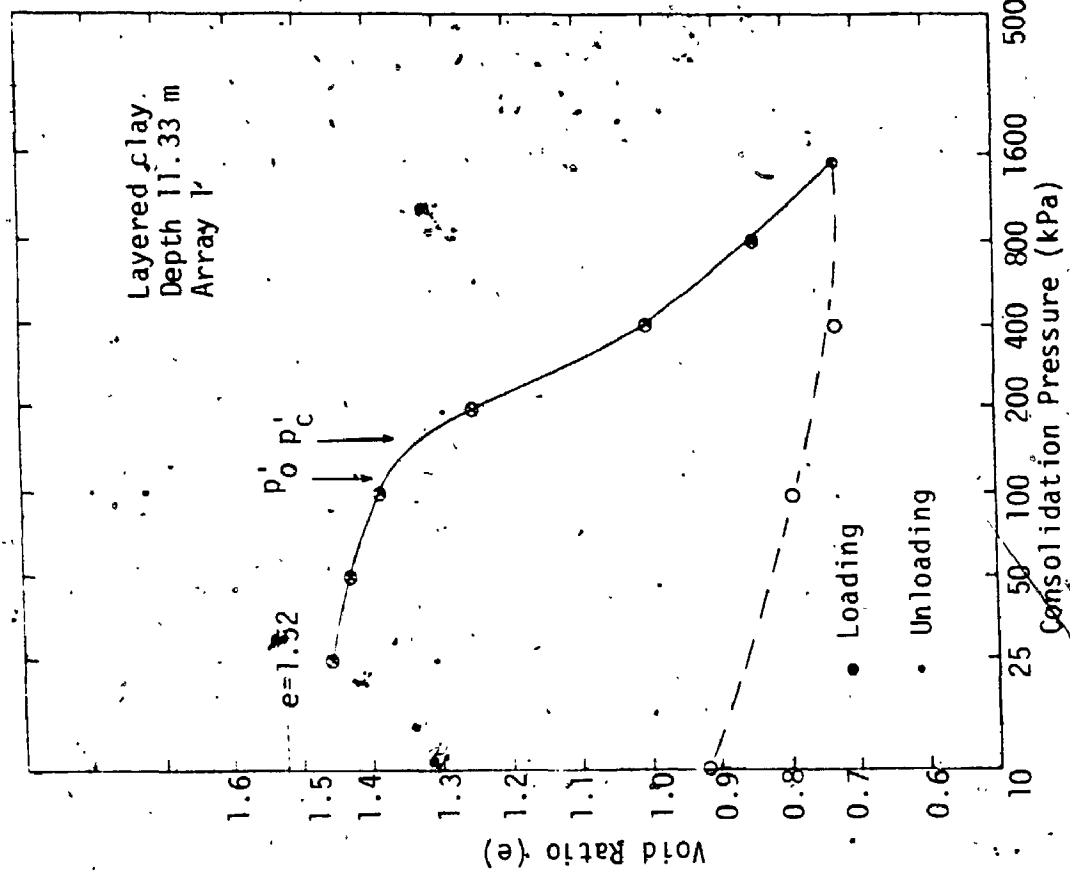


FIGURE C.6 Consolidation Curve for One Dimensional Conventional Oedometer Test

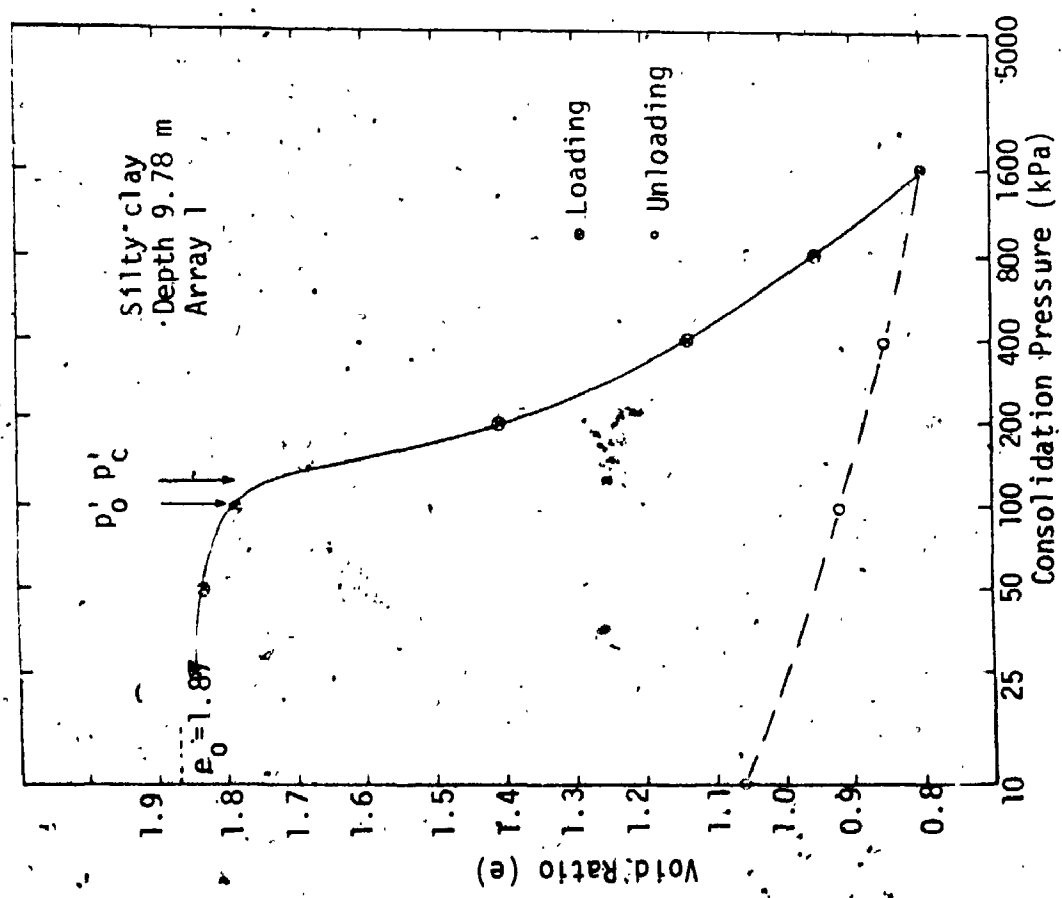


FIGURE C.5 Consolidation Curve for One Dimensional Conventional Oedometer Test

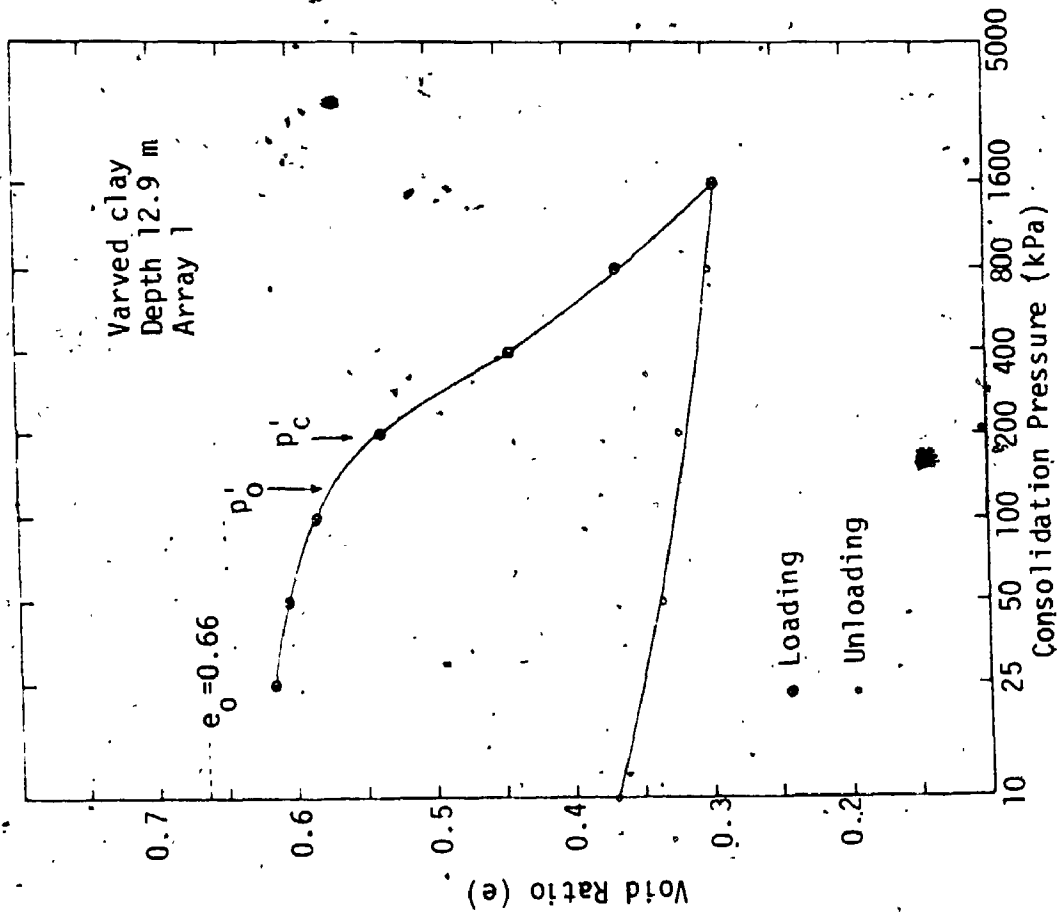


FIGURE C.7 Consolidation Curve for One Dimensional Conventional Oedometer Test

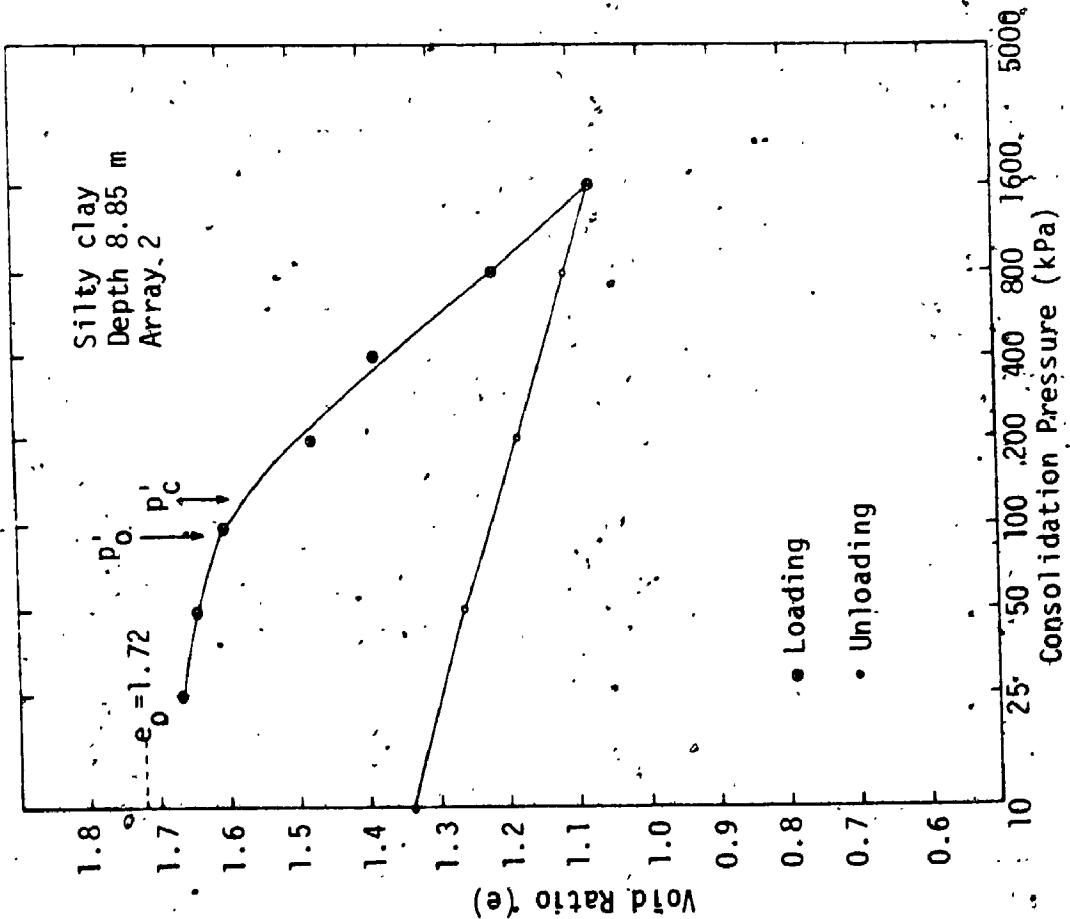
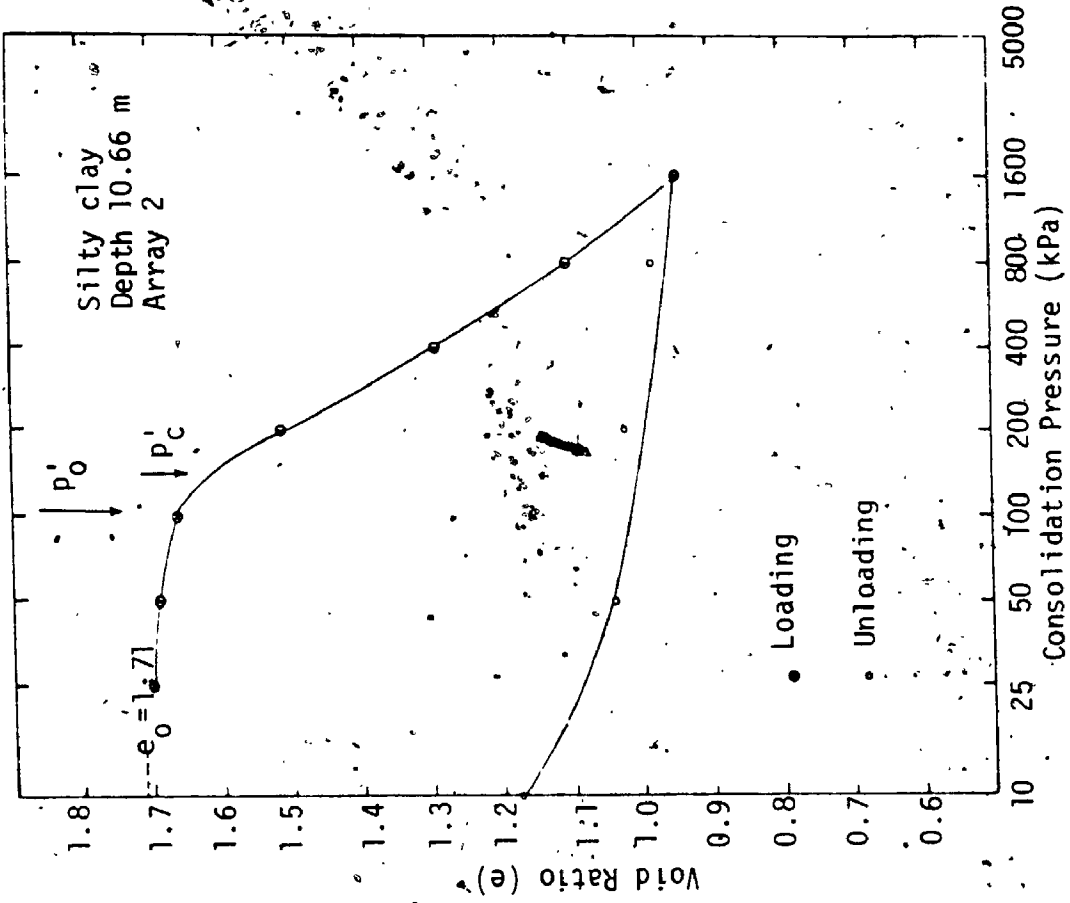


FIGURE C.9 Consolidation Curve for One Dimensional Conventional Oedometer Test

FIGURE C.8 Consolidation Curve for One Dimensional Conventional Oedometer Test

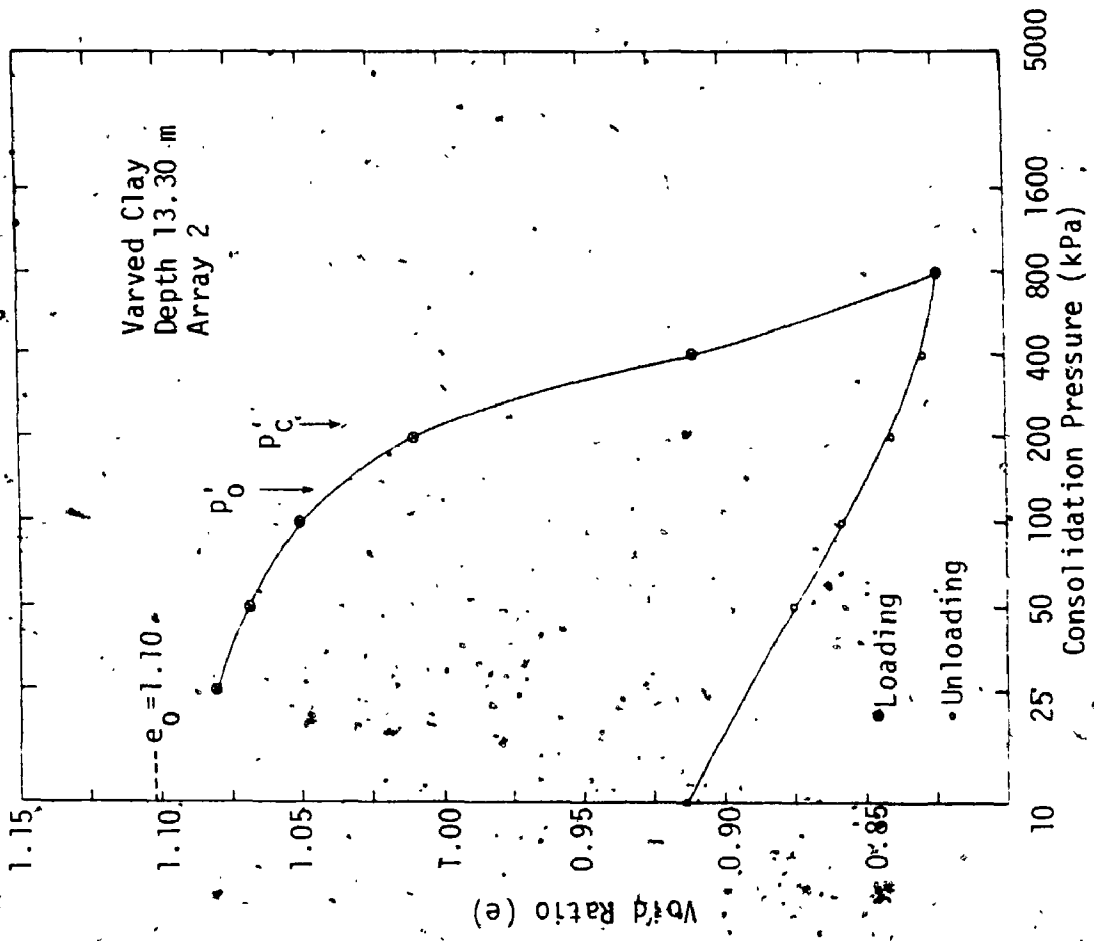


FIGURE C.11 Consolidation Curve for One Dimensional Conventional Oedometer Test 439

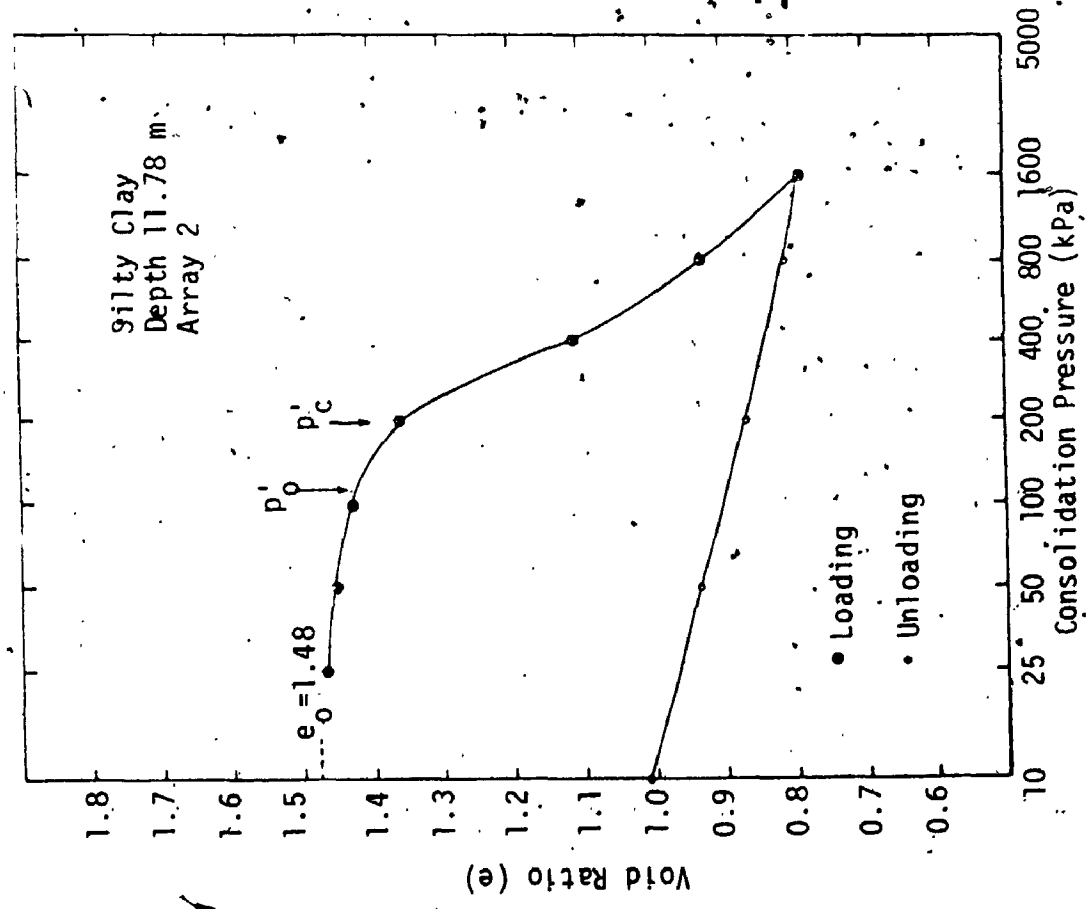


FIGURE C.10 Consolidation Curve for One Dimensional Conventional Oedometer Test

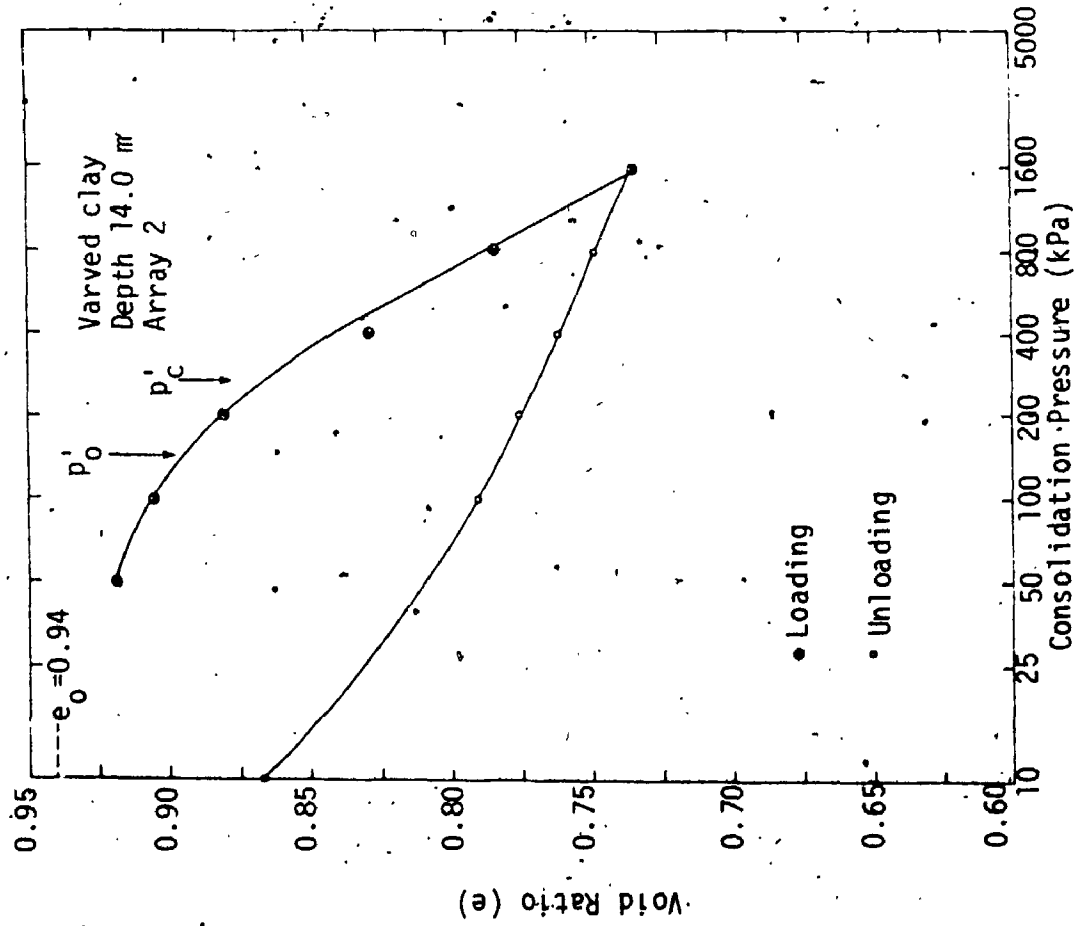


FIGURE C.12 Consolidation Curve for One Dimensional Conventional Oedometer Test

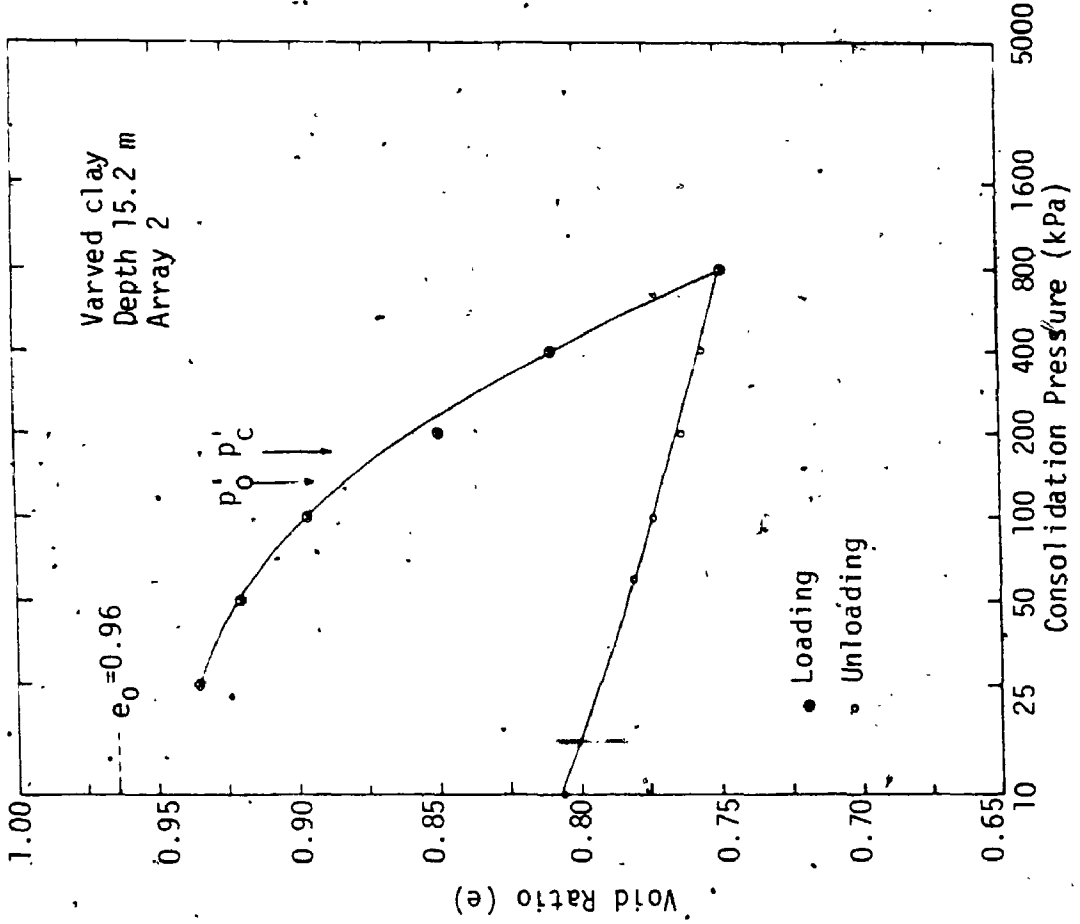


FIGURE C.13 Consolidation Curve for One Dimensional Conventional Oedometer Test

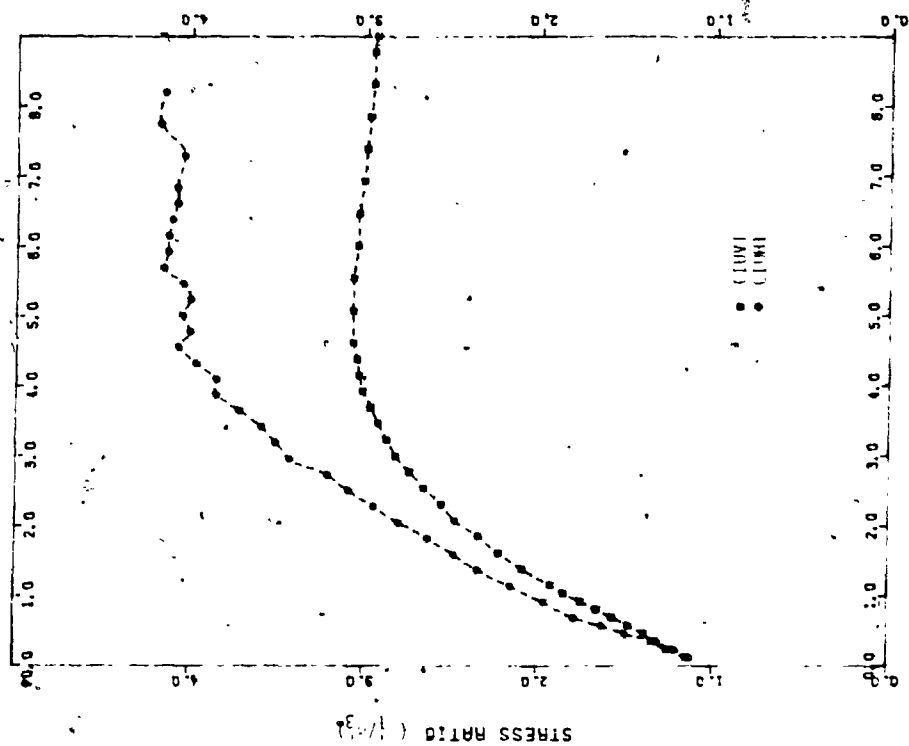


FIGURE C.15 Stress Ratio-Strain Relationship from CIU Tests on Vertically and Horizontally Oriented Silty Clay Samples

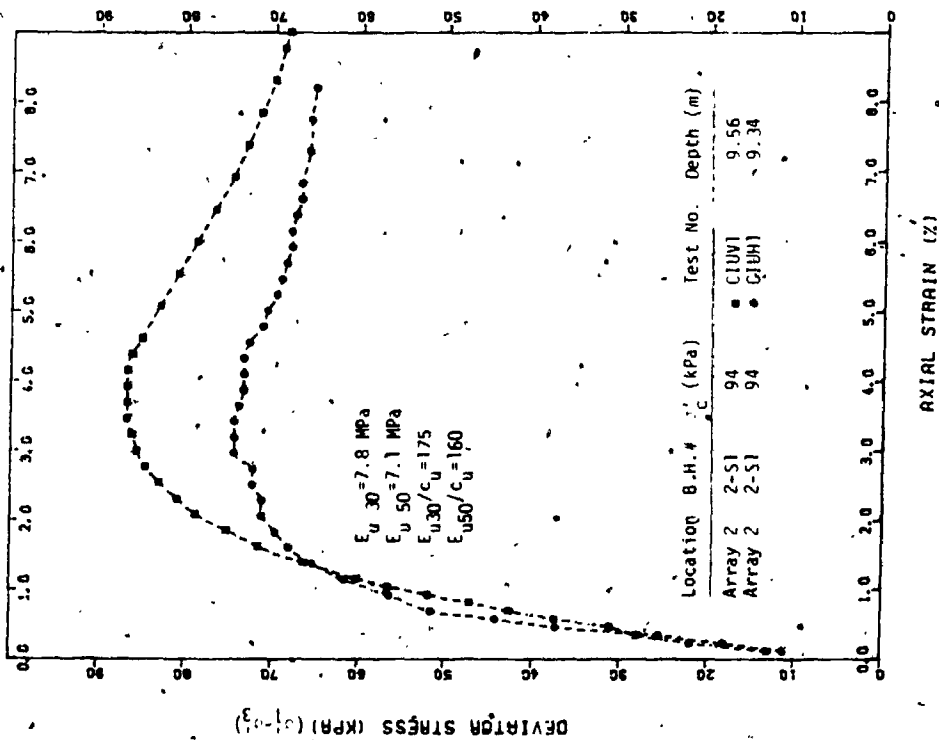


FIGURE C.14 Stress-Strain Relationship from CIU Tests on Vertically and Horizontally Oriented Silty Clay Samples

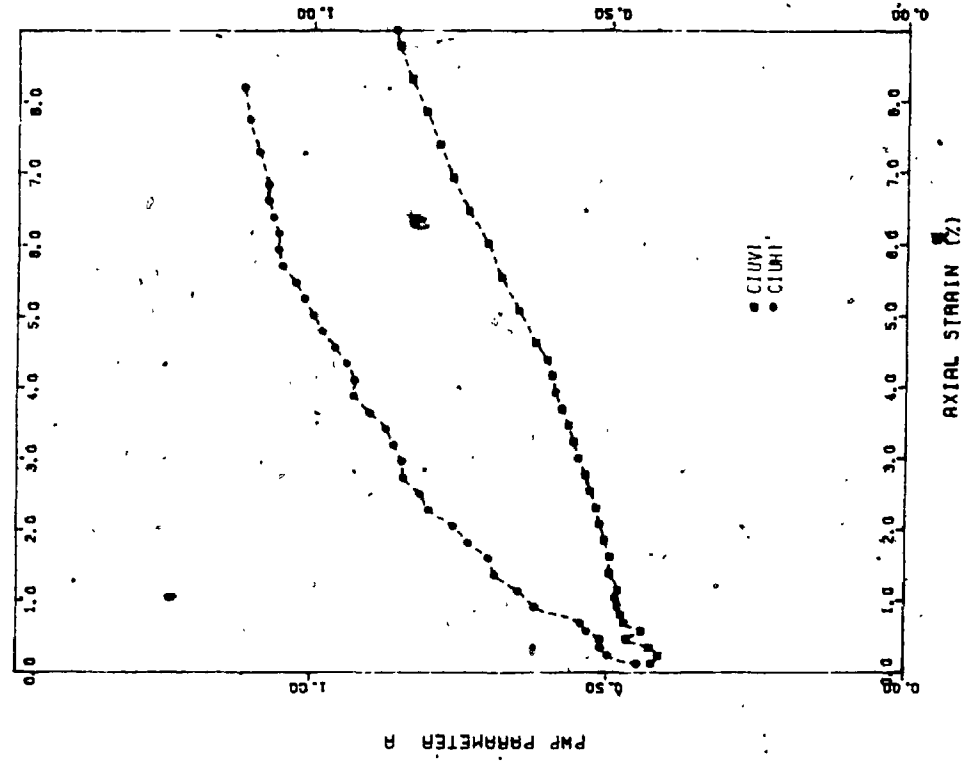


FIGURE C.17 Pore Pressure Parameter A - Strain Relationship From CIU Tests on Vertically and Horizontally Oriented Silty Clay Samples

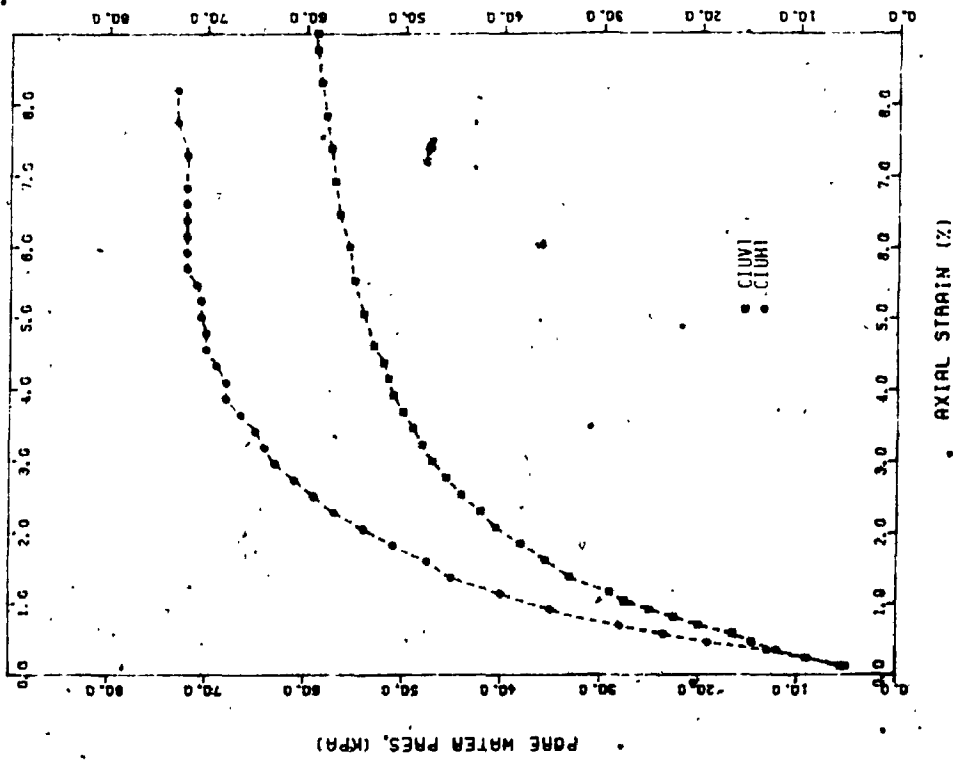


FIGURE C.16 Excess Pore Water Pressure-Strain Relationship from CIU Tests on Vertically and Horizontally Oriented Silty Clay Samples

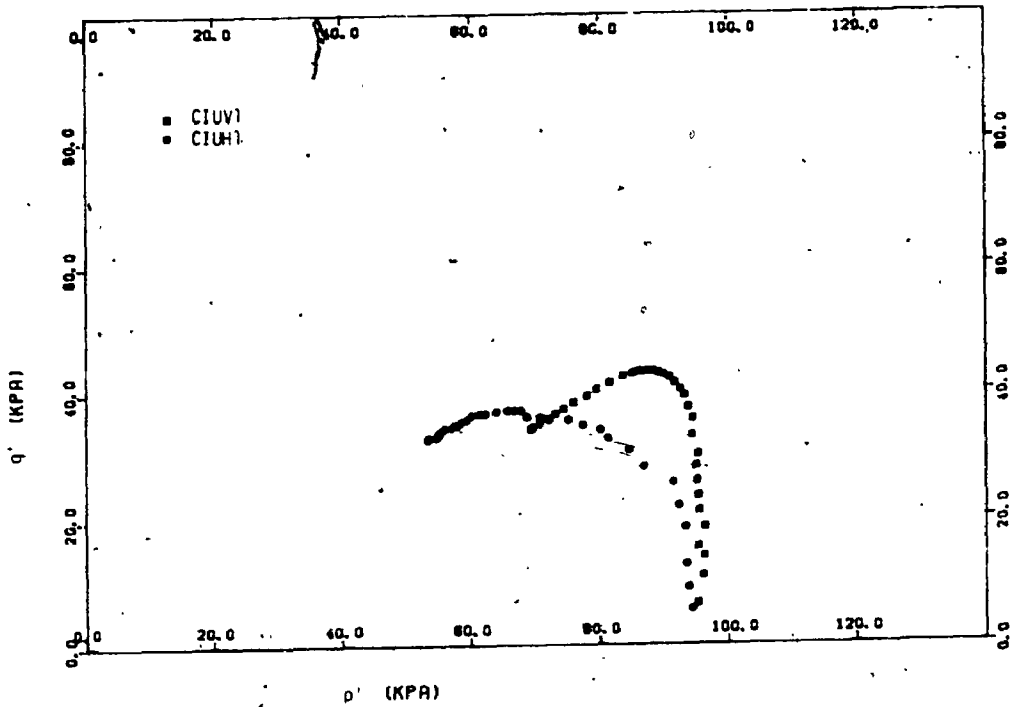


FIGURE C.18 Effective p-q Stress Path Plot from CIU Tests on Vertically and Horizontally Oriented Silty Clay Samples

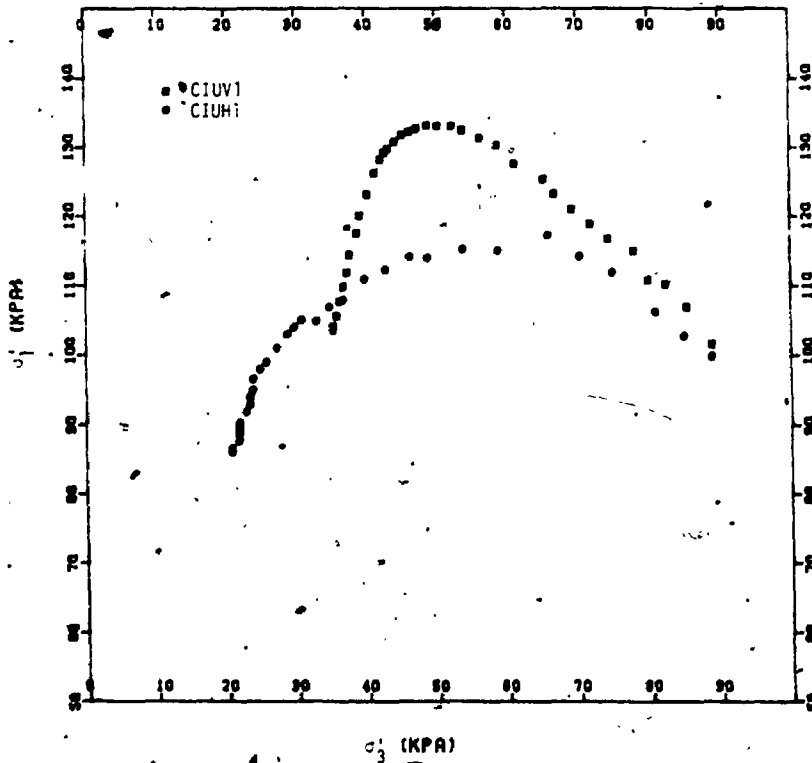


FIGURE C.19 Effective σ_1 - σ_3 Stress Path Plot from CIU Tests on Vertically and Horizontally Oriented Silty Clay Samples

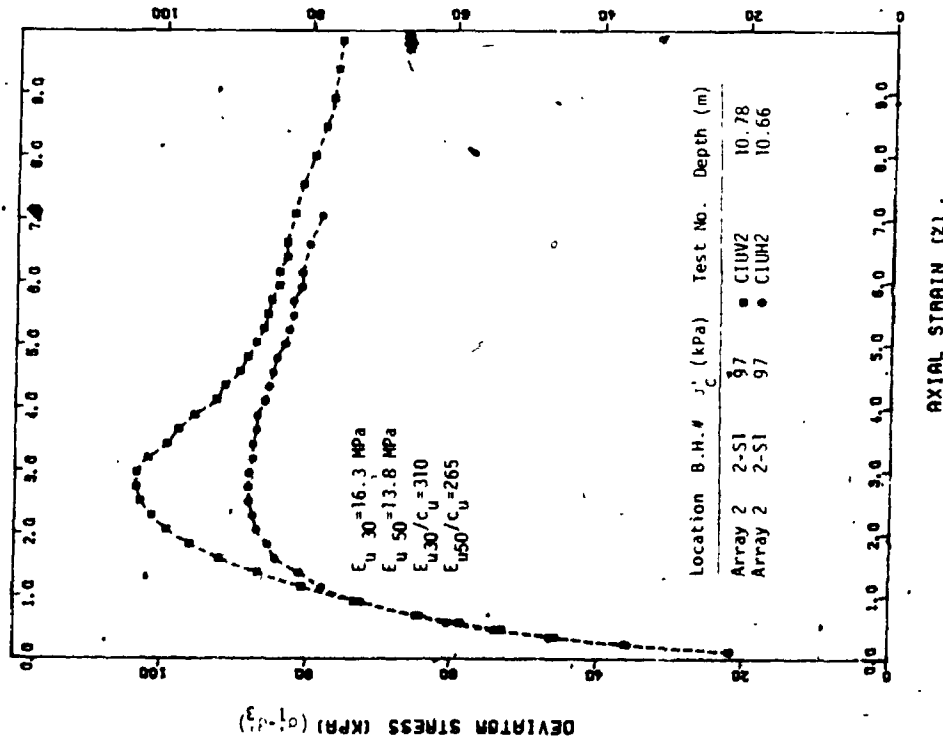


FIGURE C.20 Stress-Strain Relationship from CIU Tests on Vertically and Horizontally Oriented Silty Clay Samples

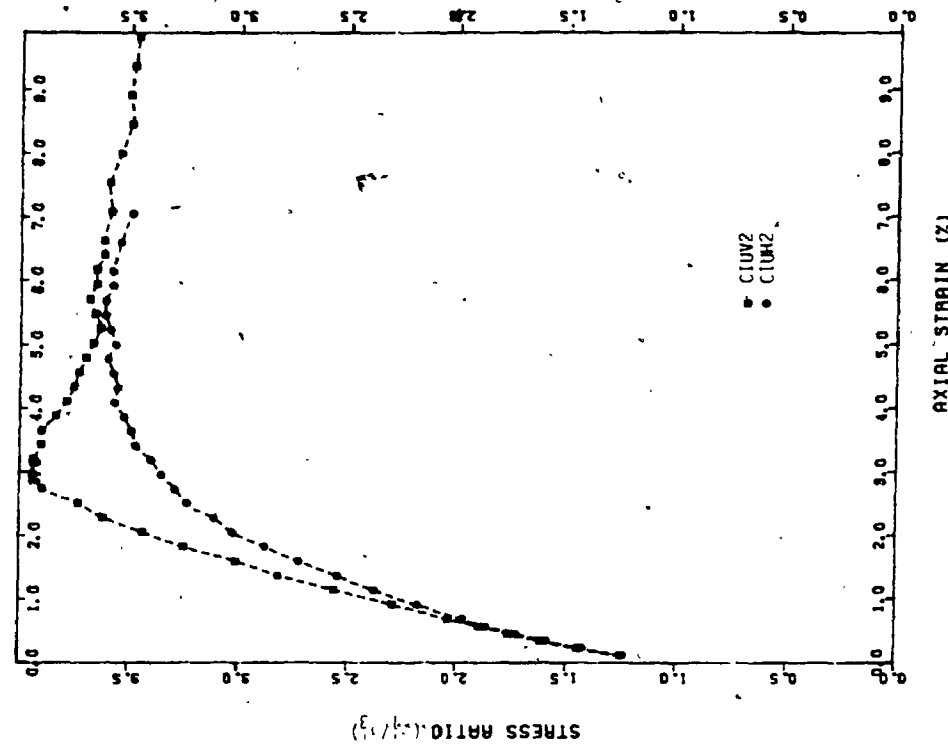


FIGURE C.21 Stress Ratio-Strain Relationship from CIU Tests on Vertically and Horizontally Oriented Silty Clay Samples

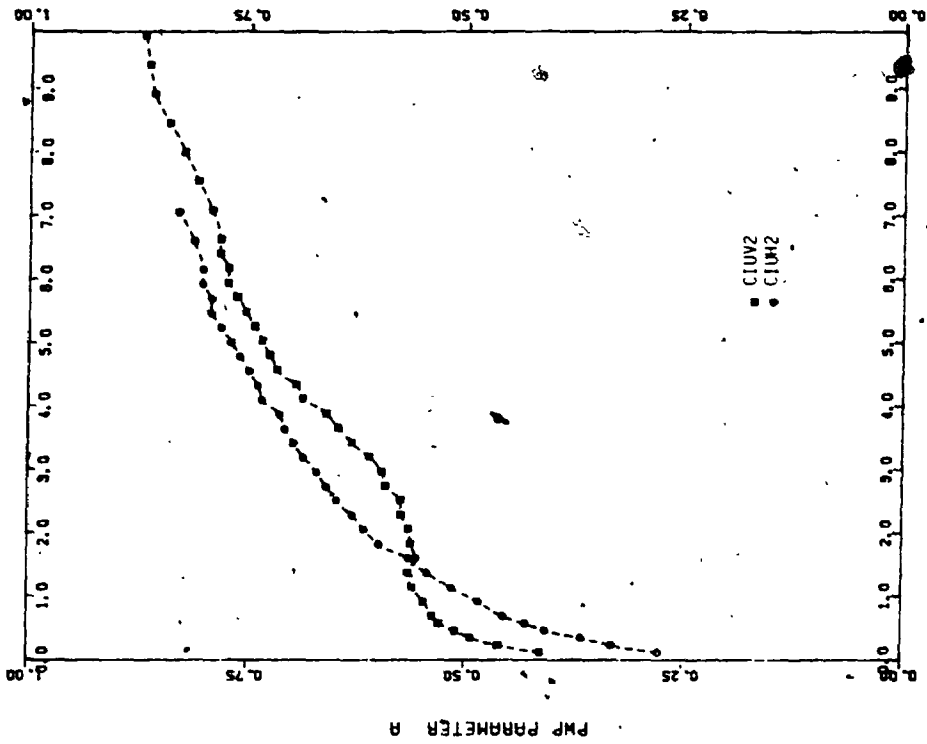


FIGURE C.23 Pore Pressure Parameter A - Strain Relationship from CIU Tests on Vertically and Horizontally Oriented Silty Clay Samples

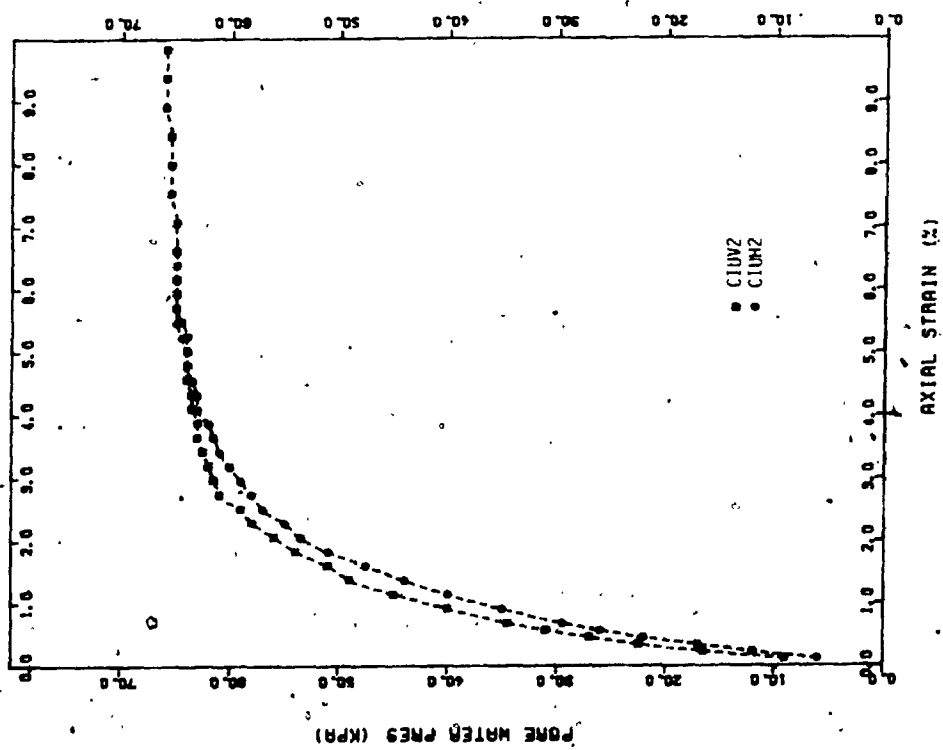


FIGURE C.22 Excess Pore Water Pressure-Strain Relationship from CIU Tests on Vertically and Horizontally Oriented Silty Clay Samples

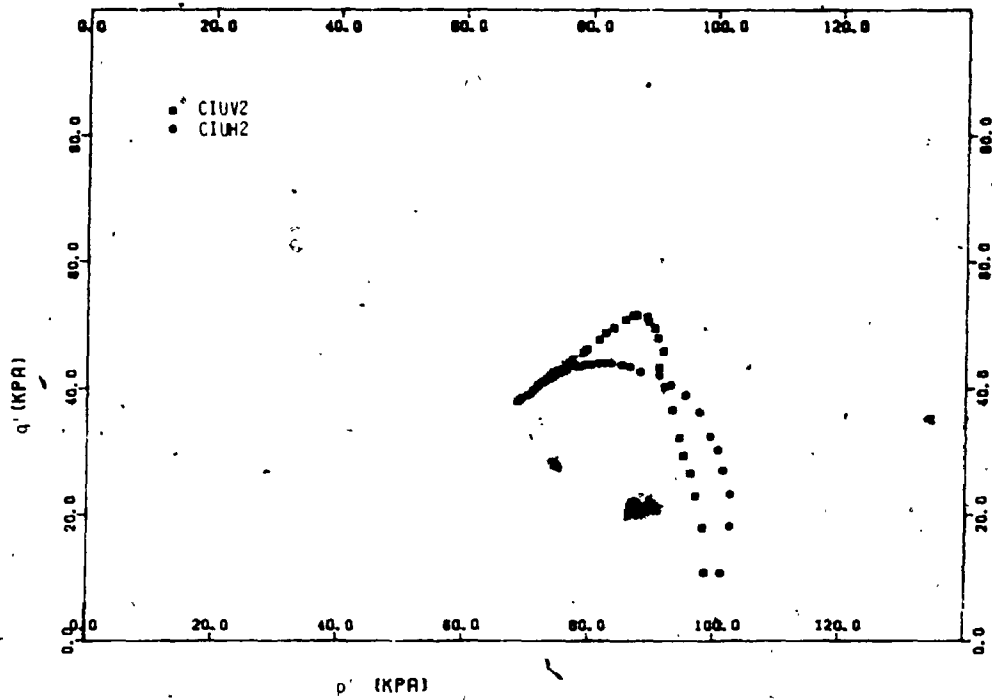


FIGURE C.24 Effective p-q Stress Path Plot from CIU Tests on Vertically and Horizontally Oriented Silty Clay Samples

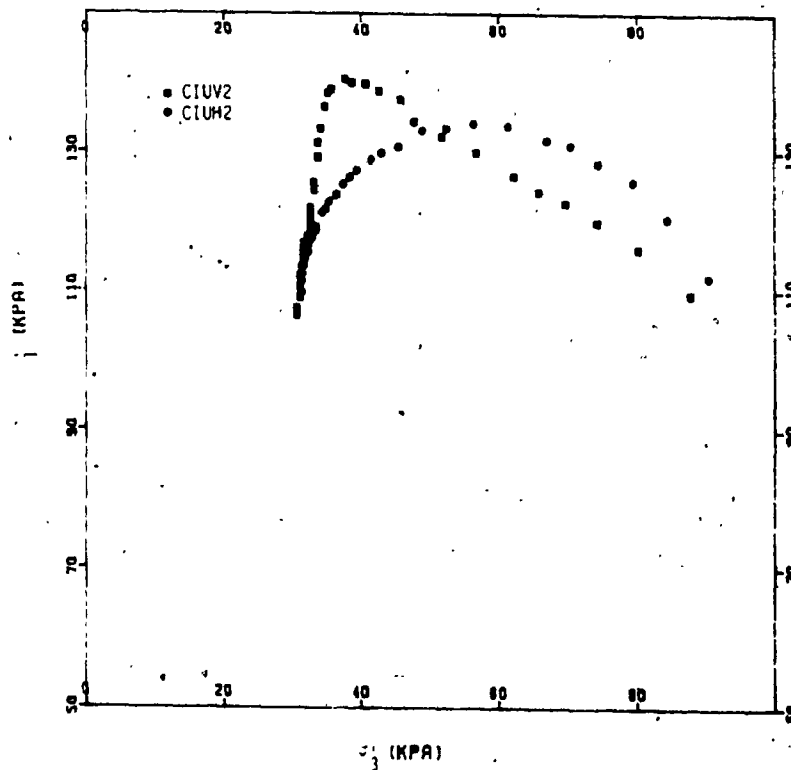


FIGURE C.25 Effective p_1 - p_3 Stress Path Plot from CIU Tests on Vertically and Horizontally Oriented Silty Clay Samples

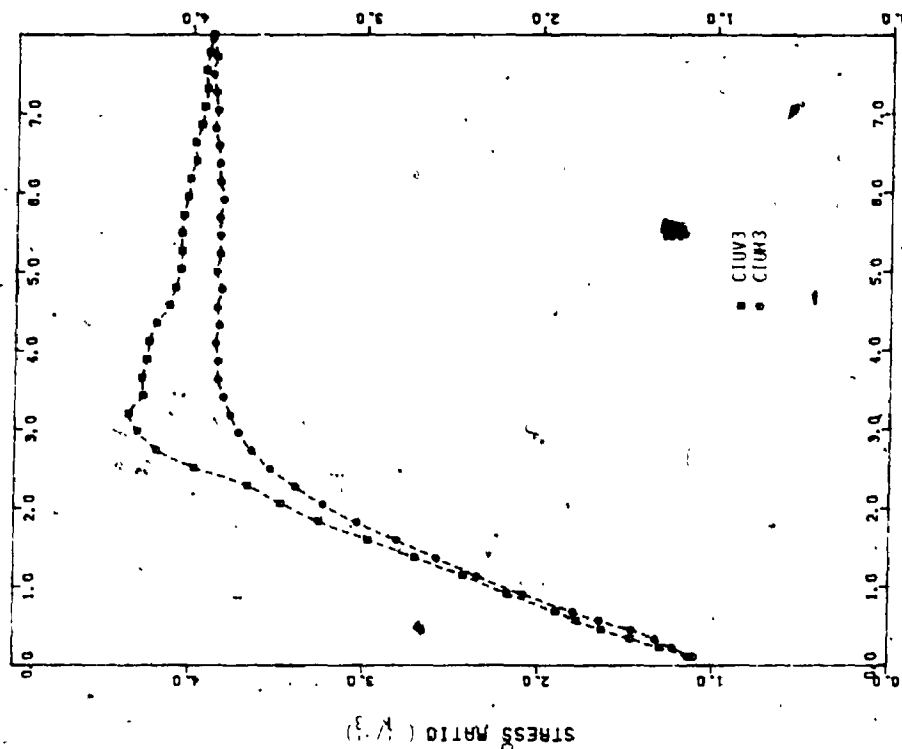


FIGURE C.27 Stress Ratio-Strain Relationship from CIU Tests on Vertically and Horizontally Oriented Silty Clay Samples

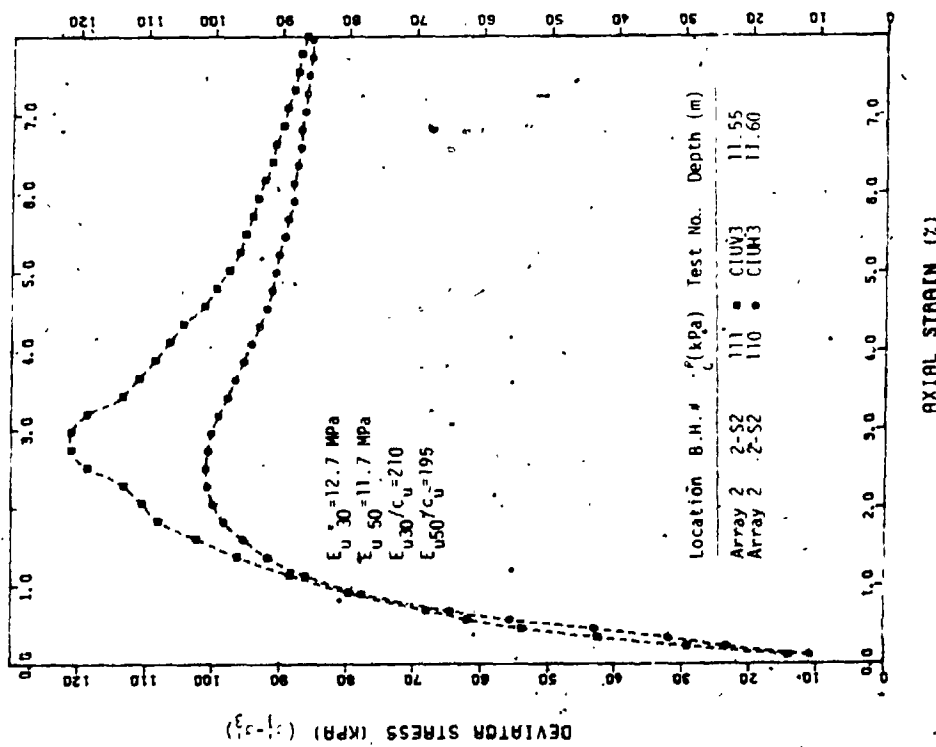


FIGURE C.26 Stress-Strain Relationship from CIU Tests on Vertically and Horizontally Oriented Silty Clay Samples.

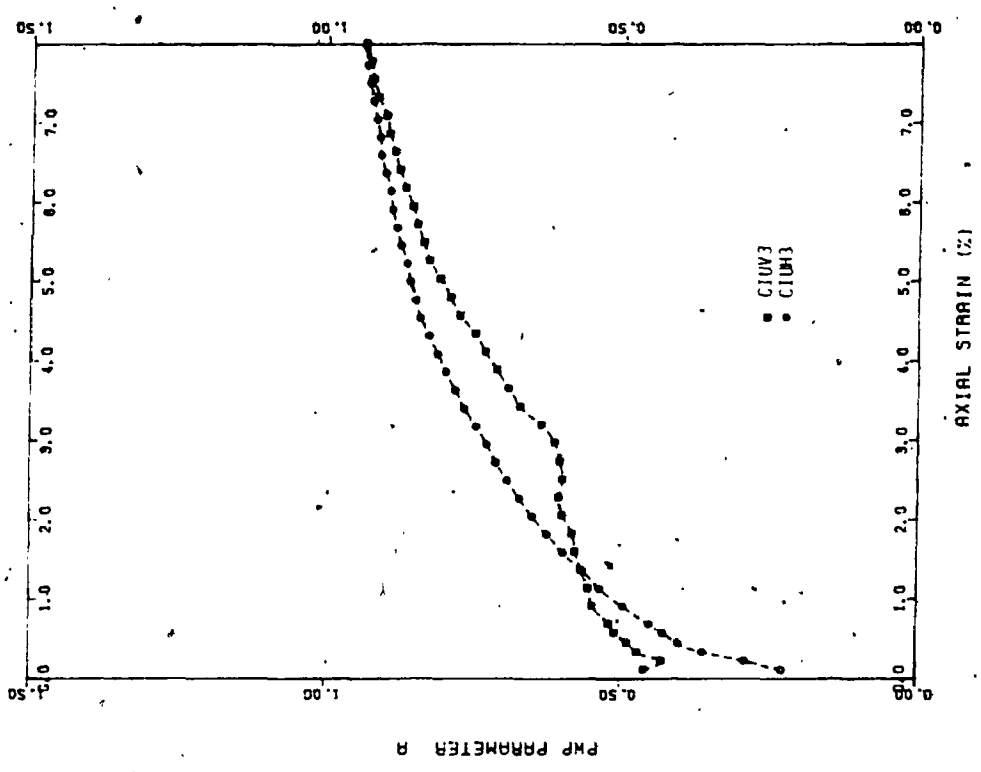


FIGURE C.29 Pore Pressure Parameter A - Strain Relationship from CIU Tests on Vertically and Horizontally Oriented Silty Clay Samples

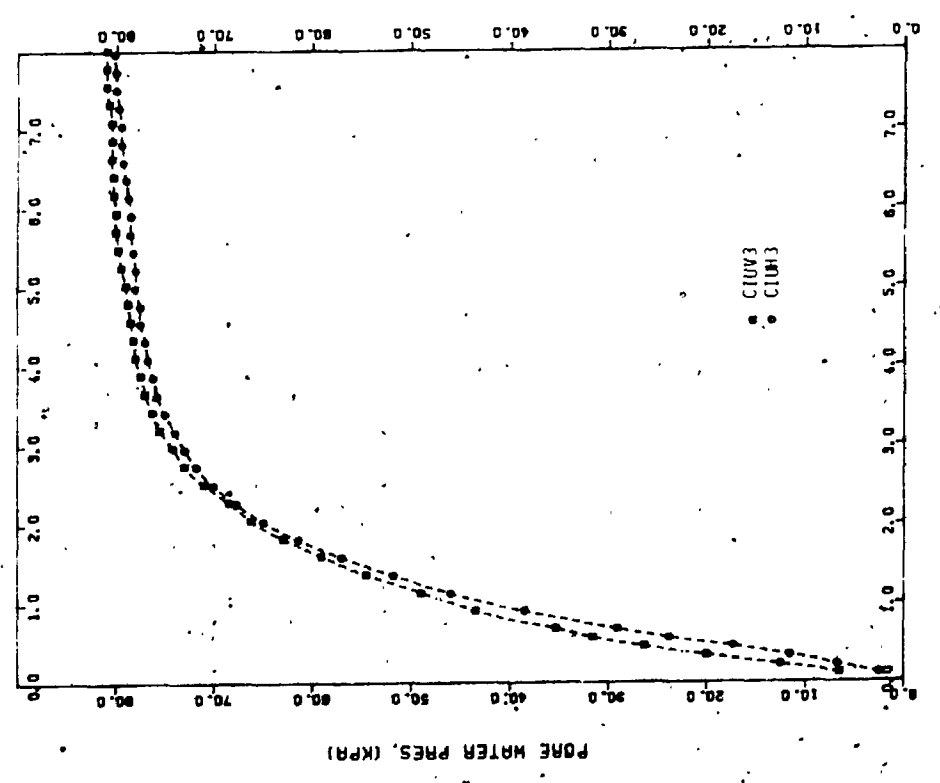


FIGURE C.28 Excess Pore Water Pressure-Strain Relationship from CIU Tests on Vertically and Horizontally Oriented Silty Clay Samples

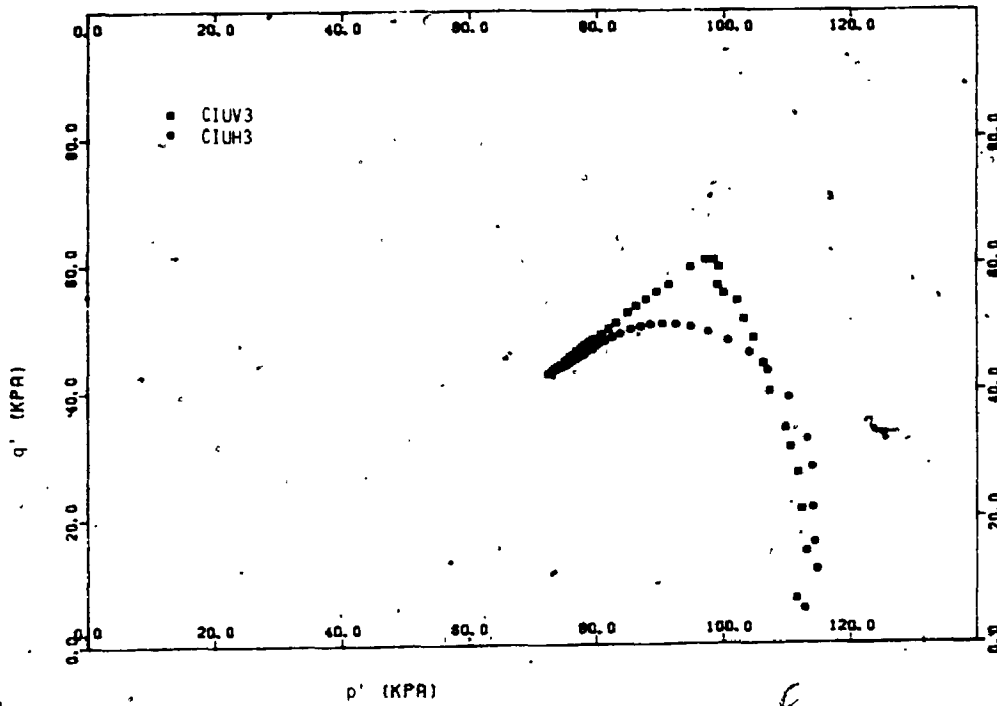


FIGURE C.30 Effective p-q Stress Path Plot from CIU Tests of Vertically and Horizontally Oriented Silty Clay Samples

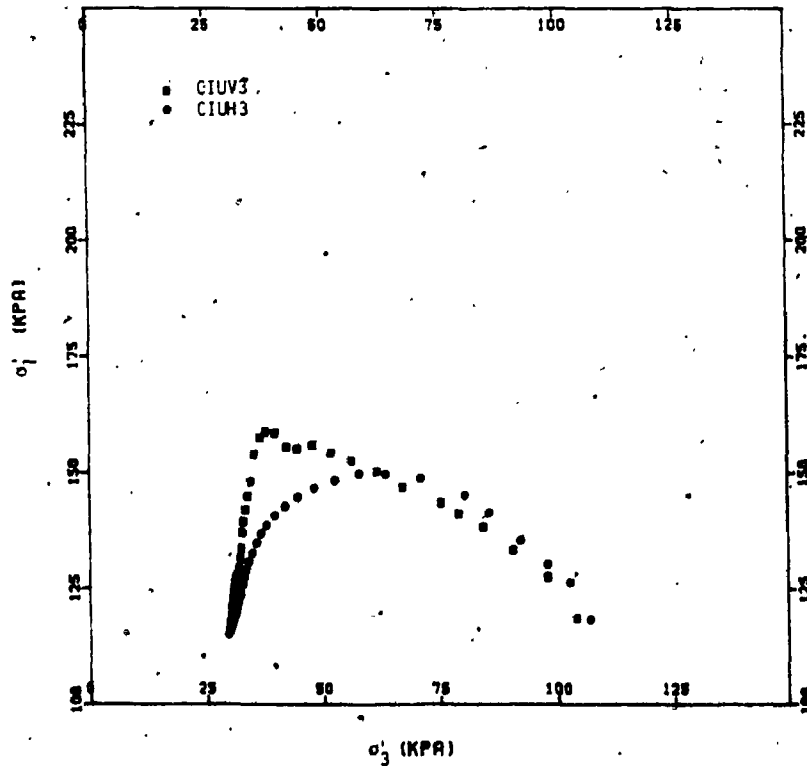


FIGURE C.31 Effective $\sigma_1 - \sigma_3$ Stress Path Plot from CIU Tests on Vertically and Horizontally Oriented Silty Clay Samples

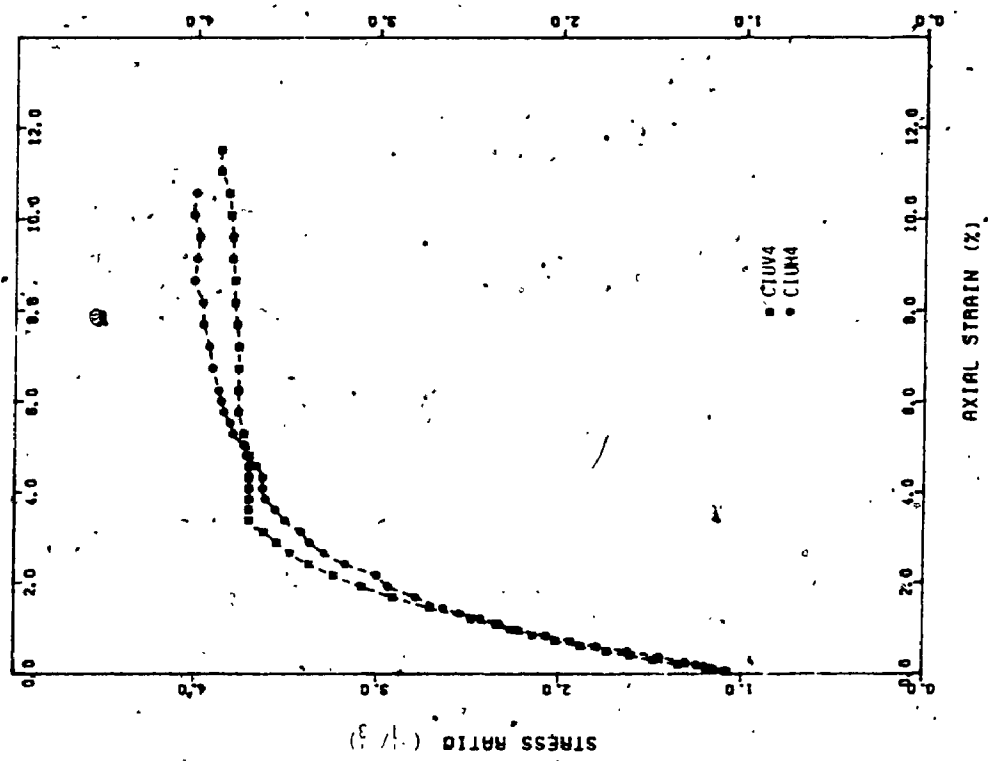


FIGURE C.33 Stress Ratio-Strain Relationship from CIU Tests on Vertically and Horizontally Oriented Varved Clay Samples

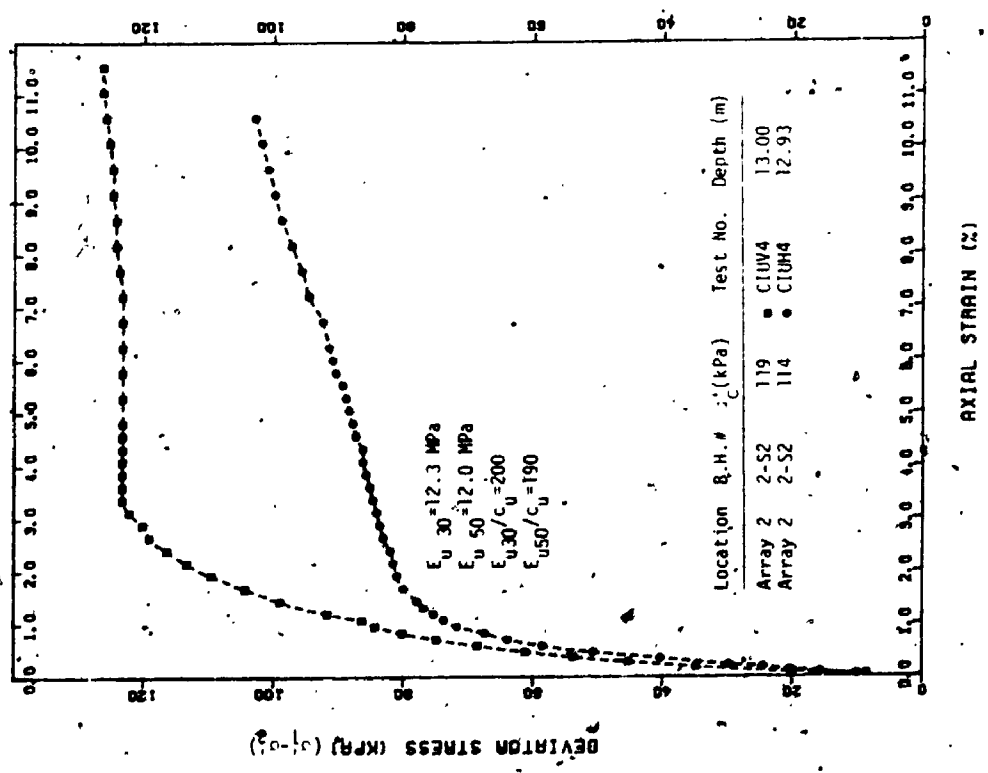


FIGURE C.32 Stress-Strain Relationship from CIU Tests on Vertically and Horizontally Oriented Varved Clay Samples

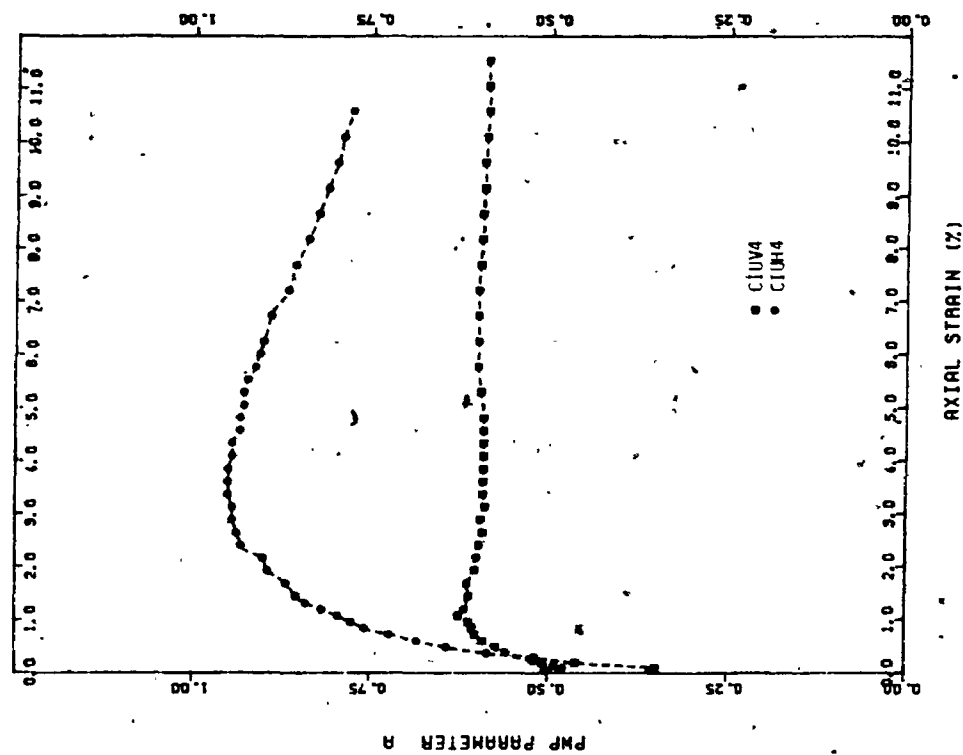


FIGURE C.35 Pore Pressure Parameter A - Strain Relationship from CIU Tests on Vertically and Horizontally Oriented Varved Clay Samples

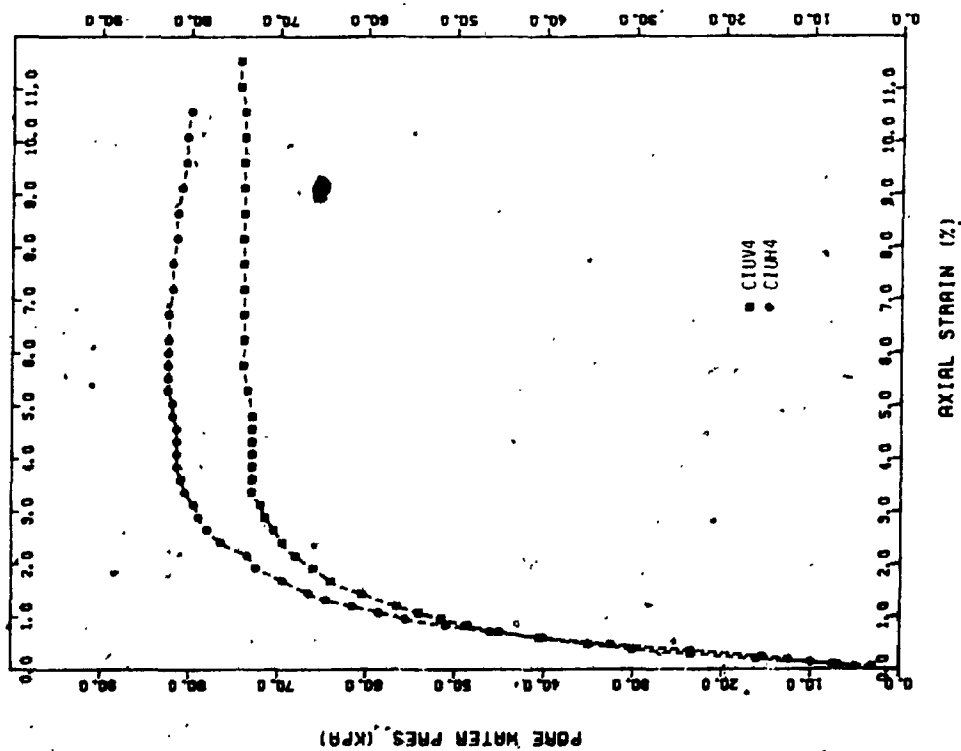


FIGURE C.34 Excess Pore Water Pressure-Strain Relationship from CIU Tests on Vertically and Horizontally Oriented Varved Clay Samples

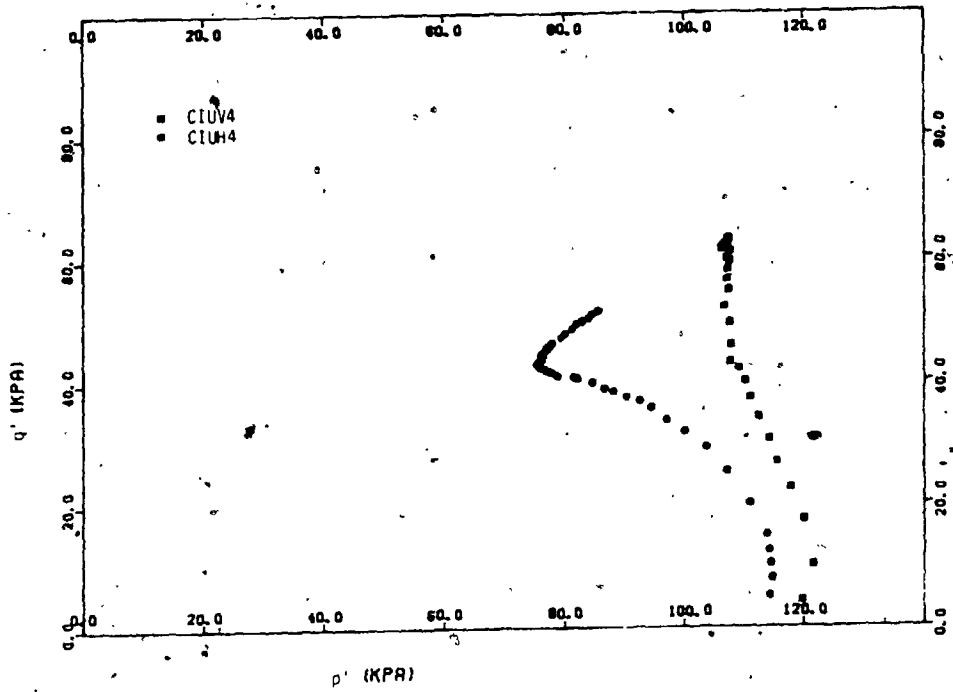


FIGURE C.36 Effective p-q Stress Path Plot from CIU Tests on Vertically and Horizontally Oriented Varved Clay Samples

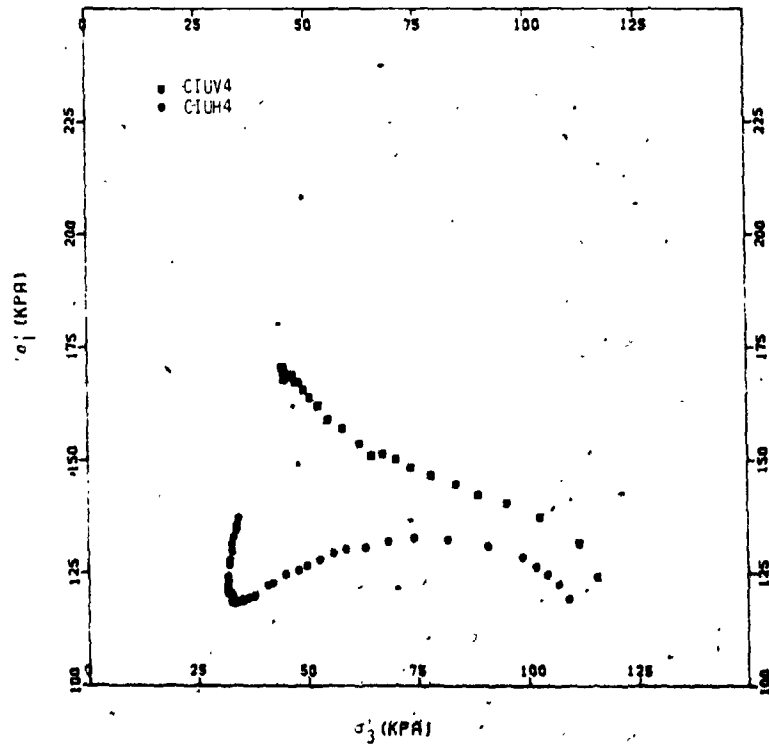


FIGURE C.37 Effective $\sigma_1 - \sigma_3$ Stress Path Plot for CIU Tests on Vertically and Horizontally Oriented Varved Clay Samples

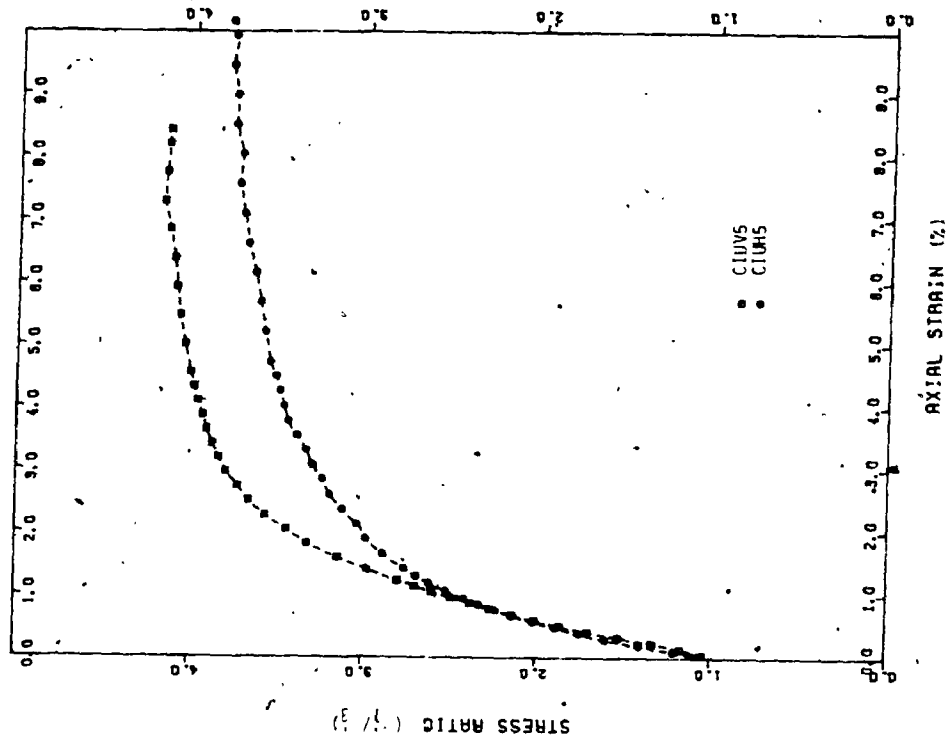


FIGURE C.39 Stress Ratio-Strain Relationship from CIU Tests on Vertically and Horizontally Oriented Varved Clay Samples

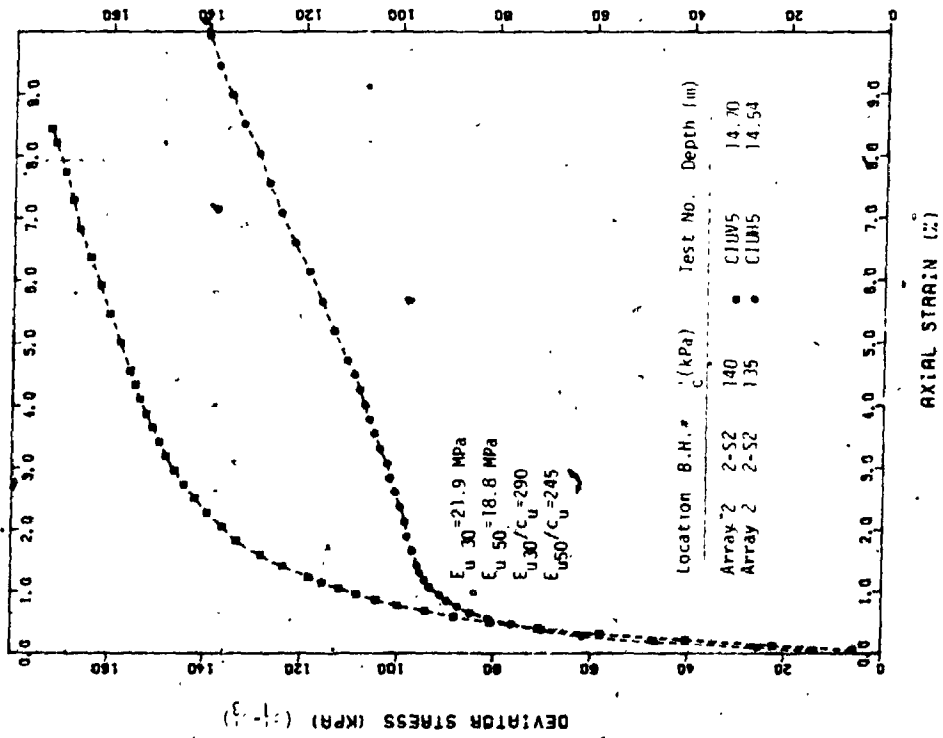


FIGURE C.38 Stress-Strain Relationship from CIU Tests on Vertically and Horizontally Oriented Varved Clay Samples

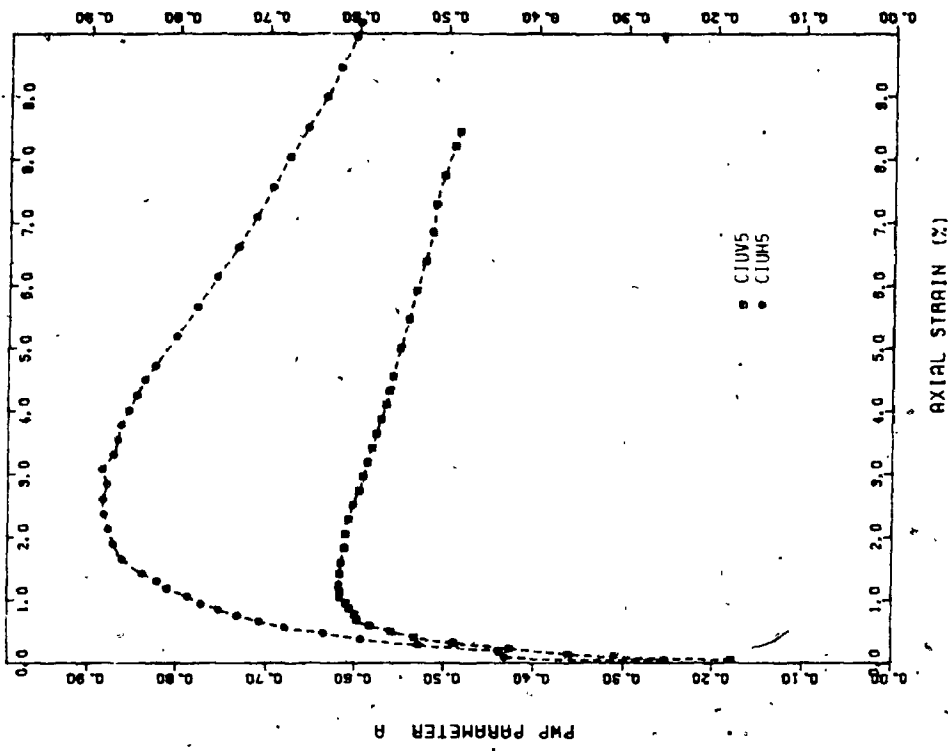


FIGURE C.41 Pore Pressure Parameter A - Strain Relationship from CIU Tests on Vertically and Horizontally Oriented Varved Clay Samples

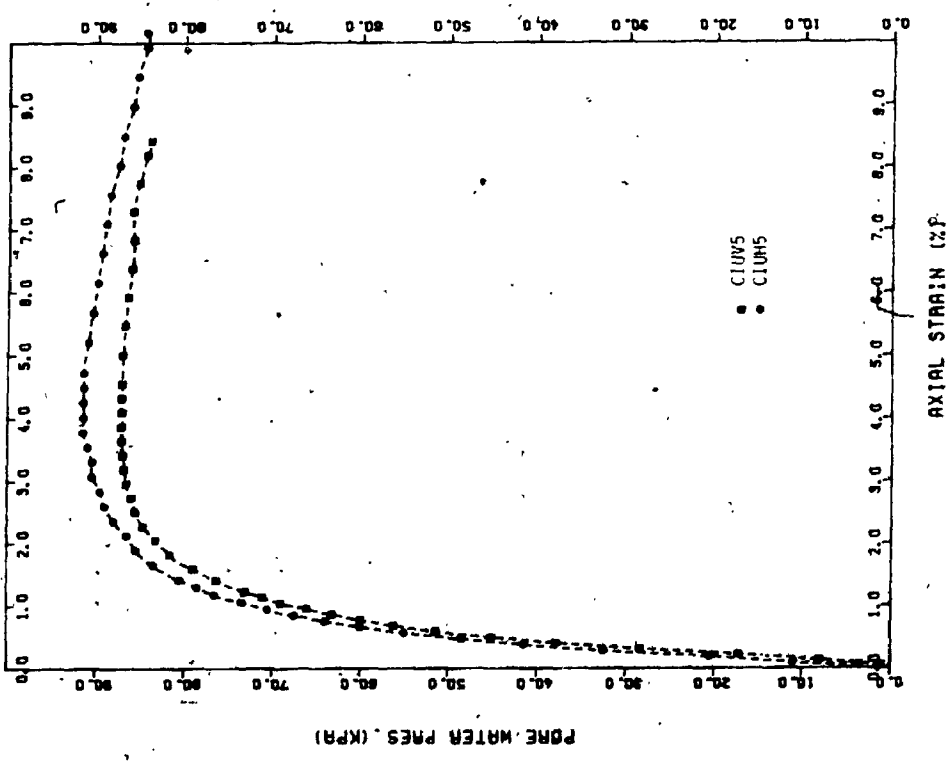


FIGURE C.40 Excess Pore Water Pressure-Strain Relationship from CIU Tests on Vertically and Horizontally Oriented Varved Clay Samples

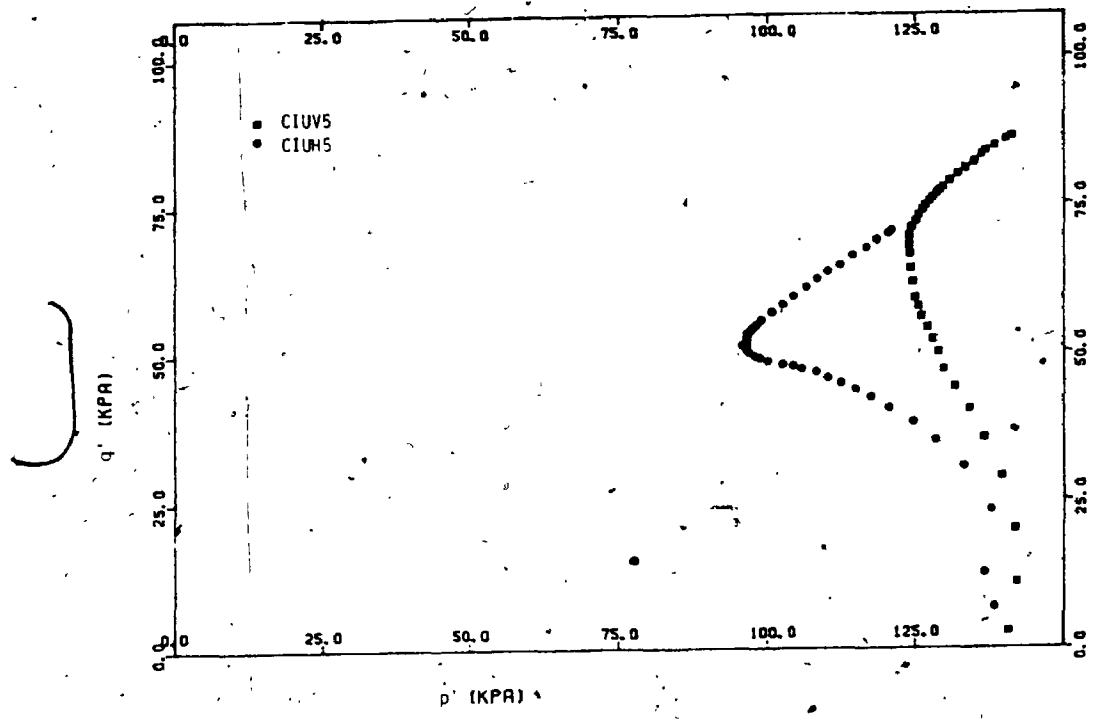


FIGURE C.42 Effective p - q Stress Path Plot from CIU Tests on Vertically and Horizontally Oriented Varved Clay Samples

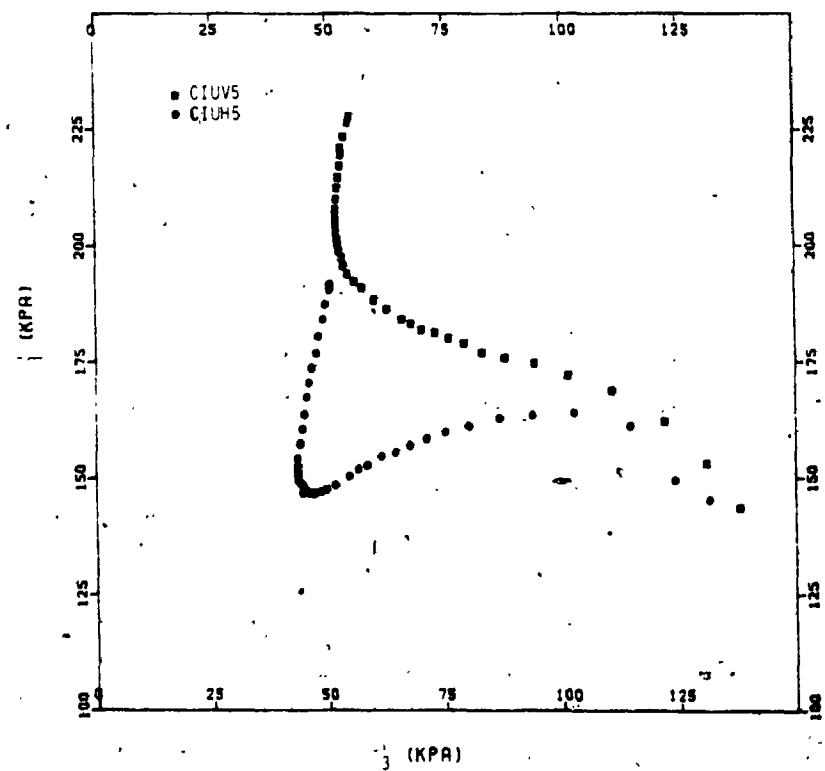


FIGURE C.43 Effective p - s Stress Path Plot from CIU Tests on Vertically and Horizontally Oriented Varved Clay Samples

APPENDIX D
CONSOLIDATION TESTS PERFORMED USING
THE ROWE CELL

D.1 DESCRIPTION OF APPARATUS

The large oedometer used at The University of Western Ontario was modified from a 152 mm (6") diameter Rowe Consolidation Cell. Complete description of the original apparatus and its usage was given by Rowe and Barden (1966). The description of the modified version was given by Becker (1981).

The Rowe Cell is comprised of three parts, the base, the ring and the cover. In the original apparatus, it is difficult to place a sample into the aluminum-bronze ring without considerable disturbance because of the need of transferring the sample subsequent to trimming. Therefore, a modification has been made on the ring of the original equipment. The ring was cut in half with the bottom half provided with a sharp cutting edge similar to the consolidation rings of the conventional oedometer. A seal is effected between the two halves by an "O" ring seal. A cross-section of the modified large oedometer is shown on Figure D.1.

The base was machined from rolled mild steel plate and provided with a central drain which can be used as a pore pressure measuring point. The central drain is covered by a 9.5 mm diameter porous stone.

By inserting a 50 mm diameter porous filter paper, the response time of the initial excess pore pressure was observed to have shortened and it also aided in saturating the sample. The top is connected to the base by eight bolts. A uniform load can be applied to the sample through a convoluted rubber bellows and the pressure is supplied by a system of mercury pots. Two holes fitted with valves on the side of the ring are used to evacuate water trapped between the sample and the upper rubber membrane. A porous disc is placed between the specimen and the rubber membrane to permit vertical drainage. A valve is provided on the cover for connection to the supply pressure system. In addition, a "bleed" valve is provided at the top of the cover for removal of air. Vertical drainage is effected by a hollow stainless steel spindle attached to the rubber membrane and passing through the cover with the sealing provided by "O" rings. The spindle in turn is connected to a flexible nylon tube to a drainage control valve. The displacement of the specimen (movement of the spindle) can be measured by a dial gauge or, alternatively, by a displacement transducer mounted to a bracket on the cover.

D.2 SPECIMEN PREPARATION AND TEST PROCEDURE

The detailed procedure followed in the laboratory in preparing the sample for the large oedometer has been presented by Becker (1981).

A brief account of the test method is given below:

- i) First, the lower half of the ring with a cutting edge is greased with vacuum grease. The grease serves the purpose of reducing the side friction during trimming and ensures a seal between the ring wall and specimen so that drainage must be through the soil sample and not the soil-ring peripheral interface.
- ii) The ring was then pushed perpendicularly through the original sample. As the ring with the cutting edge advances, excess soil is removed in a shaving manner.
- iii) The top and bottom of the specimen are trimmed smooth with the top and bottom of the ring.
- iv) The large oedometer is assembled under deaired water to minimize the entrapment of air in the system.
- v) The porous stone, lower ring with soil specimen, upper ring, base and cover are put together as shown in Figure D.1.
- vi) The cover, ring and base are bolted together in a systematic manner to ensure that tilting does not occur and thus ineffective sealing.
- vii) After the complete assembly, water that is trapped between the sample and rubber membrane is removed by the application of a small amount of pressure on top of the rubber membrane. All valves on the cover are opened and flow established to remove entrapped air. The drainage valve is then closed along with the bleed valve. The pressure head applied will cause the membrane to spread over the porous disc and "seat" it on the specimen. The water trapped between the side wall and the membrane is allowed to escape via the two valves on the

wall of the ring. After the water is squeezed out (no flow) these two valves are closed. The upper bleed valve is then reopened to remove air trapped between the cover and the membrane.

viii) The entire assembly may now be connected to the triaxial mercury pot pressure system as is done with the triaxial cell. Appropriate back pressures and supply (cell) pressures may be applied such that the required consolidation pressure is obtained.

ix) The soil specimen is now ready to be loaded in increments up to the appropriate field stress level, unloaded and repeat cycles thereof as required. In each increment of loading, the induced excess pore pressure is allowed to come to equilibrium and any displacement recorded prior to opening the drainage control valve was recorded before the start of consolidation. Continuous monitoring of both pore water pressure and displacements are carried out with a recorder. Displacement readings are also taken on the dial gauge.

D.3 COEFFICIENT OF CONSOLIDATION

The coefficient of consolidation can be determined in two ways from the results of large oedometer tests with pore pressure measurements:

- i) Based on the results of pore pressure measurements.
- ii) Based on the Casagrande logtime-displacement fitting method.

The coefficient of consolidation is defined as

$$c_v = \frac{TH^2}{t} \quad (D.1)$$

where H = length of drainage path

T = time for a certain percentage of pore pressure dissipation U

t = time factor corresponding to the above pore pressure dissipation.

The determination of c_v is conventionally based on T_{50} (50% of the average degree of consolidation) using time-displacement relationships in the Casagrande logtime fitting method and $T_{50} = 0.197$.

For determination of c_v using direct pore pressure measurement, T_{50} , the time constant at 50% dissipation of pore pressure at the base of impermeable boundary is equal to 0.38 rather than 0.197 for the case of one-way drainage.

Some inherent assumptions are made in determination of c_v and these might lead to errors in some cases. The procedure for determining c_v is to "fit" the laboratory curve to the theoretical curve at three points: zero, 50 and 100 percent of average degree of consolidation or percentage of pore pressure dissipation. The two curves may not coincide at the other points.

Although the consolidation phase ends when the excess pore pressure is zero, the sample in the consolidometer continues to deform due to secondary compression, and this 'creep movement' may have occurred

prior to the complete dissipation of pore pressure. Some interpretation of the time settlement data may be necessary in order to define T_{50} or T_{90} required in calculation of c_v . Direct pore pressure measurement in the consolidation test can remove this difficulty. It is interesting to observe that the c_v obtained from pore pressure-time relationship is generally higher than the c_v obtained from settlement-time relationship.

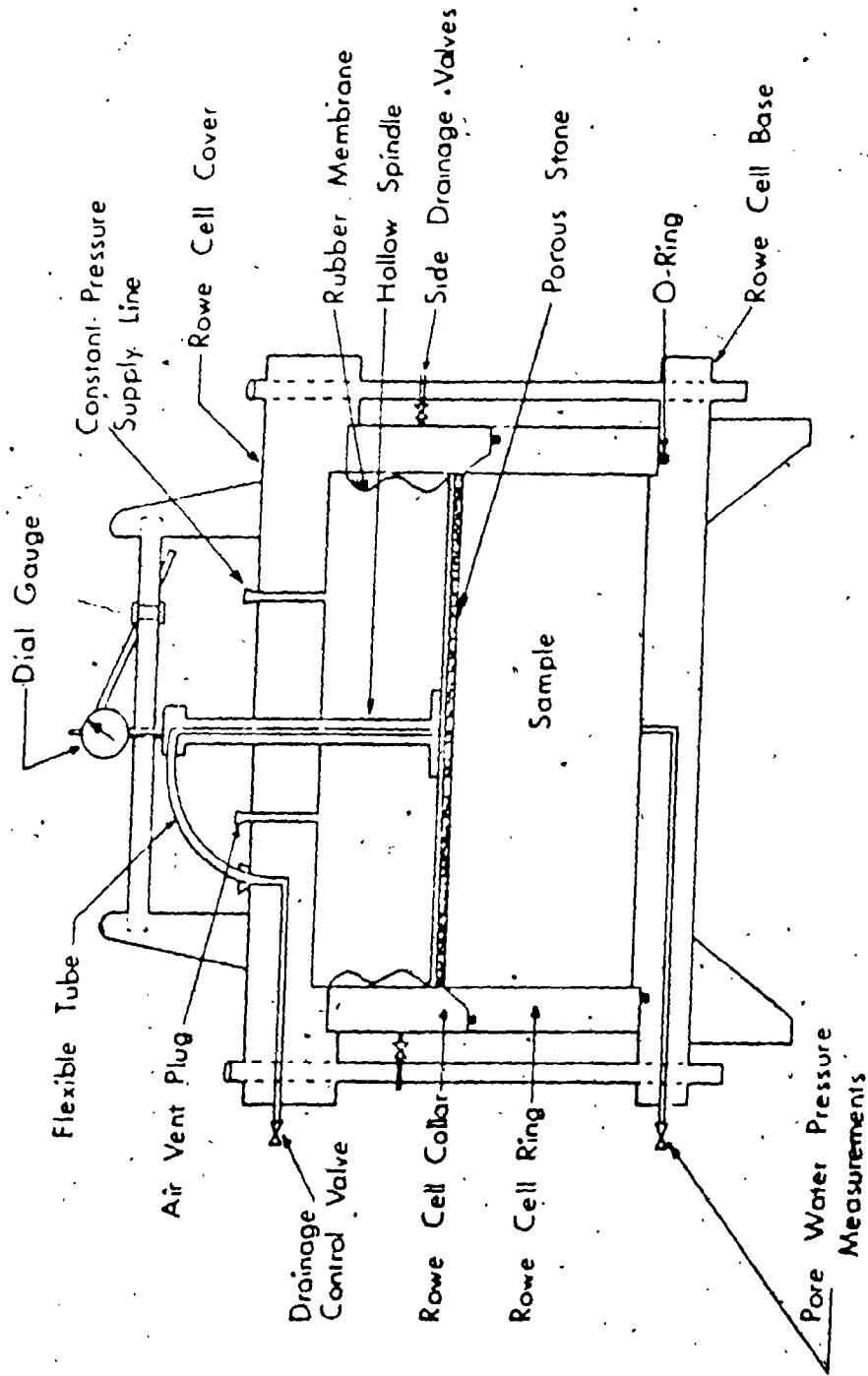


FIGURE D.1 Sectional Diagram of Large Oedometer (Modified Rowe Cell)

APPENDIX E

TESTS FOR DETERMINING ANISOTROPIC ELASTIC PARAMETERS

E.1 THEORETICAL BACKGROUND

For a cross anisotropic elastic material, the generalized stress-strain relationships can be expressed in terms of five independent elastic parameters, E_v , E_h , μ_{xx} ($= \mu_{xy} = \mu_{hh}$), μ_{zx} ($= \mu_{vh}$) and G_{zx} ($= G_{zx} = G_{vh}$). Since the elastic parameters for soil are generally different in loading and unloading, an additional set of five parameters in the unloading mode would be required to describe the deformation behaviour completely.

These ten parameters are defined as follows:

E_v, E_v^* = elastic modulus in the vertical direction for loading and unloading respectively;

E_h, E_h^* = elastic modulus in the horizontal direction for loading and unloading respectively;

μ_{xx}, μ_{xx}^* = effect of horizontal strain on horizontal strain in plane of isotropy for loading and unloading respectively;

μ_{zx}, μ_{zx}^* = effect of vertical strain on horizontal strain for loading and unloading respectively;

G_{zx}, G_{zx}^* = shear modulus in the vertical plane for loading and unloading respectively.

Those parameters which are not independent are defined as:

μ_{xz}, μ_{xz}^* = effect of horizontal strain on vertical strain for loading and unloading respectively;

G_{xx}, G_{xx}^* = shear modulus in the horizontal plane for loading and unloading respectively.

From strain energy considerations, it may be shown that

$$\frac{\mu_{zx}}{\mu_{xz}} = \frac{E_v}{E_h} \quad (E.1)$$

$$\frac{\mu_{zx}^*}{\mu_{xz}^*} = \frac{E_v^*}{E_h^*} \quad (E.2)$$

In the plane of isotropy

$$G_{xx} = \frac{E_h}{2(1+\mu_{xx})} \quad (E.3)$$

and

$$G_{xx}^* = \frac{E_h^*}{2(1+\mu_{xx}^*)} \quad (E.4)$$

E.2 FORMULATION OF STRESS-STRAIN RELATIONSHIP FOR CID TESTS

The equations for the principal strains ($\Delta\epsilon$), pore pressures (Δu) and volumetric strain (Δe) are formulated for the analysis of experimental results. These equations were presented by Lo et al. (1977).

The subscripts x, y, z are used to denote direction, v and h denote vertical and horizontal samples and subscript 1 denotes applied loading and subscript 2 denotes applied unloading.

On an incremental stress-strain basis, in terms of the five independent loading parameters, the relationships are as follows:

$$\Delta\epsilon_x = (\Delta\sigma_x/E_h) - [(\mu_{xx}/E_h)\Delta\sigma_y] - [(\mu_{zx}/E_v)\Delta\sigma_z] \quad (E.5a)$$

$$\Delta \epsilon_y = -[(\mu_{xx}/E_h)\Delta \sigma_x] + (\Delta \sigma_y/E_h) - [(\mu_{zx}/E_v)\Delta \sigma_z] \quad (E.5b)$$

$$\Delta \epsilon_z = -[(\mu_{zx}/E_v)\Delta \sigma_x] - [(\mu_{zx}/E_v)\Delta \sigma_y] + (\Delta \sigma_z/E_v) \quad (E.5c)$$

where E = modulus of deformation

μ = Poisson's ratio

G = shear modulus

ϵ = strain

σ = stress

h = horizontal direction

v = vertical direction

In equations E.5, the vertical axis (z) is taken as the axis of symmetry and the horizontal plane (x,y plane) as the plane of isotropy. Effective stresses, which directly influence soil deformation behaviour are used in the equation.

Equations for the deformation moduli and Poisson's ratios determined from results of drained triaxial tests on samples trimmed at different orientations are listed below.

(a) Vertical specimen ($i = 0^\circ$) in loading stage - Under constant cell pressure and with radial symmetry in stress system

$$\Delta \sigma'_{xv} = \Delta \sigma'_{yv} = 0$$

$$\Delta \epsilon'_{xv} = \Delta \epsilon'_{yv} = -\mu_{zx} \frac{\Delta \sigma'_{zv}}{E_v} \quad (E.6a)$$

$$\Delta \epsilon'_{zv} = \frac{\Delta \sigma'_{zv}}{E_v} \quad (E.6b)$$

Therefore,

$$\mu_{zx} = -\frac{\Delta\epsilon_{xv1}}{\Delta\epsilon_{zv1}} \quad (\text{E.6c})$$

(b) Vertical specimen ($i = 0^\circ$) in unloading stage - Under constant cell pressure and with radial symmetry in the stress system

$$\Delta\sigma'_{xv2} = \Delta\sigma'_{yv2} = 0$$

$$\Delta\epsilon_{xv2} = \Delta\epsilon_{yv2} = -\mu_{zx}^* \frac{\Delta\sigma'_{zv2}}{E_v^*} \quad (\text{E.7a})$$

$$\Delta\epsilon_{zv2} = \frac{\Delta\sigma'_{zv2}}{E_v^*} \quad (\text{E.7b})$$

Therefore,

$$\mu_{zx}^* = -\frac{\Delta\epsilon_{xv2}}{\Delta\epsilon_{zv2}} \quad (\text{E.7c})$$

(c) Horizontal specimen ($i = 90^\circ$) in loading stage - Under constant cell pressure and with radial symmetry in the stress system

$$\Delta\sigma'_{yh1} = \Delta\sigma'_{zh1} = 0$$

$$\Delta\epsilon_{xh1} = \frac{\Delta\sigma'_{xh1}}{E_h} \quad (\text{E.8a})$$

$$\Delta\epsilon_{yh1} = -\mu_{xx} \frac{\Delta\sigma'_{xh1}}{E_h} \quad (\text{E.8b})$$

$$\Delta\epsilon_{zh1} = -\mu_{xz} \frac{\Delta\sigma'_{xh1}}{E_h} \quad (\text{E.8c})$$

Therefore,

$$\mu_{xx} = - \frac{\Delta \epsilon_{yh1}}{\Delta \epsilon_{xh1}} \quad (\text{E.8d})$$

$$\mu_{xz} = - \frac{\Delta \epsilon_{zh1}}{\Delta \epsilon_{xh1}} \quad (\text{E.8e})$$

(d) Horizontal specimen ($i = 90^\circ$) in unloading stage - Under constant cell pressure and with radial symmetry in the stress system,

$$\Delta \sigma'_{yh2} = \Delta \sigma'_{zh2} = 0$$

$$\Delta \epsilon_{xh2} = \frac{\Delta \sigma'_{xh2}}{E_h^*} \quad (\text{E.9a})$$

$$\Delta \epsilon_{yh2} = -\mu_{xx}^* \frac{\Delta \sigma'_{xh2}}{E_h^*} \quad (\text{E.9b})$$

$$\Delta \epsilon_{zh2} = -\mu_{xz}^* \frac{\Delta \sigma'_{xh2}}{E_h^*} \quad (\text{E.9c})$$

Therefore,

$$\mu_{xx}^* = - \frac{\Delta \epsilon_{yh2}}{\Delta \epsilon_{xh2}} \quad (\text{E.9d})$$

$$\mu_{xz}^* = - \frac{\Delta \epsilon_{zh2}}{\Delta \epsilon_{xh2}} \quad (\text{E.9e})$$

(e) Inclined specimen ($i = 45^\circ$) in loading stage

$$\begin{aligned} \frac{\Delta \epsilon_{i1}}{\Delta \sigma_{i1}} &= \frac{1}{E_i} = \frac{1}{E_v} \cos^4 i + \frac{1}{E_h} \sin^4 i \\ &+ \left(\frac{1}{G_{zx}} - \frac{2\mu_{xx}}{E_h} \right) \sin^2 i \cos^2 i \end{aligned} \quad (\text{E.10a})$$

Therefore,

$$\frac{1}{G_{zx}} = \left(\frac{1}{E_i} - \frac{\cos^4 i}{E_v} - \frac{\sin^4 i}{E_h} \right) \frac{1}{\sin^2 i \cos^2 i} + \frac{2\mu_{xx}}{E_h} \quad (E.10b)$$

(f) Inclined specimen ($i = 45^\circ$) in unloading stage - Similar to the loading stage

$$\frac{1}{G_{zx}^*} = \left(\frac{1}{E_i^*} - \frac{\cos^4 i}{E_v^*} - \frac{\sin^4 i}{E_h^*} \right) \frac{1}{\sin^2 i \cos^2 i} + \frac{2\mu_{xx}^*}{E_h^*} \quad (E.11a)$$

where i is the angle of inclination of the axis of the specimen to the physical vertical of the clay deposit.

The shear modulus in the horizontal plane may also be determined from

$$\frac{1}{G_{xx}} = \frac{2(1+\mu_{xx})}{E_h} \quad \text{and} \quad \frac{1}{G_{xx}^*} = \frac{2(1+\mu_{xx}^*)}{E_h^*} \quad (E.11b)$$

E.3 DESCRIPTION OF THE APPARATUS AND METHOD OF MEASUREMENT

The details of the Anisotropic Parameter Apparatus and test procedures were given by Yuen (1967):

- i) The schematic layout of the testing equipment is shown in Figure E.1. The apparatus consists of a modified Geotest triaxial cell together with three transducer units which are used for displacement measurements.
- ii) The sets of the transducers and supporting units for axial and lateral measurements are shown in Figures E.2 and E.3.
- iii) The two transducers used for measuring vertical movements are rigidly supported and they are employed to measure the axial strain in the soil specimen over a gauge length equal to half the sample height (35.6 mm).

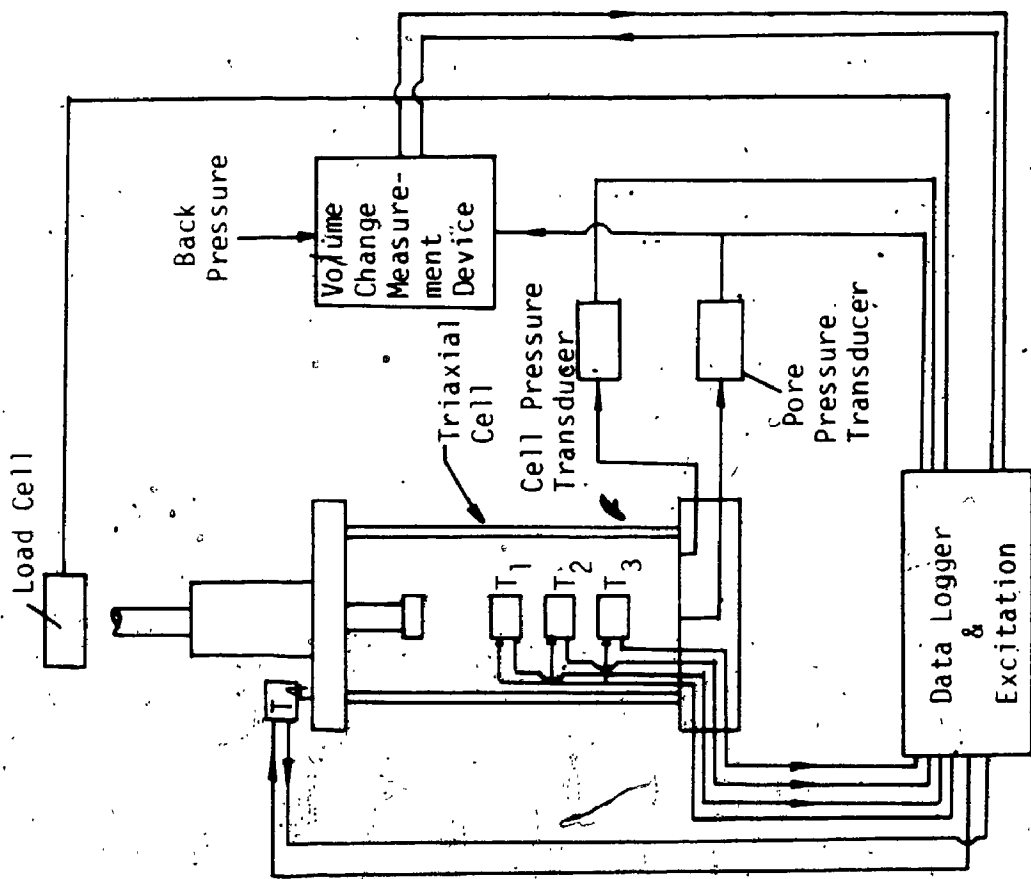
iv) Lateral strains at midpoints across the two opposite faces of the soil sample are measured by means of a transducer mounted on an aluminum bracket. The assembly is made to float in the cell fluid (a transformer oil) by attachment of three pieces of suitably dimensioned styrofoam. Since the transducer unit is floating, it would induce only very little force and movement on the sample and the chance of disturbing the test sample would be reduced.

v) The displacement transducer (LVDT) has a resolution of $0.6 \mu\text{m}$ (2.5×10^{-5} in).

vi) The samples used are square-section samples (35.6 mm x 71.2 mm) trimmed from good quality 152 mm diameter samples. Lightweight gauge points are attached to the soil sample as points of strain measurements. A silicon membrane is placed over the sample and the gauge points are sealed through the silicon membrane with silicon sealant.

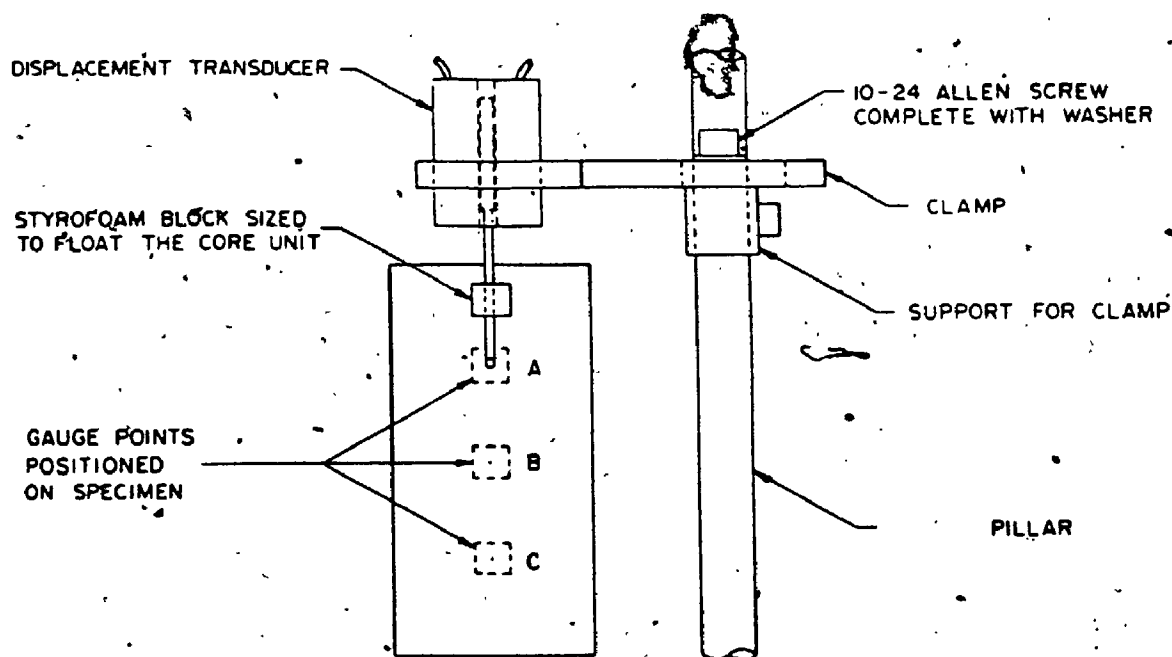
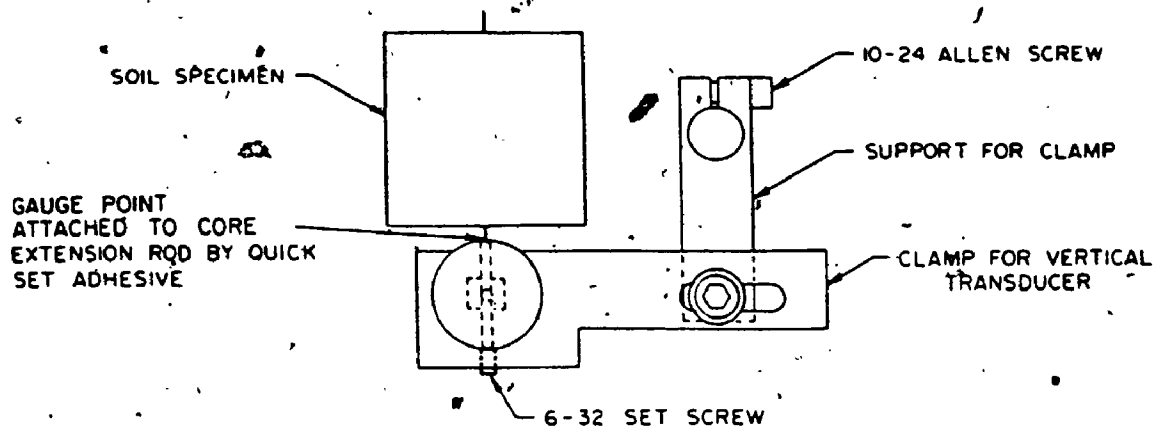
vii) When the above arrangement has been set up, the tests can be conducted in a way similar to conventional CID tests.

viii) All readout units and transducers, such as the LVDTs, pressure transducers, load cell, volume change device are electronic equipment and the data can be recorded automatically using a data-logger.



T_1 to T_4 are LVDT Displacement Transducers

FIGURE E.1 Schematic Layout of Testing Equipment



NOTES

- 1) GAUGE POINTS
A B C FOR VERTICAL DISPLACEMENT MEASUREMENT
B - FOR LATERAL DISPLACEMENT MEASUREMENT
- 2) DISPLACEMENT TRANSDUCER FOR GAUGE POINT C IS SIMILAR TO THAT FOR A.

FIGURE E.2 General Arrangement of Supports for Vertical Transducer Units (after Lo et al., 1977)

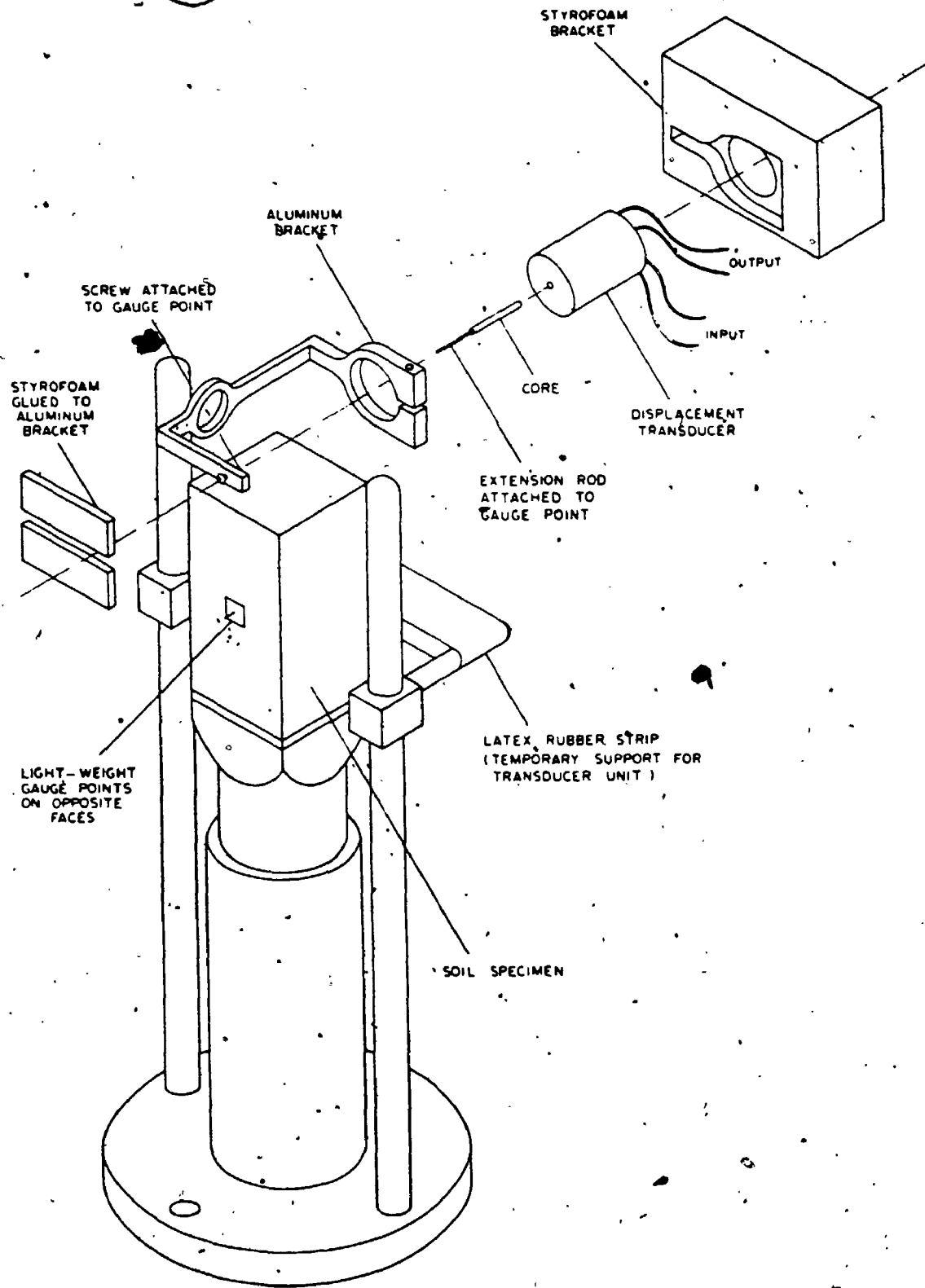


FIGURE E.3 Set-Up for Lateral Displacement Measurement (after Lo et al., 1977)

APPENDIX F
DETERMINATION OF PERMEABILITY

The coefficient of permeability of soil is not directly related to the present analysis of the tunnelling problem. However, for the sake of completeness of the laboratory testing program, the vertical and horizontal permeabilities of the silty clay and varved clay were determined.

F.1 PROGRAM OF TESTING AND PROCEDURE

The coefficient of permeability is a constant relating to the ease with which a fluid passes through a porous medium. One general laboratory method available for determining the coefficient of permeability is the falling-head method and details regarding this procedure can be found in standard texts such as 'Engineering Properties of Soils and Their Measurements' (Bowles, 1970).

The falling-head permeability apparatus consists of a permeameter and a graduated standpipe. The permeameter used is a 101 mm dia. x 101 mm high mold. The base plate of the apparatus is equipped with a porous stone and an exit tube. The cover is fixed with a vent valve and connection for attachment to the standpipe. The sample was trimmed to the desired size and was placed in the mold whose interior was greased to ensure a seal between the sample and the vertical wall of the mold. The permeameter and the sample were submerged in water with

the outlet pipe open so that water could permeate through the sample. A soaking period of 24 hours was allowed to reduce the amount of entrapped air. The permeameter was connected to the standpipe which was filled with a head of water h_1 . Care was taken to keep the system free of entrapped air. Water was allowed to flow through the sample by opening the exit tube. The hydraulic head h_2 at elapsed time t was recorded at different intervals. Temperature was also taken. The permeability, k , is calculated by the equation

$$k = \frac{aL}{At} \ln \frac{h_1}{h_2} \quad (F.1)$$

where a = cross-sectional area of standpipe

L = length of sample

A = cross-sectional area of sample

Since the objective of the tests was to assess the general characteristics of the soil permeability, only a limited number of tests was performed. The falling-head test was carried out on vertically and horizontally trimmed silty clay samples and varved clay samples so that ratio of k_h to k_v can be determined.

F.2 RESULTS OF PERMEABILITY TEST

The results of the permeability test are summarized in Tables F.1 and F.2. From the test results; the following observations can be made:

- i) The vertical coefficients of permeability of the silty clay and varved clay are of the order of 10^{-8} and 10^{-6} respectively. The higher permeability of the varved clay may be attributed to the silt layers in the soil which are more permeable than clay material.
- ii) The permeability is anisotropic. The higher horizontal permeability is a rather common phenomenon in soft clays and varved clays.
- iii) The k_h/k_v ratio is 1.7 for the silty clay and 3.2 for the varved clay.
- iv) The ratio of $k_h/k_v = 3.2$ for the varved clay is probably not representative of the entire deposit of varved clay. As the thickness of the varves increases with depth, it is anticipated that the ratio of k_h/k_v may also increase with depth as well.

TABLE F.1 RESULTS OF PERMEABILITY TESTS

Sample	Depth (m)	Vertical or Horizontal Coefficient of Permeability (cm/s)	
Silty clay	9.3	k_v	4.2×10^{-8}
Silty clay	9.1	k_h	7.3×10^{-8}
Varved clay	12.4	k_v	4.7×10^{-6}
Varved clay	12.3	k_h	1.5×10^{-5}

TABLE F.2 RATIO OF HORIZONTAL PERMEABILITY TO VERTICAL PERMEABILITY FOR SILTY CLAY AND VARVED CLAY

Sample	Average Depth (m)	k_h/k_v Ratio
Silty clay	9.2	1.7
Varved clay	12.4	3.2

(1 cm/s = 3.156×10^5 m/year)

REFERENCES

ACI Committee 504. 1982. State-of-the-Art report on sealing joints in tunnels. Concrete International, American Concrete Institute, Vol. 4, No. 6, pp. 17-27.

Alberro, J.A. and Santoyo, E.V. 1973. Long term behavior of Mexico City clay. Proceedings, 8th International Conference on Soil Mechanics and Foundation Engineering, Moscow, Vol. 1, Part 1, pp. 1-9.

Albertson, M.L., Barton, J.R. and Simons, D.B. 1960. Fluid Mechanics for Engineers. Prentice-Hall. (Civil Engineering and Engineering Mechanics Series).

Arthur, J.R.F. and Menzies, B.K. 1972. Inherent anisotropy in sand. Geotechnique, Vol. 22, No. 1, pp. 115-128.

Atkinson, J.H., Brown, E.T. and Potts, M. 1975. Collapse of shallow unlined tunnels in dense sand. Tunnels and Tunnelling, Vol. 7, No. 3, pp. 81-87.

Atkinson, J.H. and Potts, M. 1977a. Subsidence above shallow tunnels in soft ground. ASCE Journal of the Geotechnical Engineering Division, Vol. 103, No. GT4, pp. 307-325.

Atkinson, J.H. and Potts, M. 1977b. Stability of a shallow circular tunnel in cohesionless soil. Geotechnique, Vol. 27, No. 2, pp. 203-215.

Attewell, P.B. and Farmer, I.W. 1974. Ground disturbance caused by shield tunnelling in a stiff, fissured, overconsolidated clay. Canadian Geotechnical Journal, Vol. 11, pp. 380-395.

Attewell, P.B. and Farmer, I.W. 1975. Ground settlement above shield driven tunnels in clay. Tunnels and Tunnelling, Vol. 7, No. 1, pp. 58-62.

Attewell, P.B. and Woodman, J.P. 1982. Predicting the dynamics of ground settlement and its derivatives caused by tunnelling in soil. Ground Engineering, Vol. 15, No. 8, pp. 13-20, 36.

Baladi, G.Y. and Rohani, B. 1979. Elastic-plastic model for saturated sand. ASCE Journal of the Geotechnical Engineering Division, Vol. 105, No. GT4, pp. 465-480.

Barratt, D.A. and Tyler, R.G. 1976. Measurements of ground movements and lining behavior on the London Underground at Regents Park. Transport and Road Research Laboratory Report LR684.

Becker, D.E. 1981. Settlement of intermittently-loaded structures. Ph.D. Thesis, University of Western Ontario.

Belshaw, D.J. and Palmer, J.H.L. 1978. Results of a program of instrumentation involving a precast segmented concrete-lined tunnel in clay. Canadian Geotechnical Journal, Vol. 15, pp. 573-583.

Biot, M. 1941. General theory of three-dimensional consolidation. Journal of Applied Physics, Vol. 12, No. 115.

Bishop, A.W. and Green, G.E. 1965. The influence of end restraint on the compression strength of a cohesionless soil. Geotechnique, Vol. 15, No. 3, pp. 243-266.

Bishop, A.W. and Henkel, D.J. 1978. The Measurement of Soil Properties in the Triaxial Test, 2nd Edition. The English Language Book Society, Edward Arnold Ltd., London.

Bjerrum, L. and Anderson, K.H. 1972. In-situ measurement of lateral pressures in clay. 5th European Conference on Soil Mechanics and Foundation Engineering, Madrid, pp. 11-20.

Bjerrum, L., Kringstad, S. and Kummereje, O. 1961. The shear strength of a fine sand. Proceedings of the 5th International Conference on Soil Mechanics and Foundation Engineering, Vol. 1, pp. 29-37.

Bjerrum, L. and Landva, A. 1966. Direct simple shear tests on Norwegian quick clay. Geotechnique, Vol. 16, No. 1, pp. 1-20.

Bjerrum, L. and Lo, K.Y. 1961. Discussion on: Haythornthwaite, R.M. Mechanics of Triaxial Test for Soils. ASCE Proceedings, Vol. 87, No. SM2, pp. 173-176.

Bowles, J.E. 1970. Engineering Properties of Soils and Their Measurement. McGraw-Hill.

Bozozuk, M. 1973. Communications with J.H.L. Palmer at National Research Council.

Broms, B.B. and Bennermark, H. 1967. Stability of clay at vertical openings. ASCE Journal of Soil Mechanics and Foundation Division, Vol. 93, No. SM1, pp. 71-94.

Budhu, M. 1984. Nonuniformities imposed by simple shear apparatus. Canadian Geotechnical Journal, Vol. 20, pp. 125-137.

Clough, G.W., Sweeney, B.P. and Richard, J.F. 1983. Measured soil response to EPB shield tunnelling. ASCE Journal of Geotechnical Engineering, Vol. 109, No. GT2, pp. 131-149.

Cording, E.J. and Hansmire, W.H. 1975. Tunnels in soils - General Report, Session IV, 5th Pan American Conference of Soil Mechanics and Foundation Engineering, Buenos Aires, pp. 63.

Davis, E.H. 1968. Theories of plasticity and the Failure of soil masses. Soil Mechanics Selected Topics (Ed. I.K. Lee), Butterworths, Sydney.

Davis, E.H., Gunn, M.J., Mair, R.J. and Seneviratne, H.N. 1980. The stability of shallow tunnels and underground openings in cohesive material. Geotechnique, Vol. 30, No. 4, pp. 397-416.

Davis, E.H. and Poulos, H.G. 1963. Triaxial testing and three-dimensional settlement analysis. Proceedings of Fourth Australian and New Zealand Conference on Soil Mechanics, pp. 233-243.

DeBeer, E. 1964. Spanningen en vervormingen in een kleilaag rondom een cilindrische holte met horizontale as. Proceedings of 4th International Harbour Conference, Antwerpen, pp. 107-111.

DeBeer, E.E. and Buttiens, E. 1966. Construction de réservoirs pour hydrocarbures liquéfiés dans l'argile de Boom à Anvers. Étude des mouvements du sol provoqués par cette réalisation. Travaux, September, pp. 1087-1093, October, pp. 1167-1174.

Dejong, J. and Harris, M.C.H. 1971. Settlements of two multistory buildings in Edmonton, Alberta. Canadian Geotechnical Journal, Vol. 8, pp. 217-235.

Delory, E.H., Crawford, A.M. and Gibson, M.E.W. 1979. Measurement on a tunnel lining in very dense till. Canadian Geotechnical Journal, Vol. 16, pp. 190-199.

Duncan, J.M. and Chang, C.Y. 1970. Nonlinear analysis of stress and strain in soils. ASCE Journal of the Soil Mechanics and Foundations Division, Vol. 96, No. SM5, pp. 1629-1653.

Eden, W.J. 1970. Sample trials in overconsolidated sensitive clay. ASTM, SPT483, pp. 132-142.

Eden, W.J. and Bozozuk, M. 1969. Earth pressures on Ottawa outfall sewer tunnel. Canadian Geotechnical Journal, Vol. 6, pp. 17-32.

Eisenstein, Z. 1984. Private Communication.

Eisenstein, Z., El-Nahas, F. and Thomson, S. 1979. Pressure displacement relations in two systems of tunnel lining. Proceedings of Special Session on Tunnels in Soft Ground, 6th Pan American Conference on Soil Mechanics, Lima, Balkema, Rotterdam, pp. 85-94.

Eisenstein, Z., El-Nahas, F. and Thomson, S. 1981. - Strain field around a tunnel in stiff soil. Proceedings of the 10th International Conference on Soil Mechanics and Foundation Engineering, Stockholm, Vol. 1, pp. 283-288.

Eisenstein, Z. and Thomson, S. 1978. Geotechnical performance of a tunnel in till. Canadian Geotechnical Journal, Vol. 15, pp. 332-345.

Endo, K. and Miyoshi, M. 1978. Closed-type shield tunnelling through soft silt layer and consequent ground behavior. Tunnelling Under Difficult Conditions, Proceedings of the International Tunnel Symposium, Tokyo, pp. 329-334.

Ghaboussi, J., Hansmire, W.H., Parker, H.W. and Kim, K.J. 1983. Finite element simulation of tunnelling over subways. ASCE Journal of Geotechnical Engineering, Vol. 109, No. GT3, pp. 318-334.

Ghaboussi, J., Ranken, R.E. and Karshenas, M. 1978. Analysis of subsidence over soft-ground tunnels. International Conference on Evaluation and Prediction of Subsidence, Pensacola Beach, Fla., ASCE, pp. 182-196.

Hansen, J.B. and Gibson, R.E. 1949. Undrained shear strengths of anisotropically consolidated clays. Geotechnique, Vol. 1, No. 3, pp. 189-204.

Hansmire, W.H. 1975. Field measurements of ground displacements about a tunnel in soil. Ph.D. Thesis, University of Illinois at Urbana-Champaign, 334 p.

Henry, K. 1974. Grangemouth tunnel sewer. Tunnels & Tunnelling, Vol. 6, No. 1, pp. 25-29.

Hill, R. 1956. The Mathematical Theory of Plasticity. Oxford, Clarendon Press.

Hvorslev, M.J. 1949. Subsurface exploration and sampling of soils. Report on a Research Project of the Committee on Sampling and Testing, Soil Mechanics and Foundations Division ASCE, Chapter 4, pp. 83-170.

Ito, T. and Hisatake, M. 1982. Proceedings of the 4th International Conference on Numerical Methods in Geomechanics, Edmonton, Vol. 2, pp. 551-559.

Janbu, N. 1963. Soil compressibility as determined by oedometer and triaxial tests. European Conference on Soil Mechanics and Foundation Engineering, Wiesbaden, Germany, Vol. 1, pp. 19-25.

Katzenbach, R. and Breth, H. 1981. Nonlinear 3-D Analysis for NATM in Frankfurt clay. Proceedings of the 10th International Conference on Soil Mechanics and Foundation Engineering, Stockholm, Vol. 1, pp. 315-318.

Kawamoto, T. and Okuzono, K. 1977. Analysis of ground surface settlement due to shallow shield tunnels. International Journal for Numerical and Analytical Methods in Geomechanics, Vol. 1, pp. 271-281.

Kimura, T. and Mair, R.J. 1981. Centrifugal testing of model tunnels in soft clay. Proceedings of the 10th International Conference on Soil Mechanics and Foundation Engineering, Stockholm, Vol. 1, pp. 319-322.

Kuesel, T.R. 1969. Panel Discussion. Proceedings, 7th International Conference on Soil Mechanics and Foundation Engineering, Mexico City, Session IV, Vol. 3, pp. 312-320.

Kuesel, T.R. 1972. Soft ground tunnels for the BART project. Proceedings, First Rapid Excavation Tunnelling Conference, Chicago, Vol. 1, pp. 287-313.

Kulhawy, F.H. 1974. Finite element modelling criteria for underground openings in rock. International Journal of Rock Mechanics and Mining Science, Vol. II, pp. 465-472.

Ladanyi, B. 1974. Use of the long-term strength concept in the determination of ground pressure on tunnel linings. Advances in Rock Mechanics, Proceedings, Third Congress of the International Society for Rock Mechanics, II-B, pp. 1150-1156.

Ladanyi, B. 1981. Panel Discussion. Session II. Proceedings of the 10th International Conference on Soil Mechanics and Foundation Engineering, Vol. 4, pp. 613-615.

Lambe, T.W. 1973. Predictions in soil engineering. Geotechnique, No. 2, pp. 149-202.

Landva, A. 1964. Equipment for cutting and mounting undisturbed specimens of clay in testing devices. Oslo, Norwegian Geotechnical Institute, No. 56, pp. 1-5.

Law, K.T. 1975. Ph.D. Thesis, University of Western Ontario.

Law, K.T. 1981. Servo system for controlled stress path tests. Laboratory Shear Strength of Soil, ASTM, STP740, pp. 164-179.

Litwiniszyn, J. 1956. Application of the equation of stochastic processes to mechanics of loose bodies. Archiwum Mechaniki Stosowanej, Vol. 8, pp. 393-411.

Lo, K.Y. 1962. Shear strength properties of a sample of volcanic material of the Valley of Mexico. Geotechnique, Vol. 12, pp. 303-318.

- Lo, K.Y. 1965. Stability of slopes in anisotropic soils. ASCE Journal of Soil Mechanics and Foundation Division, Vol. 91, No. SM4, pp. 85-106.
- Lo, K.Y. 1972. The influence of mechanical disturbance on the consolidation of clays. Proceedings of the 3rd Southeast Asian Conference on Soil Engineering, pp. 223-232.
- Lo, K.Y. 1973. Behavior of embankment on sensitive clays loaded close to failure. Internal Report, OJT and CPR L-2, Ministry of Transportation and Communications.
- Lo, K.Y., Leonards, G.A. and Yuen, C. 1977. Interpretation and significance of anisotropic deformation behaviour of soft clay. Norwegian Geotechnical Institute, No. 117, Oslo.
- Lo, K.Y., Lukajic, B. and Ogawa, T. 1984. Interpretation of field measurements of stresses and displacements around excavations in rocks. Tunnelling in Soil and Rock, ASCE Geotech III Conference, Atlanta, Georgia, pp. 128-155.
- Lo, K.Y. and Milligan, V. 1967. Shear strength properties of two stratified clays. ASCE Journal of Soil Mechanics and Foundation Division, Vol. 93, No. SM1, pp. 1-15.
- Lo, K.Y. and Morin, J.P. 1961. Strength anisotropy and time effects of two sensitive clays. Canadian Geotechnical Journal, Vol. 9, No. 3, pp. 261-277.
- Lo, K.Y., Ng, M.C. and Rowe, R.K. 1984. Predicting settlement due to tunnelling in clays. Tunnelling in Soil and Rock, ASCE Geotech III Conference, Atlanta, Georgia, pp. 46-76.
- Lo, K.Y. and Rowe, R.K. 1982. Prediction of ground subsidence due to tunnelling in clays. Research Report GEOT-10-82, Faculty of Engineering Science, University of Western Ontario, London, Canada.
- Lo, K.Y., Wai, R.S.C., Palmer, J.H.L. and Quigley, R.M. 1978. Time dependent deformation of shaly rocks in Southern Ontario. Canadian Geotechnical Journal, Vol. 15, No. 4.
- Mair, R.J., Gunn, M.J. and O'Reilly, M.P. 1981. Ground movements around shallow tunnels in soft clay. Proceedings of the 10th International Conference on Soil Mechanics and Foundation Engineering, Stockholm, Vol. 1, pp. 323-328.
- Marsal, R.J. 1957. Unconfined compression and vane shear tests in volcanic lacustrine clay. Conference on Soils for Engineering Purposes, Mexico, ASTM, SPT 232, pp. 229-241.
- Marsland, A. 1973. Large in-situ tests to measure the properties of stiff fissured clays. Building Research Establishment Current Paper, CP1/73.

- Mesri, G., Rokhsar, A. and Bohor, B.F. 1975. Composition and compressibility of typical samples of Mexico City clay. *Geotechnique*, Vol. 25, pp. 527-554.
- Mindlin, R.D. 1948. Stress distribution around a hole near the edge of a plate under tension. *Proceedings, Society of Experimental Stress Analysis*, pp. 56-68.
- Moorhouse, W.W. 1970. Gunflint Iron Range in the vicinity of Port Arthur. *Ontario Department of Mines*, Vol. LXIX, Part 7.
- Moretto, O. 1969. Panel Discussion. *Proceedings, 7th International Conference on Soil Mechanics and Foundation Engineering, Mexico City, Session IV, Vol. 3*, pp. 325-328.
- Morton, Dodds and Partners Ltd. 1976. Study to determine load distribution and ground movements on the new sewer tunnelling system in soft clays at Thunder Bay. Prepared for the Division of Building Research, Ref. No. 76012, Rexdale, Ontario.
- Morton, J.D., Dunbar, D.D. and Palmer, J.H.L. 1977. Use of a precast segmented concrete lining for a tunnel in soft clay. *Geotechnical Aspects of Soft Clays, Proceedings, International Symposium on Soft Clay, Bangkok*, pp. 587-598.
- Muir Wood, A.M. 1969. Panel Discussion. *Proceedings, 7th International Conference on Soil Mechanics and Foundation Engineering, Mexico City, Session IV, Vol. 3*, pp. 363-365.
- Muir Wood, A.M. and Gibbs, F.R. 1971. Design and construction of the cargo tunnel at Heathrow Airport. *Proceedings, Institute of Civil Engineers*, Vol. 48, pp. 11-34.
- Niwa, Y., Kobayashi, S. and Fukui, T. 1979. Stresses and displacements around an advancing face of a tunnel. *Proceedings of the 4th International Congress on Rock Mechanics, Vol. 1, Montreux, Switzerland*, pp. 703-710.
- Norgrove, W.B., Cooper, I. and Attewell, P.B. 1979. Site investigation procedures adopted for the Northumbrian Water Authority's Tyneside Sewerage Scheme, with special reference to settlement prediction when tunnelling through urban areas. *Tunnelling '79, Institution of Mining and Metallurgy, Paper 27*, pp. 3-28.
- Oda, M. 1972. Initial fabrics and their relations to mechanical properties of granular material. *Soils and Foundations, JSSMFE, Vol. 12, No. 2*, pp. 1-18.

Oda, M. 1981. Anisotropic strength of cohesionless sands. ASCE Journal of the Geotechnical Engineering Division, Vol. 107, No. GT9, pp. 1219-1231.

Oda, M., Koishikawa, I. and Higuchi, T. 1978. Experimental study of anisotropic shear strength of sand by plane strain test. Soils and Foundations, JSSMFE, Vol. 18, No. 1, pp. 25-38.

Ohnishi, Y., Kishimoto, H., Nishigaki, Y. and Tanaka, Y. 1982. Analysis of advancing tunnel by 2-dimensional F.E.M. Numerical Methods in Geomechanics, Edmonton, Vol. 2, pp. 571-578.

Palmer, J.H.L. 1982. Private Communications.

Palmer, J.H.L. and Belshaw, D.J. 1979. Long-term performance of a machine bored tunnel with use of an unreinforced, precast, segmented concrete lining in soft clay. Paper 19, Tunnelling '79, Institute of Mining and Metallurgy, London, England.

Palmer, J.H.L. and Belshaw, D.J. 1980. Deformations and pore pressures in the vicinity of a precast, segmented, concrete-lined tunnel in clay. Canadian Geotechnical Journal, Vol. 17, pp. 174-184.

Palmer, J.H.L. and Lo, K.Y. 1974. In-situ measurement of lateral pressures using hydraulic fracturing technique. Soil Mechanics Research Report SM-2-74, The University of Western Ontario.

Peck, R.B. 1969. Deep excavations and tunnelling in soft ground. Proceedings, 7th International Conference on Soil Mechanics and Foundation Engineering, Mexico City, pp. 225-290.

Peck, R.B., Hendron Jr., A.J. and Mohraz, B. 1972. State of the art of soft ground tunnelling. Proceedings, First Rapid Excavation Tunnelling Conference, Chicago, AIME, Vol. 1, pp. 259-286.

Prevost, J.H. 1977. Anisotropic undrained stress-strain behavior of clays. ASCE Journal of the Geotechnical Engineering Division, Vol. 104, No. GT8, pp. 1075-1090.

Prevost, J. and Hoeg, K. 1976. Reanalysis of simple shear testing. Canadian Geotechnical Journal, Vol. 13, No. 4, pp. 418-429.

Pye, E.G. 1969. Geology and scenery. North shore of Lake Superior. Ontario Department of Mines.

Quigley, R.M. 1980. Geology, mineralogy and geochemistry of Canadian soft soils: A geotechnical perspective. Canadian Geotechnical Journal, Vol. 17, No. 2, pp. 261-285.

Ranken, R.E., Ghaboussi, J. and Hendron Jr., A.J. 1978. Analysis of ground liner interaction for tunnels. Prepared for Urban Mass Transportation Administration, Washington, D.C., Report No. UMTA-IL-06-0043-78-3, Illinois University at Urbana-Champaign, Dept. of Civil Engrg.

Romo, M.P. and Diazm, C. 1981. Face stability and ground settlement in shield tunnelling. Proceedings of the 10th International Conference on Soil Mechanics and Foundation Engineering, Stockholm, Vol. 1, pp. 357-360.

Rowe, P.W. and Barden, L. 1966. A new consolidation cell. Geotechnique, Vol. 16, No. 2, pp. 162-170.

Rowe, R.K., Booker, J.R. and Balaam, N.P. 1978. Application of the initial stress method to soil structure interaction. International Journal of Numerical Methods in Engineering, Vol. 12, No. 5, pp. 873-880.

Rowe, R.K. and Kack, G.J. 1983. A theoretical examination of the settlements induced by tunnelling: Four case histories. Canadian Geotechnical Journal, Vol. 20, pp. 299-314.

Rowe, R.K., Lo, K.Y. and Kack, G.J. 1983. A method of estimating surface settlement above shallow tunnels in soft soil. Canadian Geotechnical Journal, Vol. 20, pp. 11-22.

Rowe, R.K., Lo, K.Y. and Tham, L.G. 1982. The analysis of tunnels and shafts in dense oil sands. Proceedings of the 4th International Conference on Numerical Methods in Geomechanics, Edmonton, pp. 587-596.

Saada, A.S. and Townsend, F.C. 1981. State of the art: Laboratory strength testing of soils. Laboratory Shear Strength of Soil. American Society of Testing and Materials, STP 740, pp. 7-77.

Schmidt, B. 1969. Settlements and ground movements associated with tunnelling in soil. Ph.D. Thesis, University of Illinois, Urbana, Ill.

Schofield, A. and Wroth, P. 1968. Critical State Soil Mechanics. McGraw-Hill.

Streeter, V.L. and Wylie, E.B. 1975. Fluid Mechanics, Sixth Edition. McGraw-Hill Book Company.

Sweet, A.L. and Bogdanoff, J.L. 1965. Stochastic model for predicting subsidence. ASCE Journal of the Engineering Mechanics Division, Vol. 91, No. EM2, pp. 21-45.

Terzaghi, K. 1942. Shield tunnels of the Chicago Subway. Journal of the Boston Society of Civil Engineers, Vol. 29, No. 3, pp. 163-210.

Terzaghi, K. and Peck, R.B. 1948. Soil Mechanics in Engineering Practice. Wiley-Interscience, Art. 44.

Thomson, S. and El-Nahhas, F. 1980. Field measurements in two tunnels in Edmonton, Alberta. Canadian Geotechnical Journal, Vol. 17, pp. 20-33.

Tinajero, L.S. and Vieitez, L.U. 1971. Settlement around shield driven tunnels. Proceedings, 4th Pan American Conference of Soil Mechanics, San Juan, 2, pp. 225-241.

Townsend, D.L., Hughes, G.T. and Cruickshank, J.A. 1965. The effect of pore pressures on the undrained strength of a varved clay. International Conference on Soil Mechanics and Foundation Engineering, 6, Montreal Proceedings, 1, pp. 385-389.

Ward, W.H. 1969. Panel Discussion. Proceedings, 7th International Conference on Soil Mechanics and Foundation Engineering, Mexico City, Session IV, Vol. 3, pp. 320-325.

Ward, W.H., Marsland, A. and Samuels, S.G. 1965. Properties of the London Clay at the Ashford Common Shaft: Insitu and undrained strength tests. Geotechnique, Vol. 15, pp. 321-343.

Ward, W.H. and Pender, M.J. 1981. Tunnelling in soft ground - General Report. Proceedings, 20th International Conference on Soil Mechanics and Foundation Engineering, Stockholm, Session II, Vol. 4, pp. 261-275.

Yuen, C.M.K., Lo, K.Y., Palmer, J.H.L. and Leonards, G.A. 1978. A new apparatus for measuring the principal strains in anisotropic clays. Geotechnical Testing Journal, Vol. 1, No. 1, ASTM, pp. 24-33.

Zienkiewicz, O.C. 1982. The Finite Element Method, Third Edition. McGraw-Hill.

Zienkiewicz, O.C., Valiappan, S. and King, I.P. 1969. Elasto, plastic solutions of engineering problems - initial stress finite element approach. International Journal of Numerical Methods in Engineering, Vol. 1, pp. 75-100.

ADDITIONAL REFERENCES

Muckle, G. 1984. The effect of stress path on the behaviour of Thunder Bay clay. M.Sc. Thesis. University of Western Ontario.

Rowe, R.K. 1978. Soil structure interaction analysis and its application to the prediction of anchor plate behaviour. Ph.D. Thesis. University of Sydney.

Soderman, L.G. and Quigley, R.M. 1965. Geotechnical properties of three Ontario clays. Canadian Geotechnical Journal, Vol. II, No. 2, pp. 176-189.

PUBLICATIONS:

- (1) "Predicting Settlement Due to Tunnelling in Clays", Lo, K.Y., Ng, M.C. and Rowe, R.K. Proceedings of GEOTECH '84 Conference, ASCE, Atlanta, Georgia, 1984.

END

2 6 1 0 3 1 8 5

FIN